Flying GLARE®

A contribution to aircraft certification issues on strength properties in non-damaged and fatigue damaged GLARE® structures

Thomas Beumler

Flying GLARE®

A contribution to aircraft certification issues
on strength properties
in non-damaged and fatigue damaged GLARE® structures

Proefschrift

ter vergrijging van de graad van doctor
aan de Technische Universiteit Delft,
op gezag van de Rector Magnificus prof.dr.ir. J.T. Fokkema,
voorzitter van het College voor Promoties,
in het openbaar te verdedigen

op dinsdag 23 maart 2004 om 13.00 uur

door

Thomas BEUMLER
Diplom-Ingenieur der Fachrichtung Flugzeugbau
geboren te Hannover, Duitsland

Dit proefschrift is goedgekeurd door de promotoren:

Prof. ir. L.B. Vogelesang, Technische Universiteit Delft
Prof. dr. ir. M. van Tooren, Technische Universiteit Delft

Samenstelling promotiecommissie

Rector Magnificus,	voorzitter
Prof. ir. L.B. Vogelesang,	Technische Universiteit Delft , promotor
Prof. dr. ir. M.J.L. van Tooren,	Technische Universiteit Delft , toegevoegd promotor
Prof. dr. ir. J. Schijve,	Technische Universiteit Delft
Prof. Dr.-Ing. P. Horst,	Technische Universität Braunschweig, Braunschweig
Prof. Dr.-Ing. L. Schwarmann,	Chairman IASB Commitee
Dr. ir. G. Roebroeks,	Fiber Metal Laminates Center of Competence, Delft
Dr. ir. T. j. de Vries,	Airbus Deutschland GmbH, Hamburg

Published and distributed by: DUP Science

DUP Science is an imprint of
Delft University Press
P.O. Box 98
2600 MG Delft
The Netherlands
Telephone: +31 15 278 5678
Telefax: +31 15 278 5706

Cover photo taken by Jean Jodar, copyright: Airbus

ISBN: 90-407-2481-4
NUGI: 841

Keywords:
GLARE, Aircraft certification, Structural strengths, Environmental influences

Printed in The Netherlands

In memory of prof.dr.ir. Ad Vlot
* 1.11.1962 † 18.4.2002

“Your thesis will raise more questions than it will answer.”
(Ad Vlot, summer 2001)

Objective

The scope of this research is to support the type certification of the first flying GLARE structures in a civil aircraft, i.e. the A380-800, in frame of the given airworthiness requirements. The sizing process, from pre-development to structural component certification, requires a review for the GLARE application with regard to both its partly metallic and partly composite behaviour. The influences of material scatter, variable amplitude stress spectra, temperatures and ageing on the strength justification and structural certification are investigated.

Acknowledgement

Ad Vlot, Prof. Dr. Ir., Promotor, Delft University
Arjan Woerden, Ir., Fatigue Specialist, Delft University
Bob Borgonje, Ir., Fatigue & Durability Specialist, Delft University
Boud Vogelesang, Prof. Ir., Promotor, Delft University
Elke Hombergsmeier, Dipl.-Ing., Manager Materials Characterization and Simulation, EADS Forschung
Fred Pellenkoft, Ir., Fatigue Specialist, Delft University / Airbus Deutschland
Geert Roebroeks, Dr. Ir., FML Specialist, FMLC
Günther Heidenwolf, Dipl.-Ing., A380 Project Management, Airbus Deutschland
Heiner Stehmeier, Dipl.-Ing., Test Specialist, Airbus Deutschland
Henk van den Nieuwendijk, Ir., Fatigue Specialist, Airbus Deutschland
Ingo Kröber, Dipl.-Ing., Durability Specialist, Airbus Deutschland
Jaap Schijve, Prof. Dr. Ir., Promotor, Delft University
Jan Willem Gunnink, Ir., Director, FMLC
Jeroen Los, Laboratory Operator, Delft University
Johannes Homan, Ir., Fatigue Specialist, Delft University
Jos Sinke, Ir., Delft University
Lüder Schwarmann, Prof. Dr. Ing., Promotor
Marie-Theres Beumler, my daughter
Michel van Tooren, Prof. Dr. Ir., Promotor, Delft University
René Alderliesten, Ir., Fatigue Specialist, Delft University / FMLC
Rik Jan Lemmen, Fatigue Specialist, Delft University / Airbus Deutschland
Theodor Meier, Dipl.-Ing., NDI Specialist, Airbus Deutschland
Tjerk de Vries, Dr. Ir., Fatigue Specialist, Delft University / Airbus Deutschland
Thomas Repp, Dipl.-Ing., Fatigue Specialist, Airbus Deutschland
Ulrike Beumler, my wife
Viktoria Beumler, my daughter
Walter Schwarting, Dipl.-Ing., Rocket Propulsion Specialist, ASTRIUM
Walter t'Hart, Ir., Fatigue Specialist, NLR
Wilfried Kelm, Dr. Ing., Bonding Specialist, Airbus Deutschland
Willem Brugman, Ir., Material & Processes Specialist, Airbus Deutschland
Wim van der Hoeven, Ir., Fatigue & Durability Spezialist, NLR

Without the strong support or at least the tolerance of the above mentioned people this work would have been impossible.

Abstract

At the end of the second millennium did the aircraft industry decide for the first time to apply the fiber metal laminate GLARE in a large quantity on a civil transport aircraft. It was focused on an application of the material on the pressurised fuselage, the decision driven by the demand for weight saving at an affordable cost level.

GLARE material properties are linked to both, monolithic aluminium properties as well as fiber composite properties, with the preference depending on the particular strength feature under investigation. Between others, three major structural mechanic advantages compared with monolithic aluminium can be identified for fiber metal laminates, i.e. the lower density, the crack bridging capability of the fibers in presence of a fatigue crack in the particular aluminium sheets and the possibility to tailor the material according to structural mechanic requirements by appropriate orientation of the fibers.

Essential for an economic application of the material is the acceptance of `flying with undetectable fatigue damages´. This rule and it's implications on structural sizing and justification is discussed in depth in this report, leading to the particular subject of the strength behaviour of riveted joints in a fatigued condition.

Because GLARE contains an epoxy resin prone to moisture absorption, strength degradations due to environmental influences have to be taken into account. However, as for other materials, it is searched for a *realistic* exposure in order to design a structural component to the limits of the material strength and to avoid unnecessary high reserves. An outdoor exposure program is under evaluation as part of the structural investigation, which extends the time frame of this thesis. Structural components are supposed to remain for up to 6 years on a tropical exposure site. However, evaluated weight gain measurements allow extrapolations for 30 years aircraft operation and the definition of a representative accelerating ageing process.

Extensive results on particular GLARE related investigations are reported since the end of the 1980's. This thesis is compiling the available information on fatigue issues and environmental related material issues, it is extending the previous research and it interprets the material properties within the framework of the mandatory airworthiness rules.
For that purpose, two structural items which are tested by Airbus under full scale conditions are investigated concerning all particular strength properties which are required for certification or not are investigated.

The application of airworthiness regulations which are defined for monolithic aluminium are discussed for GLARE in chapter 1. While fatigue sensitive monolithic aluminium structures have a relatively long crack initiation life but a relatively short crack propagation life, GLARE shows the opposite behaviour. What does that mean for the certification of a GLARE structure? Which fatigue methods should be used for the certification and is GLARE a single load path or a multiple load path structure? Some basic rules are discussed and proposals concerning the structural certification are provided.

No type certification of a commercial passenger aircraft is accepted without test substantiation. The test pyramid is starting with elementary specimens (can be tested early in a project) and finishes with a full scale fatigue test. Chapter 2 discusses the particular influences which have to be considered for structural certification, e.g. crack initiation scatter and temperature sensitivities to crack initiation, and which have to be *re*considered for GLARE.

Chapter 3 presents all specimen types which belong to the outdoor exposure program, i.e. test series from which some specimens are shipped to a tropic exposure site and some are tested under laboratory conditions, for comparison. The relevance of the particular specimen types and their history for GLARE is briefly discussed.

A review of accelerating ageing experiences of previous researches with Fiber Metal Laminates is done in chapter 4. Diffusion coefficients for GLARE3 made of 2024T3/FM94 are determined.

First weight gain measurements which are available from the outdoor exposure test site are investigated and interpreted in chapter 5. Predictions of the weight gain of GLARE around bore holes for both, long range aircraft and short range aircraft, are performed.

Chapter 6 presents elementary specimen test results for the two tested materials, related to different ageing conditions. First experiments with specimens which have been exposed for one year outdoors are included. The crack initiation and crack propagation scatter for a row of bore holes is determined.

Chapter 7 is dealing with coupon specimens, which are representative for the full scale structure tested by Airbus. A review and calibration of crack initiation, crack propagation and residual strength methods under development by Airbus Deutschland and Delft University is performed for a prediction of the full scale behaviour. The calculated results are discussed in view of a fatigue & damage tolerance certification. Full scale test results are related to the elementary- and the coupon experiments performed in this thesis.

The outdoor exposure investigation is extended by a few panel tests, i.e. non-stiffened riveted repair panels, non-stiffened bonded repair panels and door corner cut out specimens. This analyses are collected in chapters 9 to 11.

All experiments and analysis are performed with/for GLARE composed of aluminium 2024T3 and prepreg FM94/S-glass, cured at 120°C. Due to the wide range of specimen types each of them couldn’d be provided in a high quantity, for economic reasons. Therefore just property *trends* can be provided.

The investigations performed in frame of this thesis contribute to the verification of the TU Delft / Airbus computer program ‘FML F&DT Toolbox’, which is developed at the same time.

Table of Contents

Contents (continued) page

Contents (continued) page

Riveted Joint Investigations

Miscellaneous

Contents (continued) page

List of Symbols

A	cross sectional area	[mm^2]
A	activation energy	[K]
A/C	aircraft	
A_m	stiffness matrix	[MPa]
a	half crack length	[mm]
a	material constant for maximum moisture content determination	
a_c	critical crack length	[mm]
a_i	initial crack length	[mm]
a_{av}	average half crack length	[mm]
$a_{av,c,LL}$	average half crack length, critical at limit load	[mm]
$a_{av,c,UL}$	average half crack length, critical at ultimate load	[mm]
a_{Det}	detectable crack length	[mm]
a_{lead}	lead crack length	[mm]
b	material constant for maximum moisture content determination	
b’	reference width for determination of diffusion rates between bore holes	[mm]
C	coefficient	
C	(moisture) concentration	
C_{CI}	safety factor on crack initiation life of full scale specimen PSE	
$C_{CI(Q)}$	manufacturing quality scatter factor on life for crack initiation	
$C_{CI(MS)}$	material characteristics, scatter factor on life for crack initiation	
$C_{CI(LS)}$	load spectrum scatter factor on life for crack initiation	
$C_{CI(E)}$	deteriorative environmental factor on life for crack initiation	
$C_{CI(T)}$	temperature related factor on crack initiation life	
$C_{CI(F)}$	fastener factor, to be considered for crack initiation	
$C_{CI(ST)}$	surface treatment factor, to be considered for crack initiation	
$C_{CI(S)}$	factor which considers spectrum loads for single amplitude tests for crack initiation	
$C_{CI(SC)}$	factor to consider scale effect for crack initiation	
C_{CP}	safety factor on crack propagation life of full scale specimen	
$C_{CP(MS)}$	material characteristics, scatter factor on crack propagation life	
$C_{CP(LS)}$	load spectrum scatter factor on crack propagation life	
$C_{CP(E)}$	deteriorative environmental factor on crack propagation life	
$C_{CP(S)}$	factor which considers spectrum loads for single amplitude tests on crack propagation	
$C_{CP(SC)}$	factor to consider scale effect on crack propagation	
$C_{CP(T)}$	temperature related factor on crack propagation life	
$C_{RS(E)}$	deteriorative environmental factor on residual strength	
$C_{RS(T)}$	temperature related factor on residual strength	
CA	constant amplitude (testing)	
CFH	compression filled hole	
COD	crack opening displacement	[mm]
CTE	coefficient of thermal expansion	[1/°C]
D	fastener diameter	[mm]
D, D_0	diffusion rate ; diffusion coefficient	[mm^2/s]
DSG	Design Service Goal	[flights, flight hours, years]

E	elasticity modulus	[MPa]
ECT	Edge Crack Tension specimen	
ESG	Extended Service Goal	[flights, flight hours, years]
F	force	[N]
f	factor	
F_{ad}	shear stiffness between aluminium layer and prepreg	[N/mm]
f_{corr}	correction factor for crack length through the thickness	
F_{LL}	limit load strength	[MPa]
F_{UL}	ultimate load strength	[MPa]
FML	Fiber Metal Laminate	
FWD	forward	
g	gravity	[9.81 m/s^2]
GAG	ground – air – ground (load cycle)	
G_{del}	delamination driving energy	[N/mm]
Gprep'	apparent shear modulus of GLARE3 prepreg	[N/mm^2]
h	hour	
ILSS	inter laminar shear strength	
ISA	International Standard Atmosphere, includes temperature 15°C	[°C]
ISP	threshold, no. of flights for first inspection, equals N_{TH}	[flights]
K	stress intensity	[MPa√m]
K_t	stress concentration factor	
l	length	[mm]
LL	limit load, limit load strength capability	
LR	long range	
M	number of specimens belonging to a statistical evaluated population	
M	moisture content	[%]
M_m	maximum moisture content	[%]
MSD	Multiple Site Damage	
MVF	metal volume fraction	[%]
N	rank number	
N	structural fatigue life	[cycles, flights]
$N_{A/C}$	structural fatigue life of the aircraft	[flights, flight hours, years]
$N_{A/C,I}$	aircraft flights to crack initiation for considered PSE	[flights]
$N_{A/C,P}$	aircraft crack propagation rate for considered PSE	[flights]
$N_{FS,P}$	crack propagation rate of full scale fatigue specimen PSE	[flights]
N_{DET}	flights or cycles at which crack becomes detectable	[flights, cycles]
N_{DSG}	structural aircraft fatigue life according to design service goal	[flights]
N_{ESG}	structural fatigue life acc. to Extended Service Goal	[flights]
$N_{FS,I}$	structural crack initiation life of full scale fatigue specimen PSE	[flights]
N_i	crack initiation life	[cycles, flights]
N_{iCP}	crack propagation life	[cycles, flights]
N_{LL}	no. of flight cycles, at which limit load capability is reached	[flights]
N_{TH}	threshold, no. of flights for first inspection, equals ISP	[flights]
N_{UL}	no. of flight cycles, at which ultimate load capability is reached	[flights]
NDI	Non Destructive Inspection	
NDT	Non Destructive Testing	

OAT	Outside Atmosphere Temperature	[°C]
PSE	Principal Structural Element (potentially fatigue sensitive structural item)	
Pü	probability of survival	[%]
UL	ultimate strength capability	
R	ratio minimum stress divided by maximum stress	
R	absolute temperature	[K]
R_D	ratio of fatigue damaged aluminium to total amount of aluminium	
R_{del}	critical energy release rate for delamination (delamination resistance)	[N/mm]
RH	Relative Humidity	[%]
RPT	rivet pull through	
RT	room temperature	[°C]
S	stress	[MPa]
s	standard deviation	
SEM	Scanning Electronic Microscope	
SF	scatter factor	
SMP	Structure Modification Point	
sqrt	square root	
SR	short range	
ssc	single side clad	
SSI	Structural Significant Item (identified fatigue sensitive structural item)	
t	thickness; time	[mm; h]
T	temperature	[°C]
u_{br}	crack opening displacement caused by bridging stress	[mm]
u_{∞}	crack opening displacement caused by applied stress	[mm]
VA	variable amplitude	
VT	variable temperature	
W	weight	[g, %]
w	width; weight	[mm; g, %]
WFD	Widespread Fatigue Damage	

Greek symbols

Δ	deformation	[mm]
Δp	cabin differential pressure, usually given at max. altitude	[bar, mbar]
δ_{ad}	adhesive shear deformation at delamination boundary	[mm]
δ_{fm}	extension of fibers at fatigue crack	[mm]
δ_n	random value	
γ	shear angle	
κ	slope (of SN-curve)	
μ_m	mean value	
ν	Poissons Ratio	
σ	stress	[MPa]
$\sigma_{lam.}$	Applied stress on GLARE laminate	[MPa]
σ_m	standard deviation	
σ_m	stress in metal	[MPa]
σ_{BN}	blunt notch stress	[MPa]
$\sigma_{al(\varepsilon=4.7\%)}$	stress in aluminium layers at laminate failure strain at RT	[MPa]
Σ	sum	

Terms

Damage Tolerance is the attribute of the structure that permits it to retain its required residual strength without detrimental structural deformation for a period of use after the structure has sustained a given level of fatigue, corrosion, and accidental or discrete source damage.

Design Service Goal (DSG) is the period of time (in flight cycles/hours) established at design and/or certification during which the principal structure will be reasonably free from significant cracking including Widespread Fatigue Damage.

Principal Structural Element (PSE) is an element that contributes significantly to the carrying of flight, ground or pressurization loads, and whose integrity is essential in maintaining the overall structural integrity of the airplane.

Widespread Fatigue Damage (WFD) in a structure is characterized by the simultaneous presence of cracks at multiple structural details that are of sufficient size and density whereby the structure will no longer meet its damage tolerance requirement (i.e. to maintain its required residual strength after partial structural failure).

WFD (average behaviour) is the point in time when 50% of the fleet have reached WFD for a particular detail.

Multiple Site Damage (MSD) is a source of widespread fatigue damage characterized by the simultaneous presence of fatigue cracks in the same structural element (i.e. fatigue cracks that may coalesce with or without other damage leading to a loss of required residual strength).

Multiple Element Damage (MED) is a source of widespread fatigue damage characterized by the simultaneous presence of fatigue cracks in similar adjacent structural elements.

Inspection Start Point (ISP) is the point in time when special inspections of the fleet are initiated due to a specific probability of having a MSD/MED condition.

Structural Modification Point (SMP) is a point reduced from the WFD average behaviour, i.e. lower bound, so that operation up to that point provides equivalent protection to that of a two-lifetime fatigue test. No airplane may be operated beyond the SMP without modification or part replacement.

Monitoring Period is the period of time bounded by the ISP and SMP when special inspections of the fleet can be conducted to preclude widespread fatigue damage. Note: A Monitoring Period is only applicable if there is an effective means of detecting a sub-critical crack with the special inspection.

Large Damage Capability (LDC) is the ability of the structure to sustain damage visually detectable under an operator's normal maintenance due to accidental, fatigue and environmental degradation and still maintain limit load capability with MSD to the extent expected at SMP.

Scatter Factor. A life reduction factor used in the interpretation of fatigue analysis and fatigue test results.

Test-to-Structure Factor. A series of factors used to adjust test results to full-scale structure. These factors could include but are not limited to difference in: stress spectrum, boundary conditions, specimen configuration, material differences, geometric considerations, and environmental effects.

Design Case. The strength of an aircraft structure has to be justified according to different requirements from both, static and fatigue point of view. Examples are the yield strength (static) and the maximum allowable stress in order to reach the DSG. One requirement is the toughest one to achieve, its reserve factor should be close to 1 in order to achieve the optimum weight for the component. This requirement is called the 'design case'.

Knock Down Factor. A factor which is applied on a strength value for various reasons, e.g. in order to consider environmental influences on experimental results which are performed at room temperature in a laboratory. Factors below 1 decrease strength values, factors greater than 1 increase strength values.

GLARE Grades

The GLARE which is qualified for the A380-800 aircraft is build up from alternating 2024T3 metal layers and uni-directional S-glass layers. The resin system is FM94 from supplier Cytec.

Available metal layer thickness: 0.2mm, 0.3mm, 0.4mm, 0.5mm

Standard grades:

	Prepreg Thickness	Fiber Orientation
GLARE2A	0.250mm	0°/0°
GLARE2B	0.250mm	90°/90°
GLARE3	0.250mm	0°/90°
GLARE4A	0.375mm	0°/90°/0°
GLARE4B	0.375mm	90°/0°/90°
GLARE6	0.250mm	45°/45°

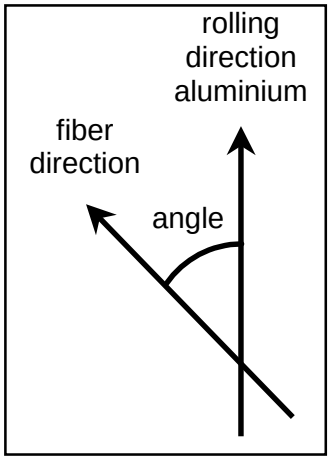

Example nomenclature: GLARE4A-5/4--.4

→ each aluminium layer: t = 0.4mm

→ 5 aluminium layers, 4 prepreg layers in GLARE4 lay-up

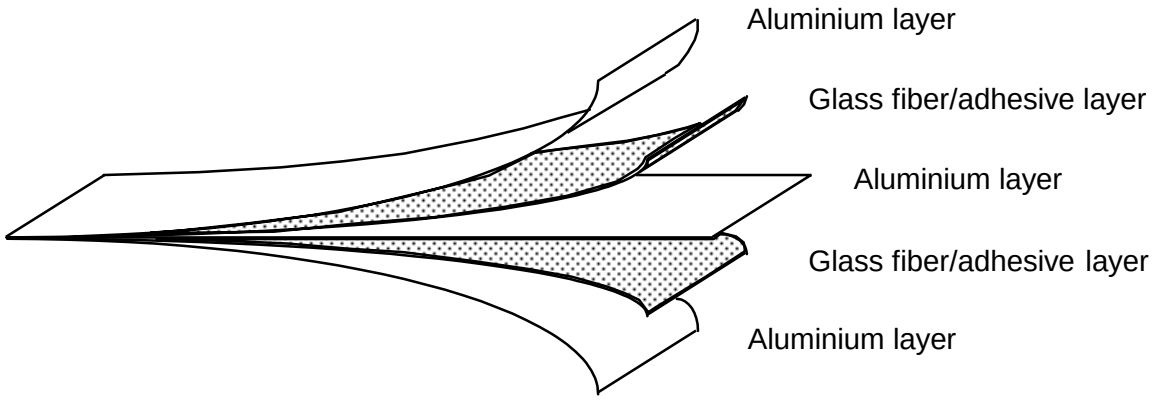

Typical material properties are compiled in table 1.

Threshold Inspection. First scheduled fatigue inspection of a PSE.

Hole. Any holes discussed in these thesis refer to drilled holes (bore holes).

Preface

Throughout the second half of the previous century service experience of aircraft operators with respect to fatigue and other types of damage has affected the ideas about designing new aircraft structures. Three noteworthy aspects should be mentioned.

(1) A number of aircraft accidents occurred due to fatigue cracks which indicated that the fatigue resistance of the structure was insufficient [1,2]. Two well-known examples are the catastrophic explosion of the De Havilland Comet fuselage in 1954 and a non-catastrophic fuselage failure along riveted lap joints in a Boeing 737 aircraft (the Aloha accident) in 1988. From the experience with failures in service it was evident that careful design against fatigue, good production techniques and reliable inspection procedures of the operator were very much needed.

(2) Operators were using the aircraft more intensively than in the past for economic reasons. Moreover, aircraft were used significantly longer than 20 years which was supposed to be a reasonable design life in the previous century.

(3) Because of the more intensive utilization of aircraft it is difficult to avoid damage of an aircraft structure. Damage can be due to fatigue cracks and corrosion, but various types of impact damage can also occur (e.g. handling damage in service, rotor burst, hailstorm, etc.).

In view of these circumstances a modern aircraft structure should be *durable and damage tolerant*. Durability includes a good fatigue and corrosion resistance. Various scenarios of how the aircraft can be used must be considered, including environmental conditions which can adversely affect the quality of the structure. Damage tolerance implies that periodic inspections are made to find damage. It also implies that sufficient residual strength of the structure must still be available if damage occurs to allow continued flying with damage until remedial action can be carried out. It should be recognized that airlines are not particularly fond on inspections for economic reasons. Actually, safety and economy quite often appear to be controversial issues. In view of safety arguments, the airworthiness authorities require that aircraft design and aircraft operation comply with official Airworthiness Requirements which for fatigue are described in the FAR 25.0571 document.

Since the application of aluminium alloy sheet material in aircraft structures around 1930, sheet materials of Al-alloys were abundantly used for transport aircraft. In the early days, limitations of the material properties of these alloys were not a serious problem. The advantages of a low specific mass and economic production technologies were attractive. Even in the present time the volume of aluminium alloys in the load carrying components of transport aircraft is in a predominant position.
In the second half of the previous century various new Al-alloys with improved properties were developed. The stress corrosion resistance of the 7000 series Al-alloys could be improved by over ageing. The fracture toughness of the 2000 series was improved by eliminating inter metallic inclusions of the material. However, improving the fatigue properties and the corrosion resistance by changing the heat-treatment and the contents of alloying elements of the Al-alloys did not lead to significant and systematic improvements. The above problem of durability and damage tolerance was not really served by modifications of the alloy system.

In the seventies interesting improvements of the damage tolerance properties were indicated in fatigue investigations on laminated sheet material built up from thin aluminium alloy sheets by adhesive bonding to a single stack [3]. However, a real break through was made around 1980 when uniaxial aramid fibers

were introduced in the intermediate adhesive layers of laminated sheet material to be built up from very thin sheets (0.3 to 0.5 mm). This hybrid fiber metal laminate (FML) was called ARALL (Aramid Reinforced Aluminium Alloy Laminates). It was primarily produced as sheet material for aircraft structures. Some different types of ARALL were developed. They showed a very high resistance against fatigue crack growth which is associated with fiber-crack-bridging in the wake of fatigue cracks. Later (around 1990) the aramid fibers were replaced by advanced glass fibers with GLARE as the trade name for this new family of FML's. Various properties were superior if compared to ARALL. Different grades of GLARE were developed for specific applications in aircraft components. A survey of the history leading to the development of GLARE was recently presented by Vogelesang [4] (see also the book by Ad Vlot [5]).

Before the aircraft industry can apply new FML's in an aircraft structure a lot of extensive research is necessary. In general terms and without attempting to be complete the following topics must be covered:

- Production of the fiber-metal laminates (FML) and quality control on the FML's.
- Collecting a large variety of material properties of the FML's.
- Production technology associated with plastic deformation (e.g. sheet metal bending) and different types of joints (e.g. riveted and bolted joints).
- Production technology associated with cutting operations.
- Various fatigue and static tests on simple notched specimens, joints, structural elements and full scale structures.
- Time dependent properties and environmental effects.

Extensive test programs are necessary for the aircraft industry to confirm the advantages of the application of GLARE in aircraft structures. These test programs are also of great interest to the aircraft operators and essential to meet the requirements of the airworthiness authorities. Moreover, the investigations should contribute to useful design data as well as to understanding of possible failure mechanisms in GLARE components. Many projects were defined and carried out in close cooperation between FMLC (Fiber-Metal-Laminate Centre of Competence), the Faculty of Aerospace Engineering in Delft, Airbus Industrie, the NLR, NIVR and Fokker Aerospace (Stork) in order to support Airbus Industrie to achieve material readiness for designing components built up from GLARE sheets.

The lay up of GLARE can be selected by the designer to meet the required thickness and properties. An important decision is to select either uni-directional or cross ply depending on the purpose of the PSE. The lowest thickness is obtained with a 2/1 lay up which will be rarely used. A common lay up for thin sheets is the 3/2 lay up with either 0.3mm or 0.4mm individual sheet thickness.

Originally GLARE was produced as sheet panels with a maximum length of 2.5 meters. In the early nineties Roebroeks [6] developed the so-called splice concept which allowed the production of much longer panels. Actually, the panels could be made as long as the length of the autoclave.
This implies that many riveted joints can be avoided which is obviously attractive. Moreover, based on the idea of the splice concept it turned out that local reinforcements could be introduced. Another option is to apply more metal layers around large cut outs which is done as part of the autoclave cycle to produce the GLARE component. A classical worry is a door in a fuselage where passengers can observe various repairs at a corner of a cabin door of flying aircraft. This problem is solved in a GLARE panel by adding GLARE doublers during the autoclave cycle.

In the mid nineties Hinrichsen suggested to produce double curved skin panels by using a curved mould in the autoclave. The same idea was also considered by FMLC and Roebroeks managed to develop this concept to production standard. This implies that a GLARE product then is manufactured rather than a GLARE sheet.

From a design point of view the GLARE technology appears to be promising for economical weight savings. A major question for the aircraft industry then is to prove satisfactory damage tolerance and durability of the GLARE components of an aircraft structure in agreement with the Airworthiness Requirements. Weight saving, durability and damage tolerance, including less inspections and repairs, are attractive for the airlines. Safety, damage tolerance and durability in the long run offer the major questions to the Airworthiness Authorities. The aircraft industry should prove that these questions are satisfactory evaluated.

The author was involved as both a PhD student at Delft University and as employee of the Airbus Deutschland GmbH in the late stages of the GLARE development. The investigation reported in his present thesis covers some parts of the above problem setting, specifically the interpretation of Airworthiness Requirements which are originally related to monolithic metal structures for GLARE.

References

[1] Structural integrity of aging airplanes. A perspective. Paper in Structural Integrity of Aging Airplanes. J.W. Mar, Eds. S.N. Atluri, S.G. Sampath and P. Tong. Springer-Verlag, 1991.

[2] Engineering Aspects of Ageing Aircraft. J. Schijve, Delft University of Technology, Technology Seminar “Ageing Aircraft”, Daimler Benz Aerospace Airbus, Hamburg, 20 Sep. 1996.

[3] Fatigue properties of adhesive bonded laminated sheet material of aluminium alloys. J. Schijve, H. van Lipzig, G. van Gestel, A. Hoeymakers, Eng. Fracture Mechanics, vol. 12, 1979

[4] Fibre Metal Laminates, the development of a new family of hybrid materials. The 19th Plantema Memorial Lecture, ICAF Symposium, Luzern, B. Vogelesang, Delft University of Technology, 2003.

[5] Glare, history of the development of a new aircraft material. A. Vlot, Delft University of Technology, Kluwer Academic Publishers, 2001.

[6] Towards Glare, G. Roebroeks, Delft University of Technology, PhD thesis, 1989

Chapter 1
Airworthiness Regulations & Aircraft Certification

Contents Page

This page intentionally left blank.

"If you would have used GLARE as fuselage material during the past 50 years and if you would now propose to fly without fibers, it would be hard for us to accept."
*Bob Eastin, FAA Fatigue Chief Technologist **

1.1 Introduction

Aircraft structures made of aluminium alloy materials do not have an infinite fatigue life and so ongoing inspections are the fate of the aircraft operator. From a design and certification standpoint the fatigue problem of aluminium structures is currently controlled by the damage tolerance design philosophy formalized in the airworthiness requirements. Aircraft fuselage skins comply with this philosophy through slow crack growth strategies allowing inspection and discovery of fatigue cracks prior to failure. This slow crack growth is obtained with a major compromise to allowable design stresses.

Airbus has selected GLARE as material for a large part of the A380 fuselage skin to overcome this drawback. The secret of GLARE is its crack bridging behaviour in the presence of fatigue cracks, by reducing considerably the effect of these cracks. This allows considerably higher design stresses form the fatigue point of view. The acceptance of GLARE from certification standpoint needs, however, an acceptance of flying with small cracks as part of the fatigue justification concept. Multiple small fatigue cracks are acceptable for airworthiness, as long as the ultimate load capability is guaranteed for crack lengths below detectable. This approach is essential for the efficient application of GLARE as primary aircraft structural material and with this the achievement of high allowable stresses and low structural weights. It has been discussed and agreed with the responsible Airworthiness Authorities for the A380 aircraft [1,2],

However, the introduction of GLARE happens in a time of ongoing discussions concerning an assessment of FAR/JAR 25.0571 for the multiple site damage (MSD) phenomenon [3]. Rulemaking task forces even consider to reinstate the safe-life requirement for certain design aspects. In the ACJ 25.0571 it is already stated that 'in practice it may not be possible to guard against the effects of multiple damage and fail-safe substantiation may be valid only up to a particular life which would preclude multiple damage'. It also mentions that 'the achievement of this [provisions to limit the probability of concurrent multiple damage] would be facilitated by ensuring sufficient life to crack initiation'. Flying with cracks is therefore a disputable concept. The current research will discuss the concept of fibre metal laminates in the frame of airworthiness requirements, especially including the aspect of environmental ageing.

Sufficient experiences with sizing processes are available for both, monolithic aluminium and composite structures. GLARE has material characteristics of both. It is demanded by ACJ 25.0571, chapter 1.1.1, how far variations of the well known procedures to maintain aircraft safety are recommendable:

** A380 Certification meeting, Toulouse, October 29, 2002*

Quote ACJ 25.0571 (1.1.1):
„ *Although a uniform approach to the evaluation required by JAR 25.0571 is desirable, it is recognised that in such a complex field new design features and methods of fabrication, new approaches to the evaluation, and new configurations could necessitate variations and deviations from the procedures described in this ACJ*.“

The above problem setting about Airworthiness Regulations and Aircraft Certification of a GLARE structure is the major theme of this thesis. The investigation is focused on two important questions which are: Fatigue of GLARE riveted joints and environmental influences on the integrity of fatigue critical GLARE components.
Basic aspects are still discussed in some detail in the present chapter (Sections 1.2-1.7). Chapter 2 starts with Design Criteria and Design Factors for Riveted Joints.
Chapter 3 describes structural elements and specimens used in the investigation on environmental effects and subjected to an outdoors exposure test program.
Chapter 4 deals with diffusion aspects associated with GLARE exposed to selected humid environments in environmental chambers, while Chapter 5 describes the diffusion behaviour based on the first outdoor exposure program weight gain measurements.
Chapter 6 covers various investigations on environmental effects and scatter as observed on elementary specimens. Similar investigations on GLARE riveted joints are presented in Chapter 7 which completes the major subjects of the present investigation. Conclusions are presented at the end of this chapter.
In Chapter 8 recommendations are made about how to continue the experiments on the specimens which will return in year 2004 and in year 2008 from the outdoors exposure site.
Some special topics associated with GLARE repair techniques, riveted and bonded, and a door corner cut out are covered in Chapter 9, 10 and 11 respectively, including the significance of environmental effects.
Finally, the last chapter, Chapter 12, summarizes the contributions of the present investigation on aircraft certification issues related to strengths properties in non-damaged and fatigue damaged GLARE structures The chapter is concluded by a number of specific conclusions.

1.2 GLARE and Fiber Crack Bridging

The most simple fiber-metal-laminate (FML) is built up from thin Al-alloy sheets with intermediate prepregs consisting of an adhesive with long fibers in the same direction. In view of the biaxial stress condition in a pressurized fuselage another type of GLARE was developed in which each layer between metal sheets consists of two fiber layers with mutually perpendicular fiber directions (90^0 cross ply). After a hot curing cycle in an autoclave a FML sheet is obtained which can be built up of different numbers of metal sheets as required, and also with different orientations of the prepregs layers with uni-axial fibers.
If a fatigue crack is initiated in a FML the cracks are growing in the metal sheets but the fibers in the wake of the crack are supposed to remain intact. These fibers are bridging the crack, which restrains crack opening, see figure 1.2.1. Moreover, part of the remote load is still passing through the fibers in the wake of the crack. As a result the stress intensity factor (K) is significantly reduced and fatigue crack growth can be very slow.

The load in the crack bridging fibers causes a shear stress on the interface between the fiber layers and the metal layers. Due to this cyclic shear stress some fatigue related delamination will occur along the crack edges, see figure 1.2.1. By using very thin metal layers there are more interfaces for the same total thickness of the FML for load transmission of the fibers into the metal layers. The shear stress is thus reduced which implies that the delaminated zone can be relatively small. The mechanism of fiber-crack-bridging and the low thickness of the metal sheets constitute the “specifics” of the FML’s.

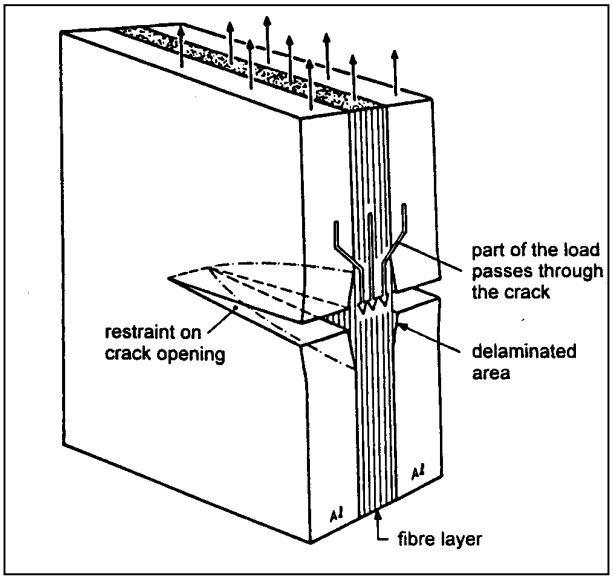

Figure 1.2.1. Intact fibers in the wake of the crack and crack edge delamination

The fatigue life of a notched element starts with a crack initiation period followed by a crack growth period until a quasi-static final failure occurs. For FML’s it is useful to define the crack initiation period as the initial part of the fatigue life as long as the crack growth is not yet significantly affected by fiber-crack-bridging. It then includes the initiation of a crack nucleus at the root of a notch and some initial crack growth. As long as the crack is short, there are no fibers in the wake of the crack, which will effectively restrain crack opening. As soon as a crack bridging becomes effective the crack should be considered to be in the crack growth period. The problem is to define a crack size, which is characteristic for the transition of the crack initiation period to the crack growth period. The size will depend on the thickness of the metal sheets and the fiber layers. It seems practical to relate the transition crack length to sizes which can be measured, even on the mating surfaces of single shear joints.

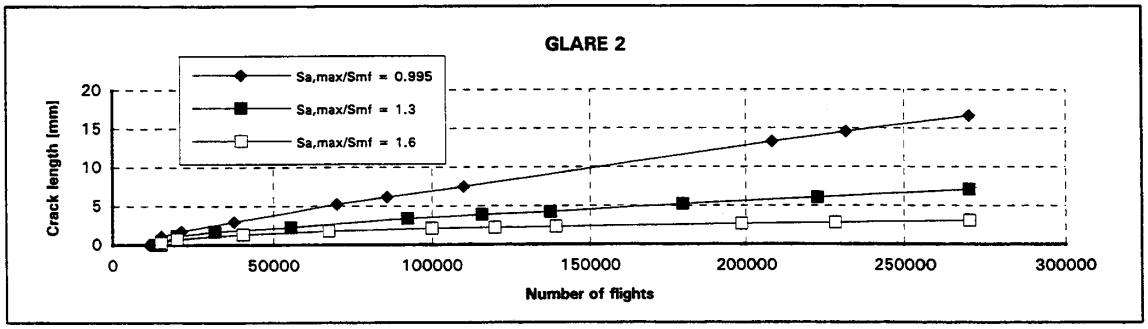

Figure 1.2.2. Crack growth curves starting at open holes (diameter 5 mm) in a 100 mm wide GLARE1 specimen loaded with miniTWIST (mean stress in flight 86 MPa) [36].

In the example above a crack nucleation occurred at about 15000 flight which was followed by crack growth until a crack length of about 1 mm at a life time of some 25000 flights. Afterwards an approximately constant and very low crack growth rate was observed. A crack length of 3 mm was reached at 200000 flights. The tendency for a constant crack growth rates has been confirmed in many

crack growth experiments both under constant amplitude (CA) loading and under flight-simulation loading.

1.3 Application of Damage Tolerance Rules

Whenever a new material is introduced in aircraft structures a lot of data and information on the new material must be available, both for designing and manufacturing of the structure and for discussions with the airworthiness authorities. In the period that ARALL was still a promising material, it turned out that FAA was considering the question whether ARALL should be treated as a metallic material or as a composite material. Nowadays, it is generally thought that the design problems and the technology of GLARE components are more similar to those aspects for metallic structures. Machining and plastic bending of GLARE is possible, which does not apply to advanced composites. However, it should be realized that the technology of machining and plastic bending of GLARE is not exactly the same technology applicable to Al-alloy sheet materials, which however, is also true for e.g. Ti-alloys. In a period of some 15 years a vast amount of data on GLARE properties, knowledge of production technology and the behaviour of GLARE components was collected. For the time being it should be expected that an Airworthiness Certification for an aircraft with GLARE in PSE's will primarily be checked on the basis of the Requirements for metallic materials.

The general purpose of JAR 25.0571 is defined in paragraph (a):
„*General.*
An evaluation of the strength, detail design, and fabrication must show that catastrophic failure due to fatigue, corrosion, or accidental damage, will be avoided throughout the operational life of the aeroplane. This evaluation must be conducted in accordance with the provisions of sub-paragraphs (b) and (e) of this paragraph, except as specified in sub-paragraph (c) of this paragraph, for each part of the structure which could contribute to a catastrophic failure (such as wing, empennage, control surfaces and their systems, the fuselage, engine mounting, landing gear, and their related primary attachments).
(See ACJ 25.0571(a))."

The structural items which contribute significantly to carry loads are so-called Principal Structural Elements (PSE), for the pressurized fuselage they are identified in ACJ 25.0571(2.2.2):
„*a. Circumferential frames and adjacent skin;*
b. Door frames;
c. Pilot window posts;
d. Pressure bulkheads;
e. Skin and any single frame or stiffener element around a cut out;
f. Skin or skin splices, or both, under circumferential loads;
g. Skin or skin splices, or both, under fore-and-aft loads;
h. Skin around a cut out;
i. Skin and stiffener combinations under fore-and-aft loads;
j. Window frames."

In order to satisfy the Airworthiness Requirements the fatigue and damage tolerance scenario follows the flow diagram presented in figure 1.3.1. If inspection is not possible on a regular basis ("impractical" according to JAR 25.0571) the safe life approach must be adopted which requires relatively large safety factors. The landing gear is the most frequently cited example. If regular inspections are possible, the

damage tolerance philosophy according to figure 1.3.1 offers the question whether the structure is a single load path or a multiple load path structure.

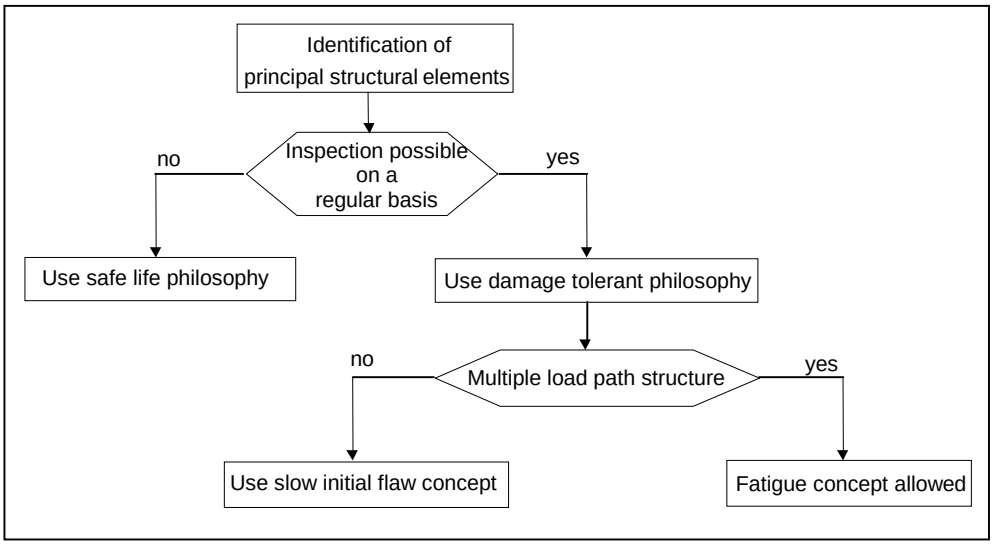

Figure 1.3.1. Flow chart defining required fatigue and damage tolerance philosophy

The theoretical definition of a single load path component is clear, if the component fails, the integrity of the structure is jeopardized. The multiple load path structure concept on the other hand suggests that failure of a single path implies load shedding to parallel elements. Such elements could be stringers, frames, or parallel wing panels. The Airworthiness Regulations distinguish between discrete and non-discrete structural items. In the latter case load shedding is a less evident phenomenon and the evaluation of damage tolerance can be a more complex problem. This applies to riveted joints, and in particular to longitudinal lap joints and circumferential single-strap butt joints. The failure scenario of riveted joints is complex as will be discussed in the present thesis.

The above steps in the flow chart are covered by the Airworthiness Requirements. Relevant paragraphs are collected on the next page. It should be noted that the 1st paragraph refers to fatigue, corrosion and accidental damage, which should not lead to a catastrophic failure. This argument is repeated in paragraph 3 for single load path discrete items referring to cracks starting from material flaws. Paragraph 4 about Damage Tolerance Analysis and Tests is the key paragraph for the aircraft industry and for the present thesis. The 5th paragraph is referring to MSD which is of particular interest for riveted joints.

A major question is which type of damage should be considered. According to the Airworthiness Requirements both accidental damage (impact damage, scratches, dents, lightning strikes) and regular damage (fatigue) should be covered. In general accidental damage is visually detectable but it must be analysed in the damage tolerance procedures in view of setting the threshold inspection periods. Fortunately, impact damage of GLARE panels in many cases does not lead to full penetration while the damage is still “readily detectable”. Moreover, the fibers restrain a subsequent extension of the damage. A worst case assumption is a complete loss of a load path, i.e. a full penetration of a stringer or a frame by rotor burst with all fibers broken. The residual strength should then be calculated with the R-curve approach.
Regular fatigue damage starts at notches, such as joints, lugs, notched sheet edges (e.g. open holes) and cut outs (doors, windows). A most prominent case is fatigue damage in riveted joints and the associated MSD. Fatigue damage in riveted joints is discussed in the following section.

Relevant paragraphs of the Airworthiness Requirements

1. About Damage Tolerance Rules

An evaluation of the strength, detail design, and fabrication must show that catastrophic failure due to fatigue, corrosion, or accidental damage, will be avoided throughout the operational life of the aeroplane. This evaluation must be conducted in accordance with the provisions of sub-paragraph (b) and (e) of this paragraph, except as specified in sub-paragraph (c) of this paragraph, for each part of the structure, which could contribute to a catastrophic failure (such as wing, empennage, control surfaces and their systems, the fuselage, engine mounting, landing gear, and their related primary attachments). (see ACJ 25.0571(a))

---

2. About safe-life evaluation:

Compliance with the damage tolerance requirements of sub-paragraph (b) of this paragraph is not required if the applicant establishes that their application for particular structure is impractical. This structure must be shown by analysis, supported by test evidence, to be able to withstand the repeated loads of variable magnitude expected during its service life without detectable cracks. Appropriate safe-life scatter factors must be applied.

---

3. About single-load path damage tolerant evaluation:

Materials and stress levels that, after initiation of cracks, provide a controlled slow rate of crack propagation combined with high residual strength. For single load path discrete items, such as control surface hinges, wing spar joints or stabiliser pivot fittings the failure of which could be catastrophic, it should be clearly demonstrated that cracks starting from material flaws, manufacturing errors or accidental damage (including corrosion) have been properly accounted for in the crack propagation estimate and inspection method.

---

4. About Damage-Tolerance Analysis and Tests: (paragraph 2.7):

It should be determined by analysis, supported by test evidence, that the structure with the extent of damage established for residual strength evaluation can withstand the specified design limit loads (considered as ultimate loads), and that the damage growth rate under the repeated loads expected in service (between the time at which the damage becomes initially detectable and the time at which the extent of damage reaches the value for residual strength evaluation) provides a practical basis for development of the inspection program and procedures described in paragraph 2.8 of this ACJ. The repeated loads should be as defined in the loading, temperature, and humidity spectra. The loading conditions should take into account the effects of structural flexibility and rate of loading where they are significant.

2.7.1 The damage-tolerance characteristics can be shown analytically by reliable or conservative methods such as the following:

a. By demonstrating quantitative relationships with structure already verified as damage tolerant;

b. By demonstrating that the damage would be detected before it reaches the value for residual strength evaluation; or

c. By demonstrating that the repeated loads and limit load stresses do not exceed those of previously verified designs of similar configuration, materials and inspectibility.“

---

5. About Multiple-Site-Damage (MSD):

“Damage at multiple sites due to prior fatigue exposure must be included (in the damage tolerance evaluation) where the design is such that this type of damage can be expected to occur.”

Under no circumstances special airworthiness rules should be established for the introduction of Fiber Metal Laminates for commercial transport aircraft. Therefore, in this thesis it is discussed how GLARE is covered within the at *present available* airworthiness requirements under consideration of particular technical aspects, e.g. material scatter and ageing effects on material properties.

It is recommended to distinguish structural GLARE items where damages are readily detectable, items which are covered by directed inspection tasks and items which will be inspected general visual. A pre-requisite for the following discussion is the knowledge, that fatigue cracks in the aluminium layers of GLARE are detectable with Non Destructive Test methods [34].

1.4 Fatigue Damages in Riveted Joints

Longitudinal riveted lap joints and circumferential single-strap butt joints in a pressurized fuselage are well-known fatigue critical elements. Fatigue cracks can start more or less simultaneously at neighbouring holes in a critical rivet row of a joint. It leads to an MSD situation which has widely been observed in fatigue tests on specimens of both aluminium sheets and GLARE. It then appears to be unrealistic to consider every rivet in a critical rivet row as a separate load path. It is more important to know that the development of fatigue damage, i.e. the crack growth, is essentially different in riveted joints of metal sheets and GLARE. As a result, detection of fatigue damage is also an essentially different question.

1.4.1. Fatigue prediction during pre-design with support of coupon tests

The development of fatigue cracks in a lap joint of monolithic sheet material will be discussed first. In a single shear joint fatigue cracks are initiated at the mating surface between the two sheets to be jointed, see figure 1.4.1a. The cracks are initially growing as a part through crack, but after some time a through crack will be present, see figure 1.4.1b. Such cracks can be detected by NDT techniques. Later if through cracks are present at neighbouring rivets holes (MSD) the ligaments between crack tips become smaller and enhanced crack growth occurs. Linking up of adjacent cracks can then occur, see figure 1.4.1c. Such a crack if it occurs in the outer sheet of a fuselage lap joint can be classified as “readily detectable”. However, if it occurs in the inner sheet, see 1.4.1d, inspection may require removal of the interior of the aircraft cabin which means that the crack is not readily detectable. In a fatigue test on a riveted joint after some more ligament failures the final failure of the specimen is imminent.
Fatigue tests on riveted lap joint specimens of monolithic sheet material have shown that the crack initiation life covering non-visible crack growth is relatively long if compared to the crack propagation life to failure. Müller observed typical ratios of crack initiation periods to total coupon specimen lives between 85% and 90% [5]. Consequently, from the 800000 fatigue cycles to failure for an A330 longitudinal lap joint coupon specimen (max. gross stress 70 MPa, squeeze force 22kN [5]), 680000 to 720000 cycles belong to the crack initiation period and 80000 to 120000 cycles to the crack propagation period. In the aircraft industry factor 5 on a constant amplitude coupon test result turned out to be conservative enough for many problems concerning the prediction of the fatigue life of the same design in a full scale structure during the pre-development phase [9]. With *fatigue life* is meant, that a probability of 95% for the concerned aircraft type fleet can be achieved to fly crack free until the Design Service Goal is met (for the investigated structural element). The high factor on the coupon result, which has to cover several uncertainties, allows to neglect a special consideration of the crack propagation part of the coupon test for the full scale prediction. Here, specimen failure equals fatigue life for the aircraft. Indeed

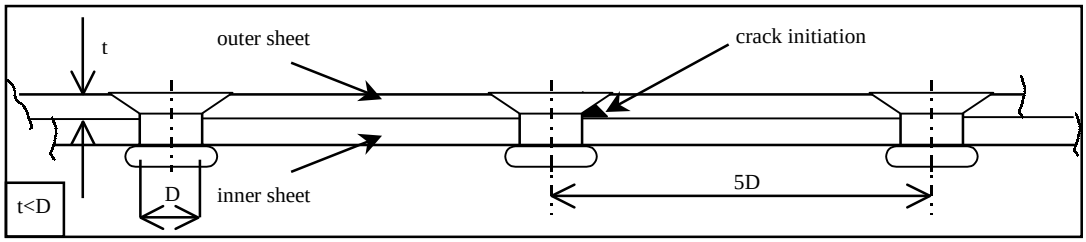

Figure 1.4.1a. Typical aluminium joint with crack initiation in upper sheet, mating surface

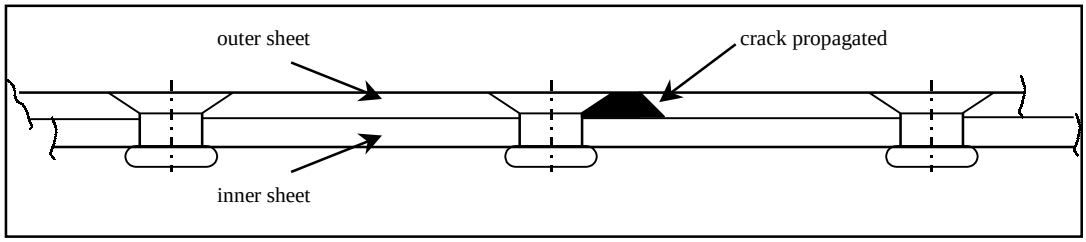

Figure 1.4.1b. Aluminium joint, small crack on fuselage surface, NDT detectable

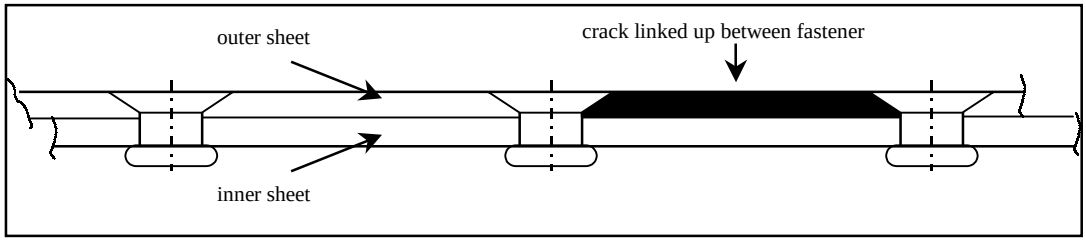

Figure 1.4.1c. Detailed visual detectable crack from outside, `readily detectable´

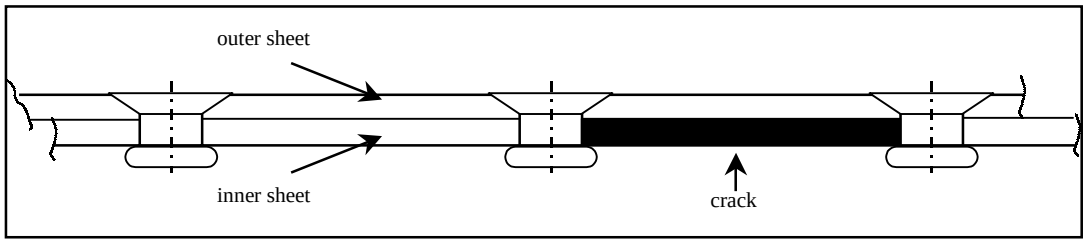

Figure 1.4.1d. Crack not inspectable from outside, not 'readily detectable'

the deviation between crack initiation and fatigue-to-failure due to the non-consideration of the crack propagation part becomes smaller with an increased safety factor.

The MSD condition of a particular aluminium coupon specimen at the end of it's "fatigue life" is one of the above mentioned uncertainties. For both, time constraints and cost reasons, micro fractographic investigations during pre-development of an aircraft are often avoided. However, cracks may initiate in one or more of the drilled holes of a coupon specimen at approximately the same time.

Two aircraft accidents have considerably affected the discussions between Airworthiness Authorities and aircraft industries. The first one was the wing failure of the F-111 in 1973 due to limited fatigue crack growth starting from an undetected large flaw in the material. Shortly afterwards a military standard of the USAF specified initial flaw sizes for threshold inspection periods of fatigue critical elements. The sizes vary from 0.005" to 0.25" depending on the inspection procedures. The second accident was a fuselage failure of an old Boeing aircraft, the so-called Aloha accident. It initiated considerable discussions, especially on multiple-site-damage (MSD) which turned out to be a common phenomenon in tests on riveted lap joints shortly before failure. Contrary to the initial damage which can be present at an early stage of an aircraft in service, MSD is fatigue damage which requires life time in service before

it can occur. Actually, the inspections of the riveted joints of the Aloha aircraft were not done according to the required standards. Anyway, the present Airworthiness Requirements imply that initial damage must be considered and a threshold inspection period should be determined based on analysis and full scale test evidence. For GLARE serious problems should not be expected in view of the very low crack growth rates in this material. But of course, if a single load path PSE would be fully damaged sufficient residual strength must be present as discussed before.

1.4.2 Inspection threshold determination supported by full scale fatigue tests

Aircraft manufacturers are obliged to perform test verified damage tolerance analysis of Principal Structural Elements for the airframe certification, ref. ACJ 25.0571, paragraph 2.7. It is also common practise for the certification of new aircraft models to carry out a full scale fatigue test, followed by residual strength tests (limit load). In the following the fatigue strength verification and the threshold determination, supported by full scale test articles, will be discussed. It is especially focused on riveted joints in pressurized fuselages.

Since 1988 the rulemaking organizations tried to specify the damage tolerance regulations further in order to avoid catastrophic failures due to cracks, which are not detectable by non-directed inspections. A distinction is made between single- and multiple load path structures on the one hand and the level of the inspectibility on the other hand. If a multiple load path structure is investigated, in which a fatigue crack can be detected by non-directed inspections, the fatigue approach is adequate to determine the threshold inspection [10]. If either a single load path structure is investigated or a multiple load path structure, in which fatigue cracks are undetectable by non-directed inspections, a crack propagation calculation is recommended for the inspection threshold determination (FAR 25.571, Amendment 96). The crack propagation method assumes manufacturing flaws in all drilled holes to account for poor manufacturing quality. Occasionally, the so-called rough flaw shall be considered, e.g. in a longitudinal joint once per frame bay. A manufacturing flaw size of 0.005 inch and a rough flaw of 0.05 inch are still to be discussed.

In the past the fatigue concept applied on a full scale test result did not really consider a multiple site damage situation. For particular PSE's it was focused on a single crack without taking adjacent damages into account. The true safety margin of the established inspection threshold remains unclear, because the residual strength capability of the structure (possibly *with* MSD) at the time of detection of a single crack is not considered. The applied scatter factor has to account for this circumstance. The initial flaw concept considers adjacent fatigue damages for the residual strength prediction (figure 1.4.2) and therefore seems to provide a more accurate prediction of the level of safety for pressurized fuselage joints.

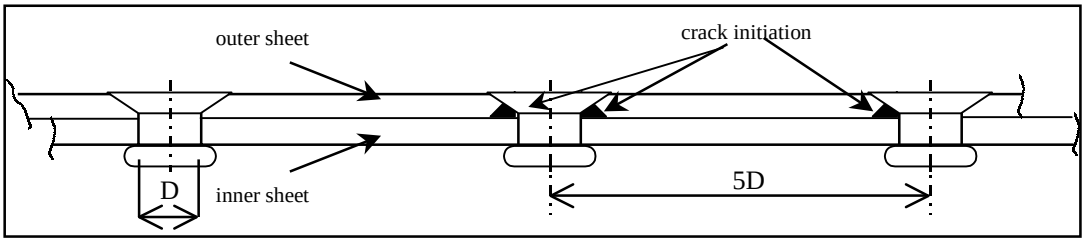

Figure 1.4.2. Multiple site damage in a riveted joint

Circumferential and longitudinal skin splices are Principle Structural Elements according to ACJ 25.0571, whose failure could result in catastrophic failure of the aircraft:

"Damage at multiple sites due to prior fatigue exposure must be included (in the damage tolerance evaluation) where the design is such that this type of damage can be expected to occur."

A lost skin panel (ALOHA) had taugh the aircraft community, that the structural aluminium joints in pressurized fuselages are without any doubt susceptible to multiple site damage. A riveted joint has a single load path character, if stiffening elements like frames or stringer can not prevent the disintegration of a panel. The airworthiness regulation distinguishes between discrete and non-discrete structural items. According to ACJ25.0571(b) the initial flaw concept is requested for single load path *discrete* items, only:
"Materials and stress levels that, after initiation of cracks, provide a controlled slow rate of crack propagation combined with high residual strength. For single load path discrete items, such as control surface hinges, wing spar joints or stabiliser pivot fittings the failure of which could be catastrophic, it should be clearly demonstrated that cracks starting from material flaws, manufacturing errors or accidental damage (including corrosion) have been properly accounted for in the crack propagation estimate and inspection method;"

However, the recommended crack pattern (0.005"/0.05") for an initial flaw calculation is arbitrary. The method can not account for the influence of hole filling on crack initiation due to different squeeze forces for aluminium fasteners or the fitting of bolts. Since the hole filling dependent factors on the crack initiation life are significant (factor >3 [5]), the advantage of the arbitrary crack lengths can be discussed. A promising alternative is the statistical evaluation of damage accumulations at all drilled holes along a rivet row [11]. If a damage accumulates to 1 at a particular location, the point of crack initiation (N_i) is reached for this drilled hole. For each individual location a crack propagation calculation follows, after its fatigue damage has been accumulated to 1. This method is recommended by the author for crack initiation calculations in riveted joints, because it combines the benefit of fatigue resistant designs and high manufacturing qualities (fatigue approach) with the conservatism of a MSD calculation for the residual strength- and inspection threshold prediction.

1.5 Fatigue Damages in GLARE Joints

1.5.1 Fatigue behaviour

The crack growth behaviour is entirely different for lap joints of GLARE, but nevertheless, the damage tolerance principle must be satisfied. Under the same external fatigue load a PSE made of GLARE performs different in crack initiation if compared to an equivalent aluminium structure. Crack initiation starts earlier in the aluminium layers of GLARE than in a monolithic structure, due to both the stiffness mismatch between aluminium layers and prepreg layers and due to the curing process related internal stress system. However, the crack propagation rates in GLARE can be orders of magnitude lower than in monolithic aluminium [8,13], depending on the crack orientation in relation to the fiber orientation. Figure 1.5.1 illustrates the behaviour of a MSD sensitive GLARE PSE, e.g. a riveted joint between two fuselage panels. Slow crack propagation occurs after the initiation period (N_i), with a corresponding gradual loss of the residual strength. At a certain time (N_{UL}) the ultimate load capability will be reached (F_{UL}). The associated crack length is the critical crack length $a_{c,UL}$. A similar relationship exists at limit load (N_{LL}, F_{LL}, $a_{c,LL}$).

Readily detectable cracks in GLARE structures will be inspected similar as readily detectable cracks in monolithic aluminium, either visual or by NDI techniques. Corner cracks at door cut outs are representative examples for such kind of structures.

As mentioned before, fatigue cracks in single shear joints always initiate on the mating surface side. Due the slow crack growth, the cracks in a riveted GLARE joint remains undetected for a long duration. Figures 1.5.2a to 1.5.2d present an experimental example, a butt strap made of GLARE2-7/6-.4 [33]. Cracks initiated randomly, as for monolithic aluminium. In some drilled holes up to four of the seven aluminium layers were found to be fatigue cracked after 180000 load cycles, but all fibers were still intact. Figure 1.5.2b provides the crack distribution of all (6) inspected holes in all aluminium layers. The crack illustrated in the mating surface layer on the left side of the hole in figure 1.5.2c is the lead crack with a length of 7.5mm. The *average* crack length is defined as the total length of all cracks divided by the number of possible fatigue critical locations: $a_{av} = \Sigma a_{ij}/12$ for this example.

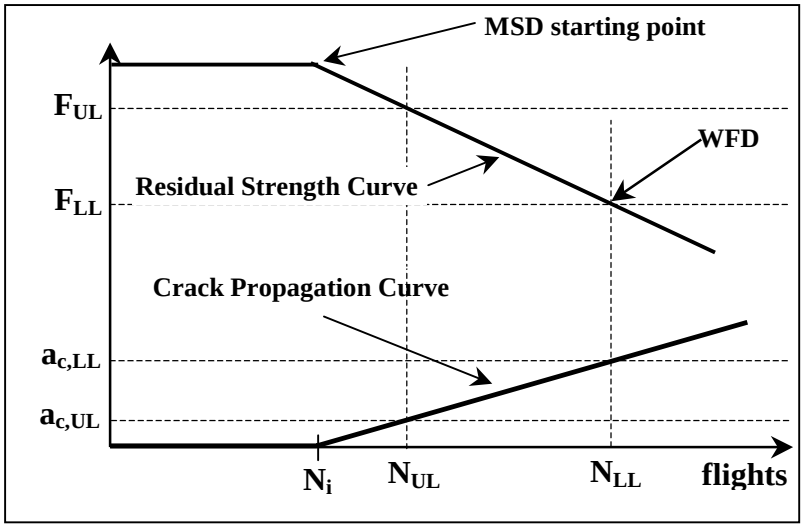

Figure 1.5.1. Schematic crack initiation, crack propagation and residual strength behavior of a GLARE structure with crack.

Figure 1.5.2d compiles some details of the crack situation in aluminium layer 1, which is the mating butt strap layer with the skin sheet. The detectable crack length is estimated to be 7mm (NDT). One crack, 8.3% of the community, exceedes the NDT inspectable crack size, thus the inspectibility for cracks of the specimen is obtained after approximately 180000 cycles. The average crack length being 3.7mm is included in diagram 1.5.2d as well. It is an indicator for the residual strength of the joint. After 180000 cycles, 9.2% of the aluminium in the GLARE butt strap (all layers) is cracked. The residual strength of the butt strap material can be calculated with the rule of Müller [5]:

$\sigma_{res.cack.} = \sigma_{BN} - R_D * MVF * \sigma_{al(\varepsilon=4.7\%)} = 625 - 0.092 * 0.651 * 420 = 599$ MPa

with the blunt notch stress σ_{BN} (net stress) from source [14]. Remark: The calculated residual strength is valid for as-received GLARE at room temperature, the fastener strength is not taken into account.

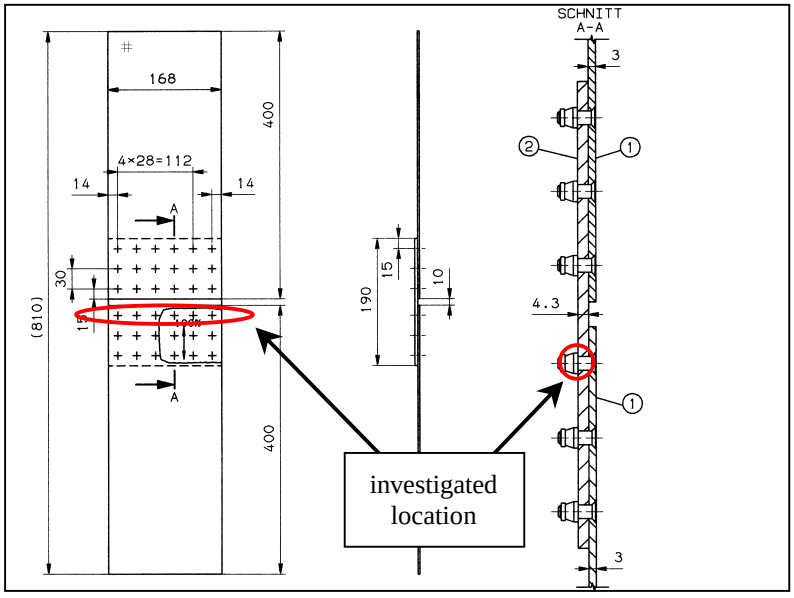

Figure 1.5.2a. Circumferential joint specimen with GLARE2-7/6-.4 butt strap

The calculated residual strength of the butt strap with cracks still exceeds the ultimate load of aircraft fuselage circumferential joints. The structure would require no inspection until 180000 cycles divided by a scatter factor. The scatter of residual strengths, determined with coupon specimens, includes always a mixture of crack initiation and crack propagation related scatter. It can be separated, if the point of crack initiation can be determined. Although the residual strength remains high beyond 180000 fatigue cycles, a repair would be required in case of a similarly cracked condition detected on an aircraft. Any further operation of an aircraft with *detected* fatigue cracks would exceed the current framework of airworthiness regulations and would require a separate section, a so-called 'Special Condition' for GLARE.

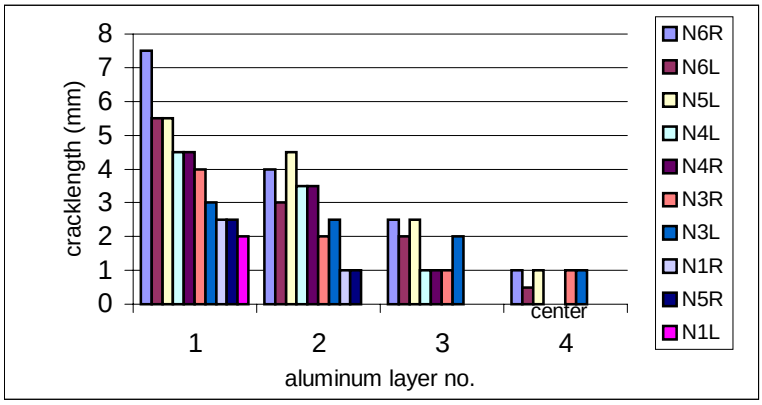

Figure 1.5.2b. Crack length distribution in a GLARE2B-7/6-.4 butt strap after 180000 cycles, the legend indicates the crack locations

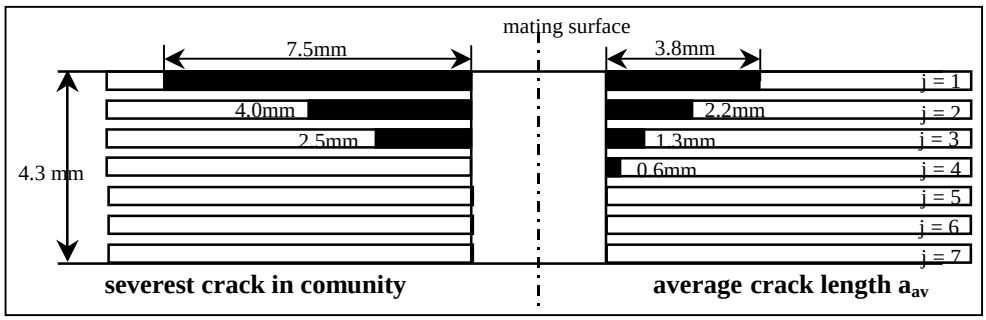

Figure 1.5.2c. Typical cracks in a GLARE2B butt strap after 180000 fatigue cycles

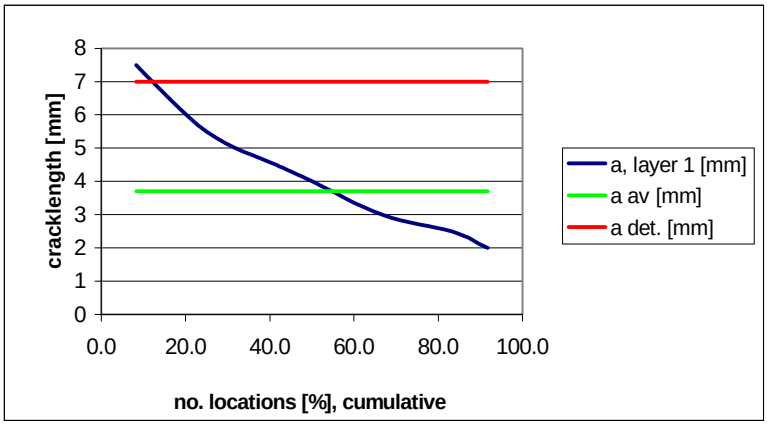

Figure 1.5.2d. The crack length distribution and the average crack length of layer j=1, after 180000 fatigue cycles

The glass fibers in GLARE are not allowed to fail under any fatigue condition. If they would, residual strength would become unpredictable. The intact fibers provide a second load path for the cracked aluminium layers. In agreement with FAR 25.571, Amendment 96, the following design philosophy is established:

1) A GLARE sheet represents a multiple load path structure under fatigue conditions (fibers intact).
2) The low crack propagation rates of GLARE support to design PSE's in a manner, that fatigue cracks become detectable before catastrophic failure of the structure.

3) When conditions 1) and 2) are fulfilled, the fatigue approach is acceptable to calculate crack initiation (ref. principle figure 1.3.1).
4) Since the crack propagation phase can be more dominating in GLARE than it is in monolithic aluminium structures (depending on the crack orientation), the crack propagation analysis should be adopted for the determination of the inspection threshold in GLARE as well.

1.5.2 Continuous airworthiness

Once the airframe is in service, fatigue inspections belong to the integrated concept of continuous airworthiness. In order to obtain an overview about the relevance of the full scale fatigue test for the fatigue strength justification and inspection threshold determination of a GLARE PSE the schematic figure 1.5.1 is extended. Two crack propagation curves should be included in the diagram, one representing the lead crack, which determines the number of flights when a crack becomes inspectable, the other curve indicating the average crack length for the determination of the residual load capability. The time to crack initiation, the detectable crack length, the ultimate load capability and the limit load capability define, in relation to the Design Service Goal (DSG, predefined, commercial life in [flights]), whether the GLARE structure has to be inspected for fatigue reasons or not. Figure 1.5.3 provides the most likely occurrence of several possible cases.

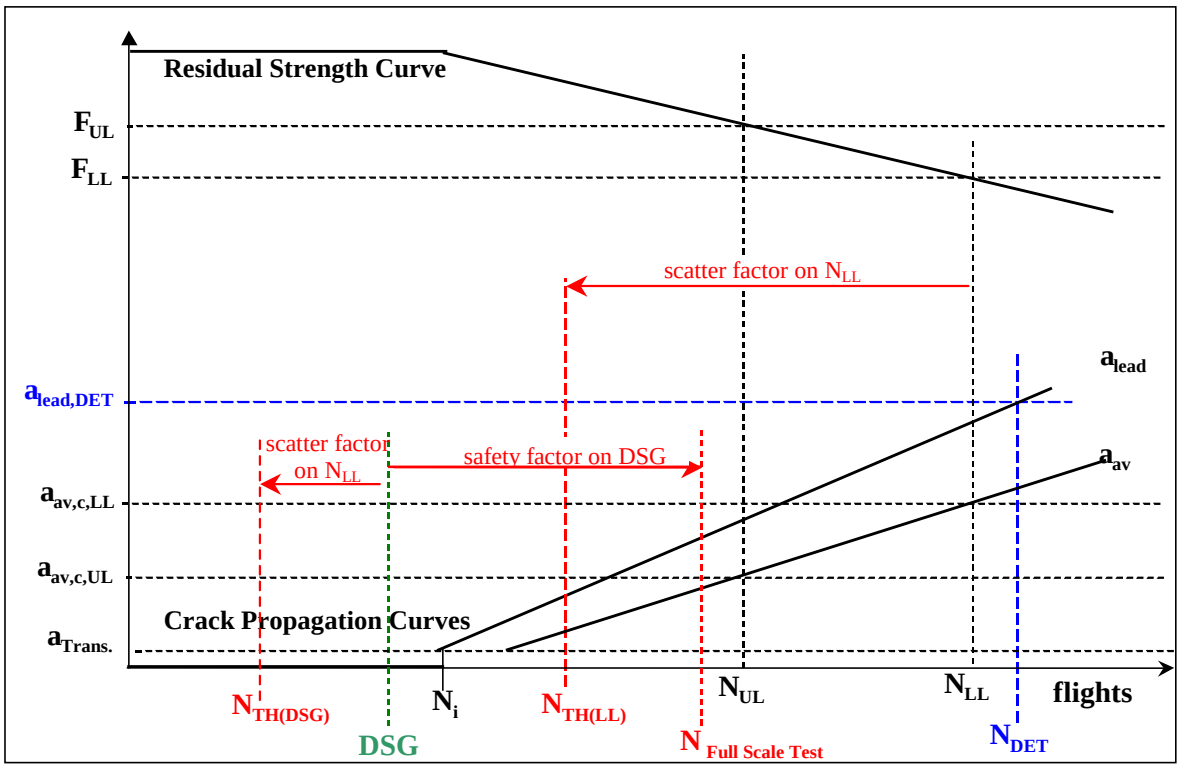

Figure 1.5.3. Case study: threshold determination for GLARE PSE (schematic, diagram not drawn in scale)

For economical reasons it is likely that not more than 2½ life times of the aircraft DSG will be simulated in the full scale test article ($N_{FullScale}$). The factor 2½ is considered as a safety factor to be applied on the full scale test article, which accounts for operational related effects on the structure which are not simulated in the hangar which hosts the full scale specimen, e.g. strength degradations due to corrosion. An aircraft structure made of aluminium is certified for the DSG when at least safety factor 2 is applied on the full scale test article. If no information about the condition of the (aluminium) structure at the end of the test is available, i.e. if no detailed tear down inspection is provided but the specimen can still carry

ultimate load, it is common practise to divide the (test verified) DSG by a scatter factor in order to calculate the first scheduled fatigue inspection. This inspection threshold is called $N_{TH(DSG)}$ in diagram 1.5.3. The applied scatter factor is predominately related to material and manufacturing quality scatter. The procedure considers that the structure is close to the point of WFD (Wide Spread Fatigue Damage) at the end of the full scale test and that it might not be able to carry limit load in case of further fatigue loading. The logic of this procedure for aluminium PSE's is easy to understand because it is accounting for the short crack propagation life of aluminium structures, relatively to the fatigue life and also in comparison to the crack growth periods for GLARE components.

The relations between the participating variables (N_i, N_{LL}, etc.) for the inspection threshold determination in GLARE are different, due to the different ratio of crack initiation life to crack propagation life. The slope of the average crack length curve (a_{av}) in figure 1.5.3 determines the number of flights for a GLARE PSE, at which the limit load capability is reached (N_{LL}). N_{LL} is the absolute minimum tolerable residual strength for the aircraft structure, since the point of WFD is reached. In order to account for material scatter, e.g. for a riveted joint, N_{LL} (full scale result) is divided by an appropriate factor for a conservative aircraft inspection threshold determination ($N_{TH(LL)}$). This inspection threshold is related to the real structural strength condition at the life time N_{LL}. Different from aluminium structures the scatter factor is primarily dependant on crack propagation, rather than on crack initiation.

In the example it is obvious that if the inspection threshold $N_{TH(LL)}$ exceeds the Design Service Goal no scheduled fatigue inspection is required during the aircraft life. On the other hand, inspection threshold $N_{TH(DSG)}$ demands a scheduled inspection at a time when the crack initiation life has not yet been reached. The significantly different thresholds are mainly related to the long crack propagation period of GLARE.

But what are the consequences for the fatigue strength justification of GLARE structures and/or for the full scale fatigue test ? It must be considered, that the point of WFD (N_{LL}) and the detectable crack length (N_{DET}) under consideration of usual NDI techniques are beyond the full scale fatigue test duration. Consequently, both values as well as the inspection threshold $N_{TH(LL)}$ can just be *calculated* values. It is therefore required to obtain crack propagation data from full scale GLARE PSE's in order to recalculate the point of crack initiation and in order to predict the point of WFD. This question requires to improve NDI techniques for the online monitoring of fatigue cracks, compared to the available techniques of the last millennium. The alternative is a rather conservative determination of inspection thresholds, which would not consider the high residual strength potential of a fatigue cracked GLARE structure.

1.6 Environmental Influences

Relevant time dependent failure modes in monolithic aluminium are corrosion and changes of the material temper. The latter is a no-go item for application as an aircraft primary structure material, e.g. particular aluminium lithium metal sheets failed to qualify because of being unstable in temper. Corrosion, on the other hand, is strongly dependent on the aircraft utilization and therefore often an isolated case. With some exception, corrosion can be detected by using appropriate inspection techniques. Fatigue inspection tasks and corrosion inspection tasks are included into the Inspection Program for an aluminium fuselage. The above mentioned exception is associated with intergranular corrosion. Because it is growing rather in the sheet plain directions then in depth, it remains undetectable for a long period, leading to an undetectable loss of strength. Aluminium materials, which are sensitive to intergranular corrosion within the DSG [years], should not be considered as a candidate for aircraft application.

Sufficient safety without an unacceptable inspection burden for the aircraft operators is provided by the establishment of dedicated corrosion inspection tasks, divided in environmental categories, dependant on location, material, surface treatment and the expected environmental condition. For example, the upper fuselage shells will be inspected less frequently from the inside than the lower shells, because all fluids follow the gravity and will be collected in the bilge area. Locations which may come in contact with aggressive fluids should be inspected in a different way different than surfaces just in contact with air [12].

Because the corrosion inspection tasks are part of the concept to maintain airworthiness of the aircraft structures, there is no special factor considered for the application on monolithic aluminium test results, full scale tests included. However, environmental influences on crack initiation [15] and/or crack propagation may be known from in-service experiences or conservative, accelerated tests. Dedicated factors can then be used during design for application on allowable stresses [16] or for application on test results conducted in a dry environment.

No environmental factors are considered for residual strength analysis and tests of monolithic aluminium structures.

Epoxy matrices of composite materials absorb moisture. The environmental humidity defines the maximum moisture level in the composite (Fick’s law) and the temperature is dictating the diffusion speed (Arrhenius equation). A high temperature leads to a lower interlaminar shear strength and can thus decrease the structural strength of the composite component. Fatigue damages in composites are mainly classified as delaminations, which have a certain size at the beginning of the aircraft service life and may grow due to the applied load spectrum. Compared with fatigue cracks and corrosion in aluminium, delaminations are more difficult to detect.

Due to the material behaviour and inspectibility, composite parts require different test procedures than metallic structures. A possibility is to test fatigue specimens in hot humid air in order to simulate the ageing influence. Before fatigue cycling, it is common practise to load the composite structure up to limit load in order to extend a possible manufacturing flaw (delamination) to its maximum possible size. If really present and detectable, the size of the delamination during the test will be monitored. For certification tests the procedure will be conducted with artificial delaminations. Residual strength tests may be conducted at elevated temperature if the design load case occurs before take-off.

If tests in humid environments are not possible for technical or economical reasons, the effects can be simulated by factors on load. However, it needs to be known, *which* accelerated ageing process is representative to simulate an aircraft life cycle. The accelerated ageing and the associated factors on dry specimens should be conservative enough, but the conservatism should not consume too much of the weight saving potential of the material. The accelerated ageing treatment must represent a realistic flight operation with the associated material temperatures, humidities and frequencies of different flight types.

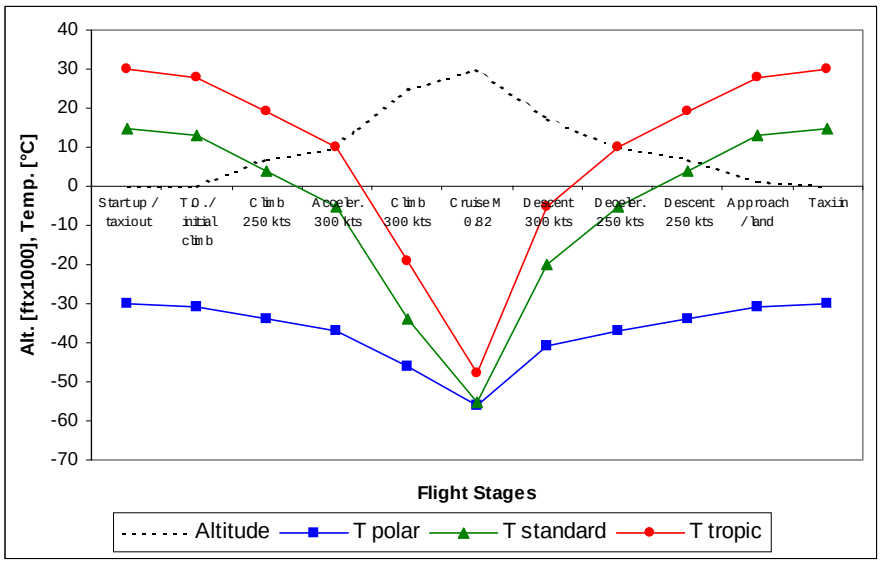

Figure 1.6.1. Ambient air temperatures during flight

Airbus Industrie evaluated a mission mix with 25% of all flights carried out in an arctic environment, 50% in a standard environment and 25% in a tropic environment [17]. The associated ambient air temperatures are plotted in figure 1.6.1 [18].

The ambient air temperature at low altitude is dependent on the hour of the day, especially for the tropic profile. Depending on the aircraft location in relation to the sun, the ground condition and the distance of the structure from the ground, as well as its insulation and paint system, a specific material temperature will evaluate. An example is presented in figure 1.7.1 [19].

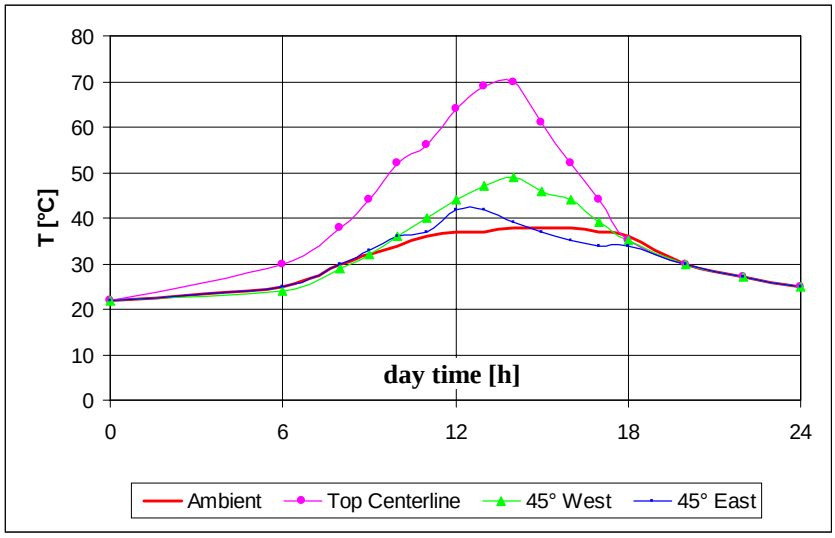

Figure 1.7.1. Black skin panel temperature measurements in the Sahara desert on BAe146 crown panel

The moisture profile at the end of the aircrafts design life, i.e. after 25 to 30 years, is an integration of all environmental humidities and temperatures flight profiles. Reversibility of the process and specific material properties have to be taken into account. Based on extensive investigations, Airbus defined a 3000 hour / 85% relative humidity / 70°C treatment for representative and conservative accelerated ageing composite tests. With this kind of exposure, pure composite structures will be saturated up to a depth of 4mm in depth after 25 years aircraft operation, which is realistic as verified by traveler specimens [32].

The previous explanations lead to the conclusion, that structures consisting of aluminium- and composite components can not be certified with the same full scale test article. Especially, loading the metallic part to limit before fatigue, as desired for the composite structure, would lead to non-conservative fatigue results due to the cold working effect in the metallic drilled holes.

Fiber Metal Laminates are material candidates for aircraft fuselage skin- and stringer applications. They will be connected to monolithic aluminium structures in any case, e.g. to frames. Very likely, monolithic aluminium structures and Fiber Metal Laminate structures, like GLARE, will be tested according to the same rules, at least in the full scale test for type certification. The relevant scatter factors for crack initiation and crack propagation as well as the knock down factors due to ageing and/or temperature have to be determined. Due to the barrier property of the outer aluminium layers for moisture absorption, the investigation can be limited to drilled holes and sheet edges. Special attention has to be paid to the environmental influence on crack propagation, since a fatigue dominated delamination zone develops around the fatigue crack in the aluminium layer of GLARE. The delamination zone may be influenced by the environment and consequently the environment may influence the crack propagation rates.
Systematic investigations of the environmental influences on GLARE edges, open holes, closed holes and riveted joints have been conducted by several researchers [20 to 30], using different acceleration methods and conditions. As a major milestone, the accumulated knowledge has been compiled in 1999 as ‘preliminary knock down factor’ list, used for the pre-design of the A380-800 aircraft [31].

1.7 Preliminary Conclusions

Due to the crack bridging properties of GLARE, the strength degradation after fatigue crack initiation is very limited. It remains limited during subsequent aircraft operations, since the crack propagation rates are low compared with monolithic aluminium.

It is an essential material property of GLARE that fibers do not fail under any fatigue condition. They provide a second load path for the fatigue cracked aluminium layers and the fatigue approach may be included in the fatigue and damage tolerance strength justification, offering additional utilization potential for the aircraft.

Multiple fatigue cracks are tolerable in a non-repaired condition, as long as they are undetectable and the ultimate strength of the concerned component can be carried. The expected fatigue crack lengths at the end of the Design Service Goal is limited, it may be undetectable with NDT methods.

The FM94/S-glass prepreg of the GLARE type which is qualified for the A380-800 is sensitive to moisture and temperature. The influences of environmental conditions have to be determined for crack initiation, crack propagation and residual strength.

A full scale test specimen, required for certification, will always contain both, monolithic aluminium and GLARE structures. For technical and commercial reasons the test will be conducted at room temperature and without artificial environmental conditions, in most of the cases.

The scatter factors of GLARE for crack initiation and crack propagation have to be determined in order to calculate the certified service life for the GLARE structures. For GLARE, the scatter of crack propagation may be equal important than the scatter of crack initiation, since the crack free life of the structure may equal the time during which the aircraft is flying with fatigue cracks.

Test-to-structure factors for GLARE fatigue and damage tolerance properties need to be developed in order to interpret coupon- and component specimens in relation to full scale test structures and the flying fleet.

NDI techniques need to be improved in order to monitor the fatigue condition of GLARE full scale structures with the target to provide crack propagation curves. These data allow the prediction of comfortable inspection thresholds.

Material properties after accelerated ageing are available from the famous GLARE Research Program, obtained from structural tests after a standardized 3000h / 85%RH / 70ºC exposure. The moisture absorption of GLARE is limited to its edges and around holes, for the far field the outer aluminium layers provide a barrier function. An analysis on *realistic* exposure is required in order to determine, whether the knock down factors obtained from the *standardized* accelerated ageing process can be decreased. Lower knock down factors provide higher weight saving potential. Decreased accelerated ageing procedures provide faster results and cheaper testing.

1.8 References

[1] Glare Application For Primary A3XX Airbus Structure
DaimlerChrysler Aerospace Airbus Document EMF-723/99, Issue 3, 2000

[2] Airbus Industrie Memo AI/EA-A 412.0674/00, C. Beaufils, 2000

[3] FAA requested TOGAA[1)] review of ARAC[2)] recommendations for prevention of WFD in the commercial fleet, May 1999

[4] Laboratory tests to simulate APU heating on GLARE3-4/3-.4, W. t'Hart, R. Diks, NLR, Report NLR-CR-99338, 1999

[5] An Experimental and Analytical Investigation on the Fatigue Behavior of Fuselage Riveted Lap Joints, R. Müller, PhD Thesis, 1995

[6] The residual strength of Glare laminates with foreign object damage, T. de Vries, Delft University of Technology, EADS Technology Seminar 2001

[7] Fatigue and residual strength effect of scratches, M. Hagenbeek, Delft University of Technology, Report B2V-00-14, 2000

[8] Fatigue crack growth of part through the thickness cracks in GLARE3 and GLARE4B coupons, A. de Koning, L. Schra, NLR, Report NLR-CR-2000.078, 2000

[9] Design of Fuselage Panels and Major Panel Joints, Th. Beumler, DaimlerChrysler Aerospace Airbus, Technology Seminar `Advanced Fuselage Design´, Hamburg, 1999

[10] Current and Future Regulations, Design Goals and Industry Standards, H.-J. Schmidt, DaimlerChrysler Aerospace Airbus Do. EMF-1/99, 1999

[11] Analysis of Aircraft Structure Regarding Widespread Fatigue Damage, H. Trey, EADS-EMF, EADS Technology Seminar 2001

[12] Daimler Benz Aerospace Airbus Technical Note TN 10003 M, chapter 3: Einteilung der Flugzeuge in Umgebungskathegorien

[13] Prediction Methods for Fatigue Crack Propagation in unstiffened GLARE, Through Cracks, J.Homan, R. Alderliesten, Delft University of Technology, Report B2V-99-40, 1999

[14] The Metal Volume Fraction Approach, G. Roebroeks, SLI Report TD-R-00-003, 2000

[15] Environmental Fatigue of Aluminium Alloy Structural Joints, R. Wanhill, J. Luccia, L. Vogelesang, NLR Report MP 81013 U, 1981

[16] Damage Tolerance Methods and Allowables, Boeing Document D6-24958

[17] General environmental conditions for strength justifications of composite structures, Airbus Industrie Document ABD0087

[18] A340-500/600 Thermal Conditions to be used for the section 15/21 stress analysis, Aerospatiale Report A3456-TN-LIGC-2267-AT, 1999

[19] Aluminium-Lithium Fuselage Application Meeting, Information provided by ALCOA, Hamburg, 1998

1) Technical Oversight Group Ageing Aircraft
2) Aviation Rulemaking Advisory Committee

[20] ARALL, Adhesion Problems and Environmental Effects, Vol. B, Environmental Effects, M. Verbruggen, Delft University of Technology, PhD Thesis, 1986

[21] The moisture absorption of Glare – an introduction, O. Tensen, Delft University of Technology, Master Thesis, 1990

[22] Verifikation und Ergänzung von Berechnungsmethoden für die statische Auslegung von GLARE-Strukturen, H. Bär, Universität Stuttgart, Diplomarbeit, 1992

[23] Thermal- and deformation induced delamination of fibre metal laminates, E Kappel, Delft University of Technology, 1992

[24] Durability of GLARE - The influence of water and temperature on the low-frequency fatigue behaviour of GLARE, E. Huijzer, Delft University of Technology, Master Thesis, 1992

[25] The effect of frequency, moisture and temperature on the constant amplitude fatigue behaviour of GLARE3, M. Deutekom, Delft University of Technology, Master Thesis, 1994

[26] Thermal Behaviour of Fiber Metal Laminates, G. Graafmans, Delft University of Technology, Master Thesis, 1995

[27] Strength of GLARE after exposure to moisture, M. Boertien, Delft University of Technology, Master Thesis, 1996

[28] Qualification testing for the GLARE panel in the A310P/F, MSN484 aircraft, W.v.d.Hoeven & L.Schra, NLR report NLR-CR-2000-115

[29] GLARE Durability Programme - Results of tests carried out at the NLR, W.v.d.Hoeven & L.Schra, NLR report NLR-CR-2000-237

[30] The influence of elevated temperature on Glare after exposure to moisture, B. Borgonje, Delft University of Technology, Master Thesis, 2000

[31] Interims Report GRP working group 1C, ‘GLARE Durability’, EADS Report no. 10L020K4200I02, Issue 1, 2001

[32] Feuchteaufnahme von dicken CFK-Laminaten im Flugbetrieb, I. Kröber, DaimlerChrysler Aerospace Airbus, Technical Note TN-EMD-B/2000-01, 2000

[33] GTO WP 1.1 / Durability Program, DaimlerChrysler Aerospace Airbus, MoM EMF-932/99, 1999

[34] GLARE Introduction in the Airbus Material Family, NDI for In-service, W. Bisle, Th. Meier, Presentation at Airbus Toulouse, 3.7.2003

[35] The effect of temperature and ageing on Glare circumferential joints, M. Ypma, Delft University of Technology, report B2V-02-46, 2002

[36] Flight simulation fatigue tests on notched specimens of fiber metal laminates, J. Schijve, F. Wiltink, V. van Bodegom, Delft University of Technology, Report LRV-10, 1994

Chapter 2
Design Criteria and Design Factors for Riveted Joints

Contents Page

This page intentionally left blank.

2.1 Introduction

The application of GLARE as a structural material requires special attention for designing a new structure. In the present chapter, the phenomena associated with the fatigue strength justification of GLARE are discussed in general terms. The procedures of collecting experimental information for this purpose are summarized first, followed by a discussion on relevant design aspects concerning material characteristics, production, fasteners, load spectra and environmental conditions. Several of these aspects are studied in subsequent chapters. This applies specifically to GLARE riveted joints and environmental influences.

Some comments on the general philosophy

Mainly influenced by commercial aspects and competition on the market an aircraft has to be designed nowadays in not more than four to five years. This period contains the concept phase, during which the aircraft configuration will be settled, the predesign phase, used for material selection and defining the rough dimensions of structural components, and the design phase including the final strength justification. Unfortunately, the slot is too short for the required engineering sequence, i.e. configuration freeze $\rightarrow$ wind tunnel tests $\rightarrow$ load preparations $\rightarrow$ strengths calculations $\rightarrow$ design. In fact this sequence should be an iterative process towards the final design, which requires more than one loop. In reality, all engineering disciplines more or less start working at the same time, guided by their experiences from former projects.

During pre-design the stressman's disadvantage is the uncertainty of the design loads, since the load specialist has not yet reliable information from the aerodynamics. The fatigue specialist requires an entire stress spectrum, but that will be derived from the static load set and therefore must be expected even later. Consequently, the fatigue specialist must contribute to the safety relevant design features for the aircraft at a moment when neither reliable load/stress information nor the associated structural responses for new developed structural components are available. An option to improve the reliability of predictions is an early start of fatigue and damage tolerance tests using structural components with new design details, e.g. material- and fastener types. It is usual to carry out constant amplitude coupon or shell tests under laboratory conditions. Transfer functions for the calibration of test results with regard to the flying aircraft are required, the so-called „test-to-structure" factors. Depending on the specimen tested, these factors should account for size, stress spectrum, frequency, material scatter, manufacturing scatter and environmental influences. The correction factors have to consider quite different aircraft utilization aspects - from short range to long range, flying in arctic or tropic environment, operation on more or less gusty routes and even some habits like the soft landings celebrated by Air France pilots.

However, these engineering correction factors need to reflect a conservative average of utilization. Designing under consideration of all worst cases means to over-design the aircraft for the majority of users which is therefore unacceptable. The determination of the particular correction factors and the translation into a test-to-structure factor requires an educated guess. Later in this chapter the engineering factors to be considered for fatigue and damage tolerance of a monolithic aluminium fuselage structure will be introduced and discussed for the application of GLARE

.

Figure 2.1.1 illustrates the relationship between the aircraft to be certified and the available test components. It has to be recognized that there is a difference between the full scale fatigue test, which is mandatory according to airworthiness regulation JAR25.571 as a certification test, and the early development tests of components and coupon size specimens.

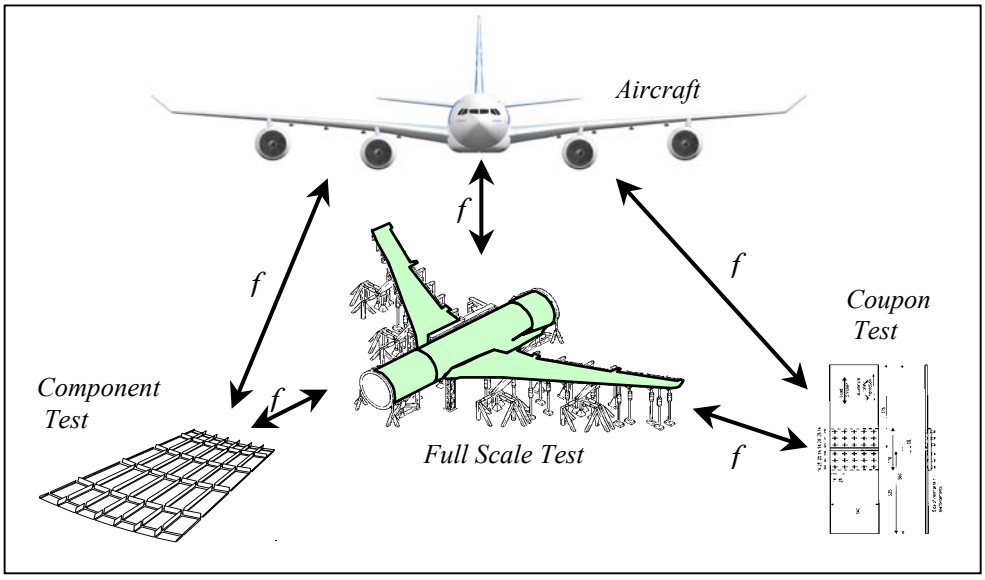

Figure 2.1.1. Correlations to be considered between aircraft structure and test results from different test articles

Appropriate factors in order to account for material scatter, load spectrum scatter and environmental influences have to be applied on test results for either the verification of the design service goal or the determination of the inspection threshold. The aircraft manufacturer looks back on a long history of experiences with aluminium structures. So-called test-to-structure factors have been developed for coupons and components, to be applied on stress or life in order to obtain results applicable to the full scale aircraft. During pre-design the factors are used for a quick evaluation of test results.

Fatigue results for small aluminium specimens (coupons) are related to final failure. The crack propagation life of the test is considered to be negligible. Consequently, the applied factors which shall link the coupon- with the full scale result are dependent on the crack initiation behaviour of the metal, not on the crack propagation behaviour. Factors 3 to 5 on the life of a constant amplitude coupon test result are commonly used in order to cover the full scale result.

The factors which have to be considered between the full scale result and the operational aircraft provide a certain safety standard, e.g. Airbus' target is to achieve a probability of survival for the monolithic aluminium structure of about 95%, i.e. only 5% of the aircraft will meet with fatigue damage before reaching the Design Service Goal. This level of safety should be kept for GLARE structures.

The full scale test result is valid for the applied mission mix, only. The aircraft will be certified for the applied load spectra, there is no factor accounting for load variations. If necessary for future aircraft derivates, an assessment for range or weight can be performed analytically. However, a conservatism can be integrated in the full scale test procedure by truncating the peak fatigue loads, in order to avoid the positive effects of plastification at the drilled holes.

Corrosion is a time- and user dependent damage, which is covered by dedicated corrosion inspection tasks. Therefore it is not considered in the full scale test evaluation as well.

Since the sizes of both, aircraft and full scale specimen, are similar, the engineering factor f between both is mainly dedicated to material scatter and the environmental influences which may decrease the material properties.

2.2 Test-to-structure factors for Fatigue Strength Justification

For a new material to be applied, the determination of the test-to-structure factors happens *during* the design phase of the new aircraft project. The learning curve improves by filling the so-called test-pyramid with results. This pyramid is limited to the full scale fatigue test on the top, which contributes significantly to the aircraft certification. Environmental influences on the strengths and stiffness of a new material in service have to be estimated with support of standardized or non-standardized tests and in-flight experiences obtained from other materials applied on earlier aircraft.

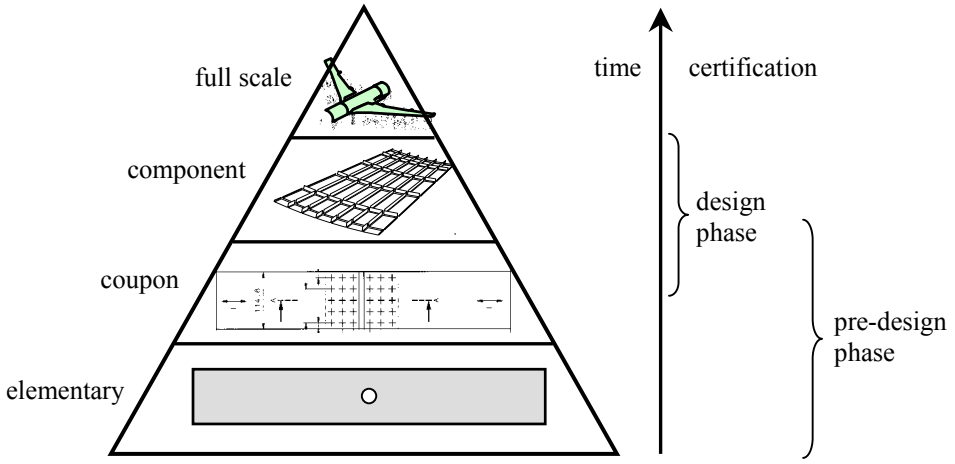

Figure 2.2.1. Test pyramid

A full scale fatigue structure due for aircraft certification is usually manufactured in the same production line as the corresponding aircraft parts. Beside the economical reason to produce the specimen with minimum costs there is the technical reason to copy the manufacturing quality of the aircraft as reliable as possible for the specimen. Since there is just one full scale structure available for testing, scatter due to manufacturing quality must be limited. Therefore it is recommended to take the specimen structure out of the production line after initial problems associated with the start of a new program are solved and the production process is running reliably.

The first new aircraft enter service almost simultaneously with the start of the full scale fatigue test. Until the test is finished and the results are evaluated, the calculated fatigue lives, inspection thresholds and inspection intervals for the particular PSE's are not validated and therefore preliminary. In terms of flight cycles it is the target to be ahead of the lead aircraft with the full scale specimen as soon as possible and thereafter to increase the lead of the test. Milestones of the full scale test are discussed and agreed with the airworthiness authorities.

The agreed milestones determine the required test speed. An accelerated load program contains a flight mission mix, ranging from „soft" to „hard" missions as well as from „short" to „long". However, the wide variation of possible flight routes and the habits of particular pilots can not be considered. Still the mission mix is a kind of average, on the conservative side.
Low loads of the test spectra are omitted at a level at which they are insignificant for the damage accumulation in order to accelerate the test. High fatigue loads are truncated for monolithic aluminium structures in order to avoid a crack initiation life improvement and/or a crack retardation effect due to local plastification, e.g at holes or a crack tip. For the latter reason the spectrum is considered to be conservative for the crack initiation- and crack propagation life in the full scale specimen structures.

Depending on the specimen size, the geographical test site location and the manufacturers philosophy, the full scale test will be conducted either in a laboratory or outdoors. Temperatures below zero degree Celsius can not be accepted, because it would make inspections uncomfortable for the test team. Consequently temperature effects have to be taken into account separately, e.g. for a material mix aluminium/titanium or for a particular material property itself.
Taking into account a maximum full scale test duration of two years, even to perform it outdoors will not simulate a realistic environmental influence of 20 to 25 years in-service operation. Anyhow, the designer is obliged to use metals, which do not experience time dependent changes of the material structure and the associated mechanical properties.

The influence of corrosion on metals is not considered for the full scale test. Corrosion is treated by special tasks in the aircraft inspection program. Corrosion in service must be detected and repaired in order to restore the certified strength of the structure. However, it is wise to test the allowable corrosion reworks on the full scale specimen.

This thesis is dedicated to determine some of the test-to-structure factors introduced in the following for a GLARE strength justification applied to commercial aircraft.

2.2.1 Fatigue crack initiation

The correlation between the full scale test- and the aircraft crack initiation life can be expressed in:

$$N_{A/C,I} = N_{FS,I} / C_{CI} \quad (1)$$

$N_{A/C,I}$: aircraft flights to crack initiation for considered PSE
$N_{FS,I}$: structural crack initiation life of full scale fatigue specimen PSE [flights]
C_{CI} : safety factor on crack initiation life of full scale specimen PSE

The safety factor C_{CI} contains several test-to-structure factors:

$$C_{CI} = C_{CI(Q)} \times C_{CI(MS)} \times C_{CI(LS)} \times C_{CI(E)} \times C_{CI(T)} \quad (2)$$

$C_{CI(Q)}$: manufacturing quality scatter factor on life for crack initiation
$C_{CI(MS)}$: material characteristics, scatter factor on life for crack initiation
$C_{CI(LS)}$: load spectrum scatter factor on life for crack initiation
$C_{CI(E)}$: deteriorative environmental factor on life for crack initiation
$C_{CI(T)}$: temperature related factor on crack initiation life

The load spectrum factor $C_{CI(LS)}$ can be set to 1 if a conservative mission mix is defined for the full scale test article. If not, it will be determined analytically in frame of an assessment analysis. Then, either the DSG or the inspection intervals or both will be decreased for the concerned aircraft.

If the full scale specimen is one of the regular assembled aircraft, factor $C_{CI(Q)}$ may be set to 1.

The above mentioned factors are considered for the relations between full scale, component and coupon tests as well. Dependencies between these specimen types require consideration of additional factors:

$C_{CI(F)}$: fastener factor, to be considered for crack initiation if different fasteners are used to compare similar structures

$C_{CI(ST)}$: surface treatment factor, to be considered for crack initiation if specimens with different surface conditions are to be compared

$C_{CI(S)}$: factor which considers spectrum loads related to single amplitude tests, including frequency effects

$C_{CI(SC)}$: factor to consider scale effect, e.g. due to stiffening elements, bi-axial loading

2.2.2 Fatigue crack propagation

Chapter 1 discussed the relevance of the fatigue crack propagation phase of the aircraft strength justification for both, monolithic aluminium and GLARE. As the determination of the inspection interval for a repair is of primary importance for *monolithic aluminium*, it is the determination of the residual strength for the *GLARE structure*, which should be always above ultimate load. The equation to be considered for the relation between the aircraft and the full scale test article looks similar as for crack initiation (§ 2.2.1):

$$N_{A/C,P} = N_{FS,P} / C_{CP} \quad (3)$$

$N_{A/C,P}$: aircraft crack propagation rate for considered PSE [flights]

$N_{FS,P}$: crack propagation rate of full scale fatigue specimen PSE [flights]

C_{CP} : safety factor on crack propagation life of full scale specimen

The safety factor C_{CP} contains several test-to-structure factors:

$$C_{CP} = C_{CP(MS)} \times C_{CP(LS)} \times C_{CP(E)} \times C_{CP(T)} \quad (4)$$

$C_{CP(MS)}$: material characteristics, scatter factor on crack propagation life

$C_{CP(LS)}$: load spectrum scatter factor on crack propagation life

$C_{CP(E)}$: deteriorative environmental factor on crack propagation life

$C_{CP(T)}$: temperature related factor on crack propagation life

The load spectrum factor $C_{CP(LS)}$ can be set to 1 if a conservative mission mix is defined for the full scale test article. If not, the inspection interval for those aircraft, which are not covered by the full scale test, will be determined analytically for aluminium structures. For GLARE PSE's an analytical assessment is necessary in order to determine the particular DSG.

Additional factors to be considered for the relations between full scale, component and coupon:

$C_{CP(S)}$: factor which considers spectrum loads for single amplitude tests, including frequency effect

$C_{CP(ST)}$: surface treatment factor, to be considered for crack propagation if specimens with different surface conditions are to be compared

$C_{CP(SC)}$: factor to consider scale effect, e.g. due to specimen width, bi-axial loading

2.2.3 Residual strength

The residual strengths of a fatigued structure is dependent on the particular failure mode and the associated material property. It can be directly linked to applied loads and measured strains close to the failure location. The failure mode must be similar for all kind of properties.

Test-to-structure factors to be considered between full scale specimen and aircraft:

$C_{RS(E)}$: deteriorative environmental factor on residual strength

$C_{RS(T)}$: temperature related factor on residual strength

Some of the most important test-to-structure factors will be discussed in the following chapters of this thesis.

2.3 Material Characteristics (ref. $C_{CI(MS)}$, $C_{CP(MS)}$)

Aluminium materials are characterized by strength properties, i.e. yield stress, modulus and strain at failure. In general terms, an aluminium alloy with a high static strength provides earlier crack initiation and faster crack propagation than an aluminium with lower static strength. The crack initiation behaviour of a metal is characterized by the shape of SN-data, the crack propagation behaviour by the shape of da/dN-ΔK-data. The scatter of these properties is an important parameter for the fatigue strength justification.

Other material characteristics of metals are linked to durability, e.g. the sensitivity to different types of corrosion and the long term stability.

GLARE is characterized by the selected metal, the selected fiber and the selected resin. Two major limits are considered for the static sizing of a component:

1) no detrimental permanent deformation at limit load (JAR/FAR25.0305)
2) no failure at ultimate load for at least 3 seconds (JAR/FAR25.0305), ultimate load equals limit load times a factor 1.5 for safety (JAR/FAR25.0303)

The combination of both, the particular aluminium type and fiber type, characterizes the stress-strain curve of the laminate. The combination 2024T3 and S-glass provides a significant second slope after yielding of the metal sheets. The second slope is dominated by the fiber property [9] (figure 2.3.1). Final failure occurs when the fiber failure strain is reached. Therefore, the GLARE material is mainly designed according to limit 1) during static sizing, with a second load path offered by the fibers if the aluminium is damaged. Then, if the fibers are bridging the damage in the aluminium sheets, the material characteristics of the resin become important. The damage size in the aluminium, the capability of the aluminium to local plastification, the fiber strength and the delamination size between the metal sheets and the fiber layers need to be balanced for optimized laminate properties.

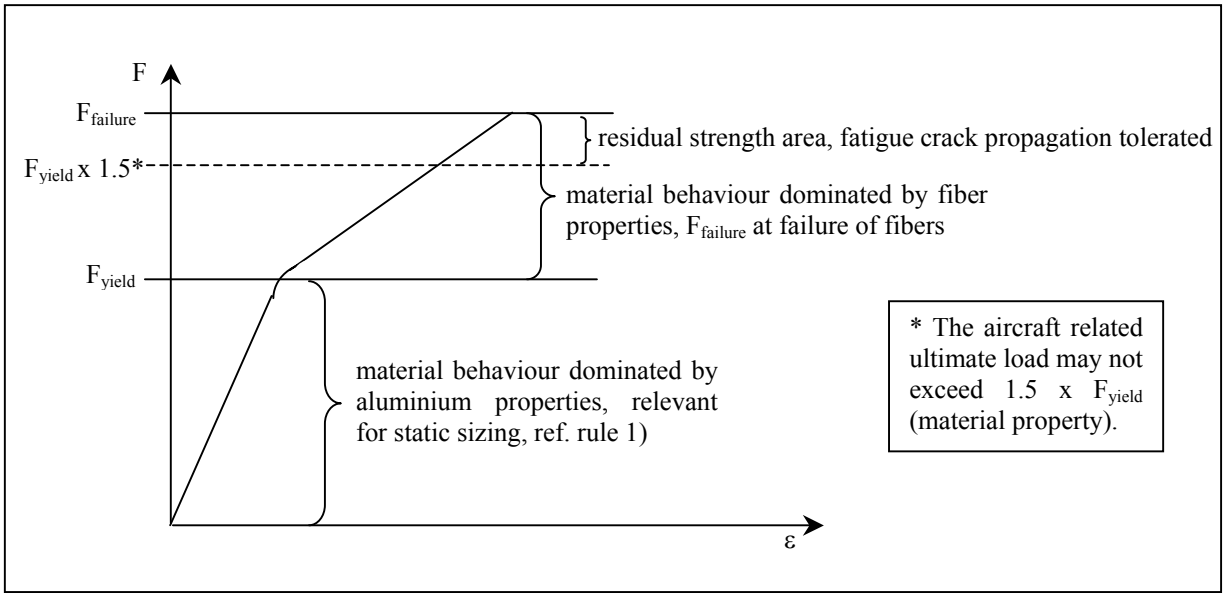

Figure 2.3.1. Typical stress-strain curve for GLARE made of 2024T3 an S-glass prepreg

The crack initiation scatter and the crack propagation scatter in the aluminium layers of GLARE will be discussed in the following chapters 6 and 7.

2.4 Manufacturing Quality (ref. $C_{CI(Q)}$)

The manufacturing quality of bore holes and the associated fastener fit in the drilled hole has a significant influence on the crack initiation life. For example, a factor 5 can be obtained on crack initiation in riveted GLARE joints by variation of the squeeze force applied to a NAS1097 fastener [3].
Airbus has developed manufacturing instructions for drilling operations and fastener installations in GLARE which produce non-damaged holes [4]. It is focused especially on a controlled feeding rate and revolution speed of the drill, which shall prevent any delamination of the laminate. For the same reason the interference fit between the drilled holes and the bolts is limited to 40 μm.

All holes in specimens which belong to this research are manufactured according to the Airbus specification [4] or very similar requirements. Details are explained together with the specimen description. Open hole specimens, produced for detailed crack initiation investigations in the laboratory, are reamed.

The drilling and fastener installation quality is similar for all GLARE specimens of the present research.

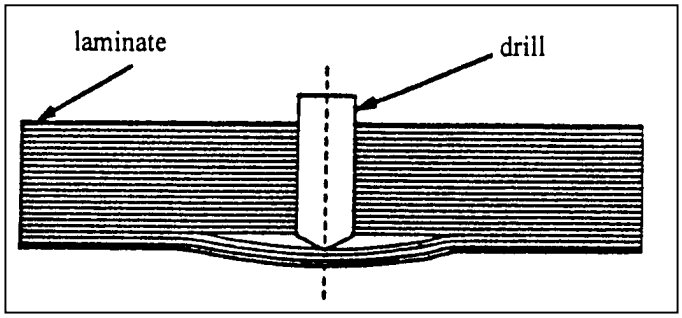

Figure 2.4.1. Delamination in GLARE caused by non qualified drilling parameters

2.5 Fastener Type (ref. $C_{CI(F)}$)

The influence of different fastener types, installed in similar designed riveted joints, has been investigated extensively by Airbus. Due to different fastener characteristics concerning hole filling, hole expansion, fastener head- and collar design, materials, stiffnesses and clamping forces, differences of factor 2 in crack initiation lives can be obtained [5].

For the present research, the same fastener types are used for all specimens as installed in the referenced full scale structures. If exceptions are made, the reasons are explained and the influences discussed together with the specimen description. Exceptions have lead to unscheduled differences concerning the fatigue crack location as discussed in chapter 7 for the riveted repair coupon specimens.

2.6 Surface Treatment (ref. $C_{CI(ST)}$ & $C_{CP(ST)}$)

Variations of the surface condition of a 2024 sheets have a negligible effect on fatigue for practical structural applications, if manufactured within the specifications of the commercial aircraft industry. Differences in fatigue lives due to various surface treatments, like phosphoric acid anodising, chromatic acid anodising or the application of primers are present, but the absolute fatigue performance in the (un-notched) far field will never decrease to an unacceptable level.
If superposed with notches, e.g. chemical milled edges or drilled holes, the notch factor introduced by the geometrical discontinuity becomes dominant. An exception is fretting corrosion, which might cause crack initiation in a riveted field but outside the hole, if insufficient sealant is applied or if the sealant is squeezed away by high clamping forces.
A careful surface preparation including cleaning and activating of the surfaces, is important for a good bond between the metal sheets and the sealant. Modern sealants provide high adhesive forces, which can influence the crack initiation lives of metal structures favourably [14]. For comparative crack initiation investigations of riveted joints it is therefore important to prepare all specimens with the same surface and sealant in the joint area.

2.7 Load Spectrum Factor (ref. $C_{CI(S)}$ & $C_{CP(S)}$)

2.7.1 Load spectrum factor on crack initiation ($C_{CI(S)}$)

The load spectrum factor $C_{CI(S)}$ is a main parameter for the consideration of particular flight spectrum characteristics on crack initiation predictions, which are based on constant amplitude SN data. It is an expression for the severity of the stress spectrum – whether it is soft, like for a commercial aircraft fuselage skin, or hard, like for a fighter aircraft wing. The target is the determination of a single amplitude stress level, which leads to the same damage as the accumulated damages of one flight (spectrum), under consideration of a Rainflow analysis. An advantage of the method is the independency of notch factors.
For monolithic aluminium, the spectrum factor $C_{CI(S)}$ is defined as the ratio between the equivalent stress and a reference stress. The latter is a mission stress which is typical for the spectrum. Certain manufacturers select the stress level which is related to flight stage `1g cruise´ superposed with the stress which develops due to the cabin differential pressure as the equivalent stress.

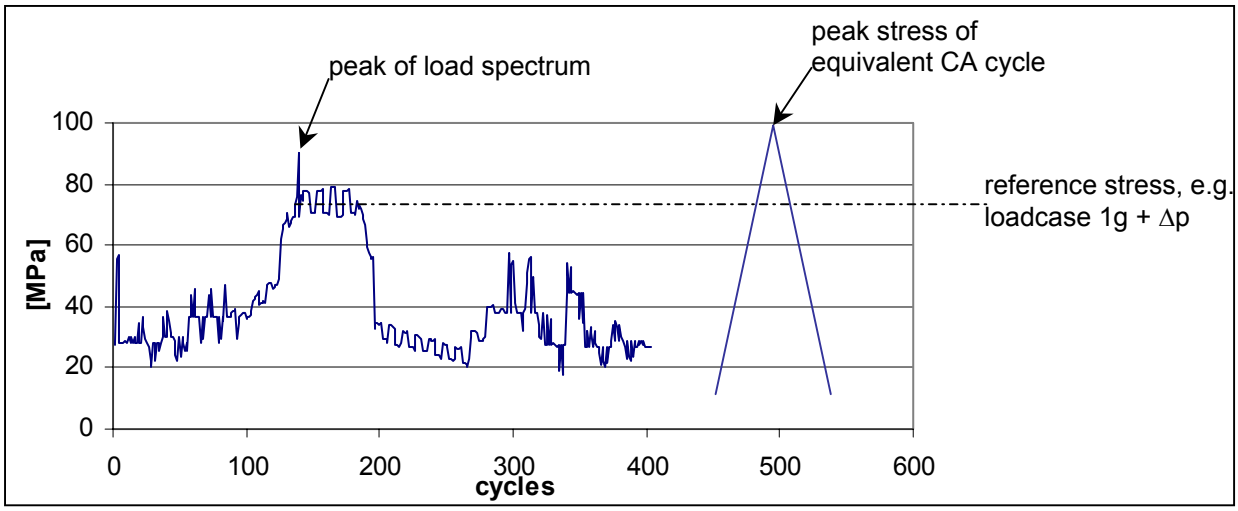

Figure 2.7.1. Typical flight spectrum and a single load cycle, both leading to the same damage

$C_{CI(S)} = \sigma_{equivalent} / \sigma_{reference}$ for a similar damage [6] (5)

A commonly selected reference stress is the so-called `1/flight´ stress level. It is the stress level, which is exceeded as often in the cumulated fatigue load envelope as the scheduled number of flights, which defines the Design Service Goal, figure 2.7.2. For rear fuselage structures, loaded in length direction, stresses due to load case '1g+Δp+10ft/s gust' turned out to be close to the equivalent stress level [2]. This is particular important for the pre-development of circumferential fuselage joints.

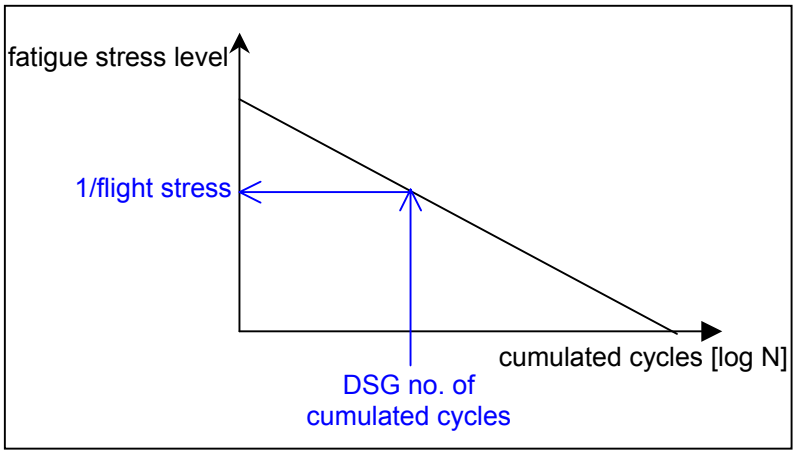

Figure 2.7.2. Determination of 1/flight stress level

For tests of full scale metallic fatigue specimens, high fatigue loads are often truncated in order to prevent local plastification, at drilled holes for instance, which may lead to postponed crack initiation, crack closure effects and consequently lower crack propagation rates. The effect can increase the fatigue life of a component by factor 2, depending on the particular stress spectrum, truncation level, material type, etc. [7]. By truncating the high fatigue loads in metals, this effect can be avoided and a conservatism is introduced. Low fatigue stresses, which do not contribute to either damage accumulation or crack propagation, can be omitted for

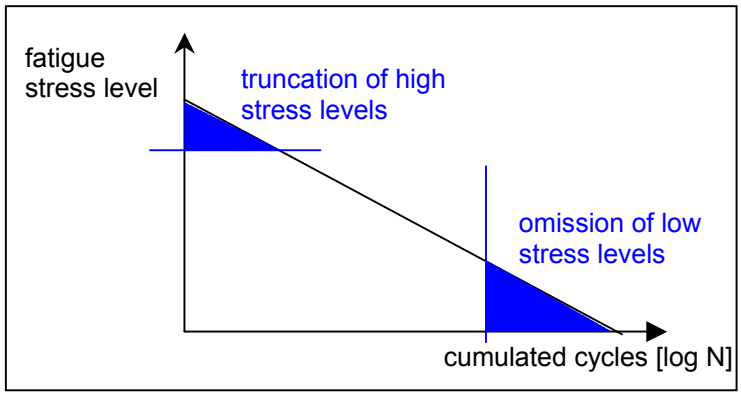

Figure 2.7.3. Truncation and omission

economical reasons, i.e. for a faster test performance. Just *one* truncation level and *one* omission level can be defined for *one* entire full scale specimen. Depending on the particular stress levels and notch factors, each PSE will be affected differently. This holds as well in case of a material mix, i.e. for structures made of both, monolithic aluminium and GLARE. Because the stress levels in the aluminium layers of GLARE are dependent not just on the applied load, but also on the stiffnesses of its ingredients and the temperature, a survey of the influence of truncation and omission on the properties of GLARE is recommended. Depending on the sizing criteria for fatigue sensitive locations and the associated maximum stresses, it is required to investigate whether the truncation and/or omission level have a different effect for monolithic aluminium and GLARE structures. If so, a compromise has to be found for the mixed material full scale fatigue certification structure.

2.7.2 Load spectrum factor on crack propagation ($C_{CP(S)}$)

In monolithic aluminium the load spectrum factor which accounts for the spectrum influence on crack propagation rates should be related to the same crack length interval:

$$C_{CP(S)} = \sigma_{equivalent} / \sigma_{reference} \quad \text{for a similar crack extension [6]} \qquad (6)$$

In explanation it has to be answered to the question, about which factor has to be applied on the reference stress (CA) in order to obtain the equivalent stress (CA) which covers the crack propagation rate related to the entire spectrum (VA) for a given crack propagation period. Due to the strong dependency of the crack propagation rate from the actual stress intensity factor the method is limited in its application for monolithic aluminium to the area between 'no crack growth' ($\Delta K_{threshold}$) and 'fast crack growth'. The constant stress intensity factor at the crack tip of a fatigue crack in GLARE even for long cracks extends the validity of the method significantly. Similar as for crack initiation, the influences of truncation and omission of loads for GLARE components in a full scale fatigue have to be investigated.

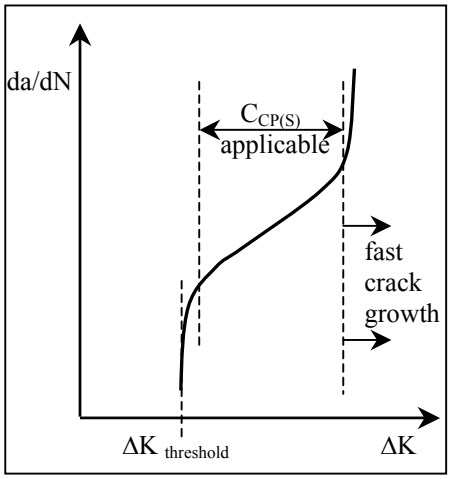

Figure 2.7.4. Typical da/dN/ΔK curve for monolithic aluminium

2.8 Size Effect ($C_{CI(SC)}$ & $C_{CP(SC)}$)

The larger the test components, the lower the size effect will be if compared to a full scale specimen. The main parameter which influences the accuracy of test results is the specimen complexity, i.e. the availability of as much as possible structural elements which allow a load distribution from one element to the other one. Stiffening elements decrease local bending significantly and have a large influence on the crack initiation life. Consequently, stiffened panels provide a better result than a coupon. A curved panel, e.g. for the simulation of a fuselage shell, increases the accuracy of a test result even more, since the curvature suppresses local bending as well.

With increasing complexity both, the test time and the costs increase. Depending on the particular boundary conditions, the stressman has to choose for either a simple but fast and cheap test (coupon), a non-stiffened panel (flat), a stiffened panel (flat) or even a curved stiffened panel. The latter one

requires a large test rig, which on the other hand allows the application of internal pressure loads and tensile loads in longitudinal and circumferential fuselage direction, in most of the cases. This test will provide the most accurate results, since the influence of bi-axial loading on fatigue can be included.

For the structures which will be investigated in this thesis the presence of both stiffening elements, stringer and stringer couplings, will have a significant influence on the local deformations under load and consequently on the crack initiation lives. The influence of stiffeners on the bending stress of a butt strap is demonstrated in a common program of Airbus and Delft University. During the pre-development phase, A3XX test shell 'XE3' has been tested by Airbus [1]. The test shell was made of aluminium skin panels jointed by a GLARE2B-7/6-.4 butt strap. The width of the panel was sufficient to accommodate three aluminium stringer on each skin panel, connected with three stringer couplings. Strain gauge measurements have been performed in the aluminium skin and at both sides of the butt strap, at the center rivet row where the frame clip was not attached. The panel was fatigued and failed during a residual strength test in the far field, in a distance of approximately a half frame bay from the joint. Thereafter, a coupon specimen was cut out of the panel, just between two stringer positions:

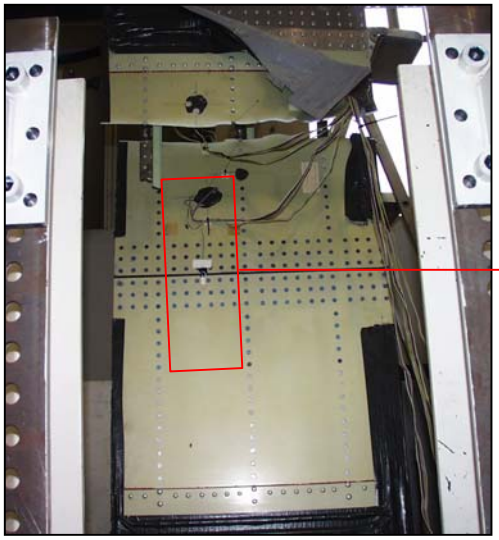

Figure 2.8.1. Circumferential joint test shell 'XE3', focus from outside, stiffener included

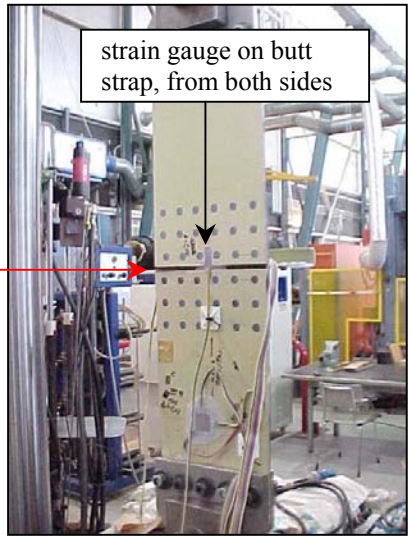

Figure 2.8.2. Cut out joint coupon from shell 'XE3' in test rig

The coupon included the strain gauges attached at Airbus. It was loaded at Delft University, and strain measurements have been performed without the stiffening influence of the stiffeners. The mating surface butt strap stresses increase by 35% for the 1/flight load, if the stiffeners do not suppress the bending.

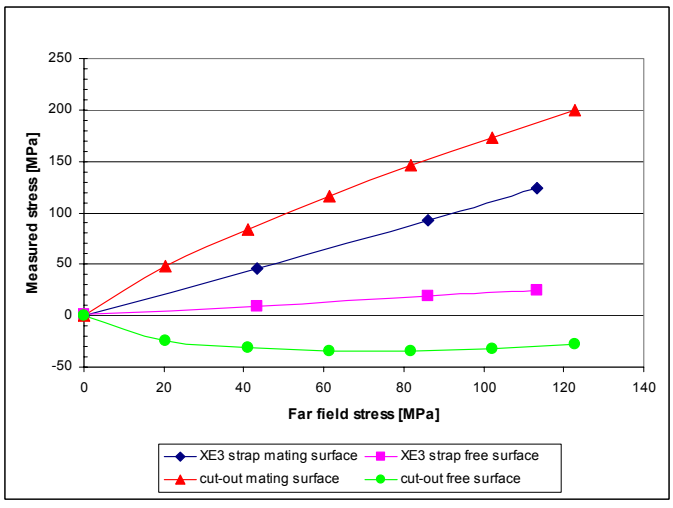

Figure 2.8.3. GLARE2 butt strap surface stresses (net) with and without stiffeners, stresses related to E=72 GPa

2.9 Temperature Influences ($C_{CI(T)}$ & $C_{CP(T)}$)

The influences of temperature on strength need to be discussed on both, the elementary level (material properties) and on the component level.

FAR/JAR 25.0613 discusses the material strength properties and allowable design stresses. According to paragraph 25.0613c, effects of temperature on allowable stresses have to be considered. Since GLARE is composed out of materials with different coefficients of thermal expansion, i.e. aluminium and glass fiber, the effect of the internal stress system due to temperature variations on different strength properties may be discussed in view of the FAR/JAR 25.0613 requirement. However, for time constrains it should be avoided to force the aircraft component designer to deal with the internal stresses in GLARE. For simplification, knock down factors have to be introduced which allow the designer to use the room temperature material properties, to be multiplied with the knock down factor if required. Especially the evaluation and application of SN-data (Wöhler curves) would be complicated if linked to the thermal stresses in the particular aluminium layers. This item will be discussed in detail in chapters 6 and 7. For simple handling, it should be the target to relate both SN-data and crack propagation curves to the *applied* load on GLARE material.

The suitability and durability of '*materials used for parts*' is discussed in FAR/JAR 25.0603 (Materials). FAR/JAR25.0603c details, that the effect of temperature has to be taken into account. On a component level it is important to consider the thermal stresses which develop between two materials of different CTE's, e.g. a riveted joint between titanium and aluminium or a repair patch made of steel, riveted on an aluminium structure. The differences of the CTE's of GLARE and aluminium are so limited, that they can be considered negligible [10, 11]. Very fatigue sensitive is a joint between either GLARE and titanium or GLARE and steel. In such a case, a detailed thermal stress analysis is recommended for the GLARE structure.

In this thesis the test-to-structure factors $C_{CI(T)}$ and $C_{CP(T)}$ do always reflect on the GLARE internal stress system, not on the thermal stresses between structural components made of different materials.

Which material temperatures have to be considered, depends on the result of a thermal analysis for the particular component. This thermal analysis is based on assumptions concerning the ambient conditions including wind speed on the ground, the material properties of the fuselage skin, the design of the concerned structure including the insulation and all connected structural parts, and it is dependent on the applied load. Figure 2.9.1 shows the result of a thermal analysis for an A380 GLARE fuselage skin top shell, for a static strength justification [12]. In a steady state condition, maximum skin temperatures close to 85ºC have been calculated for the GLARE skin. Note the absorption coefficient 0.6 used for the calculation, it does not consider the darkest possible color. The temperature decreases when the aircraft starts to move, on the outside faster than on the inside, since no air flow can transport the heat away from the structure inside the fuselage. During the take-off run, when the first significant structural loads can occur due to a start abortion, still skin material temperatures between 70ºC and 80°C have to be considered for static sizing. A start abortion can load the upper front fuselage shells significantly in compression, due to the breaking forces and the associated bending moment which develops between the nose landing gear and the main landing gear. In the aft fuselage no designing forces are considered until the wing flaps have been retracted (approximately at t=750 seconds for the A380).

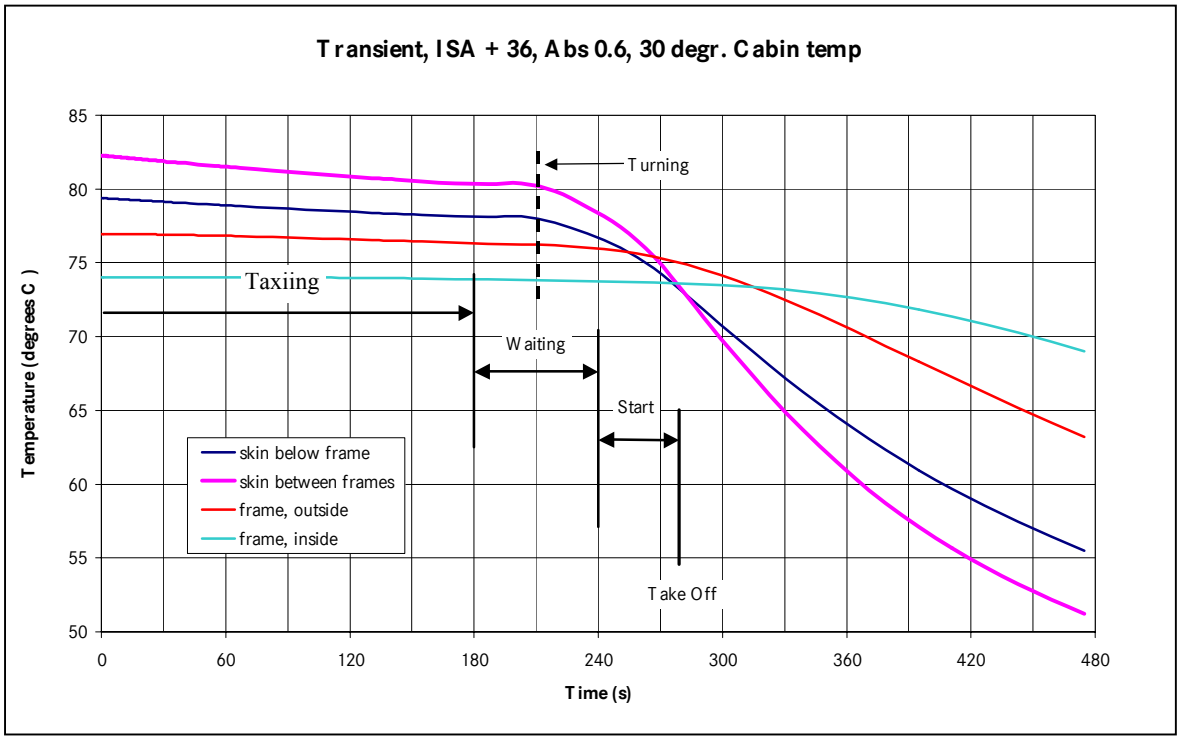

Figure 2.9.1. GLARE skin panel temperature dependent on flight mission time (temperature shown for static strength justification) [12]

Since both, the artificial circumferential joint in the A340-600 full scale test article and the riveted repair on the Megaliner Barrel are located on the aft fuselage, high temperatures during *static* loading will be not considered in this thesis. However, the influences of high temperature on material properties and allowable design stresses will be discussed occasionally.

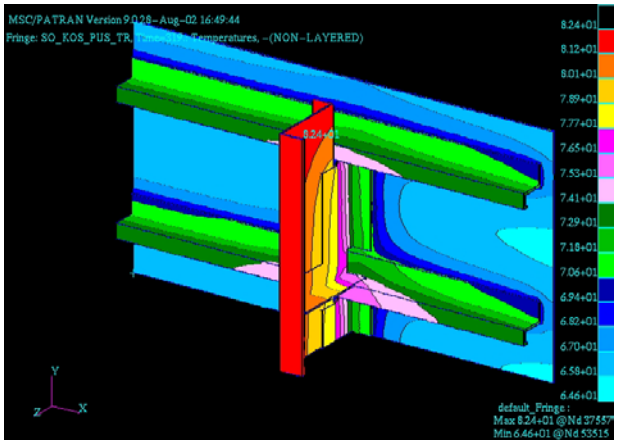

Figure 3.9.2. Temperatures in skin panel, 319 seconds after stage `engine on´ (example, static condition) [12]

The calculated stationary temperature for the early mission phases and for the *static* strength justification with loads is linked to a high outside air temperature, i.e. 51°C (ISA+36). This temperature is considered as the worst possible case. It is not applicable for fatigue. Typical fuselage skin temperatures measured in the Sahara desert have been presented in chapter 1. 70ºC skin material temperature have been measured for 'standing on ground'. This temperature is considered for the tropic flight mission as ground material temperature before taxi out.

For a pressurized fuselage, significant longitudinal fatigue stresses may appear during taxi, but no significant circumferential fatigue stresses will be present. Hence the superposition of fatigue loads and high material temperatures have to be justified mainly for PSE's loaded in longitudinal fuselage direction,

e.g. for a circumferential joint. Low material temperatures, between -30ºC and -55ºC, have to be considered for the cruise phase, during which the internal pressure is dominating the fuselage skin stresses in circumferential direction.

2.10 Environmental Influences ($C_{CI(E)}$ & $C_{CP(E)}$)

Regulations FAR/JAR 25.0603, ACJ25.0603 and 25.613 require the consideration of environmental influences on material strengths. From previous research it is understood for fiber metal laminates that moisture is absorbed in the adhesive and at the glass fiber / adhesive interface [13]. Water displaces the H+ OH- bond between fiber and adhesive and breaks the fiber bond. A reduced bond strength between fiber and adhesive can lead to shear failure in the laminate at lower applied loads than obtained in a dry condition, resulting in decreased material properties. Conservative but realistic accelerated tests must provide test-to-structure factors to be applied on any test specimen, in order to simulate an aircraft condition at the end of it's service life [years]. At a fatigue load level (relatively low stresses) it needs to be determined, whether any deterioration due to moisture can influence the crack initiation life ($C_{CI(E)}$). Crack propagation is much more complex if related to matrix ageing. High shear forces develop between aluminium and prepreg as well as in the prepreg in the vicinity of the fatigue crack. However, an investigation is required whether for practical applications the moisture absorption is faster than the fatigue crack propagation (then, the crack would propagate along a wet prepreg) or whether the crack propagates faster than the moisture travels (the crack would propagate along a dry prepreg).
In the residual strength case, different prepreg related failure modes may be influenced by moisture absorption (figure 2.10.1), along with the bond line between prepreg and aluminium.

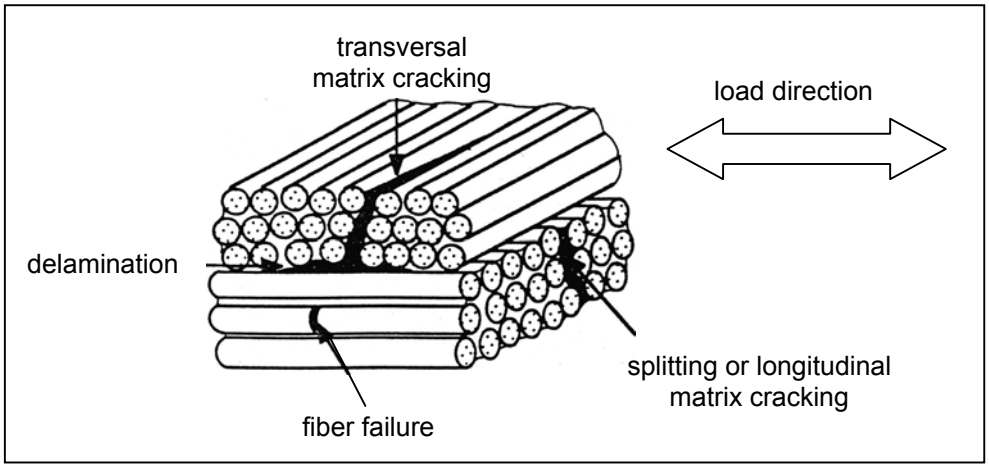

Figure 2.10.1. Failure modes in prepreg, matrix cracking and delamination can be influenced by the presence of diffused moisture

2.11 Summary

The particular physical phenomena which have to be considered for the fatigue strength justification of GLARE structures are summarized in the present chapter. In principle they can be divided in two major groups:

1) Mechanical properties of the GLARE type in the as-received condition, including manufacturing effects.
2) The influence of environmental ageing and temperature on the mechanical properties according to 1).

In the following chapters mechanical properties of two selected riveted joints will be determined by tests and developed by analysis. S*tatic* properties are included in order to determine which properties – static or fatigue – are sizing the joint under realistic ageing conditions.

Concerning environmental influences the main focus will be on *ageing* rather than on temperature. For this reason chapters 4 and 5 deal with the approximation of diffusion into the prepreg throughout the aircraft life.

Chapter 3 will introduce the selected riveted joints and those specimen types which participate in an outdoor exposure program.

The above introduced engineering factors are developed with the help of elementary specimen test results in chapter 6. The analysis will be extended to riveted joints and full scale test results in chapter 7.

2.12 References

[1] Fatigue tests on cross-butt jointed panels XE1 to XE4, A3XX, R. Hillbrecht, Airbus, Technical Note TN-ESVG-4007/01, 2001

[2] Fatigue test results of A320 and A321 circumferential butt joint panel specimens, Th. Beumler, Deutsche Aerospace Airbus Report 10D/E022K4753C04

[3] An Experimental and Analytical Investigation on the Fatigue Behavior of Fuselage Riveted Lap Joints, R. Müller, PhD Thesis, 1995

[4] Preparation of GLARE Test Specimen, Process Specification, W. Brunkhorst, Airbus Document EVM 40308.00, Issue 2, 2001

[5] Repair Assessment Guidelines, DaimlerChrysler Aerospace Airbus, Report 10X00274450C02

[6] Aerospatiale Fatigue Manual, D. Campassens, Aerospatiale Document MTS 005, Issue B, 1998

[7] Crack growth in aluminium alloy sheet material under flight-simulation loading, J. Schijve, S.Ichsan, J. Vlutters, J. Kluit, International Journal of Fatigue, Vol. 7, p. 127-136, 1985

[8] Stress-strain curves of GLARE, B. Out, Delft University of Technology, Report B2V-01-15, 2001

[9] Towards GLARE, G. Roebroeks, PhD Thesis, Delft University of Technology, 1991

[10] Thermal Behaviour of FML, Verolme, Structural Laminates Company, Report TD-R-95-24, 1995

[11] Estimation tool for basic material properties, M. Hagenbeek, Delft University of Technology, Report B2V-00-29, 2000

[12] Thermalanalyse von Rumpfbauteilen aus GLARE, S. Waitz, J. Teßmer, Deutsches Zentrum für Luft- und Raumfahrt, Bericht IB 131-2003/24, 2003

[13] ARALL, Adhesion Problems and Environmental Effects, Vol. B, Environmental Effects, M. Verbruggen, Delft University of Technology, PhD Thesis, 1986

[14] Comparison of skin/clip rivetings with sealants PR1431 and PR1827, Th. Beumler, Deutsche Airbus GmbH, Report 10F022K4751C04, 1989

[15] General environmental conditions for composites, Airbus Directive ABD0087, 2001

Chapter 3
Outdoor Exposure Test Program

Contents Page

This page intentionally left blank.

3.1 Introduction

The purpose of the present research is to investigate design sizing methods for static properties, fatigue crack initiation and propagation, and residual strength of a GLARE structure. These methods are well established for monolithic aluminium structure for which a huge data base is available, in particular 2024. The present research can provide and validate trends, and is intended to provide guidelines for the structural justification and certification of GLARE structures, while further experience for a consolidation have to be collected in the coming years by the GLARE customers.

An important aspect of the above problem setting is associated with the possibility of environmental effects on properties of GLARE structure elements as discussed in sections 2.9 and 2.10. An extensive outdoor exposure program has been set up in Queensland/Australia. The selection of the specimen types for this program is presented in this chapter, including some background information concerning the purpose and previous experience. All elementary-, coupon- and component test specimen which belong to the outdoor exposure program are similar or relevant to characteristic features of:

(1) A GLARE2 butt strap of an “experimental” circumferential riveted joint in the fuselage of the Airbus full scale test article of the A340-600, see figure 3.1.1 (the experimental joint does not occur in the regular A340-600 aircraft).

(2) A riveted repair patch applied in the Airbus full scale test article ‘Megaliner Barrel´ shown in fig. 3.1.2.

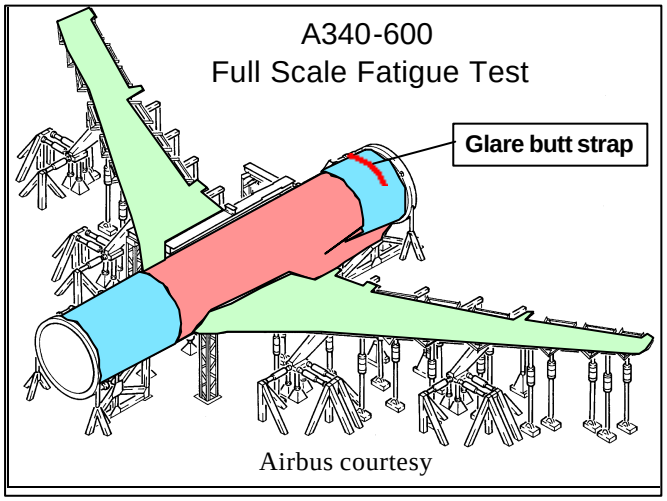

Figure 3.1.1. Sketch of the Airbus A340-600 EF2 test article, details shown on the following pages

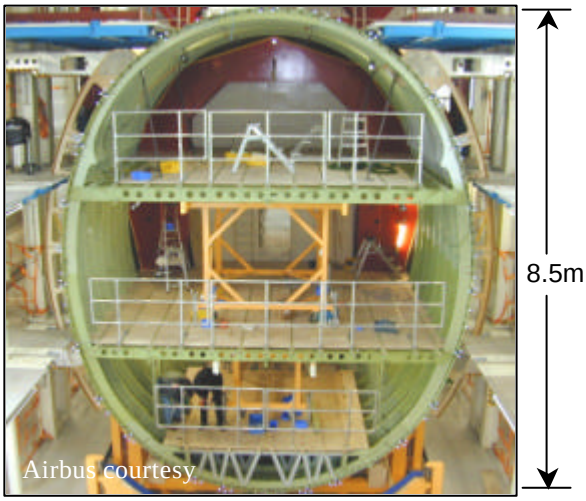

Figure 3.1.2. View on cross section of Airbus `Megaliner Barrel´, details on following pages

A survey of the coupon and component specimens discussed in this chapter is given in figure 3.1.3, which indicates a distinction between specimens related to the butt strap riveted joint and the repair patch. These elementary specimens were also investigated in the artificially aged condition for later comparison with outdoor exposure results. It will be investigated in chapters 6 and 7, how far the elementary and coupon specimens should be considered to provide either material properties (FAR 25.603) or design allowables (FAR 25.571 & FAR 25.613) and how far they are useful for structural sizing. With regard to the design criteria discussed in the previous chapter, strength values will be determined in chapter 6 based on the *elementary* specimens. Depending on the feasibility, this will be done with or without fatigue cracks. In order to determine the lower limit of strengths due to moisture absorption, material data after different hours of *accelerated* ageing will be included. The first results from *outdoor* exposure after one year ageing are available. The *joint coupon* test results will be discussed in chapter 7. Correlations of test results obtained from the different specimen types will be established, leading to test-to-structure factors. A prognosis for the influence of realistic ageing will be

performed as well, provided, the failure mechanisms after both, accelerated ageing and outdoor exposure ageing is similar. However, the final verification will be possible in the year 2008, when the outdoor exposure period and the subsequent tests are completed.

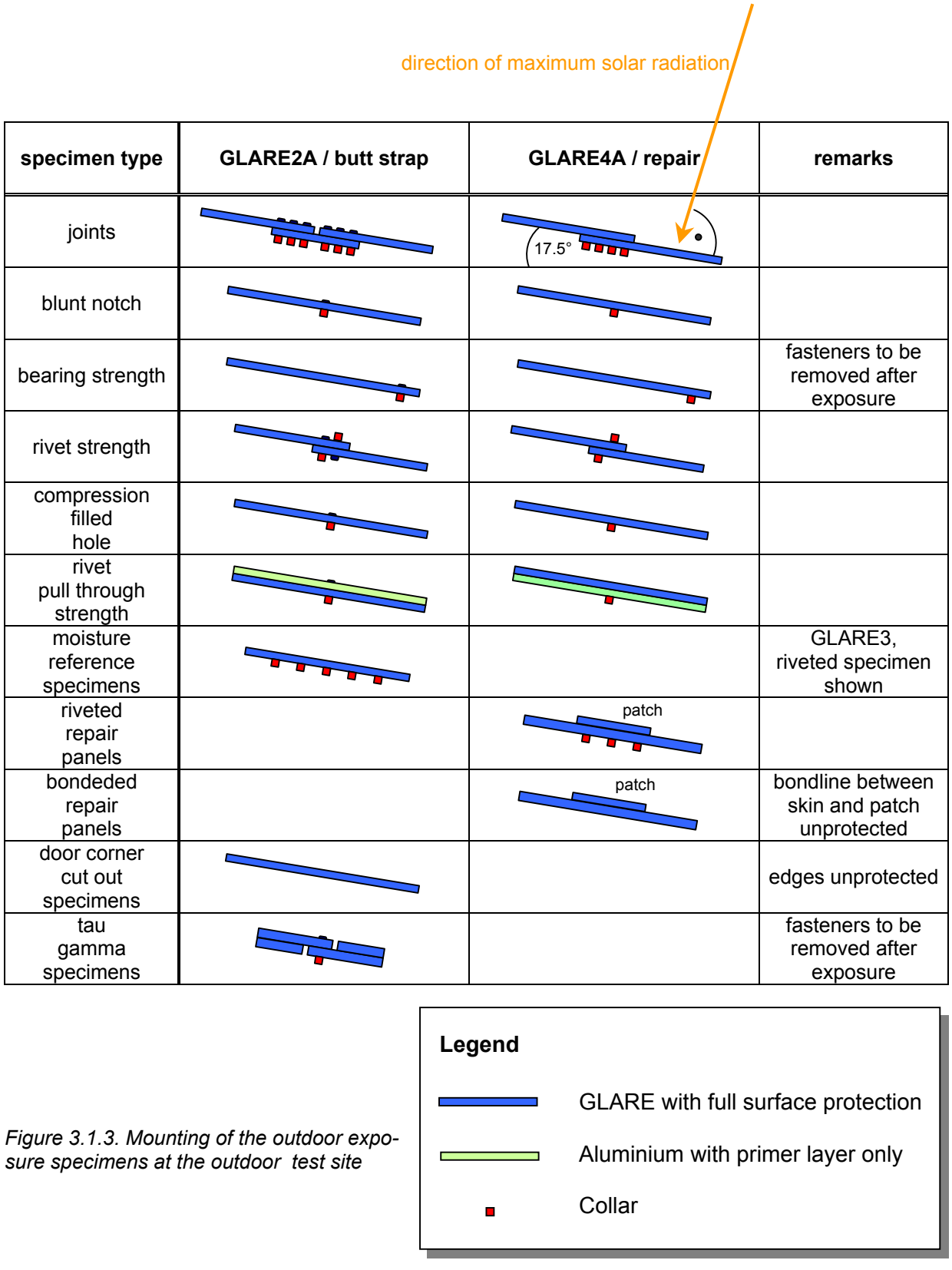

specimen type	GLARE2A / butt strap	GLARE4A / repair	remarks
joints			
blunt notch			
bearing strength			fasteners to be removed after exposure
rivet strength			
compression filled hole			
rivet pull through strength			
moisture reference specimens			GLARE3, riveted specimen shown
riveted repair panels			
bondeded repair panels			bondline between skin and patch unprotected
door corner cut out specimens			edges unprotected
tau gamma specimens			fasteners to be removed after exposure

Figure 3.1.3. Mounting of the outdoor exposure specimens at the outdoor test site

3.1.1 A340-600 EF2 experimental circumferential fuselage joint

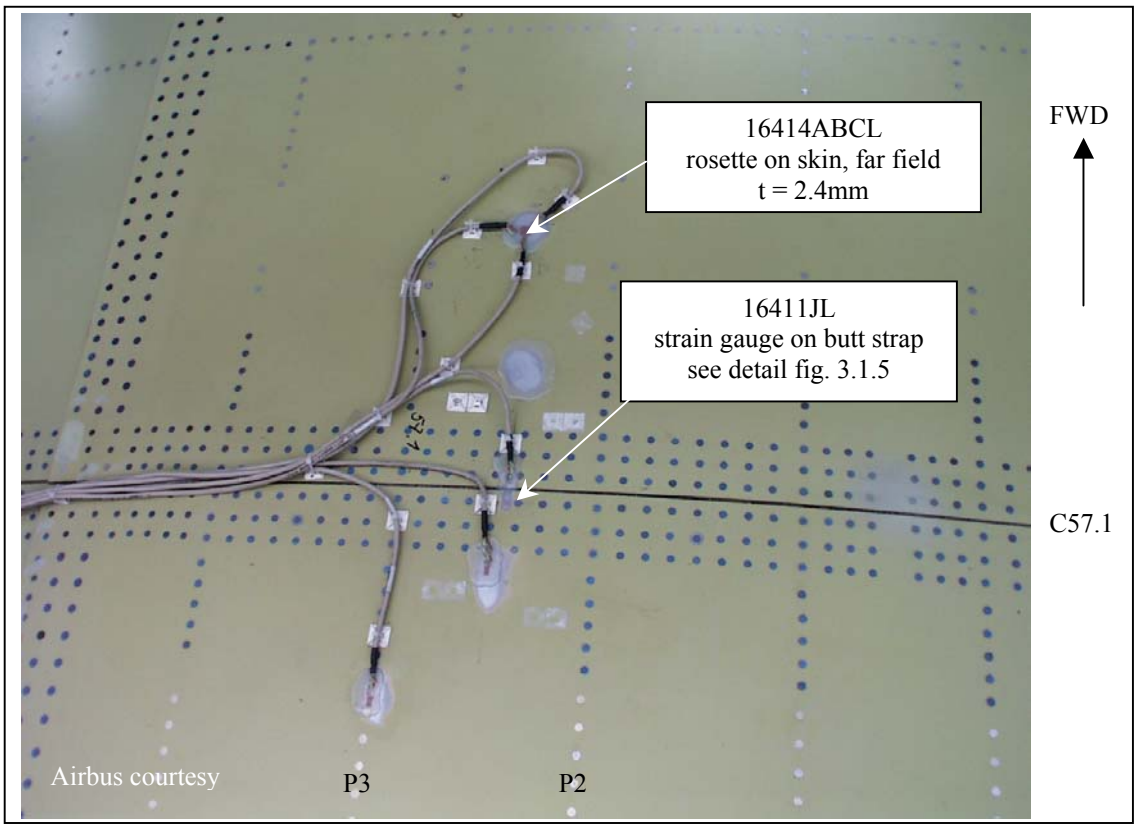

Figure 3.1.4.Top view on the fuselage of full scale specimen at frame 57.1 with the external strain gauge positions

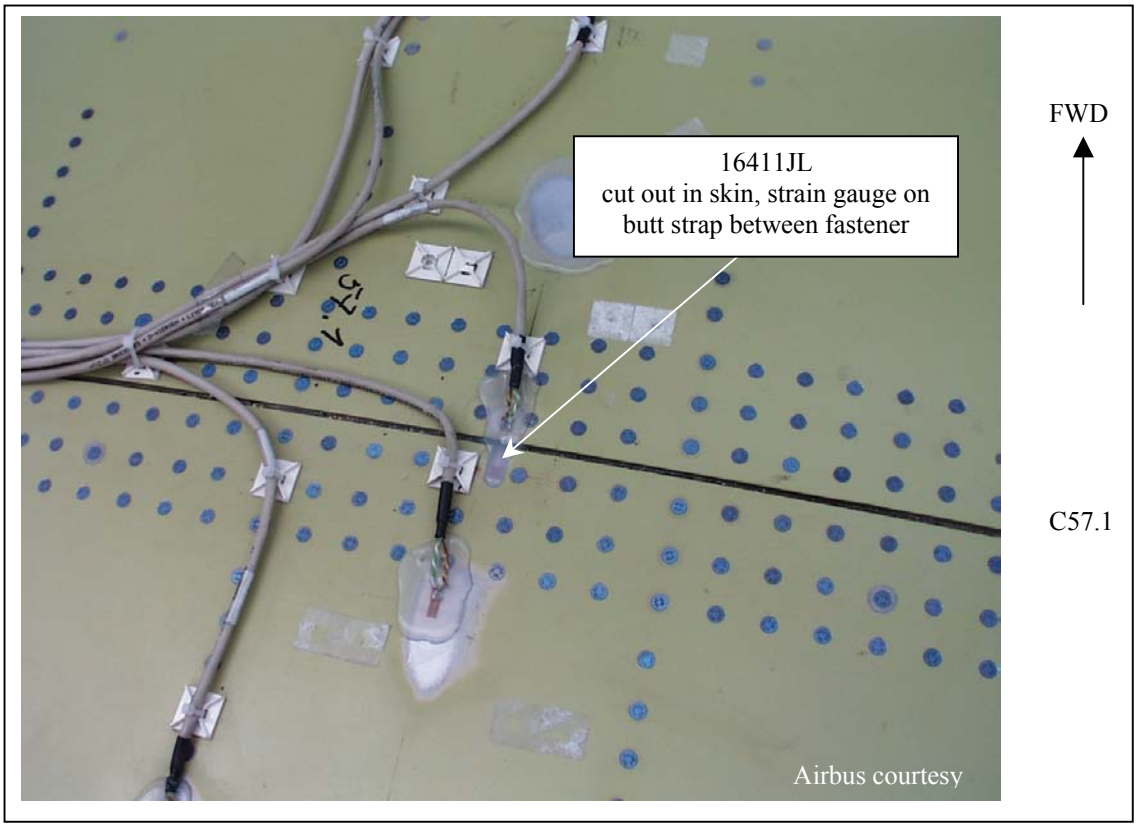

Figure 3.1.5. Detailed top view on fuselage, strain gauge 1611JL at critical butt strap location, cut out milled in the skin for access to the butt strap mating surface

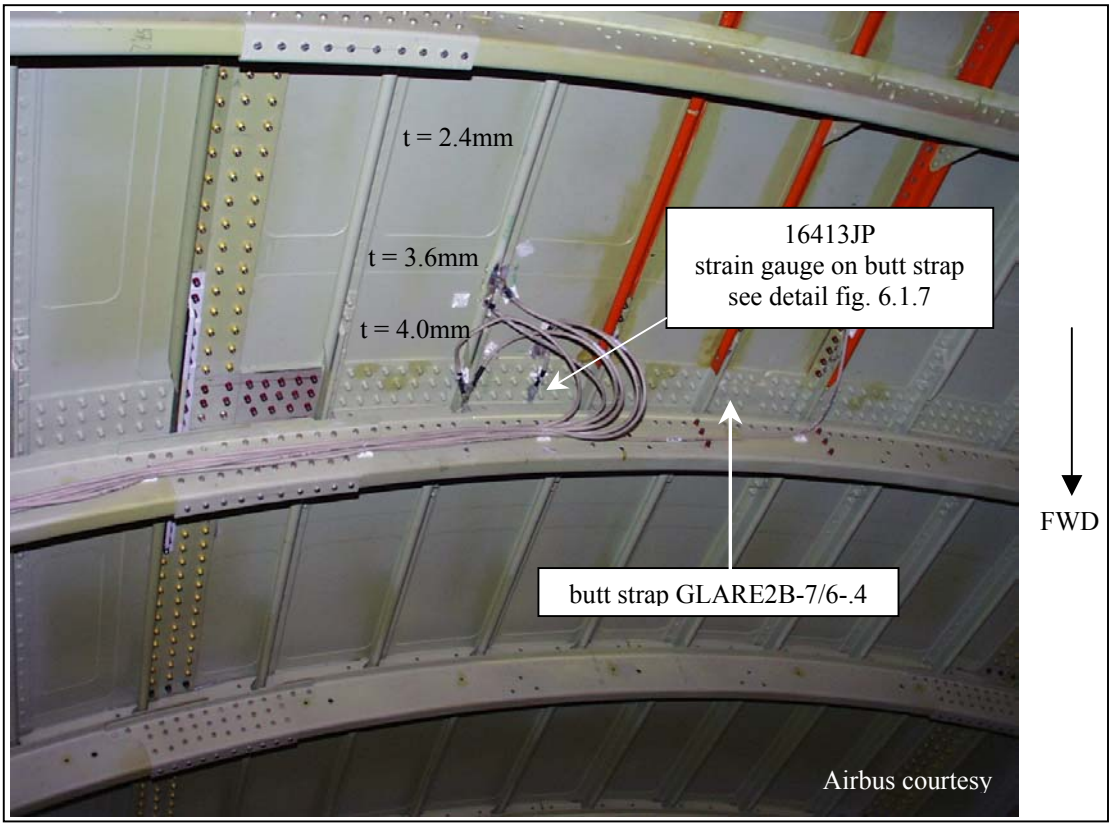

Figure 3.1.6. View on the circumferential joint with the GLARE butt strap from fuselage inside

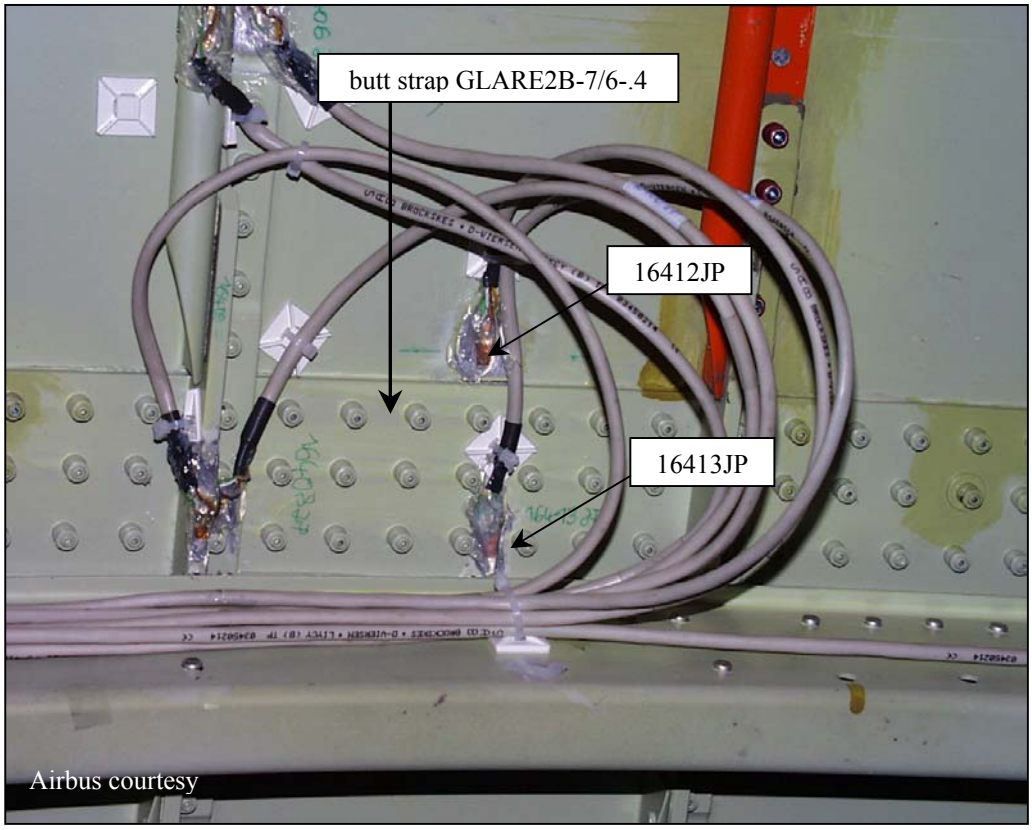

Figure 3.1.7. Detailed inside view on butt strap, strain gauge 1611JL attached opposite to 16411JL

The circumferential single strap joint connected two 2524T3 stiffened panels with three rivet rows at each side of the joint, see figure 3.1.5. The strap was made of GLARE2B-7/6-.4.

The drilled holes in the joint of the full scale specimen are automatically drilled with 5000 revolutions per minute speed and 800 mm/minute feeding rate (4,78mm, h8 tolerance). The bore hole diameters have been measured before fastener installation. A tendency towards larger hole diameters in the aluminium skin compared with the hole diameters in the GLARE2 butt strap is observed:
Measured hole diameters in aluminium skin: 4.770mm – 4.800mm.
Measured hole diameters in GLARE strap: 4.759mm – 4.790mm.

The nominal diameter of the installed DAN6-6 fastener (Hi-Lok with shear type countersunk head) is 4,801mm to 4,813mm. This results in:
Maximum interference fit in GLARE2: 4.749mm – 4.813mm = -0.054mm.
Minimum interference fit in GLARE2: 4.790mm – 4.801mm = -0.011mm.
It implies that all fasteners have been installed with a low to medium interference.

In the full scale fatigue test 50000 flights are simulated to which the experimental butt strap is also subjected. Eight different flight types have been defined by Airbus for each mission type, i.e. short range, medium range and long range mission. They are applied in blocks of 1660 flights, in a specified flight type sequence.
The condition of the butt strap is inspected repeatedly by rotating probe eddy current inspection after removal of the fasteners. A tear down inspection is planned by Airbus after finishing the fatigue test.

As shown by pictures in figures 3.1.4 to 3.1.7, strain gauges were bonded on several locations of both the butt strap and the attached skin. The purpose was to explore the local stresses in the but strap in order to simulate them with the later discussed coupon specimens (chapter 7).

3.1.2 Megaliner Barrel riveted repair

A repair situation was simulated in a GLARE4A skin panel of the Airbus Megaliner Barrel specimen. A hole was cut out with the longitudinal length of 252mm and a circumferential height of 196mm. The removed piece of the skin was supposed to be damaged for which a repair was necessary. The bonded stringer was assumed to be undamaged because stringer repair was not the aim of the investigation. Under the stringer foot, a strip of the fuselage skin remained in place as a filler, but it was cut at the edges of the hole to avoid load transfer from the skin, see figure 3.1.8.

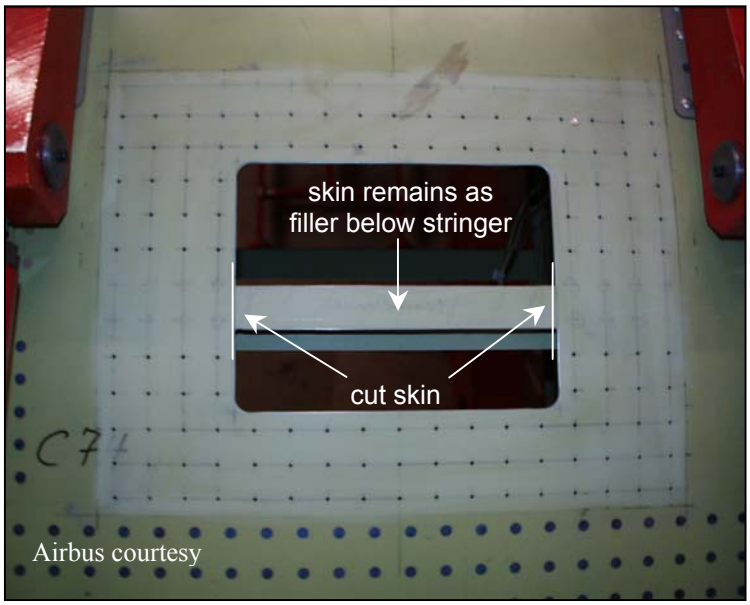

Figure 3.1.8. Cut out in GLARE4A skin of Megaliner Barrel between frames 73 and 74 at stringer 4 right hand side

A GLARE4A-5/4-.4 repair patch (single side clad) is jointed to the Barrel skin of similar material type. The repair patch is shown in figure 3.1.9. The fastener pitch is not constant due to geometrical restrictions, i,e, the position of lap joint P5 and the position of stringer P4.
Fasteners used: ASNA2026, 5.6mm Hi-Lites, installed with clearance fit. Rivet pitches and rivet row pitches: 28mm. Edge distances: 14mm.

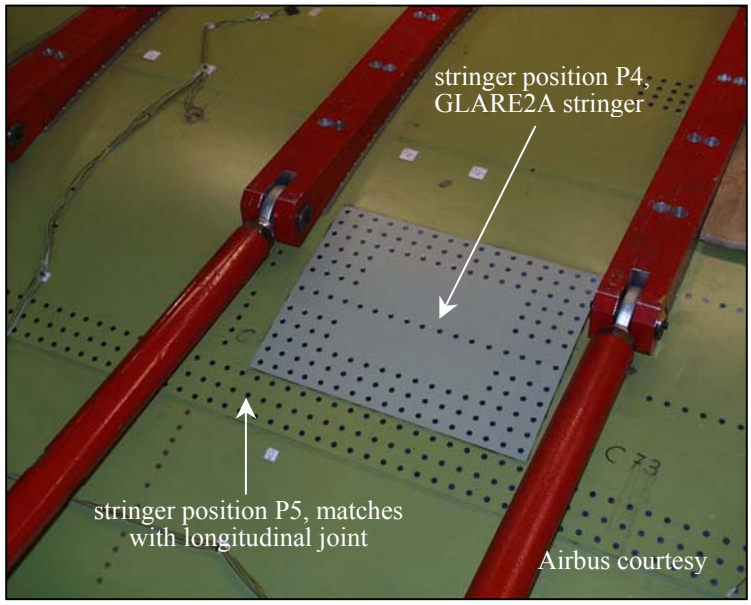

Figure 3.1.9. The GLARE4A repair patch on the Barrel

The Megaliner Barrel was fatigue loaded with 40 different flight types applied in a flight-by-flight sequence developed by Airbus. The test goal for the Barrel is 50000 flights. Between 20000 flights and 40000 flights the patch is removed for scheduled inspections and the drilled holes in both skin and patch is inspected for cracks.

3.2 Outdoor Exposure Specimen Types

3.2.1 Moisture Reference Specimens

So-called Moisture Reference Specimens (MRS) have been designed for weight gain measurements in the prepreg of GLARE drilled holes. The weight gain gives information about moisture absorption and the absorption should be studied to explore environmental effects on the properties of structural joints. The MRS dimensions are shown in picture 3.2.1.1 and a figure 3.2.1.2.
The 20 layers of S-glass/FM94 prepregs are layed up cross wise between two sheets of 0.2mm aluminium 5754-H18 (corrosion resistant). The prepregs are cut 20mm shorter in both directions (dotted line in figure 3.2.1.2) in order to manufacture a metal/metal bond at the specimen edges. Moisture absorption is not possible along those edges and is therefore concentrated at the location of the drilled holes. Because of the 20 prepreg layers, total thickness 2.5mm, a high prepreg volume is available for absorption which is still sandwiched between two metal layers as a barrier at the outer surface. Three different specimen types are produced:

- specimens without holes
- specimens with 4.8mm drilled holes
- specimens with 4.8mm holes and aluminium Lock-Bolts installed (for weight reasons)

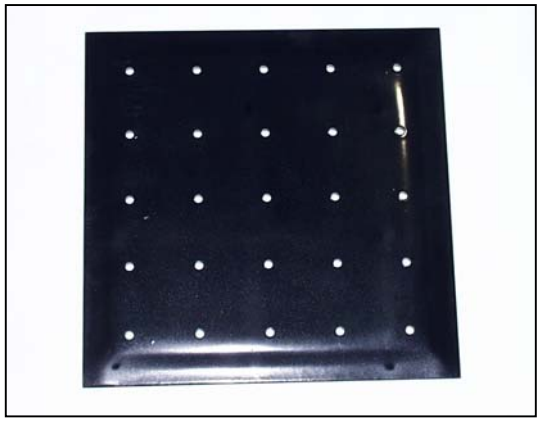

Figure 3.2.1.1. Open hole MRS specimen 8-3-PH

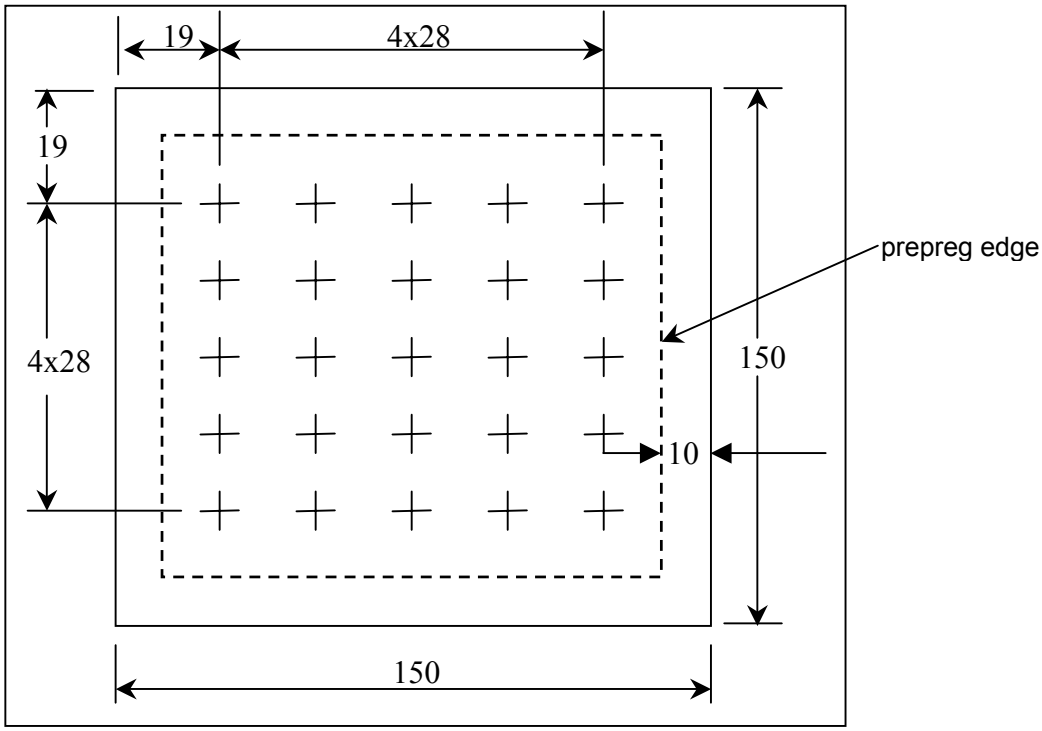

Figure 3.2.1.2. Dimensions of the moisture reference specimens

In case of painted specimens, drilling has been performed *after* painting (worst case scenario, with one exception, see figure 3.2.1.3). The aluminium Lock-Bolts have been selected in order to use light fasteners but to be able to install them with clearance fit.

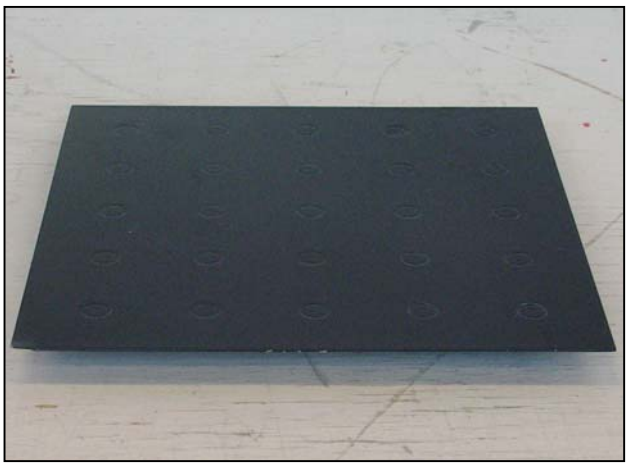

Figure 3.2.1.3. Specimen 8-9-FP, coincidently painted <u>after</u> the Lock Bolt installation

Figure 3.2.1.4. Specimens 8-5-PF and 8-7 at the outdoor exposure site

The designations and design details are contained in table 3.2.1.

3.2.2 τ-γ-Specimens

τ-γ-specimens made of GLARE2-2/1-8.0 specimens are designed with a shear overlap and width, which copies the fastener pitch and rivet row distance of the A340-600-EF2 butt strap. All edges are covered with paint. A 4.8mm hole is drilled in the specimen center, which is the only access for moisture to penetrate into the prepreg. The specimen is designed in order to investigate, whether the delamination resistance at the edge of the shear overlap is effected by specified ageing processes or not. The specimen designations are contained in table 3.2.2.

Manufacturing steps:

1) Pre-treatment of aluminium sheets and bonding to GLARE2-2/1-8.0 according to the GLARE production specification. The 8mm thick aluminium sheets are made of 2024 aluminium.

2) Drilling holes (top view on specimen:)

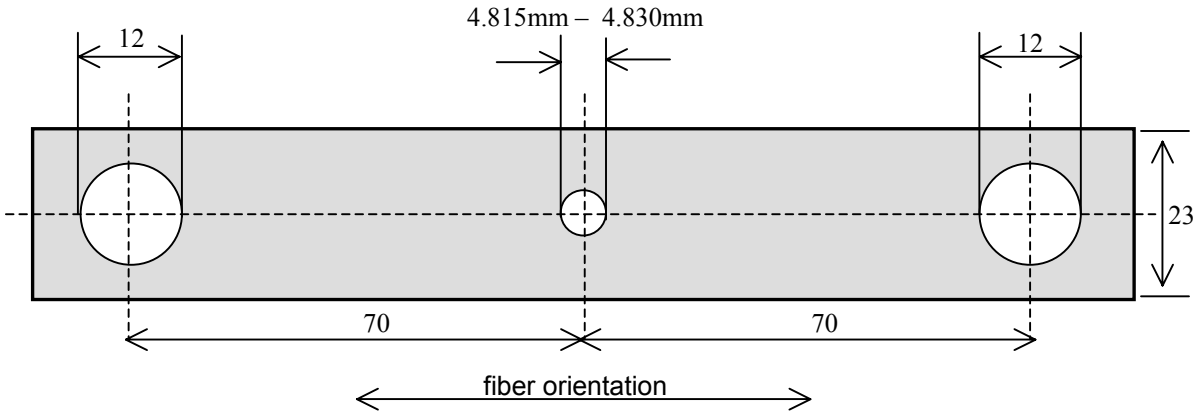

3) Milling slots, cut prepreg:

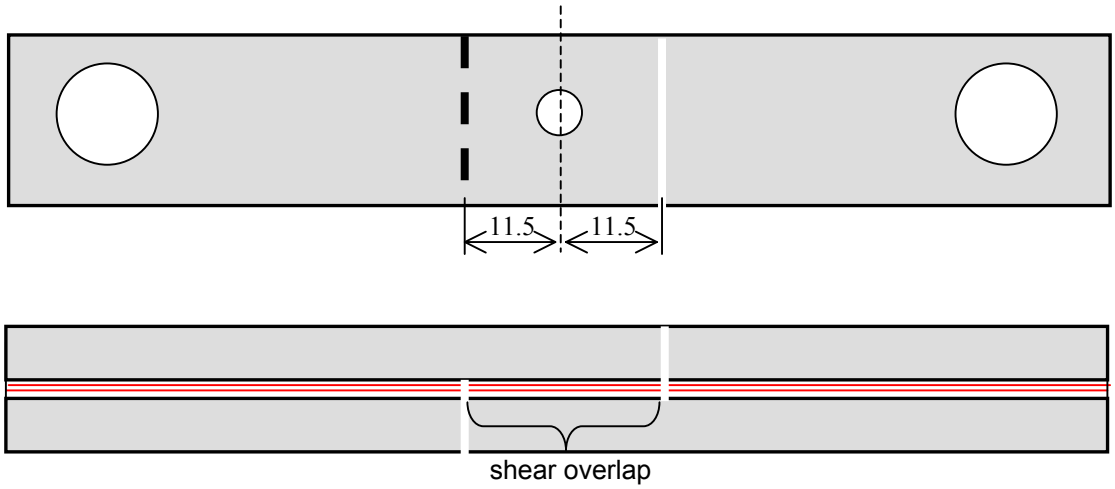

4) 4.8mm holes taped and complete surface protection system applied on specimens 14-B-7 to 14-B-24 (for exposure):

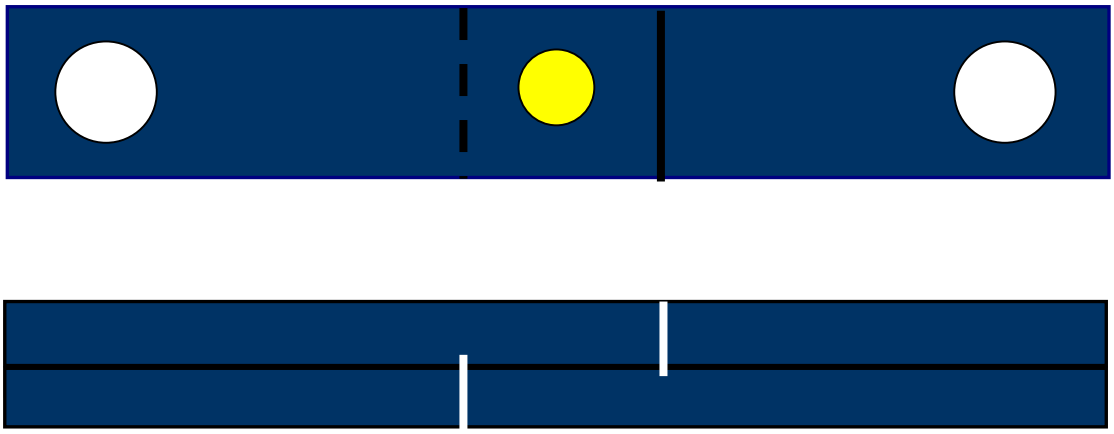

5) Tapes removed and DAN7-6 fastener installed in specimens 14-B-7 to 14-B-24, *during exposure only*, collars hand tightened. Fasteners removed before tensile test.

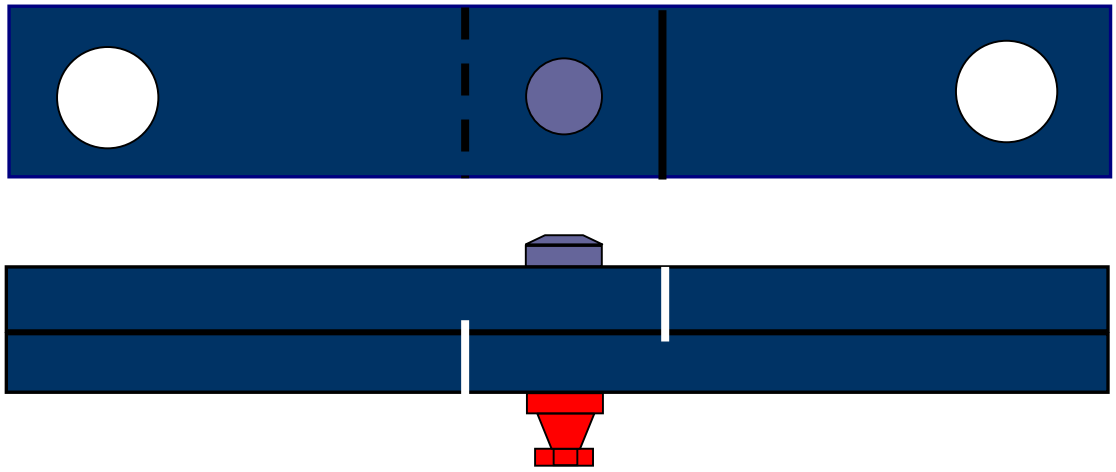

3.2.3 Riveted Joint Specimens

3.2.3.1 Circumferential joint

The material type and the dimensions of the butt strap specimen copy exactly the design of the strap in the Airbus A340-600 full scale fatigue specimen, see section 3.1.1. Experience with mixed material specimens, i.e. skin sheets made of aluminium connected to GLARE2 butt straps indicate that the *aluminium skin parts* fails under fatigue loading [11, 12, 13]. Therefore the 3.8mm aluminium skin parts which are present in the full scale specimen (section 3.1.1) are replaced by GLARE2 B-7/6-.4 in the coupon specimen. Because the skin parts serve as load introduction to the strap but not as test item, the DAN6 countersunk fasteners used for the full scale specimen were replaced by DAN7-6-6 protruded head Hi-Loks in the coupons. Collar: ASNA5075-6. The drilling parameters and hole diameters are similar in both specimens, ref. chapter 3.1.1. Fasteners are installed dry, the sheets are jointed with sealant. The tasks performed by the particular specimens are contained in table 3.2.3.1.

The circumferential joint coupon specimens are designed and manufactured to investigate crack initiation scatter and crack propagation scatter, to evaluate a crack initiation Wöhler curve and to analyse the variable amplitude behaviour of a GLARE joint compared with monolithic aluminium, to investigate the influence of variable temperature and of outdoor exposure on the crack propagation life of a GLARE joint, to investigate the residual strength related failure mode depending on the ageing condition. All investigations dealing with this specimen are collected in chapter 7.

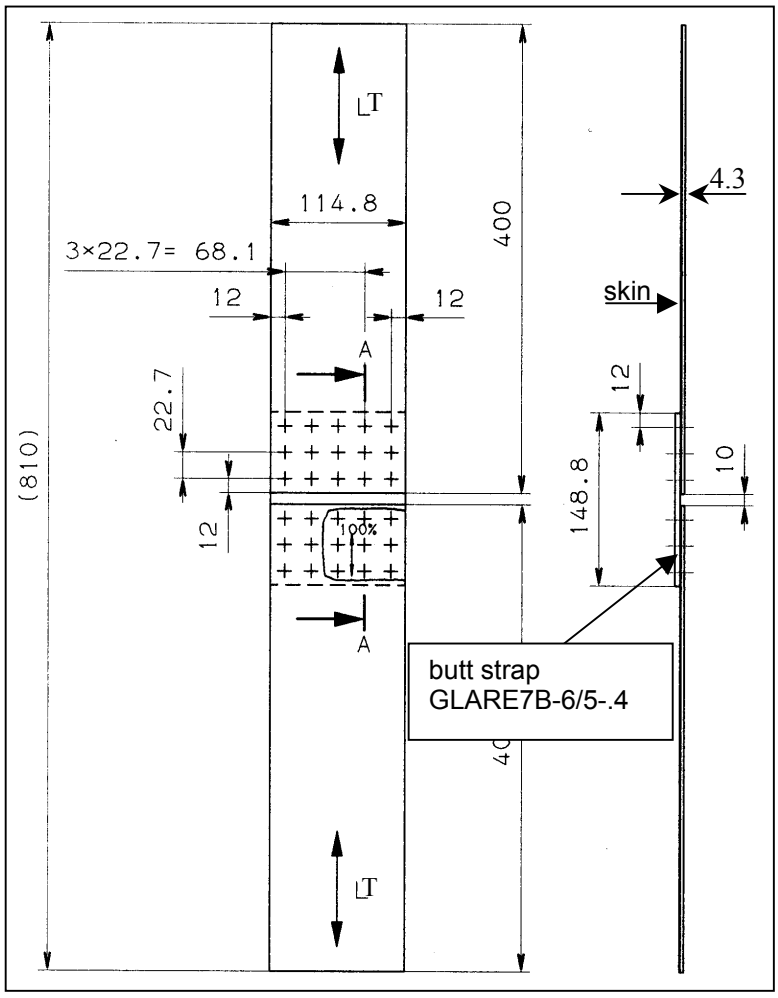

Figure 3.2.3.1. Circumferential joint coupon specimen

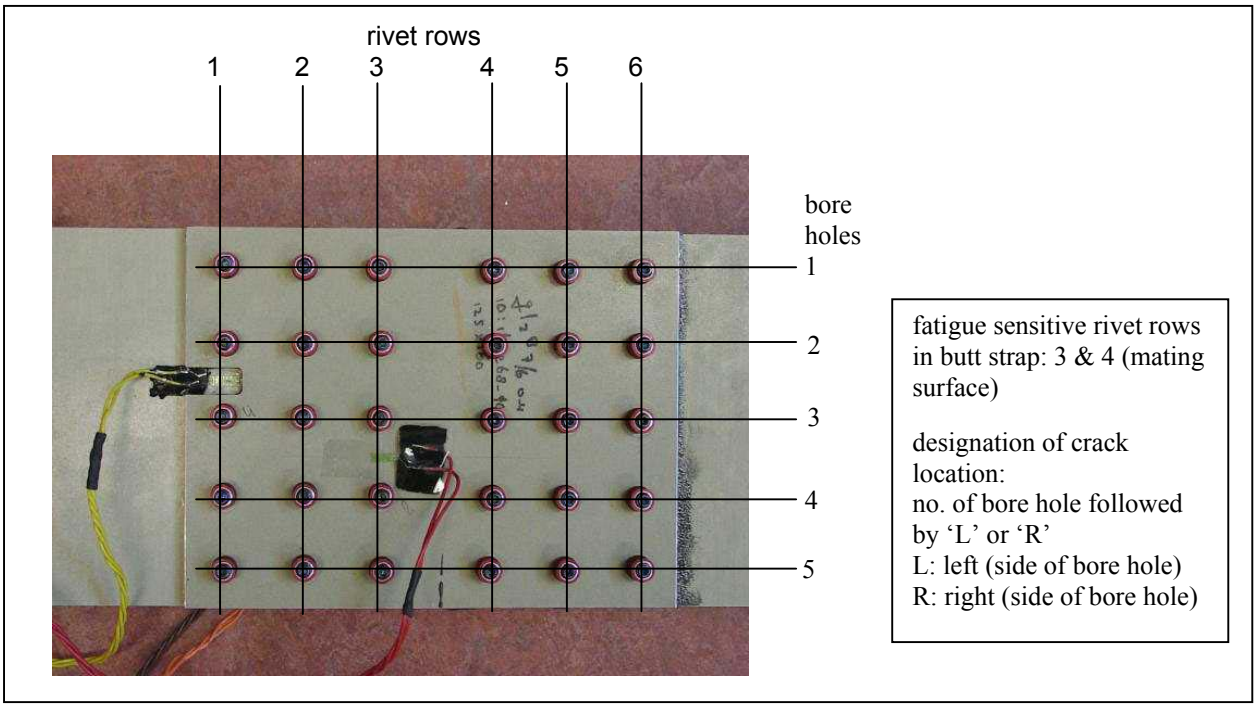

Figure 3.2.3.2. Specimen2-B-102 , rear side, view on the GLARE2B-7/6-.4 butt strap

Due to the single shear geometry bending occurs in all three parts. The highest secondary bending happens in rivet rows 3 and 4 in the butt strap. If not explicitly mentioned, crack initiation and crack propagation data belong to the mating aluminium layer of the butt strap in rivet rows 3 and 4.

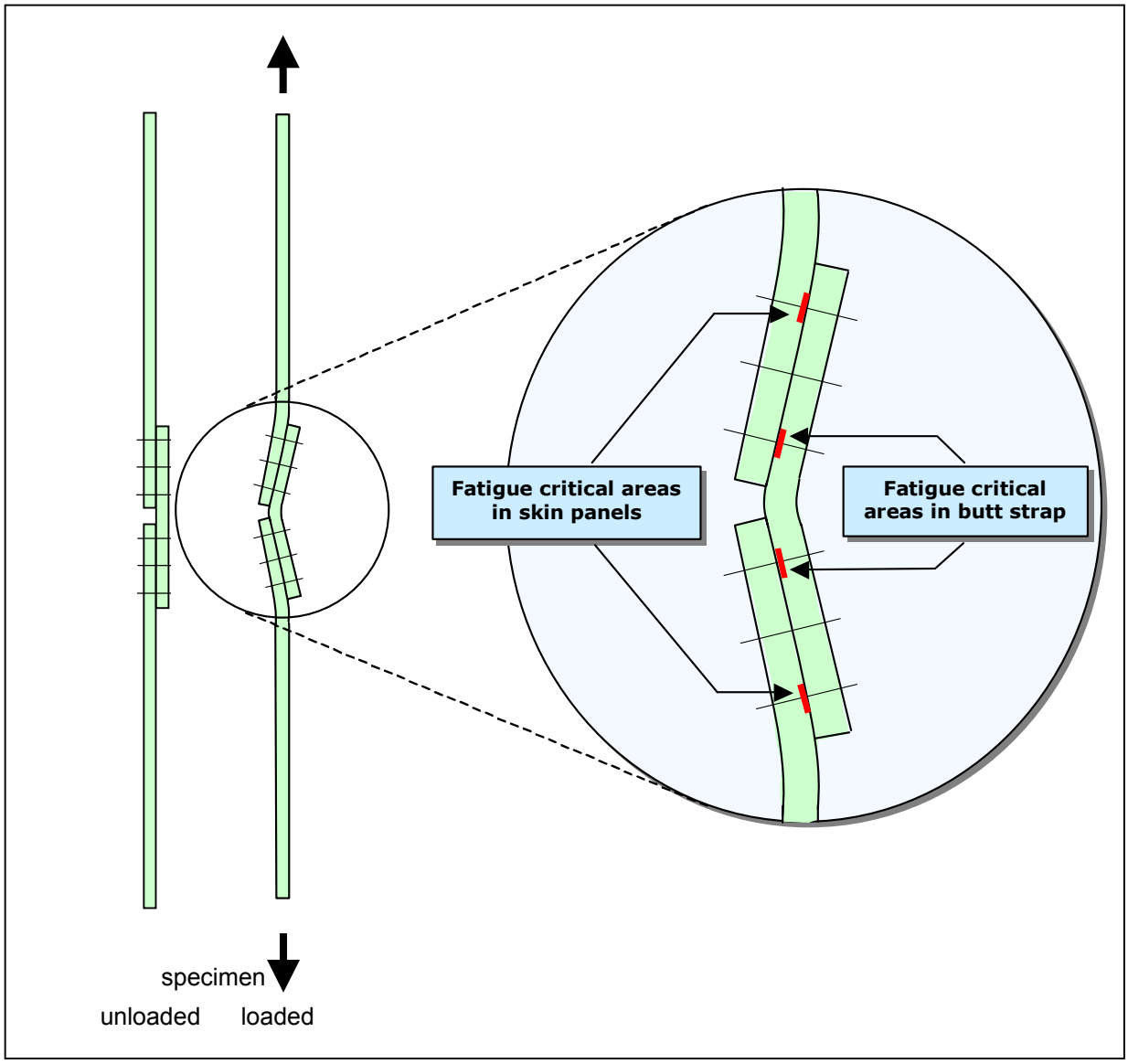

Figure 3.2.3.3. Fatigue critical locations in the circumferential joint, series 2-B-x

3.2.3.2 Repair, lap joint coupon

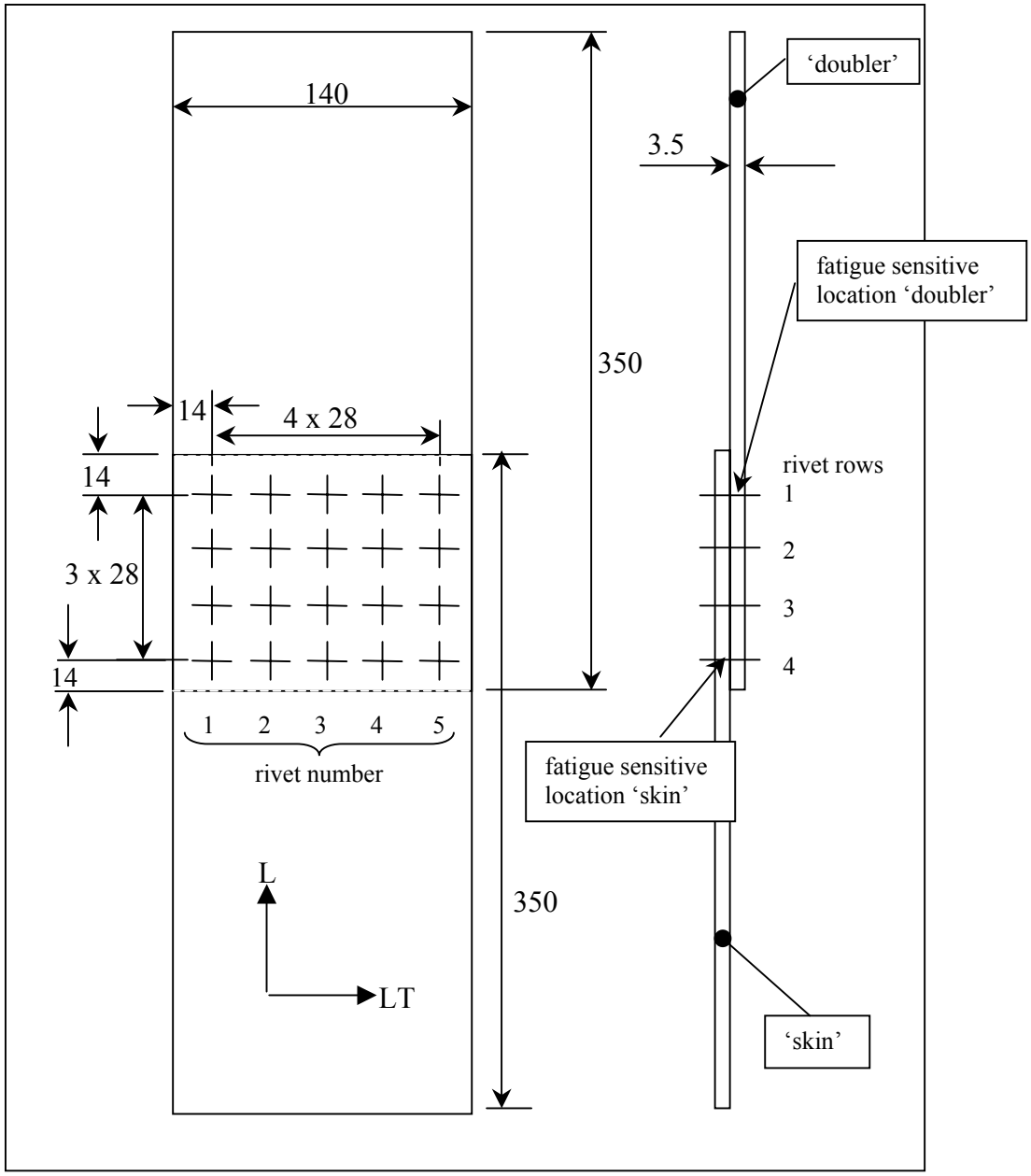

Figure 3.2.3.4. Drawing of the repair coupon specimen

The repair coupon simulates exactly the repair on the Megaliner Barrel (ref. section 3.1.2).
Skin and patch material: GLARE4A-5/4-.4, singe side clad, jointed with sealant.
Fasteners & collars: : ASNA2026 & ASNA2528-3A, installed dry. For cost reasons some specimens are fatigued with HL413VF-6-5 / HL93-6 fastener/collar. If so, it is particularly indicated.

designation of crack location:
no. of bore hole followed by 'L' or 'R'
L: left (side of bore hole)
R: right (side of bore hole)

The tasks performed with the particular specimens are contained in table 3.2.3.2.

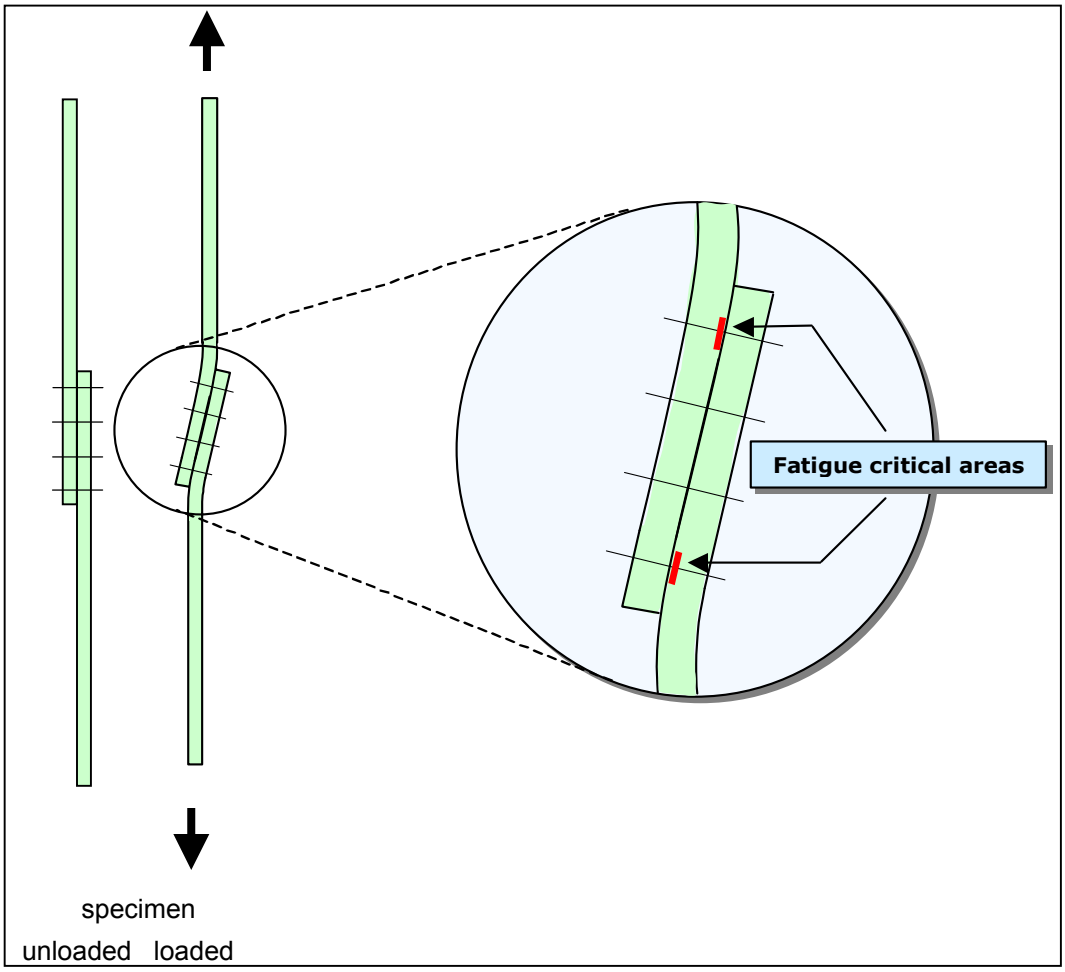

Figure 3.2.3.5. Fatigue critical locations in the longitudinal (repair) joint, series 2-A-x

If not explicitly mentioned, crack initiation and crack propagation data belong to the mating aluminium layer of the 'doubler' in rivet row 1 and of the 'skin' in rivet row 4.

3.2.4 (Tension) Filled Hole Specimens

If in a riveted GLARE structure sufficient rivet strength is provided and the fastener tilting is limited, then the blunt notch strength of the holes becomes the dominating failure criterion. These conditions apply to riveted skin/ stringer attachments or load transferring riveted joints with a high ratio of fastener diameter to clamping length [6]. The blunt notch failure is fiber dependent [6,7]. Borgonje did the first systematic blunt notch tests with GLARE3-3/2-.3 open hole specimens after different periods of exposure in a 70°C / 85%RH environment and at different test temperatures [8]. He observed a constant strength reduction of 15% at any test tempearature after 3000 hours exposure (figure 3.2.4.1). However, the strength of similar exposed specimens is not dependant on the test temperatue, see figure 3.2.4.1.

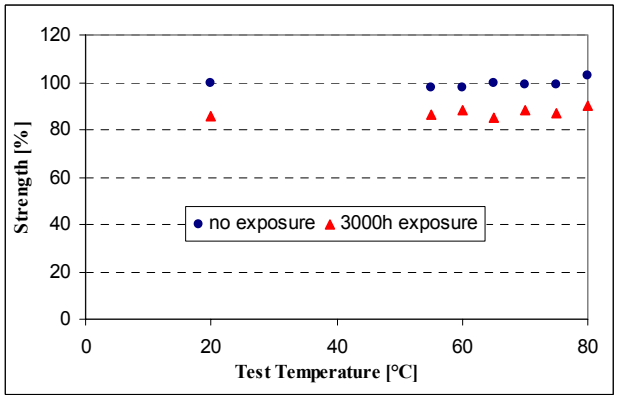

Figure 3.2.4.1. GLARE3 blunt notch strength depending on accelerated ageing [8]

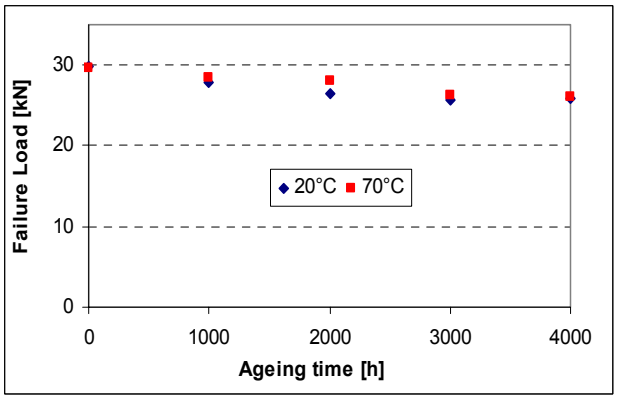

Figure 3.2.4.2. GLARE3 blunt notch strength depending on test temperature [8]

From previous research a strong dependency of the specimen width on the blunt notch strength after accelerated exposure was observed [9]. The strength of small specimens decreases more than 15%, if exposed 3000 hours in the Airbus standard environment. However, similar strength was found for blunt notch specimens of different width in the non-exposed condition. This holds for blunt notch specimens with a width ≥50mm. In the absence of other feasible explanations it must be concluded, that an edge effect due to exposure has to be considered. Neither painted edges nor applied sealant can completely prevent moisture absorption at the specimen edges. Since the environmental influence becomes smaller with an increasing size and the complexity of the structure, it is recommended either to simulate blunt notch strength with wide specimens with at least 5 holes in a row (see A310 MSN 484 GLARE demonstrator qualification tests [10]), to use single hole specimens with a width of 50mm [8], or to expose a relatively large GLARE sheet with drilled holes and to cut out the specimens after ageing. A quick milling operation is demanded in the latter case in order to avoid dry out effects in the drilled holes. As a contribution to the design of flying structures it is recommended to install protruded head bolts with clearance fit in the holes during exposure. The protruded head fastener is selected in order to avoid a dependency of any counter sunk fastener head geometry, which would increase the complexity of the investigation.

Specimens with 5 bore holes in a row are used for the investigations of accelerated and natural ageing on crack initiation, crack propagation, scatter and residual strength in this thesis. The hole diameter and the hole pitch are the same as in the butt strap in the A340-600 full scale specimen and the Megaliner Barrel repair, respectively. The holes are drilled after painting in order to keep the drilled hole clean. Fasteners are installed during ageing periods and for static strength tests. Details of the specimen designs are presented in the drawing shown in figure 3.2.4.3.

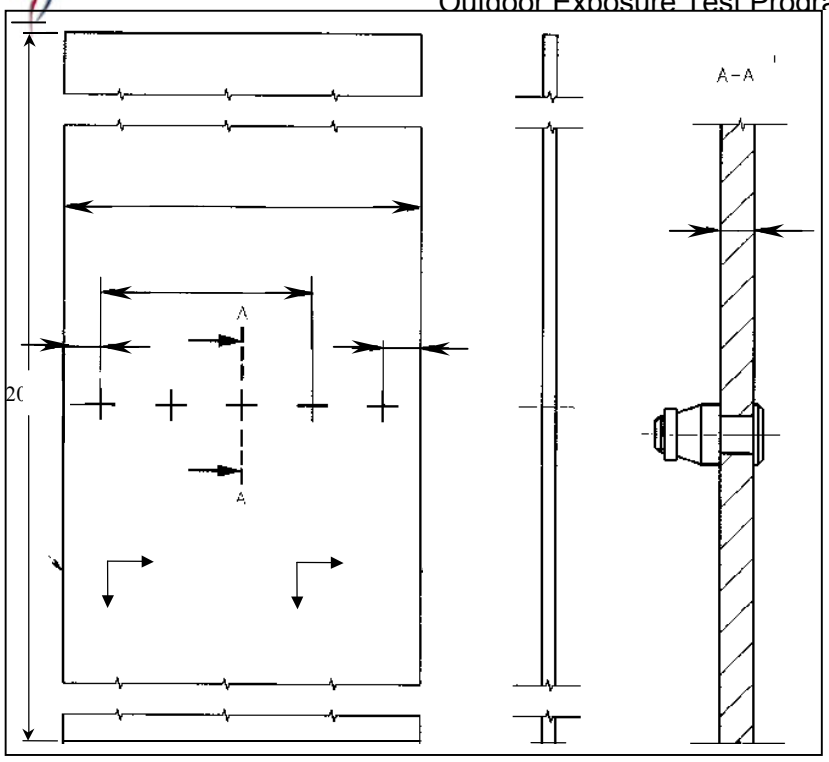

	GLARE2B	GLARE4A
designat.	3-B-x	3-A-x
t [mm]	4.3	3.5
t1 [mm]	22.7	28.0
w [mm]	113.5	140.0
fastener type	DAN7-6-3 / NSA5075-6	ASNA2026-3A-3 / 2528-3A

Figure 3.2.4.3. Filled hole specimen geometry

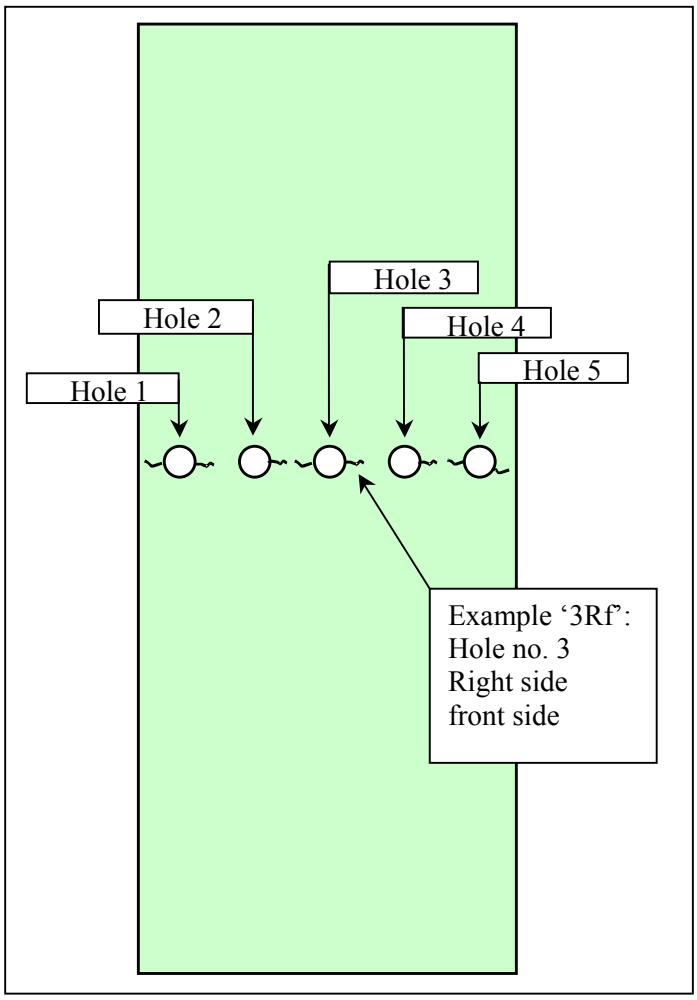

Figure 3.2.4.4.
Crack nomenclature definition:
R: right side of hole
L: left side of hole
r: rear side of specimen
f: front side of specimen

The crack nomenclature is defined in figure 3.2.4.4. The first filled hole specimen failed in the suspension during residual strength test. The problem could be solved just by decreasing the specimen width for blunt notch / residual strength testing, see figure 3.2.4.5.
The tasks performed by the particular specimens are contained in tables 3.2.4.1 and 3.2.4.2.

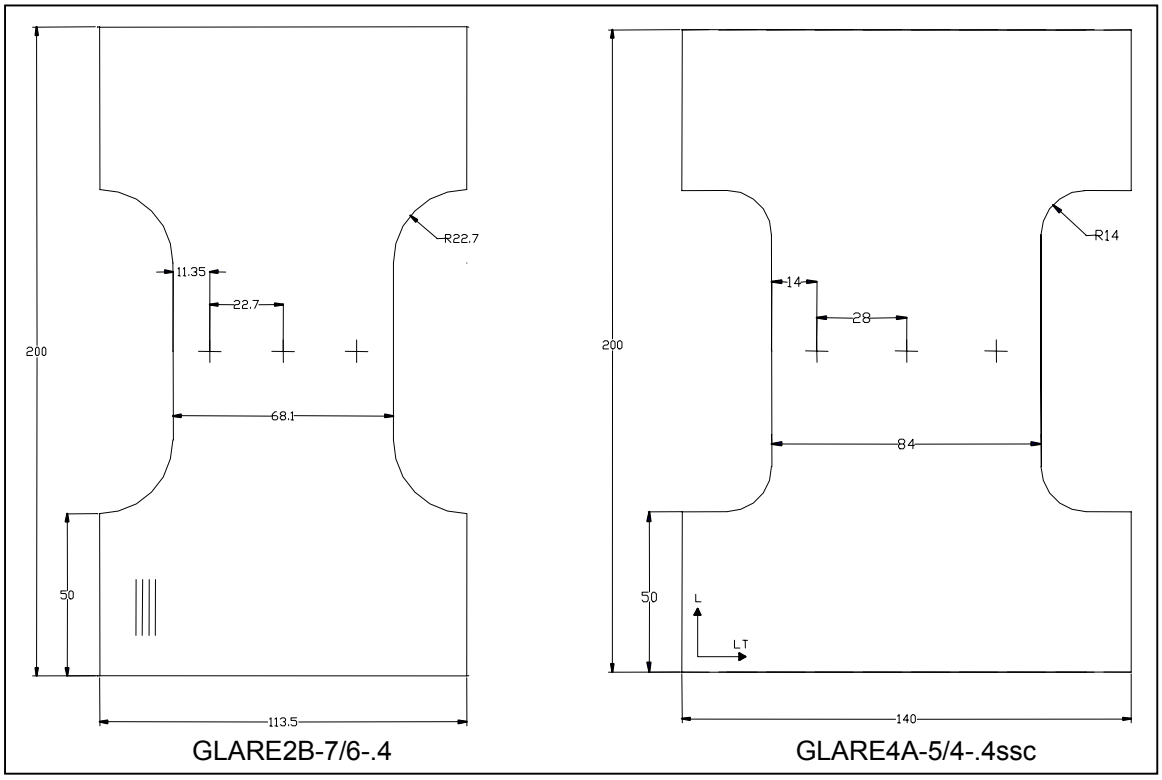

Figure 3.2.4.5. Filled hole specimen design prior to the blunt notch test / residual strength test

3.2.5 Bearing Specimens

The bearing tests are considered to provide material properties according to FAR 25.0603 rather than design allowables according to FAR 25.0613. As a design allowable they may qualify for the calculation of double shear joints because the detrimental effect of fastener tilting obtained in a single shear joint does not occur. Without fastener tilting, the bearing strength values can provide a first impression of the level of the available yield strength, but for a single shear design they would be un-conservative. For that reason the bearing strength yield properties should always be higher than the rivet strength yield properties obtained from tests according to MIL-STD-1312-4 [15] (for similar geometries). For the evaluation of data with a realistic bearing failure mode in laminates the use of a test set up according to specification ASTM-D953-87 with a clamping force applied on the specimen due to a bolt/nut torque of 0.15 Nm is demanded, see figure 3.2.5.1. Due to the clamping, an unrealistic bulging of the test material around the bolt in specimen thickness direction is prevented.

For completeness of the investigation, bearing strength tests are conducted with the A340-600 butt strap design and with the Megaliner Barrel repair design as well. Materials, specimen widths, edge distances and bore hole diameters are similar as in the full scale structures. The specimen design is presented in figure 3.2.5.1, the test matrix is given in table 3.2.5.

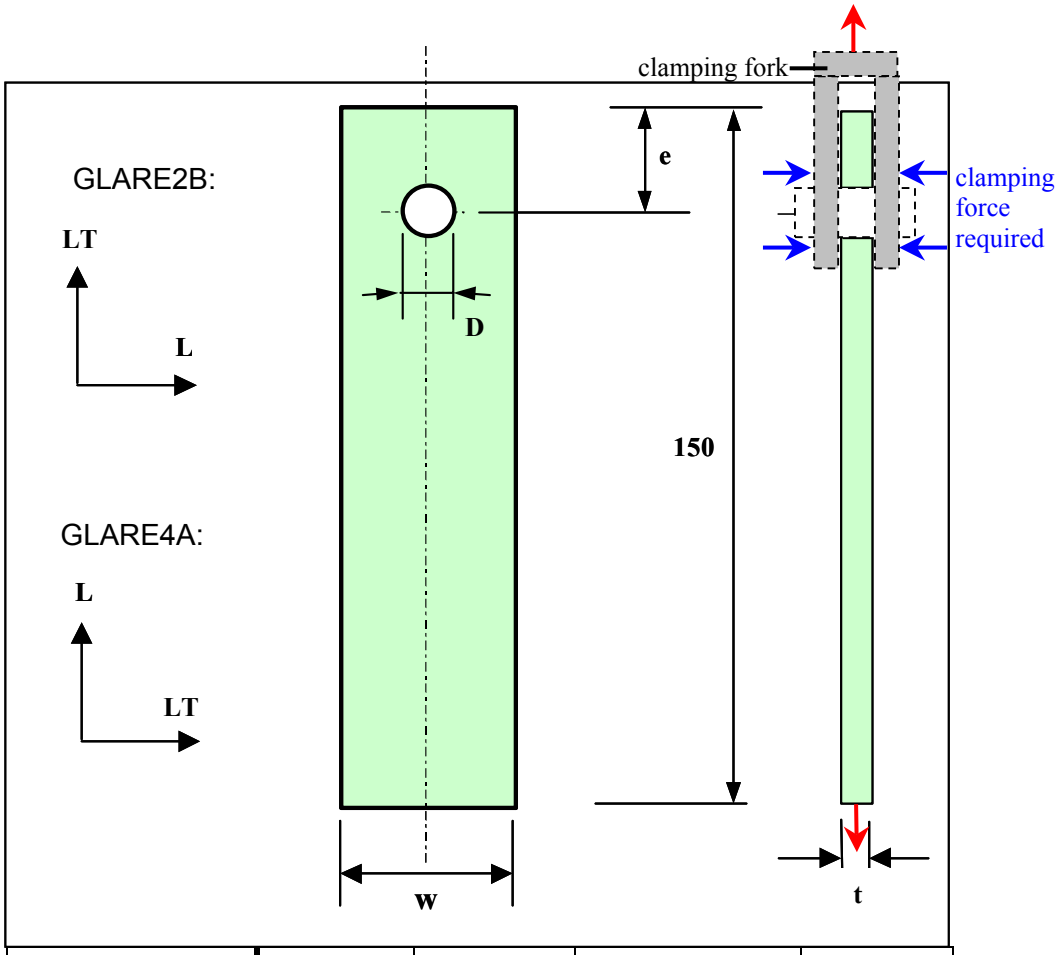

Material type	t [mm]	w [mm]	D [mm]	e [mm]
GLARE2B-7/6-.4	4.3	22.7	4.8	12.0
GLARE4A-5/4-.4	3.5	28.0	5.6	14.0

Figure 3.2.5.1. Geometry of the pin loaded hole(bearing) specimens

Specimen manufacturing: GLARE sheets have been saw cut to parts suitable for milling into the final shape. Batch numbers of the GLARE sheets used for specimen production are given in reference [23]. Before milling, small holes have been drilled at the location of the fasteners. The specimens used for outdoor exposure are then provided with a full paint system for protection, (ref. chapter 3.3).

After milling and painting the holes are drilled to their final size, after which the fasteners are installed in the to be exposed specimens for a simulation of an aircraft structure. For the GLARE2B specimens protruded head Hi-Loks with an interference fit are used, for the GLARE4A specimens countersunk Hi-Lites with a clearance fit. Hole diameters and fastener codes are given below, they copy the hole and fastener situation in the full scale specimens. The fasteners are removed before testing by unscrewing the collars and pushing the fastener out. For the test the (longer) bolt which belong to the clamping fork was pushed through the hole and the bolt was hand tightened.

Material type	designation	Hole ∅ [mm]	Fastener/collar type
GLARE2B-7/6-0.4	4-B-x	4.77 – 4.80	DAN 7-6-6 / NSA 5075-6
GLARE4A-5/4-0.4	4-A-x	5.54 – 5.57	ASNA 2026-3A-3 / 2528-3A

Because the strength of a pin loaded hole cannot properly be determined with a countersunk hole, the GLARE4A specimens have been drilled with cylindrical holes instead. During environmental exposure, a countersunk fastener is installed but with the head protruding from the hole (figure 3.2.5.2.c). To avoid damage to the hole edge by pressure from the countersunk head, the collar is not fully torqued. The “protruding countersunk head“ is expected to correspond better to the moisture absorption behavior around a fully installed countersunk fastener (figure 3.2.5.2.b), as opposed to a protruded head fastener (figure 3.2.5.2.a). The test is performed with this cylindrical hole.

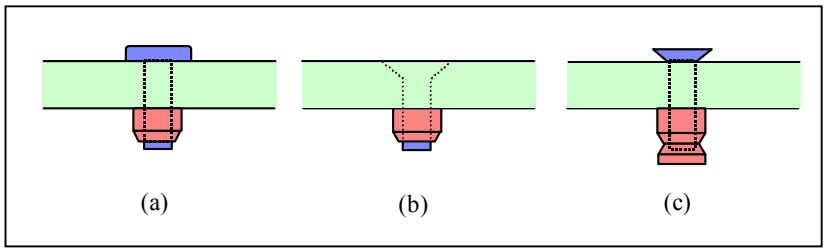

Figure 3.2.5.2. Fastener installation types

The accelerated exposure is performed in the climate chamber of the Structures and Materials Laboratory. Specimens are exposed to a 70º C, 85% RH environment for 3000 hours. One series of the GLARE2B specimens is exposed for 1500 hours.

Test procedure: By mistake, the tests with dry and accelerated aged specimens were performed according to the Fokker specification RP-00-00.030, i.e. with a 0.1mm gap between specimen and clamping tool at both sides. The specimens could deform in thickness direction with consequences explained before.
The tests were carried out on a 100 kN MTS testing machine. The test setup is shown in figure 3.2.5.3. A few exposed GLARE2B specimens were tested at 70ºC for which an oven is placed around the test setup. The temperature is monitored by a thermocouple. Testing is started 5 minutes after the desired temperature is indicated. Because the hydraulic grips cannot be used in the oven, these specimens were clamped with mechanical grips.

The bearing yield strength is determined by using the secondary modulus derived from the load-displacement diagram. This diagram is obtained by using the following test procedure:

1) The specimen is loaded to the (anticipated) yield load
2) The load is reduced to 10-20% of the yield load
3) The load is increase the load until failure

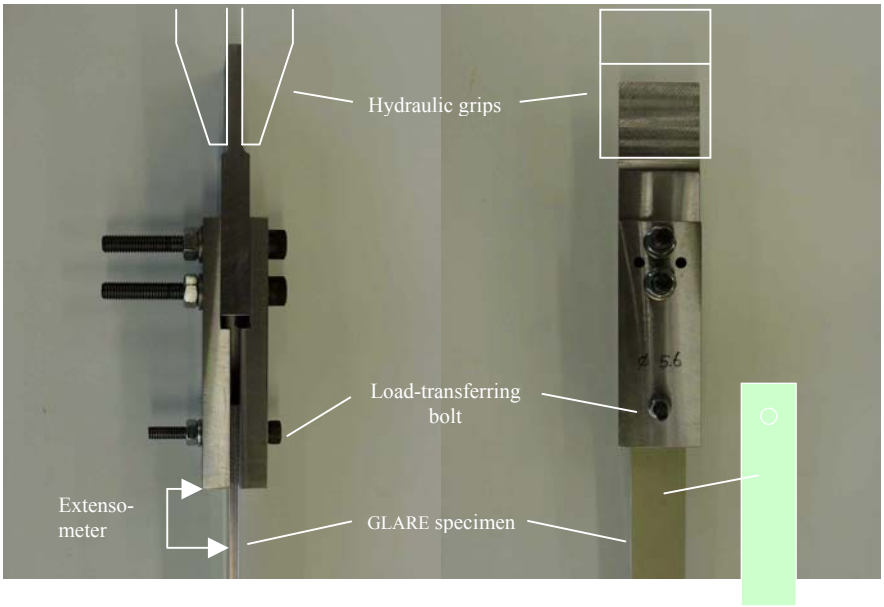

Figure 3.2.5.3. Bearing test setup

From the load-displacement diagram (see figure 3.2.5.4), the yield load is determined to be the load for 2% hole deformation. It is assumed that in this case, displacement is dominated by hole deformation:

1) Draw a line through the return part (left side) of the loop.
2) Offset this line at 0.02*D from the starting point of the curve, which if necessary, is corrected by extending the (almost) linear initial part of the curve.
3) The yield load is determined by the intersection of this line and the load-displacement curve.

The procedure is visualized in figure 3.2.5.5.

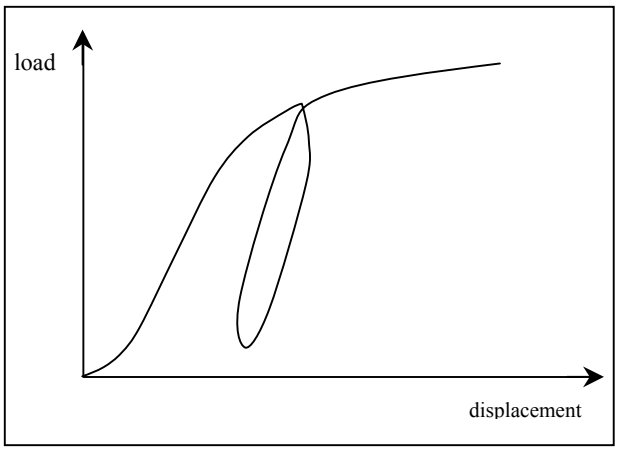

Figure 3.2.5.4. Load-displacement diagram for the determination of the secondary modulus

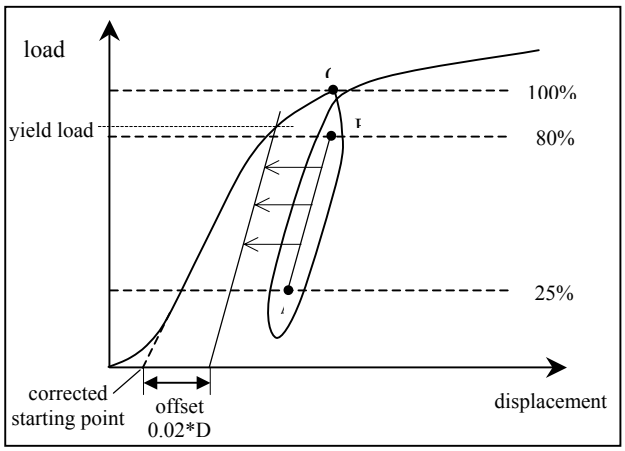

Figure 3.2.5.5. Secondary modulus method for the yield strength determination

3.2.6 Rivet Strength Tests

The rivet strength test according to MIL-STD-1312-4 [15] provides yield and ultimate strength data for a particular single shear combination of *a* sheet material and *a* fastener. The strength is usually recorded in the unit [load/fastener]. The single shear design is relevant for the strength predictions of the circumferential joint and the repair.

Due to the material characteristics of GLARE composed with 2024T3 metal, the yield values are considered as design allowables. According to the FAR/JAR 25.0305 regulation, 'no detrimental permanent deformation at limit load' is allowed which is the dominating design criterion. In case of a fatigue damaged bore hole in GLARE, the deformation of the structure at the time of the applied load may be larger than without fatigue damage. The crack opens and may exhibit a slight crack extension. After the load is released the fatigue crack closes again and no additional permanent deformation remains, compared to the condition of the structure before the load was applied. Therefore it was decided to investigate the rivet yield strength without fatigue cracks.

Specimen design:

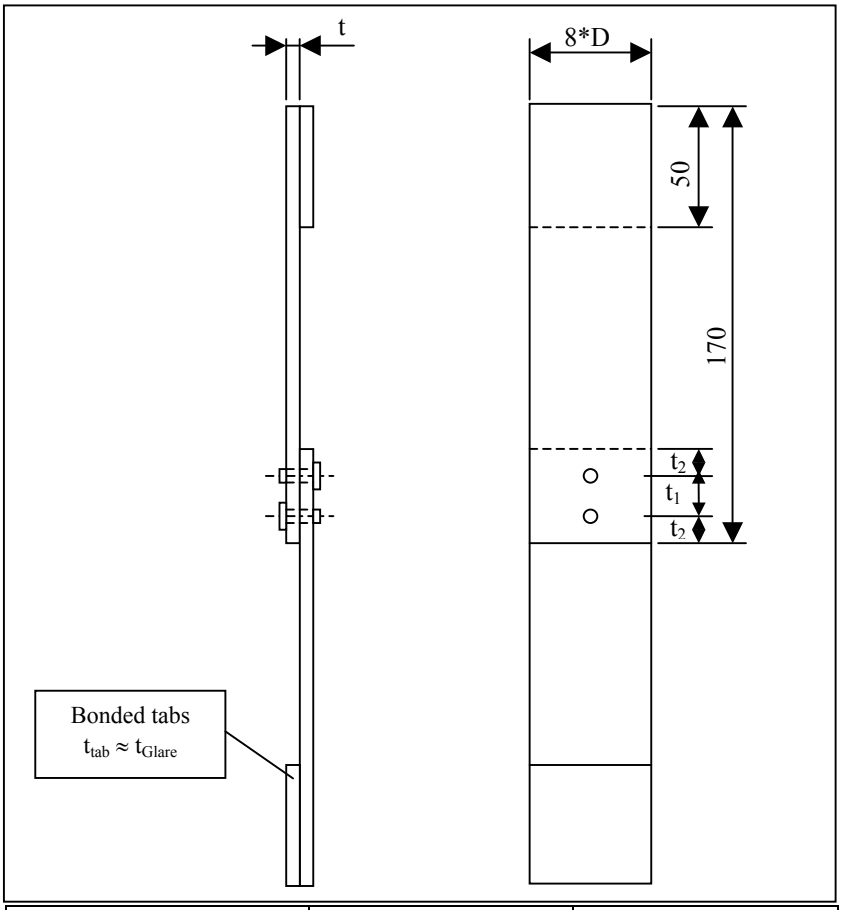

material type	t_1 [mm]	t_2[mm]
GLARE2B-7/6-0.4	22.7	12.0
GLARE4A-5/4-0.4	28.0	14.0

Figure 3.2.6.1. Rivet strength specimen geometry [15]

Hole diameters and fastener types:

material type	designation	hole ∅ [mm]	fastener/collar type
GLARE2B-7/6-0.4	5-B-x	4.77 – 4.80	DAN 7-6-6 / NSA 5075-6
GLARE4A-5/4-0.4	5-A-x	5.54 – 5.57	ASNA 2026-3A-3 / 2528-3A

Batch numbers of the GLARE sheets are given in reference [16].

Specimen manufacturing: GLARE sheets were saw cut to parts suitable for milling into final shape. Small holes were drilled at the location of the fasteners followed by application of a paint primer which fully covered the separate parts. The preliminary holes are then used to temporarily attach both parts of each specimen together, after which the specimens for the outdoor exposure were painted dark blue.

The installation of the fasteners was carried out by Delft University personnel at Airbus Bremen with an automated drilling and riveting machine. Between the mating surfaces of the panels a sealant (Naftoseal MC-630 C-2 Techkit 130) was applied. For the unexposed specimens it was originally planned to apply the sealant directly on top of the standard surface treatment of the aluminium. However, it was found that the sealant has much better bonding on the paint primer than on the standard surface. In order to have equal bond characteristics, a paint primer has also been applied onto the unexposed specimens.

Test procedure: The accelerated exposure was performed in the climate chamber of the Structures and Materials Laboratory in Delft. Specimens were exposed to a 70º C, 85% RH environment for 3000 hours. The rivet strength tests are performed on a 100 kN MTS test machine. The unexposed specimens were tested at room temperature, while the exposed specimens are also be tested at 70º C.
The method to determine the yield strength has been taken from reference [17]. It is determined using the secondary modulus, similar as described in the previous section. Exception: the off set is 0.04*D, since the specimen contains 2 fastener.

The test matrix which contains the particular rivet strength specimens and tests is given in table 3.2.6.

3.2.7 Compression Filled-Hole Tests

The compression filled-hole (CFH) test is related to pure composites. It considers the strength behaviour of the surface layers of a laminate, i.e. the metal layers in case of GLARE, close to a hole. Different from the composite layers embedded in the center of a laminate, the surface layers may escape in the out-of-plane direction by buckling during compression. Buckling of the surface layer, is restrained by the adhesive between the laminate layers and probably by the fastener as well. In principle the quality of the bonding is the main parameter to be investigated. An example of a locally buckled aluminium layer is shown in figure 3.2.7.1 at a skin/stringer riveting occurring in a shear/compression test article. However, the damage shown is a secondary failure, because it happened *after* skin and stringer buckling.

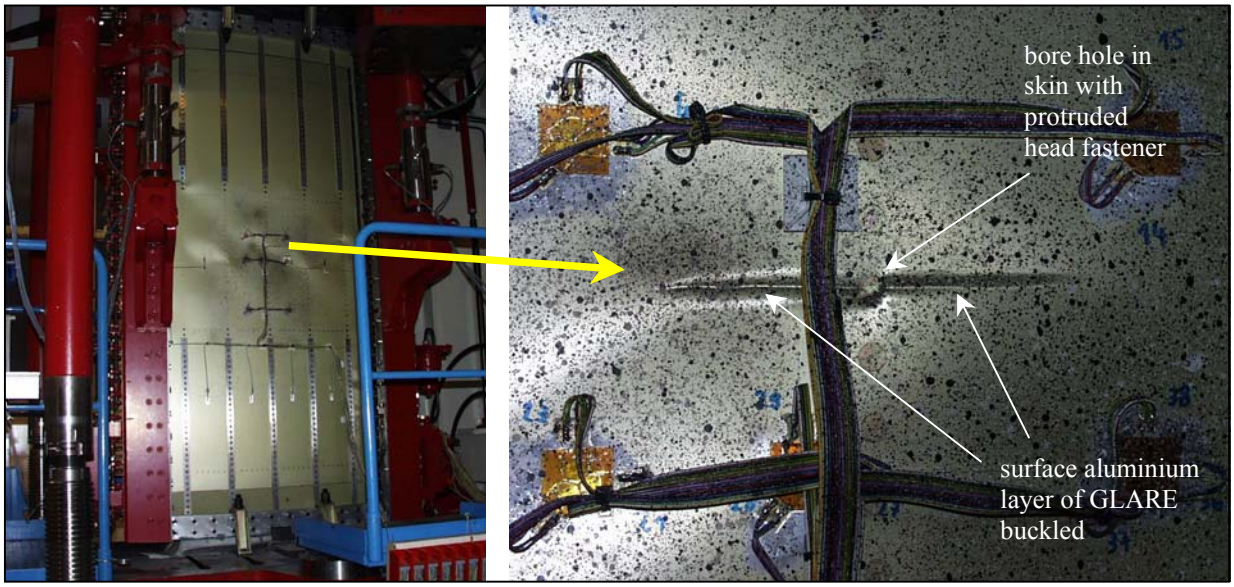

Figure 3.2.7.1. CFH (secondary) failure at Airbus / TU Delft compression/shear panel ('XT'-series)

A significant difference in CFH behaviour between both, pure composite and GLARE may be expected due to the different stiffnesses of the surface layers. The stiffness of a delaminated surface layer of a composite with a thickness in the range of 0.1mm to 0.15mm is significantly lower than the stiffness of a delaminated aluminium layer of GLARE ($t \geq 0.3$mm). Therefore a very limited influence of the CFH strength on the strength justification of a GLARE structure is expected.

Compression filled-hole tests with GLARE turned out to be very complicated. The first experience was obtained by van der Hoeven in 1999 with specimens made of GLARE3-3/2-.3 and NAS1097 fastener [10], tested without anti buckling guides. The entire GLARE laminate buckled between the clampings, always in the direction of the closing head of the countersunk fastener. Obviously, the 1.7mm thin GLARE buckled in the Euler mode before a CFH failure could happen. The shape of the countersunk fastener head causes a non-symmetric cross section stiffness of the specimen which controls the buckling direction. Later tests were conducted with different kinds of anti buckling guides, open holes , protruding head fastener or pins, e.g. a bold which is just filling the hole and not tightened [18, 19].

Still a final solution is not yet available for the present thesis, but the influence of both, fatigue cracks and environmental ageing, on the filled-hole behaviour under compression load should be investigated for the A340-600 butt strap and the Megaliner Barrel repair. Because fatigue cracks are surrounded by delamination zones, a CFH strength reduction compared with a non-fatigued hole can be expected.

For practical applications the inter rivet buckling load is reached before the compression yield strength of the concerned skin material [22]. Since inter rivet buckling means that the load tries to escape from one structural component and consequently another component will be heavily loaded, it is a common

design rule to prevent that the compression yield strength will be exceeded at ultimate load. The compression yield strength becomes a sizing limit for the CFH strength. As long as the compression filled-hole strength exceeds the compression yield strength, it will not be a design criterion for the structural component concerned. An overview about the relation between both strengths for selected GLARE materials is given in figure 3.2.7.2 [20].

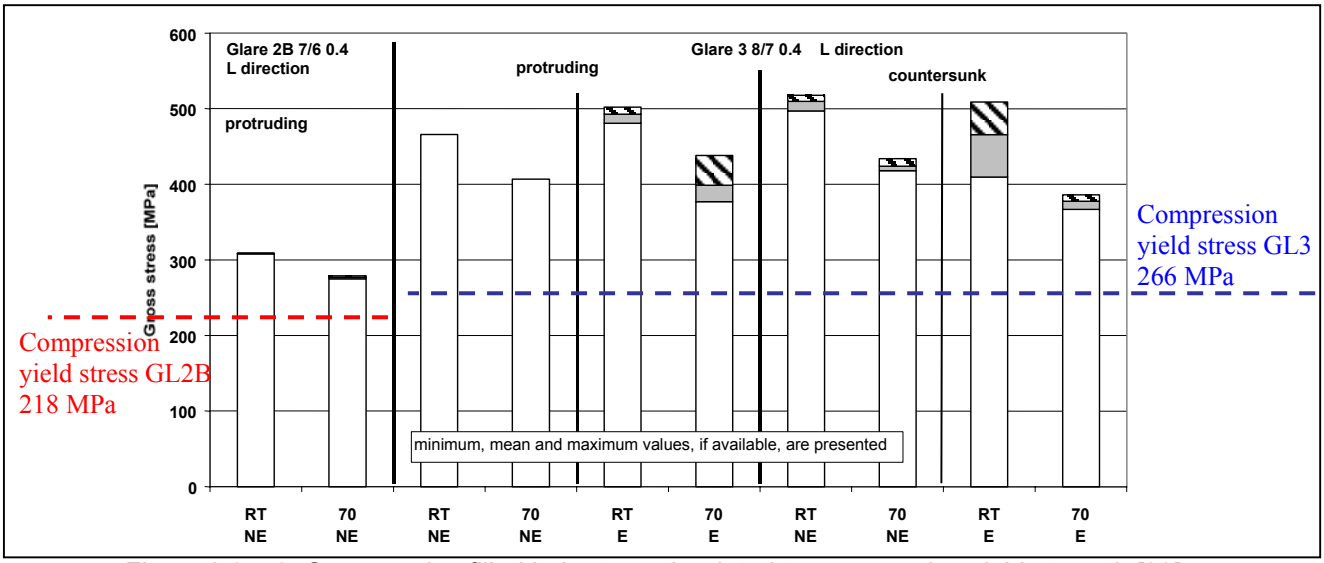

Figure 3.2.7.2. Compression filled hole strength related to compression yield strength [20]
Note1: E = `exposed´. Note 2: NE = `not exposed´. Note 3: GLARE2B is tested in L-direction.

For a commercial aircraft pressurized fuselage the compression filled-hole strength can be important for the upper shell in the front fuselage (compression during breaking which can occur at elevated temperature), the lower shell in the rear fuselage (vertical gusts and vertical maneuver) and in the vicinity of door cut outs. Both representative riveted joints which are investigated in this thesis belong to the rear fuselage upper shell, which is dominated by tensile stresses. As a rule of the thumb, the maximum static compressive stresses are 50% lower than the maximum static tensile stresses.
Due to the accumulation of local thicknesses at both structural items discussed in this thesis, i.e. the circumferential joint in the A340 full scale specimen and the repair of the Megaliner Barrel skin, it is unlikely that the compression filled-hole strength will be reached. However, in adjacent panels with a lower thickness panel buckling will occur which then will be the strength determining failure mode. The CFH strength with fatigue cracks is investigated here for completeness.
The specimen geometry for the outdoor exposure program is presented in figure 3.2.7.3. The used materials for these tests are similar as in the two full scale structures (ref. section 3.1). The specimen widths and the distances between the clampings are equal to the rivet pitch in the full scale structures. Protruded head fasteners are adopted for the GLARE2B tests, because there is no countersunk in the butt strap.

Specimen preparation: GLARE sheets have been saw cut to parts suitable for milling into final shape. During milling, small preliminary holes have been drilled at the location of the fasteners. This fixates the position of the final holes and provides easier specimen handling during painting. The specimens used for outdoor exposure are provided with the complete paint system to provide realistic protection against environmental influences, ref. chapter 3.3

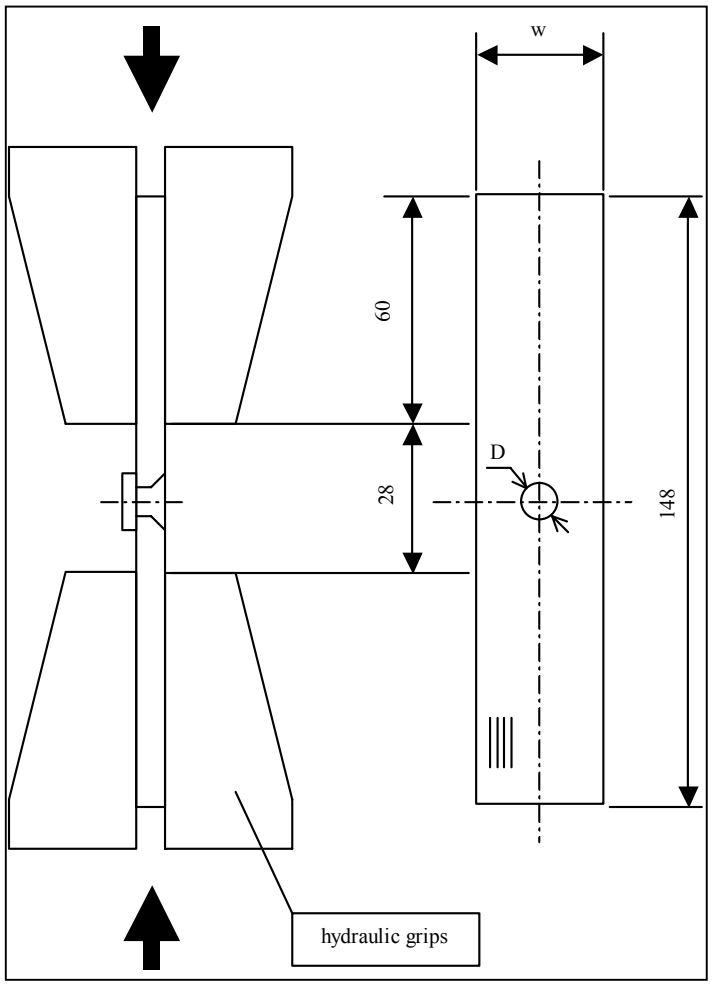

	GLARE2B	GLARE4A
designat.	6-B-x	6-A-x
D* [mm]	4.8	5.6
w [mm]	22.7	28.0
fastener type	DAN7-6-3 / NSA5075-6	ASNA2026-3A-3 / 2528-3A

* hole diameter

Batch numbers of the used GLARE sheets are given in reference [21].

The test matrix for the CFH specimens is given in table 3.2.7.

Figure 3.2.7.3. Geometry of the compression filled-hole specimens

Cracks of different lengths have been created by fatigue testing the specimens to different numbers of cycles. The cracks in the GLARE2B specimens were measured on both sides of the specimen. Due to the presence of a countersunk hole, the cracks in the GLARE4A specimens have been measured on the non-countersunk side, only.

After fatigue testing, the holes are drilled to their final size and the fasteners are installed. For the GLARE2B specimens protruded head Hi-Loks with an interference fit are used, for the GLARE4A specimens countersunk Hi-Lites with a clearance fit.

Anti-buckling guides are used along the sides of the specimen according to the method specified in [18]. Ref. [18] recommends to use steel bolts without a nut, with the head remaining free from the surface, in order to obtain local buckling rather than buckling in the area between the grips and the anti-buckling guide.
For this investigation it is decided to test the GLARE2B specimens with a DAN 7-6-6 fastener, but without the collar. By replacing the original Hi-Lok (DAN 7-6-3) by one with a longer shaft, the fastener head could remain some millimeters away from the specimen surface, while making sure that the threaded area remains outside the hole. The GLARE4A specimens contain countersunk fasteners. It would not make sense to test them without the collar, because the countersunk head would then be pushed out of the hole. They have therefore been tested with fully installed fasteners.
Specimens are tested both at room temperature and at 80º C. For the elevated temperature tests a chamber with infrared heat elements has been placed around the test setup. The temperature was monitored with a thermocouple attached to the specimen surface. The test was performed several

minutes after the surface obtained the required temperature. Due to the long time needed for heating (approximately 30 minutes), it is assumed that the specimen was then reached the specified temperature throughout its thickness.

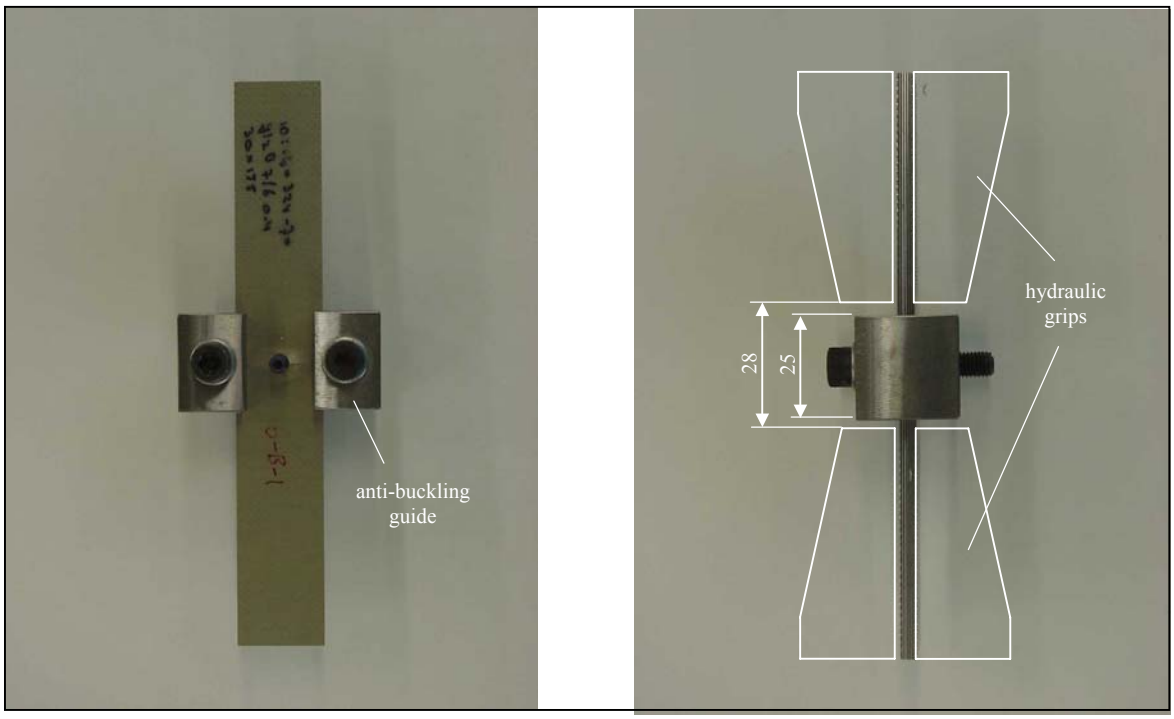

Figure 3.2.7.4. Compression filled-hole test setup

The CFH strength is determined by dividing the maximum obtained compression load by the nominal gross cross-sectional area of the specimen.

3.2.8 Rivet Pull Through Specimens

Rivet pull through failure has to be considered in case of a large through the thickness skin damage, which may extend its size due to operational loads and approaches a riveted location, e.g. a frame clip attachment. Then, high loads in radial fuselage direction can occur due to the presence of internal pressure and a bulging of the skin. This case need not to be considered for the A340-600 butt strap and for the Megaliner Barrel repair. However, previous ultimate tests with riveted single shear GLARE joints have shown severe fastener tilting, including a significant plastic deformation of the GLARE sheets. The more the fastener is tilting, the more load will be transferred by fastener tension from one GLARE sheet to the other one. Consequently, in the ultimate condition, rivet pull through may determine the joint strength. The rivet pull through tests in this thesis will deal with the influence of fatigue cracks on the rivet pull through strength.

The specimens have a standard dimension of 80 by 80 mm. They consist of two parts, one made of GLARE and the other made of 4 mm thick aluminium. They are attached to each other by one fastener in the center. For the GLARE2B-7/6-.4 specimens the fastener head is on the side of the aluminium sheet, while for the GLARE4A-5/4-.4ssclad specimens the fastener is on the side of the GLARE panel.

This is to cover both full scale design cases. In the butt joint, GLARE2B is used for the butt strap on the inside of the aircraft, thus the side with the collars. The lap joint is based on a GLARE repair panel, where the fastener head is located on the GLARE part; therefore for the RPT specimens the head is placed on the side of the GLARE panel.
Four holes are drilled around the center rivet hole at a 45° clockwise rotated position in the two sheets. Pushing pins passing through the holes, four pins from each side of the specimen, apply the load for a rivet pull through experiment. The specimen geometry is shown in figure 3.2.8.1.

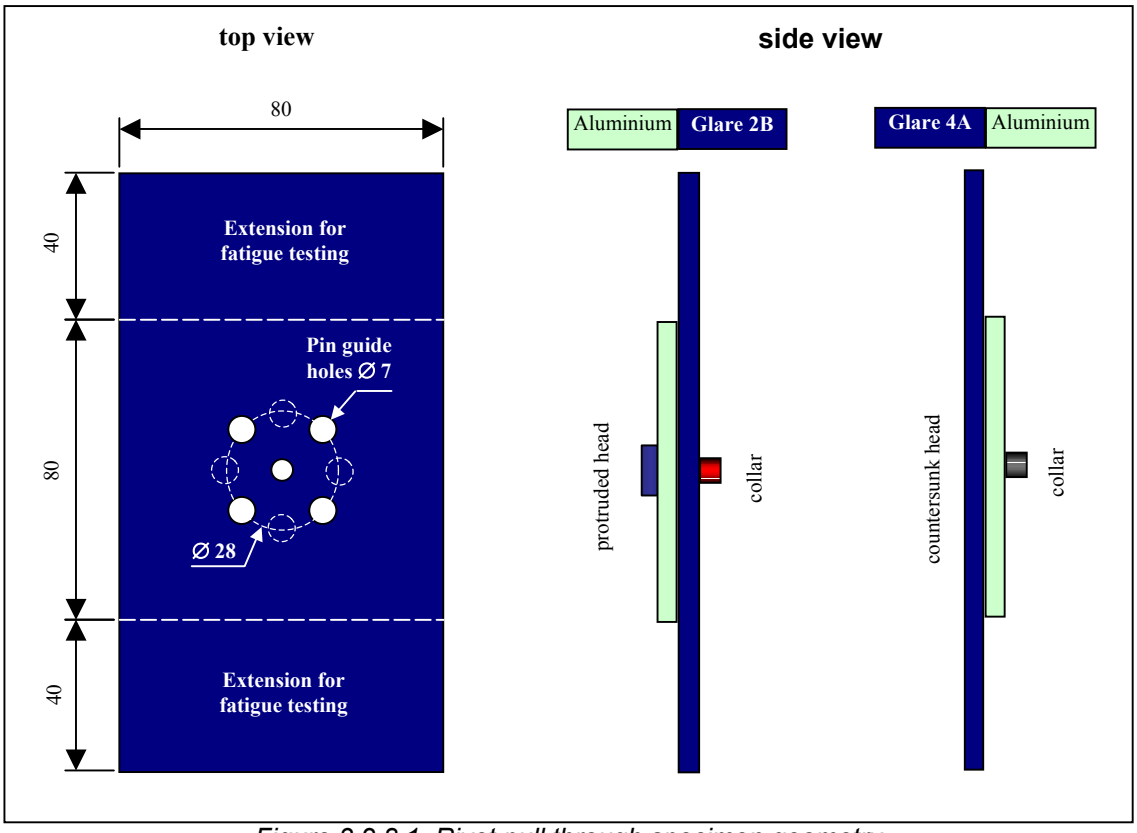

Figure 3.2.8.1. Rivet pull through specimen geometry

Because fatigue testing had to be performed before the rivet pull through tests, the GLARE sheets were extended 80mm for clamping.

The GLARE parts were cut to dimensions suitable for milling into final shape. During milling, small holes have been drilled at the location of the fastener. The specimens used for outdoor exposure are provided with an entire paint system for environmental protection and maximum heat attraction (ref. chapter 3.3).
The aluminium parts were cut to 80 x 80 mm. They have undergone a standard surface treatment, identical to that of aluminium sheet used in GLARE. This will provide sufficient protection against corrosion during outdoor exposure.

The GLARE parts are fatigue tested to create cracks of different lengths. After testing, the aluminium sheets are attached to the GLARE sheets. For the GLARE2B specimens protruded head Hi-Loks with an interference fit are used, for the GLARE4A specimens countersunk Hi-Lites with a clearance fit are used.

Hole diameters and fastener types:

GLARE type	designation	hole ∅ [mm]	fastener/collar type
GLARE2B-7/6-0.4	7-B-x	4.77 – 4.80	DAN 7-6-6 / NSA 5075-6
GLARE4A-5/4-0.4	7-A-x	5.54 – 5.57	ASNA 2026-3A-3 / 2528-3A

The four guidance holes needed for the pull through tests were drilled before testing of the unexposed specimens. These holes have not been drilled for the outdoor exposure specimens, in order to avoid corrosion or other undesirable environmental effects. When the pull through tests need to be performed, the holes can be drilled through both parts at once.
Material batch numbers of the used GLARE panels are given in [14], the test matrix is contained in table 3.2.8.

3.3 Surface Protection

In order to achieve high moisture absorption rates in the outdoor exposure specimens, a colour system is selected with high absorptivity for the range of visible wavelength from solar radiation. In this way relatively high specimen temperatures are provided. In addition, the paint system prevents corrosion damage.

Figure 3.3.1. An A321 aircraft in U.S. Airways colours in a winter evening

Painting procedure for all specimens, exceptions notified separately:

- (GLARE received with bonding primer)
- Cleaning with solvant
- Alodine application on edges acc. to Airbus specification FA 80-T-35-1101
- Application of paint primer (Type 37 035 A) acc. to Airbus specification FA 80-T-35-5002
- Activating surface acc. to Airbus specification FA 80-T-35-9127
- Application of external paint primer acc. to Airbus specification FA 80-T-35-9127
- Application of external paint coating acc. to Airbus specification FA 80-T-35-9127, paint thickness approximately 50 μm

External paint system: CA8000 U.S.Airways dark blue I6018, supplier: PRC deSotho,
purchase no. HTZ 58-71-6818-127,
solar absorbance according to AITM 2-0018: alpha(s) 0,982.

3.4 Outdoor Exposure Test Site and Specimen Mounting

The outdoor exposure and the weight gain measurements are contracted to the Defence Science and Technology Organisation (DSTO), Aeronautical and Maritime Research Laboratory, located at Innisfail, Queensland, Australia. The test site is located at 146° longitude east, 17.4° latitude south. The location is tropic and provides a realistic yet worst case environment. Very high levels of sunshine, rain fall and humidity provide conditions that are required to test a materials resistance to degradation.

Figure 3.4.1. Location of outdoor exposure site

The specimens are mounted on exposure racks provided by DSTO using aluminium channel sections to hold the edges. For reference to earlier investigations at the test site the racks are oriented 17.5 degrees to the horizontal, which provides the maximum incident solar radiation (see figure 3.1.3). All specimens are exposed to the open sky, consequently they are directly exposed to rain as well. Applicable test specifications: ASTM standards [1,2,3,4].

MRS: In order to avoid direct access of rain and associated dirt to the moisture reference specimens, they are covered under well ventilated glass according to ASTM G24-97, exposure cabinet type A [5].

Figure 3.4.2. Exposure rack with 2-B- specimens

Figure 3.4.3. Exposure rack carrying different specimen types

3.5 References

[1] ASTM E41-92, Standard Terminology Relating to Conditioning

[2] ASTM G113-94, Standard Terminology Relating to Natural and Artificial Weathering Tests of Nonmetallic Materials

[3] ASTM G147-96, Standard Practise for Conditioning and Handling of Nonmetallic Materials for Natural and Artificial Weathering Tests

[4] ASTM D618-99, Standard Practise for Conditioning Plastics for Testing

[5] ASTM G24-97, Standard Practise for Conducting Exposures to Daylight Filtered Through Glass

[6] An Experimental and Analytical Investigation on the Fatigue Behavior of Fuselage Riveted Lap Joints, R. Müller, PhD Thesis, 1995

[7] Experimental project to assess the failure mechanisms during blunt notch of Glare, Dr. Y. Meziere, Delft University of Technology, Report B2V-00-47, 2000

[8] The influence of elevated temperature on GLARE after exposure to moisture, B. Borgonje, Delft University of Technology, Master Thesis, 2000

[9] GRP WG1C progress meeting, 10.1.2002 , Th. Beumler, EADS Airbus MoM 510/02

[10] Qualification testing for the GLARE panel in the A310P/F, MSN484 aircraft, W.v.d.Hoeven & L.Schra, NLR report NLR-CR-2000-115

[11] GTO WP 1.1 / Durability Program, DaimlerChrysler Aerospace Airbus MoM EMF-932/99, Th. Beumler, 1999

[12] Fatigue test results of A320 and A321 circumferential butt joint panel specimens, Th. Beumler, Deutsche Airbus GmbH, Report 10D/E022K4753C04, 1991

[13] Fatigue test results of A330 and A340 circumferential butt joint panel specimens, Th. Beumler, Deutsche Airbus GmbH, Report 10F/G022K4753C04, 1991

[14] GLARE outdoor exposure program: Rivet pull through tests, B. Borgonje, Delft University of Technology, Interim report B2V-02-22, 2002

[15] Fastener test methods, Method 4, Lap joint shear, MIL-STD-1312-4, Department of Defense, Washington D.C., 1984

[16] GLARE outdoor exposure program: rivet strength tests, B. Borgonje, Delft University of Technology, Interim report B2V-02-15, 2002

[17] MIL-HDBK-5: 98th Meeting FIWG Minutes, Raleigh, NC, October 22, 1999

[18] Determination of the test conditions for compression filled-hole tests on Glare, W. van der Hoeven, National Aerospace Laboratory Report NLR-CR-2002-303, 2002.

[19] The influence of (thermal) ageing and temperature on compression filled-hole strength of GLARE, M. Ypma, Delft University of Technology, Report B2V-02-47, 2002

[20] Compression filled-hole tests of GLARE, M. Ypma, Delft University of Technology, Report B2V-00-50, 2000

[21] GLARE outdoor exposure program: Compression filled-hole tests, B. Borgonje, Delft University of Technology, Interims report B2V-02-28, 2002

[22] HSB 45131-01, O. Mester, L. Schwarmann, 1996

[23] GLARE outdoor exposure program: Bearing strength, B. Borgonje, Delft University of Technology, Interims report B2V-02-36, 2002

'Vorstellungskraft ist wichtiger als Wissen.'
Albert Einstein

Chapter 4
Accelerated Diffusion

Contents Page

This page intentionally left blank.

4.1 Introduction and Review

The long term behaviour of an aircraft structure is an important item for the sake of safety and economy. Matrix controlled mechanical properties of a composite may decrease when moisture diffusion reduces the glass transition temperature and the moduli of the polymer. This phenomenon is extensively investigated since the introduction of carbon fiber and glass fiber reinforced polymeric materials as aircraft structures. The questions to be answered are always the same, independent from the particular laminate and the component manufacturer:

- Which moisture content and which moisture distribution has to be considered after 20 to 30 years aircraft operation ?
- Which strength degradation is associated to the moisture distribution at the end of the aircraft life ?
- Which specimen type is suitable for diffusion simulations ?
- Which outdoor environment is representative for the investigation of diffusion trends ?
- Which type of *accelerated* ageing can be used to obtain a condition representative for the aircraft structure at the end of its operational life ?
- Will specimen subjected to mechanical tests show the same failure mode after artificial ageing as after outdoor tests.
- Will specimen subjected to mechanical tests show the same failure mode after artificial ageing as after outdoor tests.

The last question is extremely important for the determination of knock down factors that cover ageing, which can be used for the certification of aircraft structures. A change in failure mode would make accelerated aging results unreliable, which may either make the application of the material impossible or at least would require additional safety factors. This chapter 4.1 will start with an overview of experience gained from past investigations on both, pure composite and fiber metal laminates in the past. It will be used as starting point for the definition of the GLARE outdoor exposure program.

NASA deployed graphite-epoxy and Kevlar epoxy composites on aircrafts from three different operators, among them Aloha Airlines which operates 737 aircraft between the Hawaiian Islands (hot wet climate). Specimens have been exposed inside and outside the aircraft, as well as at different ground exposure sites [1]. The investigation was limited to compression-, tension-, flexure- and short beam shear specimens. Some shear strength degradation after 2 years of exposure is reported, but no reduction of tensile and compression values.
British Aerospace fitted carbon fiber tensile- and compression specimens on the wings of BAe Trident aircraft. Ground exposure and moisture assessments were included in the program. Compression properties decreased between up to 30%, depending on the fiber orientation tested [2]. Based on the weight gain measurements it was concluded, that the maximum deterioration occurs during the *first* years in service.

The University of Tokyo exposed both, glass fiber and carbon fiber specimens for three years in three different Japanese cities. Weight increase was measured upto one year of exposure, thereafter the weight decreased [3].
Extensive research on the moisture absorption phenomenon in composites is conducted and published by Springer [4]. He performed a complete transient diffusion analysis in order to simulate 20 years

service life of an aircraft in changing atmospheric conditions. His major conclusions from the analysis on the variation of moisture content and moisture distribution are:
“After 10 years of exposure to the actual (transient) environment the moisture content nearly reaches a steady state.”
“The moisture distribution never reaches a steady state but varies continuously. Nevertheless, after about 6 years most of the variations occur within a narrow layer near the exposed surface.”
“Owing to the continuous variation of the moisture distribution, the distribution from a transient ambient cannot be simulated accurately by a constant environment.”

Kröber performed diffusion calculations for carbon fiber laminates, using Springers computer software “W8GAIN” [5]. The simulation, based on meteorological data from Rome and Jakarta, revealed that no more than 4mm saturation depth can be obtained after 25 service years, from each side of the composite surface [6]. The calculation results have been verified by traveller specimens attached to a spoiler for 4 years [7]. Moisture content variations in the narrow layer, as defined by Springer, have been observed for a maximum depth of 1.4mm, due to changing seasons. These analyses resulted in the definition of an accelerated ageing procedure of 3000 hours exposure in a 70ºC / 85% relative humidity environment [8], hereafter referred to as ‘*standard accelerated ageing*’.

The diffusion rates in a composite can be described by the Arrhenius equation:

$$D = D_0 \times e^{(-A/RT)} \tag{1a}$$

or

$$D = D_0 \times e^{(-A/T)} \tag{1b}$$

, with the gas constant R included in coefficient A.

The diffusion rate D is dependant on the *ambient* temperature and the material constants A and D_0. The material constants have to be determined by test, they are different for different matrix systems.

The maximum moisture content in a matrix is dependent on the ambient relative humidity (RH):

$$M_m = a \times (RH)^b \tag{2}$$

Again, two material constants, a and b, have to be determined by tests.

Finally the moisture concentration as function from the position in the composite needs to be described. If no discontinuities are present in the material, e.g. matrix cracks, voids or delaminations, if the heat transfer through the material is governed by conduction only (Fourier’s law) and if the temperature inside the material approaches an equilibrium much faster than the moisture concentration, then Fick’s law can be used for the determination of moisture concentration. In a one-dimensional form the diffusion process reads:

$$\frac{\partial c}{\partial t} = \frac{\partial}{\partial x} \times \left(D_x \times \frac{\partial c}{\partial x}\right) \tag{3}$$

Moisture can be absorbed by a composite structure through its complete interface with the environment, so its complete surface. The one dimensional Fickian law is applicable, if the influence of the edges is negligible, i.e. if the surface of the edges is small compared to the surface of the plate.
For the determination of the constants in equation (1a, 1b and 2), it is therefore required either to work with a large thin shell or, if the volume of the environmental chamber is limited, to apply a coating at the edges in order to prevent their influence on the results. True edge sealing, however, is problematic, since sealants and paint systems absorb moisture as well. In the worst case, a correction is required for the contribution of the edges to the moisture absorption. This correction increases the numerical problem significantly, since after absorption of moisture at the edges, diffusion will occur parallel to the fiber orientations while absorption through the surface of the shell will be followed by diffusion through the thickness of the plate. Diffusion coefficients for these two directions are not identical which would require an anisotropic version of Fick's law.

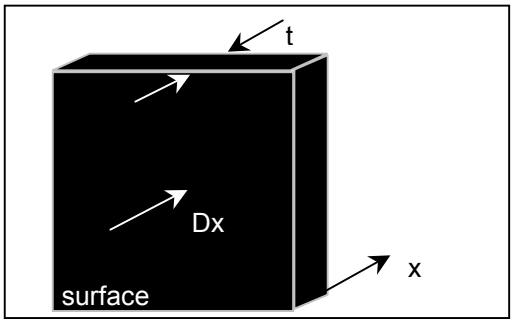

Figure 4.1.1. Composite specimen for diffusion investigations, t/l < 0.01, t/w < 0.01

The diffusion routes for moisture in FML specimens are quite different from those in pure composites. Due to the barrier function of the aluminium layers at both surfaces, moisture absorption is possible at the sheet edges and at drilled holes.

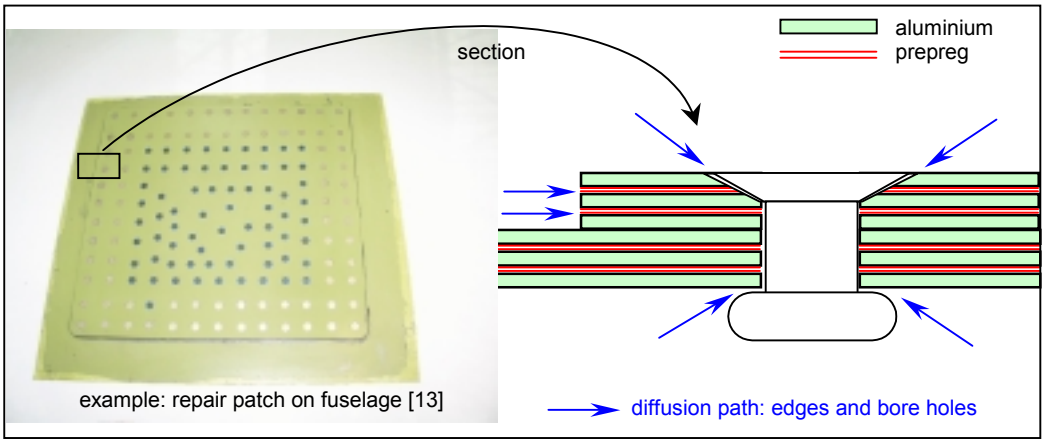

Figure 4.1.2. Diffusion path in GLARE

Summarizing the know-how on the in-service composite behaviour it can be concluded, that the physical phenoma are well understood and that tools are available for reliable diffusion predictions. The definition determination of the *real worst case* in-service conditions is complex. Depending on the available test sites, contribution of aircraft customers for in-flight tests and the assumptions of the environmental mission mix, a more or less reliable estimate of the worst-case can be made. However, uncertainties will remain, until it is possible to measure the weight increase of a composite structure, which has been operated for 20 to 30 years in a tropical environment.

Experience with the influence of the environment on Fiber Metal Laminates is not yet as well known as it is for composites. Roebroeks exposes GLARE specimens on the roof of Delft University since 1995, removing them in groups in unscheduled intervals for destructive investigation [14]. After 86 months of exposure (status February 2003) strength degradations were found of 10% for ILSS specimens, 2% for

tensile specimens and no strength reduction for A340-geometry riveted GLARE joint specimens, compared with the unexposed specimen. The results clearly indicate that there is not an identical influence of the environment on all mechanical properties and that one has to decide on the properties of interest to select the right specimen and test . Obviously, matrix dominated properties decrease (e.g. ILSS), but this effect has no influence on the tensile strength of a particular joint. For the experiments in Delft both the expected and found failure modes have to be discussed, as well as the relevance of the climate in Delft. Delft belongs to a part of The Netherlands with high pollution, due to the neighbourhood to Rotterdam, but the ambient temperatures, which determine the moisture diffusion for an significant part, are moderate throughout the year. Furthermore it needs to be determined, how many in-service flights are represented by the 86 months of exposure.
Besides the selection of the appropriate specimen type other proper decisions have to be made for a durability test program on GLARE. Due to the barrier function of the aluminium sheets ultra long exposure times have to be considered. To obtain timely results decisions have to be made early in the material selection, testing and certification process. This bears the risk that the constituents of the FML preferred by the industry change before the durability test program has been finished. This holds especially for the determination of saturation levels in the laboratory and for outdoor exposure tests. Starting in the 1980's with ARALL, research and commercialisation changed to GLARE with 2024 metal, phosphoric acid anodising, R-glass and AF163 resin. Later glass fibers selection changed to S-glass and the preferred resin to FM94, again later the phosphoric acid anodising was substituted by chromic acid anodising. This final material was qualified for the Airbus A380 application. However, the optimisation of the material did not come to an end.

Fundamental research on the durability behaviour of ARALL was done by Verbruggen [15], who solved the equations of the two-dimensional diffusion process and determined diffusion rates for both diffusion directions in the laminate. Diffusion rates are determined and reported for both directions, and the fracture mechanisms in the metal/prepreg interface have been studied. For all environments and exposure periods applied, the fracture path under mechanical loading was situated at the interface between the so-called fiber-rich and resin-rich epoxy layers, which is typical for ARALL. Warm water and salt water proved to have a larger deteriorating effect on the fiber/resin interface. An important discovery was the non-linear relationship between the maximum moisture content M_m and the relative humidity RH. Especially in warm water M_m was much higher than it was found after humid air exposure. It is important to note that the Aramid fibers in ARALL absorb moisture as well as the matrix system.

Tensen [16] repeated the evaluation of diffusion coefficients with GLARE with AF163 as matrix material. The glass prepreg in GLARE has such a high fiber content that a resin-rich layer, like in ARALL, is not present. Tensen measured the diffusion rates parallel and perpendicular to the fibers as function of temperature [16]. However, all data is obtained with warm water exposure, since major problems occurred with specimens exposed to salted air. The weight of some specimens exposed to salted air did not change, other specimens even decreased in weight. This is a normal phenomenon since the salt will extract water from the polymer by putting it under salt. Consequently, not even a trend could be observed. A similar experience has been made later by van der Hoeven [17]. After sufficient exposure time in an environmental chamber with a salt solution GLARE specimens lost weight even at 50°C.

4.1.1. Diffusion at sheet edges

Residual shear stresses develop at the sheet edges due to the different coefficients of thermal expansion at temperatures below curing temperature. The magnitude of these stresses is also determined by the difference in stiffness between the different layers. The affected area equals 4 to 5 times the laminate thickness [18]. The problem is solved numerically by an elastic plastic assessment of the Shear-Lag theory [19]. In theory the shear stress between aluminium and prepreg should be infinitively high at the singularity point/line. The shear lag theory uses a simplified model of the adhesive layer (only one element over the adhesive thickness). The singularity is therefore not captured by the model. However, by taking the plasticization effect into account it is contributed to the reality. Peel stresses result from the equilibrium equations according to the elementary bending theory, but due to the high stiffness of the aluminium they are found to be insignificant [18]. Characteristic for the shear deformation in both the resign rich layer and to some extend in the prepreg is the G-modulus. Figure 4.1.4 contains the G-modulus reduction for AF163-2K adhesive, dependent on the material temperature [18]. Note: The investigations performed by Kappel [18] cover the temperature range from 25°C to 120°C (curing temperature), values below 25°C are extrapolated.

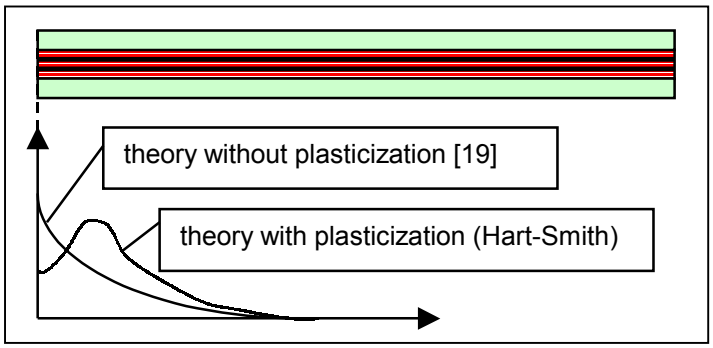

Figure 4.1.3. Shear stresses at GLARE edges, principle

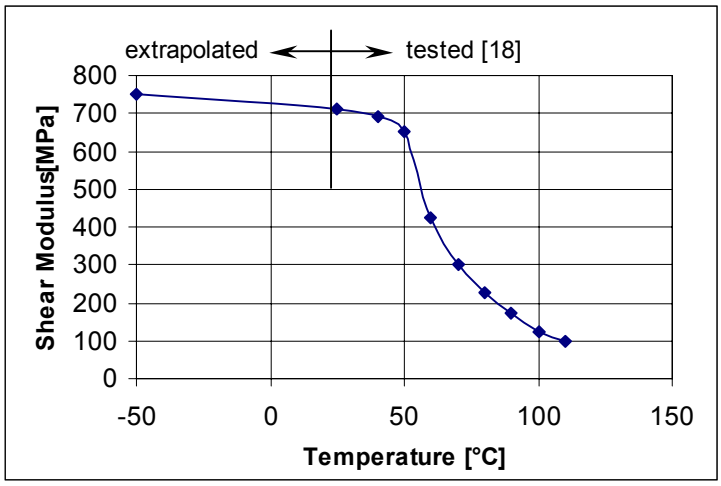

Figure 4.1.4. Shear modulus depending on temperature

GLARE is cured at 120°C in the autoclave. During its life it is subjected to the temperature envelope for commercial aircrafts which ranges from –30°C (cruise) to 70°C (standing on ground, fatigue (?)). With decreasing temperature, both the shear stress, due to the mismatch of CTE's and stiffness, and the shear moduli increase. It needs to be investigated, how the cyclic temperature variation will affect the bonding strength at the GLARE edge and whether the presence of humidity will influence the results. Preferred is a cohesive failure, adhesive failure would compromise the metal surface pre-treatment, which should be of doubtless quality after decades of metal bonding. However, if water molecules form areas of high concentrations in the prepreg, debonding between glass fibers and epoxy occurs [20].

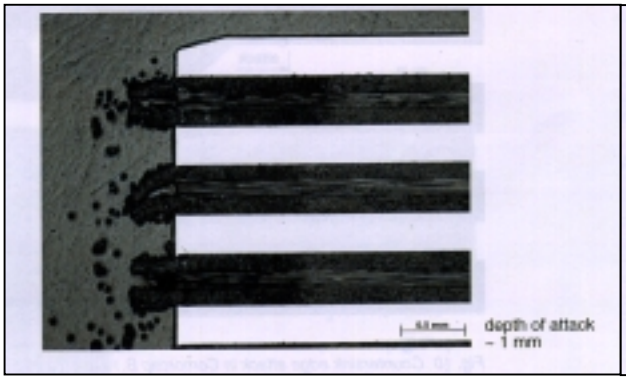

Figure 4.1.5. Edge immersed in Turco 6881 (168h) [21]

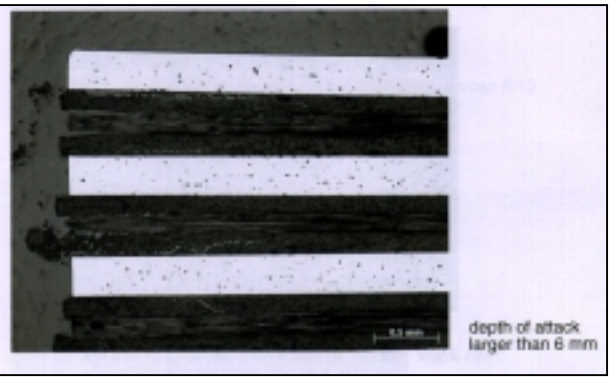

Figure 4.1.6.. Edge immersed in Comorcap B.10 [21]

The debonding of matrix and fibers was accelerated by an extreme exposure to paint stripping agents for GLARE [21]. If immersed for 168 hours, fibers decoupled at the edge and were even pushed out their internal compressive forces, see figures 4.1.5. and 4.1.6.

These tests performed in aggressive environment [21] had of course a different purpose than the investigation of the environmental influence on the material during flight service. But it proved the sensitivity of GLARE (FM94, S-glass) to environments other than humid air. The penetration depth is conform the expectations. Aerospatiale exposed a GLARE panel for two and a half years on Isle de Pelier, an island in the Atlantic Ocean. Specimens have been cut from different distances from the unprotected edges, and the glass transition temperature was measured (method see [22], chapter 5.5):

Distance from unprotected edge	Tg
5 mm	123 °C
17mm	129 – 125 °C
29 mm	129 °C

It was concluded, that moisture diffused at least 5mm into the laminate, after two and a half year outdoor exposure. Delamination or other failure modes have not been observed, except some local corrosion on the unprotected metal.

Kelm measured a similar diffusion depth (6.8 – 8.1mm) in the prepreg after 2000 hours exposure in 70°C warm water [23]. The subsequently conducted peel tests (method acc. to MBB specification QVA-Z10-46-03, see appendix U) revealed a strength reduction of 28% to 48%, depending on the GLARE type. This reduction gives an impression of the influence of moisture on a mode I failure, which can occur in a structural component in case of local additional bending.

However, the moisture *concentration* related to the distance from the specimen edge couldn't be provided by both investigations [22,23].

A shear loading, mode II, is better investigated by using a thick adhered specimen. The interlaminar fracture toughness energy G_{Ic} represents the degree of delamination resistance against shear. G_{Ic} values between 3700 and 4250 J/m^2 have been determined for the dry FM94/S-glass prepreg embedded in a GLARE-2/1 specimen [24], compared with 200 to 800 J/m^2 for a carbon prepregs. The high fracture toughness energies of GLARE give evidence for a specific delamination resistance in the shear mode, which is important for an effective crack bridging in the fatigue crack propagation case (The delamination size is balancing the load distribution between the fatigued metal and the fibers which bridge the fatigue crack.).

The influence of thermal cycles on the failure of GLARE edges has been first investigated by Graafmans [25]. 986 thermal cycles between –50°C and 80°C have been applied on GLARE3, without any sign of delamination, debonding or cracks at the specimen edges. A GLARE2 specimen with 2.6mm thick aluminium sheets was exposed in order to obtain a worst case result (the shear forces increase with the

aluminium thickness). Also this specimen passed the test without any failure. Prerequisite for undamaged specimens after thermal cycling was an accurate milling of the edges. Specimens which have not been milled but *cut* to final size, obtained small damages from the manufacturing process, which increased due to the thermal cycles.

Van der Hoeven tried to create a delamination in a prepreg by spark erosion of the outer aluminium layer in a 5/4 lay-up for a subsequent thermal- and humidity cycle test [26]. But even after 130000 cycles at 130 MPa maximum stress no delamination initiated. The procedure was changed to a constant applied peel stress by bending the specimen. Now, 1-2mm delamination growth was estimated after 1000, 2000 and 3000 alternating temperature and humidity cycles.

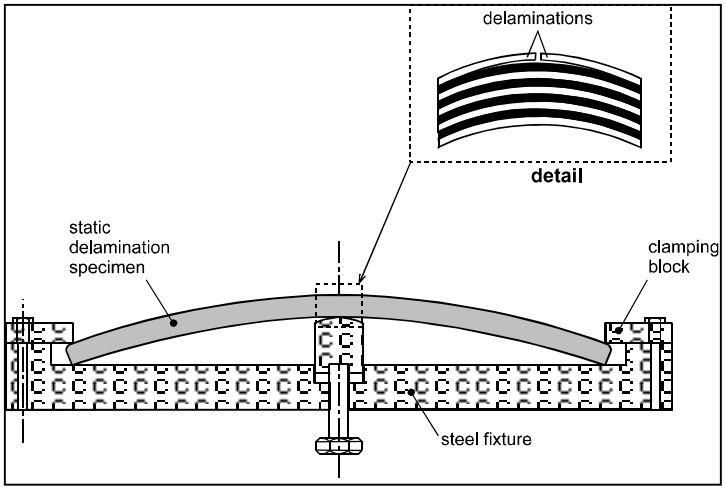

Figure 4.1.7. Static delamination tests with cyclic exposure [26]

GLARE sheet edges at fuselage skin panels can be distinguished in two categories. Free edges in the vicinity of a longitudinal joint or circumferential joint are almost free from external load. Edges at cut outs of any kind are loaded up to 200 MPa in fatigue. The latter ones should be therefore more critical, because the residual stresses (from the curing process) are superposed with high mechanical loads.

Outdoor exposure results for ARALL reinforcements riveted emergency door cut outs are available for the Fokker 100. Seven aircraft entered service in 1989 and 1990 with these reinforcements. Until the year 2000 they made 16000 to 20000 flights. An inspection threshold of 13700 flights with an interval of 2700 flights has been defined by Fokker. No finding has been reported until the year 2000, when questionnaires have been completed by operators [9].

The review of the available research and in-flight experience indicates high bonding strength of GLARE in the shear mode and limited strength in the peel mode. Information from superimposed structural and temperature loads for both, dry and wet sheet edges, are not available for GLARE but for ARALL (Fokker 100 reinforcements). The required information on GLARE should be gained by tests, since an analytical solution is not possible. In frame of this research investigations have been done with door corner cut out specimens . They are discussed further in chapter 11.

4.1.2. Diffusion in GLARE holes

Drilled holes in aircraft are usually filled with fasteners. The fit between fastener and hole edge is a major parameter for pin loaded holes. In order to limit the number of variables, it makes sense to focus on the worst case for the diffusion investigation A realistic worst-case scenario is the installation of a clearance fit bolt without sealant, but according to all other manufacturing specifications.

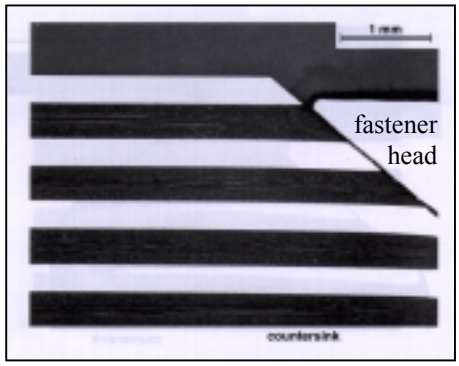

Figure 4.1.2.1. Too deep countersunk (concession) [36]

Based on the determined diffusion coefficients for GLARE in warm water, Tensen predicted iso-concentration lines of moisture around a drilled hole, depending on time and fiber orientation [16], see figure

4.1.2.2. The problem is more complex than at a sheet edge, since the fiber orientation relative to the hole edge changes continuously.

Preliminary knock down factors for different material properties due the influence of moisture uptake have been defined in frame of the GLARE Technology Program [27], all linked to 3000 hours ageing in a 70°C / 85%RH environment. It is emphasized that the standardized accelerated ageing procedure is *a defined realistic worst* case for composites, but not *the worst possible* ageing for the material. A higher maximum moisture content than the one associated to the 85% relative humidity is possible, if the ambient relative humidity is constantly higher. The moisture absorption can be accelerated if the chamber is heated to more than 70°C.

But how realistic are coupon size exposure specimens for the simulation of ageing related strength reductions in a flying aircraft GLARE structure? The design of test specimens can influence the obtained strength results significantly, especially it has to be accounted for that the protection of specimen edges against environmental influences with sealant or paint may be impossible, since both absorb moisture themselves. If the failure location of a specimen is at its edge and the influence of moisture on the edge strength shall be investigated, then coupon tests are provide reliable results. Care must be taken for the design for specimens where the edge is not the investigated location. Sufficient edge distance must be provided in order to avoid environmental influences from the edge on the test location, e.g. a drilled hole.

Van der Hoeven demonstrated the influence of a small specimen width and unprotected edges for the materials which are of interest for this research, i.e. , GLARE2B-7/6-.4 and GLARE4A-5/4-.4. holes.

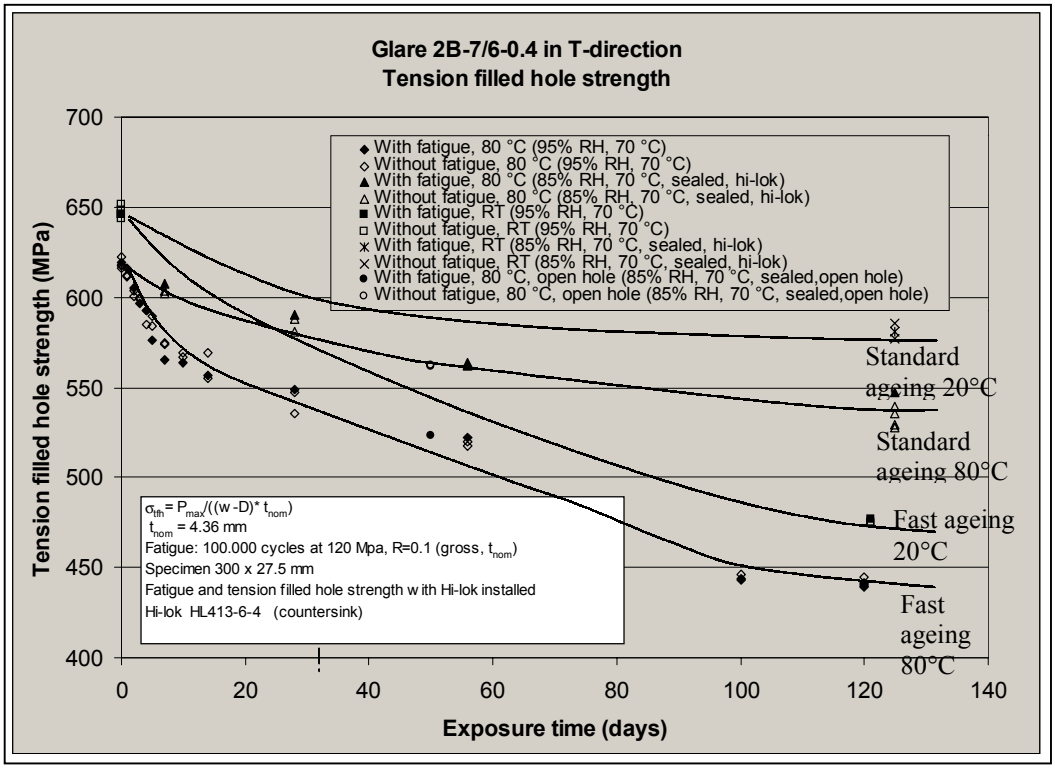

Figure 4.1.2.3. The influence of specimen width, edge protection and relative humidity on blunt notch strengthGLARE2B. [10]

The tested blunt notch specimens had a width of 27.5mm, which equals a situation in which an edge would be located between each pair of holes. The standardized accelerated ageing process has been applied on specimen with coated edges (sealant) and in addition the influence of a 'fast ageing' process, i.e. 95% RH at 70°C, with non protected specimen edges, was investigated [10]. Significant influences (knock down factors) on the blunt notch strengths have been observed, see figures 4.1.2.3 and 4.1.2.4.

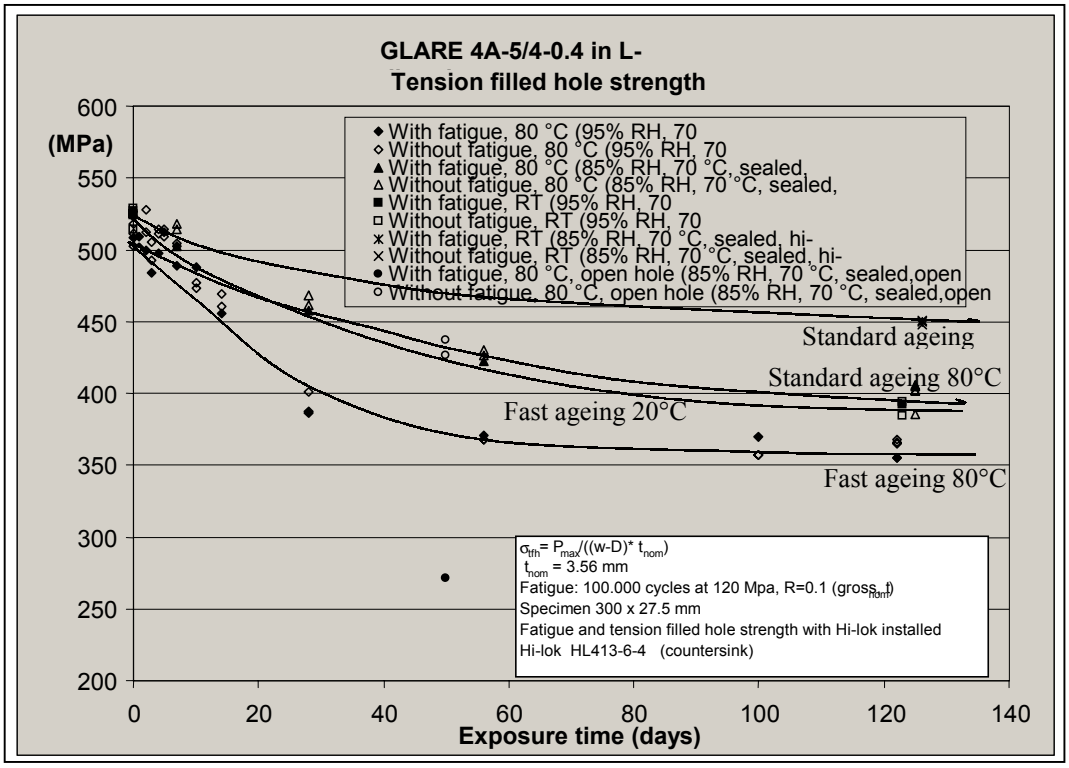

Figure 4.1.2.4. The influence of specimen width, edge protection and relative humidity on blunt notch strength, GLARE4A-5/4-.4. [10]

The historic examples discussed above show the need to test *realistic* specimen designs. Surprisingly, van der Hoevens small specimens became even strength sensitive high applied material temperature during the static test, which was not the case for Borgonje's 50mm wide specimens [11], see chapter 3.2.4. Neither did wider blunt notch specimens with 5 drilled holes in a row show significant strength reduction due to temperature in a previous investigation [12].

The complexity of the ageing phenomenon increases for fatigue crack propagation in GLARE. In a fatigue cracked condition shear stresses develop along the crack as indicated in figure 4.1.2.5. Shear stresses in the xy-plane develop between the intact fibers and the aluminium, with a maximum at the fatigue crack face (section A-A in figure 4.1.2.5). The local shear stresses depend on the delamination size and –shape. They can be different for every position along the crack face. The influences of (fatigue) delamination shapes in the vicinity of fatigue cracks is extensively discussed by Guo an Wu, who summarized the phenomenon as follows [41]: "Bridging stress acting on the boundary of the delaminated area arrests the crack by the adhesive. The extension of the bridging fibers plus the shear deformation of the adhesive in the boundary of the delaminated area should equal to the crack opening displacement contributed by both the applied and the bridging stress." The later definition is transformed into equation (4) [41]:

$$\delta_{fm}(x_i) + \delta_{ad}(x_i) = u_{\infty}(x_i) - u_{br}(x_i) + \Delta \qquad (4)$$

δ_{fm}: extension of intact fibers
δ_{ad}: adhesive shear deformation at delamination boundary
u_{∞}: crack opening displacement caused by applied stress
u_{br}: crack opening displacement caused by the bridging stress
Δ: deformation of metal (not relevant)

Note that both the previous and the present research are simplified to uni-axial stress statii and that the poisson effect on the crack opening is ignored. How ever, this has no influence on the absolute load distribution between fibers and aluminium.

A relation between the adhesive shear stress τ between aluminium and fiber prepreg is defined by Marissen [33] and prescribed in detail by de Vries [32]:

$$\tau = \left(\sigma_{Al} - \sigma_{Al,0}\right) \times t_{Al} \times \sqrt{\frac{t_{prep.}}{j \times G_{prep.}} \times \left(\frac{1}{E_{Al} \times t_{Al}} + \frac{1}{E_{prep.} \times t_{prep.}}\right)} \qquad (5)$$

(Equation for ARALL interpreted for GLARE. Difference: ARALL has two resin rich layers, GLARE has none.)

σ_{Al}: stress in aluminium layer due to applied load

$\sigma_{Al,0}$: curing stress in aluminium layer due to autoclave temperature

j: number of prepregs

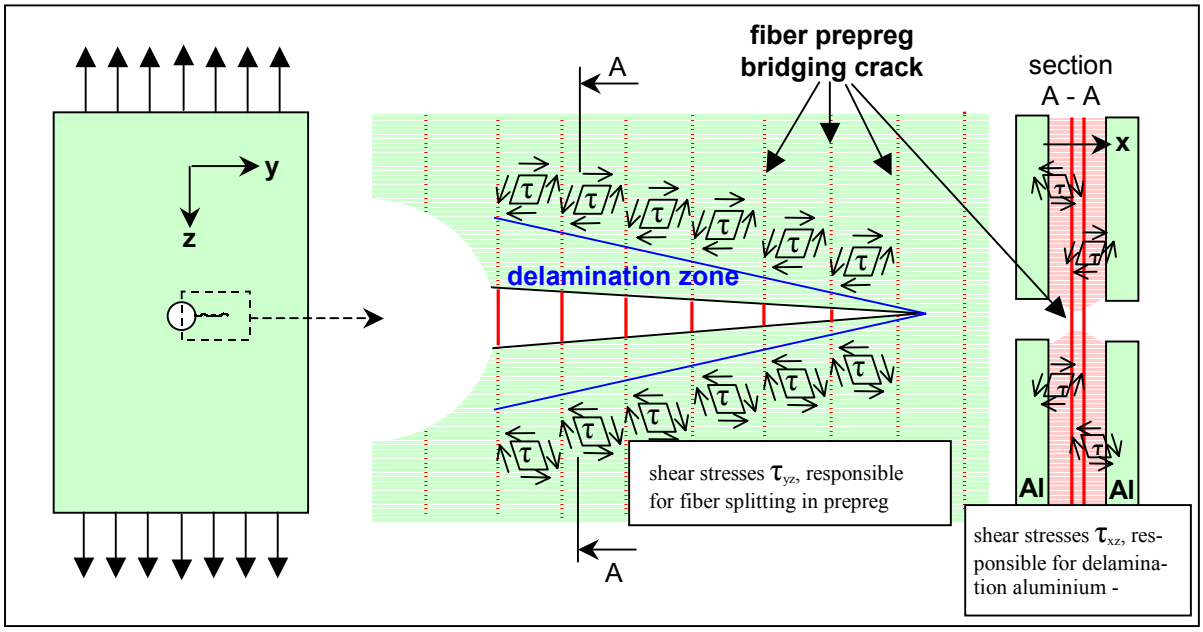

Figure 4.1.2.5. Schematic display of shear stresses in the vicinity of a fatigue crack at a hole

Shear stresses in the yz-plane (figure 4.1.2.5) develop if the elongations of the fibers are different, e.g. due to the stress gradient from the hole to the crack tip. The relative deformation between fibers in load direction causes a failure mode which is called fiber splitting. It happens short before tensile fiber failure and is considered as less representative for the discussion of crack propagation [37].

Roebroeks related the applied energy release rate G_{del}, which is material- and geometry dependant, to the 'delamination resistance' R_{del}, which is a material property and serves as 'critical energy release rate' [37]. Static delamination growth will happen, if $G_{del} > R_{del}$. The delamination resistance R_{del} has been investigated by Roebroeks for different GLARE lay-ups and especially for different resin types, but in any case in a dry material condition and at room temperature. It is a measure for the fatigue delamination size, i.e. the greater the static delamination for a standardized specimen and load, the lower the delamination resistance.

In frame of the present research it has been investigated if and to which extent absorbed moisture in the FM94/S-glass prepreg leads to larger delamination sizes and/or larger shear deformations, which both may increase fatigue crack propagation rates. The delamination size has a significant influence on crack opening according to Guo and Wu. For a practical application it must be considered that a commercial aircraft structure is operated at continuously varying temperatures, so it is almost impossible

to predict the 'average' delamination size, that develops around the crack during aircraft service. A complex test is required for clarification, Realistic specimens have been loaded with both, variable mechanical loads and simultaneously variable temperature. This test is discussed further in chapter 7.1.6.

For fatigue loads which do not lead to a delamination growth, the shear stiffness between metal and prepreg might dictate the COD and therefore the crack propagation rates for different temperatures and moisture levels. This phenomenon is investigated by dedicated crack opening measurements and presented in chapter 6.5.

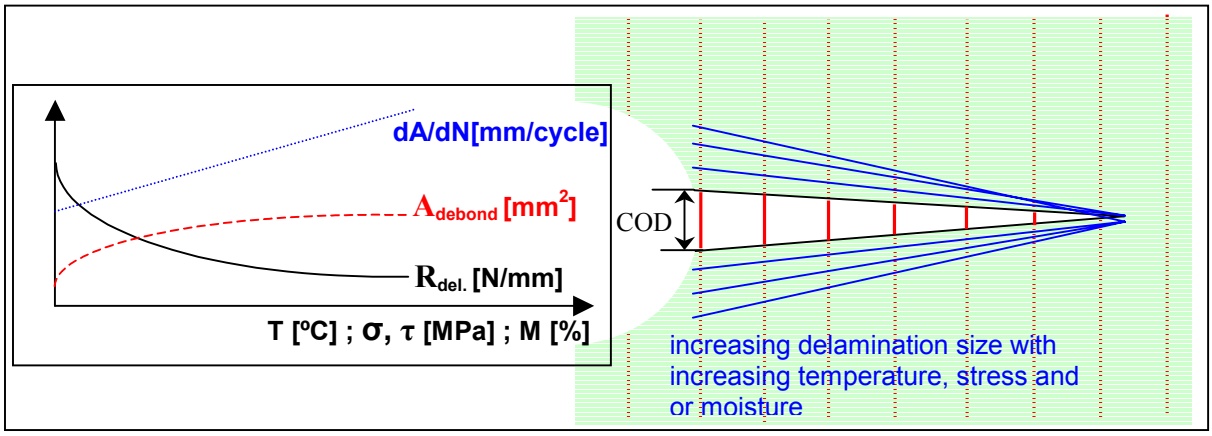

Figure 4.1.2.6. Schematic display of influencing factors on fatigue crack propagation in GLARE, model

4.1.3 Outlook for the present research

Since no diffusion coefficients are available for the FM94/S-glass GLARE type they have to be determined by a dedicated weight gain test program in humid air environment.

The lessons learned from the composite community urged the author of this research to expose GLARE specimens at least for 6 years outdoors. It is important to expose and investigate structural components, not just elementary specimens, for a representative simulation of an aircraft structure with it's complex failure modes.

The relation between the Moisture Reference Specimen weight gain curves obtained from accelerated exposure and from the exposure at the site in Australia should allow the determination of the moisture content in GLARE around a drilled hole in an aircraft structure at DSG and it should allow for the specification of a realistic accelerated ageing process.

The influence of moisture on crack propagation is believed to be very complex, since local structural mechanic loads interfere with local adhesive properties. Important is the comparison of diffusion speeds with crack propagation rates. Which is faster ?

This research will check the *extreme* condition, e.g. crack propagation in GLARE with prepreg near to saturation (chapter 6.6). Furthermore it will be investigated, whether a more *realistic* rate of diffusion causes a concern for crack propagation, or whether it may be considered as insignificant. The delamination resistance of the bond between metal and prepreg will be examined as a measure for the influence of temperature and moisture on crack propagation rates in chapter 6.5. Complex tests under variable temperature and variable loading conditions are required to simulate realistic aircraft structure conditions (chapter 7).

4.2 Diffusion Coefficients obtained from Rectangular GLARE3 Weight Gain Specimens

The availability of the diffusion coefficients A, D_0 (equation 1), and, a and b (equation 2) is essential for the calculation of specimen conditions after any kind of exposure. Equation (3) is solved in [4] for semi-infinite solids. Under the assumptions that the moisture content at the beginning of the exposure (t=0) is constant throughout the specimen and that the moisture concentration on the specimen surface at any time >0 equals the maximum moisture concentration of the ambient, equation (3) can be solved for a rectangular specimen having a similar kind of material exposed at each edge. The latter is the case for GLARE3, where 50% of the fibers are oriented parallel and 50% perpendicular to each edge. For GLARE3 it can be assumed, that the diffusion characteristics are similar at all edges, if the specimen is cut in L- and LT-direction.

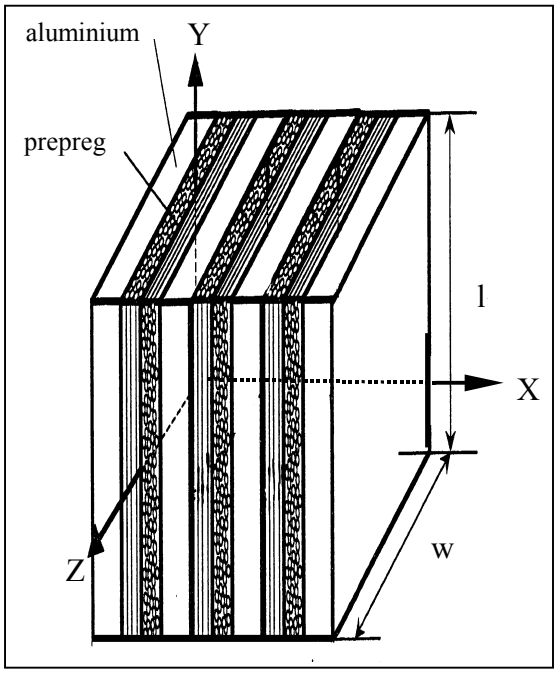

Figure 4.2.1. Rectangular GLARE3 diffusion specimen (no scale)

Four groups of rectangular GLARE3 specimens are investigated in constant climates in order to determine the diffusion coefficients. Three specimen groups are made of GLARE3-4/3-.3 (length 60mm, width 40mm, material ID 158882-39), according to Airbus test specification [31]. For comparison, a specimen made of GLARE3-4/3-.4 (length 100mm, width 25mm, as investigated by Borgonje [29]) is included in the analysis. All specimens have been dried at least 48 hours at 60°C directly before exposure. It can not be expected that this drying procedure will provide a dry laminate in the entire specimen. But the free surfaces (edges) of the prepregs, which are exposed to the particular environment of the location where the specimens are stored before test, are dried out. The procedure provides confidence to limit the prepreg condition variation prior to the exposure test to a minimum.

Due to the limited amount of exposure area of GLARE samples an extremely long exposure time is expected until saturation can be observed. On the other hand it is not possible to accelerate the diffusion process by using temperatures significantly higher than 80°C, since the glass transition temperature will decrease during exposure from between 95°C to 110°C (dry) to between 79°C to 97°C (prepreg saturated) [35]. It has to be considered that exposure at higher temperatures than 79°C may lead to fast weight gain, but just until the time t_{glass} is reached at which the prepreg changes into a glassy condition at the specimen edges. In a glassy condition the resin is considered as a barrier against diffusion and the weight gain is expected to come to a rest below the physical possible maximum moisture content, which can be achieved with exposure in the

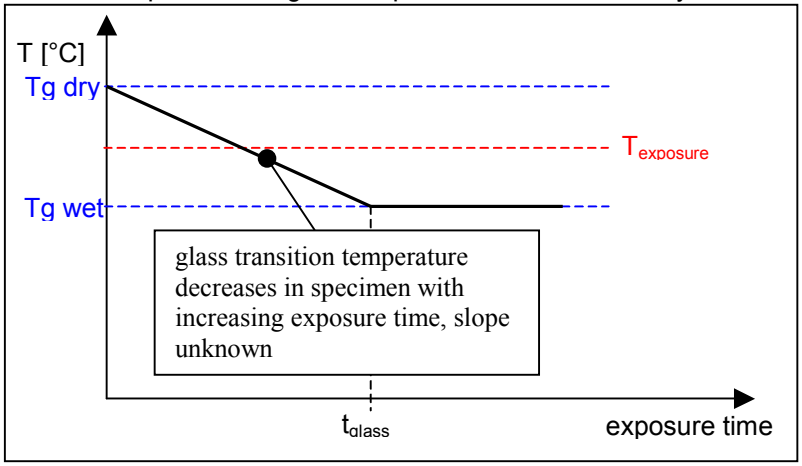

Figure 4.2.2. Schematic sketch of Tg behaviour dependant on exposure time

same humidity, but at lower temperature and after a significant longer time period.

4.2.1 Weight gain results

Table 4.2.1a-d contains the weight gain results from the rectangular specimens exposed at different humidities and temperatures. The weight gains in percentages of the prepreg dry weight, related to the square root of time, yield straight lines at the beginning of the test, as required for a Fick'ian behaviour of the epoxy (figure 4.2.3). One test specimen group is exposed above the wet glass transition temperature, i.e. at 90°C/95%RH. The weight gain behaviour changes after 1500 hours exposure and continued with a different slope than before. The exposure time t_{glass} (ref. figure 4.2.2) was obviously exceeded.

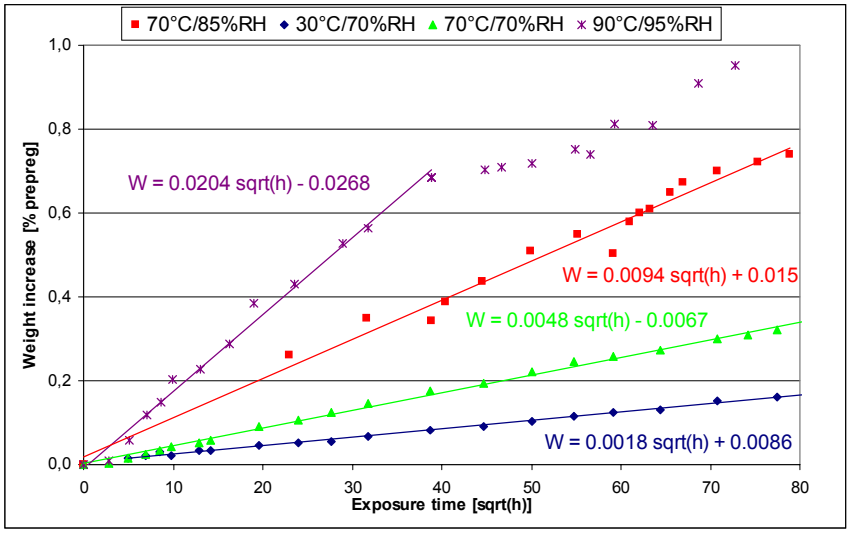

Figure 4.2.3. Weight gain results from rectangular GLARE3 specimens and non-corrected regression lines (i.e. regression lines do not intersect 0/0 in diagram)

4.2.2 Maximum moisture content

From equation (2) of this chapter can be used to derive the values for the coefficients a and b by inserting the relative humidity and the measured weight gain at a specific temperature, e.g. the 70°C/85%RH specimen and the 70°C/70%RH specimen.

In reference [34] the following equation is developed for the moisture absorption of a rectangular ARALL plate with width b and length l.

$$\frac{\sqrt{D_y}}{l} + \frac{\sqrt{D_z}}{b} = \frac{\sqrt{\pi}}{4M_m} \times \frac{M_t}{\sqrt{t}} \qquad (6)$$

This equation is also applicable to GLARE3 and it considers different diffusion rates in y- and z-direction. If D_y equals D_z the formula is simplified to :

$$M_t = 4M_m \times \frac{l+b}{l \times b} \times \sqrt{\frac{D_{yz} \times t}{\pi}} \qquad (7)$$

M_t moisture content at time t

Since the temperature used during moisturization is the same for both specimens, the diffusion speed D_{yz} is equal as well (Arrhenius). Therefore a part of equation (7) becomes constant:

$$4\times\sqrt{\frac{D_{yz}\times t}{\pi}}=C$$

The weight gain in the 70°C/85%RH specimen exceeds 0.79% prepreg weight after 8600 hours exposure. The maximum weight measured ($M_{m(70/85)}$ =) is 0.7996% prepreg weight after 15234 hours exposure. The linear regression lines obtained with the test results, figure 4.2.3, do not cross the 0% weight level. They should be corrected for the constant value in the particular weight gain equations.

The 70°C/85%RH specimen dimensions are l=100mm and b=25mm. The correction in weight is -0.015%.

$$M_{70/85}=(0.7996-0.015)\times\frac{100+25}{100\times 25}\times C=0.7846\times 0.05\times C$$

For the 70°C/70%RH specimen is found:

$$M_{70/70}=M_{m70/70}\times\frac{60+40}{60\times 40}\times C=M_{m70/70}\times 0.042\times C$$

The relation between $M_{70/85}$ and $M_{70/70}$ can be obtained from the weight gain measurements at any time, for example after 1000 hours exposure (tables 4.2.1):

$M_{70/85}$ = 0.3485 % - 0.0150 % = 0.3335 %
$M_{70/70}$ = 0.1457 % + 0.0067 % = 0.1524 %

$$\frac{0.3335}{0.1524}=\frac{0.7846\times 0.050}{M_{m70/70}\times 0.042}$$

$$M_{m70/70}=\frac{0.7846\times 0.050}{2.188\times 0.042}=0.427$$

The maximum moisture content in the prepreg of GLARE (FM94/S-glas) is 0.4% at 70%RH.

Now, the apparent coefficients a and b in equation (2) can be determined:

$0.785 = a \times 85^b$ and $0.427 = a \times 70^b$

$$\frac{0.785}{0.427}=\left(\frac{85}{70}\right)^b$$

$$b = \frac{\log\left(0.785 / 0.427\right)}{\log\left(85 / 70\right)} = 3.13$$

$$a = \frac{0.785}{85^{3.13}} = 7.02 \times 10^{-7}$$

Equation (2) now becomes:

$$M_m = 7.02 \times 10^{-7} \times RH^{3.13} \qquad (8)$$

Equation (8) describes the dependency of the maximum moisture content on the relative humidity for the investigated GLARE3.

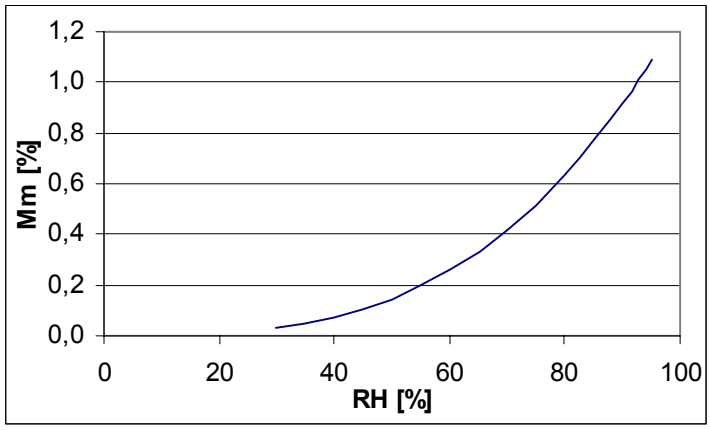

Figure 4.2.4. Maximum moisture content in prepreg related to environmental maximum humidity

For the exposure conditions used in this thesis the following results are obtained for the maximum weight gain (expressed in % of the dry prepreg weight) at different relative humidities :

Relative humidity [%]	70	85	95
Maximum moisture content in prepreg [%]	0.43	0.78	1.09

4.2.3 Determination of diffusion coefficients

If equation (7) is solved for Dyz, the moisture absorption rate at any time during the exposure can be determined. Since the applied temperature is constant for all specimens, the associated diffusion rates should be constant as well (Arrhenius equation). The diffusion rates which belong to the different exposure temperatures are calculated with equation (9) and plotted in figure 4.2.5. The calculated data are contained in tables 4.2.2a-d.

$$D_{yz} = \left(\frac{M_t}{\sqrt{t}} \times \frac{\sqrt{\pi}}{2M_m} \times \frac{l \times b}{2(l+b)} \right)^2 \qquad (9)$$

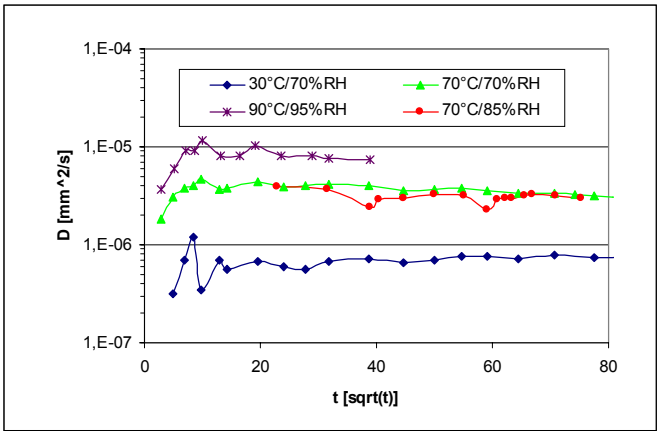

Figure 4.2.5. Diffusion rates in rectangular GLARE3 specimens, 70°C/85%RH obtained from Borgonje [29], data limited to linear diffusion behaviour (ref. fig. 4.2.3)

After initial scatter the diffusion rates converge towards constant values. For the different temperatures it is found with a linear regression of the last three data points for each curve (average):

Temperature [°C]	30	70	90
Diffusion rate GLARE3 [mm^2/s]	7,70x10^{-7}	3.35x10^{-6}	8.63x10^{-6}

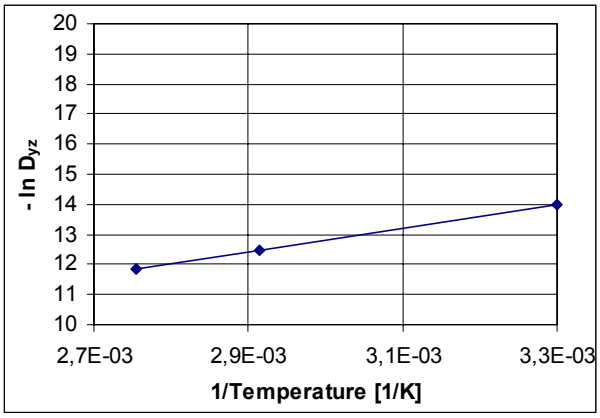

Figure 4.2.6a

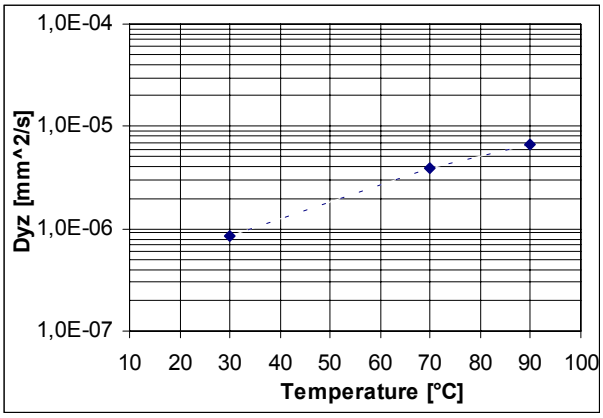

Figure 4.2.6b

Diffusion rates of rectangular GLARE3 specimens.

Figures 4.2.6a and 4.2.6b show the relationship between temperature and the diffusion rate for GLARE3 in different units. The slope of the curve equals the activation energy constant A for the rectangular GLARE3 specimens, refer to equations 1a and 1b of this paragraph:

A = 4316,6 [K]

Equation 1b is solved for the coefficient D_0 for GLARE3:

$$D_0 = D / e^{(-A/T)} \qquad (10)$$

Calculated coefficient(s) for GLARE3:

T [K]	D [mm^2/s]	D_0 [mm^2/s]
303	7,70E-07	1,18E+00
343	3,35E-06	9,77E-01
363	8,63E-06	1,26E+00

The calculated coefficients D_0 for the different temperatures vary slightly. The mean value is calculated with 1.14 [mm^2/s]. Equation (1b) reads for GLARE3:

$$D = 1.14 \times e^{\left(-4317/T\right)} \tag{11}$$

Tensen developed the relationship for diffusion rates in GLARE3 and GLARE2, parallel and perpendicular to the fibers [30]. Although he performed his tests in warm water and with GLARE which contained an AF163/R-glass prepreg, the *ratio* between the diffusion rates is considered to be valid for the FM94/S-glass prepreg as well, since it is linked to a geometrical measure, i.e. the barrier function of the fibers. The factors on diffusion rates are given in table 4.2.3, for 20°C and 60°C. They have a little scatter which is equalized by using the mean values for the present investigation.

Diffusion rate ratios, mean values:

$$\frac{D_{GLARE\,2\,parallel\ \ to\ \ fibers}}{D_{GLARE\,3}} = 1{,}865$$

$$\frac{D_{GLARE\,2\,perpendicular\ to\ \ fibers}}{D_{GLARE\,3}} = 0{,}445$$

Figure 4.2.6 is extended to GLARE2 diffusion rates parallel and perpendicular to the fibers, see figure 4.2.6.

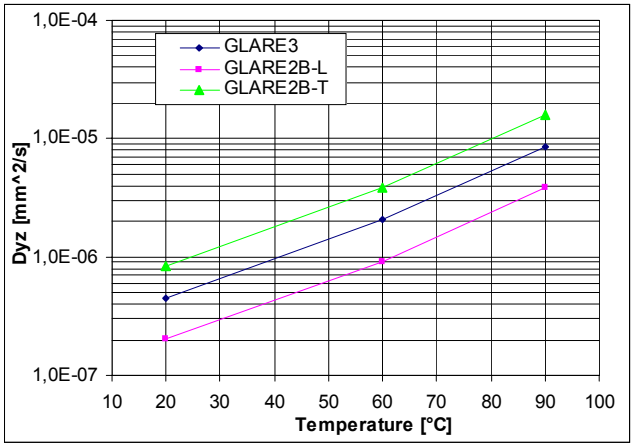

Figure 4.2.7. Apparent diffusion rates related to temperatures for GLARE2 parallel to fibers (e.g. GLARE2B-T) and perpendicular to fibers (e.g. GLARE2B-L)

If calculated with the activation energy 4316,6 [K] (obtained from the GLARE3 analysis), the following apparent diffusion coefficients become available for GLARE2 (equation (9)):

D_0 for GLARE2, parallel to fibers: 2.126 [mm^2/s]
D_0 for GLARE2, perpendicular to fibers: 0.507 [mm^2/s]

Note: The activation energy A is a physical constant related to the resin system, only. It is independent from the prepreg lay-up.

4.3 MRS Accelerated Diffusion, Empirical Investigation

Diffusion coefficients were determined in the previous section for prepreg edges with fibers oriented either parallel or perpendicular to the specimen edges. Along the circumference of a hole, the orientation of the fibers changes continuously. In order to eliminate this variable for the investigation on drilled holes, the Moisture Reference Specimens have been designed. Diffusion coefficients shall be determined from MRS exposed in environmental chambers, for a subsequent recalculation of the weight gain results for the outdoor exposure site. Note that these specimens have not been dried before exposure. Therefore, just the *slope* of the weight gain curve can be representative, not the saturation weight. Figure 4.3.1 shows the regression lines through weight gain data obtained from open hole MRS exposed in three different climates (data recorded in table 4.3.1a-c). The calculation method for the determination of weight gain in the prepreg is given in attachment D. Like the rectangular specimens, also these specimens diffusion follow the Fickean law.

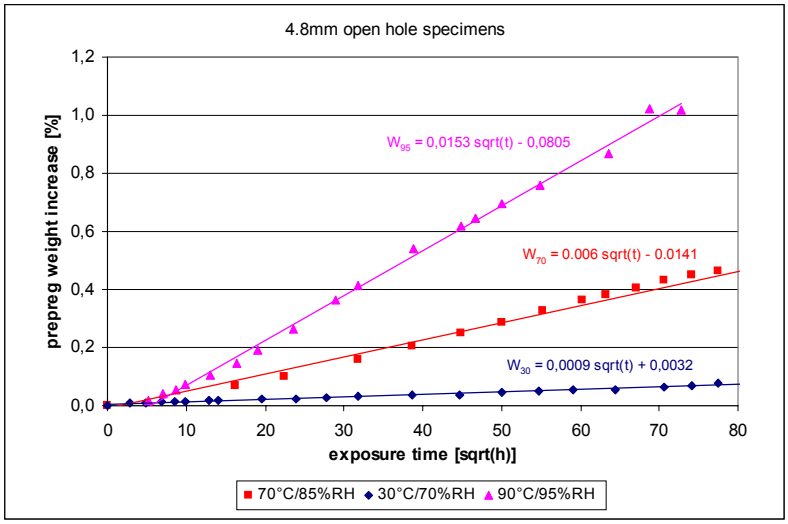

Figure 4.3.1. Accelerated ageing weight gain data for MRS, different climates, non-corrected regression lines
30°C/70%RH: specimen 8-21-H
70°C/85%RH: specimen 8-T2-H
90°C/95%RH: specimen 8-20-H

The geometric constant C in equation (7) is approximated for the edge surface of 25 drilled holes with the circumference 4.8mm x π. For simplification the width b and the length l are set equal to the quarter of the hole circumference:

b = l = 4.8 x π / 4 = 3.77mm

Geometric constant C:

$$C = (\frac{\sqrt{\pi}}{4}) \times 25 \times \frac{l \times b}{l + b} = 20.88$$

With the information of the maximum possible moisture content in the prepreg (figure 4.2.4) the diffusion rates D through the drilled holes can be approximated:

$$D = \frac{M_t \times 20.88}{\sqrt{t} \times M_m}$$

Figure 4.3.2 shows the diffusion rates for the different climates. As expected, they converge to a constant value after some exposure time. Note that the dry prepreg weight of the MRS at the beginning of the test is a calculated value, since no other procedure is possible. The relation between the diffusion rates and the temperature can be established (mean value from measurements between 1500 and 4000 hours exposure). Kröber performed a one dimensional regression analysis and solved equation (3) for D [38]. Details will be discussed in chapter 4.4. He found diffusion rates in the same order of magnitude as found with the above presented simple approach, see figure 4.3.3.

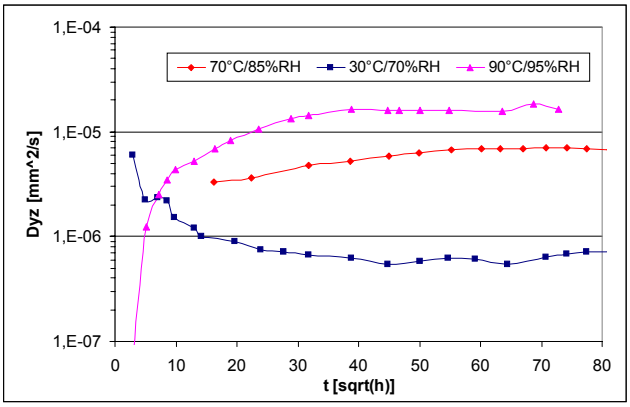

Figure 4.3.2. Diffusion rates in open hole MRS, GLARE3, approximation as expl. on previous page
$D_{30°C}$ = 5.84E-07 [mm²/s]
$D_{70°C}$ = 6.29E-06 [mm²/s]
$D_{90°C}$ = 1.61E-05 [mm²/s]

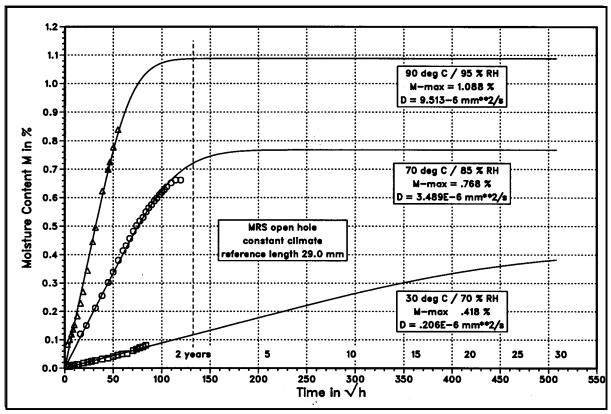

Figure 4.3.3. One dimensional regression analysis for diffusion rates in open hole MRS [38], GLARE3, tested values (dots) and calculation (lines),
$D_{30°C}$ = 2.06E-07 [mm²/s] [38]
$D_{70°C}$ = 3.49E-06 [mm²/s] [38]
$D_{90°C}$ = 9.51E-06 [mm²/s] [38]

The difference of the results is considered to be a result of the simple approximation of the geometric constant C for the hole. The Arrhenius equation for the drilled hole in GLARE at constant temperature is solved with:

$$D_{MRS} = 3110 \times e^{(-7109/T)} \quad \text{[38]} \qquad (12)$$

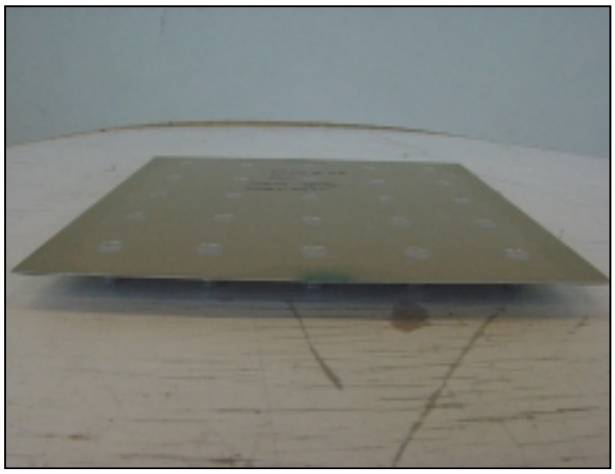

Figure 4.3.4. Specimen 8-8-F

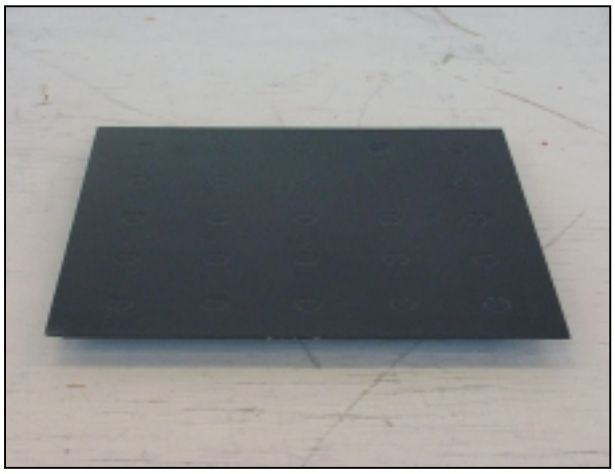

Figure 4.3.5. Specimen 8-9-PF

The determined coefficients are obtained with open hole specimens. The influence of installed countersunk aluminium Lok-Bolts (filled holes, clearance fit, specimen 8-8-F) is investigated for a better representation of an aircraft structure. Specimen 8-9-FP has been painted *after* fastener installation,

coincidently. It should behave similar in an environmental chamber, as an non-drilled specimen. No weight gain was expected .

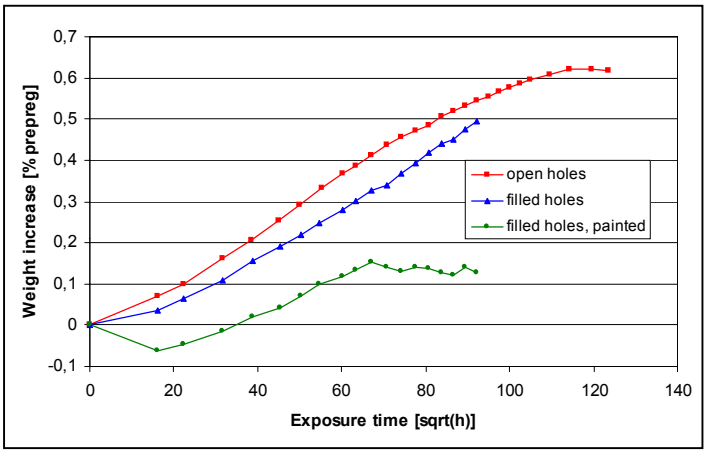

Figure 4.3.7. Accelerated ageing weight gain results, 70°C, 85%RH, specimens 8-T2-H, 8-8-F and 8-9-PF

The weight of the unpainted filled hole specimen (8-8-F) decreased at the beginning of the test, until 260 hours. Thereafter, the weight gain slopes of all specimens differ just slightly.

Weight increase / exposure time:
Open hole specimen: 6.00E-03 [%/√h]
Filled hole specimen: 5.63E-03 [%/√h]

A weight gain rate reduction of 6.2% is determined for a clearance fit filled hole compared with an open hole.

The behavior of the filled hole painted specimen is not according to the expectations. After 260 hours (16.12√h, first measurement) the specimen weight had dropped 0.061g. Thereafter, between 260 and 4508 hours (67.03√h) the specimen weight increased with a slope of 4.65E-03 [%/√h]. Above 4508 hours the weight remained almost constant.
Since the drilled holes and fasteners in specimen 8-9-PF are completely covered with the surface protection system, they are not considered to influence the weight gain results. Consequently the differences in weight are linked to processes happening in the paint. The weight reduction is obviously caused by a chemical reaction. If so, it may be concluded that the drying process of the paint system can continue also for aircraft exposed to high temperatures. The subsequent weight increase indicates diffusion into the paint, which is also epoxy based. Coincidently the weight gain into the paint is of the same order of magnitude as through the drilled holes. After approximately 4500 hours exposure at 70°C the paint is saturated.

It should be remembered that a paint system is applied on the outdoor exposure specimens for corrosion prevention. A dark blue color was selected in order to improve high solar heating. Now, after the accelerated exposure results obtained from specimen 8-9-PF, it appears that another variable has to be considered for the evaluation of the outdoor results, the drying and moisture absorption behaviour of the paint.

Weight gain results from specimens 8-8-F and 8-9-F are stored in table 4.3.2.

4.4 Moisture Concentration around GLARE Drilled Holes after Accelerated Ageing

The application of Fick's law for a through-the-thickness moisture diffusion analysis in composites has been established by Shen and Springer, [5]. Whitney verified that the total weight gain for a three-dimensional case is simply the product of three one-dimensional solutions for the total weight gain [39]. The same is true for the two-dimensional case, as investigated for the FML-application by Куснецов [40]. A simplification of the problem would be achieved, if the one-dimensional diffusion kinetics and the computer software W8GAIN, which was written by Springer for this problem, could be applied for GLARE at drilled holes.

Springers software allows for the calculation of the moisture concentration at any point in a one directional coordinate system after exposure time t. Figure 4.4.1 specifies the dimensions l and b of each prepreg which is sandwiched between two aluminium sheets in GLARE, for example in the weight gain specimens discussed in the previous chapter. Moisture penetrates through the entire lengths of the edges, in directions y, -y, z and -z. The two-dimensional calculation considers an influence of both penetration directions on the prepreg locations in the center of the specimen. However, if l>>b, the diffusion kinetics reduce to a one-dimensional problem at cross section y=l/2. With the equation for two-dimensional diffusion (13) and the diffusion coefficients determined in chapter 4.3 for GLARE3, the moisture concentration at any location z and –z for cross section y=l/2 can be calculated for different relations l/b, refer to literature [40].

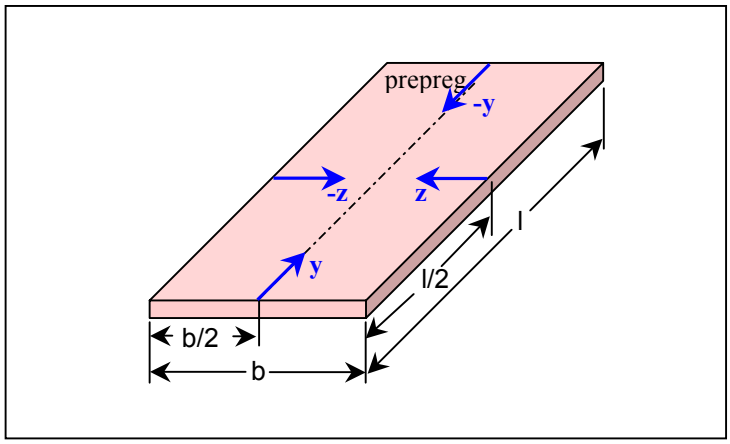

Figure 4.4.1. Rectangular prepreg between aluminium sheets (not shown) and definition of diffusion directions y and z

$$\frac{M_m - M}{M_m - M_0} = \frac{64}{\pi^4} \sum_{n=0}^{\infty} \sum_{m=}^{\infty} \frac{1}{(2n+1)^2 \times (2m+1)^2} \times e^{-\pi^2 \times \left[(2m+1)^2 \times D_y / l^2 + (2n+1)^2 \times D_z / b^2\right] \times t} \qquad (13)$$

Figures 4.4.2 and 4.4.3 compare the moisture concentration after a range of exposure times for two rectangular GLARE3 specimens of different sizes. For equal values of the exposure time t and coordinate z (at y=l/2), the relative moisture concentration c/c_m is lower for the higher l/b ratio specimen.

Examples:

c/c_m for l/b = 100mm/25mm specimen at z = 5mm after 3 month exposure: 0.43

c/c_m for l/b = 60mm/40mm specimen at z = 5mm after 3 month exposure: 0.52

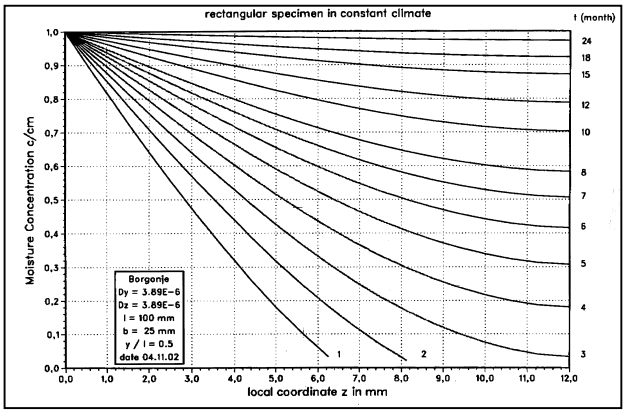

Figure 4.4.2. Moisture concentration in local direction z at y=l/2, GLARE3, l=100mm, b=25mm, 70°C/85% RH constant environment [38]

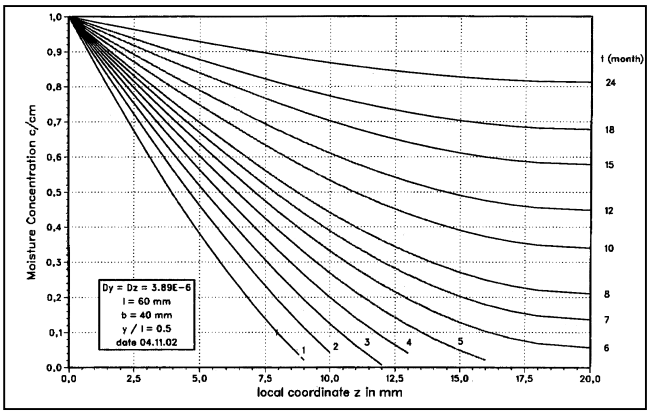

Figure 4.4.3. Moisture concentration in local direction z at y=l/2, GLARE3, l=60mm, b=40mm, 70°C/85% RH constant environment [38]

The influence of the moisture absorption in directions y and –y on the prepreg cross section l/2 is more significant for the specimen with the lower length and the greater width. An approximation of the required specimen ratio length / width for a close approximation of one-dimensional diffusion is performed for the constant climate 70°C/85%RH:

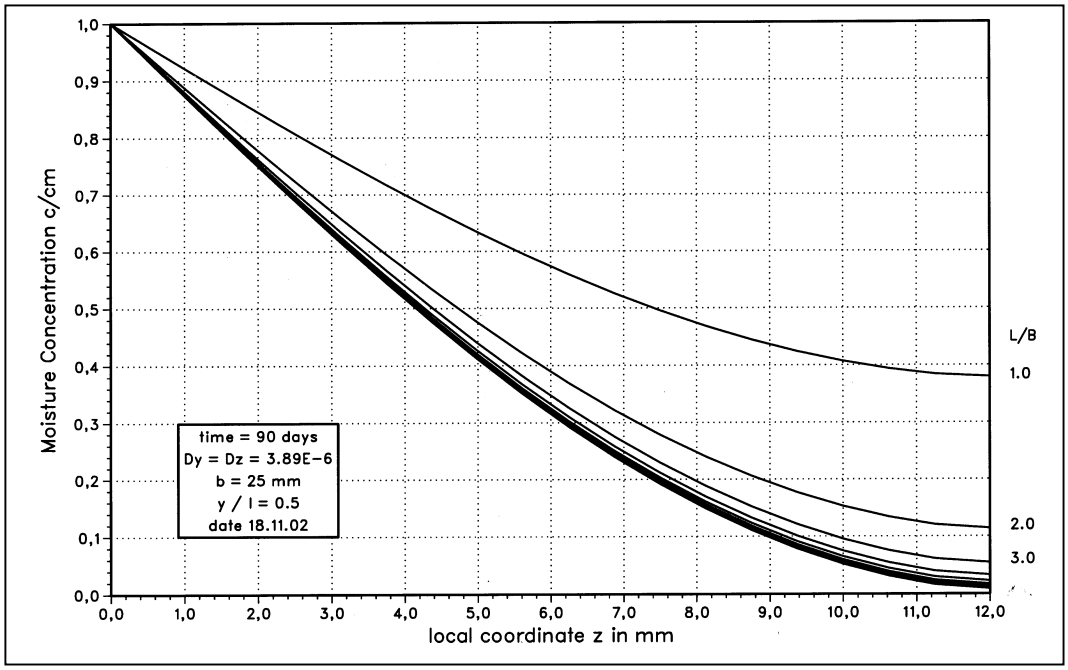

Figure 4.4.4. Moisture concentration at location y=l/2 in direction z for different length/width ratios and a constant width of 25mm [38]

The calculation results presented in figure 4.4.4 show that an influence from the short edges on the cross section l/2 is present for specimen length lower than 4 times the width. Consequently the *one-dimensional* prediction method can be used for specimens where l>4b. It is recommended for future weight gain tests with rectangular GLARE specimens, to use a length/width ratio of 100mm to 25mm or larger, but always with a length/width ratio >4.

In a second step the calculation method is calibrated with the weight gain curve for specimen MRS 8-T2-H, i.e. for the 70°C/85%RH environment, see figure 4.3.1. It is the target to predict the weight gain of a hole with the one-dimensional model as well. The diffusion kinetics in the center cross section of the rectangular specimens, (two entry points for moisture in the laminate, z and –z), are considered to be

similar between two holes. The geometrical model for a one dimensional calculation between two drilled holes is illustrated in figure 4.4.5. Weight gain calculations are performed for different reference width b', e.g. for 23.2mm, which equals the distance from one hole edge to the other, for drilled holes in a line. For the diagonal case, the nominal width between the holes equals 39.6mm. More calculations have been performed by trial and error in order to assess the measured weight gain curve.

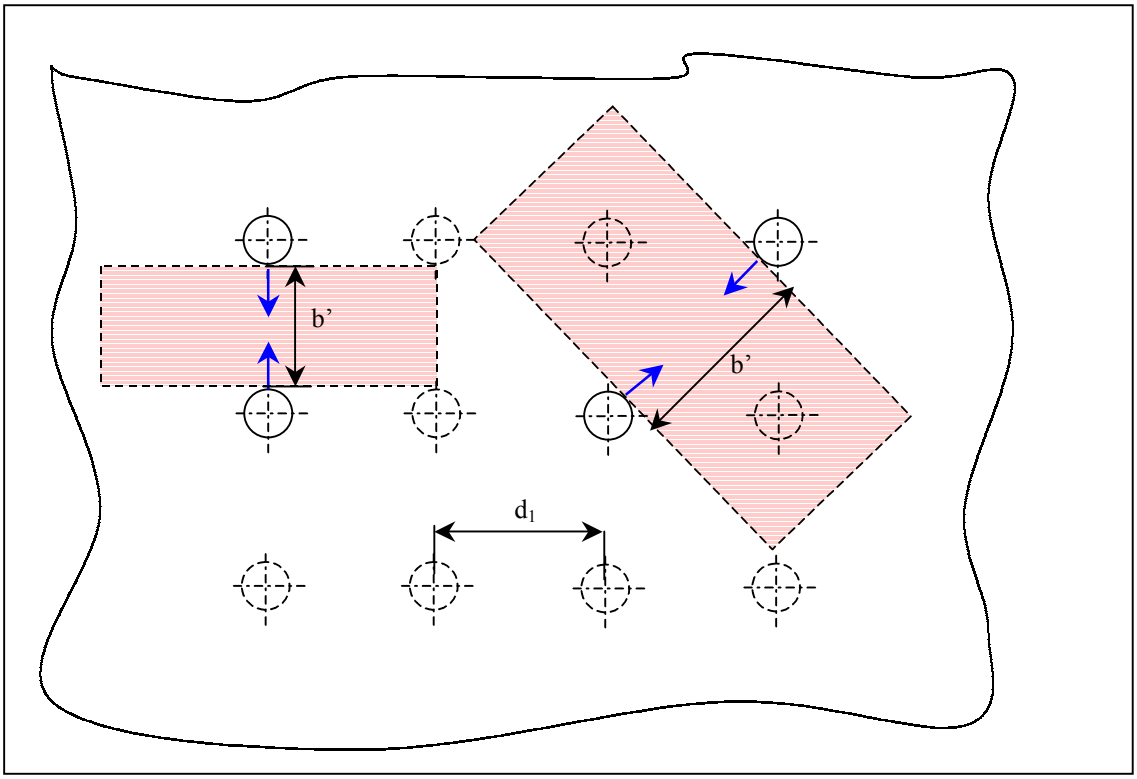

Figure 4.4.5. One dimensional approximation of moisture diffusion for bore holes withindicated rectangular specimens shown, illustration of reference width b'

27.92mm turned out to be the width with which the weight gain of MRS no. 8-T2-H can be simulated, a value very close to the nominal bore hole pitch (figure 4.4.6). The simulation width 27.92mm provides an empirical *mean* value for the determination of local moisture concentrations around the hole.

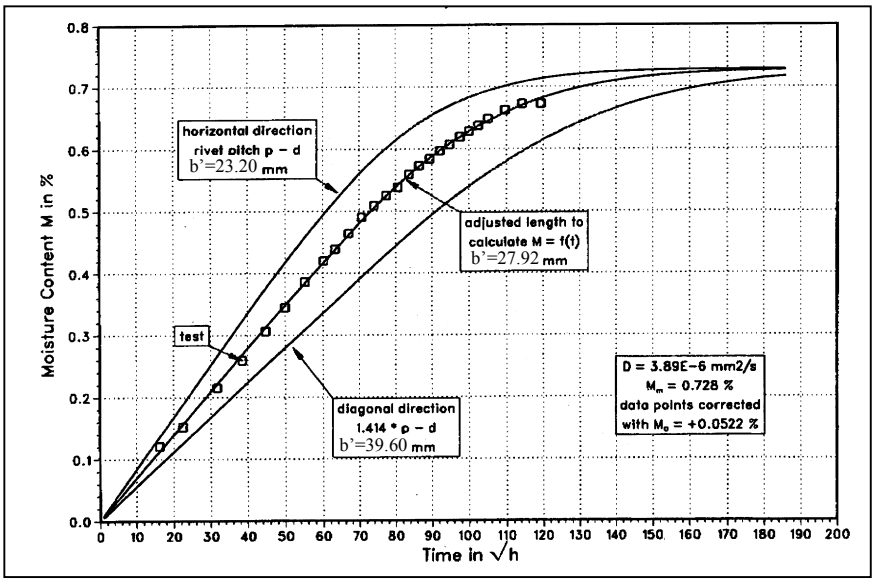

Figure 4.4.6. Moisture content as function of time for MRS 8-T2-H, 70°C/85%RH, for different reference widths b' for the simulation of diffusion through drilled holes [38]

The moisture concentration at a given distance from the bore hole edge will decrease slower in the direction of the shortest distance between two holes, compared with the mean value, since the diffusing moisture of the two drilled holes will meet after a relatively short time. The decrease is fastest for the diagonal direction between two holes. Here, it takes longer until iso-concentration lines from the two concerned holes will interfere.

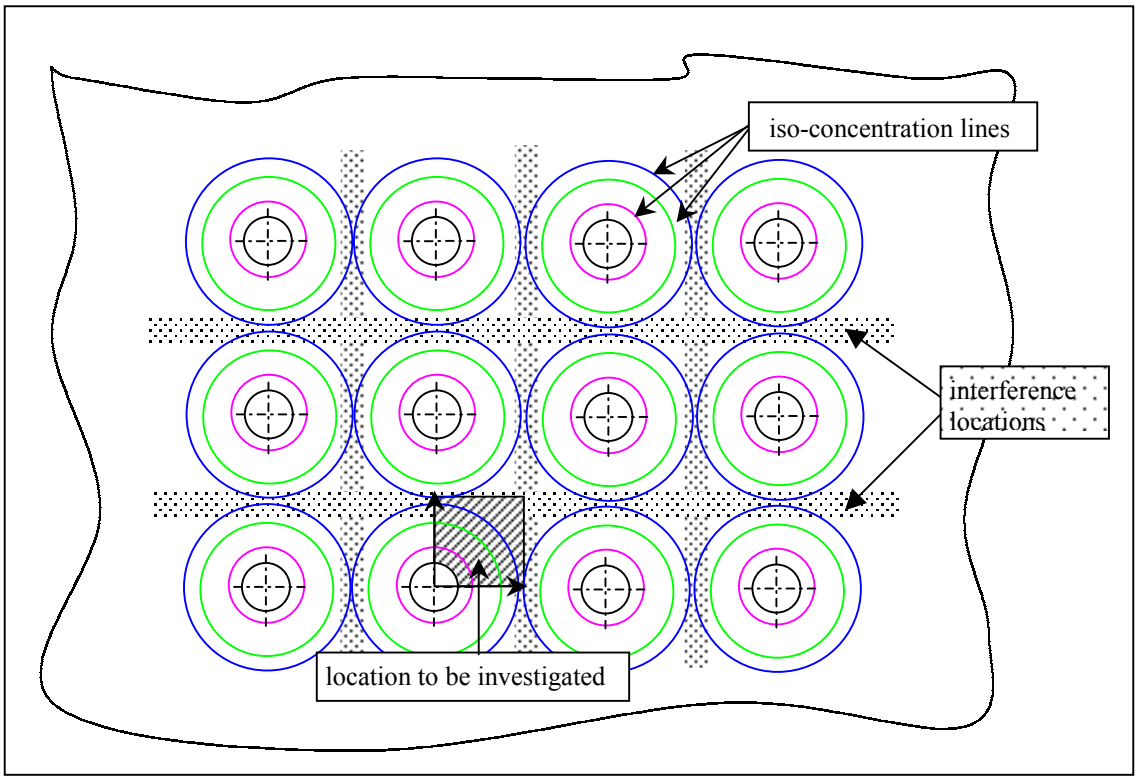

Figure 4.4.7.Top view on rivet field with 12 drilled holes with iso-concentration lines

Moisture enters from each of the hole edges and diffuses in all directions around the circumference. The diffusion rates in the different directions are dependent on the GLARE type and on the environmental and geometrical details, e.g. the hole diameter and the hole pitch. Iso-concentration curves from different holes meet in the so-called `interference locations´ (figure 4.4.7). The limits of the empirical calculation model are reached from the moment interference occurs.
This chapter and chapter 5 discuss the moisture concentration for one quarter of a hole (see grey shaded section in figure 4.4.7), which is located in a rivet field. The analysis are performed in order to understand the prepreg condition of drilled holes in structural specimens, which will be discussed in the following chapters.

As explained above, the weight gain for a moisture reference specimen with a hole diameter of 4.8mm and hole pitches of 28mm in x- and y-direction , exposed to a 70°C/85%RH environment, can be calculated with a one-dimensional diffusion model, when a reference width b'=27.92mm is used.

b' = 27.92mm for D=4.8mm and d=28mm in GLARE3 at 70°C/85%RH

The moisture concentration around the circumference of a hole varies continuously for two reasons, i.e. the changing fiber orientation and the influence of other fastener holes in the vicinity. If the first effect is neglected for simplification reasons, the moisture concentration along the radius follows equation (13) for GLARE3 due to the influence of the adjacent bore holes:

$$c_\alpha = \frac{1}{2}(c_0 + c_{45}) + \frac{1}{2}(c_0 - c_{45}) \times \cos(4\alpha) \quad (13)$$

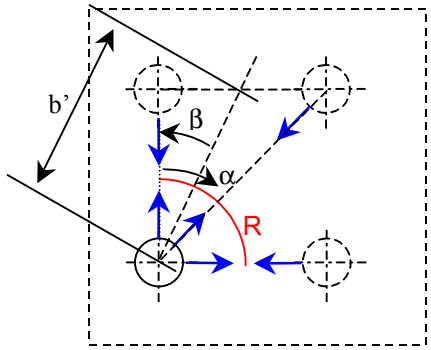

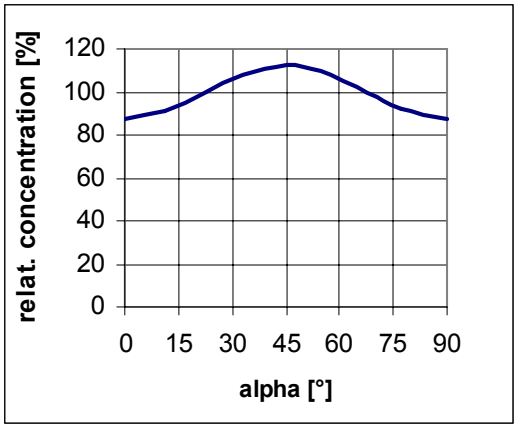

Figure 4.4.8. Relative moisture concentration distribution along at distance R around GLARE3 hole

If the reference width b' is considered as mean value for the correct weight gain prediction for the given geometry, it is representative for the moisture concentration at $\beta = \alpha/2$.

For $d_1=d_2$ (figure 4.4.5): $\beta = 22.5°$ and $\beta = 67.5°$ (for GLARE3).

The relative concentration c_b is directly related to the reference width b' and equals 100% at β. At different angles but constant distances from the drilled hole edge, the moisture concentration varies dependant on the distance to the next hole (simplified one-dimensional approach). The moisture concentrations at 0° (parallel to one fiber orientation in GLARE3) and 90° (parallel to the other fiber orientation in GLARE3) can be calculated by using the width:

$$b_{0,90} = b' \times \cos\beta \quad (14)$$

For the 45 degree direction it can be calculated with:

$$b_{45} = b_{0,90} / \cos 45 \quad (15)$$

One unpainted MRS (8-14-H56) was drilled with 5.6mm bore holes and exposed in the 70°C/85%RH environmental chamber. A slightly increased diffusion rate was expected, compared with the 4.8mm hole diameter specimens. However, after 4127 hours exposure (the weight gain experiment still continues) no considerable difference between the weight gain curve slopes was found.

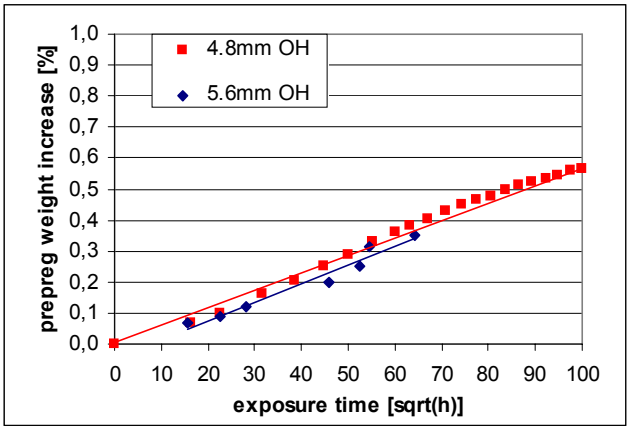

Figure 4.4.9. Weight gain comparison of MRS with 4.8mm and 5.6mm drilled holes, respectively

The characteristic widths for different geometries of specimens are calculated with the following distances [38]:

hole diameter D	hole distances d *	b' at α = 22.5°	$b_{0,90}$	b_{45}	application
4.8mm#	28.0mm	28.0mm	25.9mm	36.6mm	GLARE3, MRS
4.8mm	22.7mm	22.7mm	21.0mm	29.7mm	GLARE2B specimen

results equal almost 5.6mm drilled hole diameter * see figure 4.4.5, here: $d_1 = d_2$

The present analyses is limited to GLARE3 and GLARE2. Moisture concentration predictions for drilled holes in GLARE 4 require weight gain tests with GLARE4 specimens. However, taking the barrier function of the particular prepregs into account, lines of equal concentration for GLARE4 are expected to be between those for GLARE2 and GLARE3, see figure 4.4.10.

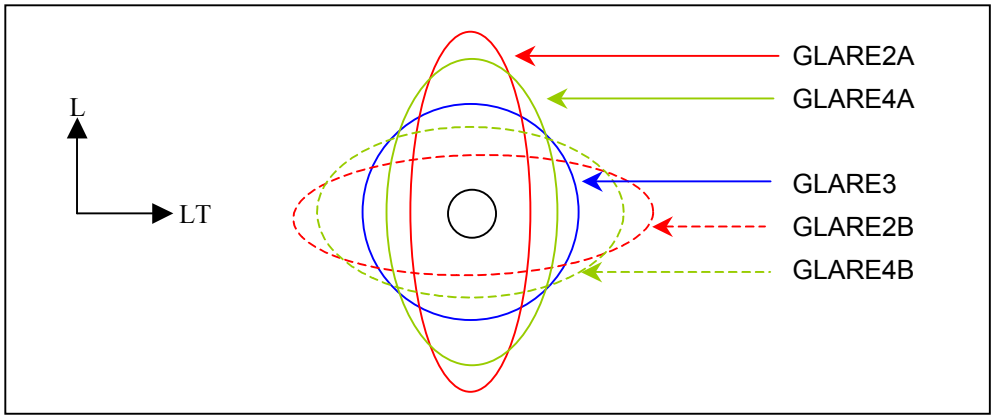

Figure 4.4.10. Iso-concentration lines around bore hole for different GLARE types, principle

Note that the method which is presented here is empirical but conservative concerning the diffusion depth around the hole. The weight increase due to moisture at a drilled hole is measured for *defined* exposure conditions and related to a one-dimensional diffusion calculation and a penetration cross section which equals the hole perimeter (constant C). Subsequently predictions are made for non-tested conditions by using the one-dimensional calculation for any direction around the perimeter. Since the area of the prepreg that will be moisturized increases with the radial distance from the hole, an effect that is not taken into account, all calculated diffusion depth for particular moisture concentration levels are slightly exaggerated. More detailed analysis may be possible with finite element models.

Approximated diffusion distribution around a drilled hole in GLARE3

- open hole, no fastener
- hole diameter: 4.8mm
- hole pitch in both directions: 28mm
- environment : humid air, 70°C, 85% RH

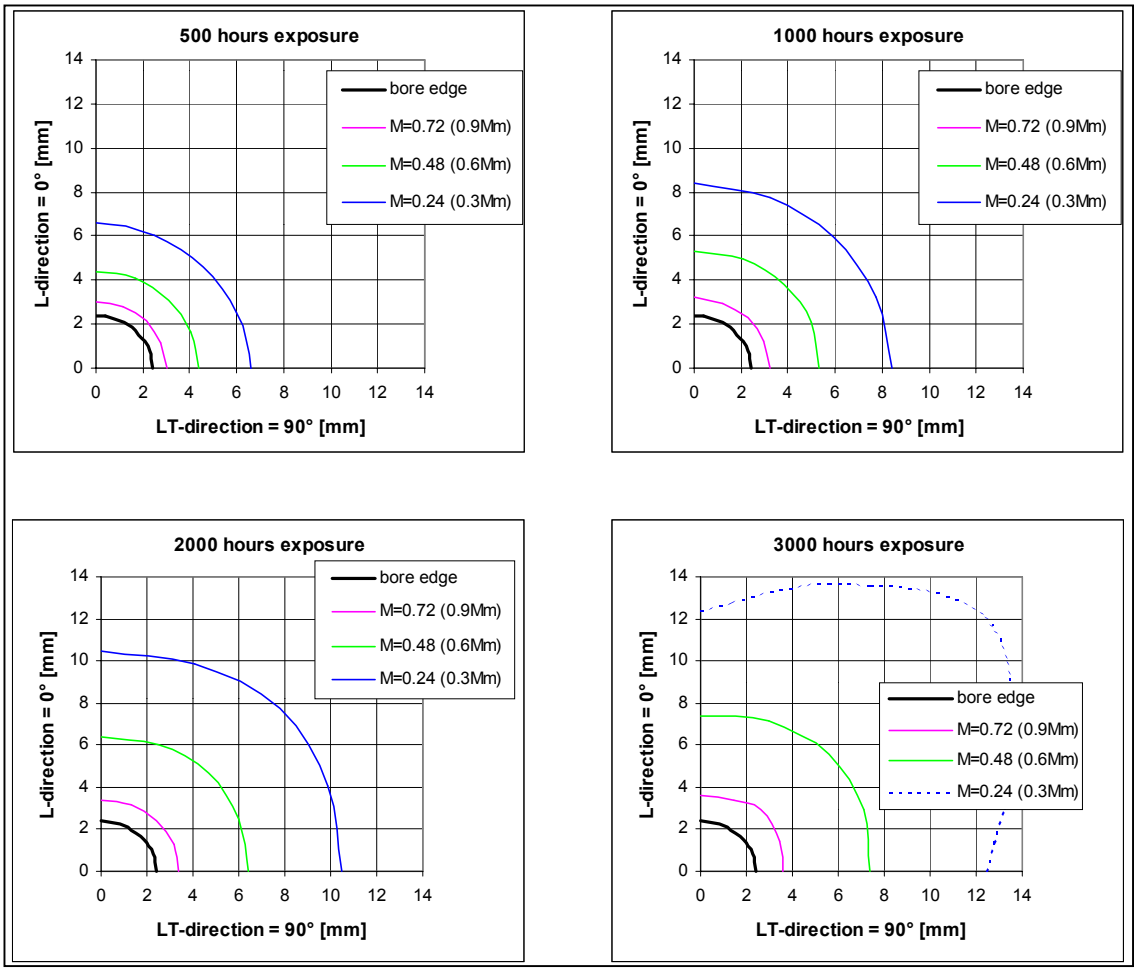

Figure 4.4.11. Approximated moisture distributions around an open GLARE3 bore hole after exposure in a 70°C/85%RH environment, Mm=0.78%, bore hole distances 28mm, different exposure times, the dotted line indicates a calculation result outside the validity of the applied empirical method. The one-dimensional moisture concentration plots used to construct these curves are contained in appendix L.

Each of the diagrams contained in figure 4.4.11 covers an area of 14mm to 14mm, which equals half a fastener pitch and half a rivet row pitch, respectively. The center of the investigated hole is located at [x,y] coordinate [0,0], with a quarter hole edge at a radius of 2.4mm. The diagonal of the x-y-diagram equals 19.8mm. The moisture which penetrates through the investigated hole interferes with the diffusion through the adjacent drilled holes at [x,y]-locations [0,28], [39.6,39.6] and [28,0]. The effect is visible in the diagram for 3000 hours exposure time. The iso-concentration line for concentration 0.24% already interfered with those coming from the holes at locations [0,28] and [28,0], but not or to a lower extend with the moisture coming from the hole at the diagonal position [39.6,39.6]. The moisture can still travel unaffected from the other holes in diagonal direction, but in direction x and y it can not. That's the reason why the blue line, which represents a moisture content of 0.24% prepreg weight, has no continuous radius around the hole any more but is bulging out in diagonal direction.

The progressing of the particular concentration lines in time is shown below:

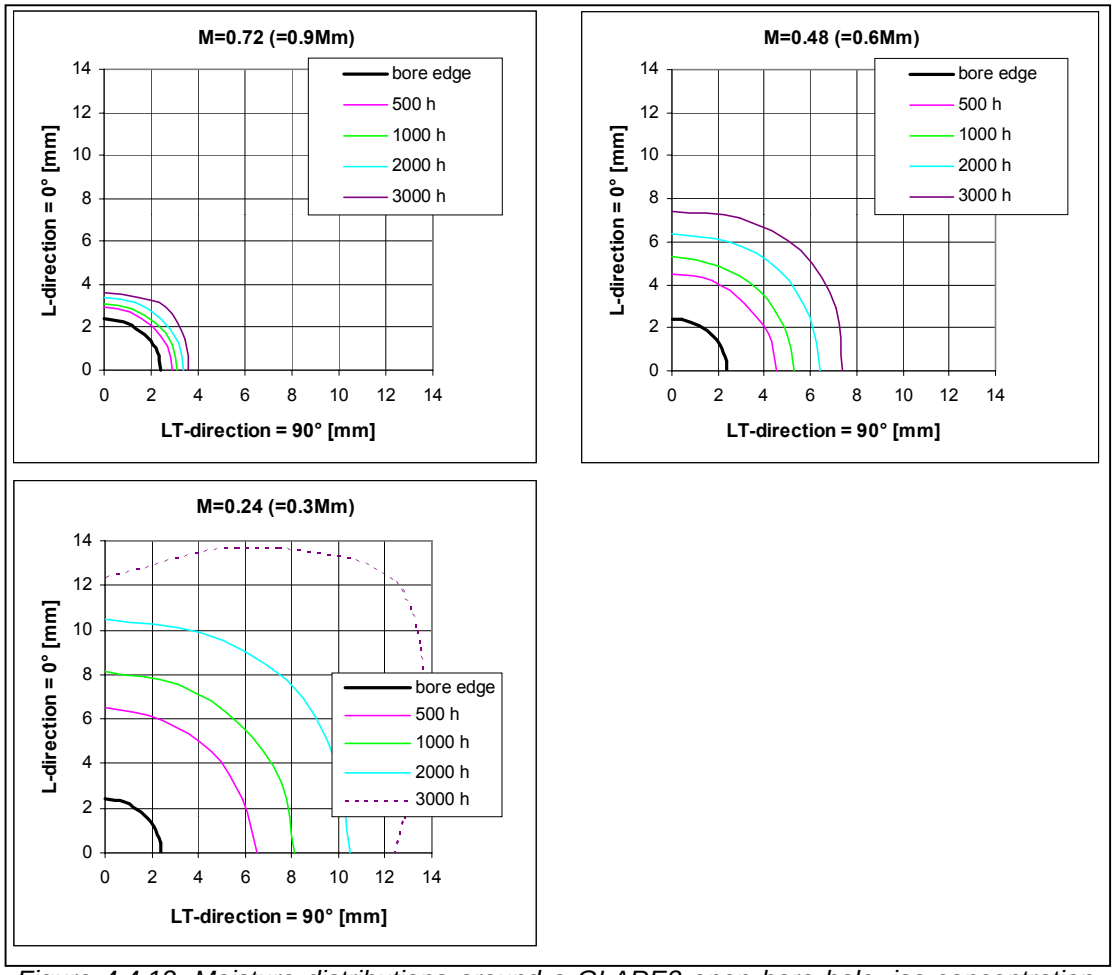

Figure 4.4.12. Moisture distributions around a GLARE3 open bore hole, iso-concentration lines as function of exposure time, environment humid air, 70°C/85%RH (Mm=0.78%), the dotted line indicates a calculation result outside the validity of the applied method

Approximated diffusion distribution around a hole drilled in GLARE3

- clearance fit fastener
- hole diameter: 4.8mm
- fastener pitch distance and rivet row distance: 28mm
- environment : humid air, 70°C, 85% RH

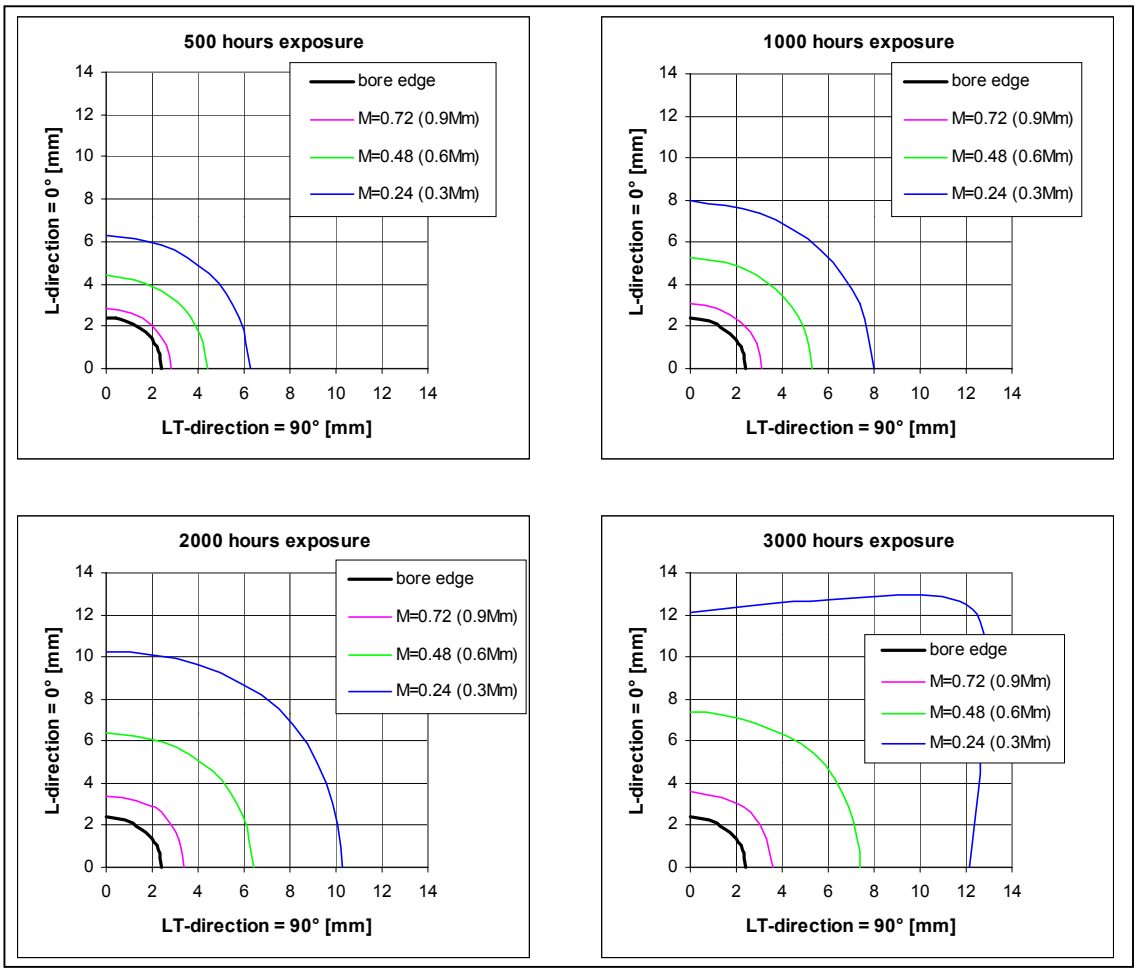

Figure 4.4.13. Approximated moisture distributions around a filled GLARE3 bore hole after exposure in a70°C/85%RH environment, Mm=0.78%, bore hole distances 28mm, different exposure times. The one-dimensional moisture concentration plots used to construct these curves are contained in appendix M.

As shown in figure 4.3.7, the weight gain decreases if a fastener are installed in the drilled holes. The influence of this reduction is considered by an assessment of the weight gain curve and the calculation of the associated b'-values.

Worth noticing are the iso-concentration lines for 3000 hours ageing and 0.72% prepreg weight. This line has already reached the interference location for the specimen without fastener – for the specimen with fastener it is still comfortably located within the half hole pitch of 14mm x 14mm.

Approximated diffusion distribution around holes drilled in GLARE3

- open hole, no fastener
- hole diameter: 4.8mm
- hole pitches in both directions: 22.7mm
- environment : humid air, 70°C, 85% RH

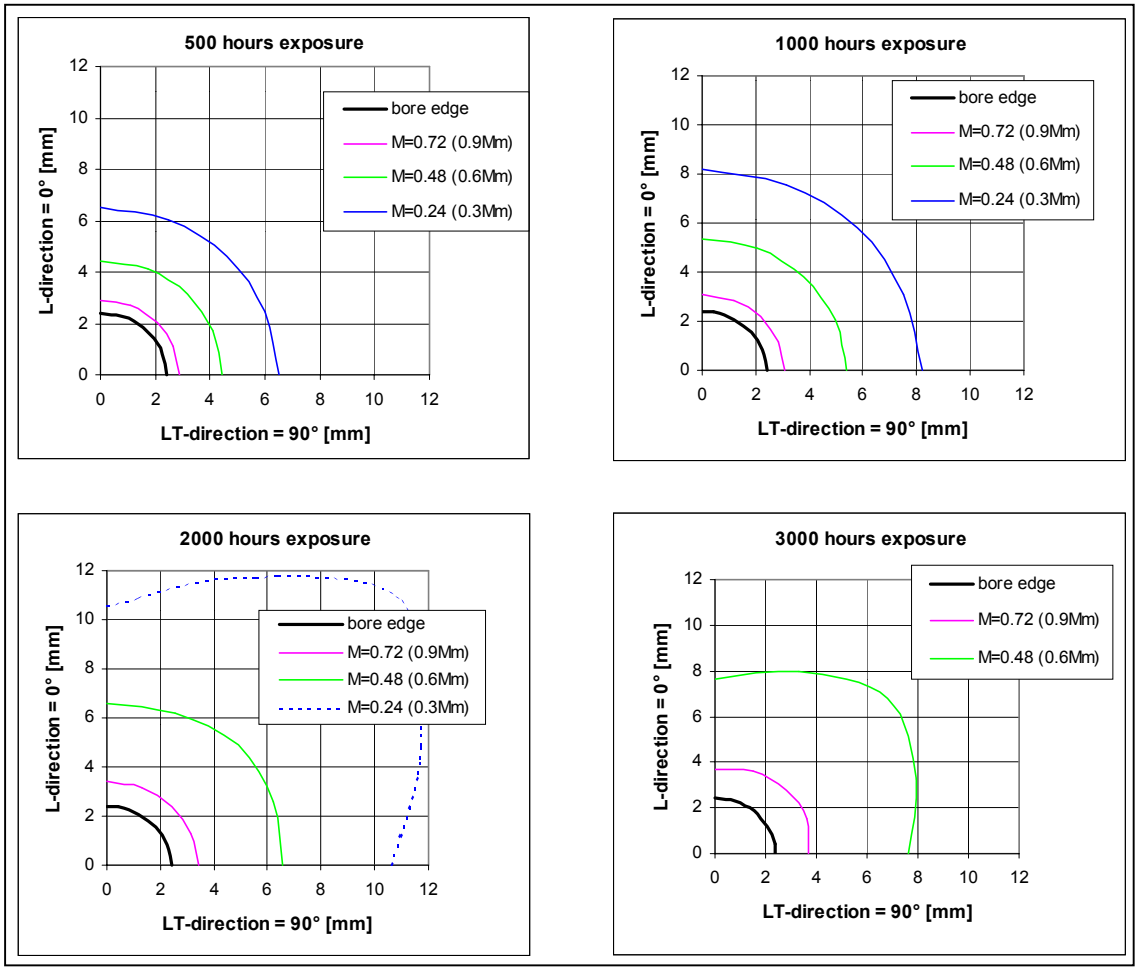

Figure 4.4.14. Approximated moisture distributions around an open GLARE3 bore hole after exposure in a 70°C/85%RH environment, Mm=0.78%, bore hole distances 22,7mm, different exposure times, dotted line indicates calculation results outside the validity of the applied method.The one-dimensional moisture concentration plots used to construct these curves are contained in appendix N.

In a field of drilled holes with distances of 22.7mm to each other, the iso-concentration lines expanding from the different holes meet earlier at the half net section, compared with a field of greater hole pitches. Note that the diagrams 4.4.14 are limited to 12mm in x- and y-direction, since the half rivet pitch is 11.35mm (16.05mm in diagonal direction). Due to the shorter distances from hole to hole, the 0.24% prepreg weight iso-concentration curve exposure already approaches the interference location after 2000 hours. After 3000 hours exposure, this concentration level is not present any more. More complex analysis would be required to determine the exact moisture level in the interference location. For the present investigations it is sufficient to know, that the entire area outside the 8mm x 8mm square has got a concentration level of ≤ 0.48% of the dry prepreg weight after 3000 hours accelerated exposure.

Approximated diffusion distribution around a hole drilled in GLARE2B

- open hole
- hole diameter: 4.8mm
- fastener pitch distance and rivet row distance: 22.7mm
- environment : humid air, 70°C, 85% RH

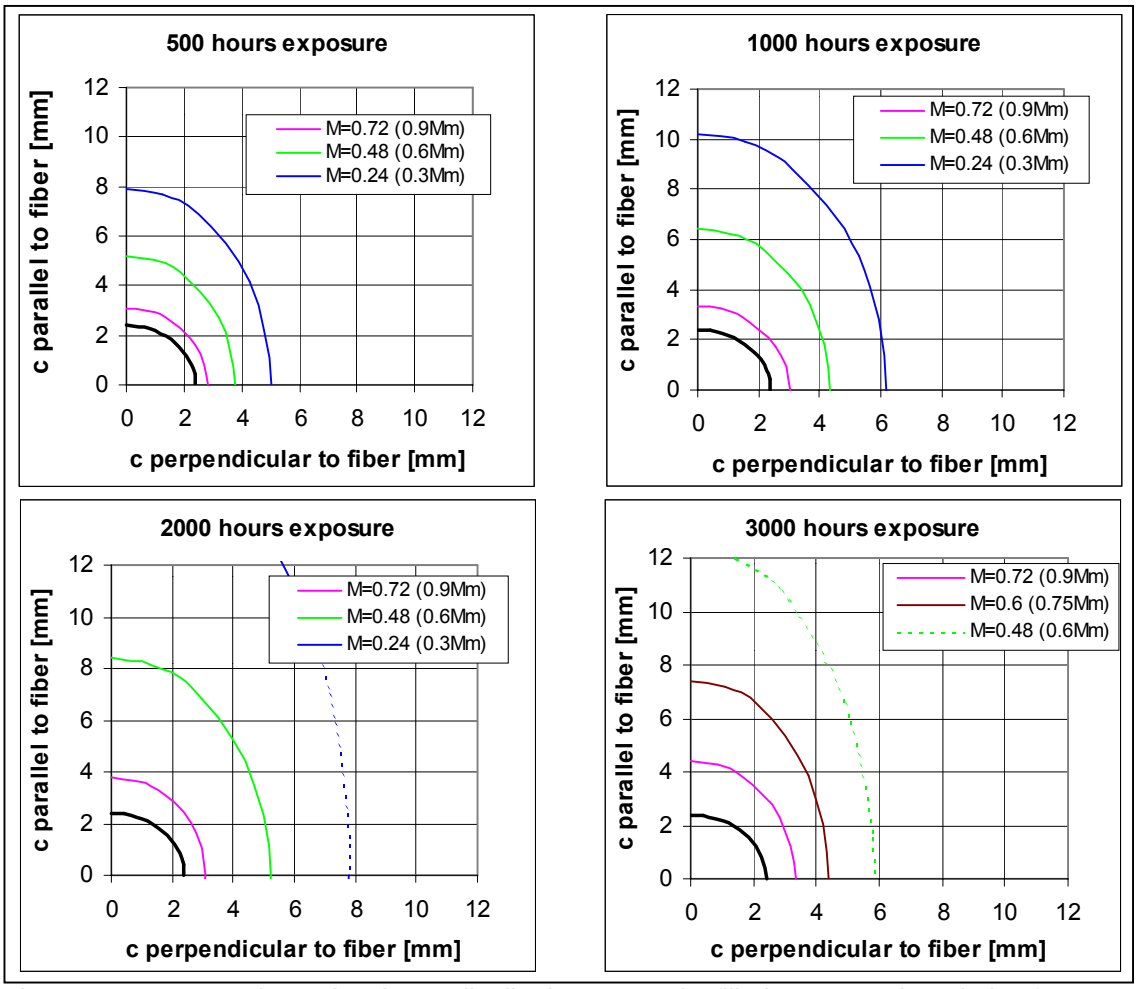

Figure 4.4.15. Approximated moisture distributions around a filledGLARE2B bore hole after exposure in a 70°C/85%RH environment, Mm=0.78%, bore hole distances 22.7mm, different exposure times, dotted line indicate calculation results outside the validity of the applied method

4.5 τ-γ-Specimen for Diffusion Depth Identification

For the interpretation of fatigue crack propagation tests it is valuable to identify the diffusion depth around a drilled hole for a particular exposure treatment. In the worst case, if the diffusion depth would equal both, a half rivet pitch and a half rivet row pitch, respectively, the entire rivet field would be considered. Dependant on the obtained moisture concentration, an effect on the adhesive forces in the laminate could influence the crack propagation rate significantly.

The open hole thick adhered specimen is designed to indicate a loss of shear strength in either the prepreg or the metal/prepreg interface at a distance of a half rivet pitch from the drilled hole, if the moisture travels so far. The bonded area equals 23mm x 23mm, representing a rivet pitch and rivet row distance associated to a 4.8mm hole. Peel forces are avoided as far as possible.

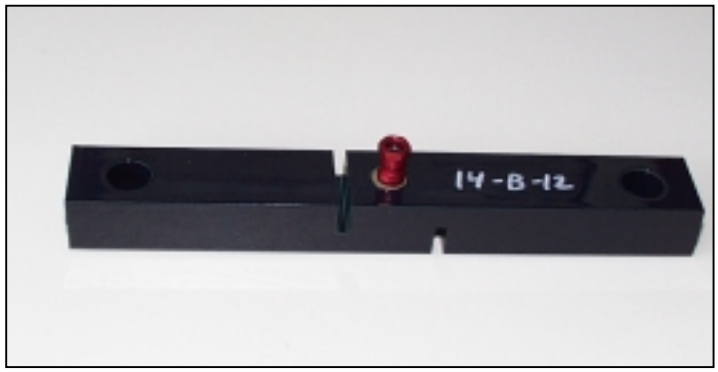

Figure 4.5.1. Thick adhered open hole specimen (fastener installed during exposure, only)

A linear elastic finite element calculation was conducted, using computer software STRESSCHECK® for the verification that the overlapping ends being the critical location. This is a prerequisite for the determination of the diffusion depth.

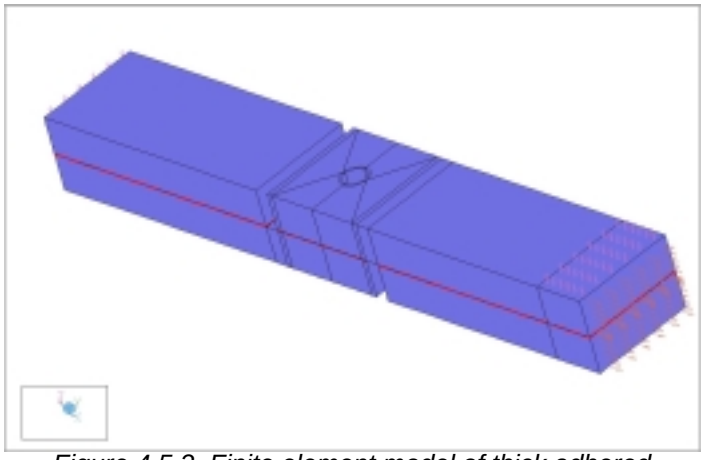

Figure 4.5.2. Finite element model of thick adhered specimen

The FE-program model is used to perform static simulations considering non-linear displacements (secondary bending) and non-linear material behaviour. The model geometry matches the test specimen geometry cut at both ends next to the load introduction holes. The rivet is not modelled because it is only attached during exposure, as contribution to reality. A linear elastic material model is selected for the bar material (aluminium, 2024). The bars are connected by a bonded prepreg (FM94/S-glass), which is modelled as a whole (not separated in matrix and adhesive layer, see thin red-coloured layer in figure 4.5.2) with an elastic-plastic material model (exemplary 5-parameter-model). The specimen is fully restrained at one end and in the axis direction of the open hole on the top of the other end, where also the axial load is introduced. The geometry is modelled by a small number of solid p-elements with high order. The prepreg layer is simulated by co-located elements in three levels. This way, plots of particular element levels allow to identify local stresses close to either the upper of the lower metal sheet.

Figures 4.5.3 and 4.5.4 show tensile stresses in the prepreg parallel to the load direction and shear stresses, respectively. The applied load is 15000 N. If compared with the hole location, the high stresses at the edge of the prepreg clearly validate, that the edge is the critical area. Consequently, any influence

of ageing on shear strength should be linked to the edge shear failure, which indicates the diffusion depth.

The fasteners which have been installed during the exposure period (see figure 4.5.1.) are removed prior to the tensile test. Via bolts inserted in the 12mm holes at the edges, specimens 14-B-1 to 14-B-4 and 14-B-6 to 14-B-12 are pulled to failure according to specification DIN54451, using a servo-hydraulic test machine. The loads at which the specimens sheared to failure are recorded in table 4.5. The average failure load for the dry specimens is 15566 N, after 3000 hours ageing in a 70°C/85%RH environment it dropped to 14470 N (average). A strength reduction of 7% is observed due to the accelerated ageing process. Since the highest shear- and tensile stresses occur on the prepreg edges, it can be concluded that this location is the origin of failure. The strength reduction indicates that moisture penetrated through the filled hole along a distance of 9.1mm, parallel to the fibers. For all specimens a failure in the prepreg is observed, i.e. either cohesive (failure in matrix) or adhesive at the fiber/resin boundary.

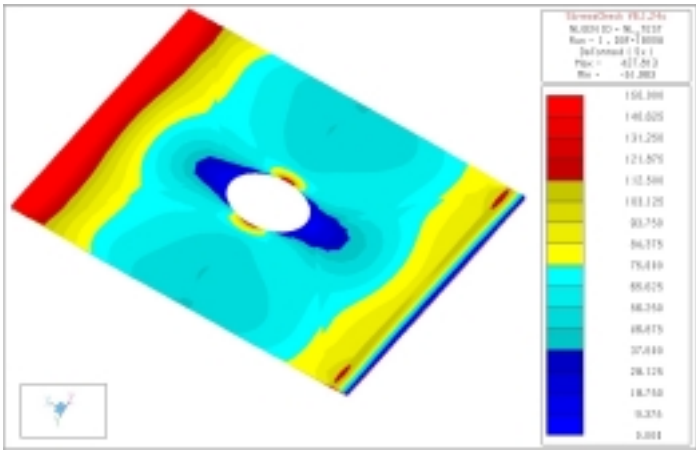

Figure 4.5.3. Longitudinal stresses in prepreg, upper side (= element level)

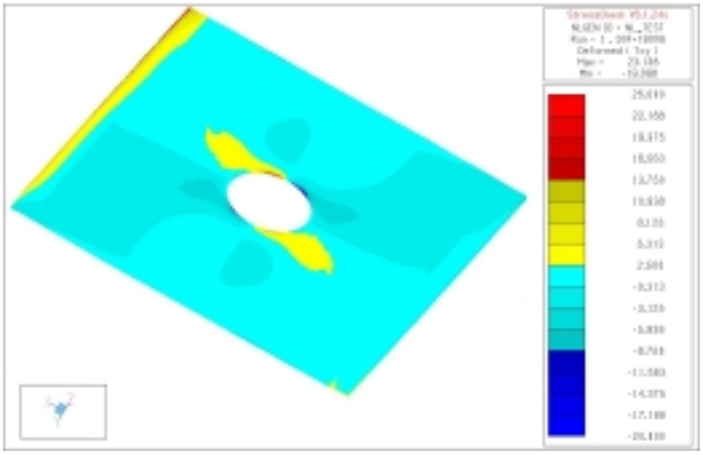

Figure 4.5.4. Shear stresses in prepreg, upper side

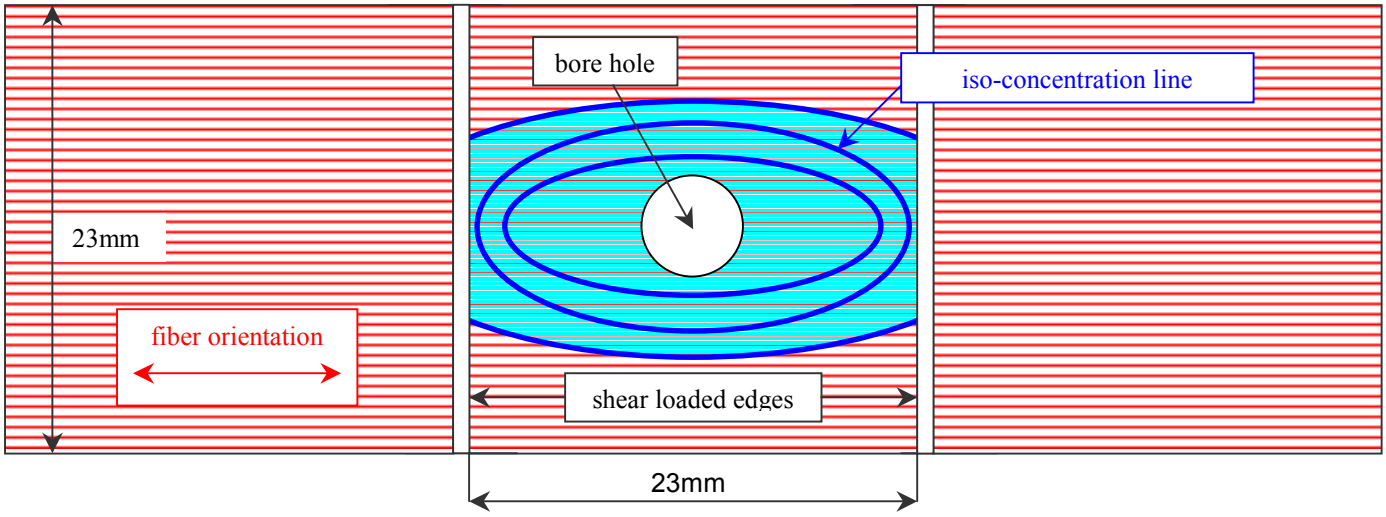

Figure 4.5.5. Schematic sketch of moisture distribution around 4.8mm hole after 3000 hours accelerated ageing, view on UD prepreg

A moisture profile for GLARE2 is calculated using the coefficients and method described in the previous paragraph, see figure 4.5.6:

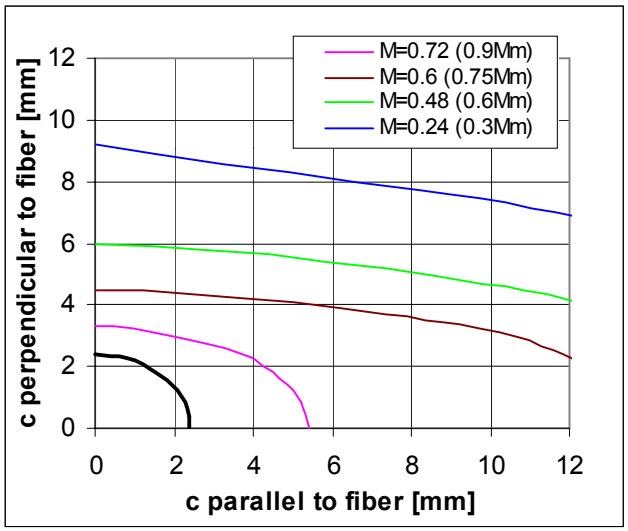

Figure 4.5.6. Calculated iso-concentration levels around GLARE2 drilled hole after 3000h / 70°C / 85%RH exposure

Parallel to the fibers, moisture travels rather fast. The moisture concentration level at the shear edges, which influences the delamination resistance and consequently the here tested strength, equals 0.6% prepreg weight and lower. Perpendicular to the fibers the moisture almost reaches the specimen edge with low concentration. The new designed specimen satisfies the predefined purpose. By variation of its design, especially the distance from the drilled hole to the shear edge, it can serve as verification tool for predicted moisture depth and the influence of moisture on shear delamination resistance. By variation of the exposure process it can be used to determine an acceptable moisture level, at which its detrimental influence on inter laminar shear strength is tolerable for structural mechanic problems.

4.6 Summary and Conclusions

Diffusion coefficients are evaluated using rectangular GLARE3 specimens of different sizes, exposed in humid air. The FM94/S-glass prepreg behaves according to the Fick'ian law. The Arrhenius equation is shown to be applicable. These conclusions are confirmed without exception for exposure temperatures up to 70°C, based on the present research.

At 90°C exposure the calculated maximum moisture content of the prepreg is obtained with a weight gain curve with a kinked slope. It is assumed, that the continuous decrease of the glass transition temperature is the reason for the behaviour of the 90°C/95%RH rectangular specimens above 1500 hours exposure. The diffusion kinetics change when the glass transition temperature is exceeded.

The relation between the maximum moisture content in the prepreg and the ambient air relative humidity is established.

Diffusion coefficients for GLARE3 are determined.

Apparent diffusion coefficients for GLARE2 are estimated with support of literature data. It is recommended to perform weight gain tests with rectangular GLARE2- and GLARE4-specimens. The specimens should have a length of 100mm and a width of 25mm.

Accelerated ageing weight gain results are obtained from Moisture Reference Specimens (GLARE3) and compared with the results obtained from the rectangular specimens. A simplified hole geometry has been considered for the calculations. Nevertheless the calculated diffusion coefficients obtained from the MRS are in the same order of magnitude as the results from the rectangular specimens. It is recommended to use the diffusion coefficients determined from the rectangular specimens for diffusion rate predictions in GLARE3 holes.

The two-dimensional and one-dimensional numerical solutions for the calculation of diffusion concentrations, as developed by Springer, are applied for GLARE3 holes. Moisture concentrations around drilled holes exposed in a 70°C/85%RH environment are estimated for different geometries in GLARE3 and GLARE2.

Observations:

- The area of maximum moisture concentration (90%Mm) around a drilled hole varies just slightly between 500 hours and 3000 hours exposure time in a 70°C/85%RH environment. The area which is moisturized at concentration levels (≤ 60%Mm) differ significantly with increasing exposure time.
- The difference of moisture concentration levels between a plate with drilled holes with fastener (bolts, clearance fit) and a plate without fastener is not significant.
- The areas around the drilled holes which are moisturized to concentration level 90%Mm is almost equal for GLARE3 and for GLARE2 perpendicular to the fibers. Perpendicular to the fibers the radii of lower concentration lines are shorter for GLARE2 than for GLARE3.

Note: The above used empirical method is linked to the tested MRS geometries.

In order to support the calculated diffusion depth some elementary investigations are performed with thick adhered specimens. Thick adhered specimens with aircraft typical dimensions and a drilled hole in the center of the specimen have been designed and tested. The specimen is representative to investigate the diffusion depth in a prepreg from the origin of a drilled hole. After 3000 hours exposure in a 70ºC/85%RH humid air environment, moisture travelled as far as 9.1mm parallel to the fibers. A concentration level of $0.5xM_m$ is calculated at the shear edges, which are the considered failure locations. 7% loss of the interlaminar shear strength is observed, failure occurs in the prepreg, not at the resin/metal interface (cohesive failure). It is concluded that the resistance of the prepreg against de-lamination due to shear loads is influenced around bore holes by accelerated exposure. If the exposure is severe enough even distances of 9mm from the hole edge are effected by strength degradations. Interesting enough, the moisture content *parallel* load direction leads to a loss of interlaminar shear strength.

4.7 References

[1] Environmental Exposure Effects on Composite Materials for Commercial Aircraft, M. Gibbins, D. Hoffman, Boeing, NASA Contractor Report 3502, 1982

[2] In-service environmental effects on carbon fibre composite material, L. Jones, British Aerospace PLC, in *Progress in Advanced Materials and Processes: Durability, Reliability and Quality Control*, edited by G Bartels and R. Schliekelmann, Elsevier Science Publishers B.V., Amsterdam, 1985

[3] Outdoor Exposure of Advanced Composites, Hiroshi Fukuda, Science University of Tokyo, Chiba, Japan

[4] Environmental Effects on Composite Materials, G. Springer, University of Michigan

[5] Numerical Procedures for the Solution of One Dimensional Fickian Diffusion Problems, G. Springer, University of Michigan, Technomic Publishing ISBN 087762-300-7

[6] Feuchteaufnahmen von dicken CfK-Laminaten im Flugbetrieb, I. Kröber, DaimlerChrysler Aerospace Airbus, Technical Note EMD-B/2000-01

[7] Feuchteaufnahmen von CfK im Flugbetrieb, I. Kröber, MBB, Vortrag zum DGLR Symposium “Entwicklung und Anwendung von Faserverbundstrukturen”, Berlin, 1987

[8] Das beschleunigte Befeuchten von CfK-Proben in künstlichem Klima. I. Kröber, DaimlerChrysler Aerospace Airbus, Technical Note EMD-B/2000-05

[9] Erfahrungen im Flugbetrieb mit FML-Strukturen, Th. Beumler, DaimlerChrysler Aerospace Airbus, Presentation EMF-417/00, 2000

[10] Fast ageing test program analysis, W. van der Hoeven, NLR, GRP WG1C progress meeting 10.1.2002 , Annex to EADS Airbus MoM 510/02

[11] The influence of elevated temperature on GLARE after exposure to moisture, B. Borgonje, Delft University of Technology, Master Thesis, 2000

[12] Blunt notch test results, W. van der Hoeven, NLR, in DaimlerChrysler Aerospace Airbus MoM EMF-932/99, 1999

[13] Fatigue and Damage Tolerance Justification of a Fuselage Repair with a GLARE3 Sheet, Concession DD-278029, Th. Beumler, DaimlerChrysler Aerospace Airbus, Technical Note TN-EMF-6/00, 2000

[14] Technical information from G. Roebroeks on SLC project SL-MR-09 (in progress), “Durability, strength after exposure”, FMLC, February 2003

[15] Aramid Reinforced Aluminium Laminates: ARALL, Adhesion Problems and Environmetal Effects, Volume B: Environmental Effects, M. Verbruggen, Delft University of Technology, PhD Thesis, 1986

[16] The moisture absorption of GLARE – an introduction, O. Tensen, Delft University of Technology, Master Thesis, 1990

[17] Moisture absorption experiments on GLARE, W. van der Hoeven, NLR report NLR-CR-2002-374, 2002

[18] Thermal- and deformation induced delamination of fibre metal laminates, E. Kappel, Delft University of Technology, Master Thesis, 1992

[19] Adhesive bonded double lap joints, L. Hart-Smith, NASA Scientific and Technical Information Facility, Report CR112235

[20] Silane Coupling Agents, I. de Haan, Delft University of Technology, 1994

[21] Immersion tests in the paint strippers Cormorcap B.10 and Turco 6881, W. t'Hart, NLR, report NLR-CR-2001-167, 2001

[22] Evaluation d'une structure en GLARE apres 2,5 ans d'exposition sur site marin Aerospatiale, Centre de Recherches Louis-Bleriot, Report DCR/M-64252-99

[23] 2000 stündige Lagerung von GLARE3 Schälproben in 70°C warmen Wasser, W. Kelm, Daimler-Chrysler Aerospace Airbus, Laborbericht K268/00, 2000

[24] Determination of interlaminar fracture toughness energy G1c on Al specimens containing FM94/S2 glass prepreg, W. Kelm, DaimlerChrysler Aerospace Airbus, Laboratory Test Report K272/01, 2001

[25] Thermal Behaviour of Fiber Metal Laminates, G. Graafmans, Delft University of Technology, Master Thesis, 1995

[26] Cold/hot soak behaviour of GLARE, W. van der Hoeven, NLR, Report NLR-CR-2000-273, 2000

[27] GLARE Preliminary Knock Down Factors, Th. Beumler, DaimlerChrysler Aerospace Airbus, Memo EMF-243/00, 2000

[28] Experimental project to assesss the failure mechanisms during blunt notch of GLARE, Y. Meziere, Delft University of Technology, report B2V-00-47, 2000

[29] The influence of elevated temperature on GLARE after exposure to moisture, B. Borgonje, Delft University of Technology, Master Thesis, 2000

[30] The moisture absorption of GLARE, O.J. Tensen, Delft University of Technology, T.Z.report, 1990

[31] Bestimmung von Diffusionskoeffizienten in GLARE3, Th. Beumler, Airbus Deutschland GmbH, Versuchsspezifikation 10L029K4800I84, 2002

[32] Blunt and sharp notch behaviour of GLARE laminates, T. De Vries, PhD Thesis, Delft Universityof Technology, 2001

[33] Fatigue crack growth in ARALL – A hybrid aluminium-aramid composite material, R. Marissen,Delft University of Technology, Report LR-574, 1988

[34] Determination of the moisture absorption of ARALL, M. Verbruggen, Delft University of Technology

[35] Bestimmung von Erweichungs- und Glasübergangstemperaturen an FM94-S2 Glasprepreg, W. Kelm, Airbus, Laborbericht K286/02

[36] Paint stripper immersion tests on GLARE (ASTM Specification F483-98), W. t'Hart, NLR, Report NLR-CR-2000-683

[37] Towards GLARE, G Roebroeks, PhD Thesis, Delft University of Technology, 1991

[38] Über die Feuchteaufnahme von GLARE, I.Kröber, Airbus Deutschland GmbH, Technische Note TN-ESGC-2003-01, 2003

[39] Three-dimensional moisture diffusion in laminated composites, J.M. Whitney, Air Force Materials Laboratory, Wright-Patterson Air Force Base

[40] А. Куснецов, А. Кротов, О. Стартев, Experimental study and modelling of moisture diffusion in composite materials, Altai State University

[41] Bridging stress distribution in center-cracked fiber reinforced metal laminates: modeling and experiment, Y. Guo and X. Wu, Beijing Institute of Aeronautical Materials, in Engineering Fracture Mechanics 63, pages 147-163, 1999

Chapter 5
Tropic Ageing

Contents Page

This page intentionally left blank.

5.1 Introduction

Predictions for the moisture absorption around drilled holes in GLARE structures which belong to civil aircraft will be performed in this chapter, based on the lessens learned about the diffusion behaviour of GLARE under accelerated ageing conditions (previous chapter) and based on outdoor weight gain measurements. A recommendation for the application of a standardized accelerated ageing process, which simulates the GLARE drilled hole condition after 30 years aircraft service will be provided.

5.2 Meteorological Data and Moisture Reference Measurements

The outdoor exposure site is located at latitude 17.4° south and 146° longitude east. In this environment the very high levels of sunshine, rainfall and humidity combine to provide the conditions that are required to test a material's resistance against degradation. Long term meteorological data indicate average daily mean ambient temperatures between 19.4°C in winter and 26.4°C in summer (table 5.2.1). The average daily maximum ambient temperatures are measured at 23.8°C in winter and 31.2°C in summer. The recorded relative humidities are steady at high levels, i.e. between 78% (autumn) and 87% (spring) for the average daily mean and between 95% and 96% for the average daily maximum.

For this research the Aeronautical & Maritime Research Laboratory provides min/max temperature and humidity readings for every particular day of the GLARE exposure project, starting with January 1, 2002. Since the weight gain measurements of the MRS are performed in intervals of a quarterly year, reliable diffusion recalculations and predictions are limited to blocks of 3 month as well. However, this interval is expected to be accurate enough to predict the moisture content after a period of 30 years exposure (aircraft DSG).

This chapter details three major topics. First it will be investigated whether it is possible to recalculate the measured weight gains from the outdoor MRS by using the equations and coefficients discussed in chapter 2. Second, the available weight gain readings will be used for long term diffusion predictions, related to both, long range and short range flight missions. The last item to be addressed is the moisture distribution around the drilled hole.

The weight gain data will be updated every quarter of a year, until January 2008, which is the end date of the outdoor exposure program. This report contains the data related to 1¼ year outdoor exposure, i.e. from January 2002 until March 2003 (included).

5.2.1. Outdoor exposure weight gain results

The outdoor weight gain results are collected in table 5.2.2. As expected from accelerated ageing specimen 8-9-FP (ref. chapter 4), all painted specimens loose weight during the initial exposure phase. Even specimen 8-7, which is not drilled and unpainted, looses some weight at the beginning of exposure, but significantly less than the painted specimens. Obviously even in the bonding primer of specimen 8-7 some chemical reactions develop.
Specimens 8-1-P and 8-2-P are not drilled but painted. All measured weight changes must be related to the paint, only (ref. table 3.2.1). Consequently, if the weight changes measured at specimens 8-1-P and

8-2-P will be subtracted from the weight changes of the open hole- and filled hole specimens, the difference must be the moisture uptake through the holes.

Note: The decrease or increase of weight at specimens 8-1-P and 8-2-P is dependent on the paint behaviour, only! The averaged weight changes obtained from specimens 8-1-P and 8-2-P is subtracted or added, respectively, on the weight changes measured for painted open hole and the painted filled hole specimens. The result is considered as the net weight gain of the open/filled holes !

A correction is required since the painted surface of the open hole- and filled hole specimens is smaller than for the non-drilled specimens: (25 x 2 x drilled hole area). This procedure considers that the diffusion processes in the paint of all MRS is similar, which is expected since all specimens have been painted in the same batch with the same paint by the same operator.

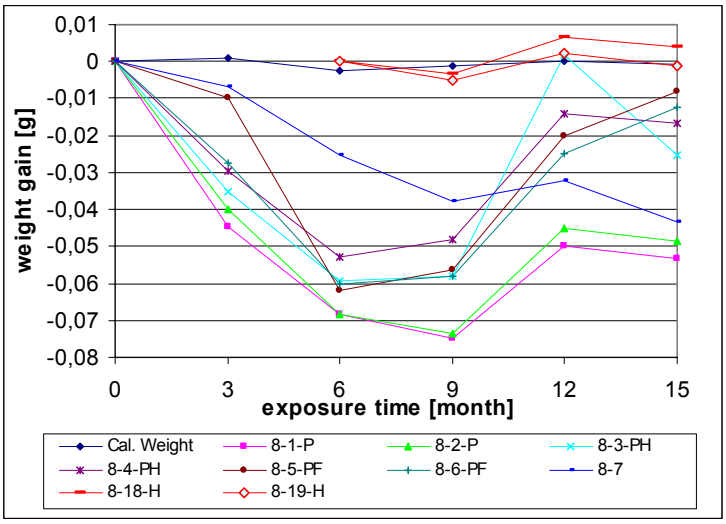

Figure 5.2.1. Weight gain of outdoor exposure MRS, starting from January 8, 2002

The painted specimen without hole, i.e. 8-1-P and 8-2-P, behave similar as the painted specimen exposed in the environmental chamber (8-9-PF, see figure 2.3.7). First the weight decreases, then it increases and finally it becomes constant. The steady state modus seems to be reached after one year of exposure, which needs to be confirmed by the future weight gain measurements. The weight gain slope of all painted specimens with holes (8-3-PH, 8-4-PH, 8-5-PF, 8-6-PF) follows the slope of painted but not drilled specimens. The behaviour of the paint dominates the weight gain in the early exposure phase, at least for 12 months. Two data points must be considered as outlaws, i.e. the weight of specimen 8-5-PF after 3 months exposure and the weight of specimen 8-3-PH after 12 months exposure. Specimen 8-7 is not drilled and its surface is covered by the bonding primer only. Unexpectedly, its weight decreases during the entire exposure period up to date. Obviously the bonding primer reacts even longer if exposed to the sun than the blue paint. Specimens 8-18-H and 8-19-H (open hole, paint primer), which have been added to the program half a year later than the others, show more or less a constant weight. It must be concluded, that the weight gain through the holes almost equals the weight loss of the bonding primer, at least for the first 9 month of exposure.

Table 5.2.3. contains the mean weight gain values of the different specimen types after different exposure times and the total amount of weight gain after subtraction of the non-drilled weight gain from the open hole- and filled hole specimens, respectively. The correction factor for the decreased amount of painted area due to the drilled holes is calculated to be with 0.9832. With the correction for the paint, the negative weight gains of the open- and filled hole specimens turn into positive values.

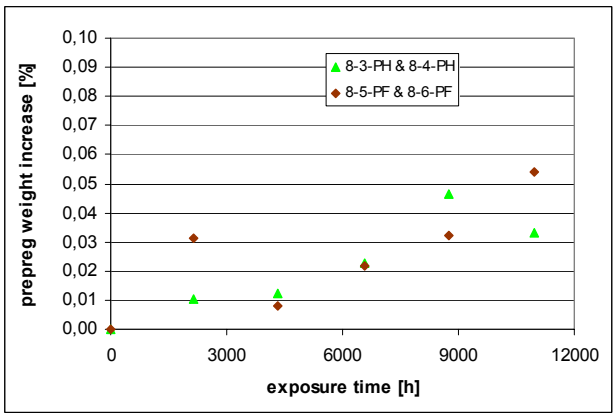

Figure 5.2.2. Outdoor exposure MRS weight gain

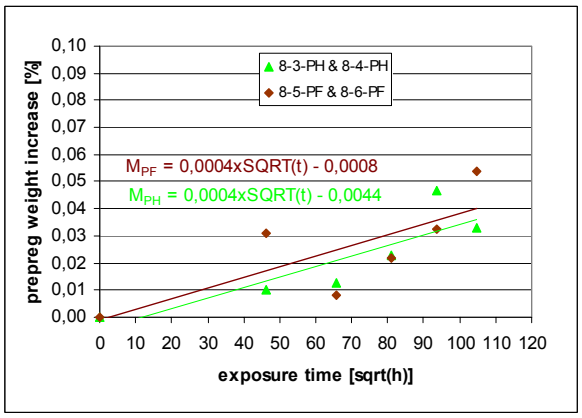

Figure 5.2.3. Outdoor exposure MRS weight gain with linear regression

Figures 5.2.2. and 5.2.3. show the prepreg weight gain related to both, [hours] and square root [hours] for the first 15 months of exposure in Queensland. Specimens 8.18-H and 8-19-H have a delay of 6 month compared with the other specimens, they are not taken into account for the present evaluation. Since the climate is not constant, no constant data increase can be expected. Figure 5.2.3 shows the weight increase of the prepreg around the holes for the open hole and filled hole specimens with paint, with the influence of the paint considered. Note that all data points are included, even the two which are classified as outlaws. Linear regression lines are included for an approximation of the weight gain after one aircraft life. It is noticed, that the regression lines through the open holes and filled holes data points, respectively, provide an almost identical slope.

5.2.2. Empirical Outdoor Weight Gain Prediction Method, Calibration

The information of maximum, minimum and average meteorological data for each particular day of specimen exposure is not sufficient for the recalculation of the outdoor weight gain according to figure 5.2.3. An integration of both, temperatures and humidities, over the entire exposure time is required. In order to limit the amount of data to an acceptable size, the weight gain measurements obtained from the period January 8 to April 8, 2002, are related to one typical Australian summer day. Attachment E contains the temperature and humidity record from January 14, 2002. Ambient temperatures and relative humidities are measured in intervals of 10 minutes, see figure 5.2.4. In order to decrease the amount of data further, the average values for each daily hour are calculated (table 5.2.4). The diffusion rates are dependent on the temperature, but yet it is unknown on which - the ambient or the specimen temperature. For an assessment, specimen surface temperatures (lower and upper surfaces) are measured over a period of five days, from March 28 to April 2, 2002. The temperature curves labeled ‘under glass’ in figure 5.2.5a are obtained from Moisture Reference Specimen 8-1-P. The temperature measurements are repeated in January/February 2003 (figure 5.2.5b). Interesting enough, it can be observed that the weather conditions in January (higher ambient temperature and higher sun radiation) increase the measured specimen temperature under glass, but decrease the free exposed specimen temperature. An unknown variable for this comparison is the wind speed, which might explain the unexpected results.

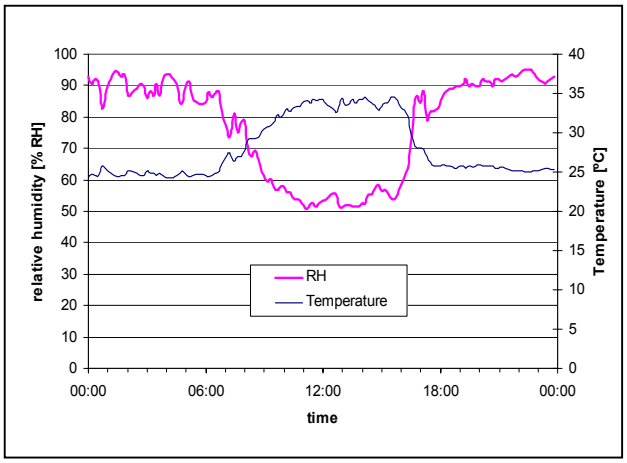

Figure 5.2.4. Ambient temperature and relative humidity on January 14, 2002, 'calibration day'

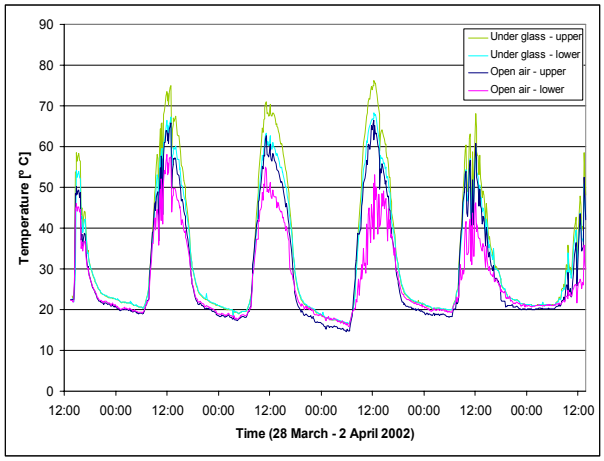

Figure 5.2.5a. Specimen surface temperatures

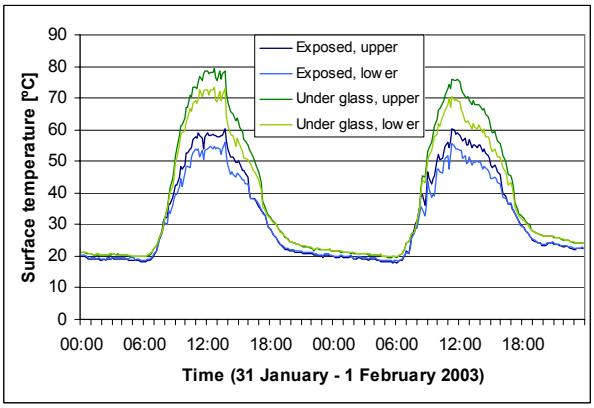

Figure 5.2.5b. Specimen surface temperatures

In March/April 2002, higher specimen temperatures are measured on the surface directed towards the sun compared with the side directed towards the ground. Peak temperatures of 75°C are measured during noon on the outer aluminium sheet, related with at maximum 34°C ambient temperature at the same day time (measured on January 14, 2002). The variations of the available meteorological data throughout the seasons 2002 are set in relation to the 30 year long term readings (table 5.2.1) in order to make an assessment on the sensibility to mistakes due to the data mix. The daily minimum, daily mean and daily maximum ambient temperatures and humidities, obtained from both records (30 years and 2002), are compared:

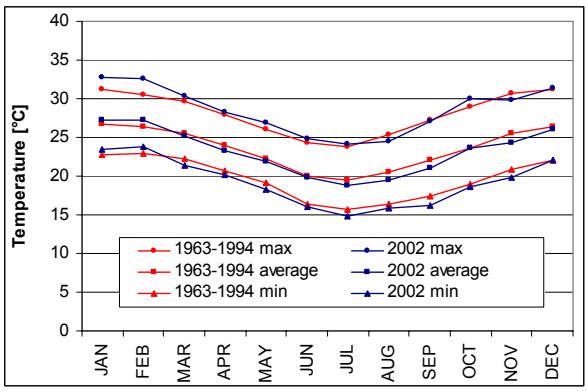

Figure 5.2.6. Comparison of ambient temperatures, daily values averaged to months

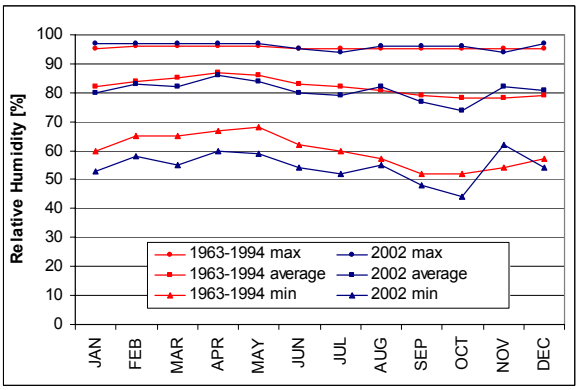

Figure 5.2.7. Comparison of relative humidies, daily values averaged to months

The temperatures and humidities measured in the exposure period so far follow the trend observed over the past 30 years. However, the maximum daily temperatures in summer 2002 have been 2°C higher than usual, while the minimum relative humidity was between 5 and 10% lower than the long term average. Both deviations belong to the daily time period from 11a.m. to 4p.m., see figure 5.2.4.
In the following all meteorological data are condensed to one typical day in any of the four seasons. Concerning the relation of the ambient temperatures on January 14 with the specimen temperatures measured from March 28 to April 2, the absolute difference between the maximum daily temperatures must be considered, if no data profile from the period March 28 to April 2 coincidently matches the data from January 14. By reviewing appendix C it is found:
Maximum ambient temperature January 14: 34.6°C.
Maximum ambient temperature March 31: 33.4°C
The maximum ambient temperatures of both days differ just slightly. It is estimated, that the ambient temperatures recorded from 11a.m. to 6p.m. on January 14 fit to the specimen temperatures recorded on March 31, approximately. The 14th of January is therefore defined as the 'calibration day' for the following exercises. Based on this assumption a temperature factor f_{MRS} is evaluated for any hour at January 14. By multiplication of the ambient temperature with factor f_{MRS}, a specimen temperature profile for an entire day becomes available. Both, factor f_{MRS} and specimen temperature T_{MRS}, are included in table 5.2.4.
The open hole weight gain, measured during the period from January 8 to April 8 2002, can be recalculated with both, the ambient temperature profile and the specimen temperature profile, in order to determine the better fit. It is important to consider, that all equations used in this paragraph are just valid for a *constant* environmental condition. This is not the case during outdoor exposure. Both, temperatures and humidities, change frequently and diffusion in reverse direction (drying) may happen. Hence, no qualitative correct result can be expected by using the simple equations. Expected is a trend, which indicates whether the ambient temperature or the specimen temperature leads to a better approximation of the reality.
Since the conditions at any particular day are slightly different, but a detailed reading is available for just *one* typical day, it is decided to consider that all days of the measurement period equal the typical day ('calibration day'). The calculation of the mass of moisture, which is transported at any hour into the holes, can be calculated by solving equation (7) from chapter 4 for ΔM_t. The calculated values will be normalized in order to compensate for the daily changing weather conditions.

$$\Delta M_t = 2M_m \times \left(\frac{l+b}{l \times b}\right) \times 2\sqrt{D} \times \sqrt{\frac{t}{\pi}}$$

with: l = b = 25 x 4.8mm x π / 4 (for 25 holes)
t = 1 hour
$D = 3110 \times e^{(-7109/T)}$, for MRS, ref. chapter 4
$M_m = 7.02 \times 10^{-7} \times (RH)^{3.13}$, ref. chapter 4

With these formulas both, the diffusion rate D and the moisture uptake ΔM_t are calculated for any particular hour of the day. The calculation is done twice, once in relation to the ambient temperatures and once in relation to the material temperatures, see table 5.2.5.

The normalized results of both calculations, i.e. the contribution of any particular hour to the moisture uptake of the calibration day in [%], are shown in figure 5.2.8. During evening and night, all calculated diffusions are lower if related to the *specimen* temperature. This is compensated during the period from 10a.m. to 3p.m., when the specimen temperatures are high which increases the diffusion speed significantly. During noon, relative humidities are as low as 52%, which corresponds to a maximum possible moisture content in the prepreg of 0.14%, see table 5.2.4. For the total calibration day, both calculated weight gain values ΔM_t are in the same order of magnitude ($1.72x10^{-2}$ [%/day] if related to the ambient temperature and $2.14x10^{-2}$ [%/day] if related to the specimen temperature, see table 5.2.5). For the further calculations a choice was to be made to continue calculations either based on the weight gain which is related to the ambient temperature or to the weight gain which is related to the specimen temperature. This question is not solved in the durability community. The relative humidity can be just provided by the ambient air. The diffusion speed at the specimen holes, however, should be related to the specimen temperature. For the present thesis it is decided to work with the *specimen* temperatures, since it leads to a more balanced normalized weight gain throughout the day.

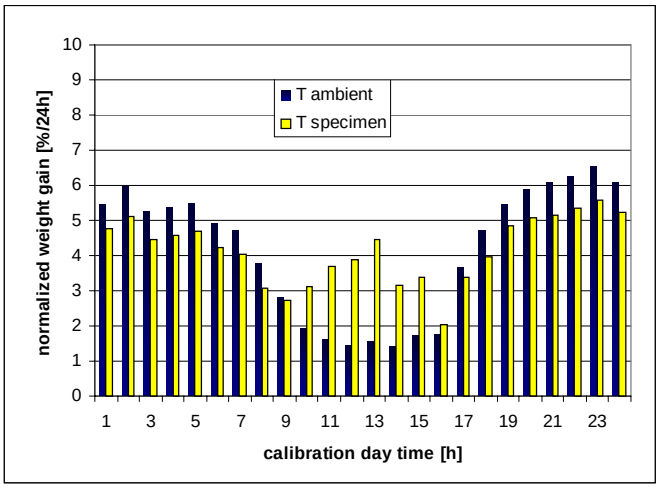

Figure 5.2.8. Normalized moisture uptake per hour for the calibration day

5.2.3. Empirical in-service weight gain predictions

From specimens 8-3-PH and 8-4-PH a weight gain related to the different seasons is calculated:

Season 2002	January 8- March 8	March 8 – June 8	June 8 – October 8	October 8 – January 8
Weight gain	$1.01x10^{-4}$ [g/day]	$3.33x10^{-5}$ [g/day]	$1.06x10^{-4}$ [g/day]	$8.79x10^{-5}$ [g/day]

If multiplied with the normalized weight gain (figure 5.2.8), the empirical weight gain for any hour of a *typical* day in any season becomes available, see figure 5.2.9. It indicates almost similar weight gain in summer and wither 2002 and slightly lower weight gain in spring. The autumn of year 2002 was an unusual dry period.

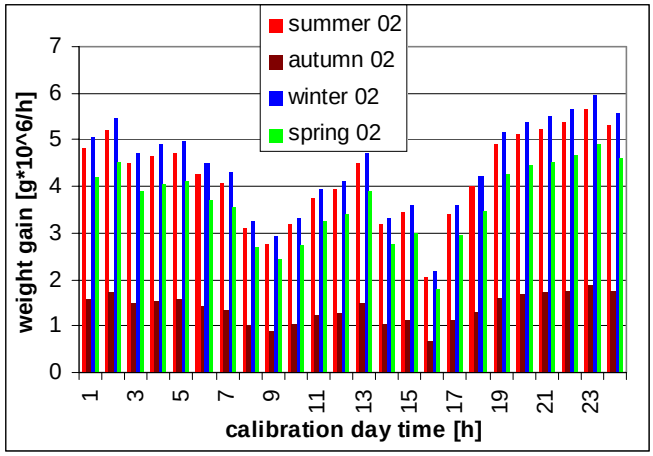

Figure 5.2.9. Weight gain per hour of typical tropical days in seasons 2002, empirical

Short range aircraft are mainly operated during the day time. A high utility aircraft mission is presented in table 5.2.6, obtained from the KLM time schedule winter 2001/2002 for flight operations between Hamburg and Amsterdam. In theory it is possible to fly the missions of one day with just one aircraft. From the same time schedule a typical *long* range mission has been taken, KLM flight 781, Amsterdam – Aruba – Curacao – Amsterdam (table 5.2.7). Figures 5.2.10 and 5.2.11 indicate the ground time for both flight missions (in yellow), during which moisture can penetrate into the GLARE prepreg.

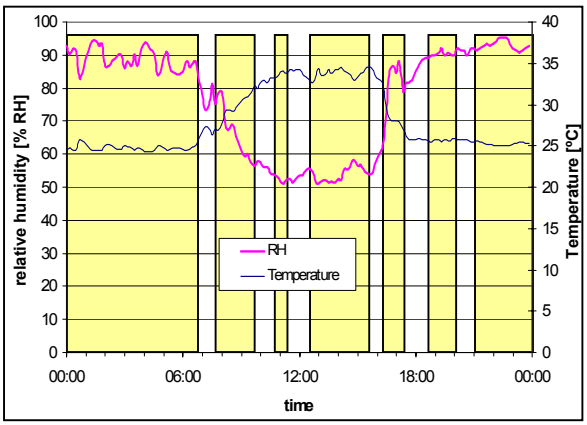

Figure 5.2.10. Short range mission, calibration day, yellow bars indicate aircraft standing on ground

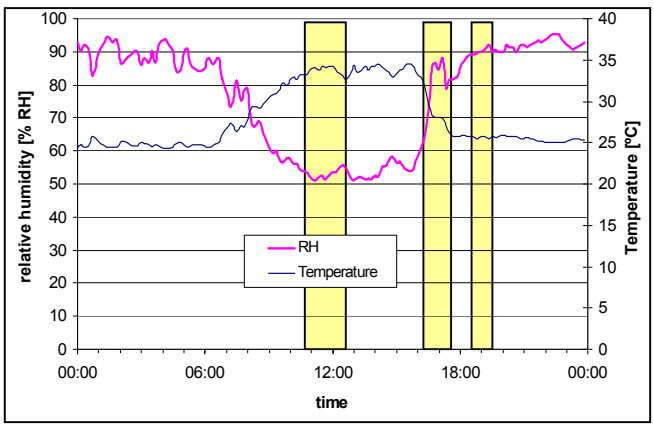

Figure 5.2.11. Long range mission, calibration day

If it is assumed that not just Aruba and Curacao, but as well Amsterdam and Hamburg would be located in the tropics, empirically the weight gain associated to the ground times can be added. Or, with other words, the weight gain during flight is subtracted from the weight gain profile for an entire day according to figure 5.2.9, since the condition of the prepreg will be frozen during flight. The calculation results are listed in tables 5.2.8 and 5.2.9 for the two flight missions, respectively. The weight gain results obtained from the continuous measurements in Australia and for the two flight missions are shown in figure 5.2.12. Note that the straight lines are approximations. In fact, the different seasons of the year lead to a cyclic weight gain curve.

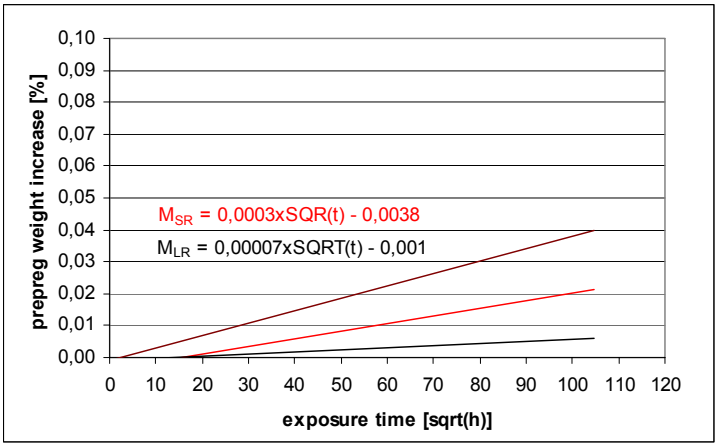

Figure 5.2.12. Empirical prediction of weight gain in filled hole GLARE3 for long range and short range mission, related to the outdoor exposure weight gain measurement period January 2002 to April 2003 (1,25 year)

It is possible to calculate the moisture uptake of the open hole MRS based on the weight gain slopes from figure 5.2.12 and the meteorological records from the 30 year measurement campaign (table 5.2.1) with the computer program W8GAIN [1] (method described in ref. [2]) :

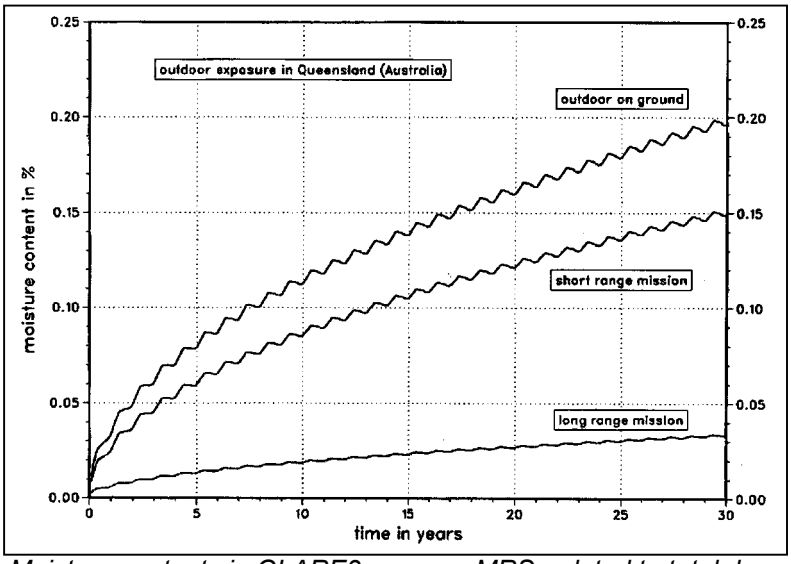

Figure 5.2.13. Moisture contents in GLARE3 prepreg, MRS, related to total dry prepreg weight, calculated for every single month with average temperature and humidity data for that month

A one-dimensional calculation of the diffusion depths for constant exposure in Queensland, the long range- and the short range mission, all for a period of 30 years, leads to the following diagram (b'=28mm):

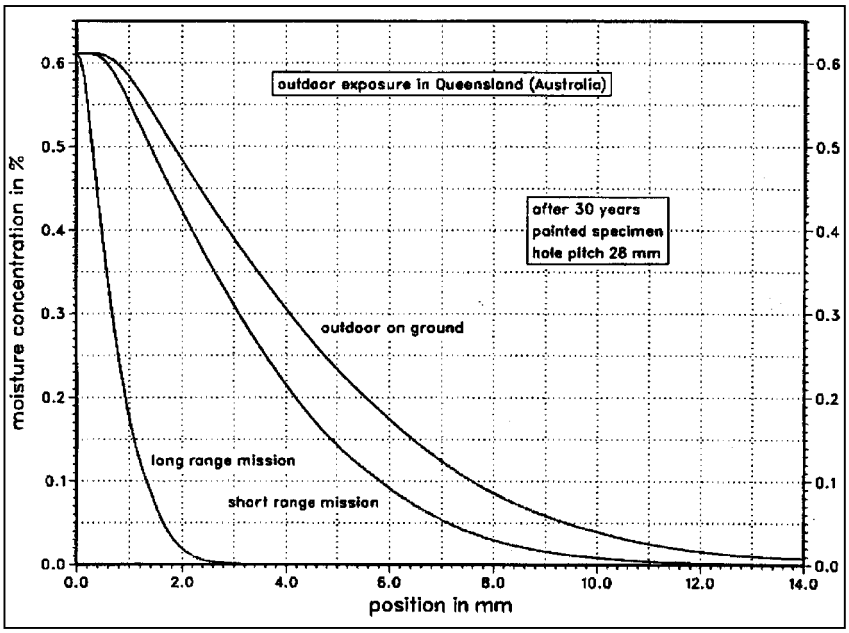

Figure 5.2.14. Moisture concentration depths in prepreg after 30 years of exposure, one dimensional calculation

The (absolute) moisture concentration of 0.62% prepreg weight at the GLARE edge (position 0mm) is a calculated average value based on the December climate in Queensland. It will change continuously close to the edge, based on the actual weather condition. According to Springer, the maximum affected depth of weather dependent moisture condition is 1.4mm (ref. chapter 4). The moisture concentrations and distributions inside the laminate are not affected.

5.2.4 Diffusion around drilled hole, flight missions

Under assumption of an equal distribution of moisture around a hole drilled in GLARE3, iso-concentration lines after different outdoor exposure times can be constructed. Figures 5.2.15 and 5.2.16 contain iso-concentration lines for 30 years of service in a tropic environment. Baseline is an open hole spacing of 28mm and a hole diameter of 4.8mm.

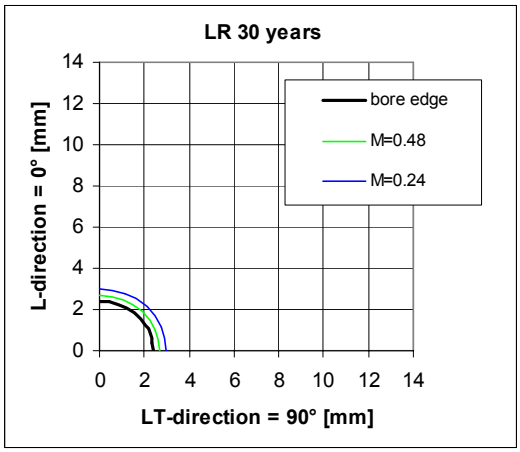

Figure 5.2.15. GLARE3 bore hole, 30 years long range mission service

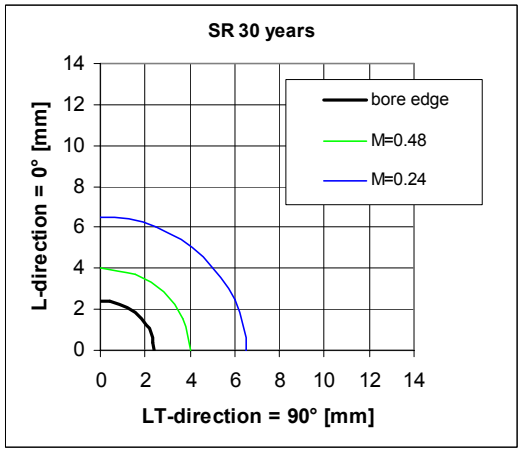

Figure 5.2.16. GLARE3 bore hole, 30 years short range mission service

The diffusion depth is so small that it is not necessary to conduct calculations for smaller hole pitches. Usual rivet pitches are 4.5 to 5.5 times the hole diameter. The iso-concentration lines from different holes do not interact for diameters of 4.8mm and higher. For comparison with the accelerated ageing condition after 500 hours exposure (70°C/85%RH), as calculated in chapter 4, is added to this paragraph.

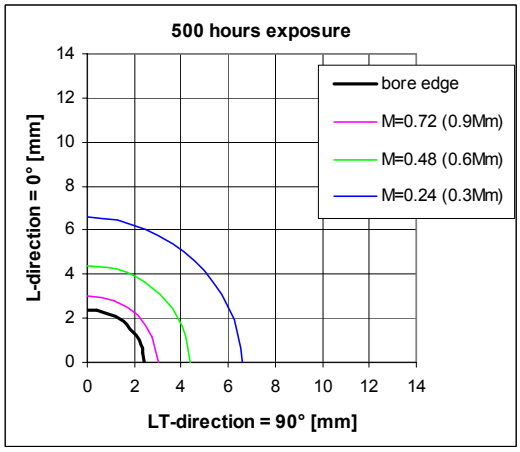

Figure 5.2.17. Iso-concentration lines around 4.8mm bore hole (pitch 28mm) after 500h constant accelerated ageing in 70°C/85%RH air

The diffusion depth and distribution after 500 hours accelerated exposure (70°C/85%RH) equals almost the condition after 30 years short range mission service.

5.3 Representative Accelerated Ageing Procedure

The standard accelerated ageing weight gain (chapter 4) is compared with the outdoor weight gain obtained from the exposure period January 2002 to April 2003, see figure 5.3.1. The following investigation will be updated in intervals up to the ultimate duration of the outdoor exposure program. The last weight gain measurement of the outdoor MRS is scheduled for January 2008.

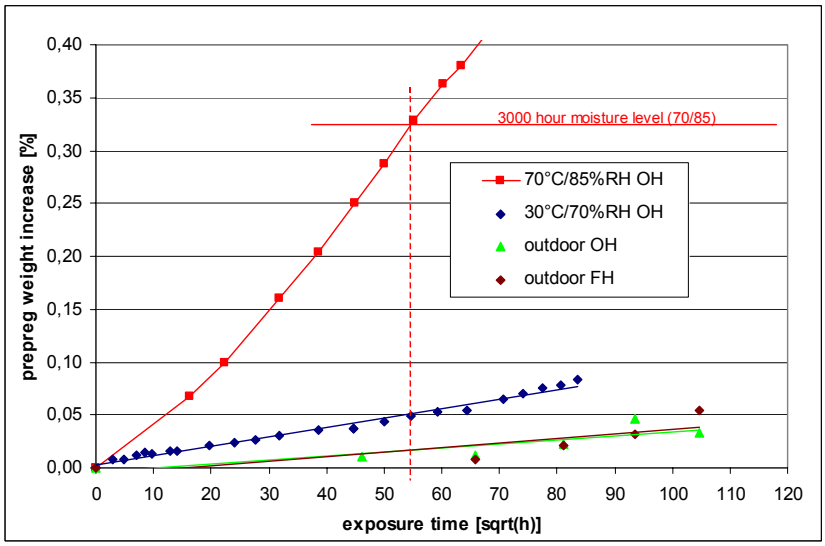

Figure 5.3.1. Comparison of standard accelerated ageing with outdoor exposure weight gain

After 3000 hours Airbus standard exposure, a ΔM of 0.32% prepreg weight has been obtained. With the associated moisture level the preliminary structural knock down factors for A380 sizing have been established [3].

The green line indicates the weight gain for 15 months open hole exposure in tropic Australia. With the obtained slope
can be calculated, that it will take 75 years in Queensland / Australia to reach the same moisture level as after 3000 hours accelerated ageing in a constant 70°C/85%RH environment.:

$T_{\Delta M=0.32\%}$ = (((0.32-0.0044)/0.0004)^2) / (365*24) = 75 [years] (equation from diagram 5.2.3)

If the observed outdoor exposure curve will maintain its slope the moisture content in the prepreg after 30 years exposure can be calculated:

$M_{30\ years}$ = 0.0004 x SQRT(30 x 24 x 365) - 0.0044 = 0.201

A moisture content of 0.201% prepreg weight equals 1281 hours accelerated exposure in a 70°C/85% RH environment. The moisture *distribution*, however, will be different at the end of both, the 30 year outdoor exposure and the 1281 hours accelerated exposure.

The calculations performed above can be repeated for different 'environmental applications':

'Environmental Application'	Time to achieve 0.32% prepreg weight[4] [years]	Prepreg weight gain (bore holes) after x years environmental exposure	Simulation of achieved weight gain in 70°C/ 85%RH environment [h]
Open hole in Queensland[1]	75	30 years: 0.201 [%]	1281
Filled hole in Queensland[1]	73	30 years: 0.204 [%]	1324
Short Range flights[2]	133	7.5 years[3]: 0.073 [%]	211
Short Range flights[2]	133	30 years: 0.150 [%]	748
Long Range flights[2]	2401	7.5 years[3]: 0.017 [%]	27
Long Range flights[2]	2401	30 years: 0.035 [%]	67

1) Permanent exposure
2) Based on filled hole data, worst case
3) Assumption: ¼ of all flights operated in tropical environment
4) Equals prepreg weight gain around drilled holes after 3000 hours accelerated exposure in 70°C/85%RH environment

5.4 Summary and Conclusions

The weight gain measurement campaign on GLARE specimens exposed in Queensland/Australia is scheduled for the period January 2002 to January 2008. Weight gain results from the first 1¼ year of exposure are used for predictions at the present stage of this thesis.

The paint system contributes significantly to the weight gain behaviour of exposed specimens, during the first months of exposure. The weight of moisture which is collected or released by the paint has to be considered for the calculation of the diffusion through the drilled holes. This circumstance leaves some concerns on the reliability of the data, which should vanish with the increased amount of incoming data until 2008.

The moisture distributions in the FM94 prepreg around holes which are drilled in GLARE3 are calculated for both, a short range mission and a long range mission. It is assumed, that diffusion is impossible during flight. The reversibility of moisture absorption by the prepreg, i.e. drying, is implicit, since it is part of the weight gain measurements obtained from the GLARE specimens exposed in Queensland.

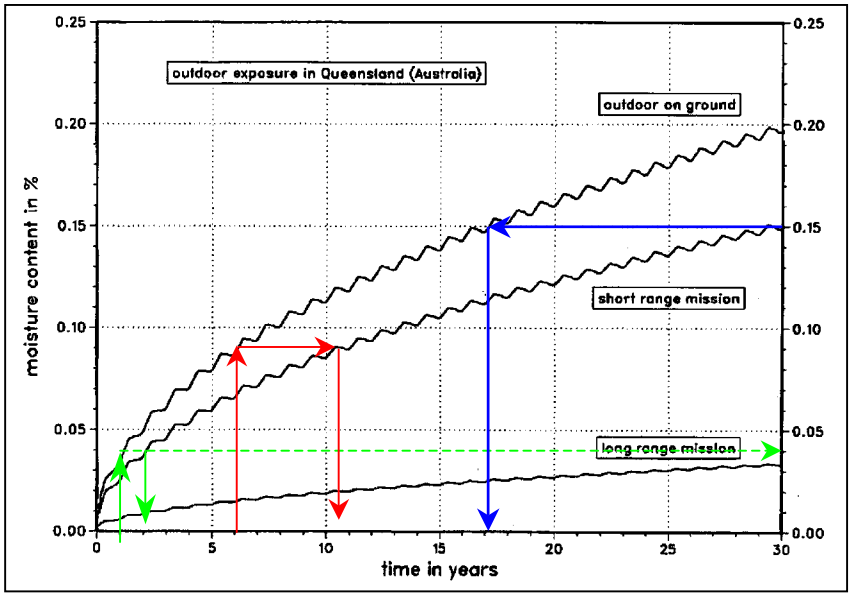

Figure 5.4.1. Determination of moisture contents for permanent outdoor exposure and in-service

One year outdoor exposure in Australia simulates two years short range aircraft operation in a tropic environment, concerning the moisture content around drilled holes, see the green arrows in figure 5.4.1. One year constant outdoor exposure exceeds already the moisture content which is present after 30 years long range flight operation.
Six years outdoor exposure in Australia simulates more then ten years short range aircraft operation in a tropic environment, see red arrows in figure 5.4.1. It would require 17 years outdoor exposure to simulate the short range mission material condition after 30 years tropic operation, see blue arrows in figure 5.4.1. The type of flight mission is extremely important for the determination of the material (moisture) condition.

According to the preliminary weight gain results it is recommended to define a representative accelerated ageing procedure for short range aircraft GLARE structures to 500 hours at 70ºC/85%RH, in order to be realistic but still conservative. The 500 hour accelerated exposure equals approximately 30 years flight operations in a tropical environment similar to Queensland/Australia. The approach is conservative, since it is not expected that any aircraft will be operated for its entire design life at the same locations.

For aircraft operated for long range missions it is recommended to consider no environmental ageing originating from tropical climates at all.

The analysis performed in this chapter (5) must be repeated in the year 2008 for a final verification of all conclusions that are linked to the moisture content of the GLARE specimens obtained from the exposure site in Queensland.

The accelerated ageing process for short range aircraft is just representative, if the failure modes after accelerated exposure are similar to those obtained from outdoor exposure results. This item is addressed in the following chapters. Most of the artificially aged specimens discussed in the following are exposed 3000 hours in a 70°C / 85% RH chamber, since the tests have been performed before the outdoor exposure weight gain data became available. The reader is requested to keep this in mind.

5.5 References

[1] Numerical Procedures for the Solution of One Dimensional Fickian Diffusion Problems, G. Springer, University of Michigan, Technomic Publishing ISBN 087762-300-7

[2] Über die Feuchteaufnahme von GLARE, I. Kröber, Airbus Deutschland GmbH, Technische Note TN-ESGC-2003-01, 2003

[3] Technische Information A380 / GLARE / MSN7^{+}, Th. Beumler, Airbus memo ESG-278/02, 2002

Chapter 6
Elementary Investigations

Contents Page

This page intentionally left blank.

6.1 Introduction

Several elementary investigations have been carried out on specimens with a simple but well defined geometry. The purpose of these elementary investigations is to obtain a better understanding of the phenomena associated with crack initiation, propagation and static strength properties of GLARE and to know how these phenomena are affected by the environment, in particular by moisture absorption and temperature. Furthermore, the attention is also focused on scatter of GLARE properties.

Similar investigations on realistic riveted joints are presented in Chapter 7.

An evaluation of the results is presented in the last section (6.14) where the significance of the observation is discussed in relation to the airworthiness requirements.

Subject		Aspects studied	Section
Fatigue	Crack initiation life	Temperature effect	6.2
		Accelerated aging	6.3
	MSD cracks	Initiation, propagation, scatter	6.4
	Fatigue cracks	Crack opening displacements	6.5
		Accelerated aging	6.6
		Temperature effect	6.7
Static strength	Blunt notch strength	Filled and open hole behaviour	6.8
	Residual strength	Fastener filled holes	6.9
		Temperature effect	6.10
		Bearing strength	6.11
		Rivet pull through	6.12
		Compression filled-holes	6.13

6.2 Crack Initiation, Temperature Influence

(ref. factor $C_{CI(T)}$)

It is the target of this test series to verify the assumption, that crack initiation in the aluminium layers of GLARE can be calculated accurately if the stress level in the aluminium sheets is known. Two aspects have to be accounted for which are the different stiffnesses and the different coefficients of thermal expansion in the aluminium- and glass fiber layers.

From the literature it is known that the crack initiation life of 2024 aluminium increases at low temperatures [54], which provides additional conservatism on a full scale fatigue test result obtained from a test conducted at room temperature. It must be investigated whether the crack initiation period is also longer at low temperatures in GLARE .

In order to avoid any geometry effect on the result, and in order to achieve a reliable crack detection accuracy, open hole specimens were made of 1.6mm 2024T3 sheet and GLARE3-3/2-.3 sheet material with an 1.4mm thickness. The specimen width is 50mm, length 400mm, and the hole diameter is 5.6mm. The holes were reamed. Crack detection was done by using the potential drop method. More details concerning the test method are presented in Ref.[1].

The target of these investigations was to determine the crack initiation fatigue life defined by obtaining a crack lengths of 1mm because this is considered to be the transition point from crack initiation to crack propagation in GLARE [6]. As discussed in Section 1.2, crack bridging becomes effective at a 1mm crack length.

Fatigue cracks at the edge of the hole are shown in figure 6.2.1 and a fracture surface in figure 6.2.2.

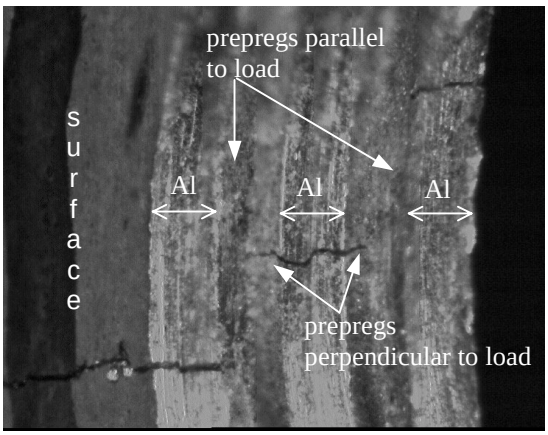

Figure 6.2.1. View into GLARE3 drilled hole, fatigue cracks in all aluminium layers and the prepregs with fibers orientated perpendicular to the load direction

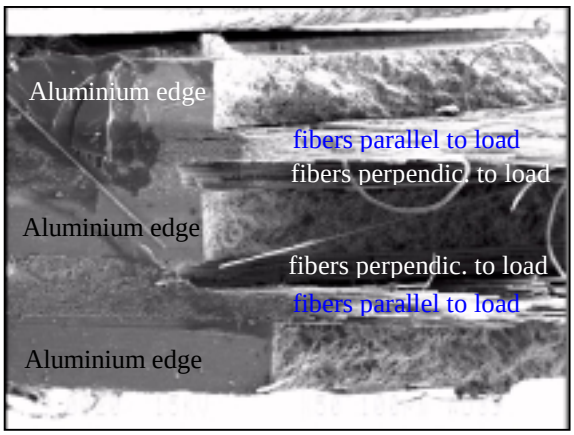

Figure 6.2.2. SEM photo of GLARE3 specimen edge after failure

Except for the final comparison of SN-curves, it is focused on the test result evaluation of the GLARE3 specimens in the following. A similar statistical evaluation has been conducted for the monolithic 2024 specimens reviewed in [2].

Constant amplitude load cycles with a stress ratio R=0.05 were applied on the specimens at different tests temperatures. Gross stress levels were selected to obtain crack initiation fatigue lives in the range between 30000 and 100000 cycles, because this range covers the most interesting fatigue life range for civil aircraft structures. On the average, a crack length increment of 0.07mm can be detected with low scatter by in situ microscopic observations on the outer aluminium sheets.. Hence, the evaluated crack initiation curves represent an accuracy of 0.07mm crack length. In all tests, cracks first initiated in the surface aluminium layers. This behaviour was also observed by previous investigators. All inner „sandwiched“ aluminium layers are supported by glass fibers at both surfaces of each layer. As a result, load transfer to fibers can occur at both sides. However, this is not possible for the outer aluminium layers. They are supported on the inner surface only. This subject is further discussed in chapter 6.9.1.

The applied gross section stress requires a correction for stiffness, for temperature and for the stress ratio, in order to allow a comparison with monolithic aluminium crack initiation data.

Calculation of stresses in the aluminium layers (σ_{metal}) due to different coefficients of thermal expansion and due to different stiffnesses of both, the 2024 aluminium sheets and the prepreg layers:

$$\sigma_{metal} = \sigma_{metal,curing} + \sigma_{metal,applied} \qquad (1)$$

$$\sigma_{metal,curing} = A_{metal} \times \Delta T \times (CTE_{laminate} - CTE_{metal}) \quad (2)$$

The stiffness matrix is calculated with:

$A_m = 0.10864 \times 10^6$ MPa. [1]

$CTE_{GLRE3-3/2-.3} = 1.68E\text{-}05$ 1/°C [4] $CTE_{2024} = 2.25E\text{-}05$ 1/°C [1]

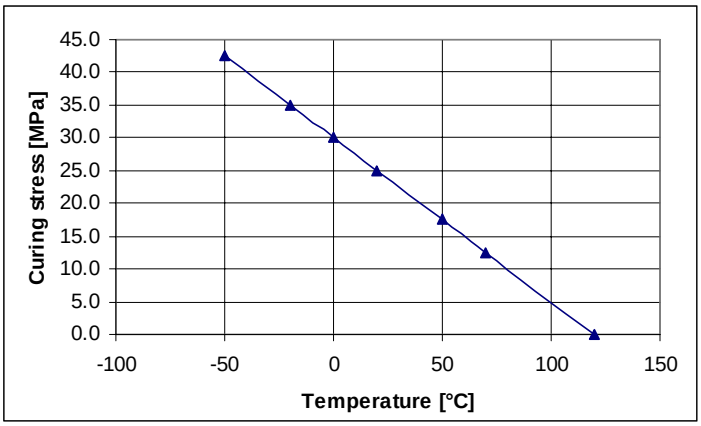

Figure 6.2.3. Curing stresses in aluminium layers of GLARE3-3/2-.3, depending on temperature. Curing temperature: 120°C

$$\sigma_{m,applied} = \sigma_t \times t_t / (t_m + (E_c/E_m) \times t_c) \quad \text{with } t_t = 1.4mm;\ t_m = 0.9mm;\ t_c = 0.5mm \text{ [GPa]} \quad (3)$$

The elasticity moduli are dependant on temperature [1]:

	-50°C	RT	70°C
E_C [GPa]	30.3	31.7	28.4
E_M [GPa]	75.3	72.4	71.0

The curing temperature for GLARE is 120°C, and room temperature in the Delft University laboratory is 20°C. Crack initiation tests have been performed at constant 70°C, room temperature and -55°C, respectively. Due to the stiffness and temperature influences, the stress ratio in the aluminium sheets differs from the applied stress ratio (R=0.05) for each specimen. An SN-curve evaluation for a particular stress ratio requires R-corrections. An empirical equation, developed by Airbus France, is used for a recalculation to R = 0.05 values for the aluminium layers in the GLARE specimens:

$$\sigma_{R0.05} = ((1-R)/0.95)^{0.6} \times \sigma_R \quad [5] \quad (4)$$

All stiffness-, temperature- and stress ratio corrected stresses in the aluminium sheets of the GLARE3 are compiled in table 6.2.1. The statistical data evaluation is performed by non-linear regression analysis with computer program ”Wöhler“, provided by Airbus Deutschland (theory according to [3]). The program calculates SN curves for different probabilities of survival (Pü) at a statistical confidence level of 95%. It demands both inputs, the applied force on the specimen and the specimen cross section area, in order to calculate the stresses by itself. Therefore, a fictitious applied force is calculated for program “Wöhler”

in order to simulate the correct stress levels in the aluminium sheets of the GLARE. The calculation results are shown in table 6.2.1.

The calculated mean stress increases by 6 MPa if GLARE3 is cooled from 70ºC to room temperature. Accordingly, a minor decrease in fatigue life at room temperature can be expected. A comparison of SN data in the range between 30000 and 100000 cycles revealed a similar order of magnitude indeed. No sufficient data for a reliable statistical evaluation are available outside this range. In figure 6.2.4 the room temperature data are plotted in the 70ºC diagram. All data points except one at a low stress amplitude fit into the 70°C scatter band. Because all results belong to the same population, they can be evaluated statistically in one batch, see figure 6.2.5.

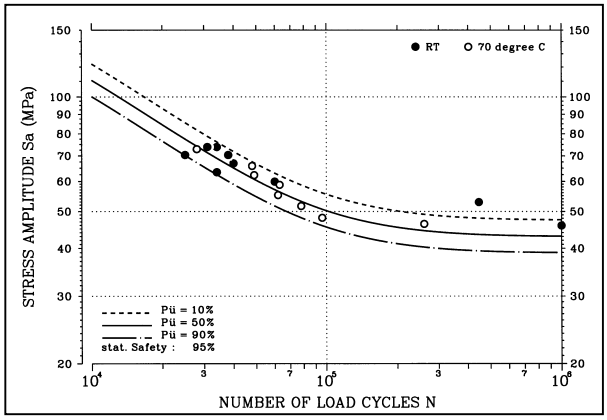

Figure 6.2.4. Crack initiation in GLARE3-3/2-.3, comparison room temperature & 70ºC, gross stresses in aluminium layers, R=0.05

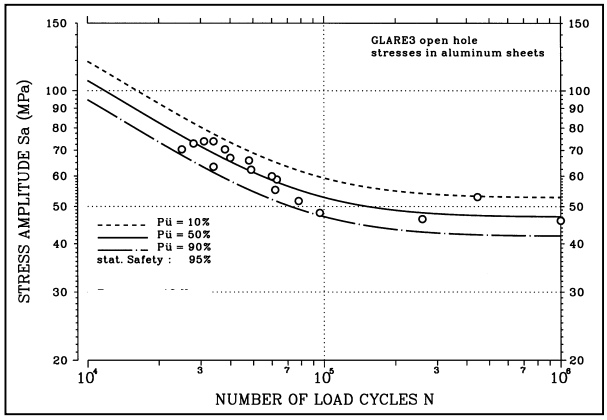

Figure 6.2.5. Crack initiation in GLARE3-3/2-.3, room temperature and 70ºC, gross stresses in aluminium layers, R=0.05

The results on the influence of low operational temperature, to be considered during the cruise phase of a commercial aircraft, are plotted in figure 6.2.6. The crack initiation life at -55ºC is systematically larger in comparison with room temperature values. A similar behaviour is observed for monolithic 2024 [1]. It can be concluded that the favourable influence of the low temperature on 2024T3 overcompensates the influence of the calculated additional tensile stresses in the aluminium layers of GLARE. Based on these results, a crack initiation test conducted at room temperature is conservative with regard to the temperature spectrum to be considered for a commercial aircraft fuselage skin.

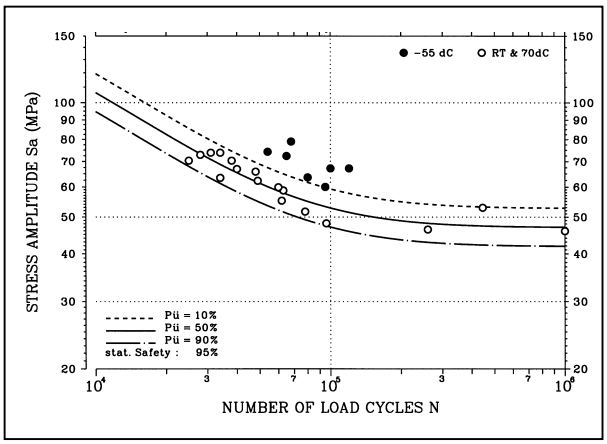

Figure 6.2.6. Crack initiation in GLARE3-3/2-.3, influence of low temperature, gross stresses in aluminium layers, R=0.05

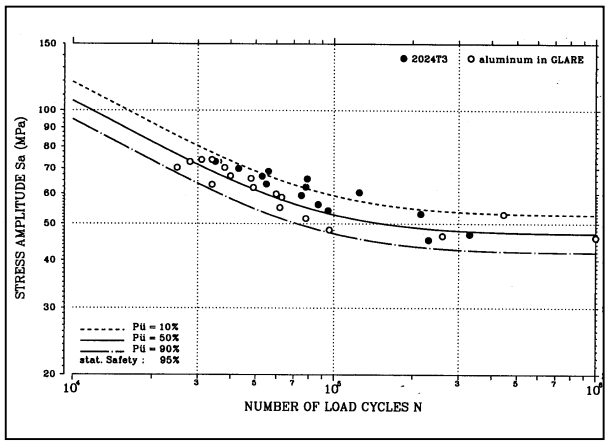

Figure 6.2.7. Crack initiation in GLARE3-3/2-.3 and 2024 T3, room temperature & 70ºC, gross stresses in aluminium layers, R=0.05 [2]

A similar evaluation of crack initiation results has been performed on 1.6mm monolithic aluminium 2024T3 specimens [1,2]. As for GLARE3, the crack initiation data at both room temperature and 70ºC fit

into the same scatter band. Figure 6.2.7 presents the comparison of monolithic aluminium 2024 and the aluminium layers in GLARE3. The data points obtained from monolithic aluminium are located at the upper range of the aluminium-in-GLARE scatter band. A longer life to crack initiation is observed for monolithic aluminium. With regard to the calculated stress levels in the aluminium sheets of the GLARE3 the results match with the expectations. At this stage of the investigation it was recommended to repeat the crack initiation tests with GLARE specimens and bonded metal specimens for comparison. It was proposed to manufacture the bonded metal specimens with sheets belonging to the same production lot as the GLARE. This way both, the possible scatter in the metal and the difference in detectable crack lengths (POD sensitivity) can be eliminated.
The proposed investigation has been conducted as a successor of the here presented results by the Dutch National Research Laboratories [7]. The crack initiation results of both bonded thin aluminium layers and aluminium-in-GLARE match quite well.

For a prediction of crack initiation in an aircraft structure, based on few constant amplitude data points, the knowledge of the slope of the SN-curve between 50000 and 10000 cycles is important. As indicated in figure 6.2.7, the slope of the GLARE results is very similar compared with the behaviour of monolithic aluminium. For selected data points on the 50% probability curve in the desired range of life cycles the slope κ is calculated. For GLARE3:

$$\kappa = \frac{\log 100000 - \log 28000}{\log 73 - \log 55} = 4.49$$

For monolithic aluminium 2024T3:

$$\kappa = \frac{\log 100000 - \log 36000}{\log 73 - \log 58} = 4.44$$

Both results fit to the slope known from literature for aluminium structures, i.e. 4.5 [8].

6.3 Crack Initiation, Accelerated Ageing Influence

(ref. factor $C_{CI(E)}$)

Because the point of crack initiation in the aluminium layers of GLARE can be accurately correlated by accounting for the stiffness and temperature effects, there should be no influence due to ageing of the epoxy matrix. This prediction was verified by Schra [7]. Both, exposed and unexposed specimens show a similar crack initiation behaviour, see figure 6.3.

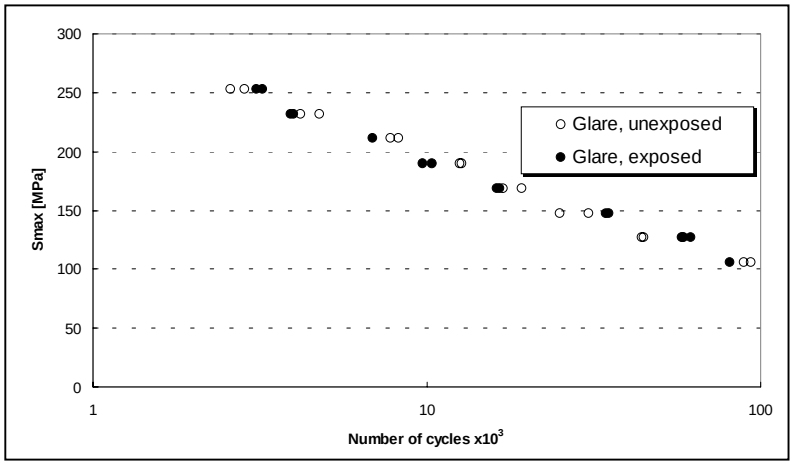

Figure 6.3, Influence of ageing on crack initiation in GLARE3 [7]

6.4 MSD Crack Initiation and Crack Propagation Scatter

(ref. factors $C_{CI(MS)}$ & $C_{CI(MS)}$)

Scatter of crack initiation and crack propagation of a GLARE structure are significant for the evaluation of the fatigue life obtained in the full scale test. Traditionally, “scatter of fatigue properties” is investigated at either a constant stress levels or a constant fatigue life as obtained in large numbers of tests on elementary specimens. Schijve investigated the crack initiation- and crack propagation scatter in ARALL and GLARE for wing spectra [17]. He observed a limited scatter of both crack initiation life and crack propagation rates, obtained in several single hole specimens. Even crack growth rates from two cracks initiated at the same side of the same hole did not show a different crack growth behaviour. Obviously the fibers located close to fatigue damage carry the major part of the load in the wake of a crack, and it thus may be expected that multiple fatigue damages do not readily interact.

It is generally observed that the ‘fatigue’ scatter decreases at high stress levels and increases at low stress levels [55]. If compared with monolithic aluminium, lower material related scatter is expected for the aluminium layers in GLARE, because the stress levels in these sheets should be higher in an optimised aircraft structure. The trend is verified by Schijve [17]. The present investigation will focus on the scatter of multiple sites in one structural element. For GLARE it is of importance in view of the very slow crack propagation rates which follow the crack initiation period, also in view of the residual strength, which is dependent on the fatigue damage rate R_D, which will be discussed in the following chapters for different material properties.

For the consideration of the MSD phenomenon on scatter, just a few specimens are used, but all fatigue sensitive locations will contribute to the statistical evaluation. The specimens should be as wide as possible. A relation between the number of fatigue sensitive locations and the fatigue life is known from monolithic aluminium. The more fatigue sensitive locations present, the lower the fatigue life of the component [18]. This behaviour is based on the higher probability of crack initiation with the increased number of fatigue sensitive locations, followed by load- and crack interaction and subsequently a relatively low fatigue live, i.e. specimen failure. The item has been discussed in chapter 1 of this research.

Three GLARE2B-7/6-.4 specimens have been used for the initial scatter investigation, i.e. no. 3-B-1 (manufacturing ID 140324-1), no. 3-B-10 (manufacturing ID 140324-10) and no. 3-B-11 (manufacturing ID 140324-11). The specimen width was 113.5 mm and the hole diameter 4.8 mm (see figure 3.2.4.3). Each specimen thus provided 20 potential fatigue sensitive locations (5 holes x 2 hole edges x 2 specimen sides). Because of the large number of fatigue critical locations an MSD scenario can be simulated which is relevant to the A340-600 single-strap butt joint discussed in Chapter 3. The advantage of the open holes is the optimal visibility for early crack initiation. Because of the pitch between the holes (22.7 mm) and the slow crack growth in GLARE it is expected that the mutual interaction of different holes will be limited.

The surface condition of all specimens is “as received” (chromic acid anodised and primed). The specimens were tested in a servo-hydraulic testing machine under constant amplitude load and room temperature until predefined numbers of cycles. Details of the test loads are given in table 6.4.1 and the crack growth records of the three specimens in tables 6.4.2 to 6.4.4 respectively. The crack length measurements have been made with a digital camera after loading the specimens to the maximum

fatigue load. The cracks are opened by S_{max} of the fatigue load, see the picture in figure 6.4.1. Due to opening of the crack a measurement accuracy < 0.1mm is possible [20]. Note that the two fatigue cracks in figure 6.4.1 originating from adjacent holes pass by without linking up. The crack initiation and crack propagation measurements have been limited to the outer aluminium layers of the GLARE2 sheets, layer 1 and layer *7.*

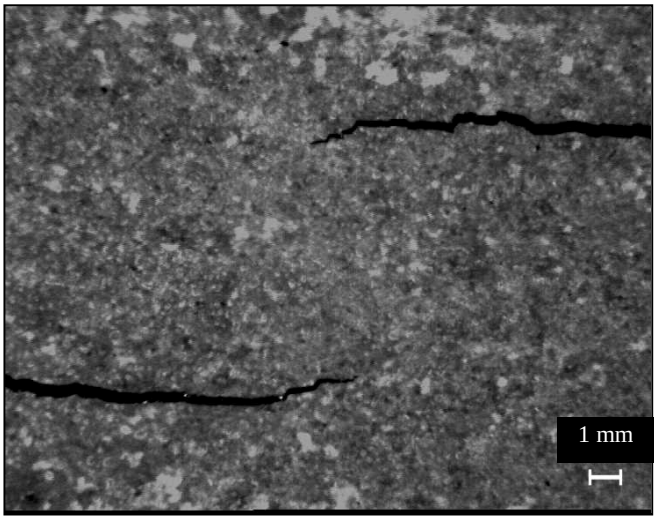

Figure 6.4.1. Crack tips 1Rr and 2Lr on specimen 3-B-11 after 60000 cycles

Crack bridging becomes effective at a crack length of approximately 1mm [21]. At a smaller crack length the propagation is rather fast. At a larger crack length the crack growth rate is expected to be constant as observed in other investigations [22,23].

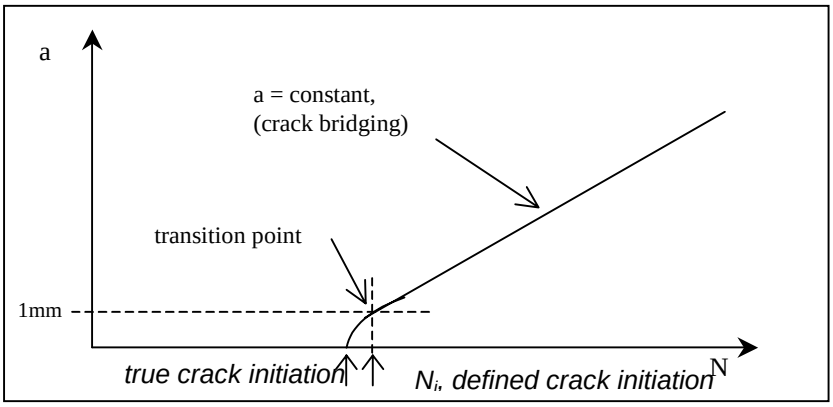

Figure 6.4.2. Crack propagation behaviour of aluminium sheets in GLARE

The transition point from non-bridged to bridged crack propagation is defined the point of crack initiation N_i.

6.4.1. Specimen 3-B-1

Specimen 3-B-1 was tested at a nominal gross stress S_{max} = 140 MPa (R = 0.1). Crack length measurements were performed between 20000 and 160000 cycles. The results for the front side are given in table 6.4.2 and in figure 6.4.6.

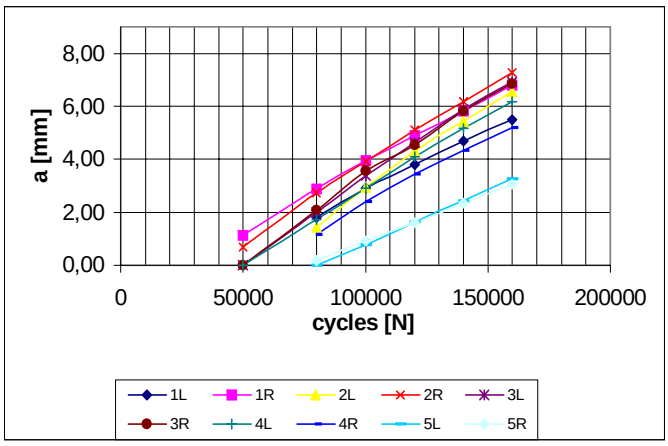

Figure 6.4.3. Crack propagation measurements specimen 3-B-1, front side

The crack propagation rates are almost constant. A linear extrapolation of each particular curve to a=1mm is performed in order to determine the point of crack initiation (equivalent life concept, see table 6.4.3). The results are presented in figure 6.4.4.

Mean crack initiation life specimen 3-B-1:

$$N_{i\,mean} = 10^{\frac{\Sigma \log N_i}{m}} \qquad (5)$$

With m = 10: N_{imean} = 68894 cycles

Standard deviation:

$$s^2 = (m * \Sigma(\log N^2) - (\Sigma(\log N))^2) / m^2 \qquad (6)$$

Standard deviation on life, extrapolated to a = 1mm: s_e = 0.116

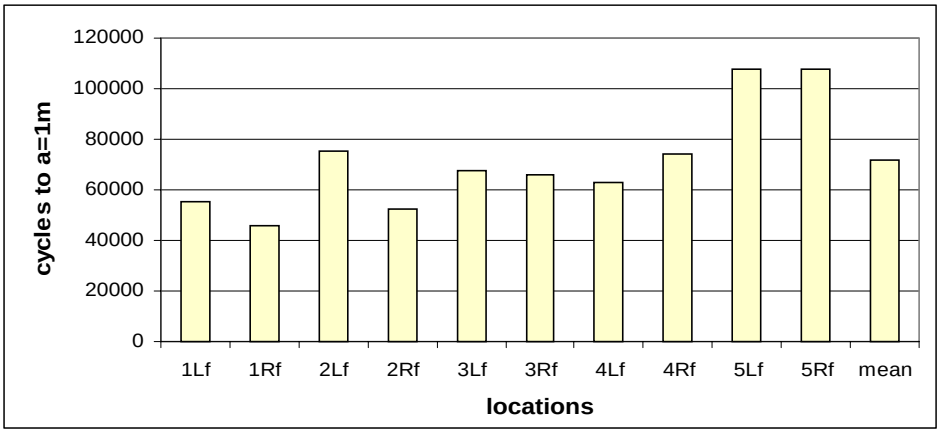

Figure 6.4.4. Extrapolated crack initiation life for specimen 3-B-1 (a_i=1mm)

The crack initiation lives are plotted in figure 6.4.5 in a normal probability graph in which a Gaussian distribution becomes a straight line. The probability of crack initiation can be calculated for the particular occurrence according to Goβe [24]:

$$Pci = 100\text{-}100 * (3n\text{-}1) / (3m+1) \qquad (7)$$

In this equation m is the number of data (m = 10 in this case) and n is the rank number of the data if they are listed in a sequence of increasing magnitude. The results are plotted in figure 6.4.5 with the

probability of exceeding N_i according to equation (5) along the vertical axis and N_i along the logarithmic horizontal scale.

The standard deviation for the number of cycles at crack link-up is calculated as well, for the later discussion of the results. This value contains a considerable portion of crack propagation for GLARE.

Crack link up is associated with crack length a = 9mm (table 6.4.3) . The standard deviation is: s_l = 0.074

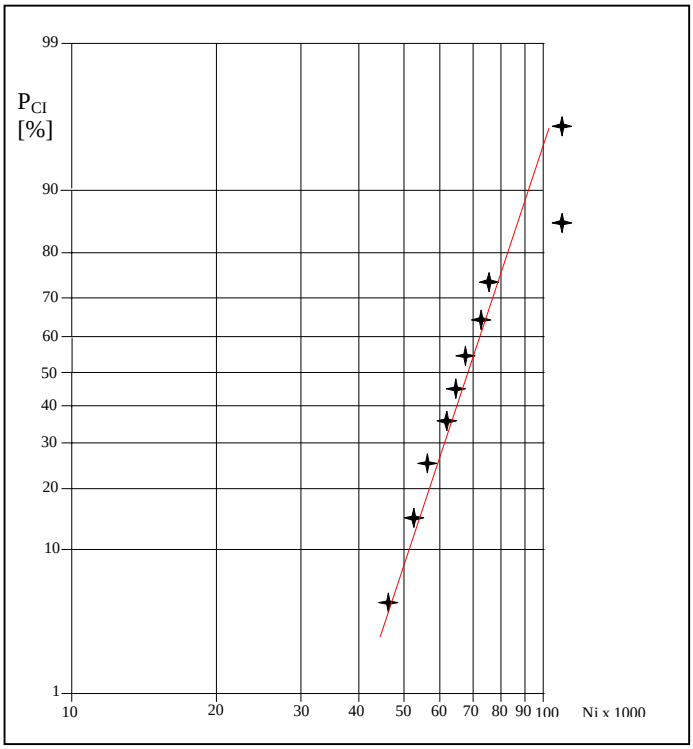

Figure 6.4.5. Probability of number of fatigue cycles to obtain crack length 1mm, specimen 3-B-1

6.4.2. Specimen 3-B-10

Crack length measurements on specimen 3-B-10 at 218 MPa nominal gross maximum stress are performed after 15000, 30000 and 45000 load cycles. Measurement results from both sides are presented in table 6.4.5 and figure 6.4.6:

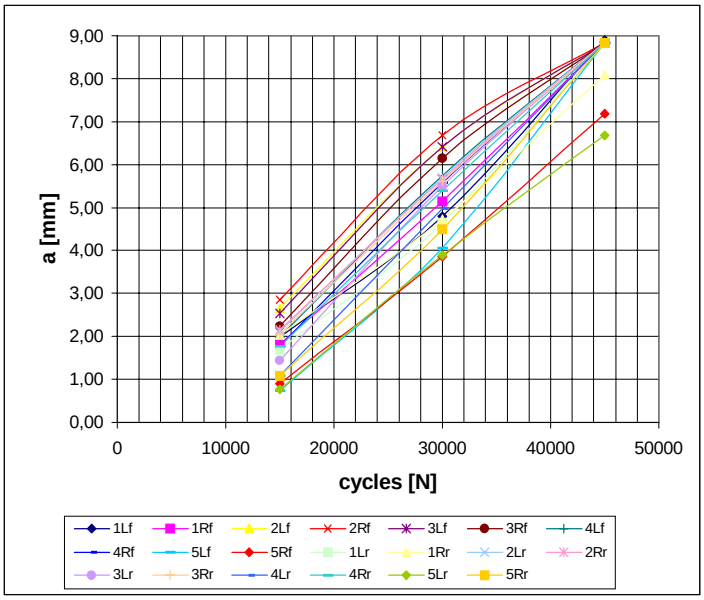

Figure 6.4.6, crack propagation measurements specimen 3-B-10

The linear extrapolation of the crack propagation curves to a=1mm is based on the data points at 15000 and 30000 cycles, since the slope of some curves decreases above 30000 cycles. The shape of these curves is explained by the fact, that some cracks had already linked up when inspected after 45000 cycles. Therefore, the maximum possible crack length is recorded at 45000 cycles, although probably it has been reached earlier.

Consequently the crack propagation curve for those cracks which initiated early, e.g. crack 2Rf, decreases above N = 30000 cycles.

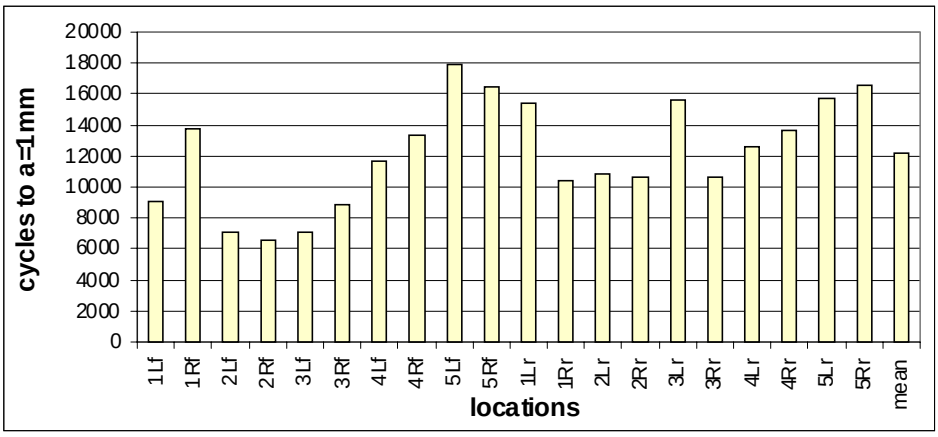

Figure 6.4.7. Extrapolated crack initiation life for specimen 3-B-10 (a_i=1mm)

Mean crack initiation life, equation (5), n = 20: N_{imean} = 11694 cycles

Standard deviation on life, a = 1mm (6): s_e = 0.129

The standard deviation for cycles at link-up, a = 9mm, (table 6.4.6) is: s_l = 0.080

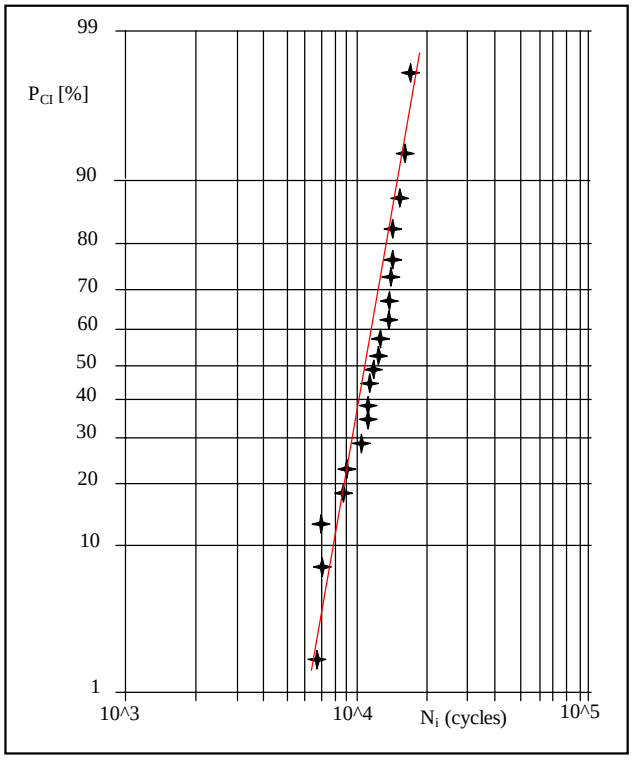

Figure 6.4.8. Probability of number of fatigue cycles to obtain 1mm crack length, specimen 3-B-10, equation (7), table 6.4.7

6.4.3. Specimen 3-B-11

Crack length measurements on the third specimen (3-B-11) tested at a nominal gross stress S_{max} = 178 MPa (R = 0.1) are performed after 15000, 30000, 45000 and 60000 load cycles. Measurement results from both sides are presented in table 6.4.8 and figure 6.4.9:

Figure 6.4.9. Crack propagation measurements specimen 3-B-11

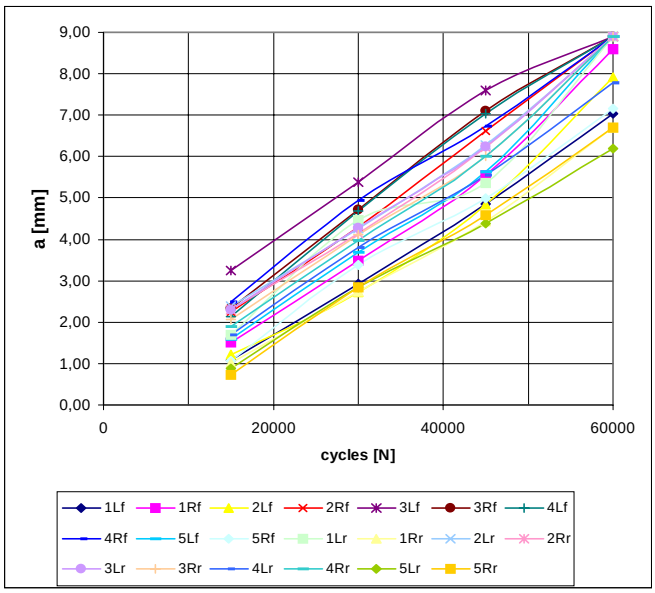

Extrapolation of the crack propagation curves to a=1mm, using the data points from 15000 to 45000 cycles, leads to the crack initiation distribution presented in table 6.4.9 and figure 6.4.10.

Mean crack initiation life, equation (5), n = 20:
N_{imean} = 10674 cycles
Standard deviation on life, a = 1mm (6):
s_e = 0.349

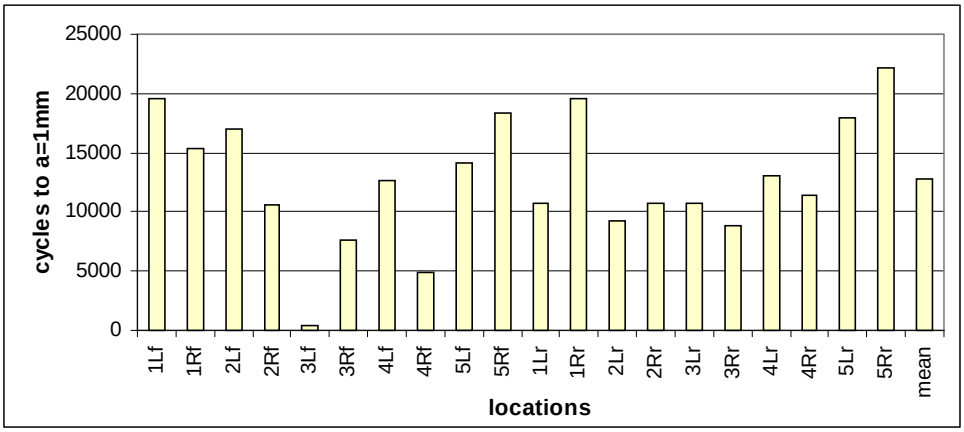

Figure 6.4.10. Extrapolated crack initiation for specimen 3-B-11 (a_i=1mm)

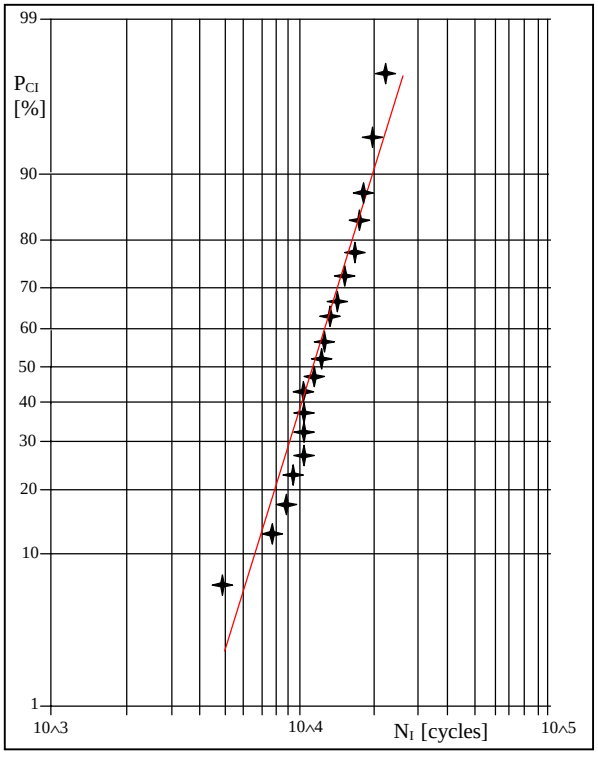

Standard deviation for cycles at link-up,
a = 9mm, ref. table 6.4.9: s_l = 0.023

Figure 6.4.11. Probability of number of fatigue cycles to obtain 1mm crack length, specimen 3-B-11, equation (7), table 6.4.10

The above three specimens are associated with the A340-600 full scale test article. If the single-strap butt joint is tested as a non-stiffened coupon, very high stresses develop at the mating surface of the butt strap. Strain gauge readings at the joint coupons (specimen type 2-B-) record 280 MPa in the net section of the critical rivet row. These strain gauge readings do not consider the thermal stress left from the curing process. In order to understand the behaviour of the butt strap, specimens 3-B-10 and 3-B-11 were tested at a high cyclic load. The gross stress in the aluminum layers including the thermal stresses are calculated to be 372 and 317 MPa respectively (see Appendix B). Taking into account a notch factor of approximately 3, the local stress regime around the holes exceeds the yield strength right in the first fatigue load cycle. Compressive residual stresses due to plastic deformation decrease the effective stress amplitude and consequently increase the crack initiation life of aluminum structures [15] around bore holes. It is expected that the approximately similar crack initiation lives of specimens 3-B-10 and 3-B-11 result from this plasticity effect, i.e. from a larger plastic zone in specimen 3-B-10, which was tested at a significantly higher load level.

6.4.4. The width effect

Thirty-eight GLARE2B and twenty-four GLARE4A specimens with five holes each are investigated within this outdoor exposure program. For the majority of specimens a tendency of earlier initiation at the center holes in relation to the other four holes was observed. For clarification of the load distribution in specimen width three strain gauges are bonded on specimen 3-B-16 close to holes no. 3, 4 and 5, see figure 6.4.12 (fastener installed, fastener head partly milled away). Strain measurements have been performed up to 107 kN, corresponding to the fatigue load of specimen 3-B-10.

Figure 6.4.13 shows the measured strains multiplied with an elasticity modulus of 72000 MPa for a conversion into stresses. Curing stresses are not considered. Higher stresses are measured at hole 4 compared with hole 5 and at hole 3 compared with hole 4. It is observed that specimen 3-B-10 was fatigued above the yield stress for the particular aluminium sheets. For specimen 3-B-1, which is tested with 69.1 kN maximum fatigue load (σ_{gross}=140 MPa) the stress level increases by 19% from hole no. 5 to hole no. 3, which is a considerable margin. It should be concluded, that a part of the observed crack initiation scatter for the five-hole specimens is linked to the variation of the stress level in the width direction.

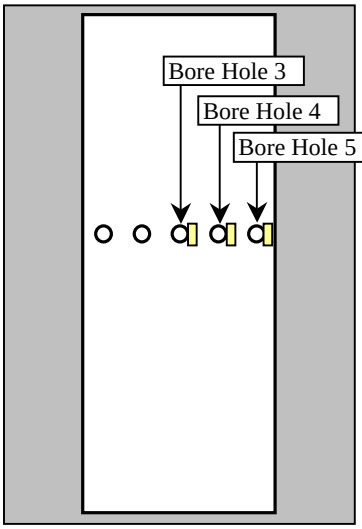

Figure 6.4.12. Strain gauge positions specimen 3-B-16

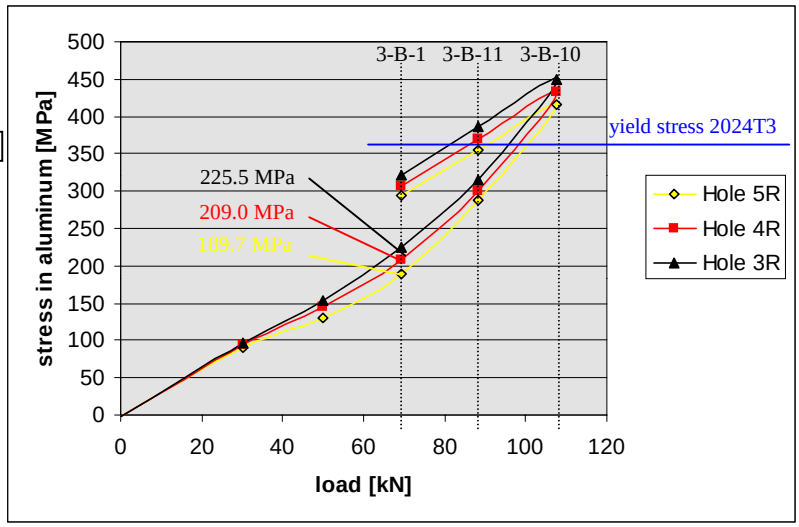

Figure 6.4.13. Measured stresses on specimen 3-B-16

In view of the latter effect additional tests with the same material but just one single open hole have been conducted. Ten specimens at two different stress levels, $S_{max\ applied}$ = 110 MPa and 140 MPa, respectively, were fatigued until crack initiation. After each interval of 1000 cycles the specimens have been inspected for cracks with the potential drop method. The crack initiation results are presented in figures 6.4.14 and 6.4.15 and tables 6.4.11 to 6.4.14.

The mean value of the fatigue life for S_{max} = 140 MPa is 45056 cycles at crack detection and 60250 cycles at 1mm crack length. The logarithmic standard deviations are 0.051 and 0.045 respectively. The mean crack initiation life related to 1mm crack length for the wide and the single hole specimen are in the same order of magnitude, i.e. 71500 cycles for the 5-hole specimen and 60250 cycles for single hole specimen. However, the scatter differs significantly, i.e. a standard deviation of 0.116 for the wide specimen and 0.045 for the single hole specimen. It is concluded, that the major contribution to the crack initiation scatter is associated with the stress deviation along the width of the 5-hole specimen and the minor part with scatter of material properties.

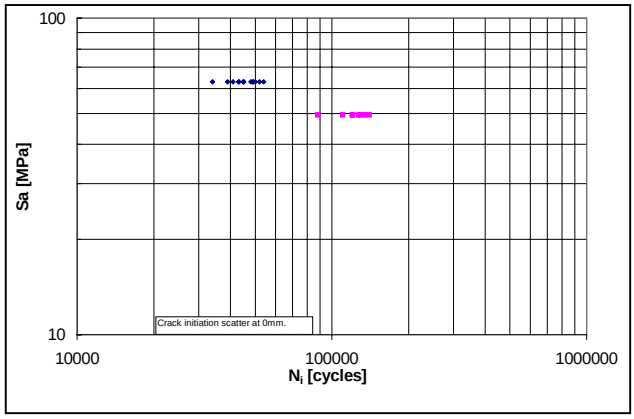

Figure 6.4.14. Crack initiation results obtained from single open hole specimens, first detection

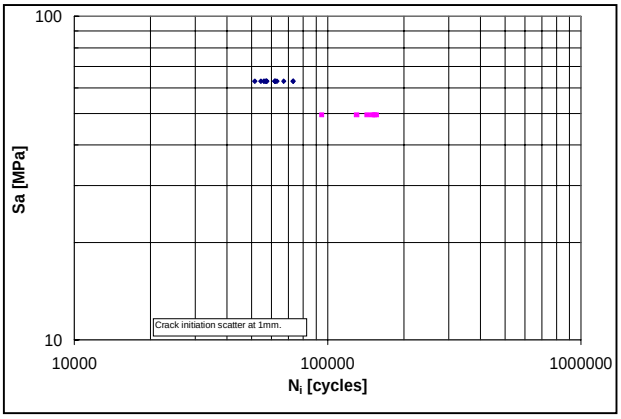

Figure 6.4.15. Crack initiation results obtained from single open hole specimens, a=1mm

6.4.5. Crack propagation, results and statistical evaluation

The curves which are plotted in figures 6.4.3, 6.4.6 and 6.4.9 indicate almost constant crack propagation rates, as expected from previous investigations [21, 22, 25]. In order to determine the crack propagation rate scatter, the following evaluation is made for the three specimens:

- Calculation of the da/dN-values between the available measurement points for each particular crack.
- Calculation of the mean value of the da/dN-values obtained in the first step.
- Calculation of the standard deviation of log(da/dN) of the mean values of the previous step.

The da/dN mean values of the individual cracks are plotted for the three specimens in figures 6.4.16 to 6.4.18 (data collected in tables 6.4.15 to 6.4.17) and the logarithmic standard deviation of these values for each specimen are given in figures captions.

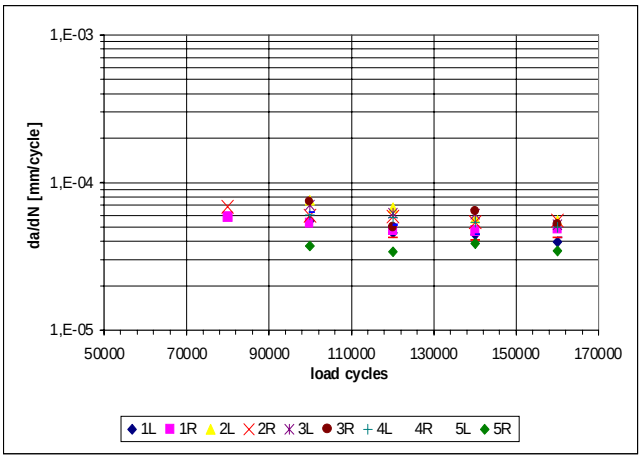

Figure 6.4.16. Crack propagation rates specimen 3-B-1, max. gross stress 140 MPa Crack propagation rate logarithmic standard deviation: s = 0.077

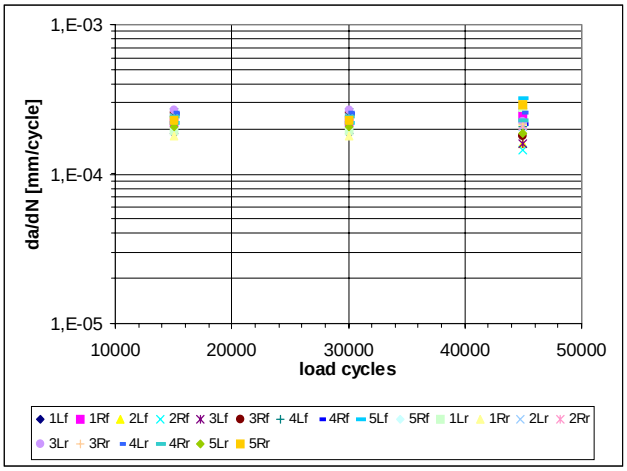

Figure 6.4.17. Crack propagation rates specimen 3-B-10, max. gross stress: 218 MPa.Crack propagation rate logarithmic standard deviation: s = 0.038

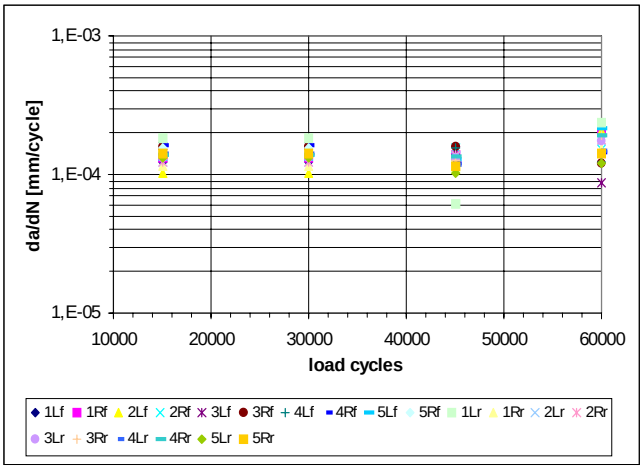

Figure 6.4.18. Crack propagation rates specimen 3-B-11, max. gross stress 179 MPa. Crack propagation rate logarithmic standard deviation: s = 0.037

6.4.6. Discussion of open hole scatter results

Standard The logarithmic standard deviations of fatigue lives between 10^5 and 10^6 cycles are usually below 0.2 for monolithic aluminium coupon specimens with holes, if the holes are produced according to the aircraft industry standard manufacturing instructions [26]. Standard deviations below 0.2 are defined as low scatter, above this value as high scatter. However, the standard deviation then applies to *failure* of the specimens. The standard deviation is thus affected by scatter of the fatigue crack initiation period and the crack growth period. When the specimens fails, all cracks have linked up, either due to fatigue or in the static mode. Recently developed analysis methods allow to separate the crack initiation and crack propagation parts and to decrease the scatter by calculation of high numbers of randomly evaluated MSD scenarios [26]. The mean values for both, crack initiation and crack propagation lives, are lower for the MSD analysis than the fatigue lives which have been determined with the coupon specimens.

The crack initiation period of a monolithic aluminium riveted joint is in the order of 85% of the fatigue life until failure [15], and thus it covers the major part of the fatigue life. This is different for a riveted GLARE joint, because the cracks in GLARE intend to initiate earlier but its crack propagation life is significantly longer compared to riveted joints of monolithic aluminium [1].

In the present investigation it was decided to use five-hole coupon specimens for a scatter investigation in order to consider the multiple side damage phenomenon. The crack propagation curves for adjacent cracks are parallel for at least crack lengths up to 6mm, which is 2/3 of the half net section between two holes (net section from hole edge to hole edge: 18mm; half net section: 9mm). Due to this behaviour it is justified to consider any particular crack initiation as an independent occurrence which then provides one independent input for a statistical analysis.

If a comparison is requested between scatter of SN-data for monolithic aluminium joints and for GLARE joints for a similar structural performance level, then the standard deviations at the fatigue life at crack link-up in GLARE should be used, i.e. 0.074, 0.080 and 0.023 for specimens 3-B-1, 3-B-10 and 3-B-11, respectively. In this case, scatter for similar structural conditions would be compared, which is failure of the aluminium. The scatter data for GLARE are below comparable values for monolithic aluminium joints, but it is obviously associated with the dominating crack propagation phase in the GLARE joints rather than to crack initiation. Such a simple comparison would not be satisfactory for the *crack initiation* fatigue life in aircraft structures made of GLARE and the interpretation of full scale fatigue tests.

The standard deviations for crack initiation, based on the transition crack length of 1 mm, are 0.116, 0.129 and 0.349 for the three GLARE specimens, respectively. Scatter of the first two specimens is acceptable, but the standard deviation for specimen 3-B-11 is significantly larger. This high standard deviation is caused by a single particularly early crack initiation of crack 3Lf with a calculated point of crack initiation at 467 load cycles. This seems to be comparable to the 1.27mm rough flaw case, which has to be considered occasionally to account for processing or handling errors [27]. Without including the result of crack 3Lf, the logarithmic standard deviation for specimen 3-B-11 drops to 0.157 (for 1mm crack length), which is a similar order of magnitude as obtained for the other specimens.

As described in section 6.4.4, a tendency was observed towards first crack initiation at the centre hole of the specimens with a row of 5 holes followed by later crack initiation at the outer ones, i.e. holes 1 and 5. This behaviour was also observed in previous investigations [25]. It was related to a slightly inhomogeneous stress distribution along the specimen width. The influence of this discontinuity was investigated in [26] and it was found that the simplification of using the remote field stress instead of the local stress at the crack initiation site may lead to a non-conservative prediction of the fatigue life. However, the results of the present tests on the single hole specimens should also be considered here. It was shown that the logarithmic standard deviation in these GLARE specimens with two crack initiation locations (front and back side) is as low as 0.045. A comparison with the results of specimen 3-B-1 (5 holes) with the single-hole specimens tested at 140 MPa leads to interesting results. The different *net* stress levels and the different K_t-values require attention. With the dimensions of the two types of specimens the results are:

Specimen 3-B-1: $\sigma_{net} = \sigma_{gross}$ x 114.8mm / (114.8mm-5x4.8mm) = 177.0 MPa

Single hole specimen: $\sigma_{net} = \sigma_{gross}$ x 50mm / (50mm-4.8mm) = 154.9 MPa

The stress concentration factors are calculated with the Heywood equation [29]:

$$K_t = 2 + \left(1 - \frac{D}{w}\right)^3 \qquad (8)$$

which leads to K_t = 2.49 for specimen 3-B-1 and K_t = 2.74 for the single hole specimen. The peak stress at the hole edge then becomes:
Specimen 3-B-1: σ_{peak} = 177 x 2.49 = 441 MPa
Single hole specimen: σ_{peak} = 154.9 x 2.74 = 424 MPa
which implies a difference of 4%. The difference should have a small effect on the comparison of the fatigue lives. The effect is estimated by using the Basquin relation $S^k N$ = constant. The slope factor k can be obtained from the single hole specimen fatigue lives (a = 1 mm) for 110 MPa and 140 MPa (see tables 6.4.12 and 6.4.14) which leads to:

$$\kappa = \frac{\log 137583 - \log 60250}{\log 140 - \log 110} = 3.42$$

The mean fatigue life of the single hole specimens (60250 cycles, table 6.4.12) is then corrected for the local stress conditions of the 3-B-1 specimens to a crack initiation fatigue life of:

$N_i = (441 / 424)^{3.42}$ x 60250 = 68920 cycles

This result should be compared to the mean crack initiation life observed from the five holes in specimen 3-B-1 which is 71481 cycles (Section 6.4.1). Apparently, the agreement is very good. In other words, the local peak stress was useful for indicating the severity of the cyclic stress for crack initiation in GLARE. Actually, this should be expected because in both types of specimens crack initiation is the same phenomenon occurring in the same aluminium sheets. The larger scatter of crack initiation occurring in the test on specimen 3-B-1 is associated, at least for some part, with the inhomogeneous stress distribution in the width direction.

The practical significance of the previous results for fatigue critical elements in a GLARE structure depends on the characteristic aspects of these elements, representative stress levels in the aircraft structure and relevant loading cases. In view of representative stress levels a distinction should be made between structural items with a low load transfer and bending, e.g. a frame clip attachment to a fuselage skin, and on the other hand, joints with a high load transfer and a high bending load, such as longitudinal lap joints and circumferential lap joints.

From the analysis of the data obtained so far it can be concluded that a nominal design stress level of 140 MPa can be a most relevant design stress level for aircraft GLARE structures. A mean crack initiation life of 71500 cycles followed by very slow crack growth indicate that GLARE will be a useful material for aircraft fuselages. Furthermore, the aluminium layers are still below yield in an open hole specimen (see appendix B), but it should be recommended to check the crack initiation behaviour of additional specimens tested at the same load level. For this purpose, the outdoor exposure program includes 10 blunt notch specimens which have been cycled up to different numbers of cycles at the same load level. In view of the almost constant crack growth rate and the low scatter the crack initiation, it is expected that these specimens will confirm the present results.

The average crack lengths of all specimens with 5 holes, including specimen 3-B-1, tested at S_{max} = 140 MPa as obtained at the end of the test are presented in figure 6.4.19 (data in table 6.4.18). The results

are found along an almost straight line. It can thus be concluded that the cracks in all specimens initiated with low scatter within a narrow life period.

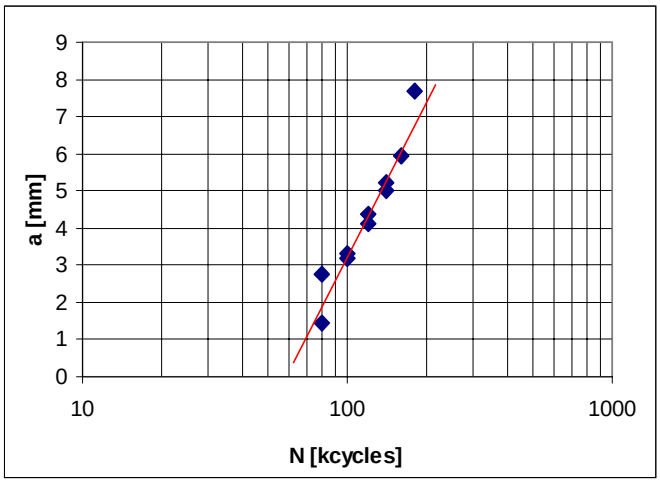

Figure 6.4.19. Average crack lengths of different specimens dependent on load cycles

The crack propagation rates obtained in the three specimens tested at different stress levels are presented in figure 6.4.20. because the crack growth rate were almost constant the mean values are plotted in this figure over the period in which measurements were obtained.

If the crack propagation rates da/dN are plotted versus the applied stress levels, the results form almost a straight line, see figure 6.4.21. This behaviour confirms the observations from de Koning, Schra, Alderliesten and Homan [8,9], for through cracks and for part through the thickness cracks.

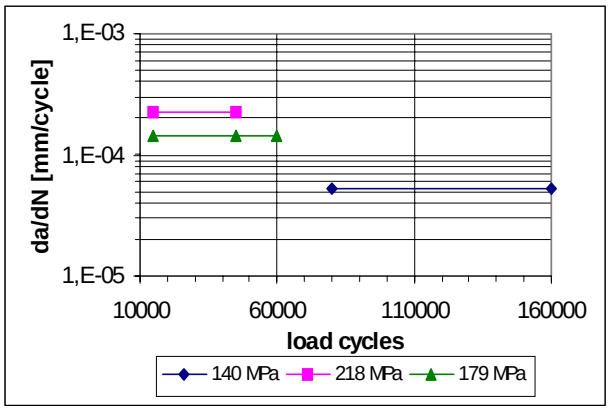

Figure 6.4.20, Crack propagation rates obtained from specimens 3-B-1, 3-B-10 and 3-B-11

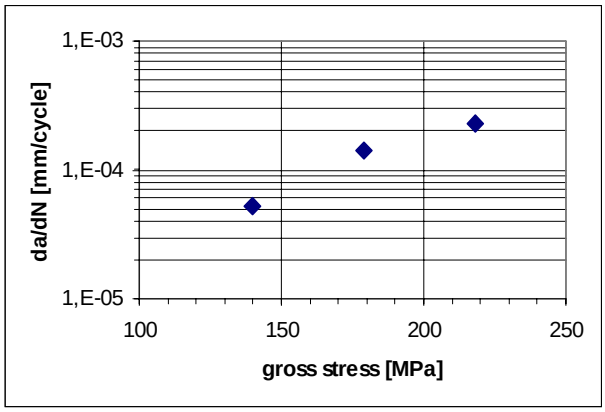

Figure 6.4.21. Crack propagation rates dependent on stress level

The results obtained in the fatigue tests on the GLARE specimens with open holes have shown a systematic behaviour. The crack initiation life was similar for the specimens with 5 open holes and for specimens with a single open hole for an equal peak stress at the edge of the hole. Secondly, the effect of the stress level indicated a value of the slope factor of the SN data which is of a similar magnitude as found for 2024-T3 notched elements. Finally, with respect to scatter of the crack initiation life, the data showed rather low values of the standard deviations of log(N), i.e. 0.077, 0.038 and 0.037 for the three stress levels used in the tests. A limited scatter is typical for fatigue crack propagation in aluminium alloys, but it is instructive to know that this is also true for the aluminium layers in GLARE. It indicates that the metal layers in the hybrid fiber-metal laminates still behave as metal layers. An additional knock down factor for scatter of fatigue crack growth in GLARE seems not to be necessary.

6.5 Crack Opening Measurements at Fatigue Cracks

The significance of the crack bridging mechanism, the size of the delamination zone and the delamination resistance was briefly discussed in chapter 4.1.2. At least two effects are distinguished, which are both linked to the adhesive forces between prepreg/metal and resin/fiber, respectively, as well as to the shear modulus of the prepreg:

1) The delamination resistance influences the fatigue delamination size between metal and prepreg, the effective crack bridging stress, probably the COD and consequently the stress intensity factor on the crack tip.
2) The shear stiffness of the prepreg influences the crack opening (without necessarily an extension of the delamination size).

If there is an influence of moisture which has been absorbed by the prepreg on the crack propagation rate in the aluminium layers, it should be dependent on both properties, the delamination resistance (responsible for the fatigue delamination size) and the prepreg shear stiffness (indicating the load distribution between fibers and aluminium for any load cycle). For an experimental investigation of this phenomenon it would be useful to saturate a prepreg around a drilled hole and to perform crack propagation and crack opening displacements with the structure thereafter. However, the problem of very long required exposure times is encountered for moisture penetration in the yz-plane of a GLARE prepreg.

In this chapter COD measurements are discussed for a qualitative investigation of the expected phenomena. In order to establish fatigue cracks with different fatigue delamination areas around the fatigue cracks fast, GLARE3-3/2-.4 specimens according to figure 6.5.1 are fatigue cycled to the similar crack length 2a=40mm at different constant material temperatures. Then, COD measurements are performed in order to measure the expected influence of the delamination size. The different delamination sizes should influence the fatigue crack propagation rates, independent from the origin of the delamination size, e.g. temperature, adhesive degradations due to moisture in the prepreg or both.

In a second step, one specimen (including the a.m. fatigue cracks and with a given fatigue delamination size) is accelerated aged in a 70°C/85%RH environment. In intervals of 500 hours, 1000 hours, 1500 hours and 3000 hours COD measurements are performed. An increase of displacement after ageing would indicate an influence of the shear deformation in the prepreg (assumption for low stress levels: without delamination size extension) and consequently an influence on the aluminium crack tip stress intensity for any fatigue load cycle.

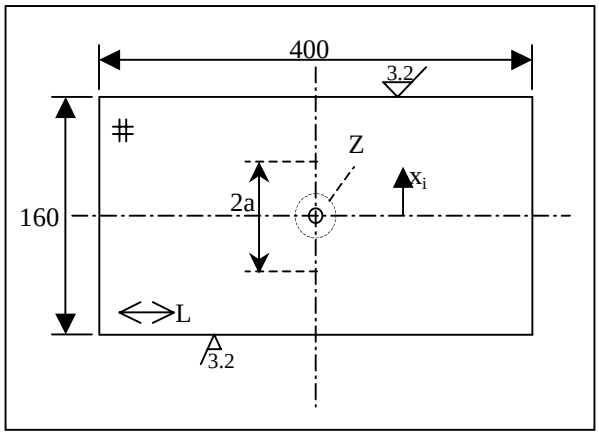

Figure 6.5.1. Open hole specimen design for COD measurements

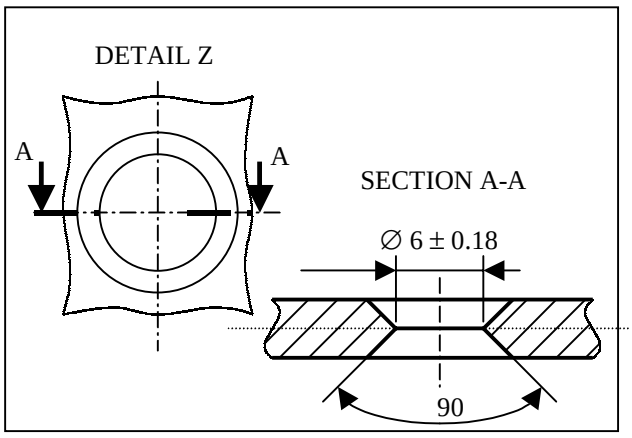

Figure 6.5.2. Bore hole design in COD specimen for COD measurements

The crack opening displacement is measured at the location of the hole in the center of the specimen. All specimens are fatigue cycled at 140 MPa applied stress. Specimens 1a and 1b are fatigued at room temperature, specimen 2 is fatigued at 70°C and specimen 3 at –30°C.

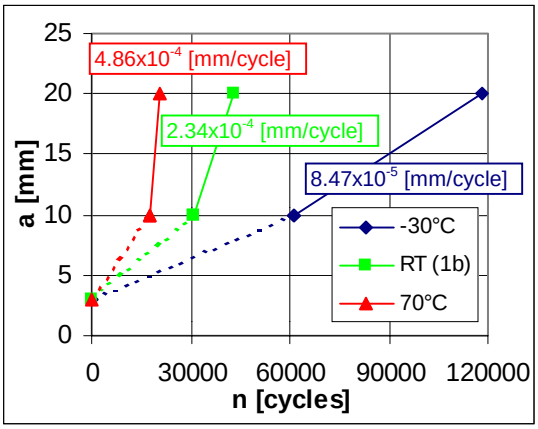

Figure 6.5.3. Crack propagation at different temperatures, all specimens not exposed

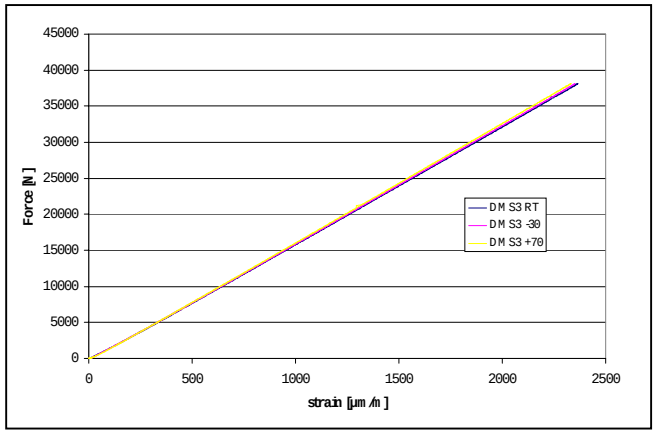

Figure 6.5.4. Specimen 1a, far field strain measurement at different temperatures (without fatigue crack)

As known from previous research [39] crack propagation rates decrease with decreasing test temperature. The crack propagation curves from the present research confirm the trend, see figure 6.5.3. Fatigue cycles are recorded at 2a=20mm and 2a=40mm. The first part includes the crack initiation life, it is consequently less reliable for a crack propagation rate determination. The average crack propagation rates which are plotted in figure 6.5.3 are calculated between a=10mm and a=20mm crack lengths.

The influence of temperature on the elasticity modulus of the material is determined before a comparison of displacements at different temperatures is performed. As shown in figure 6.5.4, no influence of temperature on the tensile elasticity modulus can be measured in the undisturbed GLARE sheet.

The crack opening displacements are measured at the center line of the drilled holes. At specimen 1a it is measured without applied force and without temperature compensation of the strain gauge (see curves at F = 0 kN in figure 6.5.5) at different material temperatures. Compared with room temperature, the crack is closing at –30°C and it opens at 70°C. The behaviour is explained with the internal stress system of the GLARE3 ingredients. Two contradicting effects have to be considered. First, the entire GLARE sheet is shrinking with decreasing material temperature and the crack opening should be reduced. On the other hand, the fatigue crack faces are mechanically free ends, at which the constraining curing stresses in both, the fibers (compression without crack) and metal (tension without crack) can be released. Due to this strain release, an equilibrium of forces and displacements develops, which keeps the fatigue crack open within the measured material temperature range, ref. figure 6.5.5.

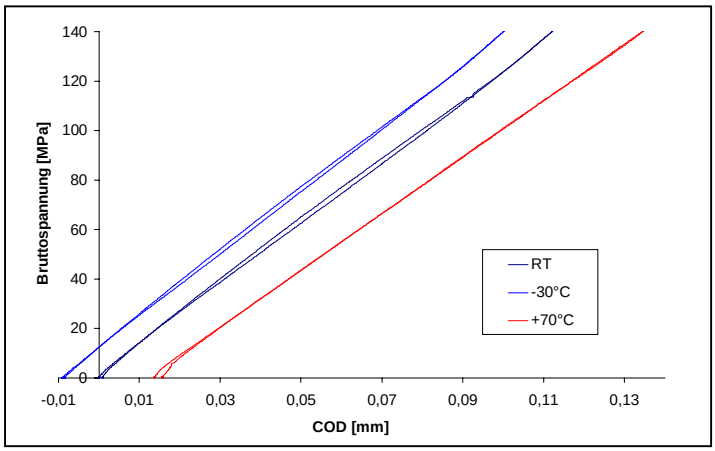

Figure 6.5.5, specimen 1a, absolute displacements at different temperatures

Compared with room temperature the crack opening displacements due to shrinking or expansion corresponding with an applied stress of 12 MPa reduction at –30°C and +15 MPa applied stress increase at 70°C.

Low temperature decreases crack opening and consequently the stress intensity at the crack tip. A high temperature increases crack opening and stress intensity. This behaviour is representative for a fatigue cracked aircraft GLARE structure. The crack opening displacement almost neutralizes the curing stresses in the aluminium in the vicinity of the crack, as demonstrated in the following. The blue line in figure 6.5.6 shows the crack opening displacement as measured on specimen 1a without external loads for –30°C, ≈20°C and 70°C. It is extrapolated to 120°C. However, the COD measurement has been set to 0mm for the room temperature value, at which in fact the crack is already open. Theoretically, the crack is closed at 120°C. That's why the blue curve is moved downwards in diagram 6.5.6, until the COD equals 0mm at 120°C. The purple line shows the theoretically true crack opening, related to material temperature. The purple line in figure 6.5.7 (dS_{cod}) shows the stress levels which need to be applied on the laminate at the different temperature levels, in order to reverse the stress opening displacements contained in figure 6.5.6. The calculation of this curve is done similar as for the displacements shown in figure 6.5.6, but now using the delta *stresses* at a constant COD. Since the displacement curves for specimen 1a are almost parallel for the three tested temperatures, the delta stresses are almost independent from the crack opening.

The green line in figure 6.5.7 represents the curing stress in the aluminium layers of the laminate in the non-notched condition (chapter 6.2). If the applied stress which is required to close the crack (dS_{cod}) is superposed with the curing stress in the aluminium layers (Sc, non-notched condition), it results in the curing stress in the aluminium layers which has to be considered for crack propagation analysis at different temperatures (Scc). It turned out, that this stress almost equals to zero, i.e. it should not be considered for crack propagation analyses. The remaining influences on fatigue crack propagation rates are the fatigue delamination size, the shear stiffness of the prepreg at the metal/prepreg interface and the reduction of crack propagation rates in 2024T3 aluminium at temperatures below freezing (ref. chapter 6.2).

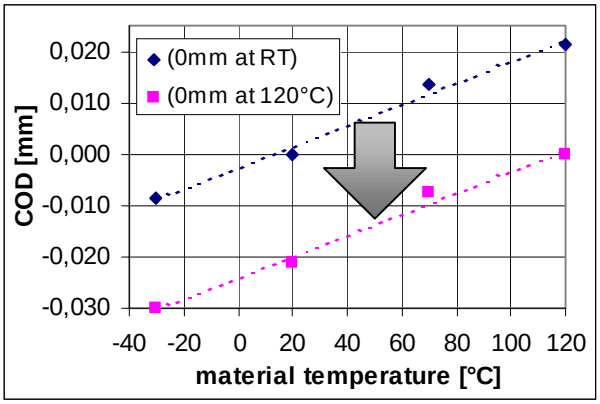

Figure 6.5.6. COD measurement results without external load, extrapolated for 120°C (blue line) and moved to COD = 0mm at 120°C (pink line)

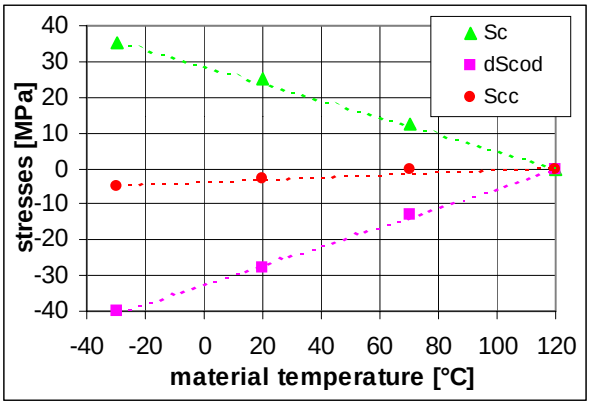

Figure 6.5.7. Curing stress far field(Sc) superposed with crack opening stress (dS_{cod}) equals curing stress in cracked condition (Scc)

If fatigue cracks are introduced at a low temperature, the size of the delamination zone is smaller than for cracks introduced at a high temperature [44]. The size of the delamination zone (A_{del}) is characterized by the length of the delaminated fibers at the tip of the fatigue crack. For the present test series it was found that:

$$A_{del.}\text{ (fatigue at –55°C)} < A_{del.}\text{ (fatigue at RT)} < A_{del.}\text{ (80°C)}.$$

Diagrams 6.5.8 to 6.5.10 contain the crack opening displacements for specimens 3, 1b and 2, respectively, each measured at *three different material temperatures*. Since the data for specimen 1b (fatigued at RT) are lost, figure 6.5.7 contains data after 500 hours exposure in 70°C / 85%RH environment.

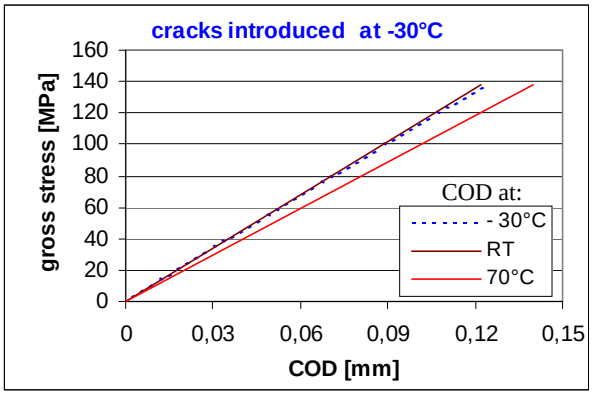

Figure 6.5.8. Specimen 3, COD at different material temperatures

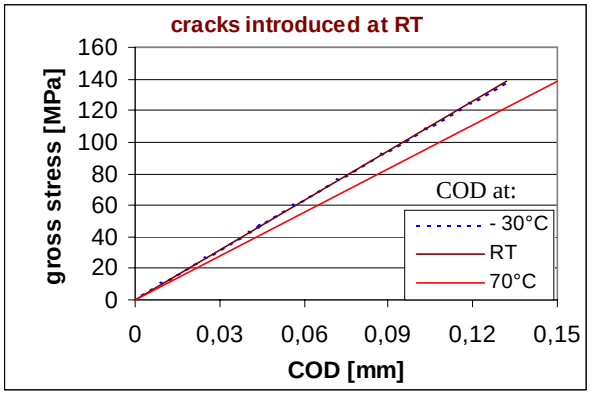

Figure 6.5.9. Specimen 1b after 500h exposure COD at different material temperatures

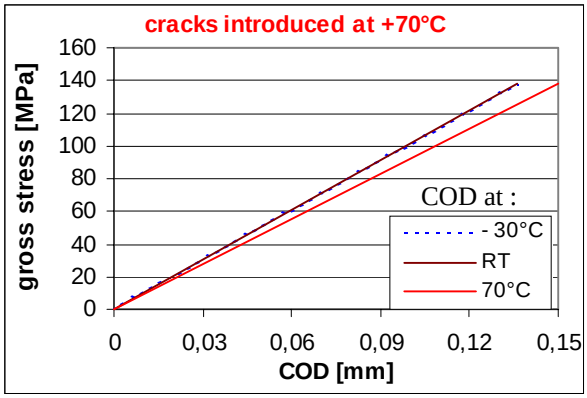

Figure 6.5.10. Specimen 2, COD at different material temperatures

The displacement plots for all specimens are similar at both, -30°C material temperature and room temperature. The displacements increase at 70°C, i.e. the shear deformation at the crack face increases. It does not change below room temperature, independent from the delamination size, which is in line with literature [14]. The available curves are now compared at *constant COD test temperatures* in figures 6.5.11 to 6.5.13. Each diagram collects the data from three different specimens, i.e. specimens with different fatigue delamination sizes:

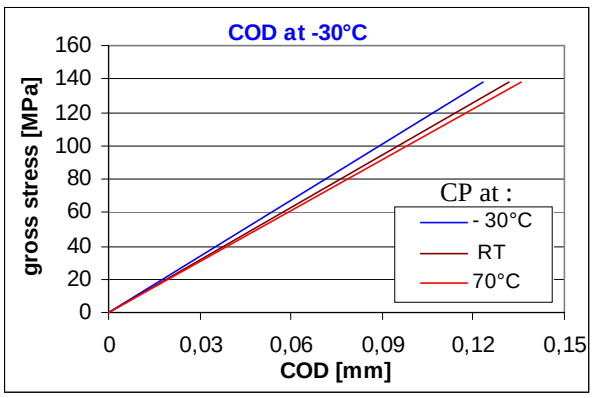

Figure 6.5.11. COD at –30°C for specimens 3, 1b, 2, specimen 1b exposed 500h at 70°C/85%RH

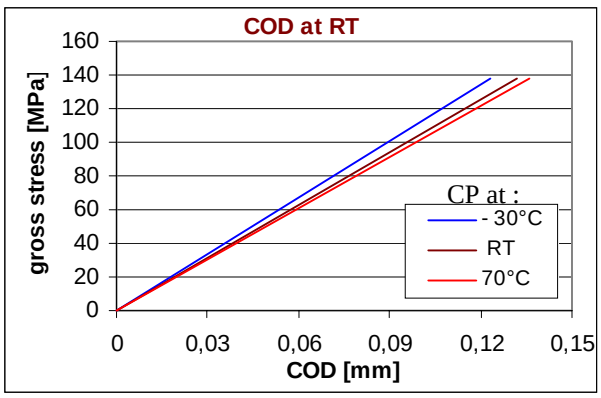

Figure 6.5.12. COD at RT for specimens 3, 1b, 2, specimen 1b exposed 500h at 70°C/85%RH

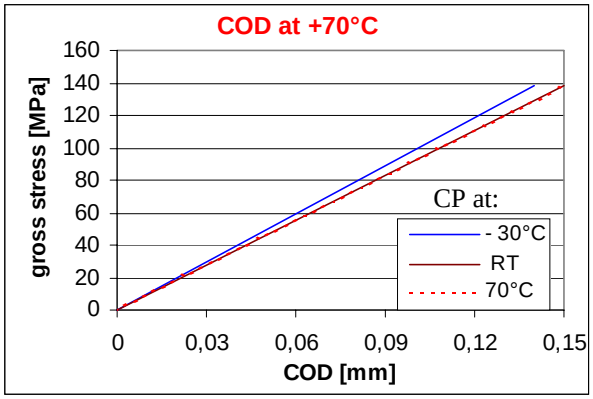

Figure 6.5.13. COD at 70°C for specimens 3, 1b, 2, specimen 1b exposed 500h at 70°C/85%RH

At all temperatures the displacement is the largest for specimen 2 (fatigued at 70°C), followed by specimen 1b (fatigued at room temperature) and specimen 3 (fatigued at –30°C). Obviously, the fatigue delamination size has an influence on the crack opening displacement, since it is the only variable in this comparison. It is observed at all test temperatures, that the displacements of specimens 2 and 1b are much closer to each other than the displacements of specimens 1b and 3.

The different slopes of the COD-versus-Force curves indicate the influence of temperature on the shear modulus G. Marissen developed an equation which related the shear modulus of the resin rich layers between the aluminium and the fibers in ARALL to the crack opening displacement [56]. His equations do not consider the delamination size.

$$COD = 2 \times \frac{E_{Al}}{E_{lam}} \times \sigma_{lam} \times t_{Al} \times \sqrt{\frac{t_{ad}}{j \times G_{ad}} \times \left(\frac{1}{E_{Al} \times t_{Al}} + \frac{1}{E_{ar} \times t_{ar}} \right)} \qquad (9)$$

j: number of bonds between aluminium sheets and prepregs

t_{ad}: thickness of resin rich layer

G_{ad}: shear stiffness of adhesive

E_{ar}: tensile elasticity modulus for aramid fibers

t_{ar}: thickness of aramid fiber prepreg

A resin rich layer is not present in the qualified GLARE with FM94/S-glass prepreg. Therefore, equation (9) is transformed into a solution, which relates the COD to the prepreg thickness:

$$COD = 2 \times \frac{E_{Al}}{E_{lam.}} \times \sigma_{lam.} \times t_{Al} \times \sqrt{\frac{t_{prep.}}{j \times G_{prep.}'} \times \left(\frac{1}{E_{Al} \times t_{Al}} + \frac{1}{E_{prep.} \times t_{prep.} \times n} \right)} \qquad (10)$$

j: number of contact surfaces between aluminium sheets and prepregs

$t_{prep.}$: thickness of one prepreg

$E_{prep.}$: tensile elasticity modulus for FM94/S-glass prepreg

n: number of prepregs

Equation (10) is solved for $G_{prep.}'$ in equation (11), here called the *apparent* shear modulus (of the entire prepreg. In fact the problem has to be distinguished between the fibers oriented in – and perpendicular to the load direction. Here it will be calculated with one value $G_{prep.}'$) :

$$G_{prep.}' = \frac{t_{prep.}}{j \times \left(\frac{COD \times E_{lam.}}{2 \times \sigma_{lam.} \times t_{Al} \times E_{Al}} \right)^2} \times \left(\frac{1}{E_{Al} \times t_{Al}} + \frac{1}{E_{prep.} \times t_{prep.} \times n} \right) \quad (11)$$

Figure 6.5.14 shows a cut through a fatigue damaged GLARE3 sheet, it is a magnification of section A-A in figure 4.1.2.5. One fiber prepreg is bridging the fatigue cracks in the aluminium sheets, since it is oriented parallel to the load direction. The other prepreg orientation is perpendicular to the load, it does not contribute to fiber bridging. The delaminated fiber length l_{fiber} is elongated by the length δ_{fm} due to the external applied load. The mean fiber volume of the FM94/S-glass prepreg is 73%, the low resin contend prevents a formation of a resin rich layer between metal and fibers. Shear deformation can be discussed just for the prepreg itself. At the boundary of the delamination a shear stress τ and a shear deformation δ_{ad} develops in the prepreg, resulting in the shear angle γ.

In the following it is assumed for simplification, that the shear stresses and shear deformations are similar for both prepregs which are sandwiched between the aluminium sheets.

Marissen developed for the calculation of the local shear stress in the prepreg [56] (equation adapted for GLARE):

$$\tau = (\sigma_{Al} - \sigma_{Al,0}) \times t_{Al} \times \sqrt{\frac{t_{prep.}}{j \times G_{prep.}'} \times \left(\frac{1}{E_{Al} \times t_{Al}} + \frac{1}{E_{prep.} \times t_{prep.} \times n} \right)} \quad (12)$$

$\sigma_{Al,0.}$: curing stress in aluminium sheets

Since the curing stress equals zero at the crack/prepreg interfaces (ref. figure 6.5.7), it is considered:

$\sigma_{Al.} = 0$ MPa

Equal elasticity moduli are used for all temperatures in the following calculations, since no different moduli are measured in the far field (ref. figure 6.5.4).

Further it is given:

$$\gamma = \frac{\tau}{G_{prep.}'} \quad (13)$$

and

$$\delta_{ad} = t_{prep.} \times \tan(\gamma) \quad (14)$$

Equation (4) in chapter 4.1 introduced the equilibrium of elongations at location x_i of the crack:

$$\delta_{fm}(x_i) + \delta_{ad}(x_i) = u_{\infty}(x_i) - u_{br}(x_i) \quad (15)$$

For the present investigation the right side of equation (15) equals the crack opening displacement at the center of the specimen ($x_i = 0$):

$$u_{\infty}(x_{i=0}) - u_{br}(x_{i=0}) = COD$$

Equation (7) reads then:

$$\boxed{\delta_{fm}(x_i) + \delta_{ad}(x_i) = COD} \qquad (16)$$

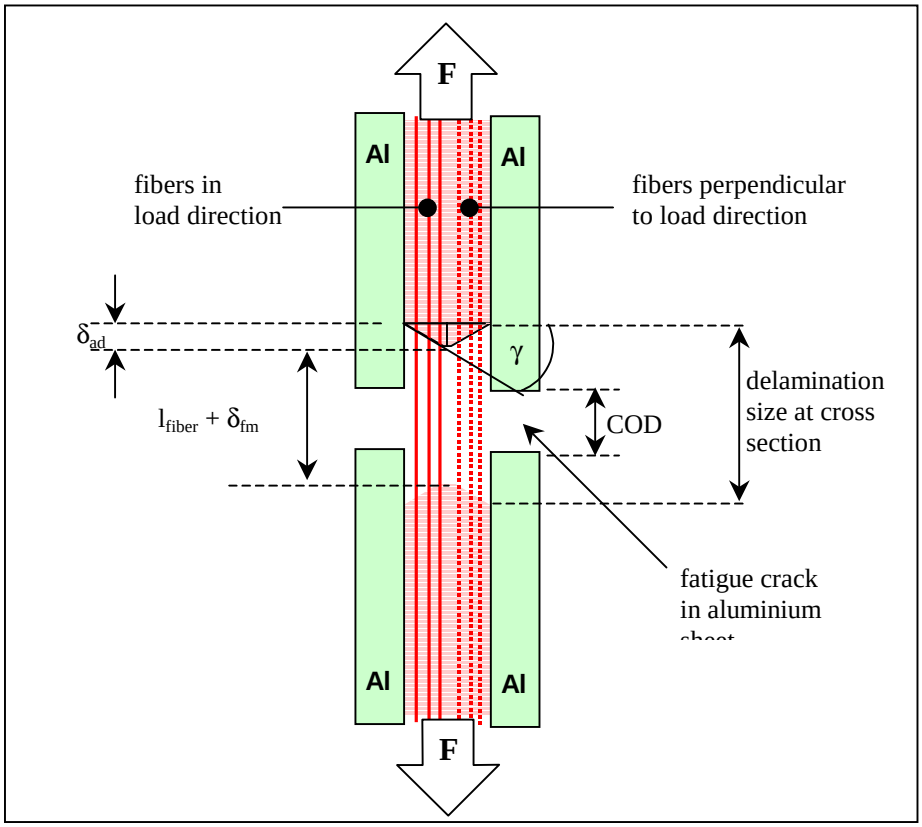

Figure 6.5.14. View in model of fatigue cracked GLARE3-2/1 laminate under tensile load. Empirical model: Higher loads and longer boundary length at metal interface compared with prepreg center line. Un-symmetric lay-up of GLARE3 not considered.

Equations (11, 12, 13, 14, 16) are applicable to calculate both, the extension of the intact fibers between the delamination boundaries (δ_{fm}) and the prepreg shear deformation (δ_{ad}) at the center of the specimen (x_i=0). Figure 6.5.15 contains the calculated elongations at room temperature for specimens with different delamination sizes. The calculated shear deformation is different for the three specimens, which should not be the case since it is not dependent from the delamination size and all other parameters which have to be considered are constant as well. The calculated difference is caused by the apparent G-modulus, which contains the above discussed uncertainty of the non-symmetric GLARE3 lay-up. In figure 6.5.16 the adhesive shear deformation is set to 0.035mm for all specimens (mean value). The blue bars indicate the different elongations of the fibers due to the different delamination sizes.

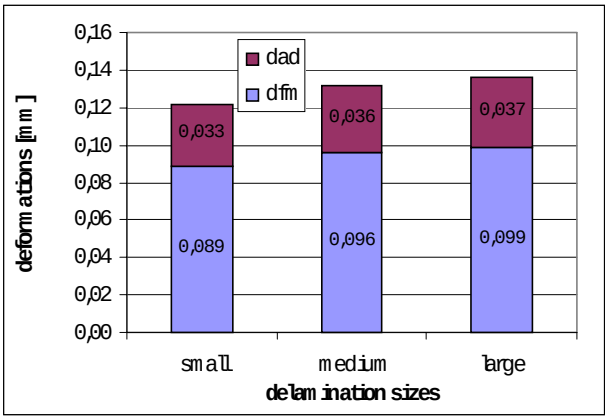

Figure 6.5.15, fiber elongations at room temperature for specimens with different delamination sizes, data based on COD plot acc. to figure 6.5.12

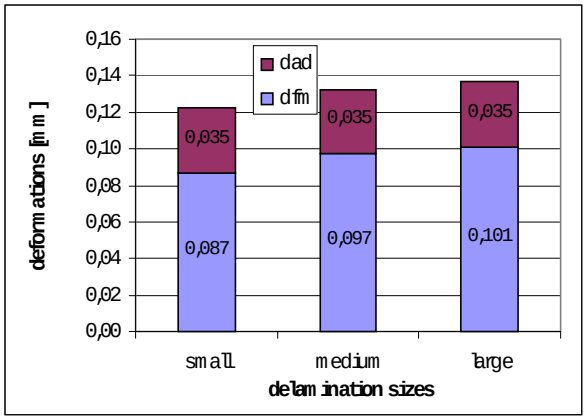

Figure 6.5.16, fiber elongations at room temperature for specimens with different delamination sizes, corrected

The larger the fiber elongation δ_{fm} – the higher the crack opening displacement and the higher the crack propagation rates (at similar temperature). Consequently the delamination size provides a kind of history effect for the following structural load cycles, i.e. even a low load can result in a relatively high crack growth rate, if it coincides with a large fatigue delamination size.

Figure 6.5.17 contains the calculated shear stresses at the metal/prepreg interfaces, for the different delamination sizes and at different material temperatures. Again, it is not distinguished between the local different fiber orientations.

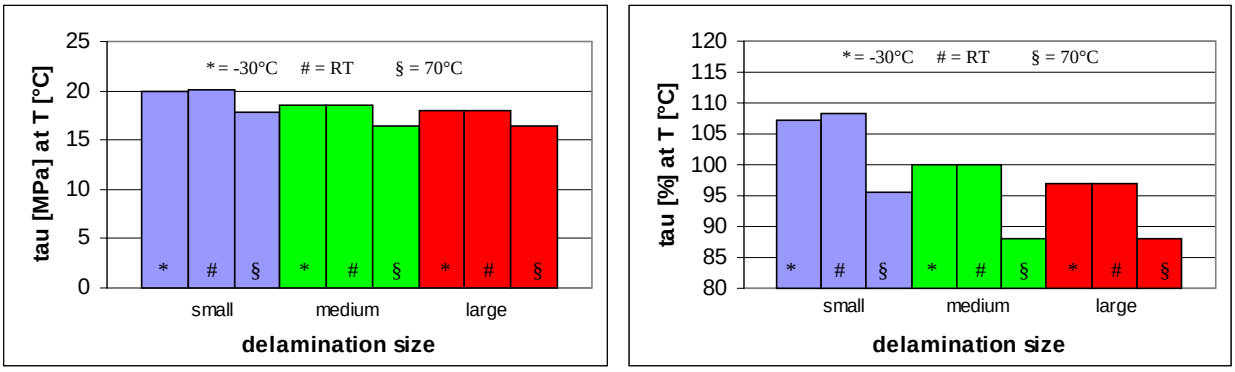

Figure 6.5.17. Apparent calculated shear stresses at metal/prepreg interfaces of GLARE3, related to different fatigue delamination sizes and material temperatures, applied stress 140 MPa, fatigue crack lengths 2a=40mm. Medium fatigue delamination size at RT set to 100%.

Independent from the delamination size, a significant reduction of shear stress is observed at 70°C material temperature. This stiffness behaviour coincides with a larger local prepreg deformation, a larger COD and an increased stress intensity factor on the crack tip, without necessarily a delamination extension.

Marissen introduced a correction factor on stress intensity for medium size fatigue crack lengths [57] :

$$C = \sqrt{h \times \tan(h) \times (\pi \times a / h)} \qquad (17)$$

with:

$$h = \left(\frac{1}{t_{Al.} \times E_{Al.}} \right) \times \sqrt{\frac{t_{prep.}}{j \times G_{prep.}} \times \left(\frac{1}{E_{Al} \times t_{Al}} + \frac{1}{E_{prep.} \times t_{prep.} \times n} \right)} \qquad (18)$$

The correction factors C due to different fatigue delamination sizes and shear stiffness (at different material temperatures) can be calculated using equations (17) and (18). Figure 6.5.18 shows the correction factors to be considered for stress intensity, with the condition 'medium delamination size at room temperature' set to 1.0.

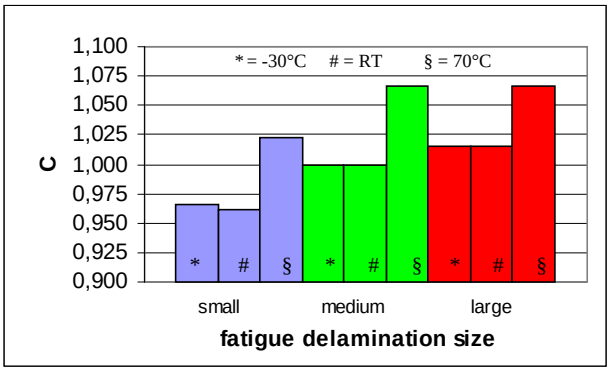

Figure 6.5.18. Correction factors on stress intensity factor for GLARE3 at 140 MPa, distinguished between different delamination sizes and material temperatures

From the investigation above it is concluded that both, the delamination size and the shear stiffness can contribute to crack opening and to crack propagation rates significantly. For example, from delamination size small$^{\#}$ to delamination size large$^{\#}$, both compared at room temperature, a correction on stress intensity of 5.6% is considered. At a given delamination size the reduction of prepreg shear stiffness can lead to an increased stress intensity at the aluminium crack tip of the same order of magnitude, e.g. 6.6% from medium delamination size at room temperature to medium delamination size at 70°C.

Note that all data presented in this paragraph are strongly dependent on the tested material, the hole diameter, the fatigue crack length and the applied load level.

The reason for the particular present delamination sizes and shear deformations can be different. Here they are introduced by fatigue loading and COD measurements at different temperatures in order limit the test time. But if the presence of moisture in the vicinity of a fatigue crack has the same detrimental influence on the fatigue delamination size and/or on the shear deformation as the high temperature, than a detrimental influence on the crack propagation rates is considered as well. Fatigue delamination sizes after accelerated ageing will be discussed in chapter 6.6 on blunt notch specimens and further in chapter 7, on riveted joints.

The influence of *accelerated* exposure on shear deformation and shear stiffness is investigated using specimen 1b. As previously mentioned, the measurement data without exposure are lost. The table below compares the crack opening displacements after 500, 1000, 1500 and 3000 hours exposure* at 140 MPa applied load and room temperature:

Exposure* time	500 h	1000 h	1500 h	3000 h
COD [µm/m]	132	133	138	140

* 70°C / 85%RH

The crack opening displacement did not vary up to 1000 hours exposure but increased by approximately four percent after 1500 hours exposure and about five percent after 3000 hours exposure. The specimen was fatigued with 42760 cycles at 140 MPa maximum stress before exposure, during which a fatigue delamination zone developed. The development of this delamination zone is considered to be a fatigue process, i.e. the entire load *spectrum* defines the delamination damage size and not a *single* load [48]. Under consideration of this principle it is concluded that the four additional load cycles performed for COD measurements at 140 MPa did not increase the delamination size. Consequently there is an influence of the moisture on the shear stiffness concluded. The influence of accelerated ageing on the shear deformation measured at the hole of the here discussed specimen is shown in figure 6.5.19.

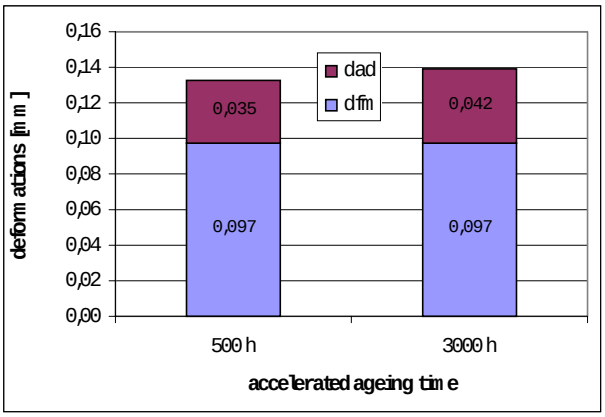

Figure 6.5.19. Influence of accelerated ageing (70°C/85%RH) on shear deformation d_{fm} at bore hole of GLARE3 specimen, specimen previously fatigued at RT (medium delamination size)

6.6 Crack Propagation, Accelerated Ageing Influence

(ref. factor $C_{CP(E)}$)

Crack propagation rates in both, laboratory air and water, have been investigated at room temperature and different load frequencies by Deutekom [36]. Since her notched GLARE3 specimens (prepreg: AF163, R-glass) was unexposed at the beginning of the crack propagation test, a comparison between the crack propagation rates and the diffusion rates is necessary in order to correlate the diffusion depth with the crack lengths. The crack propagation rates (da/dN) in terms of mm/cycle were depending on the frequency but apparently not systematically on the environment, see figure 6.6.1. More detailed information is gained if the crack propagation rates are presented in millimeter per hour and compared to the relevant diffusion speed, see figure 6.6.2. Tensen [48] determined a diffusion rate of 1.94 $x10^{-8}$ [mm/s] in 20ºC water, equal to $6{,}9x10^{-5}$ [mm/hour]. This value is approximately the diffusion rate obtained in Deutekom's specimens. The crack propagation in all her specimens was faster than the diffusion speed, see figure 6.6.2. As a consequence, different crack propagation rates due to an environmental effect should not be expected. Actually, she measured the effect of the frequency on crack propagation in GLARE3. For the frequencies below 1 Hz, Deutekom used a trapezium load shape instead of a sinusoidal one. At these low frequencies, the crack propagation rates increased from $4.0x10^{-4}$ mm/cycle to $6.5x10^{-4}$ mm/cycle.

In order to provide information concerning the crack propagation of GLARE with a wet prepreg, specimens have to be exposed either with a process that provides faster diffusion than crack propagation, or specimens have to be exposed to an ageing process which allows the moisture to penetrate deep into the laminate before starting the crack propagation test. In the latter case it is possible that cracks are growing from an area with a high moisture concentration towards locations with a lower moisture concentration.

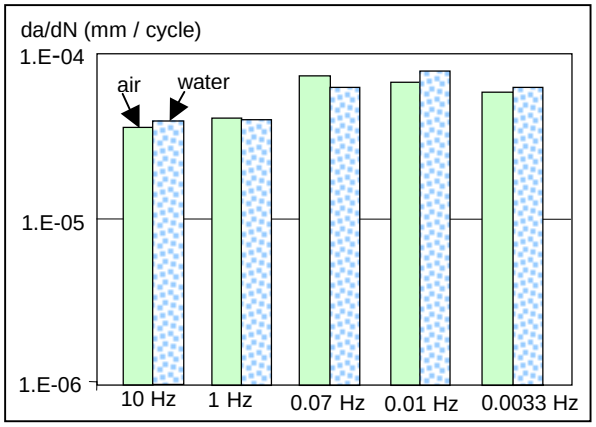

Figure 6.6.1: Crack growth rate in mm/cycle. Different frequencies, 20°C, data from [36]

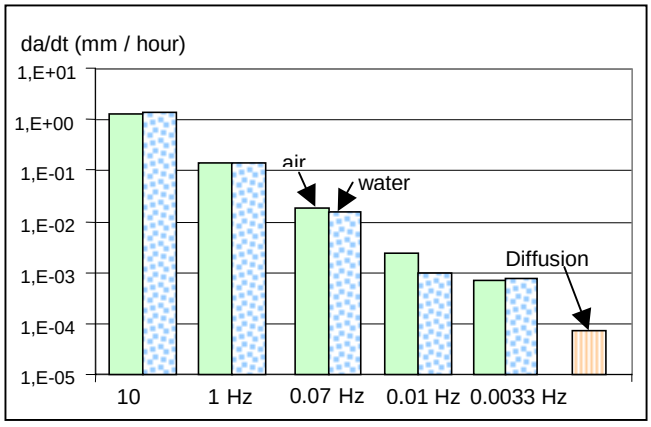

Figure 6.6.2: Crack growth rate and diffusion speed in mm/hour. Different frequencies, 20°C, data calculated from data in [36]

Van der Hoeven [12] performed both Center Crack Tension and Edge Crack Tension (ECT) crack propagation tests on specimens which were aged for 3000 hours before testing in fatigue (prepreg: FM94, S-glass). He also tested specimens aged for 1000 hours before testing and aging for again 1000 hours was repeated two times later during the crack growth experiment (environment 70°C / 85%RH).

In these tests, from the very beginning, the matrix in the vicinity of the crack has been wet. The da/dN data in figures 6.6.3 and 6.6.4 are copied from [12].

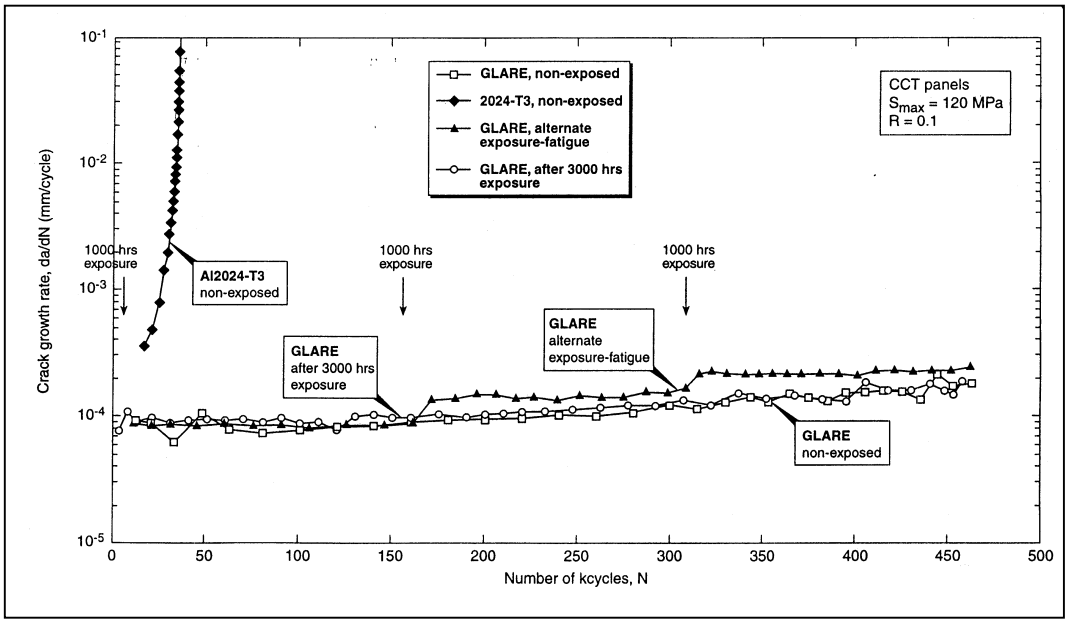

Figure 6.6.3. Crack propagation rates in CCT panels after different accelerated exposure treatment [12]

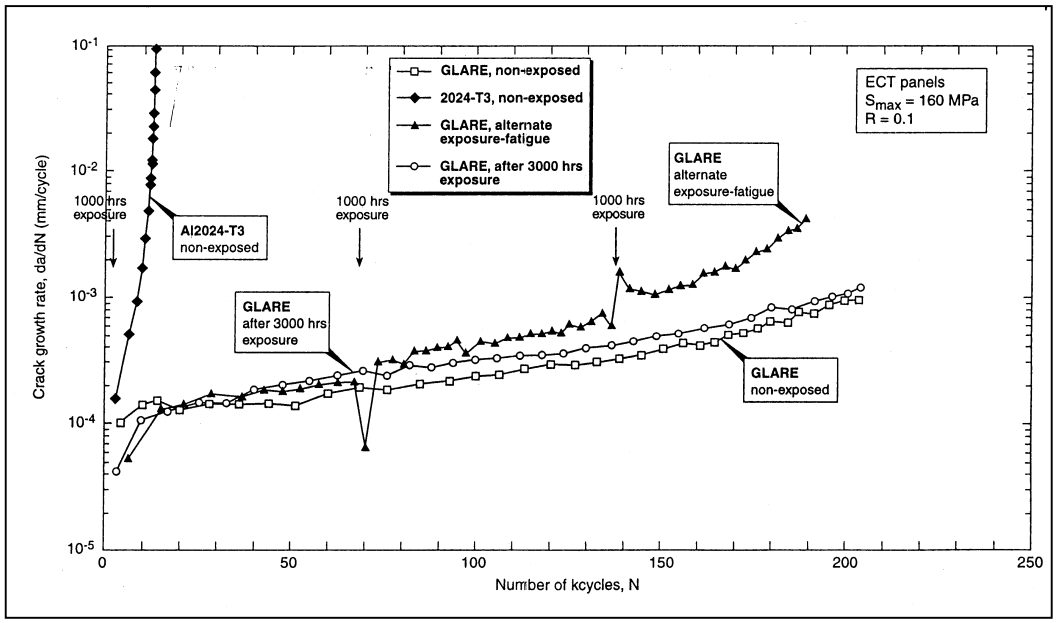

Figure 6.6.4. Crack propagation rates in ECT panels after different accelerated exposure treatment [12]

The initial saw cuts had a length of 5mm. A very limited increase of crack propagation rate is observed for the 3000h aged specimens, compared with the non-aged. After each 1000 hours exposure, the crack propagation rate increases and it remains on the new level. After alternate exposure, the crack propagation curve continues with a new but constant slope. It can be assumed, that the weakened bond due to the presence of water molecules close to the fatigue crack leads to increased delamination zones, which in return increases the crack opening angle and therefore the crack propagation rate. Thus, the `history effect´ discussed in Section 6.5 becomes evident. Van der Hoeven's fracture delamination size measurements support this theory. He exposed CCT specimens with fatigue cracks of approximately 9mm length with 3000 environmental cycles (see figure 6.6.5) followed by fatigue testing

to a crack length of approximately 40mm [38]. In another test three times an exposure of 1000 environmental cycles was applied after approximately 9mm, 14 to 18mm and 26 to 29mm crack lengths have been obtained. Each cycle included both a temperature variation and a humidity variation, see figure 6.6.5. At a crack length of 2a equal to approximately 40mm, the delamination sizes were compared. Van der Hoeven studied both through cracks and part through cracks.

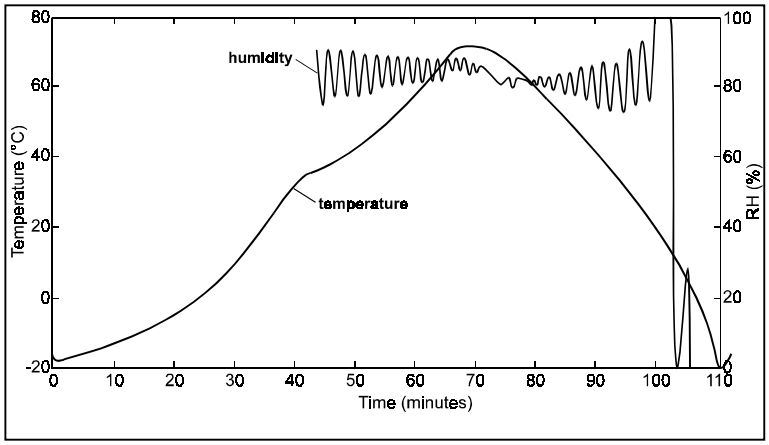

Figure 6.6.5. Applied environmental cycle [38]

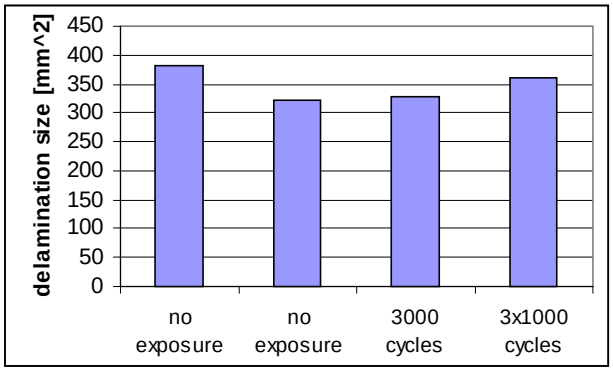

Figure 6.6.6. Influence of accelerated ageing on delamination size of through-the-thickness specimens, da/dN =4x10^{-5} to 1x10^{-4} [mm/cycle], data obtained from [38]

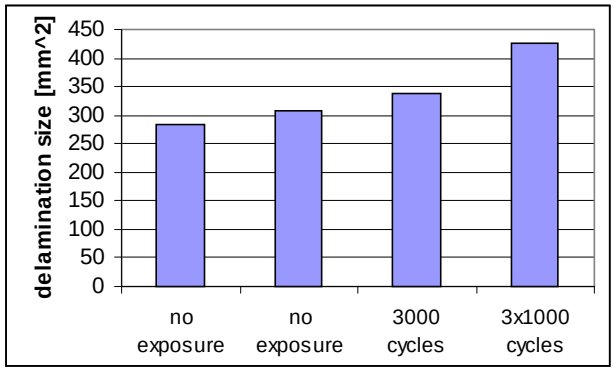

Figure 6.6.7. Influence of accelerated ageing on delamination size of part-through-the-thickness specimens, da/dN =3x10^{-5} to 4x10^{-5} [mm/cycle], data obtained from [38]

The data in figure 6.6.6 for the through cracks do not give clear indications. These cracks had relatively high crack propagation rates. The results for the part through cracks with a much lower crack growth rate show a trend towards larger delamination areas for the specimens exposed with 3000 cycles *before* testing which is even more significant for the alternately exposed specimens.

The results from [12] and [38] should not have a significant impact on the sizing of GLARE aircraft structures because all tests showed a very limited influence of accelerated ageing, and if any, it was observed for long crack lengths (>10mm). Structural details of a real aircraft structure have to be taken into account. In a single shear joint, for example, peel stresses develop which may be more detrimental in combination with moisture than observed for the elementary specimens. Furthermore, local stresses in a single shear joint can be higher than tested by van der Hoeven [12].

A review of the previous investigations leads to the conclusion that the maximum allowable load to prevent a certain level of delamination in the vicinity of a fatigue crack depends on the moisture content. Obviously a wide range of results can be produced, depending on the choice of accelerated ageing

treatment. It should be recalled that the open hole moisture reference specimen required 12000 hours exposure to saturation in the Airbus standard environment. Knowledge of realistic diffusion phenomena in GLARE is mandatory for a reliable prognosis of the influence of moisture on crack propagation. Therefore it was decided to perform some further accelerated tests on the type of specimen already investigated as a dry specimen, 3-B-1, i.e. a GLARE2 specimen with a row of 5 open holes.

Specimen 3-B-37 has been aged for 4296 hours (70°C/85%RH) in order to investigate an extreme case. No fasteners were installed in the holes during ageing. Similar to specimen 3-B-1, this specimen was tested S_{max} = 140 MPa (gross stress). The crack propagation rate increased by a factor 3, compared to specimen 3-B-1, see figure 6.6.8.
Another specimen 3-B-38 has been aged for 523 hours (70°C/85%RH) with fasteners installed (low interference fit). The crack propagation rate matches the results obtained from the dry specimen 3-B-1, see again figure 6.6.8.

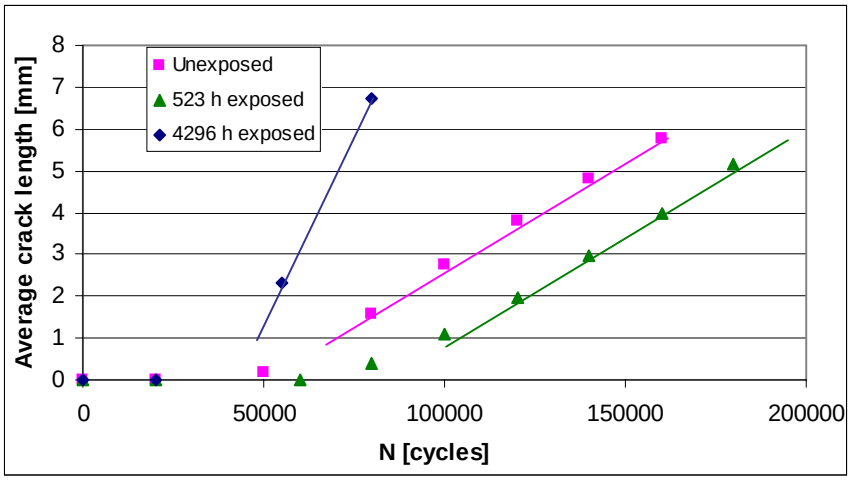

Figure 6.6.8. Crack propagation rates after ageing, GLARE2B specimens (test series 3-B-x)

The moisture level around the hole after 4296 hour exposure at 70°C/85%RH increases the crack propagation rates significantly, the moisture level after 523 hours exposure does not.
In figures 6.6.9 and 6.6.10 a comparison is made between the calculated moisture distributions in the prepreg layer of both specimens after accelerated exposures. The cracks propagated perpendicular to the fibers. It is assumed, that the crack bridging mechanism, which is influenced by the local moisture in the prepreg, becomes active not earlier than after 1mm crack length (from the hole edge) has been obtained. The crack tip in specimen 2-B-38 (Figure 6.6.9) is already below the 75% maximum moisture level at a crack length of 1 mm and it is growing towards a more dry prepreg. However, after 4296 hours exposure in the other specimen, 2-B-37, the 1 mm crack tip is still at the location where the prepreg has 90% of the maximum possible moisture concentration, see figure 6.6.10. The 75% moisture concentration is reached at a distance of 2.8 mm from the hole edge and the 60% after 5.5 mm from the edge. The crack in the aluminium top layer of this specimen propagated during the entire crack growth period in contact with a relatively wet prepreg. This has two physical consequences:

a) The thick adhered specimen, which is discussed in chapter 4.5. indicates that the shear delamination resistance decreases for moisture levels which are calculated for specimen 3-B-37. The decreased delamination resistance is considered to be the major reason for the larger delamination zones and consequently a larger crack opening displacement, a higher stress intensity factor at the tip of the crack, and thus a higher crack growth rate.

b) The shear stiffness of the prepreg is decreased after more than 3000 hours accelerated aging, see chapter 6.5. Also this will lead to a decreased shear stiffness with similar consequences although to a less extent.

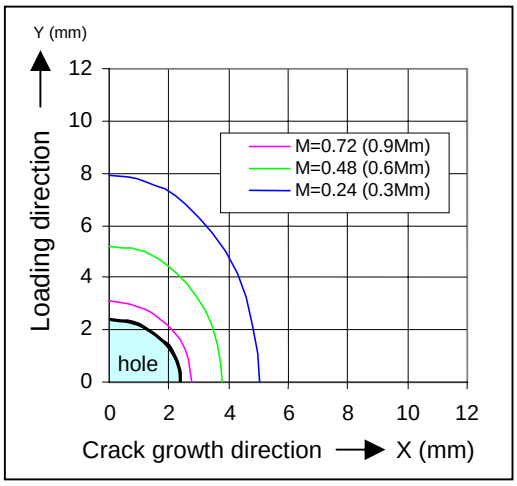

Figure 6.6.9. Calculated moisture concentration level around GLARE2B bore hole after 523h exposure (70°C/85%RH), closed hole

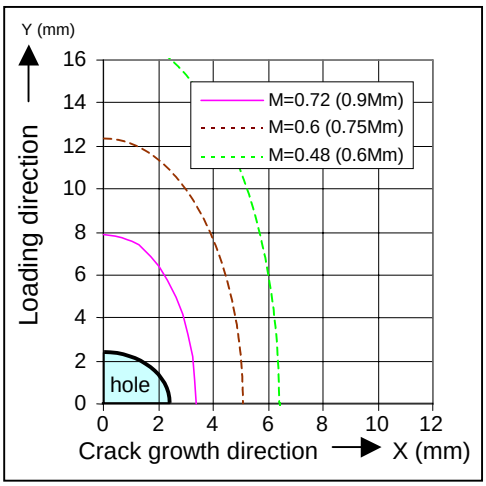

Figure 6.6.10. Calculated moisture concentration level around GLARE2B bore hole after 4296h exposure (70°C/85%RH), filled hole

After fatigue crack length inspections, one outer aluminium layer of each specimen has been etched away for a delamination and diffusion inspection. Pictures are shown in figures 6.6.11 and 6.6.12. The FM94 prepreg contains a blue colour additive for identification reasons. If exposed in humid air, the blue additive vanishes and the original, brown colour of the fiber/adhesive prepreg becomes visible. After 4296 hours exposure these brown areas can be clearly identified around the holes. Perpendicular to the fibers a diffusion depth of approximately 4.8mm from the hole edge can be measured, parallel to the fibers approximately 8.5mm is measured for specimen 3-B-37. Comparing the picture with the diagram in figure 6.6.10 leads to the conclusion that a moisture level above 60% to 80% of the maximum moisture content becomes visible by etching.

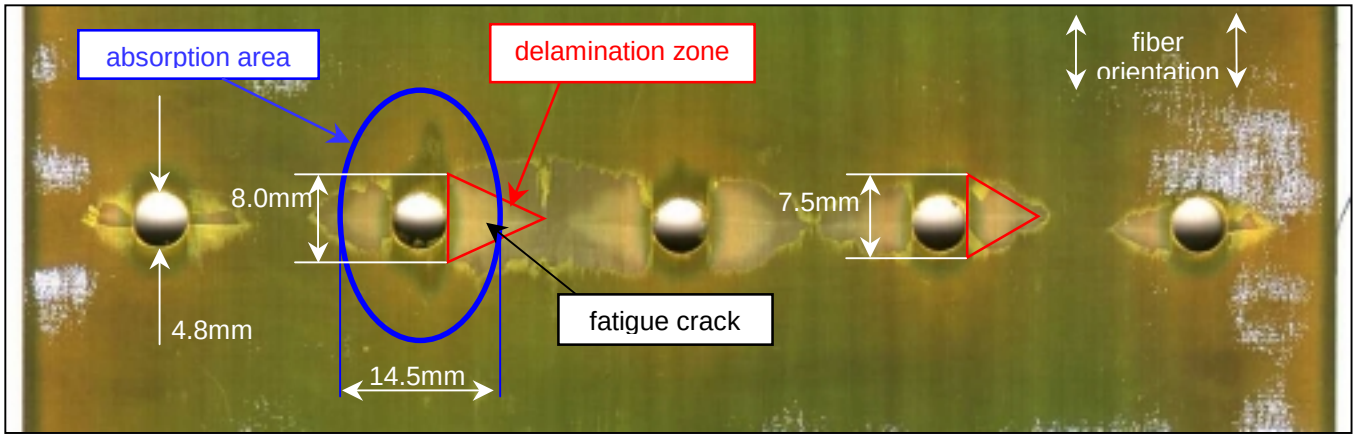

Figure 6.6.11. Specimen 3-B-37, view on first prepreg- and second aluminium layer after 4296 hours ageing at 70°C/85%RH (open hole) and subsequent fatigue crack propagation testing

In a similar way as from the open holes, moisture diffuses into the prepreg from the unprotected edges. The diffusion fronts from the outer two holes and the edges merge into one aged area at both sides of specimen 3-B-37. Picture 6.6.11 emphasises the importance of either sufficient edge distance for aged blunt notch specimens or the necessity of a perfect sealing of the edges. The other specimen in figure 6.6.12 after 523 hours exposure with filled holes revealed that no more than 0.5mm of the prepreg changed its colour around the holes and from the edges. This is in accordance with the calculations, see the diagram in figure 6.6.9.

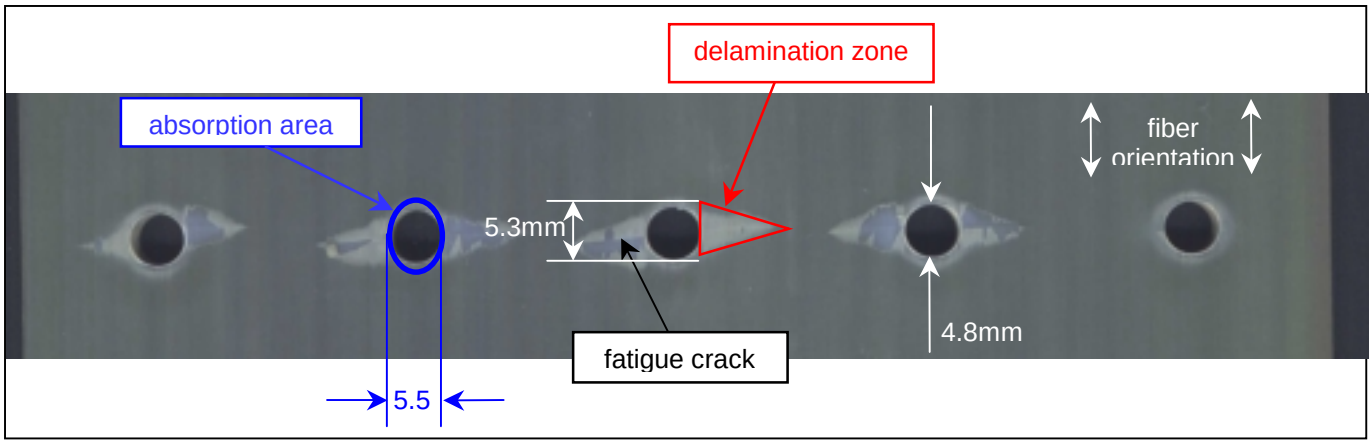

Figure 6.6.12. Specimen 3-B-38, view on first prepreg- and second aluminium layer after 523 hours ageing at 70°C/85%RH (filled hole, clearance fit) and subsequent fatigue crack propagation testing

In conjunction with the higher moisture concentration in specimen 3-B-37, larger delamination sizes are observed for similar crack lengths. The right triangle in figure 6.6.11 and the triangle in figure 6.6.12 belong to a fatigue crack of a similar length. A delamination width of 7.5mm can be measured for the specimen which has been exposed for 4296 hours, compared with a 5.3mm delamination width after 523 hours accelerated exposure.

It is an important observation that the fatigue delamination shapes are triangular, independent from the moisture content. Under these conditions, similar equations for the calculation of stress intensities in the aluminium layers crack tips can be used [58].

Chapter 5 specifies a realistic accelerated exposure of no more than 500 hours in an environmental chamber filled with 85%RH and 70°C warm air. At this exposure level, no acceleration of fatigue cracks compared with dry specimens is observed.

$C_{CP(E)} = 1$

Specimens 3-B-25 to 3-B-27 and 3-B-34 to 36 are now exposed outdoors without previously being fatigued. They are available to provide open hole crack propagation curves after a tropical exposure. The point of crack initiation for these specimens should be related to non-aged specimens with care because corrosion attack on the aluminium may cause early crack initiation.

6.7 Crack Propagation, Temperature Influence

(ref. factor $C_{CP(T)}$)

The effects of the load frequency, the temperature and the environment on the fatigue behaviour of GLARE were discussed in the previous chapters. Obviously such effects should be considered if the results of a full-scale aircraft structure are evaluated. A full-scale on an aircraft structure is carried out in one specific environment and temperature variations occurring in each flight in service are not simulated. This problem is considered in the present section.

Bär [39] observed a similar temperature effect on fatigue crack growth in GLARE as shown previously in figure 6.5.3, but Bär used many more data points. His results obtained at room temperature in laboratory air are presented in figure 6.7.1. The constant crack growth rates for three temperatures are shown in this figure. The growth rate increases for an increasing temperature.

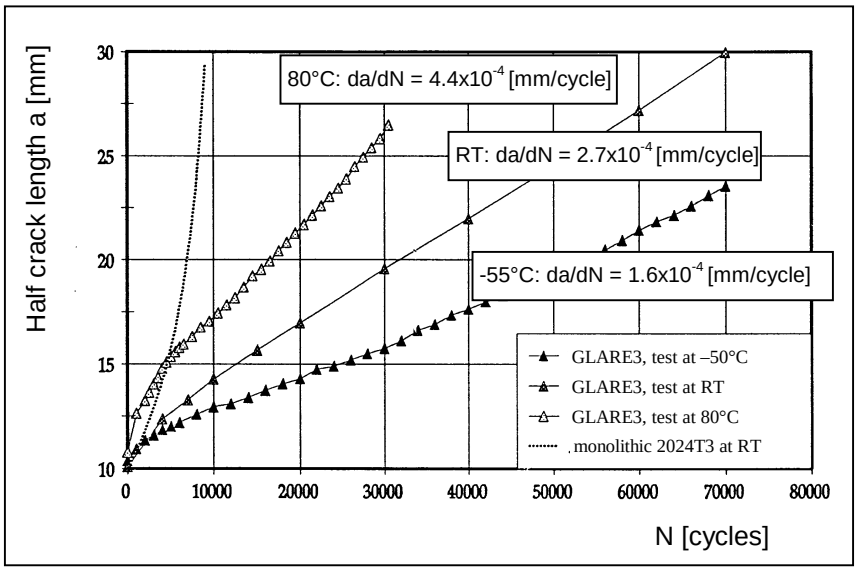

Figure 6.7.1. Crack propagation depending on material temperature, CCT specimen, GLARE3, AF163, R-glass, $\sigma_{max.}$ = 140 MPa R=0.1 [39]

A similar behaviour is observed by Brenninkmeijer for a crack in a sheet which was repaired with a bonded patch [40]. Obviously the crack bridging capability is dependent on the temperature of the resin, with and without fibers in the bond line.

Bär also investigated the delamination shapes around the fatigue cracks by etching away the outer aluminium layer. He found increasing delamination areas with increasing temperature, which he attributed to the decreasing stiffness and shear modulus of the prepreg. Some information is added to this subject by the COD measurements in section 6.5.

Deutekom tested a notched GLARE3 specimen in 60ºC warm water at 0.07 Hz / $\sigma_{max.}$ = 120 MPa [36]. The relevant diffusion rate obtained from [37] is 9.41×10^{-7} [mm/s].

Recalculation in [mm/h]: 9.41×10^{-7} [mm/s] x 3600 [s/h] = 3.38×10^{-3} [mm/h]

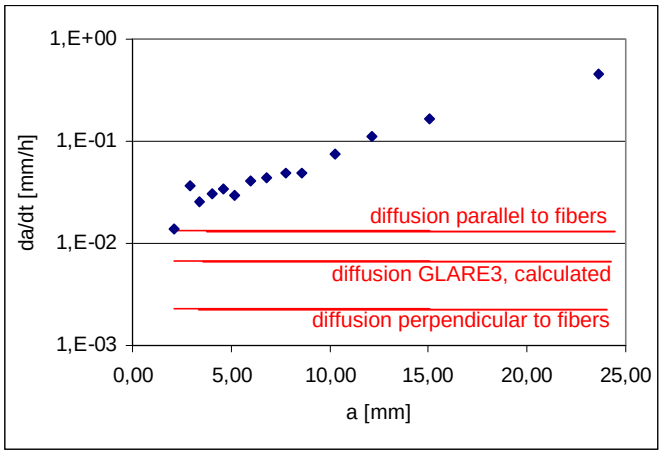

Figure 6.7.2. Crack propagation rates (blue dots) [36] and diffusion speeds [37] in 60ºC warm water, 0.07 Hz, AF163 prepreg, fatigue crack is faster than diffusion

This diffusion speed is still below the crack propagation rates at 0.07 Hz, see figure 6.7.2. Influences obtained from this test must thus be related to the temperature only. Different from tests which Deutekom performed at 20ºC in water and different from Bär's tests performed in laboratory air, the crack propagation rates increased with crack length and time in 60°C warm water. The selected medium seems to influence the material behaviour. It appears to be more realistic to concentrate on the experiments carried out in laboratory air at different temperatures.

Most commercial aircraft operate in moderate climates, like in Europe or North America. From the temperature profile of a civil aircraft flight mission it can be expected, that a delamination size associated to room temperature or negative temperatures (cruise segment of the flight) will develop in a flying GLARE component. Any full scale test conducted at room temperature would then provide conservative results. However, for the pre-flight ground case and early flight case in a tropic environment, a material temperature of 70°C should be considered (chapter 1). It needs to be investigated, whether the crack propagation rates at high material temperatures but low fatigue stresses or the crack propagation rates at low temperatures but high fatigue stresses will dominate. Therefore, comparative crack propagation calculations for a non-bending low load transfer structure (through-the-thickness crack) with a complete fuselage load spectrum have been carries out, both with consideration of a temperature effect on da/dN and without this effect. A short-range load spectrum for an A330 aircraft, longitudinal skin stresses at frame 58, calculated with a finite element analysis (finite element CQUAD4 580031), was selected for the investigation [42].

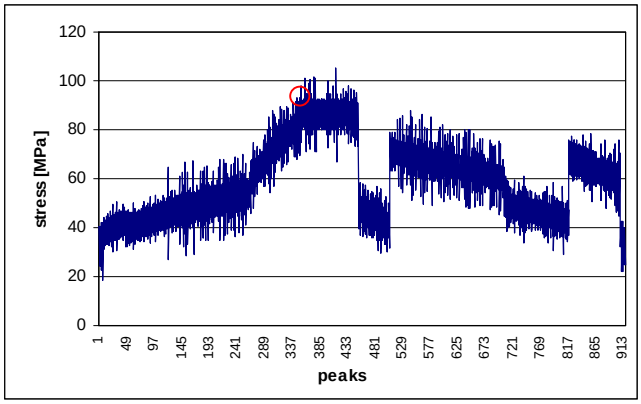

Figure 6.7.3. Short range stress spectrum no. 551

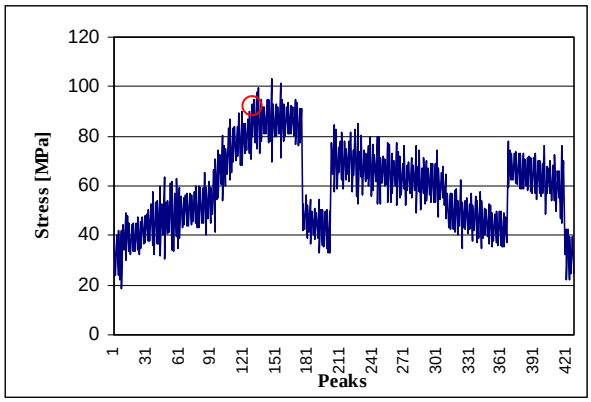

Figure 6.7.4. Short range stress spectrum no. 601

Red circles indicate stress peak, at which 100% cabin differential pressure is reached.

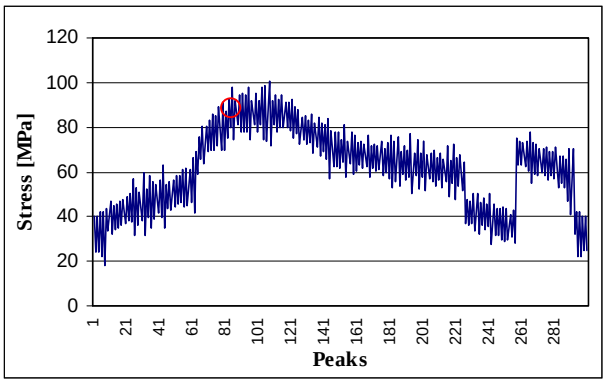

Figure 6.7.5. Short range stress spectrum no. 631

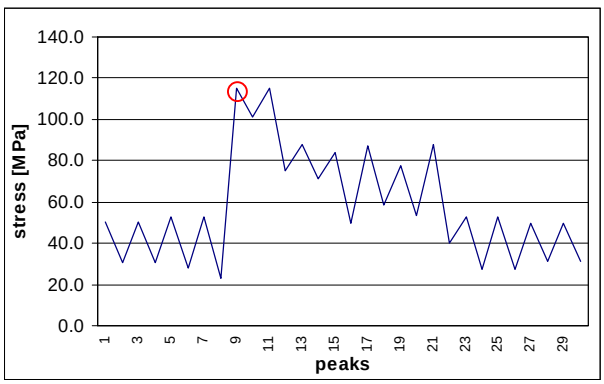

Figure 6.7.6. Short range stress spectrum no. 751

Red circles indicate stress peak, at which 100% cabin differential pressure is reached.

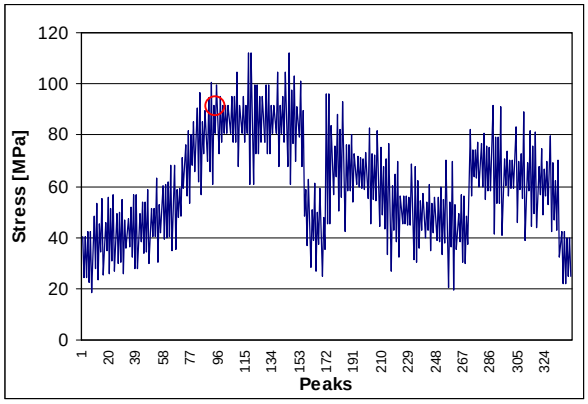

Figure 6.7.7. Short range stress spectrum no. 762, red circle indicate stress peak, at which 100% cabin differential pressure is reached.

For an efficient calculation time, the spectrum is reduced to five flight types from the envelope, which together represent 8790 flights from the 40000 flights of the Design Service Goal (DSG). Details about the selected flight types are collected in [43]. The stress histories of the five flight types are presented above.

The computer program “JOINT” (release 0.41) of the Delft University has been provided with the crack propagation data derived from the crack growth curve for room temperature obtained by Bär [39]. By trial and error, the 140 MPa stress level is increased and decreased in order to simulate the da/dN curves at temperatures of 80ºC and -55ºC, respectively. It was determined, that the stress level has to be increased by 15 MPa in order to match the 80ºC crack propagation curve and that it has to be decreased by 20 MPa in order to match the -55ºC crack propagation curve. With a slope for crack propagation rates depending on stress levels for different temperatures provided by Alderliesten [44], da/dN data for the entire stress spectrum become available, see figure 6.7.8.

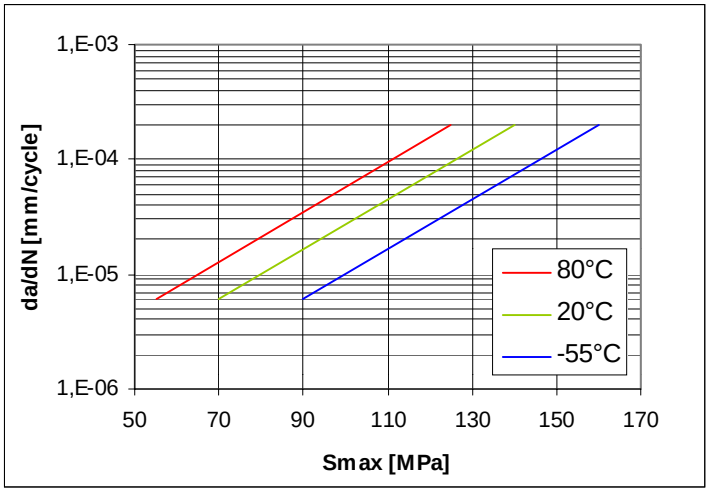

Figure 6.7.8. Crack propagation rates for different stress levels and temperatures obtained from literature [44], slopes calibrated according to literature [39]

The crack propagation calculations were made as a cycle-by-cycle summation of crack growth increments. The initial crack length was assumed to be 2a = 5.6 mm in view of simulating a crack occurring at a frame clip / skin attachment. Without accounting for the temperature effect on the crack growth rate values the result was that after 10 x 8790 flights the crack had grown from a = 2.8 mm to 7 mm [43].

In the second calculation the temperature effect was introduced. All stress peaks of pre-flight- and early flight cycles were increased by 15 MPa, and all stress peaks for the cruise and descent cycles decreased by 20 MPa. The switch from 80ºC- to -55ºC da/dN data is made at the load cycle, at which the full internal fuselage pressure is reached. The calculation showed that the crack lengths for 87900 flights increased from a = 2.8 mm to 5.5 mm [43].

Discussion:
According to the analysis described above, the influence of the increased crack propagation rates at high temperatures is overcompensated by the influence of the low crack propagation rates at low temperatures. Therefore, a crack propagation test performed at room temperature would be conservative for a commercial aircraft application. However, the analysis is physically not correct because it is based on *constant* temperature crack propagation rates. As explained in chapter 6.5, each crack develops its own delamination size, depending on the material temperature, which in return influences the crack propagation rates. It has not yet been determined which delamination size will develop in the case of continuous temperature variations, and which crack propagation rate might then be obtained. On the other hand, two significantly conservative arguments are included in the analysis. For the variable temperature calculation all stress cycles up to the full internal fuselage differential pressure is reached are supposed to occur under 80ºC conditions. This assumption is conservative for two reasons - first because the temperature adopted is higher than assumed for fatigue (see chapter 2), and second because the internal pressure condition is reached at 30000 ft altitude, which equals 15 to 20 minutes time from taxi out. During this time, the material temperature drops significantly below 70ºC. At least room temperature can be expected for the aircraft skin. According to reference [45], 25% of all flights shall be considered as tropical. Here, for simplification, all flights have been calculated as tropical.
It can be expected, that the built-in conservatisms are more severe than the uncertainties. A final proof can be given by variable temperature / variable load tests. This item is discussed in chapter 7.

6.8 Single Hole Blunt Notch Investigations (no outdoor exposure specimens)

The blunt notch strength is an important property for the fatigue and damage tolerance justification, because the failure strength without fatigue damage is the starting point for a residual strength versus fatigue damage curve (see section 1.5.2). This curve becomes a design allowable.
During the past decades, various blunt notch test programs were conducted which did not reveal a clear trend concerning the influences of accelerated aging on the blunt notch strength [10, 11, 12]. The variables are manifold, i.e. specimens were exposed with open holes and with filled holes, blunt notch tests were conducted with and without fastener, specimens of different widths were exposed (edge influence), specimens were tested with a single hole or more holes and with different hole diameters, and different GLARE types and different lay-ups were used. A systematic compilation of these data is strongly recommended.
In frame of this thesis, another test program has been carried out. Single open hole specimens manufactured from different GLARE types have been exposed to different artificial exposure conditions, after which static blunt notch tests have been carried out. This part of the investigation is discussed in section 6.8.1. The influence of moisture on the blunt notch failure mode mechanism is considered in section 6.8.2.

6.8.1 Systematic single hole blunt notch strength test results

The specimen geometry is shown in figure 6.8.1.1. Except for one test series, all specimens are exposed with open holes as a worst case condition. The specimen width is sufficient to exclude an influence on the test results due to exposure of the edges. All specimens are pulled to failure with a fastener installed. Both, the yield strength and the ultimate strength are recorded.

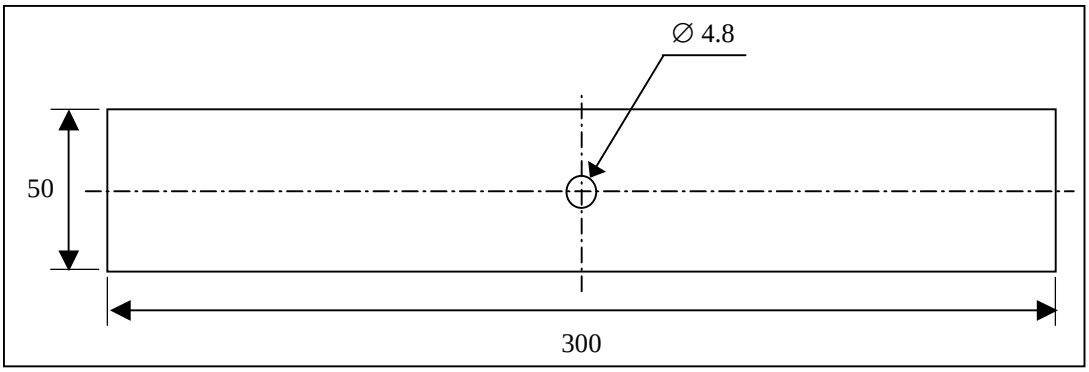

Figure 6.8.1.1. Blunt notch specimen used for static tests on different GLARE types

The test matrix is shown in the table below. In the first test series, accelerated ageing occurred during exposure times of 0, 500, 1000 and 3000 hours in 70°C/85%RH environment. The blunt notch strength results should provide input data for worst-case blunt-notch knock down factors for different GLARE types. One GLARE3 test series is exposed with a clearance fit filled hole for comparison.

Test matrix, number of specimens used.				
material	exposure time (70°C/85%RH)			
	0	500	1000	3000
GL2B-7/6-.4, open hole	5	5	5	5
GL3-3/2-.3, open hole	5	5	5	5
GL3-3/2-.3, with fastener*	5	5	5	5
GL4A-5/4-.4, open hole	5	5	5	5
GL4B-5/4-.4, open hole	5	5	5	5
	exposure time (70°C/70%RH)			
	0	4272	8544	25633
GL3-3/2-.3, open hole		5	5	5
* clearance fit protruded fastener installed during exposure				

A second series of open hole GLARE3 specimens is exposed in a 70°C / 70%RH environment for three different periods, which are 4272 hours (removed from the environmental chamber in June 2003), 8784 hours (removed in December 2003) and 25633 hours (to be removed in December 2005). These exposure times have been calculated with the diffusion coefficients evaluated in chapter 4. The criterion is to obtain the same moisture *weight gain* around the holes as for the 500h, 1000h and 3000h exposure in the 70°C/85%RH environment. The moisture *distribution* around the holes, however, will be different for the two environments. A comparison of the blunt notch strength should indicate whether the moisture distribution influences the blunt notch strength. Note that the weight gain around the holes can not be measured, just calculated, due to the presence of specimen edges which absorb moisture as well.

All test results are recorded in table 6.8.1. The specimens to be exposed to 25633 hours could not yet be included. The yield strength results as obtained in the static blunt notch test are plotted in figures

6.8.1.2 to 6.8.1.5 as a function of the exposure time. The allowable design stresses [16] are also indicated in these figures.

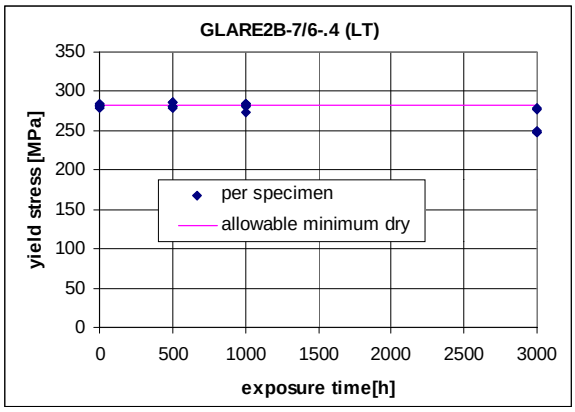

Figure 6.8.1.2. Yield strength GLARE2 after exposure in 70°C / 85% RH air

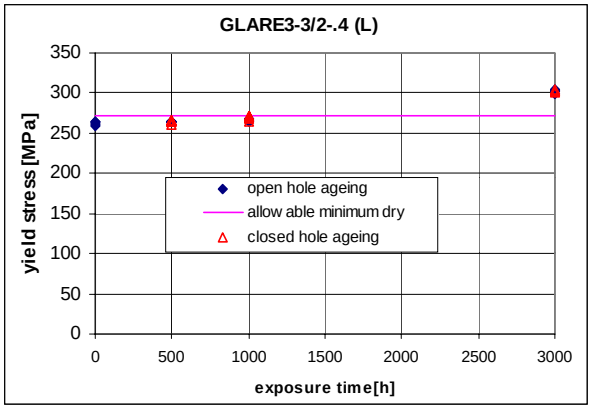

Figure 6.8.1.3. Yield strength GLARE3 after exposure in 70°C / 85% RH air

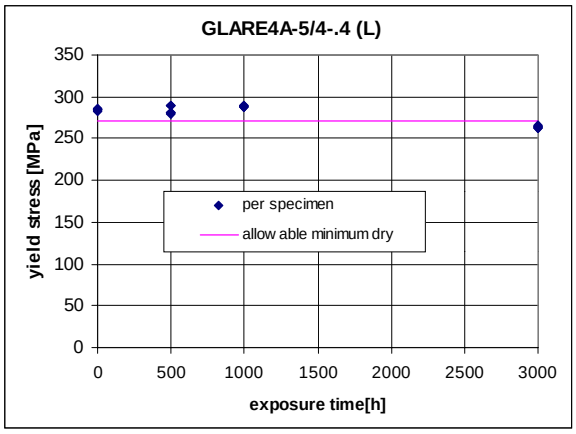

Figure 6.8.1.4. Yield strength GLARE4A after exposure in 70°C / 85% RH air

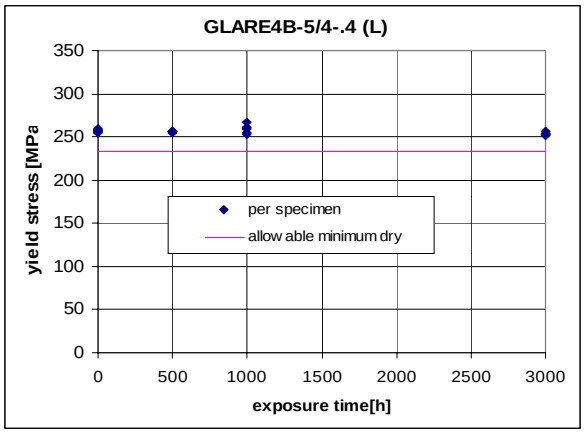

Figure 6.8.1.5. Yield strength GLARE4B after exposure in 70°C / 85% RH air

The yield strengths of these GLARE materials are almost insensitive to accelerated ageing, which is expected because the yield strength of GLARE is primarily a metal related property. The GLARE3 blunt notch results are slightly below the recommended allowable value from literature, even unexposed. Small reductions of the yield strength are also recorded for GLARE2B and GLARE4A after 3000 hours exposure in the 70°C / 85% RH environment, both of them loaded in the main fiber orientation. The GLARE2B strength even drops below the design allowable after 3000 exposure hours. However, if the conclusion about representative accelerated ageing according to chapter 4 is considered, i.e. the application of 500 to 1000 exposure hours, no knock down factor on yield strength remains.

The blunt notch strength results for all GLARE types are compiled in figure 6.8.1.6. If the strength is plotted as a percentages, the strength does not always show a continuous decrease with exposure time, see figure 6.8.1.7. Regression lines for structural sizing purposes, after skipping the less systematic results for 1000 h, are shown in figure 6.8.1.8. A clear knock down factor ranking is obtained after 3000 hours ageing, with the larger knock down factors for both GLARE4 types, followed by GLARE2 (test in fiber orientation) and finally GLARE3. Obviously the GLARE types with a higher fiber volume in the loading direction are more sensitive to long exposure periods. This conclusion is the only one about knock down factors which can not be explained neither with the yield/ultimate strength ratio nor with the load carrying fiber volume fraction.

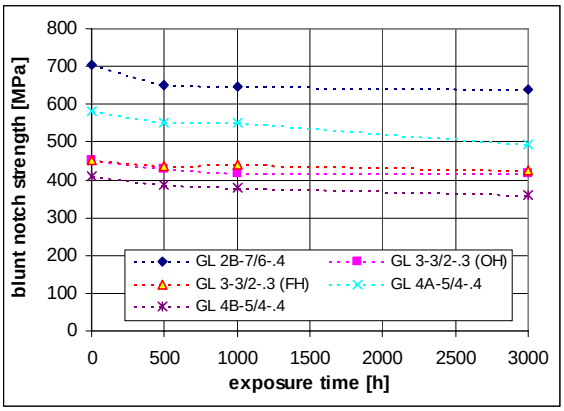

Figure 6.8.1.6. Blunt notch strength(net) after exposure in 70°C / 85% RH environment

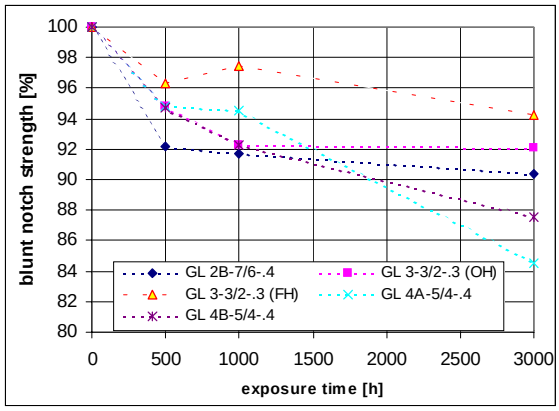

Figure 6.8.1.7. Blunt strengths in [percentage], exposure in 70°C / 85% RH environment

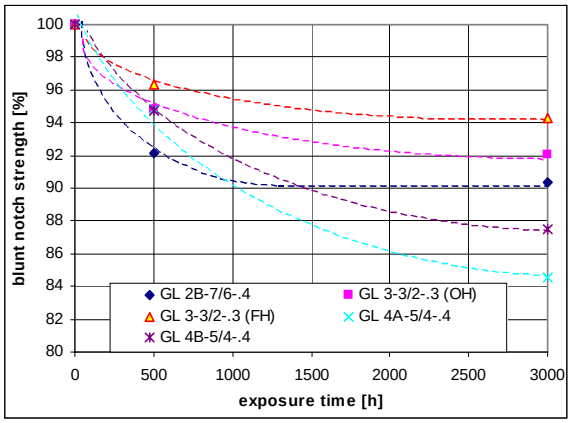

Figure 6.8.1.8. 'Engineering' knock down curves for blunt notch strength, related to 70°C / 85% RH environment, 3000 hours ageing included

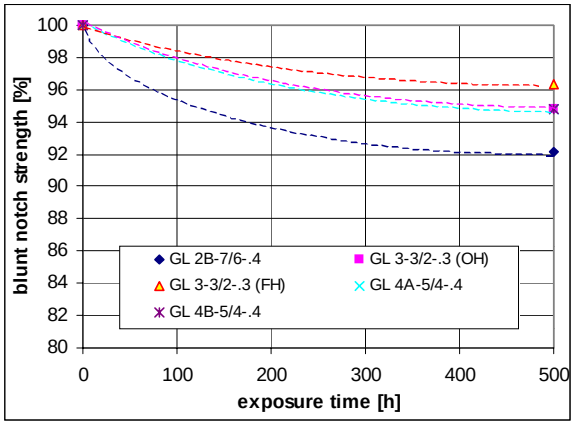

Figure 6.8.1.9. 'Engineering' knock down curves for blunt notch strength, related to 70°C / 85% RH, limited to 500 hours accelerated ageing

The moisture absorption rates decrease in GLARE3 with the fastener installed during exposure by 2% after 3000 hours, compared with the open hole.

If the moisture *content* will be the driving factor for the knock down factor values and not the moisture *distribution*, a matrix for structural sizing as shown in figure 6.8.1.9 can be developed under the consideration of at maximum 500 hours accelerated ageing for representation of a short range aircraft life. The curves in figure 6.8.1.9 contain the test results related to 500 hours accelerated ageing without consideration of the later measurements. Note that the GLARE4 results match exactly the GLARE3 open hole (ageing) results. Now, the worst result is observed for GLARE2, i.e. a knock down factor of 8% related to 500 hours ageing at 70°C / 85%RH.

Five specimens are exposed with open holes in a 70°C/70%RH environment for 4270 hours in order to absorb the same amount of moisture as similar specimens after 500 hours exposure in the 70°C/ 85%RH environment. Five more specimens are exposed in the 70°C/70%RH environment for 8784 hours in order to absorb the same amount of moisture as similar specimens after 1000 hours exposure in the 70°C/85%RH environment. Figure 6.8.1.10 contains the results obtained from all GLARE3 specimens exposed with an open hole. The 70/70 results after 4270 hours ageing are included at the x-position of 500hours in the diagram (the x-axis is related to the 70°C/85%RH environment), results for 8784 hours exposure in the 70/70 environment are included at the 1000 hour position. The scatter of the 70/70 results is higher than for the 70/85 results, but if mean values are calculated, the strength values after 4270 hours exposure in a 70°C/70%RH environment match quite well with the results after 500

hours exposure in a 70°C/85%RH environment, see figure 6.8.1.11. However, after 8784 hours exposure in the 70°C/70%RH environment, which equals 1000 hours exposure in the 70°C/85%RH environment concerning the moisture *content*, the blunt notch strength did not decrease further.

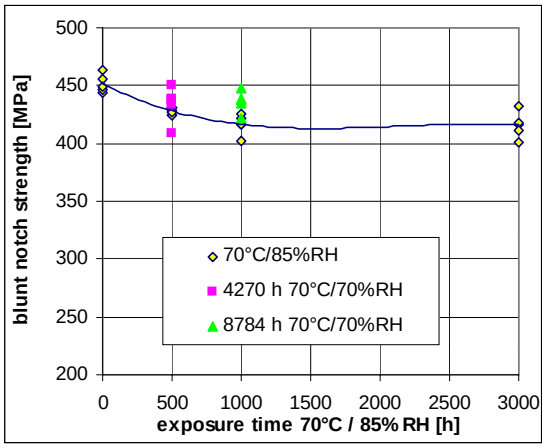

Figure 6.8.1.10. GLARE3 open hole exposure, test results from specimens exposed at 70°C / 85%RH and specimens exposed in a 70°C/ 70%RH environment

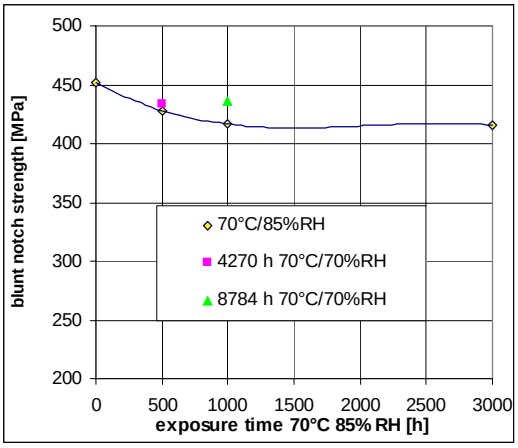

Figure 6.8.1.11. GLARE3 open hole exposure, mean values from results shown in 6.8.1.10

The strength reduction due to exposure of GLARE in hot / wet air is obviously dominated by the moisture concentration in the prepreg within a distance of 4mm from the hole edge. For illustration see figures 6.8.1.12 to 6.8.1.15.

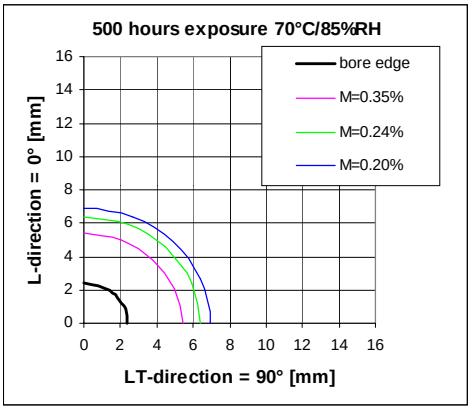

Figure 6.8.1.12. Iso-concentration lines for blunt notch specimens, 500 hours exposure in 70°C/85%RH

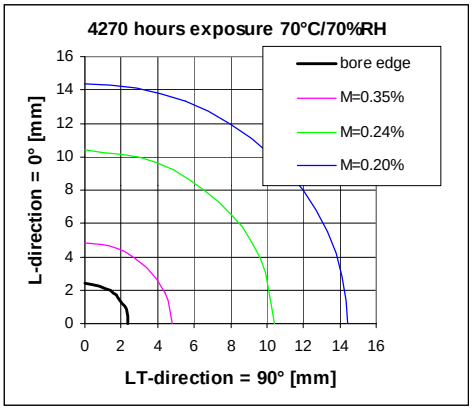

Figure 6.8.1.13. Iso-concentration lines for blunt notch specimens, 4270 hours exposure in 70°C/70%RH

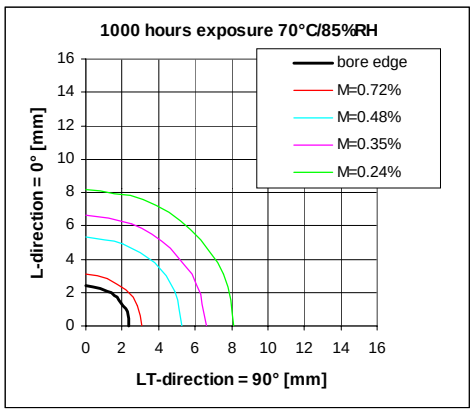

Figure 6.8.1.14. Iso-concentration lines for blunt notch specimens, 1000 hours exposure in 70°C/85%RH

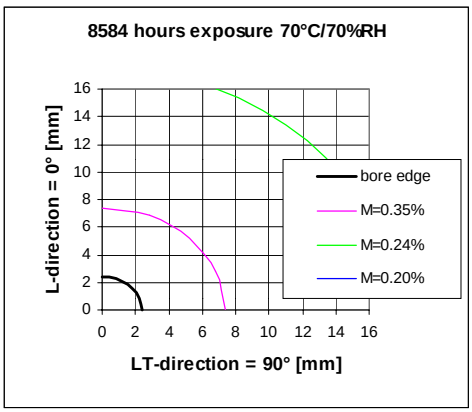

Figure 6.8.1.15. Iso-concentration lines for blunt notch specimens, 8584 hours exposure in 70°C/70%RH

Figure 6.8.1.12 shows the calculated moisture distribution after 500 hours accelerated exposure in a 70°C/855RH environment, which equals approximately the prepreg condition after 30 years short range aircraft service, see section 5.2.4. The moisture concentration equals 0.35% at a distance of approximately 3mm from the hole edge. The moisture concentration decreases fast outside the 3mm (+2.4mm) radius. Towards the bore hole higher moisture concentrations are present, because the maximum can be 0.78% in the 85% relative humidity environment.
If the specimens are exposed 4270 hours in the 70°C/70%RH environment, the iso-concentration of 0.35% is calculated in a slightly lower distance from the edge than in the 500h / 70°C / 85%RH condition, see figure 6.8.1.13. A large portion of the moisture diffuses deep into the laminate. Towards the hole the moisture concentration can increase at maximum to the value of 0.4%, see chapter 4.
Although the moisture concentrations outside and inside the 3mm (+2.4mm) radius are quite different, the blunt notch strength results are similar for the two conditions discussed above.
After 8584 hours exposure in the 70/70 environment the radius for 0.35% moisture concentration increases from approximately 5mm (from center hole, after 4270 hours exposure time) to 7.5mm, see figure 6.8.1.15. The blunt notch strength is not effected by this shift. Note that inside this radius the moisture concentration is almost similar as after 4270 hours ageing. The majority of the moisture which diffused between 4270 hours and 8584 hours into the prepreg disappeared into the depth of the material, with low concentration levels.
This is quite different after 1000 hours ageing in the 70°C/85%RH environment. At the position where 0.35% moisture content is calculated after 500 hours exposure it is already 0.48% after 1000 hours exposure, see figure 6.8.1.14. The relatively short exposure at high humidity accumulates the majority of the moisture in the close vicinity of the hole.
It must be concluded at this point that the 500 hour / 70°C / 85%RH accelerated ageing process remains the most realistic and most economic test in order to simulate a realistic aircraft structure condition. Longer exposure time in the same environment leads to unrealistic conservative strength results due to high moisture concentration close to the hole edges. Longer exposure times in lower humidity environments may lead to a more representative moisture distribution in the prepreg around the hole but it does not influence the blunt notch strength.

Based on the single hole blunt notch specimen results it is recommended for short range aircraft structures to consider a knock down factor of 4% at room temperature for ageing on blunt notch strength, if GLARE3 and GLARE4 materials are used. A knock down factor of 8% is recommended for a GLARE2 application. Long range aircraft structures made of GLARE require no knock down factor (ref. chapter 5).

6.8.2 Aspects of blunt notch failure mode after accelerated ageing

The moisture distribution around both, GLARE3 and GLARE2, is approximated in chapter 4. An engineering guess is done concerning the shape of the iso-concentration lines around GLARE4 holes. It is common understanding that the fibers provide a more significant barrier function against moisture diffusion into the resin if oriented perpendicular to the diffusion path rather than if they are located parallel to the diffusion path. The effect of moisture in the matrix is either a reduction of the resin strength itself (cohesive failure under load) or a reduction of the fiber/resin interface adhesive strength. At first sight, one may conclude that the detrimental effect should be more pronounced if the tensile loaded net section is dominated by fibers oriented perpendicular to the load direction, i.e. moisture can

travel fast into the net section. According to this assumption, the influence of moisture on blunt notch strength should be smaller in GLARE2B (loaded in LT-direction) than in GLARE3, for example. The strength reduction in GLARE4A would be expected to be less than the strength reduction for GLARE4B (both tested in L-direction).

Both assumptions appear to be wrong as proven by the tensile tests discussed in the previous section 6.8.1. After 3000 hours accelerated exposure, the strength of GLARE4B(LT) dropped more than the strength of GLARE3(L) and the strength of GLARE4A(L) dropped more than the strength of GLARE4B(L). It is also unexpected that the strength of GLARE4A(L) drops more than the strength of GLARE2B(LT), under the assumptions discussed above. For these two materials, the same trend was found by van der Hoeven, see figures 4.1.2.3 and 4.1.2.4. Both test series (the present and van der Hoevens) resulted in a knock down factor of 11% for GLARE2B(LT) and 14% for GLARE4A(L) after 3000 hours accelerated exposure, although the specimen geometries and test conditions have been quite different. Note that van der Hoeven covered several variables at the same time, i.e. edge protections and fatigue influences.

From the unexpected order of knock down factors between the different GLARE types which contribute to the investigation performed in section 6.8.1 it must be concluded, that it is not the diffusion into the net section of a blunt notch specimen, which is driving the failure strength, but obviously the diffusion in the loading direction.

Meziere investigated the failure mode in GLARE3 blunt notch specimens [13]. He describes the failure sequence as follows:

- 70% failure load: plasticising of the aluminium layers
- 75% failure load: beginning of the (fiber) splitting at the edge of the hole
- 90% failure load: increase of splitting length and debonding appearance between the aluminium layers and the glass layers in load direction
- increase of the debonding size and failure in the matrix
- fiber failure and failure propagation into the aluminium leads to the final failure

(end of quotation).

The key point of the analysis is the fiber splitting between those fibers which are cut by drilling the hole and those which are not. A significant shear load develops between these fibers, *in* the loading direction, and not in the net section. It was not possible to visualize the extent of the fiber splitting in the loading direction with the NDT methods applied. Later in this thesis the fiber splitting phenomenon was observed in a statically loaded joint specimen, see figure 7.1.8.18 in order to get an impression of the splitting extension at the left and right hand side from holes in load direction.

The testing procedure of Meziere has been repeated here for the blunt notch specimens after accelerated ageing in the 70°C/85%RH environment. GLARE4A specimens exposed for 0, 500, 1000 and 3000 hours were subsequently pulled to yield, or to 70%, 80%, 90% and 98% failure load, respectively. Then, the specimens were cut in the net section and prepared for observation in the Scanning Electronic Microscope (SEM). According to the above theory, the SEM pictures should not show indications of fiber splitting in the net section. The SEM pictures from all specimens are collected in attachment O where each page contains pictures from four specimens exposed for different time periods but loaded to a similar load level. The magnifications are between 20 and 150. At the yield load level, no damage is visible at all, independent of the ageing time. This observation agrees with the yield strength results discussed in the previous chapter. The first considerable damage in the net section close to the hole is observed at 70% failure load after 3000 hours exposure. White marks around the fibers indicate a cohesive failure between fibers and resin, very dark areas seem to be pulled out fibers

(loose fibers pulled out during the destructive preparation of the specimen). Reviewing all pictures it must be concluded, that there is no ranking of the specimen condition which fits to the load and ageing treatment. Pronounced fiber splitting, for example, is noticed for the 80% failure load specimen after 500 hours exposure. The worst condition of all seems to apply to the specimen exposed 3000 hours and then pulled to 80% failure load. Severe delaminations in the vicinity of the aluminium layers are observed. But, the specimen which is pulled to 90% failure load after 3000 hours exposure is in a better condition than the one mentioned before. And even the 3000h/98% specimen looks better than the 3000h/80% specimen.

Three pictures with a magnification of 1000x for specimens of the 3000 hours aging series are shown on the last page of attachment O. A good focus on porosity is presented in both, the yield load and the 70% failure load pictures. Some discontinuities are observed in the yield load specimen prepreg close to the metal interface. The size of these discontinuities is similar to the size of the porosities in the center of the prepreg. It may be questioned whether it is a starting delamination, which would be in contradiction with Mezieres conclusion, or whether it is porosity close to the adjacent metal layer. Clear matrix cracks are detected at both, 70% failure load and 98% failure load.

Summarizing, there is indeed no evidence from the SEM pictures to support a failure mechanism at both sides of the hole in the net section *perpendicular* to the loading direction. Consequently, it is concluded that the diffusion *in* the loading direction has a significant influence on the blunt notch strength. The argumentation can also be related to the discussion of the influence of delamination on the fatigue crack opening in section 6.5. In the blunt notch case, fiber splitting between load carrying and non-load carrying fibers seems to happen at lower applied loads if the resin is wet. During an increasing load, the fiber splitting extends and the possibility that locally disconnected fibers start failing is increased. The local fiber failure is the beginning of the final blunt notch failure of the specimen.

In view of the above arguments, it is logical that the blunt notch strength of GLARE2B(LT) is more affected by diffusion than for GLARE3, and also that GLARE4A(L) is more affected than GLARE4B(L). As a complementary investigation it is recommended to repeat tests with thick adhered specimens with fibers oriented perpendicular to the load direction.

6.9 Residual Strength of Filled Hole Outdoor Exposure Specimens

(ref. $C_{RS(E)}$)

In this section, the effect of moisture absorption on the residual strength of blunt notch specimens with fatigue cracks is considered. For this purpose, residual strength tests are carried out on blunt notch specimens which are pre-conditioned by artificial aging. Blunt notch knock down factors of 15 % were obtained in previous investigations after 3000 hours accelerated ageing in a 70°C / 85% relative humidity environment [10, 11, 12] and systematic experiments have already been discussed in chapter 6.5 of this thesis.

For a GLARE riveted joint, Müller found a linear relation between the lost metal area because of fatigue cracks and the residual blunt notch strength [15], see the discussion in section 6.9. In the present thesis the percentage of the aluminium area lost due to fatigue cracks is called the “fatigue damage rate “, R_D. The experiments of Müller were carried out on dry specimens, but the problem is more complex if environmental influences are present. Two scenarios are obvious. The fatigue crack may propagate faster than the moisture can penetrate in crack direction. This can apply if the moisture penetrates

slowly if the aircraft is operated in a low moisture environment (e.g. for long range aircraft operations), or because the surface protection system prevents moisture absorption. Moreover, the fastener may prevent moisture penetration. The wet prepreg area will then be limited to the location of the fatigue crack, and it will not significantly affect the fatigue de-lamination and crack growth. These conditions are similar to the conditions of the specimens of the outdoor exposure test program including fatigued blunt notch specimens.
The second possibility is a fast and deep moisture penetration compared with a low crack propagation rate. This can be relevant if either the structural stress level is low and the aircraft is operated in short range missions or if the surface protection system and the fastener fit allows good access of the humid air to the prepreg. The fatigue cracks in the aluminium layers then propagate along wet prepregs. It is the worst case situation as indicated by the investigation of Borgonje [10]. The condition can be simulated by *accelerated* ageing of *previously* fatigue cracked blunt notch specimens.

Fatigue cracks at the hole edges in a GLARE specimen initiate in the outer aluminium layers first [1]. For a correct determination of the cracked metal fraction the crack lengths in all metal layers must be known. It implies that the relation between the average crack lengths of the two outer aluminium layers with visible cracks and the inner aluminium layers with invisible cracks, requires attention. This aspect is covered in section 6.9.1. Results of the residual strength after accelerated aging of blunt notch specimens are presented in section 6.9.2.

In the present thesis the percentage of aluminium cross section lost by cracks in the aluminium layers, (which was called `percentage of aluminium lost´ by Müller, is defined here as `fatigue damage rate´ R_D.

6.9.1. Crack length distribution through the thickness of filled hole specimens (outdoor exposure specimens)

The blunt notch specimen no. 3-B-1 with a row of five open holes (see the discussion in section 6.4.1) was the first specimen scheduled for residual strength testing. After fatigue testing the average crack length in the two outer aluminium layers was 7.68 mm. In the residual strength test, failure occurred in the clamping area, see figure 6.9.1. Trials with bonded taps and different clampings remained unsuccessful. It was then decided to decrease the specimen width by two rivet pitches. All GLARE2B specimens have then been milled to a width of 68.1mm in the test area (see figure 3.2.4.5) and failures in the clamping are were avoided. The investigation of the fatigue crack length is thus limited to the holes number 2, 3 and 4. Specimen 3-B-4 was selected for a fractografic investigation of the crack length in all aluminium layers after failure in the residual strength test. The specimen has been fatigued until 120000 cycles at 69.1 kN maximum load (max. net stress 180 MPa) with the initial width (5 holes). With the video technique the crack length was measured for the two outer sheets and the five holes. The average length was 4.38mm. After milling the specimen to a width of 68.1mm, fasteners were installed and the residual strength test was performed at room temperature. Failure occurred at a maximum load of 143.2 kN.

Figure 6.9.1. Specimen 3-B-1 after residual strength test

Figure 6.9.2. Milled specimen, shown after failure

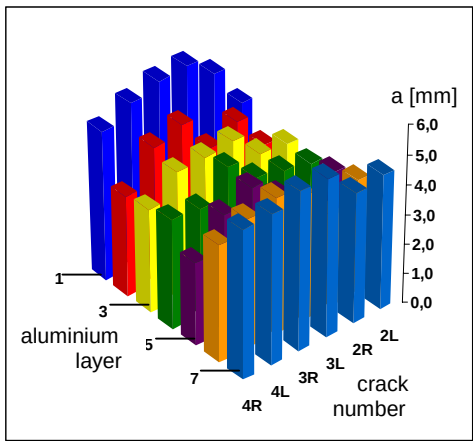

Figure 6.9.3. Crack pattern in 7 layers

The specimen was then stored in an oven at 350º C for 4 hours, which burns the epoxy and leaves the clean aluminium sheets. The fracture surface was investigated under an optical microscope. The crack lengths in all metal layers could be measured due to a clear difference between the fracture surface appearance of the fatigue crack and the statically failed ligaments. The results for the cracks in the seven aluminium layers at both sides of the three holes are plotted in figure 6.9.3 (data in table 6.9.3, mean values). The results illustrate that the longer cracks occur in the two outer layers 1 and 7. The standard deviation for the crack lengths in each aluminium layer is determined. Standard deviations for each aluminium layer is calculated between 0.4mm and 0.7mm, refer to tables 6.9.1 and 6.9.2.

For a conservative prediction of the residual strength based on the length of the visible cracks in the two outer layers only, it is necessary to assume a relatively large ratio between the crack lengths of the inner and outer aluminium layers, in order to account for a relatively high non-cracked metal area. In this way a larger damage rate is adopted. For the evaluation of the ratio, the crack lengths values of the aluminium layers 2 to 6 are related to the crack lengths measured in layers 1 and 7. The comparison is

done in percentages of crack length for each fatigue sensitive location, with the crack length measured in layers 1 and 7 set to 100 percent. The results are contained in table 6.9.4. For each inner layer the largest crack is considered to arrive at a conservative percentage of the crack length and the values for the inner layers are averaged. Due to the uneven number of aluminium sheets in the laminate, the ratio for the center layer (no. 4) is calculated twice, once in relation to layer no.1 and once in relation to layer no. 7. The conservatively averaged crack lengths of the inner aluminium layers compared with the crack lengths of the outer aluminium layers amounts to 86%. This factor 0.86 obtained with specimen 3-B-4 will be used for the crack lengths estimation of the inner aluminium layers in the other GLARE2-7/6-.4 specimens.

6.9.2. Residual strength of filled hole specimens

Four specimens of GLARE2B with open holes have been cycled in a dry condition at a maximum load of 69.1 kN up to different crack lengths. The number of cycles, the crack length obtained in layers 1 and 7, as well as the averaged crack lengths in these layers have been compiled in table 6.9.5. Another four specimens were exposed with fasteners in a 70°C / 85%RH environment for 2997 hours and then subjected to the same series of fatigue tests. Residual strength tests were carried out on all specimens with fasteners installed. As a reference, two sets of three specimens, without exposure and with the above exposure respectively, however both without fatigue loading, were also tested to determine the static strength of the undamaged blunt notch specimens. For the exposed specimens, no more than two days passed by between removal from the environmental chamber and the residual strength test.

The obtained average crack lengths for the outer aluminium layers are corrected with the evaluated factor (ref. chapter 6.9.1) for the inner layers:

$$f_{corr} = n_{outerlayers} + n_{innerlayers} \times 0.86) / n_{layers} \quad (17)$$

$f_{corr} = (2 + 5 \times 0.86) / 7 = 0.900$

The corrected average crack lengths can be then calculated with:

$$a_{corr} = a_{av} \times f_{corr} \quad (18)$$

This corrected average crack length is now considered to be applicable to all (seven) aluminium layers. Finally, the ratio of aluminium damage R_D is calculated in relation to the net section of the 3-hole specimen to be:

$$R_D = 100 - 100 \times (w_{net} - 3 \times 2 \times a_{corr}) / w_{net} \quad \text{with } w_{net} = 53.7\text{mm} \quad (19)$$

$$R_D = 100 - 100 \times (w_{net} - 6 \times a_{corr}) / w_{net} \quad w_{net} = 53.7\text{mm} \quad (19)$$

Tables 6.9.6 and 6.9.7 contain the corrected average crack lengths and the ratios of aluminium damage due to fatigue cracking for the particular specimens. They include also the obtained failure loads and the residual stresses, related to the net section.

$$\sigma_{RS} = F_{failure} / A_{net} \quad A_{net} = 230.9\text{mm}^2 \quad (20)$$

Figure 6.9.4 shows the relation between non-aged and aged residual strength results. The non-fatigued specimens reach a blunt notch strength of 710 MPa (dry) and 697 MPa (aged, 3000h, 70°C, 85%RH), both values are averaged from three specimens, respectively, with low scatter. Although the aged specimen blunt notch strength decreases by 6% compared with the non-aged specimens, both values are higher than the design values recommended from literature:

- typical blunt notch stress (no ageing influence): 673 MPa [16]
- typical blunt notch stress divided by 1.1, equals B-value, equals design value: 612 MPa.

A linear regression analysis for the residual strength related to the remaining aluminium portion after fatigue cracking is performed, as initially evaluated by Müller [15]. Knock down factors in relation to the remaining metal fraction are obtained by division of the two functions for both, aged and non-aged:

$$C_{RS(E)} = \frac{662.73 - 2.4921 R_D}{688.23 - 1.7002 R_D} = 0.9641 - 0.0014 R_D$$

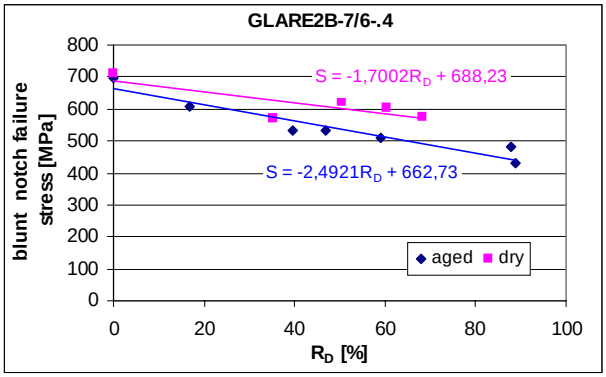

Figure 6.9.4. Filled hole residual strength test results and linear regression 3000h / 70°C /85%RH

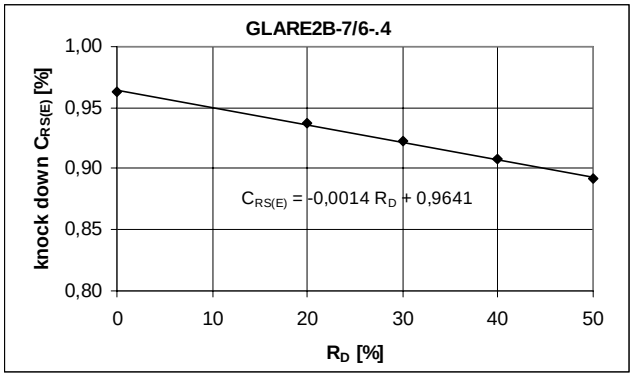

Figure 6.9.5. Knock down factor on 4.8mm filled hole residual strength, GLARE2B-7/6-.4, low interference, 3000h / 70°C /85%RH

The curve for fatigue crack lengths between zero and 50% aluminium net section reduction R_D is plotted in figure 6.9.5. The knock down factor without fatigue crack is significantly lower than the value obtained for the single hole specimen in section 6.8. The explanation is associated with the interference fit of 30 to 40 microns of the fasteners installed in all GLARE2 specimens of the outdoor exposure program. In the case of a GLARE2 application on short range aircraft it is recommended to repeat these tests with clearance fit fasteners installed and 500 hours accelerated exposure (70°C/85%RH).

The above described investigation has also been carried out on GLARE4A-5/4-.4ssclad specimens (ref. section 3.2.4). Note that the ASNA2026 fastener used for the GLARE4A specimens are countersunk fastener. Crack length measurements have been limited to the non-countersunk side, i.e. aluminium layer no. 5. The countersunk shape of the drilled requires a different evaluation of the crack lengths in the particular layers than presented above for the cylindrical holes in GLARE2 because the net section is not constant for all aluminium layers. Associated to this thesis, seven GLARE4A blunt notch specimens with ASNA2026 fasteners have been tested under off-axis *(load direction not parallel to fiber orientation)* conditions and fatigue crack lengths have been measured in all aluminium layers [52].

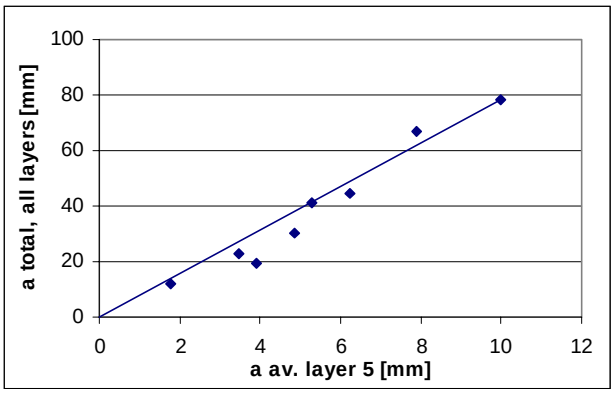

Figure 6.9.6. Relation between average crack length in layer 5 (non-countersunk side) of GLARE4A specimens and the total crack length in all layers

Based on these measurements it is possible to establish a relation between the average crack length measured in layer 5 of the laminate and the total crack lengths in all five layers as shown in figure 6.9.6. The average crack lengths for layer 5 of the specimens are contained in tables 6.9.8 to 6.9.10. The relation between the average crack lengths in layer 5 and the average crack lengths in the other layers is linear, as indicated in figure 6.9.6. The factor to be considered for the cracks in layers 1 to 4 in relation to the crack length measured in layer 5 can be calculated from the available data. Coincidently, the factor is again 0.86, the same value as obtained for the (non-countersunk) GLARE2 specimens. The calculated net section for the 3-hole specimen under consideration of the countersunk is 224.6 mm^2 which is slightly smaller than for the non-countersunk specimens.

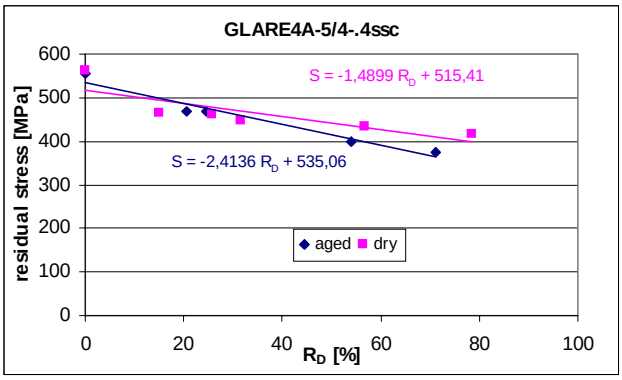

Figure 6.9.7. Filled hole residual strength test results and linear regression GLARE4A

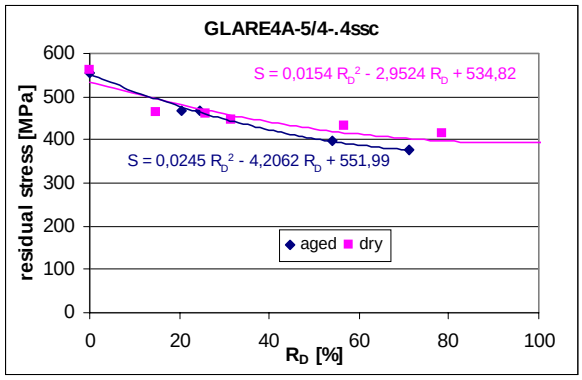

Figure 6.9.8. Filled hole residual strength test results and polynomic regression, GLARE4A

Only one non-fatigued specimen, no. 3-A-14, was available for the determination of the aged blunt notch strength. The specimen failed at 554 MPa net stress, while the average result of the three non-fatigued and non-aged specimens (no. 3-A-7 to 3-A-9) is 561 MPa. In view of the single result for the aged specimen it is unrealistic to see a significant difference between the aged and non-aged specimens in the non-fatigued condition. No knock down factor due to ageing is observed at R_D=0%. However, the results fit well to the qualified material properties:

Typical blunt notch stress (no ageing influence): 579 MPa [16].

Typical blunt notch stress provided with 90% probability (ref. FAR25.0615), design value: 526 MPa [16].

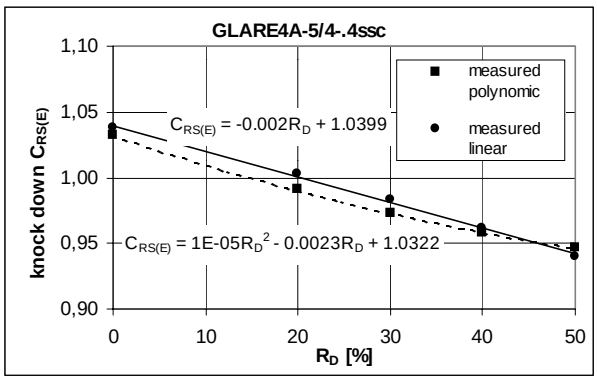

Figure 6.9.9. Linear and polynomic regression analysis, residual strength knock down factor due to 3000h aging in 70°C/85%RH environment

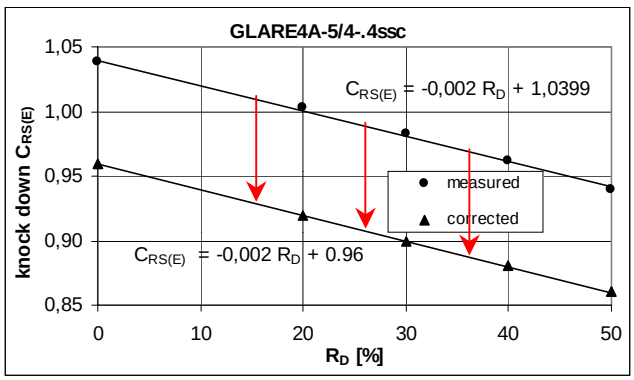

Figure 6.9.10. Knock down factor on 5.6mm filled hole residual strength, GLARE4A, 3000h / 70°C / 85%RH, clearance fit, measured and corrected values

A better approximation for the obtained residual strength values is observed for a polynomial regression compared with a linear regression, compare figures 6.9.7 and 6.9.8. The calculated blunt notch strengths at R_D=0% are closer to each other for both, the non-aged and the aged condition. The polynomial regression leads to slightly higher knock down values, see figure 6.9.9. For the practical relevant damage ratios, R_D<20%, all knock down factors are in the order between 0.99 and 1.04, i.e. a knock down factor need not really be considered. However, this conclusion might leave an un-conservative approach for data from other investigations. For practical and conservative application a correction with the linear curve is recommended according to the conclusions from chapter 6.8.2. Figure 6.9.10 contains a linear residual strength curve parallel to the measured data, but shifted downward in order to agree with the blunt notch strength at (R_D=0%) with a knock down factor of 0.96. As an example, it implies that at R_D=20% a knock down factor of 0.92 should be considered for aircraft component sizing in view of the results of standard accelerated ageing on the residual strength. Note: The iso-concentration lines which have been calculated for 3000 hours ageing (see chapter 4) are applicable for the non-fatigued specimens, only. For the fatigued specimens high moisture concentrations must be considered around the cracks, since the fatigue loads have been applied *prior* to the accelerated exposure. This procedure is conservative for practical applications because a significant portion of the aircraft life [years] will happen before fatigue crack initiation, i.e. moisture will be absorbed *without* fatigue crack in the first part of the structural life.

6.10 Residual Strength, Temperature Influence

(ref. factor $C_{RS(T)}$)

The blunt notch strength is the residual strength without fatigue damage and the sensitivity to temperature is very limited then [9]. Borgonje found no reduction at all, see figure 3.2.4.2. The final failure in both cases, blunt notch and residual strength after fatigue, is associated with fiber failure. Because the fiber strength is affected to a low extent by the temperature and because interlaminar shear effects due to bending are not considered for elementary specimens, it can be concluded, that the residual strength after fatigue will not drop more than the blunt notch strength.

This conclusion is of minor importance with regard to aircraft structures, but it may be relevant for an assessment of low load carrying holes. A more important investigation on the temperature effect applies to single shear joints where the hole is loaded by shear due to fastener tilting. This topic follows in section 7.1.8.2.

6.11 Bearing Strength

In the present section the effect of an exposure to accelerated aging on the bearing strength of joint with a double shear fastener is explored.
A similar test program is used for checking the effect of accelerated aging on the strength of a riveted lap joint with two fasteners. In this case, the fasteners are loaded in single shear and tilting of the fastener is possible.

6.11.1 Bearing strength

The experiments are carried out with the test set-up described in section 3.2.5. Two GLARE materials were involved: GLARE2B-7/6-.4 and GLARE4A-5/4-.4ssc. The ratio of D/w was the same for both grades: D/w = 0.2 but the size was different, i.e. D = 4.8mm for GLARE2B-7/6-.4 and D = 5.6mm for GLARE4A-5/4-.4ssc. The thicknesses were also different, i.e. 4.5 and 3.6 mm respectively. The accelerated exposure occurred again at 70°C in an 85%RH environment.
The test results are contained in tables 6.11.1 and 6.11.2. The mean values of the yield strength and the ultimate strength, which were obtained in 4 similar tests, and the corresponding standard deviation are presented in the table below.

Mean values for GLARE2B-7/6-.4 specimens							
exposure	temp.	σ_{yield}			σ_{ult}		
		[MPa]	[%]	s	[MPa]	[%]	s
none	RT	525	100	27.2	864	100	6.5
3000 h acc.	RT	499	95.0	42.9	786	91.0	10.9
1500 h acc.	RT	467	89.0	50.3	792	91.7	9.9
3000 h acc.	70º C	361	68.8	52.0	715	82.8	17.9
Mean values for GLARE4A-5/4-.4ssc specimens							
none	RT	570	100	7.0	867.0	100	15.1
3000 h acc.	RT	530	93.0	16.9	762.0	87.9	4.8

The bearing yield stress and bearing yield load are plotted for the different exposure treatments in figures 6.11.1 and 6.11.2 respectively.

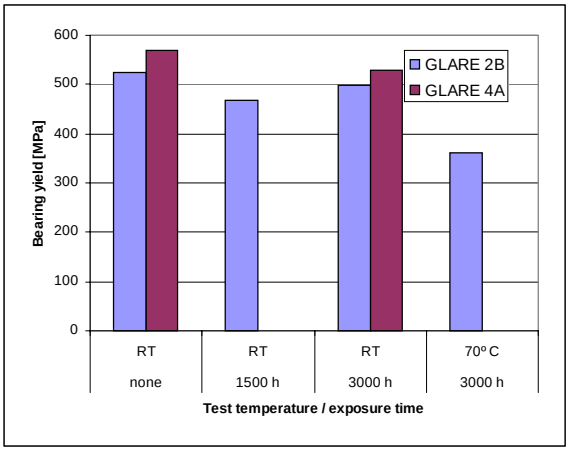

Figure 6.11.1. Bearing yield stresses

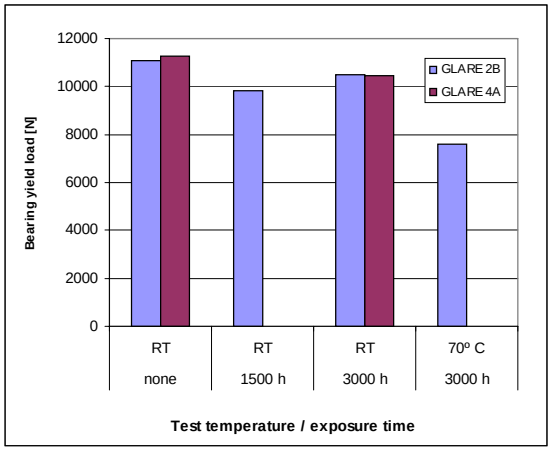

Figure 6.11.2. Bearing yield loads per fastener

The results of the GLARE2B specimens show a significant decrease in bearing yield strength after accelerated exposure. After 1500 hours of exposure this is 11.0%, but after 3000 hours the decrease is only 5.0% on average. When tested at 70º C, the bearing yield strength after 3000 hours of accelerated exposure is decreased by 31.2%. The values for standard deviation indicate high scatter for yield strengths. Possible causes are differences in clamping and inaccuracies in yield strength determination, which was done manually.

For the GLARE4A specimens, the influence of 3000 hours of exposure is quite similar. On average, the yield strength is decreased by 7.0% at room temperature.
The higher strength values of the GLARE4A specimens compared with GLARE2B are according to the expectations, they are explained by the larger D/t ratio and the presence of fibers perpendicular to the loading direction.

The failure mode was the same for all specimens. Failure occurred as a combination of bearing failure and shear-out . The failure load is obtained when no further increase of the load is possible.

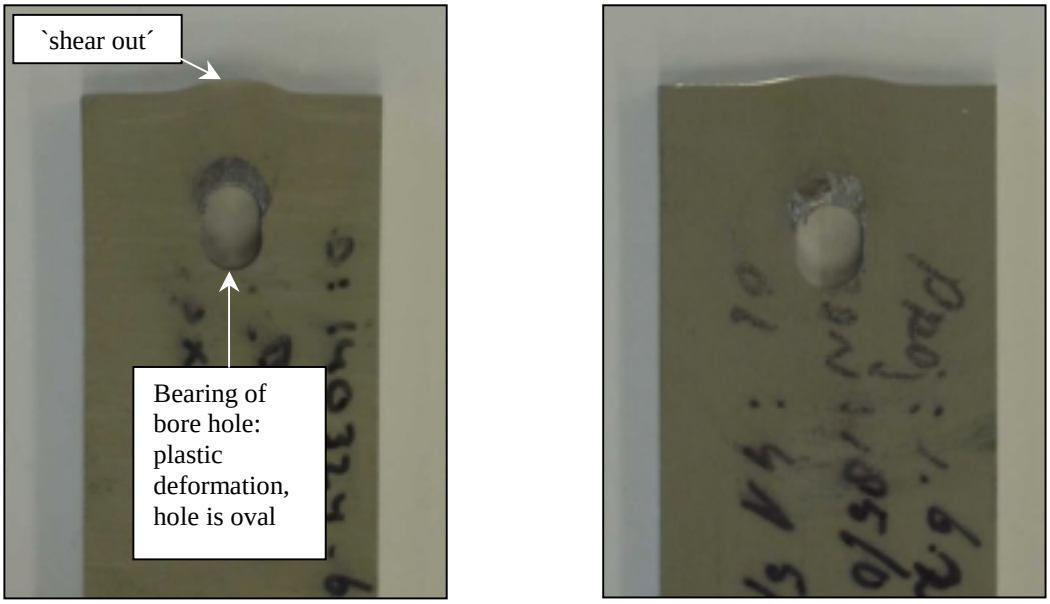

Figure 6.11.3. Failure mode of GLARE2B (left) and GLARE4A (right) specimens

A typical load-displacement diagram recorded during testing is given in figure 6.11.4. It clearly shows the loop used to determine the secondary modulus. Two different displacement measurements were made: the displacement measured by the testing machine and the displacement measured by the extensometer on the specimen, see section 3.2.5. The extensometer data are preferred because they better represents the deformation of the hole. An extremely large displacement is measured by the testing machine for a specimen tested at 70ºC (see figure 6.11.5). Probably it is caused by slip in the mechanical grips which had to be used instead of the hydraulic grips because of using the oven. However, slip in the grips has no influence on the extensometer measurements.

The bearing values found are generally lower than those obtained in previous tests [50]. This is especially true for the bearing ultimate strength values which are 15 to 20% lower. The more interesting yield strength values are about 2% lower only.

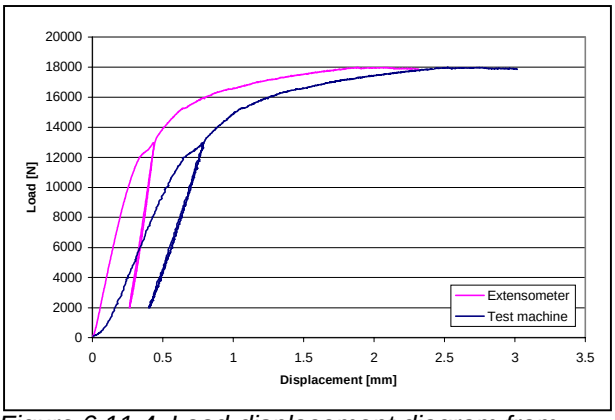

Figure 6.11.4. Load-displacement diagram from specimen 4-B-1

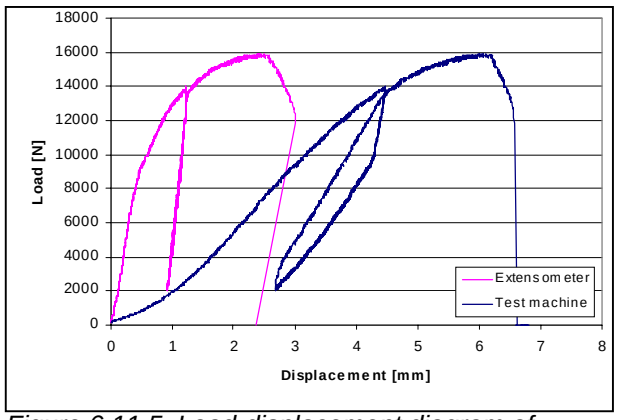

Figure 6.11.5. Load-displacement diagram of specimen4-B-17, showing large displacements measured by test machine

The bearing values found are generally lower than those obtained in previous tests [50]. This is especially true for the bearing ultimate strength values which are 15 to 20% lower. The more interesting yield strength values are about 2% lower only.

The main explanation for the higher values in the previous investigation is associated with the specimen clamping in the test tool. Due to this clamping, buckling of the surface aluminum layers is prevented, which leads to a large increase of the bearing strength. Another reason is the larger e/D ratio of 3, compared with 2.5 used in this investigation (e is the so-called head distance between the center of the hole and the top edge of the specimen).

Bearing tests were also covered in the GLARE qualification program performed by National Aerospace Laboratory NLR [51]. In those tests, a similar test setup was used as in the present investigation, i.e. with an 0.1 mm spacing between specimen and test tool. The specimen geometry was slightly different; a hole diameter of 6.35 mm and e/D ratios of 2.0 and 3.1 were used. The laminate lay-ups were also different, but identical GLARE types were used. Similar exposure conditions were adopted, i,e, 3000 hours / 70°C / 85%RH in all cases.

Figures 6.11.6 and 6.11.7 show a comparison between the NLR and TU Delft results of the GLARE2B and GLARE4A specimens respectively. The results are plotted for different values of e/D because this ratio is thought to have a significant influence on the results. The comparison of GLARE2B results in figure 6.11.6 show the TU Delft data positioned in between the values obtained by the NLR for the e/D=2 and e/D=3.1 specimens. This could be expected with the e/D=2.5 of the TU Delft specimens. The GLARE4A results in figure 6.11.7 show a less consistent relation between the results for different e/D ratios. Particularly the drop of the bearing yield strength at room temperature for increasing e/D

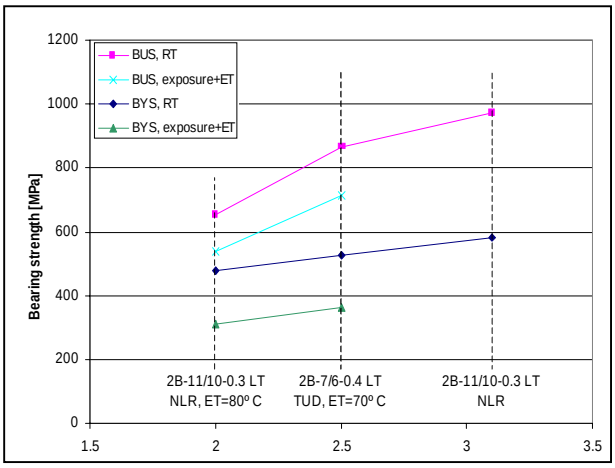

Figure 6.11.6. Comparison of GLARE2B bearing data from different sources

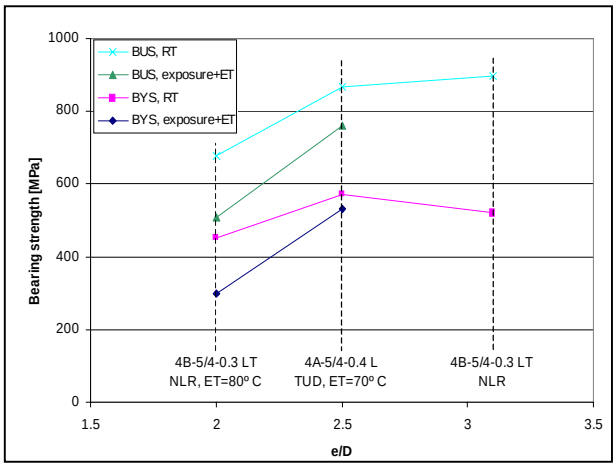

Figure 6.11.7. Comparison of GLARE4A bearing data from different sources

does not agree with expectations. At first sight, the values at e/D=3.1 seem to be too low, but it may also be that the values at e/D=2.5 are too high.
The NLR tests show the same large decreases in bearing strength when testing at elevated temperature after accelerated exposure, see figures 6.11.6 and 6.11.7.

6.11.2 Rivet strength tests

The so-called *rivet strength* property is more realistic for the determination of the single shear riveted joint strengths because it simulates the influence of fastener tilting on the test result. The test procedure is explained in chapter 3.2.6. All results of dry specimens and the specimens exposed for 3000 hours in a 70ºC/85%RH environment are recorded in tables 6.11.3 and 6.11.4.
The failure modes are different for the GLARE2B and GLARE4A specimens. The GLARE2B specimens show tilting of the fasteners and failure of the protruded fastener head (figure 6.11.8). The collars are hardly deformed and remain attached to the fasteners.

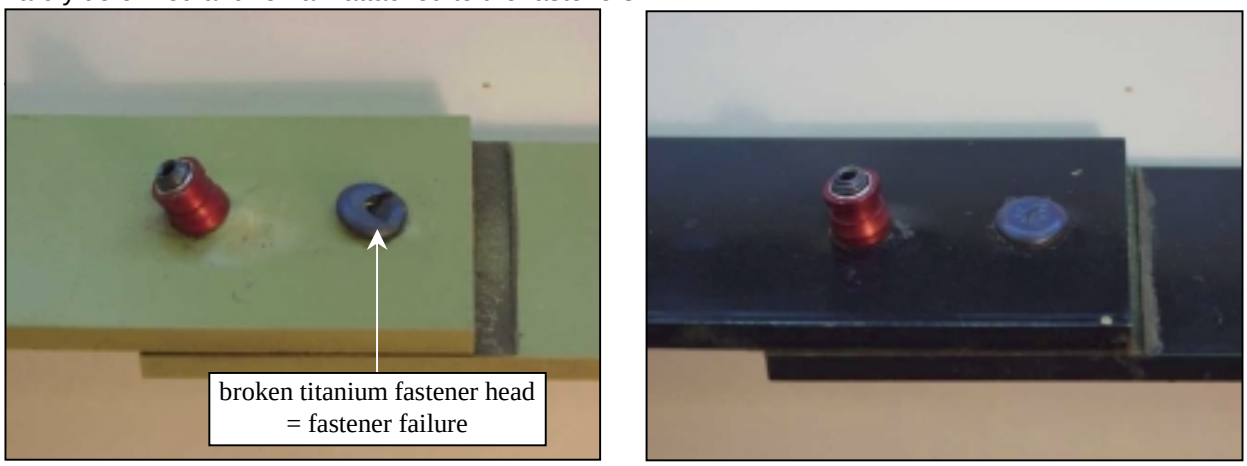

Figure 6.10.8. Failure of unexposed (left) and accelerated exposed (right) GLARE2B

The GLARE4A specimens show fastener tilting as well, but due to the countersunk, the fastener heads are pulled through the first layers of the laminate (figure 6.11.9). The fastener heads remain intact. The collars sometime deform but in all cases the collars remain attached to the fasteners.

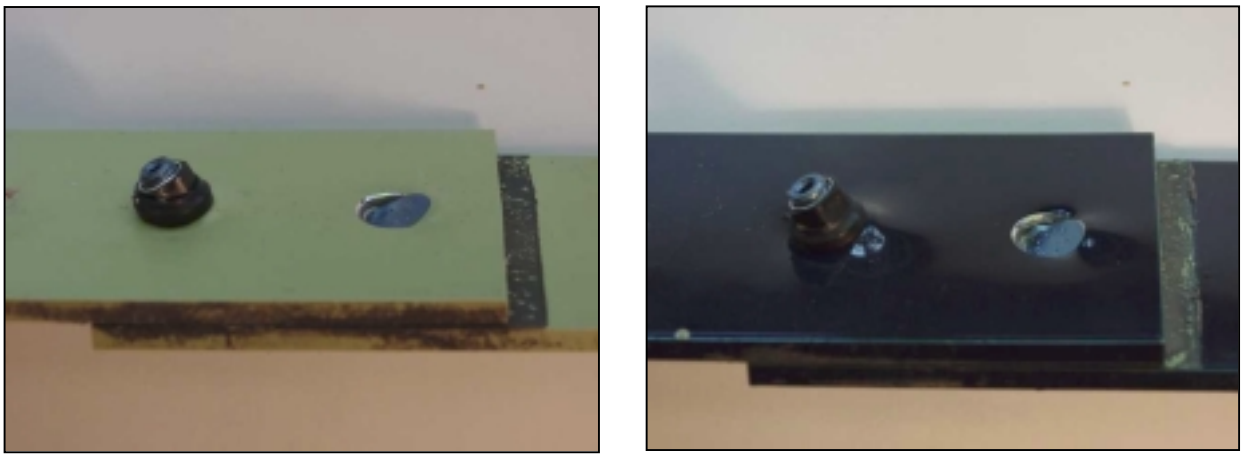

Figure 6.11.9. Failure of unexposed (left) and accelerated exposed (right) GLARE4A specimens.

Noteworthy differences between the failure modes of the exposed and unexposed specimens are observed. The average strength values expressed in loads per fastener are shown in figures 6.11.10 and 6.11.11.

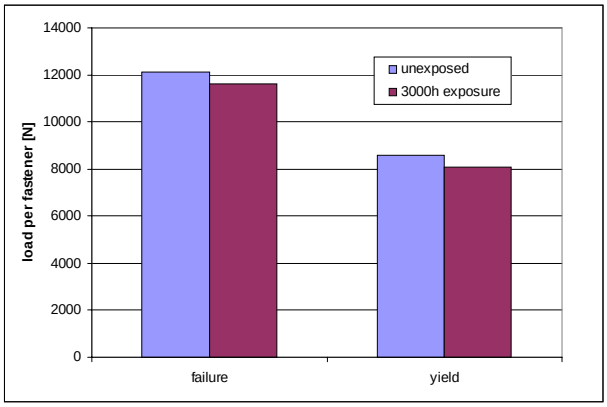

Figure 6.11.10. Rivet strength of DAN7-6 fastener and NSA5075-6 collar in GLARE2B-7/6-.4

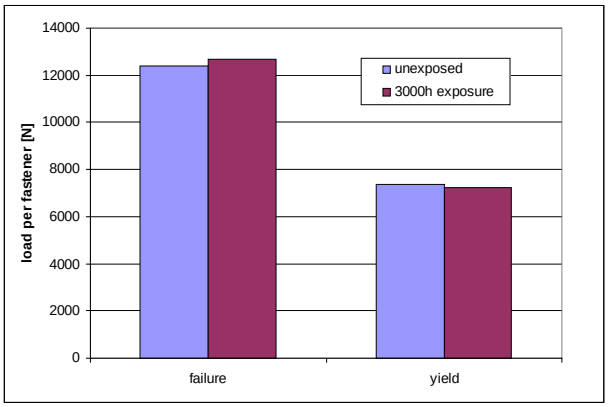

Figure 6.11.11. Rivet strength of ASNA2026-3A fastener and ASNA2528-3A collar in GLARE4A-5/4-.4

Discussion

At the time when the A340 was developed, the 4.8mm and the 6.4mm fastener were standardized and available to the Airbus Industry. The 4.8mm Hi-Lok is a widely used fastener in the A330/A340 series, which sometimes lead to an undesirable ratio between the clamping thickness and the diameter of a fastener. The substitution of a 4.8mm fastener by a 6.4mm fastener is often not a good solution, due to geometric space restraints. The space between two stringers, for example, is limited and almost not variable. Consequently, the use of the 4.8mm may not be an optimal solution, but still the best choice under the given circumstances. For the circumferential joint described in section 3.1.1 and tested as part of the A340-600 full scale structure, the ratio between the thickness of the clamped material and the fastener diameter is:

$t_{clamping}$ / D = 2 x 4.3mm / 4.8mm = 1.79

The failure load of GLARE2B / DAN7-6 combination is just 30% above the yield load, approximately. This ratio implies that the *ultimate* load determines the joint strength and not 1.5 x yield. However, it was not a failure of the GLARE material. The fastener head failed and the failure mode was associated with the strength of the collar. Actually this failure mode was not a topic of the investigation of the present thesis.

The 5.6mm fastener has been (re-) standardized for the A380, which offered more flexibility to the designer for optimization of the structures. The relation of clamping thickness to fastener diameter for the GLARE4A repair discussed in this thesis is calculated:

$t_{clamping}$ / D = 2 x 3.5mm / 5.6mm = 1.25

For this material / fastener combination, the quotient ultimate strength / yield strength is higher than 1.68, which means that the GLARE properties are sizing the joint by the yield strength.

The rivet strength tests show that accelerated exposure causes a minor reduction of the failure and yield strength of the GLARE joints. These reductions can be explained by moisture absorption of the epoxy resin which lowers the modulus of elasticity. The resin therefore offers less support to the rest of the

laminate and the fastener. This leads to earlier hole deformation and tilting of the fasteners. Due to tilting and subsequent bending forces, the fasteners are partially loaded under tension.

For the GLARE2B specimens, a reduction of 5.9 % of the yield load is found after 3000 hours accelerated ageing. For the GLARE4A specimens, the reduction of the yield load is 1.6 % only. In view of these small decreases after accelerated exposure, it is expected that the specimens which are exposed outdoors will also show minor reductions of the yield values in tests at room temperature. The reader who is interested in a further discussion of rivet strength in GLARE is referred to literature [49].
A comparison of the bearing yield strength per fastener (figure 6.11.2) with the yield rivet strength (figures 6.11.10 and 6.11.11) demonstrates the significant influence of fastener tilting. The allowable load per fastener at room temperature decreases by approximately 30% for both material/fastener combinations. The influence of ageing, even 3000 hours at 70°C and 85% relative humidity, is very limited. The results confirm that the bearing strength properties are not decisive for sizing of single shear joints.

6.12 Rivet Pull Through Strength

The distance between the inner and outer rivet row of a GLARE riveted lap joint indicates the length (l) of the parts of the joint which are clamped on one another. A large value of l combined with a relatively small fastener diameter (D) is a potential configuration for severe fastener tilting and ultimately a failure by rivet pull through (RPT). This behaviour for a high l/D ratio is expected for the circumferential joint described in section 3.2. However, if the value of l/D is low, which applies to the riveted repair (see section 3.2), a moderate fastener tilting will occur which finally could be followed by a blunt notch failure.
Because fatigue cracks at rivet holes are expected at the end of the aircraft life, the influence of these cracks on the rivet pull strength should be considered. Moreover, the environmental conditions should also be investigated. These topics are the subject of the present section. The rivet pull through strength may also become a sizing criterion if a GLARE sheet is jointed to a very stiff back-up structure, e.g. for a fuselage at the level of the passenger floor.

Test procedure

The fatigue cracks are introduced by testing the GLARE specimen described in section 3.2.8 with open holes. Cracks of different lengths in the range of 1 to 10 mm have been created. The rivet pull through tests were performed on a 100 kN MTS test machine with the setup shown in figure 6.12.1 which deflects the GLARE specimen from the 4mm thick aluminum sheet. The fastener is thus loaded in tension. Two types of GLARE were involved, GLARE2B and GLARE4A.
Specimens have been tested both at room temperature and at 70º C. For the elevated temperature tests a temperature chamber is placed around the test setup. The temperature was monitored with a thermocouple attached to the specimen surface. The test was performed 10 minutes after the surface obtained the required temperature to be sure that the specimen was heated throughout the full thickness.

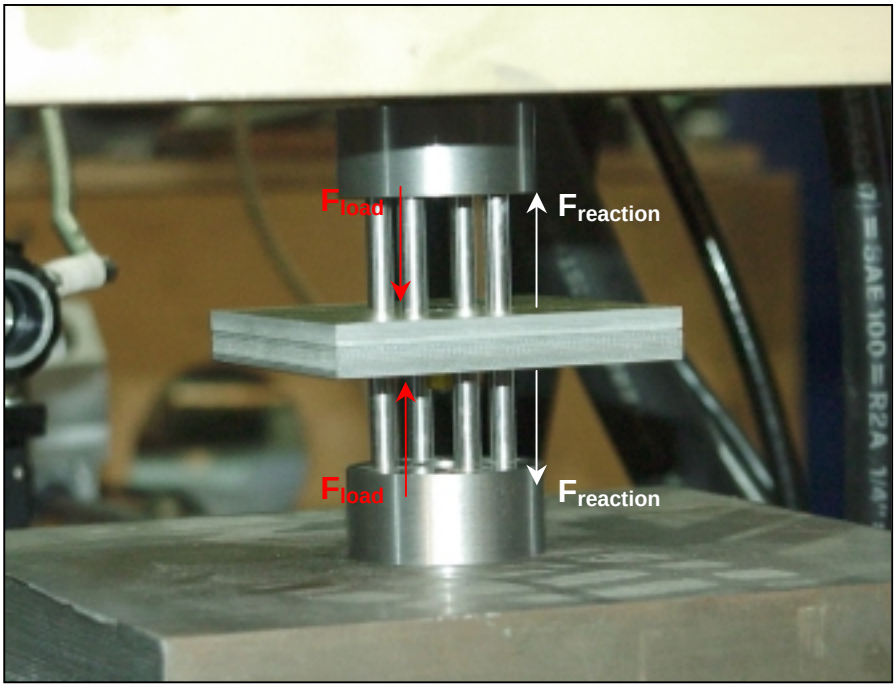

Figure 6.12.1. Rivet pull through test set up, fastener in center of specimen

Fatigue loading

Fatigue cracks of different lengths at both sides of the hole have been created by fatigue testing the specimens with different numbers of cycles. A detailed listing of fatigue test data is given in table 6.12.1. The cracks are measured on the outside aluminium layers with the camera system, which provides measurements of high accuracy [46]. The cracks in the GLARE2B specimens are measured on both sides of the specimen. Due to the presence of a countersunk hole, the cracks in the GLARE4A specimens are measured on the non-countersunk side, only.

Strength

The results of the RPT tests are given in table 6.12.2. The ultimate rivet pull through load of each specimen is plotted in figure 6.12.2 as a function of the average crack length. The results show that both crack length and elevated temperature hardly affected the RPT strength of the GLARE2B specimens. However, the GLARE4A specimens show an almost linear decrease of RPT strength for an increasing value of the crack length, and another reduction due to the elevated temperature of 70°C. The different behaviour of the two GLARE types is associated with the different configurations of the specimens and the resulting failure modes. In the GLARE2B specimens, the failure occurred in the collar of the fastener and not by a pull through mechanism. In the GLARE4A specimens pull through of the fastener head through the GLARE laminate occurred, see figure 6.12.3. The different behaviour was expected, since the 4.8mm fastener in the 4.3mm thick GLARE2B is the critical item, compared with the 5.6mm fastener installed in the 3.5mm thin GLARE4A.

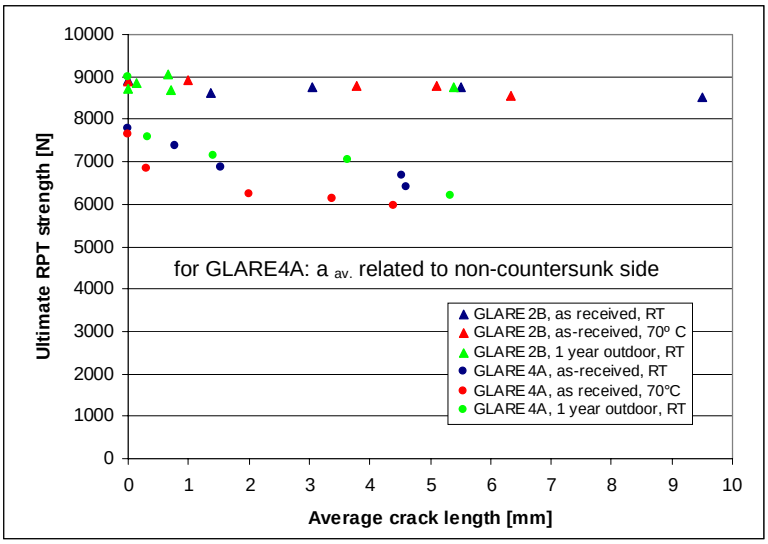

Figure 6.12.2. Rivet pull through strength vs. average crack length

Due to the fastener failure, the RPT strength of the GLARE2B specimens is hardly influenced by elevated temperature, neither by temperature nor by one year outdoor exposure. The RPT strength of the GLARE 4A specimens is decreased by elevated temperature, due to the lower resistance of GLARE against deflection, caused by the decreased interlaminar shear strength. Therefore the fastener is more easily pulled through the GLARE laminate. An influence on the pull through strength after one year of outdoor exposure was not indicated.

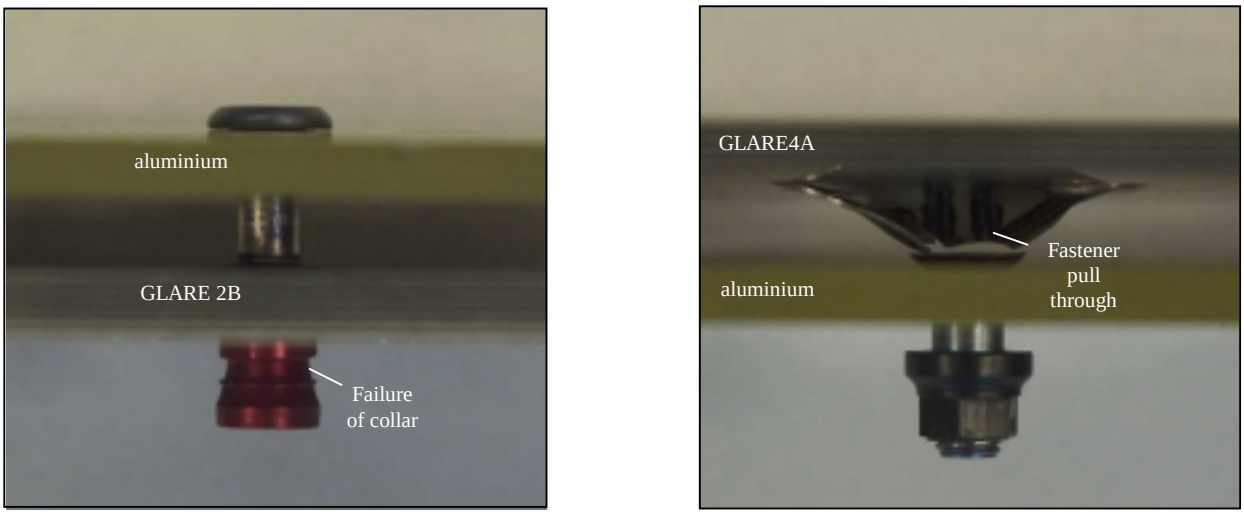

Figure 6.12.3. Typical failure modes of GLARE2B (left) and GLARE4A (right) specimen

Failure of the specimens without fatigue cracks was influenced by the four holes drilled for the pins which push the sheets apart, see figure 6.11.4. The failure path occurred in the narrowest area between

the fastener hole and the four guidance holes. But if fatigue cracks were present, the failure starts from the tips of the two fatigue cracks.

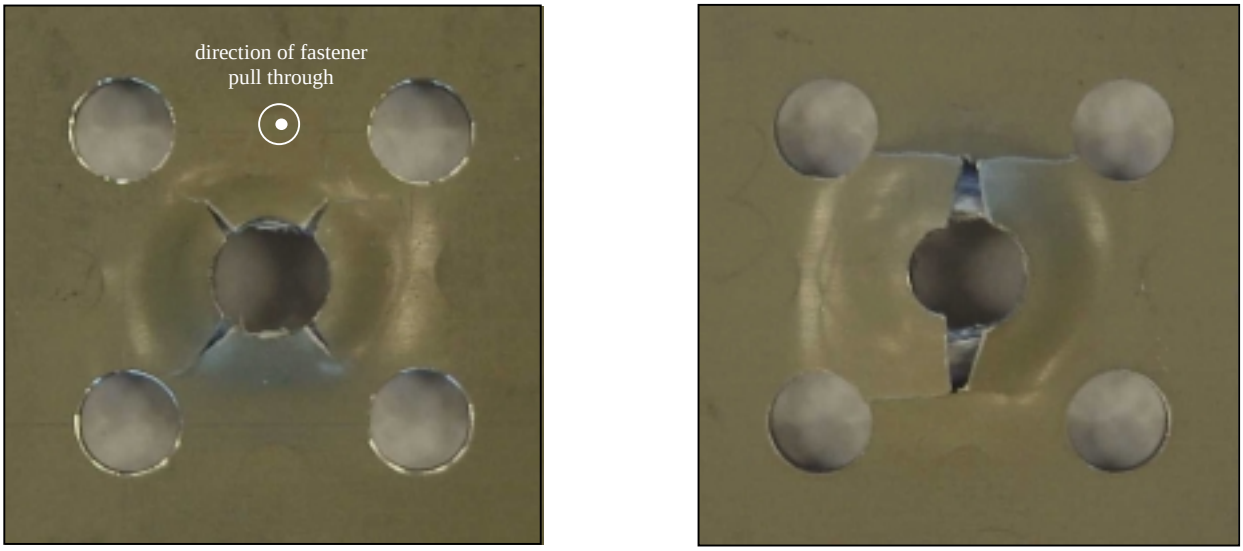

Figure 6.12.4. Typical failure of GLARE4A specimen, without cracks (left) and with cracks (right)

The GLARE4A data are related to the fatigue damage ratio R_D, for practical use. Crack lengths in the particular (5) aluminium layers are determined according to the method presented in chapter 6.9 and related to a rivet pitch of 28mm. The results are presented in figures 6.12.5 and 6.12.6.

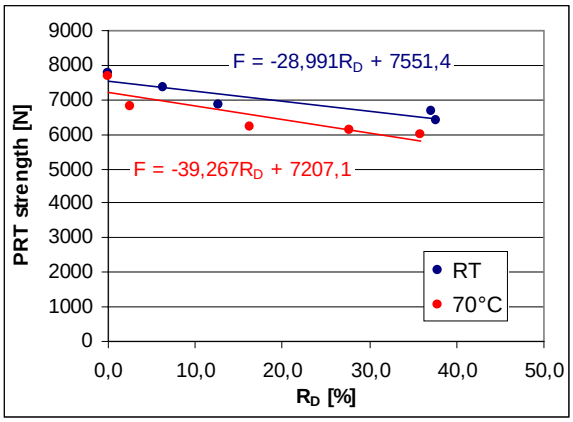

Figure 6.12.5. GLARE4A-5/4-.4 RPT strength

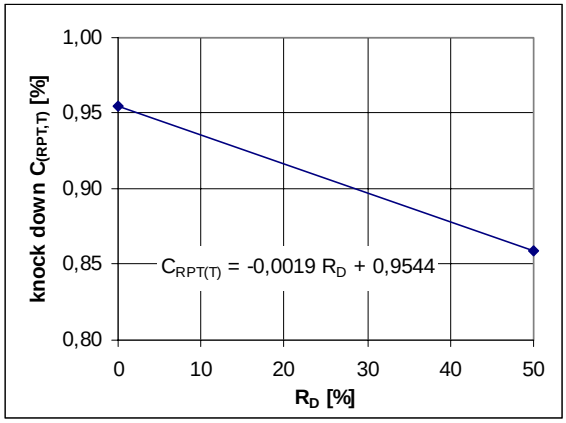

Figure 6.12.6. Temperature related knock down factor for GLRE4A / ASNA2026 specimens

Load-displacement diagrams

The load-displacement diagrams of the GLARE4A specimens tested at room temperature exhibit a number of peak loads which is attributed to the fastener head being pulled through each successive aluminum layer. If the diagram of specimens with cracks (fig. 6.12.7) is compared to the diagram of the specimen without cracks (fig. 6.12.8), it can be seen that the initial peak loads are almost equal. The reduction of RPT strength for the specimens with cracks is a consequence of the lower load needed to pull the head through subsequent aluminum layers.

The load-displacement diagrams of the specimens tested at 70º C show a more steady increase of the load to failure. There is only one clear peak load at which the specimen fails. The maximum load is again higher for the specimen without cracks (fig. 6.12.9) than for a specimen with cracks (fig. 6.12.10). The more continuous load-displacement curves can be explained by weakening of the epoxy which reduces the transverse support of the thin aluminum layers. It thus is easier to deform the GLARE sheet

by the fastener. It also leads to a lower pull through strength. The presence of cracks further lowers the RPT strength.

The out of plane stiffness of GLARE around the hole is important for the rivet pull through failure. This failure mechanism, which includes a local plasticising of the aluminum and a variable resistance of the laminate against bending (the latter depending on the prepreg condition), is similar the failure mode a of three point bending interlaminar shear specimen. The ILSS specimen strength is significantly decreased by elevated temperature [47], but it is relatively insensitive to moisture diffusion if tested at room temperature. It is therefore decided to conduct no tests after accelerated exposure, but to add some rivet pull through specimens to the outdoor exposure lot for final verification.

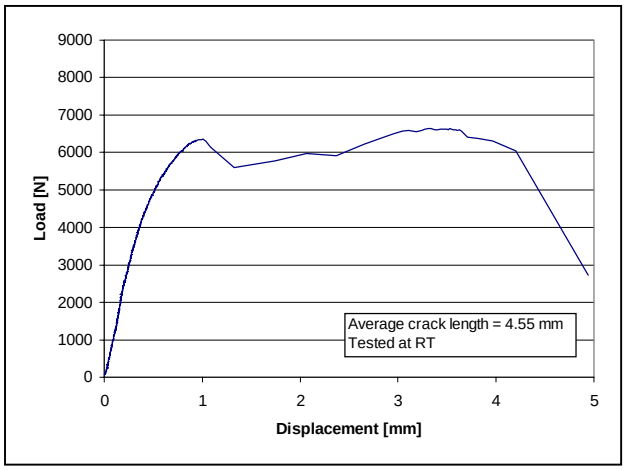

Figure 6.12.7.
Load-displacement diagram of specimen 7-A-1

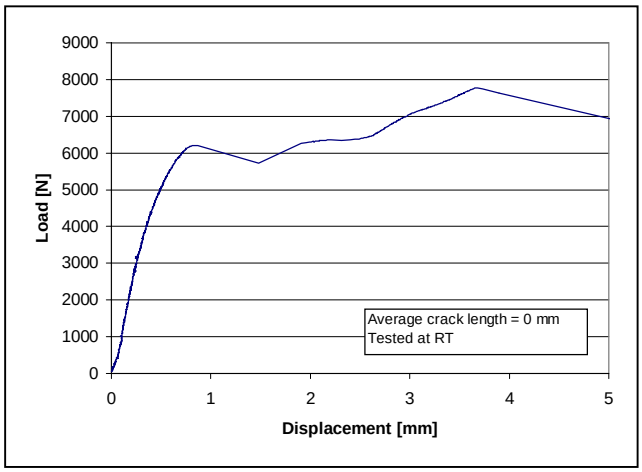

Figure 6.12.8.
Load-displacement diagram of specimen 7-A-3

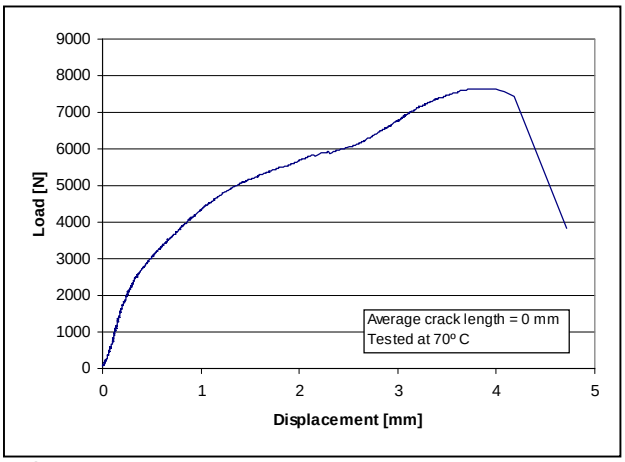

Figure 6.12.9.
Load-displacement diagram of specimen 7-A-6

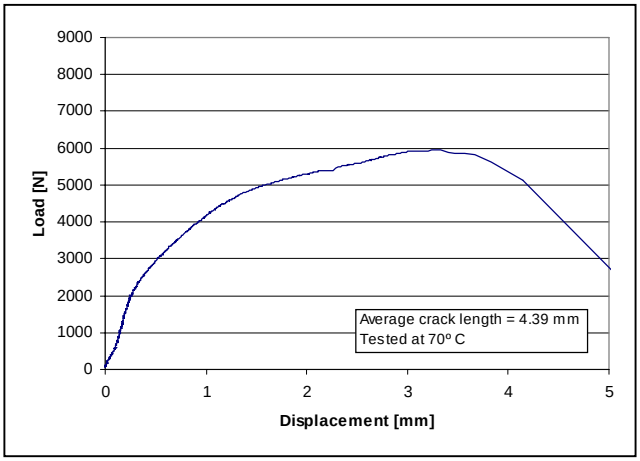

Figure 6.12.10.
Load-displacement diagram of specimen 7-A-10

6.13 Compression Filled-Hole Strength

Compression filled hole specimens with fatigue cracks have been tested at room temperature (RT) and at 80°C. The test set up and the specimen geometry are presented in section 3.2.7 where the specimen geometry is shown in figure 3.2.7.3. The hole to width ratio was D/w=0.2 (w = 22.7 mm for GLARE2B and 28mm for GLARE4A). The purpose of the tests was to see whether buckling of the detached aluminium layers would occur under a compression load. The temperature of 80°C is considered to be the worst case for non-aged material because the adhesive forces, which prevent buckling of the outer aluminium layer, decrease with temperature. Six specimens after one year outdoor exposure in Australia could already be included in the present evaluation of the data.

The fatigue crack lengths in the compression filled-hole specimens are given in table 6.13.1 and failure stresses in table 6.13.2. Figure 6.13.1 shows the gross stress failure stress as a function of average crack lengths. One GLARE2B specimen and all three GLARE4A specimens tested at 80º C failed in the specimen clamping area. They are not contained in figure 6.13.2.

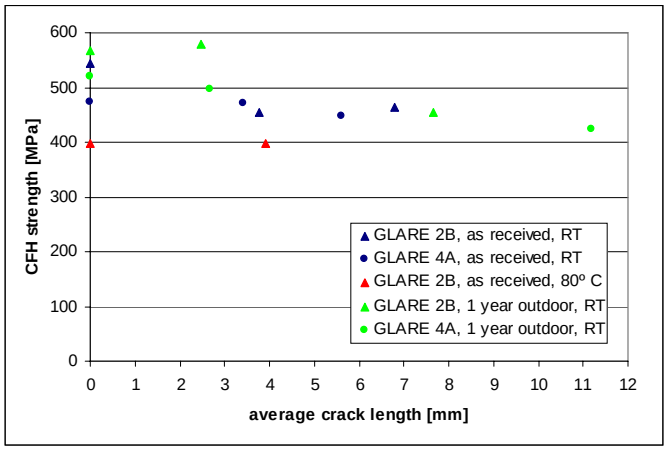

Figure 6.13.1. Compression filled hole gross failure stress versus average crack lengths

The GLARE2B specimens tested at room temperature show a more significant drop in compression strength in the presence of cracks than the GLARE4A specimens. No strength reduction due to one year outdoor exposure is observed. Due to failure at the clamping area for most specimens tested at 80º C, the information gained from these tests is very limited. The two valid results of the GLARE2B specimens show no influence of crack length. The compression strength values are however significantly lower than those at room temperature.

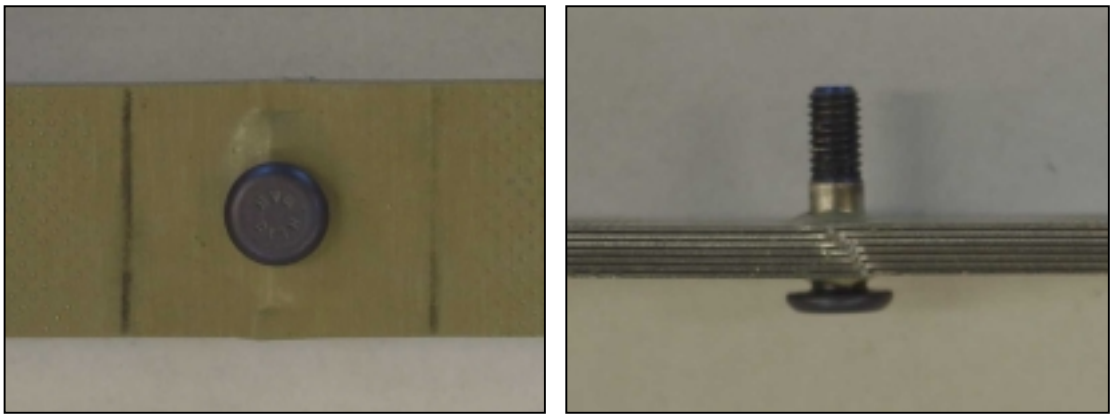

Figure 6.13.2. Desired failure mode of GLARE specimens

A failure mode is illustrated by figure 6.13.2 which shows local buckling of the entire laminate at the net section of the specimen. The other relevant failure mode is local buckling of just one of the outer

aluminum layers. The distance between the specimen clamping and the anti-buckling guides provided the correct failure mode for all specimens tested at room temperature. At 80º C however, failure often occurred between the edge of the specimen clamping and the anti-buckling guide, see figure 6.13.3.

The obviously decreased stiffness of the laminate at high temperature is at least partly compensated by the stiffness of the titanium bolt, which covers a large portion of the center specimen section and supports the aluminium layers of the GLARE to keep their position, in relation to each other.

A few specimens show deformation caused by torsion (figure 6.13.3, right). The cause of this phenomenon is unknown.

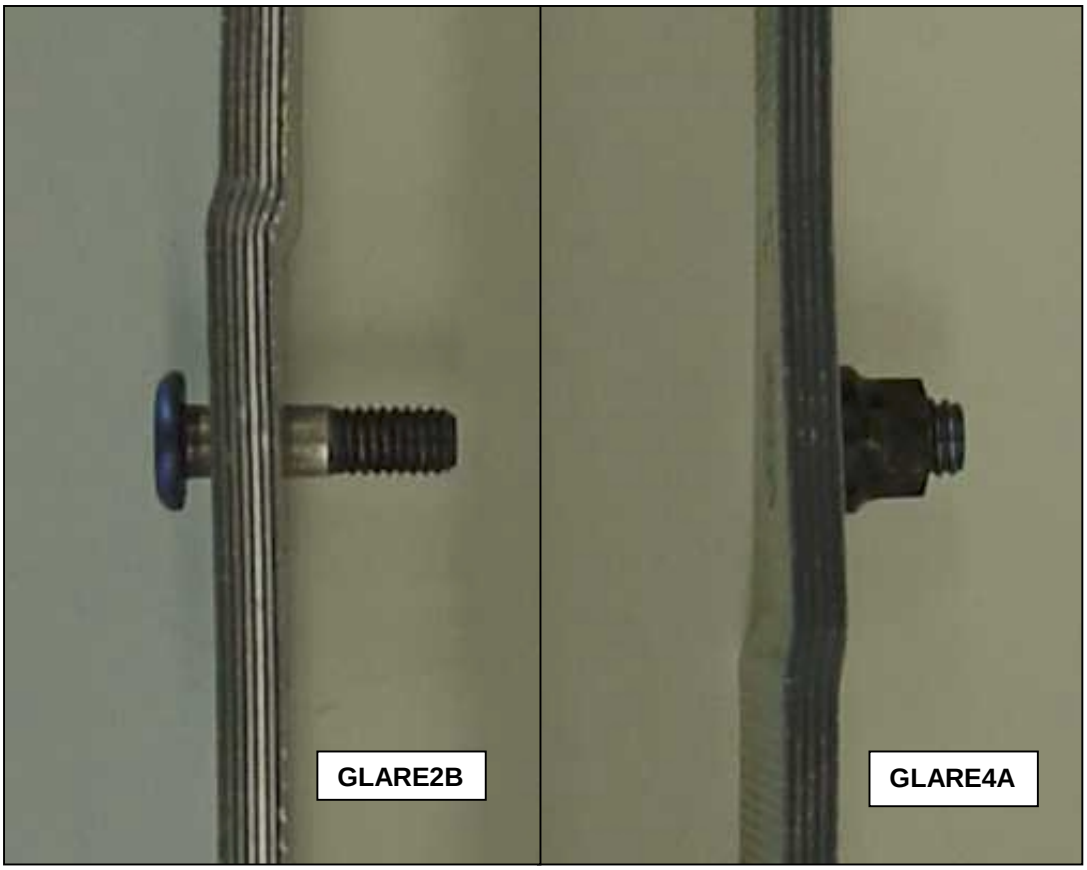

Figure 6.13.3. Incorrect failure mode for GLARE specimens

The most likely argument why the GLARE4A specimens buckled near the edge of the clamping of the specimen instead of the location of the hole is associated with the collar of the fastener. Due to its firm attachment to the surface layer and its large base area, it will certainly play a role in preventing the occurrence of local buckling.

The gross failure stress is related to the fatigue damage ratio R_D in figure 6.13.4. R_D is calculated in the same way as explained in chapter 6.9, i.e. a 14% lower fatigue crack length is considered for the center aluminum layers than measured on the outer aluminum layers. All compression filled hole strengths results, without and with fatigue cracks, which buckled in the net section, exceed the compression yield design strength for the GLARE materials involved. If the compression yield strength is not exceeded in the compressive limit load case, compression filled hole strength can not become a design case.

Because the compression filled-hole strength discussed here is relevant to the rear fuselage structure at room temperature, it is recommended to test the returning outdoor exposure specimens after 2 and 6 years respectively at room temperature.

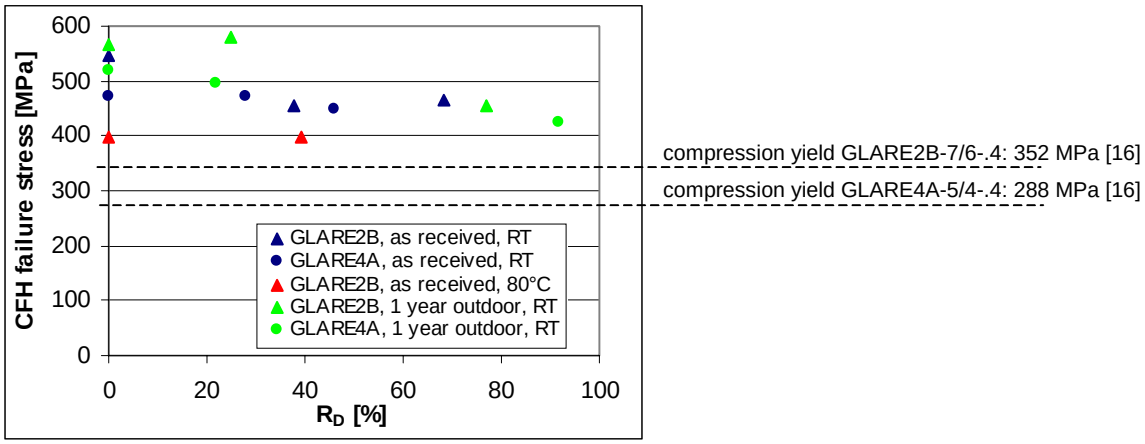

Figure 6.13.4. Compression filled hole gross failure stress versus fatigue damage rate, related to specimen width

6.14 Conclusions on Elementary Investigations

In the previous sections of this chapter various investigations on elementary GLARE specimens were discussed which covered crack initiation, crack propagation, fatigue life, scatter, static strength and residual strength if fatigue cracks are present. A major question discussed was how these properties are affected by moisture absorption and temperature, a problem which is relevant to short range aircraft (see chapter 5). In the present section, the experience obtained in the previous sections is recapitulated and evaluated in the light of the FAR/JAR airworthiness requirements and relevant knock-down factors. The various topics are discussed in the order of the table in the introduction of this chapter, starting with fatigue aspects followed by static strength problems including residual strength.

Crack initiation, temperature influence

Applicable: JAR/FAR 25.0571 (Fatigue & damage tolerance)

It has been observed that the influence of temperature on crack initiation in the aluminium layers of GLARE is negligible in the range between room temperature and 70°C. The test results fit in one scatter band. The effect of an elevated temperature need not be considered for the application of results of crack initiation test performed at room temperature.

The effect of a low temperature on crack initiation in the aluminium layers of GLARE (made of 2024T3 metal) is similar as for monolithic aluminium specimens. Crack initiation is significantly postponed if tested at a *constant* low temperature, e.g. –55°C. The lower fatigue sensitivity of the aluminium layers and the increased stiffness of the matrix at low temperature overcompensate the higher stress level in the aluminium layers of GLARE introduced by the mismatch of the coefficients of thermal expansion. It should still be recommended to investigate the influence of temperature variations as they occur in real flights under realistic service-simulation load histories.

The stress level in the aluminium layers of GLARE3 after cooling down from the curing temperature can be calculated. The crack initiation life of the aluminium layers in GLARE can then be predicted by using a monolithic aluminium SN-curve. A problem of obtaining the crack initiation life of GLARE specimens is offered by detecting a small crack in GLARE which defines the crack initiation life of GLARE specimens. The detection sensitivity depends on the GLARE thickness. A more logical approach recommended here is to carry out SN tests on laminated specimens of thin bonded metal layers without fibers and to use these data for predictions on GLARE crack initiation endurances.

.

From the elementary investigations in section 6.2 it is concluded, that no detrimental test-to-structure factor $C_{CI(T)}$ has to be applied on crack initiation results obtained in a full scale fatigue test performed at room temperature.

$C_{CI(T)} = 1$

Crack initiation, accelerated ageing influence

Applicable: JAR/FAR 25.0571 (Fatigue & damage tolerance)

There is no influence of prepreg moisture absorption on crack initiation in open holes (section 6.3). It is concluded that the influence of ageing on crack initiation need not be considered for any GLARE structure. The interpretation of full scale test results conducted in a dry environment does not require a correction. The environmental test-to-structure factor $C_{CI(E)}$ to be applied on full scale crack initiation test results is 1.0.

$C_{CI(E)} = 1$

Crack initiation and crack propagation scatter

Applicable: JAR/FAR 25.0571 (Fatigue & damage tolerance)

An inhomogeneous stress distribution in the width direction of the five-hole specimens has been observed due to edge effects. The associated crack initiation scatter can be separated in material- and MSD-related scatter. Analysis of the results indicated a relatively low standard deviation of the crack initiation fatigue life with scatter following a Gaussian distribution (Section 6.4). It appears that the material scatter obtained in fatigue tests on single hole specimens is lower than obtained in tests on monolithic aluminium specimens. The scatter data obtained from the five-hole specimens are considered to be representative for MSD situations at relevant stress levels for an aircraft fuselage. In view of the low scatter for the GLARE specimens, it is considered to be conservative to adopt a test-to-structure factor due to material scatter on crack initiation life ($C_{CI(MS)}$) which is equal to 1.0 for GLARE compared with monolithic aluminium.

$C_{CI(MS)} = 1.0$

The crack propagation scatter in the aluminium layers of GLARE was observed to be relatively low. Moreover, there are no reasons why scatter should be larger than for monolithic aluminium. As a consequence, it is not necessary to use a higher scatter factor on the crack propagation life for the GLARE PSE inspection threshold periods than for monolithic aluminium structures. Again the test-to-structure factor due to material scatter on crack propagation life ($C_{CP(MS)}$) equal 1.0 appears to be conservative for GLARE compared with monolithic aluminium.

$C_{CP(MS)} = 1.0$

If a full scale fatigue test is carried out on an aircraft structure which contains both monolithic aluminium and GLARE components, the validated operational life of the GLARE parts at the end of the test is larger than for the aluminium components if the GLARE parts are cracked but can still carry ultimate load. This conclusion is based on the low crack propagation scatter in GLARE which is lower than the crack initiation scatter in monolithic aluminium.
If the GLARE components are not fatigue damaged, they are validated for at least the same service goal than the aluminium parts of the same structure. This conclusion from the present elementary specimen investigation requires further verification for riveted joints, a topic addressed in chapter 7.

Crack propagation, accelerated ageing influence

Applicable: JAR/FAR 25.0571 (Fatigue & damage tolerance)
Fatigue crack propagation in GLARE in the dry condition is dependent on the test frequency. Propagation rates increase at frequencies below 1 Hz. Coupon- and component tests are often performed at test frequencies higher than 1 Hz. Based on the investigations performed by Deutekom [36] it is recommended to consider a factor $C_{CP(S)} = 1.6$ for the crack propagation in a full scale PSE operated at the same stress levels but a lower frequency than applied in the fatigue tests.
For the influence of moisture in the prepreg on fatigue crack propagation in the aluminium layers of GLARE it is essential to know, whether the moisture is ahead of the crack (diffusion rates higher than crack propagation rates) or vice versa. For a strength balanced aircraft structure it is recommended that fatigue cracks should not occur earlier than after one DSG in the full scale specimen, which is equal to half the DSG for the aircraft if a factor 2 is applied on the full scale result. Expressed in time, 10 to 15 years exposure have to be considered before fatigue crack propagation should be allowed. Consequently, a fatigue crack would then propagate along a wet prepreg.
The weakened bond due to the presence of moisture in the prepreg increases the de-lamination size and hence the crack propagation rate. After 4296 hours accelerated exposure (open hole, 70ºC/85%RH), crack propagation rates increase by a factor 3 at a net stress level of 175 MPa. After 500 hours accelerated exposure (filled hole, 70ºC/85%RH, similar to the short range aircraft condition after 30 years service), no increase of crack propagation rates compared with the dry specimen has been observed. It is concluded from elementary tests:

$C_{CP(E)} > 1$ for specimens which are exposed more than 500 hours in 70°C/85%RH environment

If there is any technical issue, an extension of the present program is recommended. A technical relevance can be considered if either the weight gain curves obtained from the MRS specimens at the exposure site increase significantly, or if structural specimens which return from the exposure site show unexpected fast crack propagation rates.

$C_{CP(E)} = 1$ for the crack propagation calculation of aircraft structures

The fatigue de-lamination shape of both, non-aged and aged specimens, is triangular. This information is of interest for de-lamination- and crack propagation prediction models.

Crack propagation, temperature influence

Applicable: JAR/FAR 25.0571 (Fatigue & damage tolerance)
It was shown that the fatigue crack propagation in GLARE depends on the temperature and the applied stress level (section 6.7). The crack propagation rate increases significantly at high temperatures and

decreases significantly at low temperatures. The flight- and temperature missions for structural components of a particular aircraft type have to be analysed. A simplified calculation has been performed for an A330 PSE, but experiments on the temperature effect has been done for *constant* temperature tests. If there is no interaction between varying conditions it was calculated that the low crack propagation rates at low temperatures overcompensate the high crack propagation rates at high temperatures. Based on this analysis of the constant amplitude crack growth rates for different temperatures it was concluded that:

$C_{CP(E),\ T<RT} < 1 < C_{CP(E),\ T>RT}$

A more complex analysis on riveted joint loaded under a variable temperature is presented in chapter 7.1.6.

The blunt notch strength

In the blunt notch tests on specimens with a central hole it was shown that specimens of GLARE2 (fibers in load direction) were more sensitive to ageing than specimens of GLARE3. Secondly, GLARE4A(L) is more sensitive to ageing than GLARE4B(L). It is important to realize that diffusion in the fiber direction occurs faster that perpendicular to the fiber direction. In the wet condition, fiber splitting can then occur in the loading direction if the fibers are in the same direction. As a consequence, a more critical situation can arise at the edge of hole because the fibers were cut by drilling of the hole.

Environmental knock down factors for blunt notch are important for residual strength investigations because they provide the data point without fatigue damage for the residual strength versus fatigue damage curve. Based on the results of the blunt notch investigation, it is recommended to apply a blunt notch knock down factor of 0.96 for GLARE3 and GLARE4 and of 0.92 for GLARE2 to consider realistic ageing effects on short range aircraft.

A long term experiment which involves accelerated ageing has been started. A similar moisture weight gain shall be achieved around the holes of blunt notch specimens by exposing them in two different climates. The experiment has a duration of 3½ years exposure time and three levels of weight gains are incorporated. Results from the first level are available. It turned out that the knock down factor for specimens which have been exposed for 500 hours in a 70°C/85%RH environment and the knock down factor for specimens which have been exposed for 4270 hours in a 70°C/70%RH environment are similar. It can be concluded, that the moisture *distribution* is not the strength determining variable for blunt notch, since it is different in the comparison. Obviously a particular moisture concentration close to the hole edge is responsible for the obtained blunt notch strength level. For the present problem this moisture concentration is estimated with >0.35% prepreg weight up to 4mm distance from the hole. A further confirmation of the preliminary assumptions are possible in December 2005 when further specimens will leave the environmental chambers.

Crack opening displacement tests are evaluated in order to conclude, which phenomenon has which influence on the crack propagation rates. A distinction is made between the fatigue delamination size which develops around the fatigue crack and the shear deformation in the fiber prepreg at the delamination boundary. It is concluded:

- If the fatigue delamination size increases either due to high material temperature or due to ageing effects at the fiber/resin or resin/metal bond line, this has a considerable effect on the fatigue crack opening displacement and on the crack propagation rates.
- A reduction of the prepreg shear stiffness due to high material temperature has a considerable effect on the fatigue crack opening displacement and on the crack propagation rates as well.

- An influence on the shear stiffness and on crack opening displacement is observed due to ageing effects.

Correction factors C to be considered for stress intensities at the aluminium layers crack tip are calculated for different delamination size, in relation to the tested material and crack length. It is recommended to extend this analysis for different materials, crack length and stress levels.

Residual strength, temperature influence

Applicable: JAR/FAR 25.0571 (Fatigue & damage tolerance)

The influence of elevated temperature on elementary residual strength specimens is considered as negligible. Test results from coupons will be discussed in chapter 7.1.8.2.

Residual strength, ageing influence

Applicable: JAR/FAR 25.0571 (Fatigue & damage tolerance)

A distinction is made between a fatigue crack propagating ahead of the moisture penetration area in the prepreg and vice versa. If the crack length exceeds the moisture penetration depth, it is expected that either the average crack length in the aluminium layers or the maximum knock down factor found for an *un-fatigued* hole after accelerated exposure, determines the residual strength. The opposite scenario, a cracked hole in a wet prepreg location, is investigated.

The ratio between the crack lengths in the five inner layers and the two outer layers of GLARE2B-7/6-.4 is 0.86 after 120000 load cycles at a maximum net stress of 180 MPa. The crack length scatter through the thickness is low.

All obtained blunt notch values (*static strength*, without fatigue damage) were within the qualification limits [48, 49, 16] - the GLARE2B values are close to the mean strength values, the GLARE4A results are located close to the B-values. An environmental knock down factor of 15% as proposed in [9] can not be confirmed in all cases. The outdoor exposure residual strength specimens have been milled to a 3-hole width prior to residual strength testing, thus eliminating any edge effect. This and the interference fit used in the GLARE2 specimens is considered as the reason for the low knock down factors on blunt notch after 3000 hour accelerated ageing.

For the residual strength of *fatigue damaged* holes just moderate environmental knock down factors ($C_{RS(E)}$) are identified for of the GLARE material due to accelerated ageing. The environmental factors have to be multiplied on the determined residual strengths of fatigue cracked holes in the dry condition. The results represent a worst case situation, since the material has been severely aged *after* fatigue crack propagation, i.e moisture with a high concentration had access to the prepreg close to the fatigue crack. This situation is much more severe than what happens to an aircraft structure.

Test to structure factors to be considered on the residual strength of a full scale PSE in order to simulate the aging influence on a short range the aircraft strength, related to 3000 hours accelerated ageing (70ºC/85%RH):

GLARE2B butt strap:	$C_{RS(E)} = 0.96-0.0014xR_D$	(fastener installed with interference fit)
GLARE2B butt strap:	$C_{RS(E)} = 0.92-0.0014xR_D$	(fastener installed with clearance fit)
GLARE4A repair:	$C_{RS(E)} = 0.96-0.002xR_D$	(engineering solution)

Bearing strength

Applicable: JAR/FAR 25.0603 (Materials).

The bearing strength is a material property useful for quality assurance purposes. It provides limited information about the static strength of a GLARE aircraft structure.
The outdoor exposure bearing specimens are tested after accelerated ageing at room temperature and at 70°C (fatigue temperature for flight phase 'taxi out'). The specimens are tested according to the specification defined for this program, i.e. with gaps between the loading device and the specimen. The gap allows out of plane deformations of the GLARE around the pin, which is not the desired failure mode for quality assurance and which is not realistic for aircraft structures. The bearing results presented in chapter 6.11 have no direct practical use. For the specimens which will return from the outdoor exposure site it is strictly recommended to test the bearing strength according to the Airbus specification, i.e. the specimen has to be clamped by hand tightened torque applied on the bolt ! The results can then be related to rivet strength results.

Rivet strength

Applicable: JAR/FAR 25.0305 (Strength and deformation), JAR/FAR 25.0615 (Design properties)
JAR/FAR 25.0305 (a) prescribes: *"The structure must be able to support limit loads without detrimental permanent deformation*. *At any load up to limit loads, the deformation may not interfere with safe operation."* Local permanent deformations at hole edges do not interfere with a safe aircraft operation. In both monolithic aluminium and GLARE, local plastic deformations do not have a detrimental influence on the ultimate strength of a joint. Therefore, JAR/FAR 25.0305 should be considered as a *guideline* for rivet strength values, and not as a mandatory design limit.
The GLARE2B-7/6-.4 / DAN7 fastener combination was tested in the dry condition and after 3000 hours exposure at room temperature. The ultimate strength was determined by fastener head failure in all tests. Failure occurred approximately 30% above yield load, consequently the ultimate load is the design criterion of the those joints, and not the criterion 'no failure at 1.5 x yield load'. Both, yield and failure load, decreased by approximately 6% after 3000 hours accelerated ageing.
The GLARE4A-5/4-.4ssc / ASNA2026 combination failed in a rivet pull through mode at the countersunk side. In this case, the yield strength determines the static strength allowable stress level. The strength reduction after 3000 hours accelerated ageing was in the range of material property scatter.
According to the diffusion analysis in chapter 5.1, a rivet strength reduction due to outdoor exposure should not be expected. If this conclusion is confirmed in the year 2008 by tests on specimens from the outdoor exposure site, no knock down factor due to (realistic) ageing has to be considered for the residual strength properties of the joints.

Rivet pull through strength

Applicable: JAR/FAR 25.0615 (Design properties)
The rivet pull through failure is especially relevant to GLARE structures because it is a frequently occurring failure mode if high strength fasteners are used which leads to severe fastener tilting and GLARE deformation. It was observed for 3.5mm thick GLARE4A specimens manufactured with 5.6mm ASNA2026 countersunk fasteners. The rivet pull through strength decreases gradually for extended fatigue cracks. The reduced strength was approximated with a linear regression:

$$RPT\ [N] = 7551.4\ [N] - 29\ [N] \times R_D$$

A PRT strength reduction of 8% is observed for a fatigue damage rate of 20%.

The influence of ageing is considered as negligible. The first results after one year outdoor exposure in Queensland/Australia did not show any environmental degradation. The influence of elevated temperature (70°C) was investigated, although high axial loads on fuselage skin fasteners are unlikely to occur during the pre-flight ground cases and early flight stages. A linear function of the temperature related knock down factor ($C_{RPT(T)}$) was developed for the GLARE4A/ASNA2026 combination:

$C_{RPT(T)} = 0.9544 - 0.0019 x R_D$

The 4.8mm diameter NSA 5075 collars failed in the 4.3mm thick GLARE2B. No relevant RPT strength reduction was observed at 70°C material temperature and after one year accelerated ageing. The strength reduction due to the presence of fatigue cracks is negligible for practical application.

It is still recommended to investigate the rivet pull through behaviour of thin GLARE lap joints with different fastener types and R_D<20% (practically relevant order of magnitude) at room temperature without ageing.

Compression filled-hole strength

Applicable: JAR/FAR 25.0615 (Design properties)

The compression filled-hole strength at room temperature exceeds the compression yield strength for both tested GLARE/fastener combinations. This is valid for the as-received specimens and specimens after one year outdoor exposure.

The failure mode changes from `compression filled-hole´ to `inter rivet buckling´ at 80°C, a worst case scenario. For the GLARE2B material the compression yield strength could be reached even at 80°C for fatigue damage rates up to 90%. It is assumed that this condition will cover all possible ageing influences. The investigation of compression filled-hole strength of the thinner and thus less stiff GLARE4B specimens was not successful at 80°C, due to a shift of the failure mode.

The strength after 1 year outdoor exposure matches with the non-exposed values, i.e. no degradation due to one year outdoor exposure is observed.

For an aircraft component loaded in compression, the filled-hole failure mode is not a design case.

Some final comments

Two types of aging have been adopted for the present investigation: (1) Accelerated aging in an environmental chamber with a controlled humidity and temperature, and (2) An outdoors exposure in Australia under tropical conditions. The results available at the moment and evaluated in this thesis are not the end of the present investigations. The experiments on the elementary specimens described in the present chapter have contributed to the understanding of the behaviour of GLARE specimens and structural items. The results have given indications about aircraft structural conditions where the validation of the airworthiness requirements may meet with uncertainties requiring knock-down factors, and other conditions where this will not be necessary. The philosophy will be developed further in Chapter 7 on riveted joints. However, more information from the presently ongoing research investigations will become available in the future. It may lead to certain reassessments of the procedures how to evaluate the results of full-scale flight simulation tests on complete aircraft structures as well as how to deal with the airworthiness of a fleet of aircraft in service.

6.15 References

[1] Fatigue Crack Initiation and Early Crack Growth in Glare at Different Temperatures, O. Kieboom, Delft University of Technology, Thesis, 2000

[2] The development of crack initiation curves for GLARE bore holes and riveted joints, Th. Beumler, B. Borgonje, Delft University of Technology, Report B2V-01-34, 2001

[3] Ermittlung dynamischer Festigkeitskennlinien durch nichtlineare Regressionsanalyse, M. Gecks, F. Och, aus: Probleme der Festigkeitsforschung im Flugzeugbau und Bauingenieurwesen, Herausgegeben von M. Esslinger und B.Geier, 1977

[4] Estimation Tool for Basic Material Properties, M. Hagenbeek, Delft University of Technology, Report B2V-00-29, 2000

[5] Fatigue Manual, Aerospatiale Aeronautique, Report MTS 005, issue B, 1996

[6] Prediction Methods for Fatigue Crack Propagation in unstiffened GLARE – Through Cracks, R. Alderliesten, J. Homan, Delft University of Technology, Report B2V-99-40, 1999

[7] Application of fatigue life data for aluminium alloy 2024T3 to GLARE laminates, L. Schra, NLR, Report NLR-CR-2002-185, 2000

[8] Fatigue of Metallic Materials – Theory, D. Duprat, Aerospatiale Fatigue Trainings Course, 1998

[9] Interims Report GRP Working Group 1C, 'GLARE Durability', EADS Document 10L020K4200I02, Issue 1, 2001

[10] The influence of elevated temperature on Glare after exposure to moisture, B. Borgonje, Master Thesis, Delft University of Technology, 2000

[11] Qualification testing for the GLARE panel in the A310P/F, MSN484 aircraft, W.v.d.Hoeven & L.Schra, NLR report NLR-CR-2000-115

[12] GLARE Durability Programme - Results of tests carried out at the NLR, W.v.d.Hoeven & L.Schra, NLR report NLR-CR-2000-237

[13] Experimental project to assess the failure mechanisms during blunt notch of Glare, Dr. Y. Meziere, Delft University of Technology, Report B2V-00-47, 2000

[14] MBB Unternehmensgruppe Transport- und Verkehrsflugzeuge, "MBB Handbuch Werkstoff- und Verfahrenstechnik", Teil 75

[15] An Experimental and Analytical Investigation on the Fatigue Behavior of Fuselage Riveted Lap Joints, R. Müller, PhD Thesis, 1995

[16] The Metal Volume Fraction Approach, G. Roebroeks, SLI Report TD-R-00-003, 2000

[17] Flight –Simulation Fatigue Tests on Notched Specimens of Fiber Metal Laminates, J. Schijve, F. Wiltink, V. van Bodegom, Delft University of Technology, Report LRV-10, 1994

[18] Handbuch Strukturberechnung

[19] Finite Element Calculations for a Stringer Reinforced Butt-Joint, J. Seegers, Delft University of Technology, 1992

[20] Blunt notch and sharp notch behaviour of Glare laminates, T. de Vries, PhD Thesis, Delft University of Technology, 2001

[21] Development of an empirical fatigue crack growth prediction model for Fibre Metal Laminate GLARE, R. Alderliesten, Thesis, Delft University of Technology, 1999

[22] Fatigue crack growth of part through the thickness cracks in GLARE3 and GLARE4B coupons, A. de Koning, L. Schra, NLR, Report NLR-CR-2000.078, 2000

[23] Prediction methods for fatigue crack propagation in unstiffened GLARE – through cracks, J. Homan, R. Alderliesten, Delft University of Technology, Report B2V-99-40, 2000

[24] Richtlinien für die rechnerische Ermittlung der Lebensdauer von Bauteilen des A300, W. Goße, Deutsche Airbus GmbH, 1969

[25] FOD at a row of rivet holes and lap joints including WFD, T. de Vries, P. Hooijmeijer, report B2V-00-23, Delft University of Technology, 2000

[26] Airbus Industrie Fatigue and Damage Tolerance Guidelines, Section D, Methods of Analysis

[27] Current and Future Regulations, Design Goals and Industry Standards, DaimlerChrysler Aerospace Airbus Technology Seminar, H.-J. Schmidt, 1999

[28] Fatigue Training Course, Aerospatiale Document, D. Duprat

[29] Damage and Fatigue Crack Growth of Aircraft Materials and Structures, Delft University of Technology, 1999

[30] New Methodology to meet Initial Flaw Criteria and Widespread Fatigue Damage Criteria, DaimlerChrysler Aerospace Airbus Technology Seminar, H. Trey, 1999

[31] Fatigue test results of A320 and A321 circumferential butt joint panel specimens, Th. Beumler, Deutsche Airbus GmbH, Report 10D/E022K4753C04, 1991

[32] Fatigue test results of A330 and A340 circumferential butt joint panel specimens, Th. Beumler, Deutsche Airbus GmbH, Report 10F/G022K4753C04, 1991

[33] da/dN curves for 2024T3clad and 2024T351clad, supplier Alcoa and Pechiney, L&LT, t=1.6mm, 1989-1994, 30 test samples, sources: DCAA, AS, DLR, FH-HH, e-mail H. Stehmeier, Airbus Deutschland GmbH

[34] Engineering Information from G. Roebroeks, FMLC, 2001

[35] Estimation Tool for Basic Material Properties, M. Hagenbeek, Delft University of Technology, Report B2V-00-29, 2000

[36] The effect of frequency, moisture and temperature on the constant amplitude fatigue behavior of GLARE3, M. Deutekom, Delft University of Technology, Thesis Report, 1994

[37] The moisture absorption of Glare – an introduction, O. Tensen, Delft University of Technology, Thesis Report, 1990

[38] Cold/Hot soak behavior of GLARE, W.v.d.Hoeven, NLR report NLR-CR-2000-273, 2000

[39] Verifikation und Ergänzung von Berechnungsmethoden für die statische und dynamische Auslegung von GLARE-Strukturen, H. Bär, Universität Stuttgart, Diplomarbeit, 1992

[40] The effect of moisture ingress on the bonded repair effectiveness, R. Brenninkmeijer, Delft University of Technology, Thesis Report, 2000

[41] ARALL, Adhesion Problems and Environmental Effects, Vol. B, Environmental Effects, M. Verbruggen, Delft University of Technology, PhD Report, 1986

[42] Stress spectra for A330 SR, frame 58, longitudinal stresses
E-mail from N. Ohrloff, DaimlerChrysler Aerospace Airbus

[43] Crack Propagation Justifications for Aircraft Fuselage Riveted Joints under Consideration of Operational Temperatures, Th. Beumler, Delft University of Technology, Report B2V-01-07, 2000

[44] The influence of temperature on the fatigue crack propagation behaviour of GLARE, R. Alderliesten, FMLC Report TD-R-02-16, 2002

[45] General environmental conditions for strength justifications of composite structures, Airbus Industrie Document ABD0087

[46] Crack measurement methods for fatigue investigations on Glare outdoor exposure specimens, B. Borgonje, Delft University of Technology, Report B2V-02-14, 2002

[47] Presentation on ILSS strength, G. Roebroeks, SLI, GLARE workshop, Delft 4.8.2000

[48] Bridging stress distribution in center-cracked fiber reinforced metal laminates: modeling and experiment, Y. Guo and X. Wu, Beijing Institute of Aeronautical Materials, in Engineering Fracture Mechanics 63, pages 147-163, 1999

[49] Strength of riveted joints, J. Homan, Delft University of Technology, Report B2V-98-39, 1998

[50] Determination of bearing strength, GRP project 1.5.1.1, P. Broest, P. Nijhuis, Delft University of Technology, Report B2V-00-39, September 2000.

[51] Qualification testing of semi-finished flat Glare products, W. van der Hoeven, P. Nijhuis, NLR National Aerospace Laboratory, Report NLR-CR-2002-146, 2002.

[52] GLARE outdoor exposure program: Blunt notch strength, B. Borgonje, Delft University of Technology, Report B2V-02-40, 2003

[53] The significance of flight-simulation fatigue tests, J. Schijve, Delft University of Technology, Report LR466, 1985

[54] Fatigue of Metals, P. Forrest, Pergamon Press, Oxford, 1962

[55] Fatigue predictions and scatter, J. Schijve, Delft University of Technology, Report LR696, 1992

[56] Fatigue crack growth in ARALL – A hybrid aluminium-aramid composite material, R. Marissen, Delft University of Technology, Report LR-574, 1988

[57] Towards GLARE, G. Roebroeks, Delft University of Technology, PhD thesis, 1992

Chapter 7
Riveted Joint Investigations

Contents Page

This page intentionally left blank.

7. Riveted Joint Investigations

The step from the investigations on elementary specimens discussed in the previous Chapter 6 to investigations on coupon specimens in the present chapter is important because these specimens contain design details of the real structure. The meaning of elementary properties is extended to the coupon specimen, e.g. bearing load and by-pass load. Hence the coupon delivers design values (FAR 25.0613) instead of material properties (FAR 25.0603).
A problem of coupon testing is the more complicated inspection for fatigue damage. This is especially true for single shear riveted specimens if fatigue crack initiation or propagation of invisible cracks must be recorded.

The present chapter is dealing with riveted coupon specimens which simulate (1) the experimental A340-600 butt strap (test series 2-B, see section 3), and (2) the riveted repair at the Airbus Megaliner Barrel (test series 2-A). Crack initiation, crack propagation and the residual strength behaviour, with and without ageing effects, are investigated. Calculation methods for these properties are defined and verified. Available methods for monolithic aluminium structures are considered. A survey of the investigations is given in the table below.

Subject	Aspects investigated	Section
Fatigue	Scatter of crack initiation and propagation	7.1.1
	Crack initiation SN curves	7.1.2 and 7.1.3
	Fatigue crack propagation	7.1.4
	Miner rule predictions, crack initiation and propagation	7.1.5
	Temperature effect	7.1.6
Static strength	Yield strength of joint	7.1.7
	Residual strength of joint with fatigue damage	7.1.8

Predictions on the strength of the joints in the structure in relation to justifying airworthiness requirements are discussed in section 7.2.
A survey of the conclusions of the present chapter is presented in section 7.

7.1 Riveted Joint Strength Justifications

7.1.1 Riveted joint crack initiation and crack propagation scatter

A low scatter of both, crack initiation and crack propagation, has been verified with elementary specimens in section 6.4. The present section describes an investigation on scatter observed in fatigue tests on the circumferential joint specimen described in section 3.2.3.1, i.e. a riveted single-strap butt joint with the GLARE7B-6/5-.4 butt strap as the fatigue critical element of the joint. Due to secondary bending fatigue cracks are initiated in the mating aluminium layer of the butt strap in rivet rows 3 and 4 (figure 3.2.3.2). These cracks are invisible from the specimen surface sides. An online crack propagation monitoring technique was adopted by employing crack wire foils which were bonded by Airbus Deutschland between each pair of holes in rivet rows 3 and 4. It implies that crack initiation and crack growth of a maximum of 16 fatigue cracks in one specimen can thus be recorded. Each foil contains either 20 or 10 parallel wires with a spacing of 0.25mm, see figure 7.1.1.1. Three foils can be bonded between two adjacent holes, see figure 7.1.1.2. During fatigue crack growth the crack wires produce an electrical signal when failing due to crack opening. These signals and the corresponding cycles are recorded during the test. As a result a curve with the crack length versus the number of cycles is obtained, an example of the recorded crack propagation curved is presented in appendix V.

In order to prevent damage of the crack wire foils due to clamping of the sheets, parts of the mating aluminium layer of the 'skin' is milled away, see figure 7.1.1.3. The skin sheets and the butt strap sheets

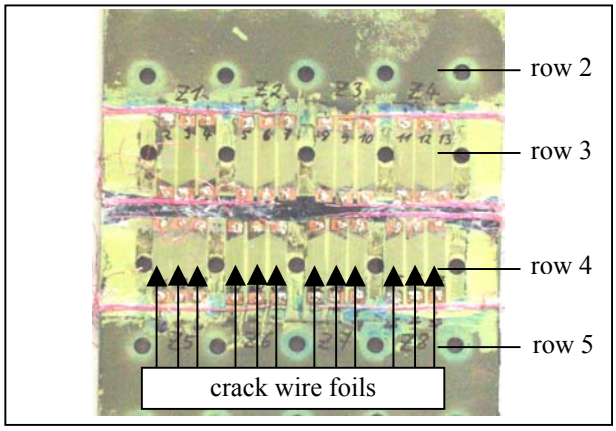

Figure 7.1.1.1. Crack wires bonded on butt strap

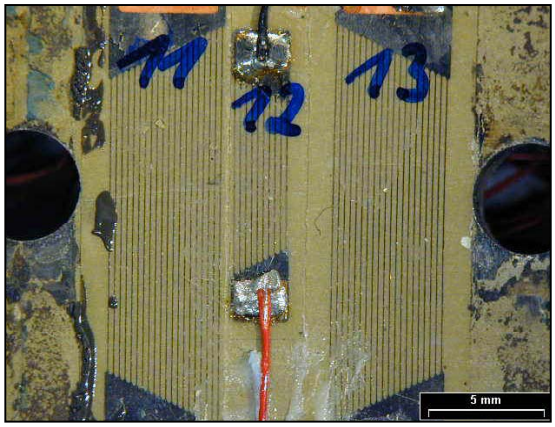

Figure 7.1.1.2. Specimen 2-B-80, crack wire foils no. 11, 12 & 13 between drilled holes

are jointed with DAN7-6-6 fasteners, dry installed, but sealant is applied close to rivet rows 1,2,5 and 6.

Four constant-amplitude tests (R = 0.1) were carried out on specimens 2-B-28, 2-B-79, 2-B-80 and 2-B-81 respectively. The maximum applied fatigue load is listed in the table below. An example of tests results is given in appendix V. A practically linear crack growth with an approximately constant crack growth rate was generally observed, which appears to be characteristic for GLARE. The crack propagation curves for all crack foils are contained in reference [19].

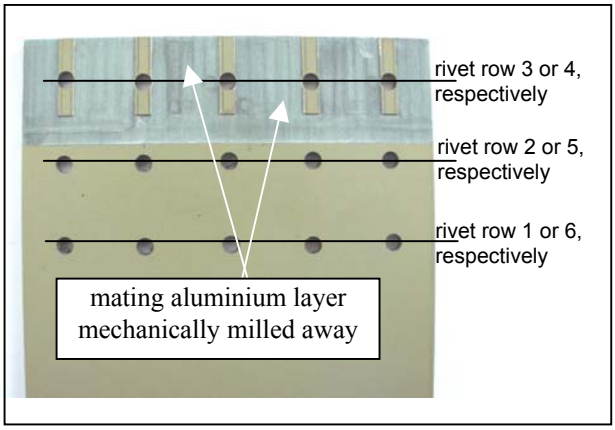

Figure 7.1.1.3. Skin sheet milled in rivet rows 3 and 4 adjacent to location where crack wires are bonded on the strap, specimen 2-B-28

specimen no.	2-B-28	2-B-79	2-B-80	2-B-81
max. load [kN]	32.5	38.9	38.9	28.1

The scatter analysis is performed in a similar way as for the open hole specimens. For each fatigue crack, the initiation life (N_i), i.e. the life for a crack length a=1mm, and the average crack growth rate (da/dN) is determined. The average crack growth rate is calculated from two data points, (a_1,N_1) and (a_2,N_2) which are the first and the last pair of data of a specific crack. The average crack growth rate then becomes ($N_2 - N_1$) / ($a_2 - a_1$). This slope of the crack growth curve is then used to interpolate (or extrapolate) the fatigue life for a crack with a length of 1 mm with the linear equation:

$$N_{a=1mm} = N_1 - (a_1 - 1) \times \frac{N_2 - N_1}{a_2 - a_1} \quad (1)$$

The results for each specimen and rivet row are contained in tables 7.1.1.1 to 7.1.1.4 and in the following figures. Both, the mean crack initiation lives related to 1mm crack length (N_{mean}) and the logarithmic standard deviations (s) are calculated.

$$N_{i,mean} = \Sigma N_i / m \quad (2)$$

$$s^2 = (m * \Sigma(\log N^2) - (\Sigma(\log N))^2) / m^2 \quad (3)$$

The two rivet rows of the same specimen are evaluated separately and together, see the results in table 7.1.1.5. With one exception, i.e. the standard deviation for rivet rows 3 and 4 of specimen 2-B-81, all standard deviations are below 0.2. The standard deviation 0.21 for specimen 2-B-81 is caused by the late crack initiation recorded by foil 25, i.e. 212000 cycles, see figure 7.1.1.6a. Ignoring this crack, the standard deviation for rivet row 4 would decrease to 0.18 to 0.12, and for rivet rows 3 and 4 from 0.21 to 0.17. A similar trend is observed for foil 5 of specimen 2-B-79.

Specimen 2-B-79 was the first one tested. Because the sealant did not harden, it was decided to investigate specimen 2-B-80 at the same load level (with hardened sealant). A comparison of the crack initiation results, i.e. 12000 cycles for specimen 2-B-79 and 10250 cycles for specimen 2-B-80 (50% probability of crack initiation), indicates a small trend of earlier crack initiation without hardened anti fretting compound. The influence of the load carrying or non load carrying sealant, however, is limited for the crack wire specimens to the area around rivet rows 1 and 2 and 5 and 6, respectively, because no sealant is applied along rivet rows 3 4 after crack wire attachment. The item will be further discussed in chapter 7.1.2.9

The crack initiation distribution follows the Gaussian law if the results yield a straight line in a diagram, which contains the crack initiation life in a logarithmic scale on the x-axis and the probability of occurrence in a Gaussian scale on the y-axis. The probability of crack initiation can be calculated for the particular occurrence according to Goβe [8]:

$$P_{ci} = 100\text{-}100 * (3n\text{-}1) / (3m+1) \quad (4)$$

With n as the rank number of the N_i-values in an increasing order and m as the total number of results. The results are plotted in figures 7.1.1.4c to 7.1.1.7c. All crack initiation data follow a Gauß distribution. If compared with crack initiation data from monolithic aluminium riveted joints [20,21,22], the scatter in

GLARE is lower or equal. The *absolute* crack initiation data may be influenced by the milled 'skin' sheets. They are compared with data obtained from non-milled sheets in paragraph 7.1.2.

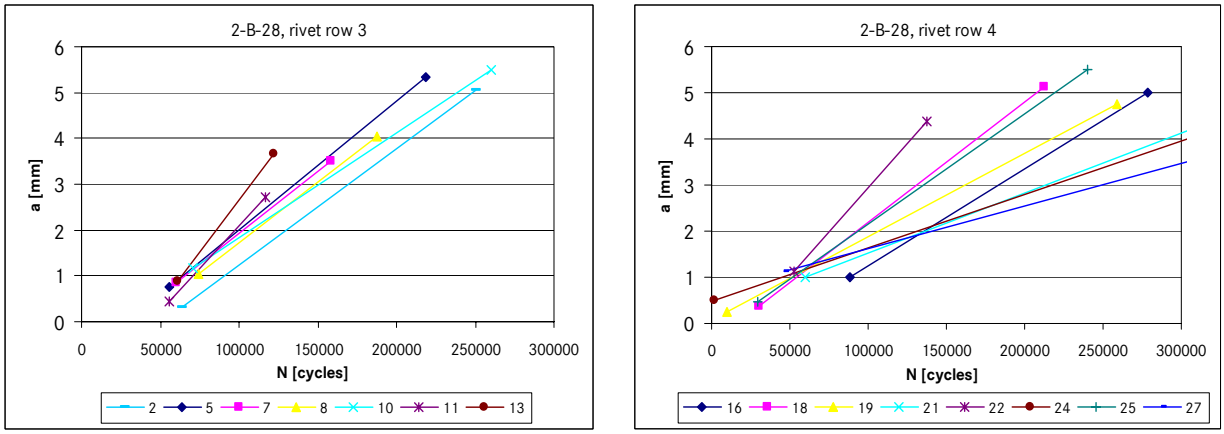

Figure 7.1.1.4a. Crack propagation curves for foils bonded on specimen 2-B-28, Fmax. = 32.5 kN

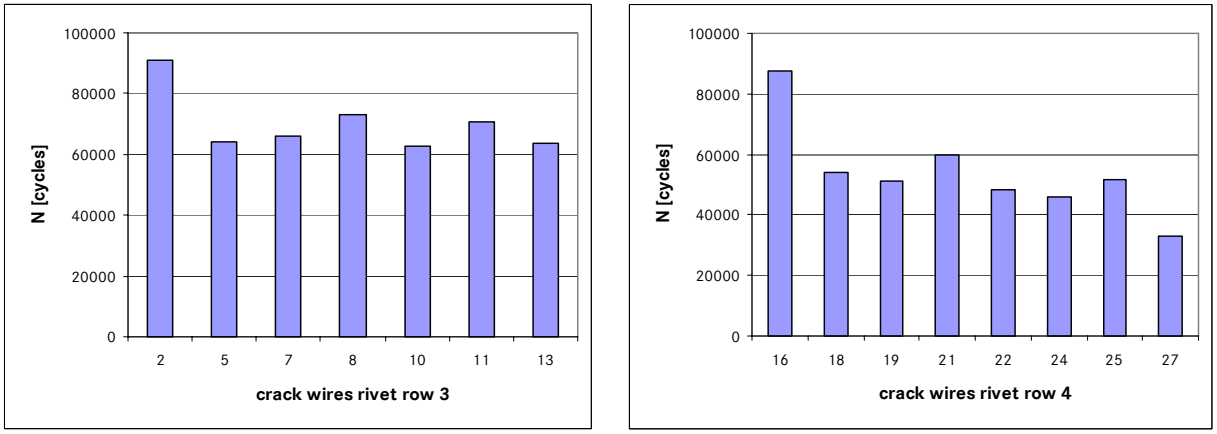

Figure 7.1.1.4b. Specimen 2-B-28, crack initiation life related to a = 1mm

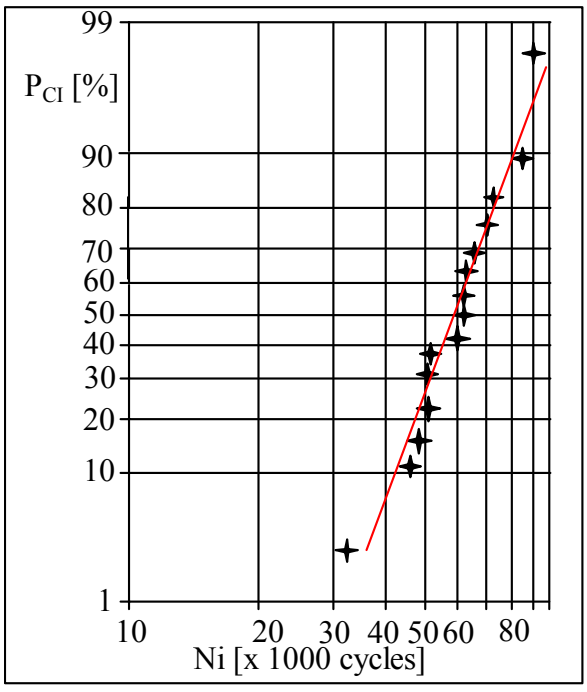

n	Pci [%]	Ni [cycles]
15	4,3	33246
14	10,9	46022
13	17,4	48563
12	23,9	51255
11	30,4	51510
10	37,0	53909
9	43,5	60000
8	50,0	62832
7	56,5	63677
6	63,0	63982
5	69,6	66168
4	76,1	70613
3	82,6	73100
2	89,1	87599
1	95,7	91203

Figure 7.1.1.4c. Specimen 2-B-28, crack initiation distribution, a=1mm

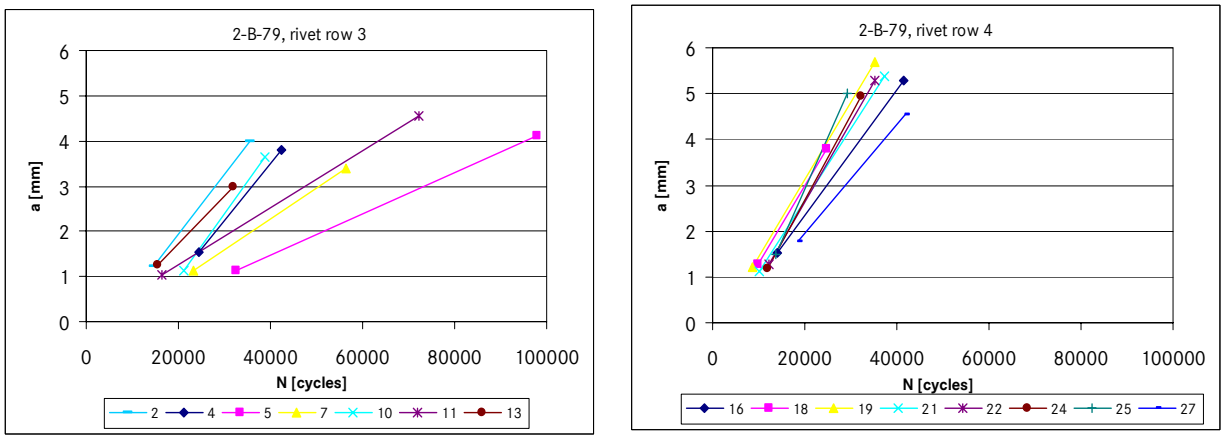

Figure 7.1.1.5a. Crack propagation curves for foils bonded on specimen 2-B-79, Fmax. = 38.9 kN

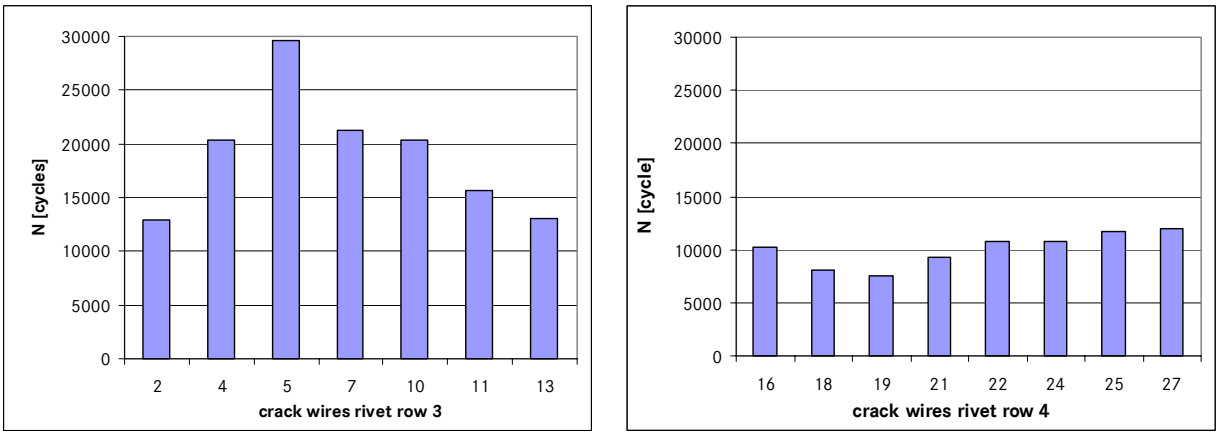

Figure 7.1.1.5b. Specimen 2-B-79, crack initiation life related to a = 1mm

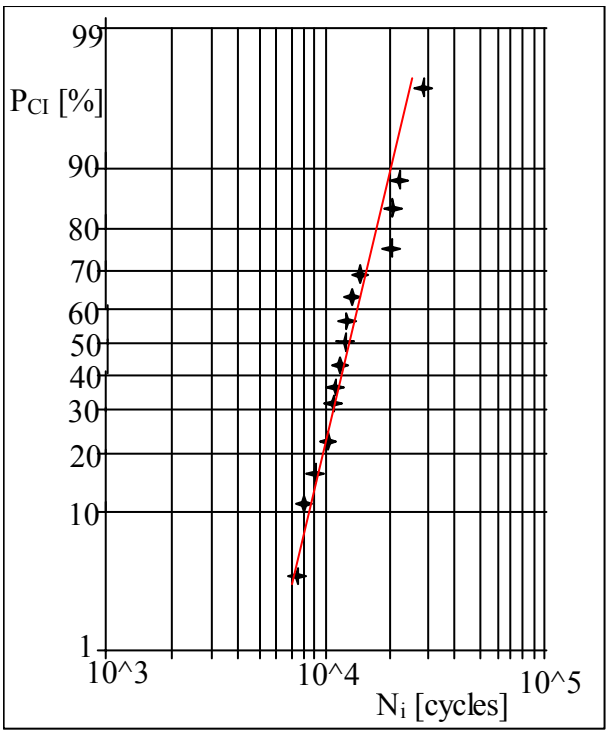

n	Pci [%]	Ni [cycles]
15	4,3	7564
14	10,9	8091
13	17,4	9308
12	23,9	10269
11	30,4	10795
10	37,0	10797
9	43,5	11673
8	50,0	12005
7	56,5	12960
6	63,0	13030
5	69,6	15664
4	76,1	20325
3	82,6	20360
2	89,1	21242
1	95,7	29622

Figure 7.1.1.5c. Specimen 2-B-79, crack initiation distribution, a=1mm

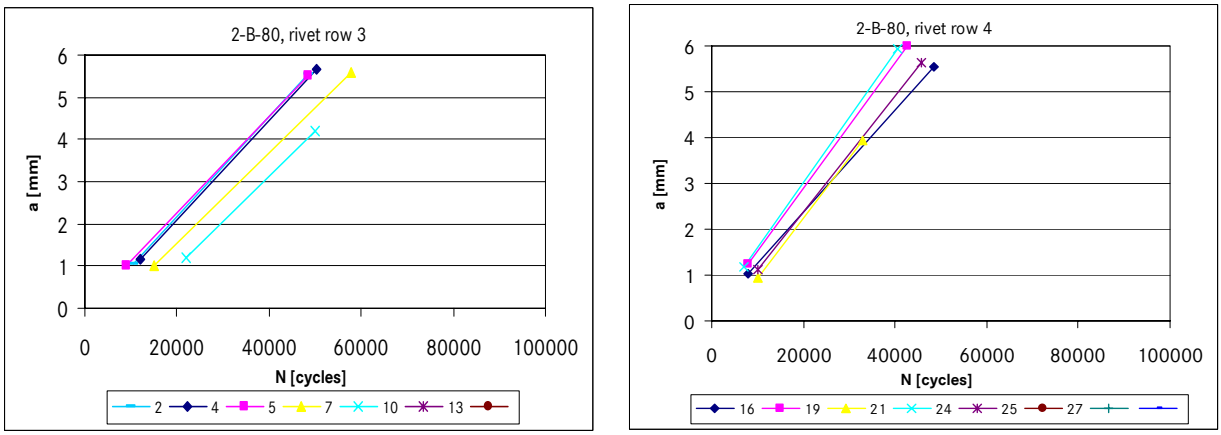

Figure 7.1.1.6a. Crack propagation curves for foils bonded on specimen 2-B-80, Fmax. = 38.9 kN

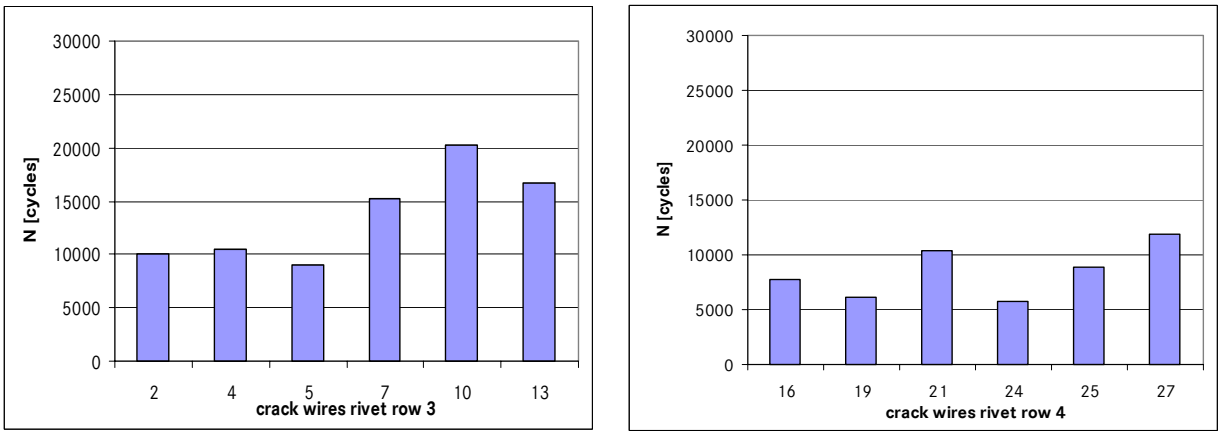

Figure 7.1.1.6b. Specimen 2-B-80, crack initiation life related to a = 1mm

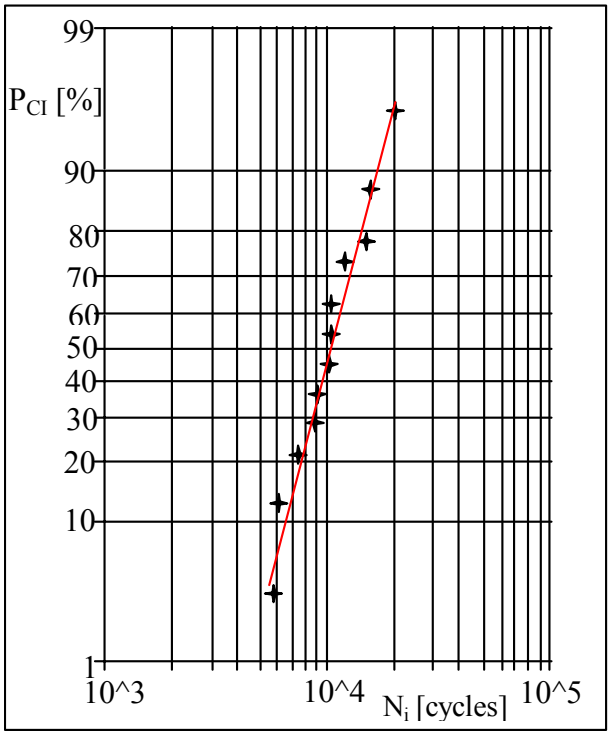

n	Pci [%]	Ni [cycles]
12	5,4	5742
11	13,5	6187
10	21,6	7691
9	29,7	8898
8	37,8	9002
7	45,9	10113
6	54,1	10388
5	62,2	10541
4	70,3	11893
3	78,4	15190
2	86,5	16690
1	94,6	20174

Figure 7.1.1.6c. Specimen 2-B-80, crack initiation distribution, a=1mm

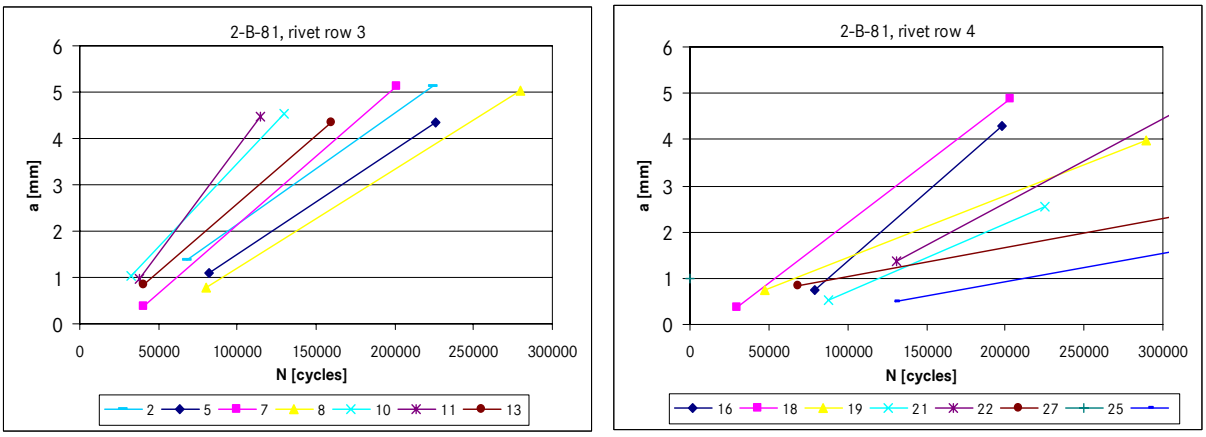

Figure 7.1.1.7a. Crack propagation curves for foils bonded on specimen 2-B-81, Fmax. = 28.1 kN

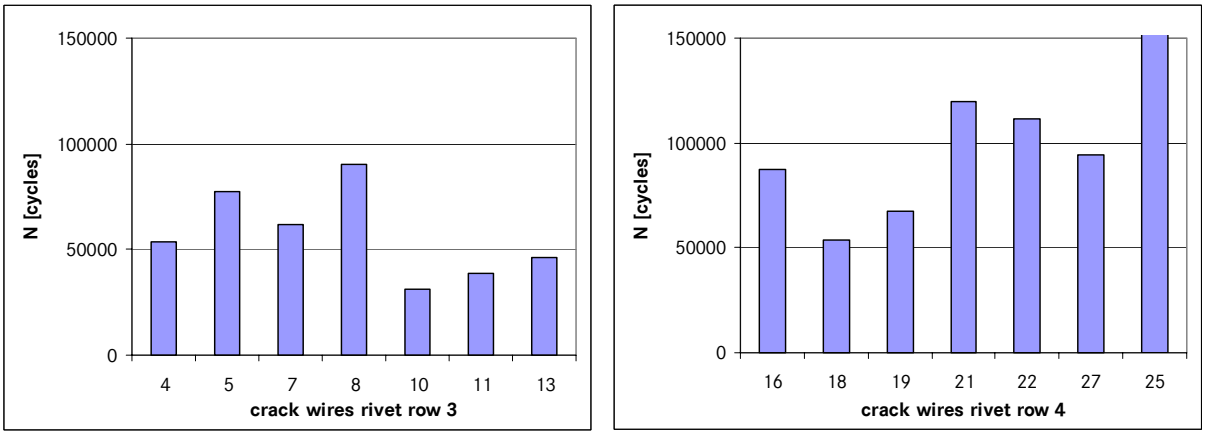

Figure 7.1.1.7b. Specimen 2-B-81, crack initiation life related to a = 1mm

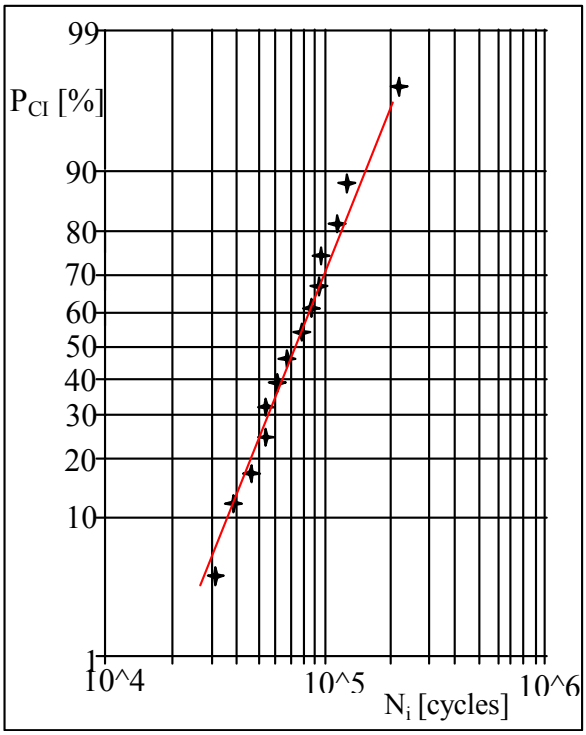

n	Pci [%]	Ni [cycles]
14	4,7	31559
13	11,6	38687
12	18,6	46431
11	25,6	53426
10	32,6	53948
9	39,5	61603
8	46,5	67123
7	53,5	77708
6	60,5	87259
5	67,4	90459
4	74,4	94019
3	81,4	111171
2	88,4	119451
1	95,3	212765

Figure 7.1.1.7c. Specimen 2-B-81, crack initiation distribution, a=1mm

Tables 7.1.1.1 to 7.1.1.4 include the crack propagation rates da/dN for the particular cracks and the logarithmic standard deviations per specimen and rivet row. All standard deviations are between 0.03 and 0.19, with the exception of rivet row 4 of specimen 2-B-81. Here, two cracks (foils 25 and 27) propagated extremely slow, which increased the standard deviation to 0.25. Without taking foils 25 and 27 into account, the standard deviation would drop to 0.14.

During the application of the crack wire foils by the Airbus test engineers, they observed that the rivet holes of the critical rows 3 and 4 were not drilled at exactly the same distance to the edge of the skin (the edge distance is indicated in the photo in figure 7.1.1.8) A possible effect on the crack growth rates is explored in figures 7.1.1.8 to 7.1.1.11.

Coincidently the edge distance scatter is *relatively* low for the lower loaded specimens (2-B-28 and 2-B-81), a deviation of <± 0.75mm was measured. For these specimens, no clear relation between the edge distances and the crack propagation rates can be found.

The edge distance tolerances are significantly larger for the other two specimens, see figures 7.1.1.13 and 7.1.1.14. For both, deviation of ± 1.38mm have been measured. A clear trend is observed showing higher crack propagation rates at holes with short edge distances and lower crack propagation rates at holes with large edge distances. These results match with the expectations, because the bending moment of the butt strap increases towards its center line. Hence, the holes closer to the butt strap (and –specimen) center line should fatigue first and should experience faster crack propagation.

Due to the mismatch of hole edge distances, a geometry related scatter is superposed on the material scatter. If separated from one another, the standard deviations would be lower than the values given in table 7.1.1.5. In conclusion it is expected that the crack propagation scatter (*material related*) for the investigated riveted GLARE joint is lower/equal than for monolithic joints.

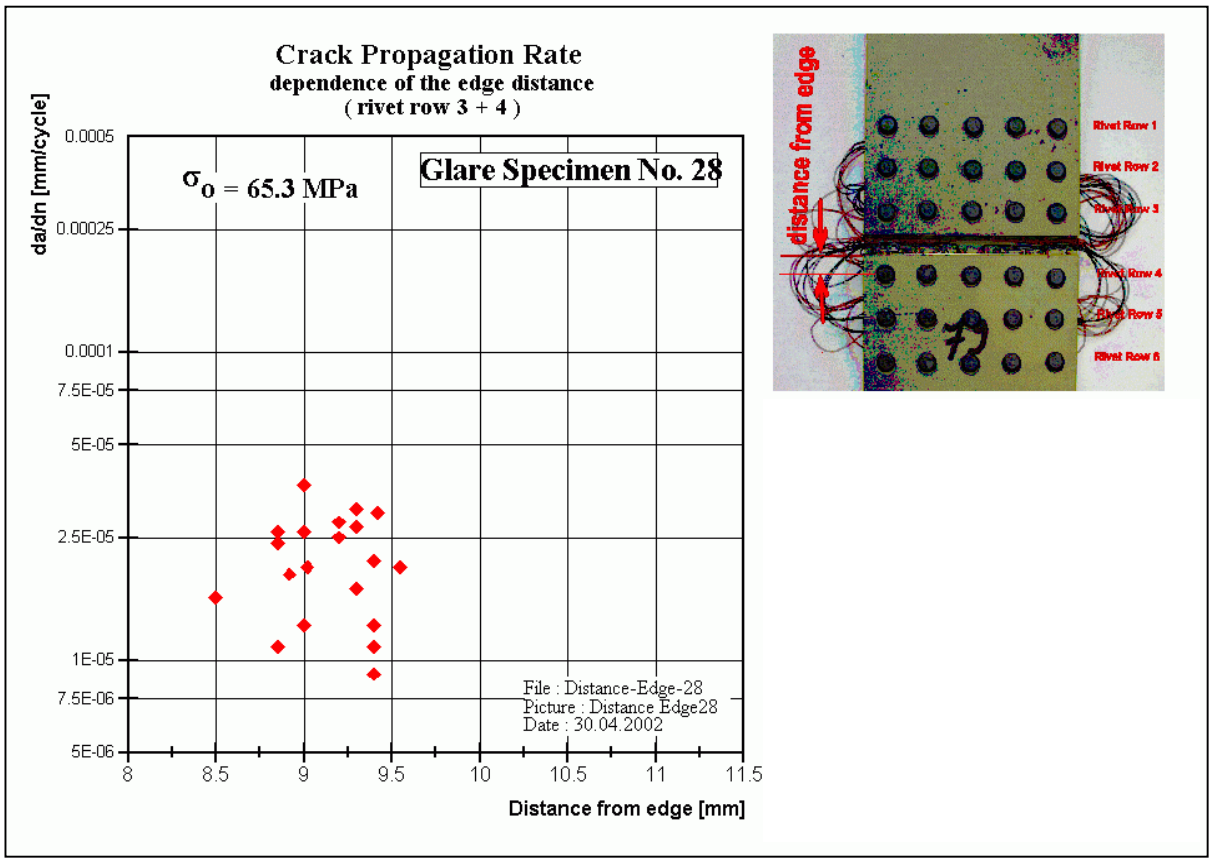

Figure 7.1.1.8. Specimen 2-B-28, crack propagation rates related to the edge distance

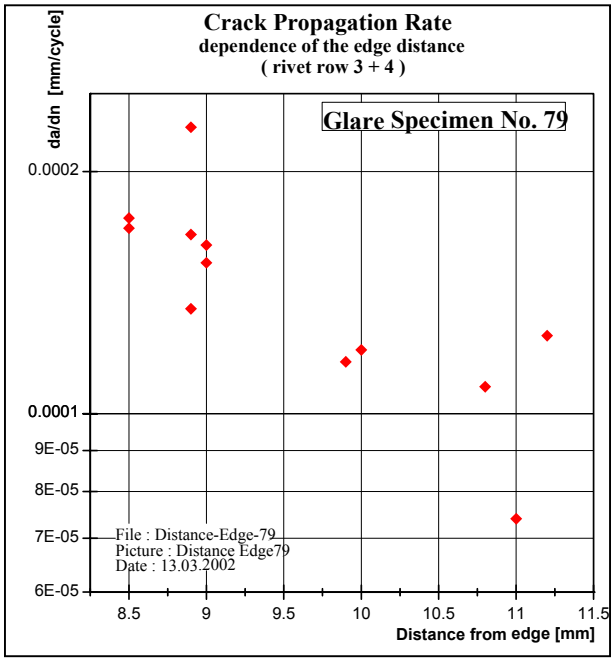

Figure 7.1.1.9. Specimen 2-B-79, crack propagation rates related to the edge distance

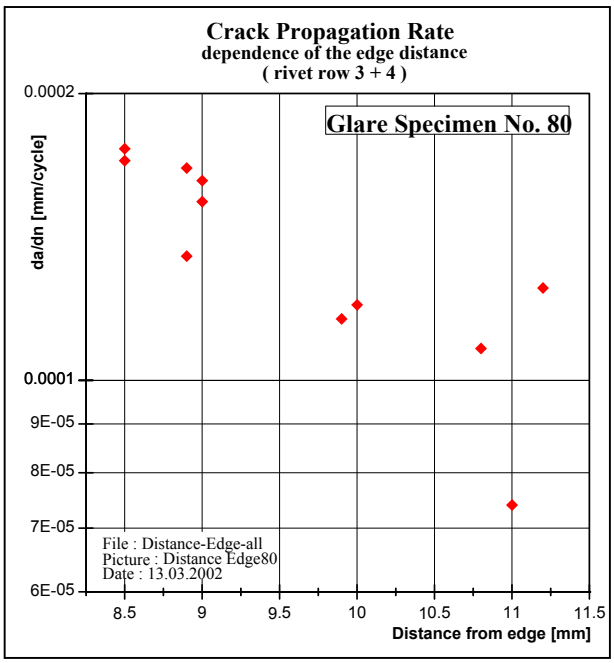

Figure 7.1.1.10. Specimen 2-B-80, crack propagation rates related to the edge distance

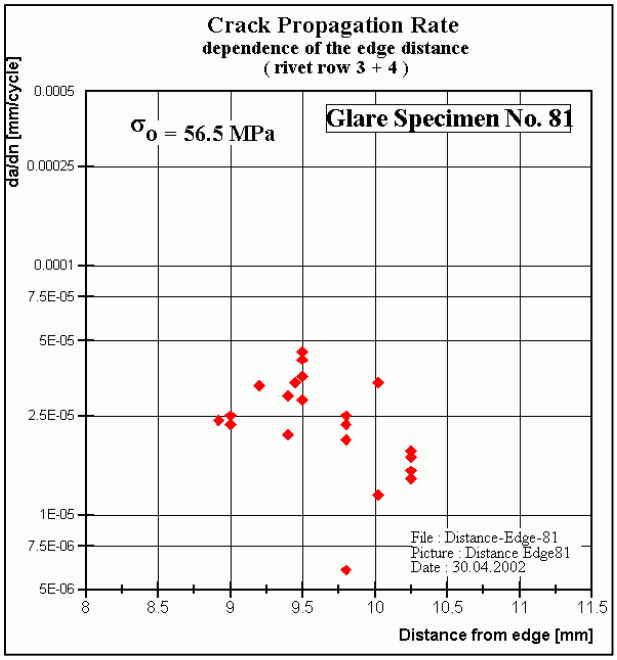

Figure 7.1.1.11. Specimen 2-B-81, crack propagation rates related to the edge distance

7.1.2. The development of crack initiation curves, circumferential joint, coupon specimens

The development of crack initiation curves for single shear riveted GLARE joints is much more complicated then for open hole specimens, due to the poor inspectibility. Fatigue testing of riveted GLARE specimens until they fail provides useless data, because a major portion of the life to failure belongs to the crack propagation phase, rather than to the crack initiation life. A SN-curve for a riveted joint needs to be developed by cycling different specimens at different load levels until the average crack length of all possible fatigue sensitive locations on the mating surface is ≤1mm, with regard to the equivalent crack length. Due to the additional bending, the average crack length is representing just the highest loaded aluminium layer, the one on the mating surface. All other layers will initiate later and will show smaller cracks.

Average crack length: $$a_{av} = \frac{\sum_{i=1}^{j} a}{j}$$ j = number of fatigue sensitive locations (5)

The average crack length is a logic measure, because the residual strength of the joint is dependent on it [1] and because the residual strength of a fatigued joint is a design criterion (ref. chapter 1).

Airbus and Delft University have developed a philosophy to use monolithic aluminium joint SN-data for the prediction of crack initiation in GLARE in order to have the benefit of a considerable amount of data already available and in order to avoid a similar extensive development of SN-data for GLARE specimens [2, 3]. It is essential to consider the temperature- and stiffness-related stresses in the aluminium layers of GLARE, as discussed for the open hole specimens in chapter 6.2. However, it has to be proven, that the method also applies to riveted joints. It implies that crack initiation curves for riveted joints have to be generated for similar specimens of both GLARE and monolithic aluminium.

7.1.2.1. The equal slope concept

An important detail for the correct prediction of crack initiation under variable amplitude conditions is the extrapolation from available constant amplitude test data, generated at a *particular* stress ratio, to crack initiation data of *different* stress ratios. The SN curves for different stress ratios in a log σ_{max} versus log N diagram are parallel lines in the finite life regime as illustrated by figure 7.1.2.1. The slope factor is approximately 4.5 for aluminium structures [4]. The problem considered in this section is whether a similar description applies to GLARE specimens.

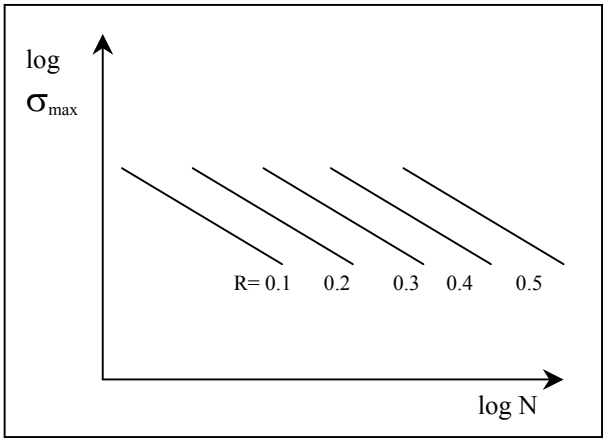

Figure 7.1.2.1. Aluminium SN data dependent on the stress ratio [4]

Crack initiation data for GLARE structures are preferably linked to applied stresses in order to give the reader a quick overview about the fatigue strength in a similar format as used for monolithic aluminium. Due to the stiffness and the temperature influences different stress ratios are obtained for the particular aluminium layers in GLARE compared with the stress ratio applied on the laminate. An example is

calculated for the open hole GLARE3 specimens discussed in chapter 6.2. The stress ratio for the applied cyclic stress was R = 0.05.

The calculated slope for the *applied stress* SN-curve of the GLARE3 specimens is 4.1 which corresponds to the blue line in figure 7.1.2.2. For reasons mentioned before, the stress levels are higher in the aluminium sheets compared to the applied stress. As a result, the ratios for the aluminium layers range from 0.23 to 0.29 at room temperature (R_{alu}) and for the aluminium layers the slope becomes 5.1 (red curve in figure 7.1.2.2). These results can again be corrected for the stress ratio value of R=0.05 which then reveals a slope factor of 4.6 (green line in figure 7.1.1.2). The correction for the R-value is made according to the method presesented in [14].

The equal slope concept is a simple method to relate the influence of different stress ratios to the fatigue life or the allowable stress level of monolithic aluminium structures. A series of similar fatigue specimens manufactured from monolithic aluminium, which are tested at different stress levels but at the same stress ratio, will form one of the lines shown in figure 7.1.2.1. It provides the slope for all curves at different stress ratios than the tested one.

The same procedure performed with GLARE would give an SN-curve related to the *applied* stresses, but not related to the stress levels which are present in the aluminium layers of the GLARE material. For the aluminium layers, data points at *different* stress ratios would be obtained which then require a correction for either the R-value or the stress in order to obtain parallel lines. The problem can be mathematically solved for elementary specimens, but it adds to the complexity of developing a data basis for GLARE. The problem becomes even more complex for single shear riveted joints with different stress levels in the aluminium layers due to secondary bending.

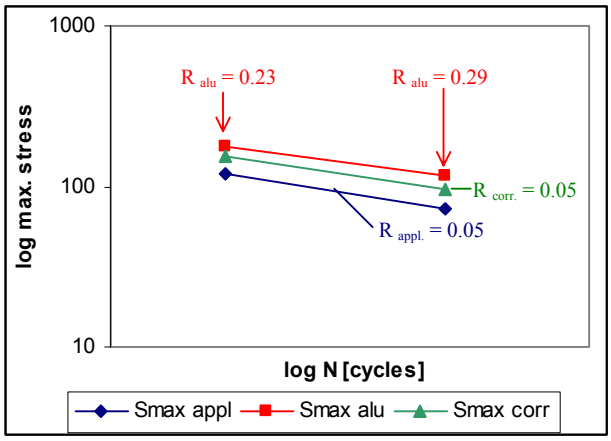

Figure 7.1.2.2. SN-data and the associated R-values for GLARE3 according to the open hole tests, see chapter 6.2

The example shown in figure 7.1.2.2. gives an impression about the differences between both the *applied* stress ratio on a GLARE laminate and the resulting stress ratios in the particular aluminum layers of the same laminate. The differences should be accounted for in any computerized calculation of GLARE structures.

If SN curves of similar specimen, but made from different materials (i.e. monolithic aluminium and GLARE made of the same aluminium alloy) are compared (the aluminium reference joint concept), different slopes have to be expected if the applied stresses on the specimens are the same. However, the differences between the *slopes* of the SN-curves are moderate for the calculated example in figure 7.1.2.2, i.e. 4.1 related to the applied stresses and 5.1 related to the stresses in the particular aluminium layers of the laminate. For a quick hand calculation of a crack initiation curve for a particular GLARE structure during the pre-design phase of an aircraft it is acceptable to adopt the slope of the SN-data of a comparable aluminium structure for the GLARE structure as well. The benefit of this conclusion will be demonstrated in section 7.1.2.3 where an SN curve for a riveted GLARE joint will be constructed.

7.1.2.2. Inspection methods for riveted joints

The detection of cracks in the mating surface layers of single shear riveted joints with a length ≤1.0 mm is a challenging target for NDT experts. Specimens should preferably not be disassembled for inspection. However, the available methods are limited. The following research is performed with the circumferential joint specimens introduced in chapter 3.2.3.1, in which cracks initiate from the hole edges. This crack location is observed if the fastener diameter is small in comparison to the clamping length, and consequently the clamping force is relatively low. In other cases, if the clamping force is large, cracks may initiate outside the holes [5] which requires other inspection methods. The following techniques have been investigated for an accurate crack lengths measurement:

- Eddy current from outer surfaces
- X-ray
- X-ray of loaded specimens
- Microscope after dismantling specimens
- Microscope after dismantling specimens and bending the particular part in order to open the cracks
- Microscope after dismantling specimens, application of dye penetrant and bending the particular part in order to open the cracks
- Eddy current inspection of the mating surfaces, after disassembly of the specimens, using a Nortec pencil probe, model no. 916056, diameter: 3.2 mm, range: 50 kHz to 1 MHz

Different crack lengths were obtained with these techniques. Unfortunately it was impossible to establish a systematic correlation between the crack lengths obtained from the different inspection methods. The most reliable detection method is the eddy current inspection using a pencil probe. It is necessary to disassemble a specimen for the inspection. The eddy current results were calibrated with crack length measurements made with a video camera on specimens under load. This provides accurate crack length results. The correlation between the two variables is shown in figure 7.1.2.3. It was concluded that 0.85 mm had to be added to the crack length obtained from eddy current measurements in order to obtain the correct values. For more details the reader is referred to report [6].

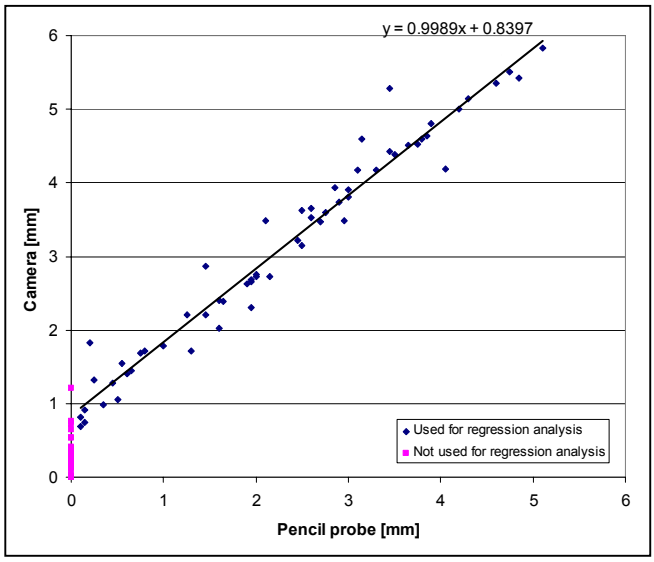

Figure 7.1.2.3. The relation between the crack length measured with the video camera and the crack length indication of the eddy current probe

Airbus NDT experts advise to cluster the short cracks which are measured with eddy current as follows in order to achieve a statistical reliability of 95% probability of detection (linked to the crack length thresholds):

- ❖ no NDT indication: set a = 1.5mm
- ❖ NDT indications ≤ 1.5mm: set a = 1.5mm
- ❖ NDT indications ≤ 2.0mm: set a = 2.0mm
- ❖ NDT indications ≤ 2.5mm: set a = 2.5mm
- ❖ NDT indications > 2.5mm: set crack length to measured value

Taking the above explained limitations into account, the minimum crack length which can be obtained from the measurements with 95% probability of detection is 1.5mm, i.e. it is 0.5mm longer than the defined transition crack length from crack initiation to crack propagation. Consequently, if shorter cracks are discussed in the following chapters, the reliability of the data is lower (than required for in-service NDI).

7.1.2.3 Construction of a crack initiation curve for the circumferential GLARE joint butt strap

Due to secondary bending, the mating surface of the GLARE2B-7/6-.4 butt strap at the location of the two inner rivet rows is the highest loaded location. Two rivet rows (no. 3 and 4 in figure 3.2.3.2) with five holes each have been investigated, which implies 20 potential crack initiation results per specimen because of crack locations on the left hand side and right hand side of each hole. The crack lengths of the potential 20 locations are averaged :

$$a_{av} = \frac{\sum_{i=1}^{20} a}{20} \qquad (6)$$

With the (applied net stress) open hole crack initiation curve as reference, it was searched for the first data point of the joint crack initiation curve. Due to the complex influences of design, fastener type, manufacturing qualities and other details on the crack initiation life of a riveted joint, it is recommended to consider results from similar structures for the first trial. The here discussed problem was related to a kind of design which has been tested previously by Airbus [7], although for other reasons. Three specimens with the same butt strap, fastener pitch and row distances as used for this research, but with aluminium skin parts and different fastener types have been disassembled after different numbers of fatigue cycles at 99.9 MPa applied net stress, related to 4.3mm thickness. From these results a crack initiation life of approximately 30000 cycles has been recalculated.

For this research, specimen no. 2-B-48 has been cycled at 38.9 kN maximum load, which corresponds to the same stress level as used previously by Airbus, to 30000 cycles (R=0.1). Cracks have been measured at all holes with the EC probe. All particular crack lengths are contained in table 7.1.2.1. The average crack length is calculated with 2.02mm, which is exceeding the target value of 1mm.

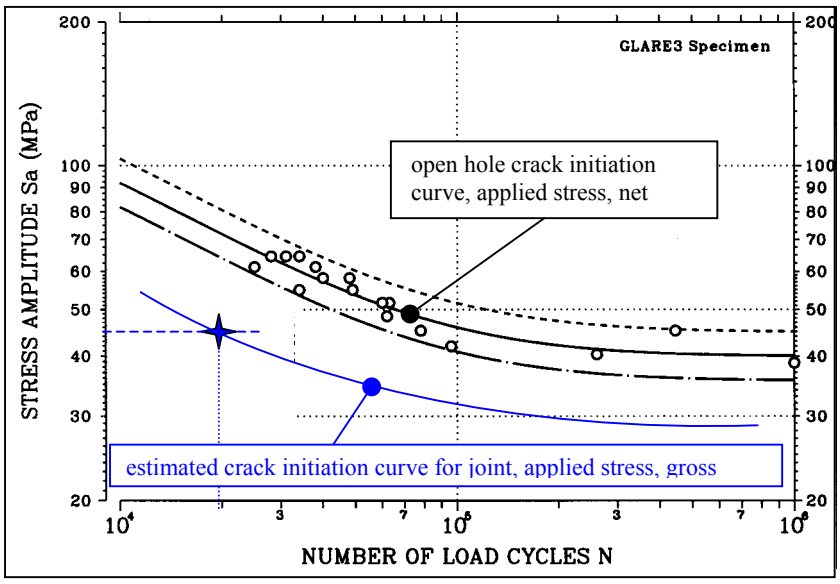

Figure 7.1.2.4. Estimated crack initiation curve for the circumferential joint, related to applied stress

Five more specimens have been cycled 20000 times under the same conditions. Crack lengths between 1.50mm and 1.93mm have been obtained, see table 7.1.2.1. The calculated mean value is 1.60mm, thus closer to the transition crack length of 1mm. The first data point for the crack initiation curve for the mating surface of the butt strap was defined with (N_{appl}=20000 / σ_a=45 MPa) and a line parallel to the crack initiation curve for the open hole specimens was drawn through this point, see figure 7.1.2.4.
The constructed crack initiation curve for the riveted joint has been used for the definition of other load / load cycle combinations to be tested. Specimens have been disassembled after the pre-defined test sequence and the average crack lengths in rivet rows 3 and 4 have been determined with the eddy current technique:

specimen no.	predefined max. load F_{appl} [kN] (R=0.1)	predefined number of cycles to disassembly N_{appl}	obtained average crack lengths a_{av} [mm]*
2-B-41	49.4	15000	1.50
2-B-43	35.0	45000	1.50
2-B-39	31.6	70000	1.50
2-B-42	26.3	170000	1.58
2-B-45	25.1	400000	1.66

* detailed crack lengths records contained in table 7.1.2.1

The combination 28.5 kN / 100000 cycles has been tested with 5 specimens, an average crack length of 1.57mm could be determined (table 7.1.2.2). The length of the cracks in these specimens was measured by a microscope only. Consequently the results may be less reliable than the values listed in table 7.1.2.1. The available crack initiation data were used to establish a crack initiation curve with a regression analysis [12] for the mating surface layer of the GLARE2B-7/6-.4 butt strap, associated with an average crack length <1.66mm, see figure 7.1.2.5.

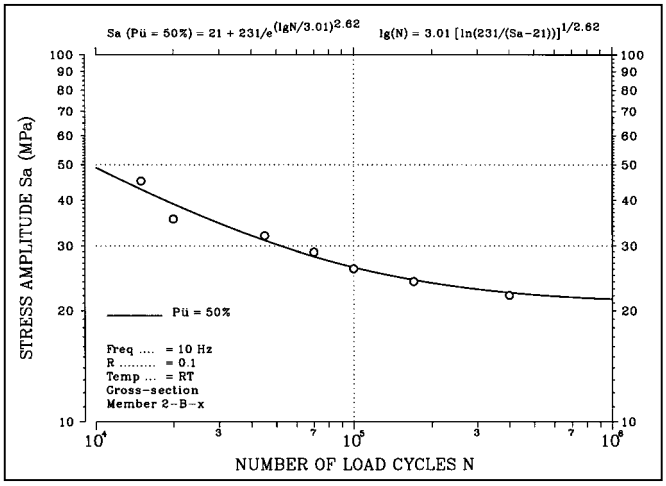

Figure 7.1.2.5. Crack initiation curve for rivet rows 3 and 4 of butt strap, mating surface layer, related to applied gross stress, all cracks initiating at holes, crack lengths <1.66mm, $R_{applied}$ = 0.1

7.1.2.4 Sensitivity of results related to inspection method

The measured crack lengths are strongly dependent on the availability and accuracy of the crack length measurement technique. Considering the recorded crack lengths in tables 7.1.2.1 and 7.1.2.2, the accuracy of 1.66mm crack length associated to the crack initiation curve in figure 7.1.2.5 is dominated by 'no findings' which have been clustered into 'crack length 1.5mm' for conservatism (industry recommendation). A sensitivity study is performed assuming that really no crack was present when the inspector found no indication by using the Nortec pencil probe (optimistic approach). The majority of the 1.5mm-values change to value 0mm (see tables 7.1.2.3 and 7.1.2.4) and the *average* crack lengths decrease accordingly.

specimen no.	predefined max. load F_{appl} [kN] (R=0.1)	predefined number of cycles to disassembly N_{appl}	obtained average crack lengths a_{av} [mm]*
2-B-41	49.4	15000	0.60
2-B-53 to -57	38.9	20000	1.04
2-B-43	35.0	45000	0.53
2-B-39	31.6	70000	0.83
2-B-7 to -11	28.5	100000	0.57
2-B-42	26.3	170000	0.68
2-B-45	25.1	400000	0.91

* detailed crack lengths records contained in table 7.1.2.3

The average crack lengths are much smaller now but consequently the scatter of the results is higher. In order to design a crack initiation curve based on a *constant* crack length for all particular data points, a statistical analysis is required. In the procedure for this purpose, several specimens were fatigue tested to the same number of cycles. The values of the crack lengths then recorded allow the determination of a mean crack length and the crack lengths which will be obtained with 10%, 50% and 90% probability at the given number of cycles. All specimens were now tested with F_{max} = 38.9 kN up to a life of 20000 cycles for this investigation, see table 7.1.2.3.

A statistical investigation similar to the elementary specimen scatter evaluation (chapter 6.4) is performed. The probability of crack initiation is calculated for the particular occurrence according to Goβe [8]:

$$P_{CL} = 100 * (3n-1)/(3m+1) \qquad (7)$$

The calculation is performed in table 7.1.2.5 and the results are presented in figure 7.1.2.6.

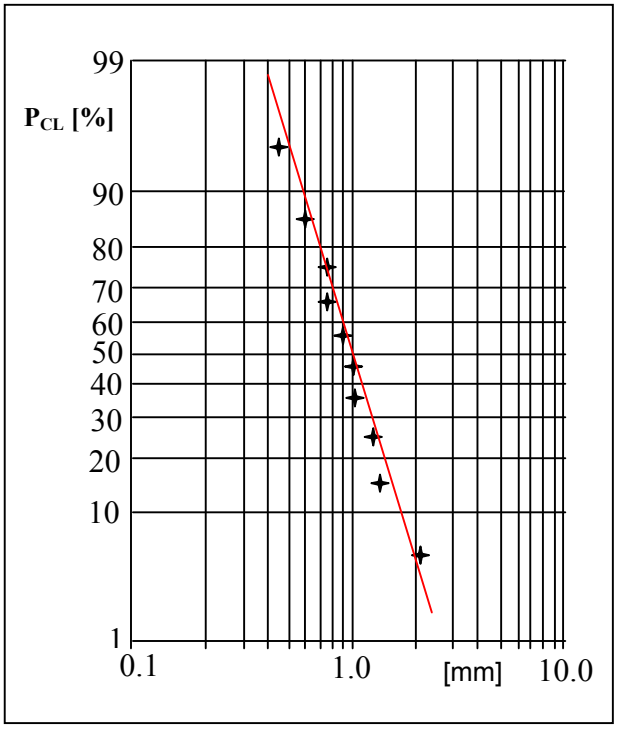

Figure 7.1.2.6. Probability of crack length after 20000 cycles at F_{max} = 38.9 kN

The results follow a Gaussian distribution.

The straight line in diagram 7.1.2.6 indicates the following crack lengths
(after 20000 cycles / F_{max} = 38.5 kN):

- 0.6mm with 90% probability of occurance,
- 1.0mm with 50% probability of occurance,
- 1.7mm with 10% probability of occurance.

In order to evaluate crack initiation curves related to constant crack lengths, all data points need to be recalculated to the above determined three crack lengths. Each value N_{appl}, at which the test has been stopped, has to be either increased or decreased, until it fits to the 0.6mm, 1.0mm and 1.7mm average crack length, respectively.

Crack propagation rates are required for this calculation. Due to the non-effective crack bridging behaviour for small crack lengths, crack propagation is supposed to follow da/dN-ΔK curves for monolithic aluminium. An indication for the crack propagation rates at low crack length for tests at F_{max} = 38.9 kN are provided by specimens 3-B-1, 3-B-48, 3-B-49 and 3-B-53 to 3-B-57. They have been fatigued to different number of cycles and cracks have been measured after disassembly. Between 0.58mm and 1.69mm average crack length a propagation rate of 1.11E-04 mm/cycle has been observed, which can serve for the recalculation of crack initiation life N from a_{av}=1.04mm to 0.6mm, 1.0mm and 1.7mm, respectively. Note: In order to obtain average crack lengths shorter than 1mm, the crack propagation curve presented in figure 7.1.2.7 is based on the non-clustered values, i.e. as reported by the EC-inspector and without clustering. The probability of detection is now below 95%.

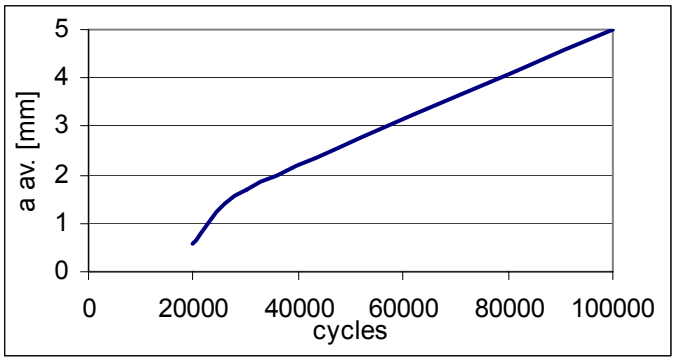

Figure 7.1.2.7. Average crack propagation curve at butt strap inner layer, crack from hole, for F_{max} = 38.9 kN

For the determination of crack propagation rates at the other load levels, the obtained da/dN value for 38.9 kN maximum test load is related to a stress intensity value according to the Forman equation for 2024T3 material, obtained from literature data [9]:

Equation:
$$\frac{da}{dN} = \frac{2.01x10^{-8}(\Delta K)^{2.7}}{(1-R)x2256-\Delta K} \quad (8)$$

The R-value is related to the *gross stress* of the concerned aluminium layer in the butt strap, corrected by the curing stress for GLARE2 for a delta temperature of 100°C, which equals 62 MPa [10]. Based on the stress measurements in the net section at F_{max} = 38.9 kN, it is 228.8 MPa between two holes on the aluminium sheet (see figure 7.1.2.10, strain gauge no. 1, E=72GPa).

$$\sigma_{gross} = \sigma_{net} - \sigma_{appl} \; x \; (1-A_{gross}/A_{net}) \quad (9)$$

Temperature correction:

$$\sigma_{gross,temp} = \sigma_{gross} + 62\ MPa \quad (10)$$

Calculation of stress ratio in aluminium sheets of GLARE butt strap (applied R=0.1):

$$R_{al} = (0.1 * \sigma_{gross} + 62\ MPa) / \sigma_{gross,temp} \quad (11)$$

For F_{max} = 38.9 kN :

σ_{gross} = 212.2 MPa

$\sigma_{grosstemp}$ = 274.2 MPa

R_{al} = 0.30

ΔK for 1.11E-04 mm/cycle and R=0.30 (equation 9): ΔK = 340 N/mm$^{3/2}$

The stress intensity factors for specimens tested at other load levels F can be approximated by accounting for the different stress levels:

$$\Delta K_F = \Delta K_{38.5kN} * \sigma_{grosstempF} / \sigma_{grosstemp38.5kN} \quad (12)$$

The values of da/dN for each load level can then be obtained with equation (8). The measured stresses, calculated stresses, R-values, stress intensities and crack propagation rates are contained in table 7.1.2.6 for all specimens. With the crack propagation rates being available for all load levels, the applied number of load cycles N_{appl} can be recalculated to the number of cycles required to obtain 0.6mm crack length ($N_{0.6}$), 1.0mm crack length ($N_{1.0}$) and 1.7mm crack length ($N_{1.7}$). A presupposition for this method is that the material scatter is similar for all applied stress levels.

$$N_{0.6} = N_{appl} - (a_{av}-0.6)/(da/dN) \quad (13)$$

$$N_{1.0} = N_{appl} - (a_{av}-1.0)/(da/dN) \quad (14)$$

$$N_{1.7} = N_{appl} - (a_{av}-1.7)/(da/dN) \quad (15)$$

The calculated lives are contained in table 7.1.2.6 and evaluated with computer program 'Wöhler' in figure 7.1.2.8. Each curve equals a probability of survival $P_ü$ of 50%.

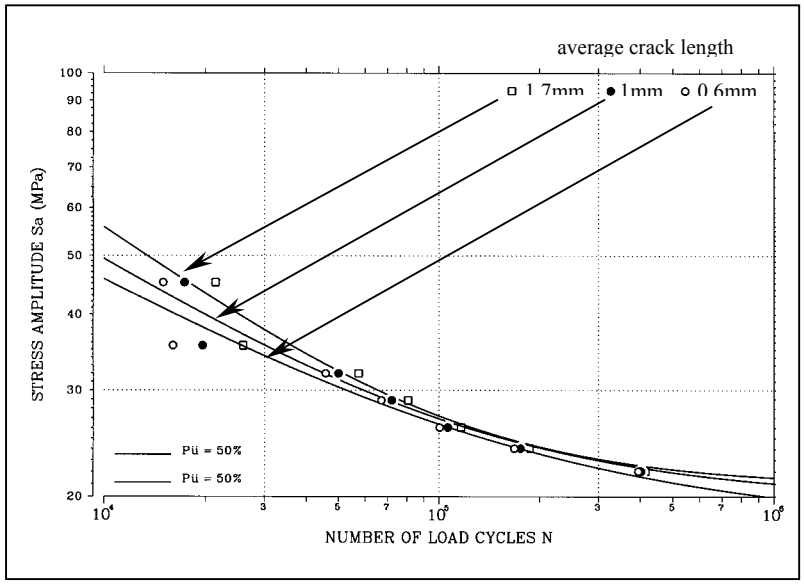

Figure 7.1.2.8. Crack initiation curves for 0.6mm, 1.0mm and 1.7mm crack lengths in but strap mating layer, related to gross stress in laminate, $R_{applied}$ = 0.1

7.1.2.5 Crack initiation prediction with aluminium reference joint method

An almost similar designed joint as investigated in GLARE2B material has been manufactured from monolithic aluminium 2024T3 and tested by Airbus [11], in order to provide a reference SN-data according to the method described in reference [2]. Differences compared to the GLARE joint are the 'skin' thickness - 3.8mm instead of 4.3mm - and the fastener heads – countersunk instead of protruded head. The GLARE2B specimens have been manufactured with high interference fit, the aluminium specimens with a low interference fit. The countersunk in the aluminium 'skin' parts has no influence on the crack initiation results, because the butt strap is the critical item of the investigated structure. Up to 173000 load cycles all aluminium specimens failed in the butt strap in rivet rows 3 or 4. At lower fatigue loads and thus higher fatigue lives they failed in the gross section between rivet row 3 and 4. The results are evaluated with program 'Wöhler' according to [12], see results in figure 7.1.2.9.

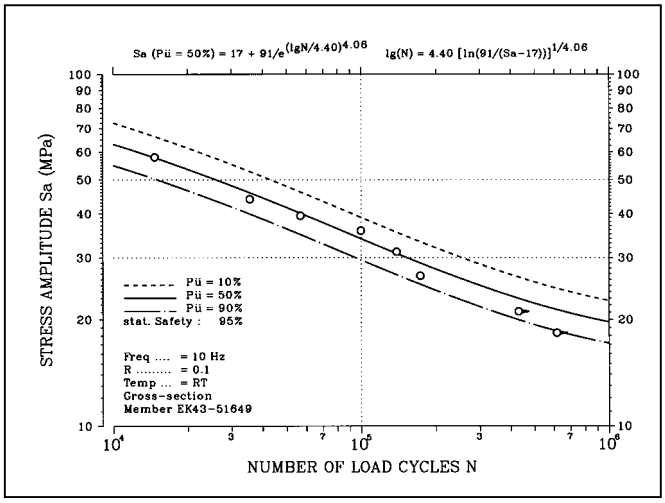

Figure 7.1.2.9. SN-data for monolithic aluminium reference joint, gross stress amplitudes related to 4.3mm thickness, cycles to failure, R=0.1

The 'stress similarity concept' is based on the assumption that riveted joints made of the same material, which experience the same stress level in the hole edge have the same crack initiation life. The method has been extended and programmed for GLARE by Delft University [2,3] in cooperation with Airbus Deutschland. The following assessments compared with the verified method for monolithic aluminium [13] have to be considered for the calculation of stresses in the aluminium layers of GLARE:

- The stiffness of the ingredients prepreg and aluminium has to be taken into account. The curing stress has to be considered.
- The stress ratios shall be calculated according to [14].
- A correction factor for the bending stress prediction for both, the GLARE joint and the aluminium joint, has to be considered (see section 7.1.2.6)
- A factor on the crack initiation life has to be taken into account for different fastener types or fastener fits (between reference joint and GLARE joint) [15].

The constant amplitude crack initiation calculations for the GLARE2B butt strap are discussed in section 7.1.2.7.

7.1.2.6. Bending stress correction

The stress similarity method used in the Delft University / Airbus computer program 'FML DTToolbox' is based on the peak stress method. The value of σ_{peak} is calculated for each individual aluminium layer in GLARE and related to SN-data available from an aluminium reference joint at the same σ_{peak} – value.

$$\sigma_{peak} = \frac{s}{s - D_0}\left[K_{thole}(1-\gamma) + K_{tpin}\gamma + K_{tbending}K_b\right]\sigma_N \; C_1 \; C_2 \qquad (16)$$

The factors C_1 and C_2 consider the stiffness of the GLARE ingredients and the curing stress respectively. They are equal to 1 for the aluminium reference joint. The factor k_b represents the stress ratio between the secondary bending stress and the applied stress. It has a significant influence on the σ_{peak} – value and consequently on the crack initiation.

Releases 93 and higher ones of the computer program 'FML DTToolbox' allow external data to be imported for both the applied stresses and the bending stresses related to the GLARE joint. Bending stresses may be obtained either analytical, e.g. by using Schijves neutral line model [16, 17], or from strain measurements. The measurements are preferred for the present study in order to avoid an additional variable for the recalculation of the crack initiation point for the GLARE joint. Specimen 2-B-102 was selected to conduct strain measurements in the non-fatigued condition.
The strain gauge readings are very sensitive to the particular location, at which they are positioned [1]. For this research it was observed that all cracks initiate in the net section, therefore strain gauges have been bonded in rivet row three between two fasteners at both sides of the strap. A small cut out has been milled in the skin part in order to allow access to the mating surface of the strap, see figure 7.1.2.10.

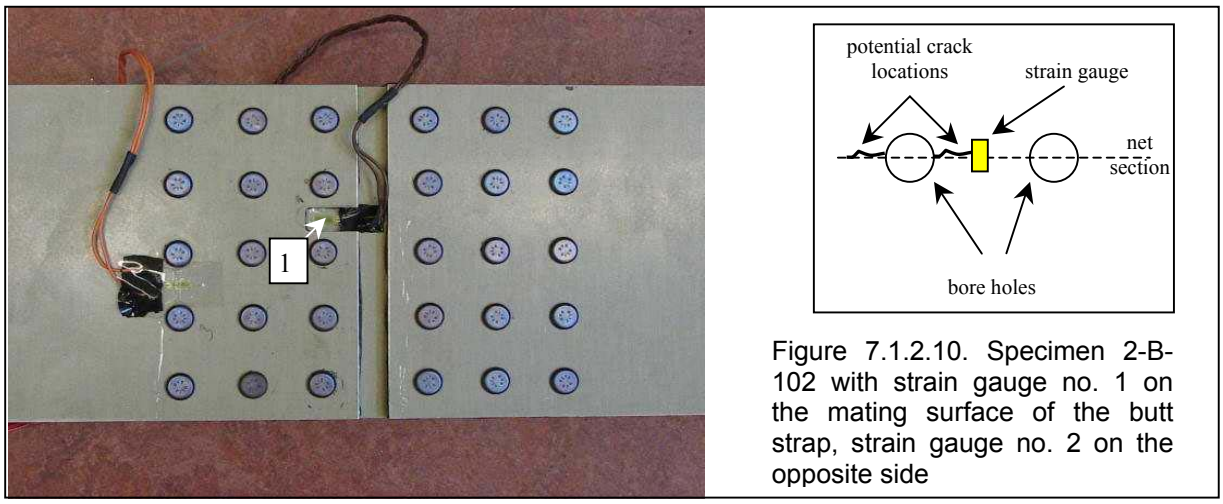

Figure 7.1.2.10. Specimen 2-B-102 with strain gauge no. 1 on the mating surface of the butt strap, strain gauge no. 2 on the opposite side

The measured strains in the net section of the mating aluminium layer are recalculated to gross stresses. Thermal stresses in order to take room temperature into account are not included. The bending stresses are calculated by subtraction of the applied stress from the butt strap gross stress:

$$\sigma_{bending}^{1)} = \sigma_{measured}^{2)} - (F_{appl.} / A_{gross}^{3)}) \qquad (17)$$

1) bending stress contribution in mating aluminium layer 2) gross stress in mating aluminium layer
3) laminate gross section

The applied specimen loads, the applied gross stresses, the bending stresses (gross) and the bending factors k_b for the mating aluminium sheet of the GLARE2B-7/6-.4 butt strap at rivet rows 3 and 4 are presented in table 7.1.2.7. Both, the applied stresses and the bending stresses serve as input data for crack initiation calculations using the TU Delft / Airbus computer program 'FML DTToolbox'.

7.1.2.7 Joint calculations

The SN-curve according to figure 7.1.2.8 and the normal stress / bending stress relations according to table 7.1.2.7 are used as input for crack initiation calculations with the computer program 'DTToolbox'. An MSD scenario is used which implies that a random multiple site damage situation is selected for cracks at the five holes of the specimen. The crack initiation life is then calculated. In view of possible scatter of the initial MSD situation a large number of this MSD scenario is analyzed. It turns out that the calculated results converge for approximately 100 randomized MSD scenarios.

The aluminium specimens (designation EK43-51649) have been manufactured with a clearance fit, while the GLARE specimens have been manufactured an with interference fit. The program considers a crack initiation life extension of factor 1.18 for this difference, according to the Airbus Repair Assessment Program [15].

For the calculation of the bending stress ratio k_b in the reference joint, release 93 uses the neutral line model as developed by Hartman and Schijve [16,17]. However, cooperative investigations at Airbus and Delft University demonstrated that the calculated bending stresses according to the neutral line model are more and more conservative for an increasing load on the specimen. A circumferential joint specimen with the similar design as the outdoor exposure series 2-B, but with 4mm monolithic aluminium skin parts and GLARE2B-7/6-.4 butt strap was manufactured by Airbus and strains on the butt strap have been measured, similar as discussed for specimen 2-B-102. For comparison the stresses have been calculated at Airbus with the neutral line model of Schijve which is programmed in computer program 'SEBIANSJ' [18]. For the ratio ($k_{b\ measured}$ / $k_{b\ calculated}$) factors between 1.0 and 0.6 were found, see triangles in figure 7.1.2.12.

Figure 7.1.2.11. Joint specimen for bending investigations, aluminium skin sheets, GLARE2 butt strap

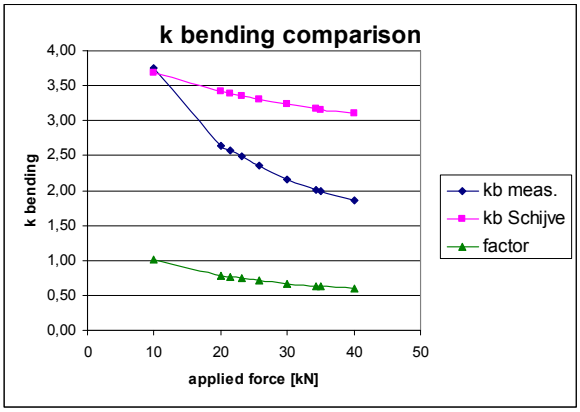

Figure 7.1.2.12. Bending factors and ratio between the measured and the calculated bending

The *calculated* bending factor with the neutral line model has to be corrected for a reliable stress level prediction. The software 'FML DTToolbox' allows to correct factor k_b for the aluminium reference joint with a constant value. For the present investigation factor 0.75 is considered (mean value obtained from measurements). With the aluminium reference SN-curve according to figure 7.1.2.9 as input, the crack initiation curve for 1mm average crack length according figure 7.1.2.8 will be predicted in the mating aluminium layer of the GLARE butt strap. Five calculations are performed, for applied maximum stresses of 55, 59.4, 66, 77 and 88 MPa, respectively. The numerical results are contained in table 7.1.2.8, compared with the crack initiation test results. Figure 7.1.2.13 contains the *tested* crack initiation curves for the GLARE2B strap (a_{av}= 1.0mm) and the *calculated* crack initiation data. The listings of the particular calculation results including the crack initiation distribution for 100 MSD scenarios shown in attachment A. The calculated results fit close to the 50% probability curve obtained from the tests. The DTToolbox is predicting the crack initiation in the butt strap accurately.

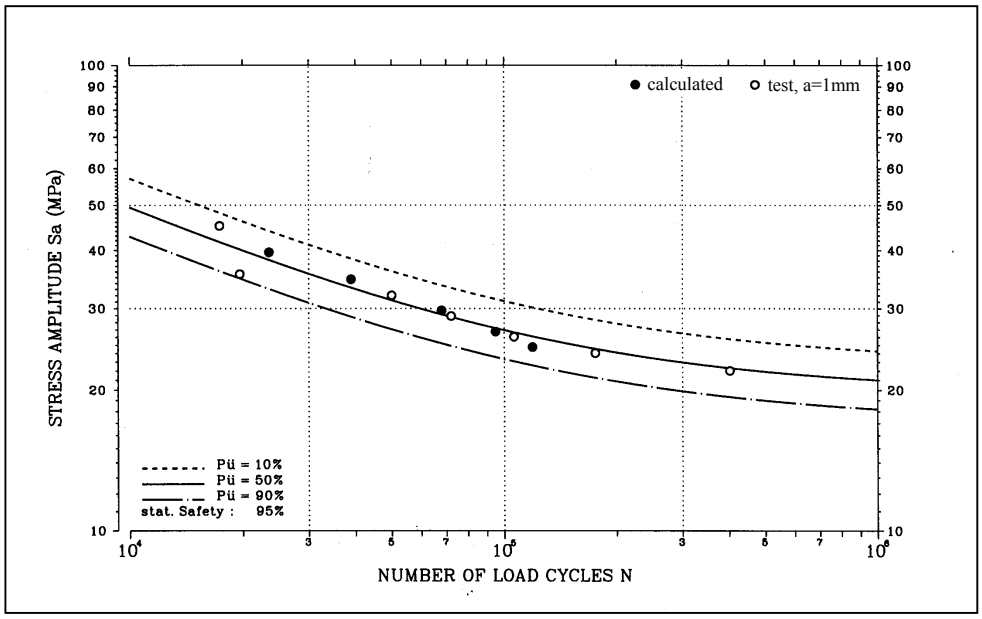

Figure 7.1.2.13. Specimen series 2-B-, measured and calculated crack initiation data related to mating aluminium layer of GLARE2B-7/6-.4 butt strap, applied gross stresses shown

7.1.2.8 Comparison of SN results of the crack wire specimens with SN_i-curve

The crack initiation results from specimens 2-B-28, -79, -80 and –81 with crack wires discussed in Section 7.1.1 are compared with the test results presented in the preceding section in 7.1.2.14. The crack initiation life of the crack wire specimens exhibit a trend to lower crack initiation lives. The trend can be explained by the local reworking of the inner skin sheet aluminium layers, which will cause more rivet tilting, and consequently higher bearing loads in rivet rows 3 and 4.

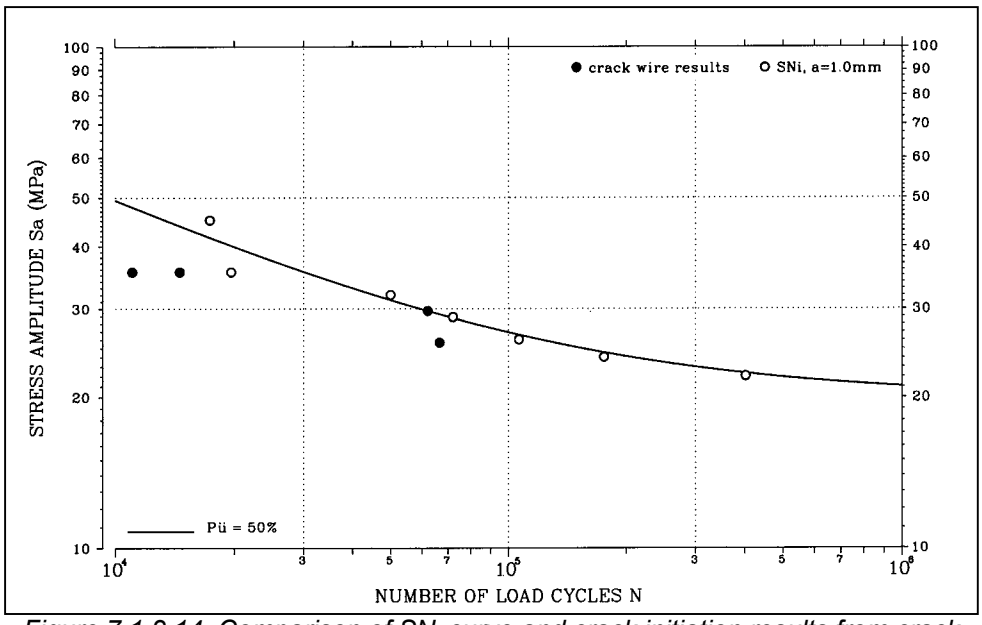

Figure 7.1.2.14. Comparison of SN_i-curve and crack initiation results from crack wire specimens (a=1mm), related to applied stresses, $R_{applied}$=0.1

7.1.2.9 Surface condition and sealant bonding properties

The scatter of crack initiation of identical specimens is a surface condition problem [28]. Several riveted joint specimens have been disassembled for a fatigue crack inspection. After fastener removal it was observed that high forces are required to separate the sheets of the painted specimens, but this was not the case for the unpainted ones. A detailed investigation of the specimen surfaces shows different failure modes of the sealant. The sealant failure was a cohesive failure in the painted specimens, whereas it was an adhesive failure at the butt strap in the non-painted specimens. On the non-painted specimens, the majority of the remaining sealant was attached to the 'skin' parts after disassembly.

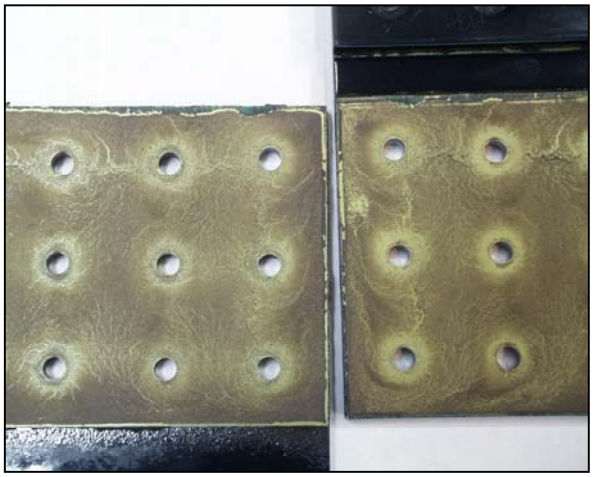

Figure 7.1.2.15. Painted specimen after disassembly, cohesive failure in sealant

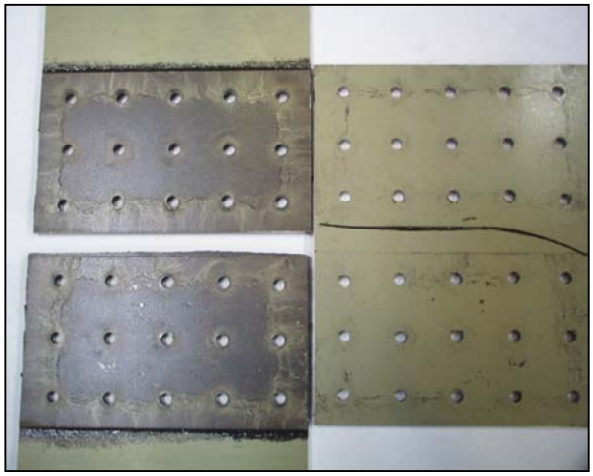

Figure 7.1.2.16. Unpainted specimen after disassembly, adhesive failure between sealant and metal

All specimens left the material workshop with bonding primer on the outer surfaces. The specimens due for outdoor exposure got a paint primer on top, then the sheet surfaces have been activated and sealant was applied before the sheets have been jointed with fasteners. Further painting procedures did not influence the condition of the joint area.

The specimens which were not planned for the outdoor exposure program still got a paint primer. The surface protection system in the joint area is similar compared with the painted specimens. However, the non-painted specimens are manufactured in a different batch. The low forces required to separate the sealed sheets (after removal of the fasteners) can have just one reason, i.e. it is likely that the butt strap surfaces have not been cleaned carefully enough before the wet assembly.

The influence of hardened or non-hardened sealant on the present research has been investigated. The load which can be transferred by adhesion from one sheet to the other one should decrease the load transfer through the fastener. Then, the pin load is decreased but the by-pass load is increased, which may affect the crack initiation life. Figure 7.1.2.16 with a magnification of the lower left part in figure 2.1.2.17 shows the available fatigue results from both, painted and unpainted circumferential joint coupons tested with a maximum load of 39.8 kN. The data represent average crack lengths for the mating layer of the butt strap in rivet row 3 and 4. The results are given in tables 7.1.2.9 and 7.1.2.10. The results cover both the crack initiation and the crack propagation period. The cracks have been measured after disassembly of the joint. Fatigue results from crack wire specimens 2-B-79 and 2-B-80 (with reworked 'skin' parts for wires) are included for comparison.

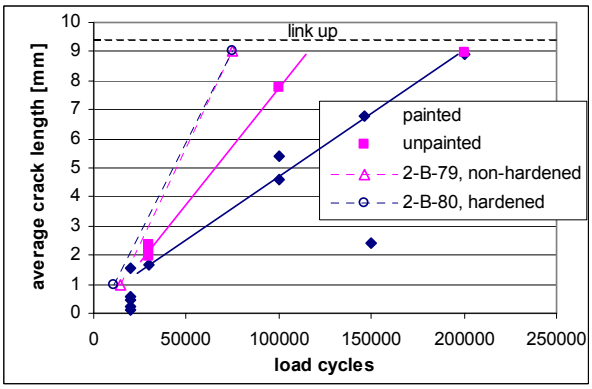

Figure 7.1.2.16. Crack propagation data from specimen series 2-B, painted and non-painted, including crack wire specimens –79 and -80

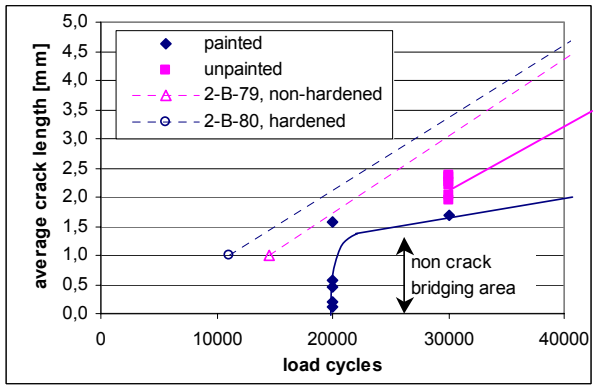

Figure 7.1.2.17. Magnification of figure 7.1.2.16

A trend for both, crack initiation and crack propagation, is observed for the painted specimens (see figure 7.1.2.16) with several measurements performed even at crack lengths before effective crack bridging. The full line in figure 7.1.2.17 is an approximation of the crack propagation curve for the short crack lengths area. Note that all involved test data are representative to discuss the influence of sealant, because all data are obtained from the first disassembly cycle! For the unpainted specimens (low adhesive sealant forces) slightly longer crack lengths are measured after 30000 cycles, compared with the painted specimens. There are insufficient data available to draw a crack propagation curve for the unpainted specimens at short crack length, but the diagrams indicate that the influence on crack initiation is in the range of scatter.

As discussed in the previous chapter, the crack initiation lives of the crack wire specimens is reduced due to the milling of the 'skin' parts, see also figure 7.1.2.17.

Trend lines are drawn for the different specimens between the average crack lengths 1.5mm and 9mm (figure 7.1.2.16). Note that at approximately 9.5mm cracks link up, the value is floating due to the non regular hole pattern. The crack propagation rates are significantly lower than for the crack wire specimens.

Just two reliable data points are available for the non painted specimens at longer crack length. One crack length matches exactly the painted result, at 200000 cycles (figure 7.1.2.16). If this point is valid, there is no difference between good and poor sealant adhesive forces required for the determination of crack propagation rates. Another data point is available at 100000 cycles / 7.8mm average crack length, which does not fit to the one discussed before. A crack propagation curve through this particular data point, as shown in figure 7.1.2.16, would result in a crack propagation life reduction of factor 2 for the specimens with low adhesive forces between the mating surfaces at the investigated load level.

A similar comparison of available crack propagation data is done for the 2-A specimen series, i.e. the riveted joint coupons. More data are available to draw a line through the crack propagation results obtained from different specimens. A clearer trend is observed concerning an earlier crack initiation of the unpainted specimens. The factor on life is approximately 1.5. As well, a clear distinction of the crack propagation rates can be made.

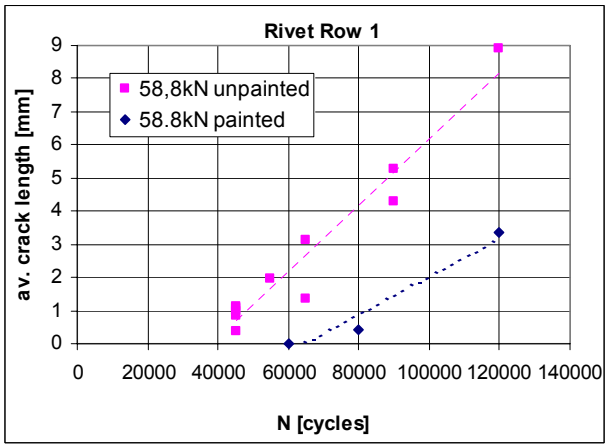

Figure 7.1.2.18. Crack propagation rates in specimens 2-A, upper GLARE sheet, lower aluminium layer (fastener: HL413VF-6 & collar HL93-6)

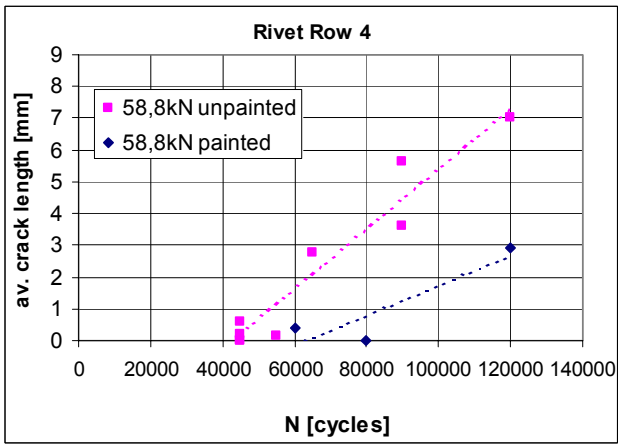

Figure 7.1.2.19. Crack propagation rates in specimens 2-A, lower GLARE sheet, upper aluminium layer (fastener: HL413VF-6 & collar HL93-6)

For the unpainted repair coupons with presumably low sealant adhesion, the crack propagation rates increase compared with the painted specimens. Obviously, if sealed properly, the intact aluminium layer from the opposite GLARE sheet, which is attached to the fatigued aluminium layer of the investigated GLARE sheet, provides a (limited) crack bridging effect similar as the glass fibers in GLARE. Note: The cracks in the 2-A-series specimens develop *around* the holes, they do not initiate *from* the holes. The particular data are recorded in table 7.1.3.1, see specimens 2-A-2 to 2-A-6 and 2-A-31 to 2-A-34. A detailed discussion of crack propagation in the 2-A series specimens follows in chapter 7.1.4.3.

The available data are not sufficient for a final conclusion of the influence of high or low adhesive qualities of sealants between mating surfaces of GLARE sheets. It is recommended to perform a dedicated experiment, if a practical reason is given, i.e. if aircraft are coincidently delivered with not-hardened anti fretting compound. For this research it is important to record:

- The crack initiation curve for the circumferential joint (figure 7.1.2.13) is established with painted specimens, i.e. including an industry representative surface preparation and good adhesion between GLARE and sealant. The surface quality is similar as for the full scale specimen A340-600-EF2.
- The crack initiation curves discussed in this research are obtained from measurements after disassembly of the specimens. After the first crack inspection, the specimens have always been assembled dry. Therefore, if a crack propagation curve is measured with one and the same specimen, i.e. if it is disassembled for crack measurements more than once, the resulting curve is similar to a curve with non hardened sealant.
- The crack propagation curve in figure 7.1.2.7 is performed with data resulting from the first measurement of different specimens. It is representative for a high adhesion joint.

The observations discussed in this section have some practical relevance. Most of the previous researches on riveted GLARE joints have been performed without a paint primer on top of the bond primer, which may cause a low adhesion between the components. Consequently, most of the evaluated crack propagation results may be rather conservative. For realistic future crack propagation investigations of riveted GLARE joints it is recommended to apply paint primer on the GLARE surface and to take care during the surface cleaning and activation operations.

Based on the *available* data it is recommended to consider a surface treatment factor on the crack initiation life ($C_{CI(ST)}$) for single shear joints where no good adhesive properties are expected between

the mating sheets, either due to the surface preparation or non hardened sealant. It is recommended to investigate the subject further.

$C_{CI(ST)}$ = 0.66 (no load transfer by adhesive forces through anti fretting compound)

A factor 1.3 is recommended for multiplication on the crack propagation rate for a specimen without expected high adhesive forces transferred by the sealant. For GLARE, this factor is linked to the top aluminium layer of the laminate.

$C_{CP(ST)}$ = 1.3

7.1.3 The development of crack initiation curves, lap joint

The fatigue cracks in the riveted repair coupons, test series 2-A, initiate simultaneously in the mating aluminium layer of the top GLARE sheet in rivet row 1 and in the mating layer of the bottom GLARE sheet in rivet row 4, if the fastener/collar combination HL413VF-6/HL93-6 is installed. As explained in chapter 3, these fastener have been selected as substitution for the much more expensive ASNA 2026 fastener, which are the standard in the A380. Fatigue cracks did not initiate at the edge of the hole,

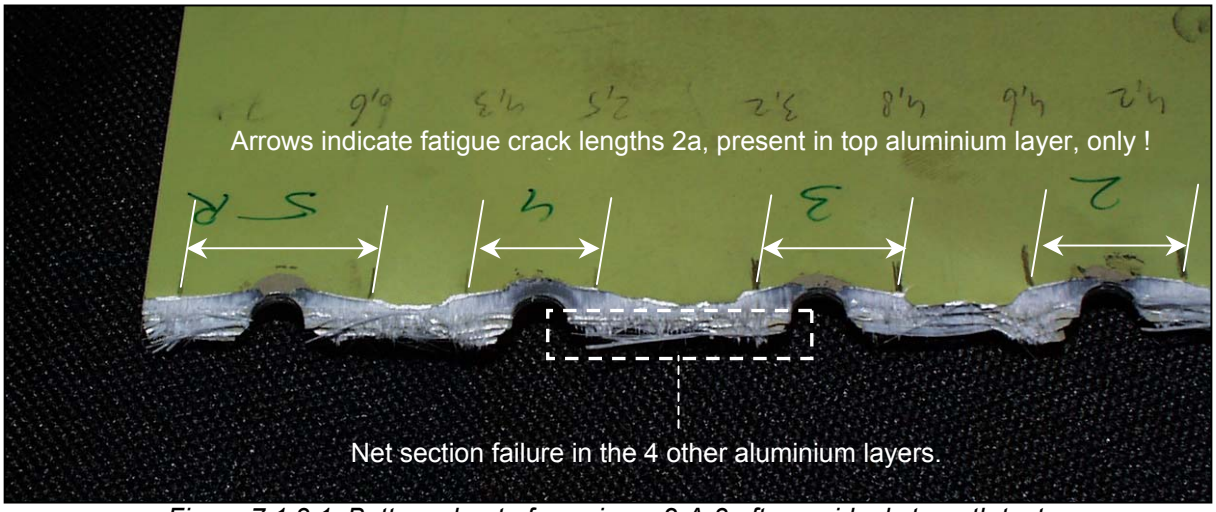

Figure 7.1.3.1. Bottom sheet of specimen 2-A-3 after residual strength test, rivet row 4(HL413VF fastener)

but around the hole in some distance of the edge. Figure 7.1.3.1 shows the fatigue cracks in the mating layer of rivet row 4 in the bottom GLARE sheet of specimen 2-A-3, after the residual strength test. In the static test the fatigued aluminium layer failed in the fatigued cross section, the others failed in the net section. A magnification shows fretting fatigue as likely reason for the crack initiation:

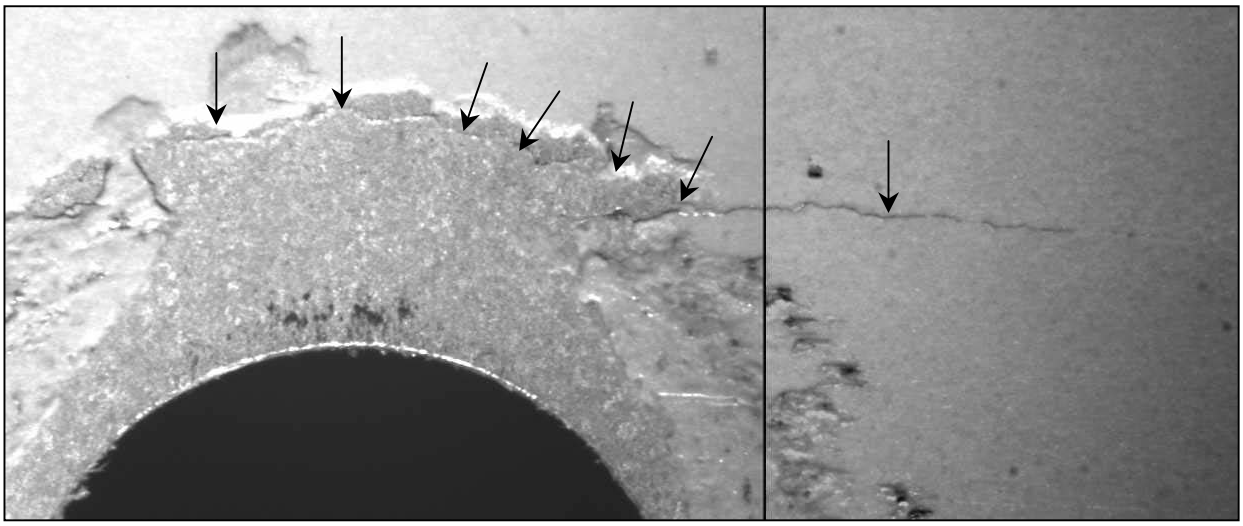

Figure 7.1.3.2. Specimen 2-A-4, fatigue crack around hole, fretting fatigue

The crack pattern *around* a hole is very rarely detected in monolithic aluminium in full scale structures, but occasionally in coupon specimens [42]. In order to determine the relevance of the present results it is important to compare the failure mode with both, the riveted repair panel (specimen series 11-RR) and with the Megaliner Barrel repair. It will be done in the following chapters.

The size of the initial crack length a_i must be reconsidered if fatigue cracks are initiated outside the fastener hole due to fretting. In such a case, it should not be expected that a small through-the-thickness crack in the mating surface layer will rapidly propagate until it reaches a crack length approximately equal to the hole diameter. Fretting is damaging the sheet surfaces in the area around the hole and the fretting fatigue crack will propagate into the depth until the first aluminium layer is cracked through. Subsequently the crack will propagate perpendicular to the load in both directions left and right of the fastener.
From the structural strength and safety point of view, crack initiation *outside* the holes is preferable because it weakens the *gross* section of the sheet material and not the *net* section. No decrease of residual strength is expected if the fatigue crack length does not exceed the hole diameter. It is thus decided to define the starter crack length to be `zero´ when it reaches the tangents to the hole parallel to the load direction, see figure 7.1.3.3. From then on, the crack lengths are measured and recorded in a similar way as if they propagate from the edge of the hole. Results are presented in table 7.1.3.1.

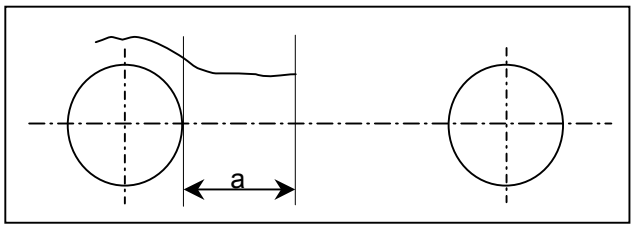

Figure 7.1.3.3. Fatigue crack length definition for specimen series 2-A fatigued with HL413VF-6 fastener

A crack initiation curve can now be established with the same trial-and-error method used for the GLARE butt strap, i.e. under consideration of the slope of the open hole SN-curve. The resulting crack initiation curve for the repair coupon is called ‘apparent’ for reasons just explained. Crack initiation data can be generated with the results from specimens 2-A-2, 2-A-4, 2-A-6, 2-A-19, 2-A-21 and 2-A-22.

Figures 7.1.3.4 and 7.1.3.5 show the apparent crack initiation data for the applied gross stress ('applied', laminate, R=0.1) and for the particular aluminium layers ('Sa', R=0.1 in aluminium layer). Numerical data are given in table 7.1.3.2. All cracks show an average length lower than or equal to 1mm, according to the definition in figure 7.1.3.3.

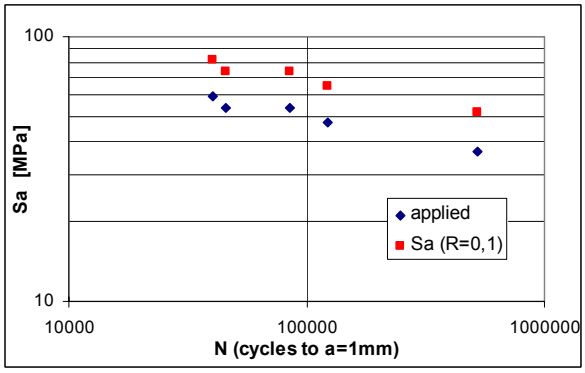

Figure 7.1.3.4. Apparent crack initiation data for repair coupons, upper sheet, rivet row 1, mating aluminium layer (fastener: HL413VF)

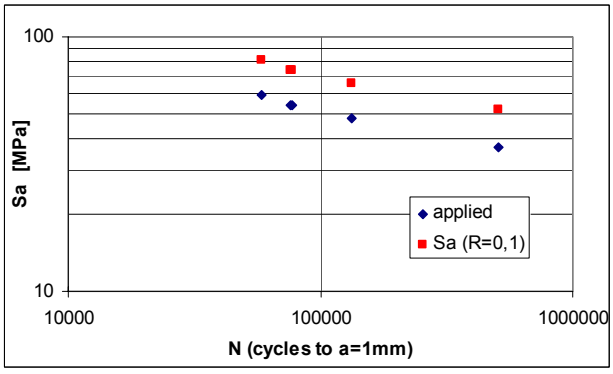

Figure 7.1.3.5. Apparent crack initiation data for repair coupons, lower sheet, rivet row 4, mating layer (fastener: HL413VF)

The painted specimens 2-B-43 to 2-B-48 were fatigue tested at the Delft University to different numbers of load cycles with ASNA2026 fastener installed. The specimens were exposed in Queensland for one year and shipped back to Delft in May 2003 for residual strength testing. Details of the structural loads are discussed in chapter 7.1.8.2. The specimens were not disassembled before the residual strength test. After final failure in rivet row 1 of the top sheet (similar as for specimens tested with HL413VF-6 fastener) it was observed that all fatigue cracks initiated *from* the hole edges. The particular crack lengths at the holes in all aluminium layers of specimens 2-A-44 (40000 fatigue cycles), 2-A-46 (80000 fatigue cycles) and 2-A-48 (120000 fatigue cycles) are given in tables 7.1.3.3 to 7.1.3.5. Due to the countersunk hole, the net section is different in all aluminium layers. The hole diameter for each sheet at each hole position is presented in the tables as well. A relation between the average crack length and fatigue cycles can be established for the fatigue test load $F_{max.}$ = 58.8 kN at a stress ratio 0.1, see figure 7.1.3.6.

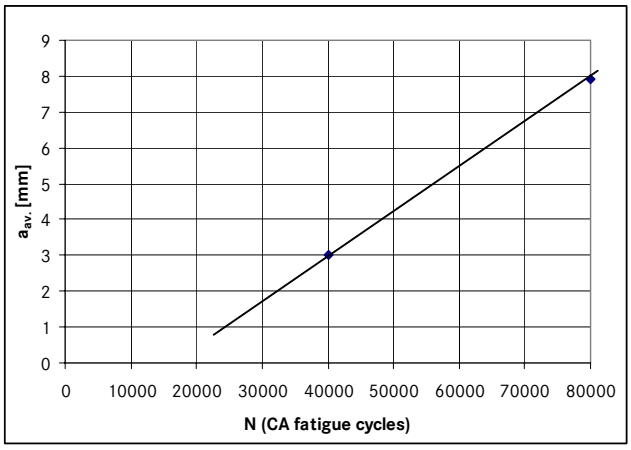

Figure 7.1.3.6. Specimens 2-A fatigued with ASNA2026 fastener, crack initiation life of mating layer of top sheet, rivet row 1

One millimeter average crack length from the hole edge in the mating layer of the top sheet in rivet row 1 is obtained after 23000 constant amplitude fatigue cycles. This result is compared in figure 7.1.3.7 to the SN-data from the specimens which failed outside the holes. A similar slope of the SN curve is assumed for both failure modes. The conclusion is that crack initiation *at* the holes with ASNA2026 fastener occurred earlier than crack initiation *around* the holes with HL413VF fastener. Figure 7.1.3.8 shows the same trend for rivet row 4 in the lower sheet.

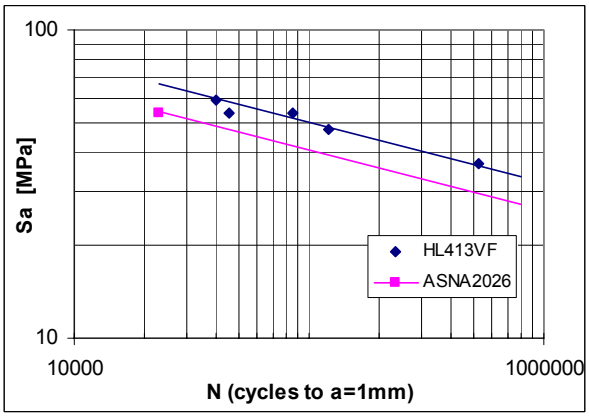

Figure 7.1.3.7. Apparent crack initiation data for repair coupons, upper sheet, rivet row 1, different fastener types and failure modes

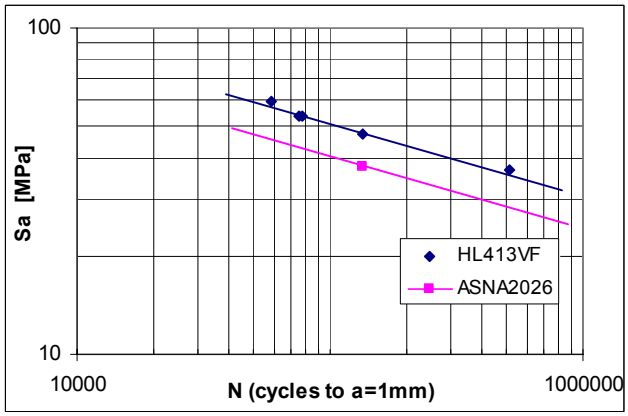

Figure 7.1.3.8. Apparent crack initiation data for repair coupons, lower sheet, rivet row 4, different fastener types and failure modes

The phenomenon is analyzed by investigating cross sections of the fasteners of specimens 2-A-1 and 2-A-43. Parts of rivet row 3 are cut out of the specimen and cross sections are made through the center line of the fasteners. Pictures obtained in the SEM are shown in figure 3.1.3.9. It should be kept in mind that both specimens have been loaded (static) before the SEM investigation was done, i.e. specimen 2-A-1 up to 198.2 kN and specimen 2-A-43 up to 197.5 kN. At these load levels they failed in the upper sheet along the fatigue cracks in rivet row 1. Some fastener tilting happened which left the fastener in a position slightly out of the center, which is visible in the top view on the top of the fastener heads in figure 3.1.3.9. Rivet row 3 was selected for the destructive investigation because a visual inspection left the impression that this is the rivet row with the minimum fastener tilting.

The 5.6mm Hi-Lite fastener has an excellent fit in the hole, see the right lower picture in figure 7.1.3.9. Both, the countersunk head and the cylindrical shaft fit neatly into the hole. The fastener head is in one loft with the outer surface of the GLARE.

The 5.6mm Hi-Loks (HL413VF) do not fit into the top sheet hole (lower left picture in figure7.1.3.9). Apparently the top sheet was drilled to a larger diameter than the bottom sheet, which is impossible to perform in one manufacturing step. Large gaps on both sides of the fastener are visible close to the top sheet. The fastener head is pulled much further into the laminate compared with the Hi-Lite. As a consequence, the edges of the upper sheets are locally clamped on the lower sheet with relatively high forces, see the blue arrows in the lower left picture. As a result, the top sheet deforms some millimeters away from the edge and a small gap is remaining (red arrows). There is no homogenous clamping force at the sheet surfaces. Where the gaps develop just a limited portion of load can be transferred by friction from one GLARE sheet to the other one. The friction will concentrate around the hole, a situation which contributes to the observed fretting fatigue damage. Furthermore, the 4.8mm collar which is screwed on the HL413VF provides just 70% of the clamping force which is guaranteed by the manufacturer for the ASNA2528 collar (min. tension preload: 1100 lbs). Apparently the lower clamping force allows more relative movement between the mating sheets in the load direction, which contributes to the local fretting as well.

Because all specimens with HL413VF fastener show crack initiation *around* the hole and all specimens fatigued with Hi-Lites failed *at* the hole, it is concluded that a systematic manufacturing error is the reason for the different results. The specimens were manufactured in different batches.

net section failure in rivet row one at static test

adhesive sealant failure

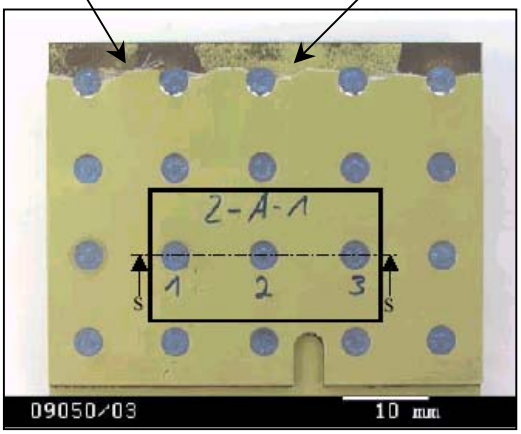

residual strength failure in rivet row 1 after fatigue and 1 year outdoor exposure

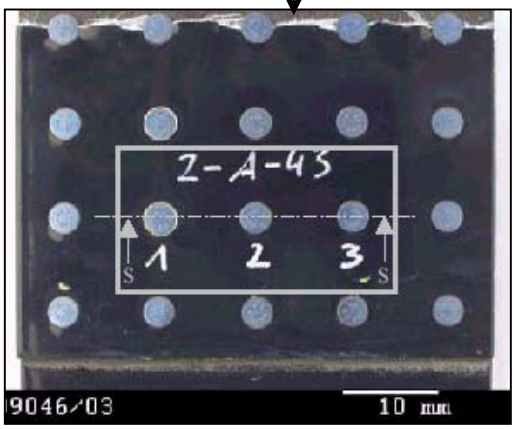

view on fastener 1

view on fastener 2

fastener too deep in laminate

The upper sheet has a larger hole diameter than the lower sheet.

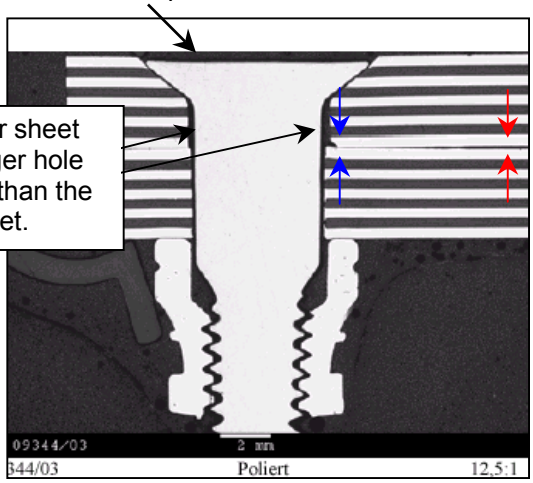

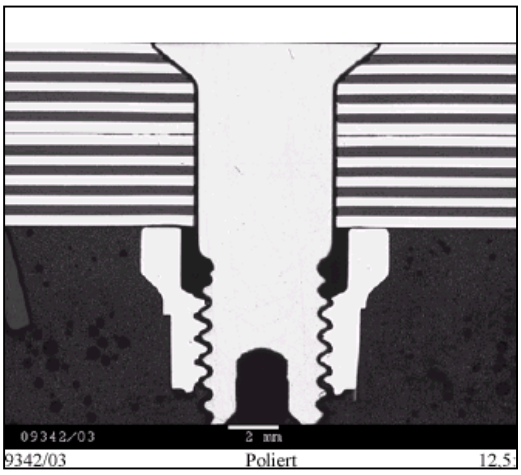

Figure 7.1.3.9. Observations after the static failure of specimens 2-A-1 (left) and 2-B-43 (right) [37]

7.1.4 Fatigue crack propagation in riveted joint coupons

7.1.4.1 Fatigue crack propagation in butt strap (coupon), mating surface aluminium layer

Five constant amplitude crack initiation calculations have been performed in chapter 7.1.2 for the calibration of TU Delft / Airbus computer program 'FML F&DT Toolbox' (release 0.93) for the present problem. The crack initiation results of 100 MSD scenarios for each calculation (stress level) are recorded in appendix A.

The software continues with crack propagation calculations for all fatigue sensitive locations in all aluminium layers, i.e. for the 2-B specimen series: 100 MSD x 5 holes x 2 sides per hole = 1000 fatigue sensitive for each aluminium layer. The theory used is explained in [39], the crack propagation rates are similar for all fatigue sensitive locations in a particular aluminium layer. One MSD scenario of hundred for each stress level, which allows the determination of the crack propagation rate for the mating aluminium layer of the GLARE2B-7/6-.4 butt strap, is plotted in appendix F.

Calculated crack propagation rates in mating butt strap layer:

applied maximum stress [MPa]	crack propagation rate [mm/cycle]
55	3.27E-05
66	8.00E-05
77	1.80E-04
88	3.27E-04

The calculated crack propagation rates are compared with available test data from the trial-and-error specimens (EC inspection, chapter 7.1.2) and from the crack wire specimens (chapter 7.1.1).

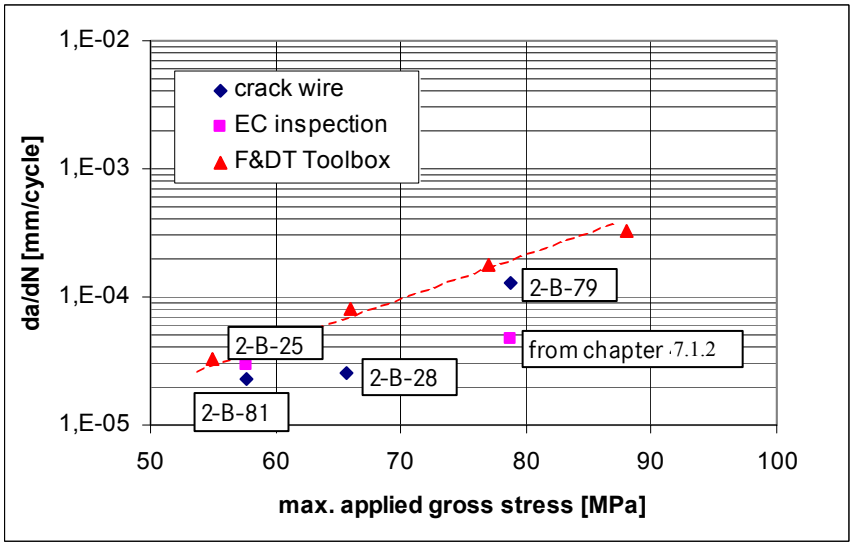

Figure 7.1.4.1, CA crack propagation results of rivet rows 3 and 4, mating surface of circumferential joint butt strap, related to average crack length, all specimens not aged.

The calculated crack propagation rates for the mating aluminium layers are conservative if compared with the test results. The FML F&DT Toolbox is applicable for conservative predictions for the highest loaded aluminium layers of single shear GLARE joints. However, additional investigations of the same kind are recommended for the future in order to increase the confidence in the software further.

7.1.4.2 Crack propagation through the thickness in circumferential joint butt strap (coupon)

Optional the stresses in the particular layers are calculated with the neutral line model (developed by Hartmann and Schijve [16]). For example, figure 7.1.4.2 shows the calculated bending and normal gross stresses in the 7 aluminium layers of the circumferential joint coupon (2-B-series) at 38.9 kN applied load, for rivet rows 3 and 4. The thermal stresses are not included.

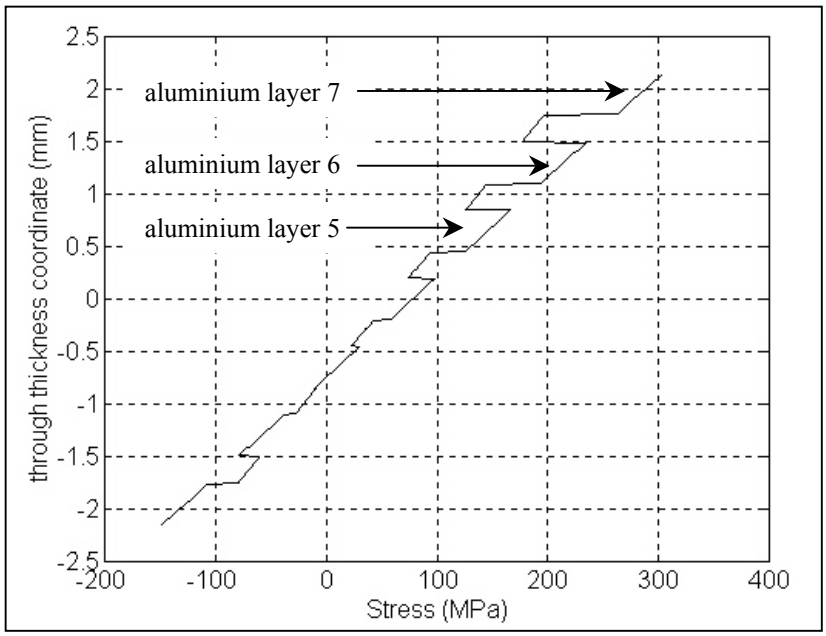

Figure 7.1.4.2. Stresses in the butt strap aluminium layers at 38.9 kN, aluminium layer 7 = mating layer

The crack lengths in the particular aluminium layers of specimen 2-B-85 butt strap are measured after 100000 fatigue cycles at 38.9 kN maximum load. The measurement results are contained in figure 7.1.4.4 for all fatigue sensitive locations of rivet row 3 and in figure 7.1.4.5 for all fatigue sensitive locations of rivet row 4 in [mm]. In rivet row 3 some cracks in layer 7 (mating layer) extend the half net section width by far. These cracks passed by, see figure 3.4.1 in chapter 3. Link-up is observed for crack no. 2R with no. 3L and for crack 1L with the specimen edge. In rivet row 4 more cracks linked up, i.e. 2R with 3L, 3R with 4L, 4R with 5L and 5R with the edge. In order to obtain an overview about the relationship between the crack lengths in the different layers at each fatigue sensitive location the maximum crack length (layer 7) is set to 100%, and the crack lengths in the other layers below are expressed as a percentage of the crack length in layer 7. These result are presented in (figures 7.1.4.6 and 7.1.4.7). Cracks which linked up in layer 7 are not considered because the crack length in % for the deeper layers would not represent a correct correlation.

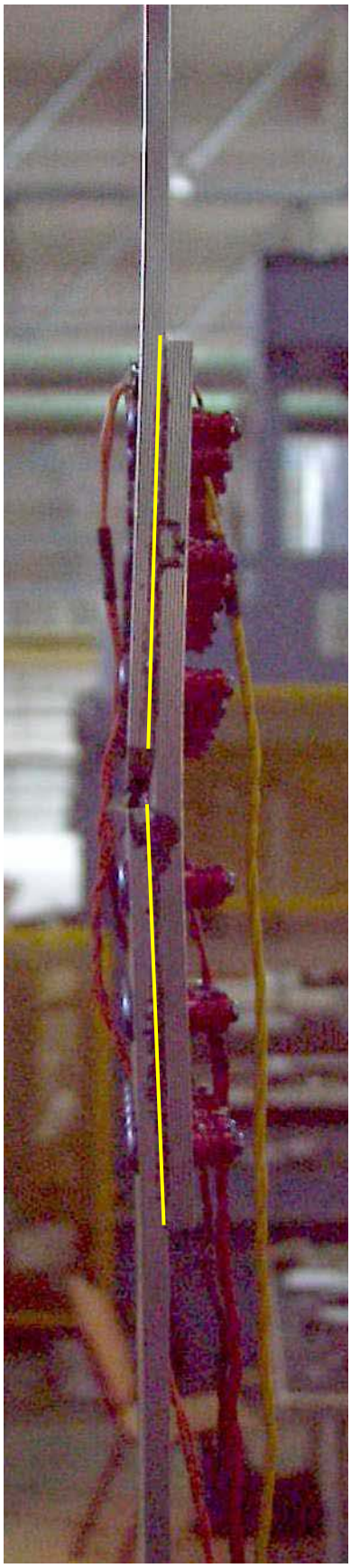

Figure 7.1.4.3. Deformation of the circumferential joint specimen at 38.9 kN load

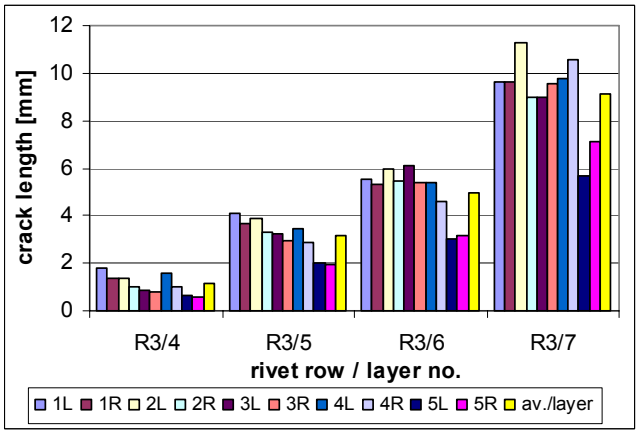

Figure 7.1.4.4. Butt strap crack length in all layers, specimen 2-B-85, rivet row 3

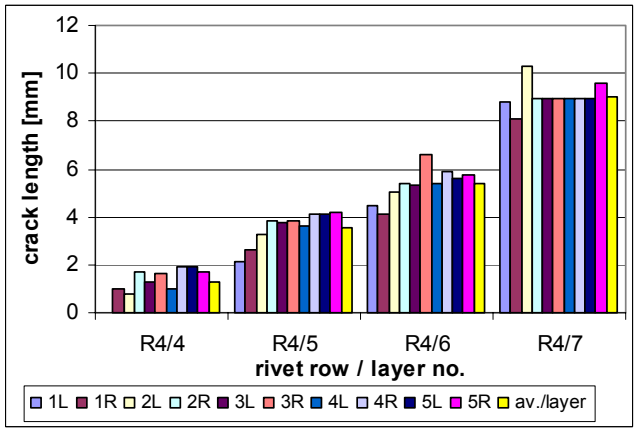

Figure 7.1.4.5. Butt strap crack length in all layers, specimen 2-B-85, rivet row 4

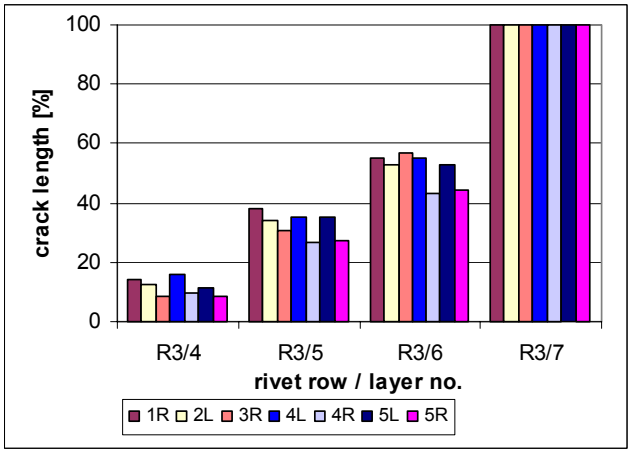

Figure 7.1.4.6. Relative butt strap crack length in all layers, specimen 2-B-85, rivet row 3

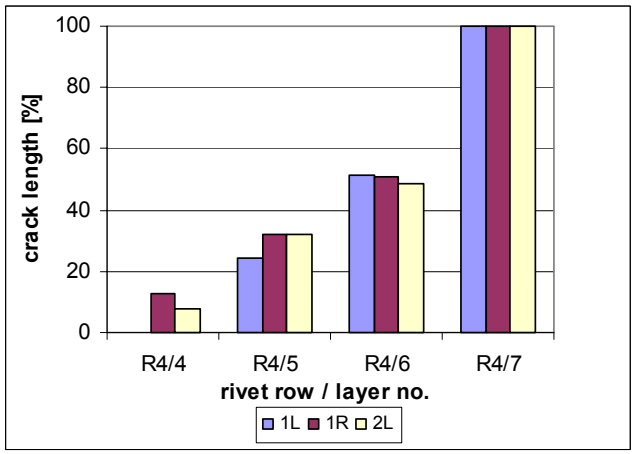

Figure 7.1.4.7. Relative butt strap crack length in all layers, specimen 2-B-85, rivet row 4

The crack lengths in the sixth aluminium layer is approximately 50%, in the fifth layer approximately 30% and in the fourth layer approximately 10% of the crack lengths measured in layer 7. With the conservative assumption of a constant crack length relation between the aluminium layers, independent from the particular crack length in layer 7, a plot of the fatigue damage rate R_D versus the average crack length in layer 7 can be established.

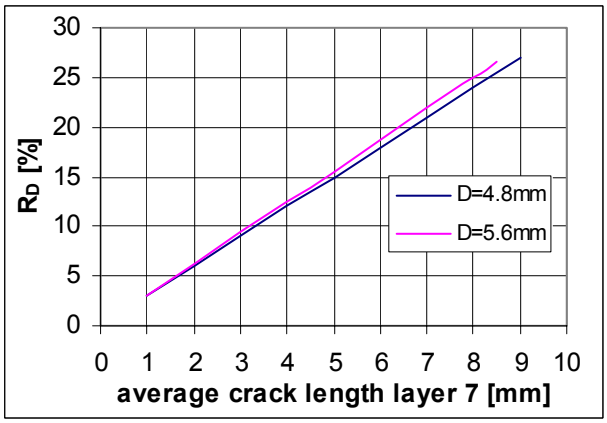

Figure 7.1.4.8. Fatigue damage rates in the butt strap related to the average crack length in the net section of the mating aluminium layer (GLARE2B-7/6-.4)

7.1.4.3 Fatigue crack propagation in repair coupon specimens

Available crack propagation data for those specimens which fatigued *around* the hole are contained in figure 7.1.4.9. The numerical data particular data can be found in table 7.1.4.1. Conservative regression lines are drawn through the data points for the later use for a full scale structure crack propagation prediction (chapter 7.2).

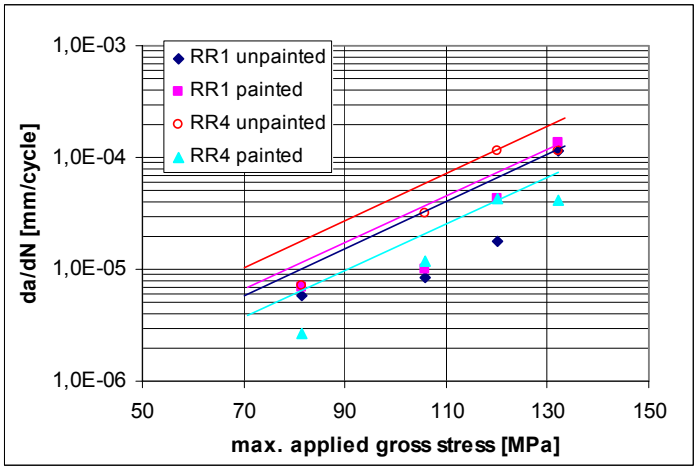

Figure 7.1.4.9. Crack propagation rates in mating layers of riveted repair coupons, with engineering (=conservative) trend lines, all specimens not exposed, all specimens fatigued with HL413VF-6 fastener

The crack propagation rates in the repair coupons are significantly lower compared to the GLARE2 butt strap for two major reasons:

a) The bending stresses are significantly lower in the 4 rivet rows because of the 3.5mm thin repair sheet.

b) The crack propagation, initiated by fretting, is limited to the mating aluminium layer (see next paragraph), the layers below are not affected and can consequently compensate the missing load path.

Figure 7.1.4.10 shows an approximation of the crack propagation rates *from* the hole edges, using crack propagation results from a single available stress level and the same slope as in the diagram above. A distinction between rivet rows 1 and 4 has not been made because the fatigue damages in specimens 2-A-44 and 2-A-46 are very similar (see tables 7.1.3.3 and 7.1.3.4).

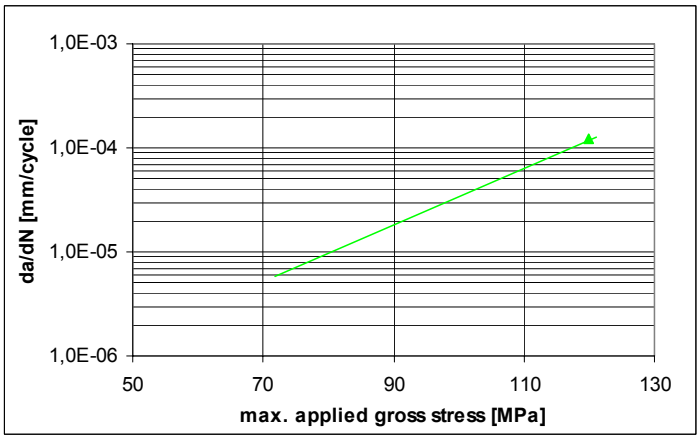

Figure 7.1.4.10. Crack propagation rates from holes of riveted repair coupons, mating aluminium layers, with engineering (=conservative) trend lines, all specimens not exposed before crack propagation tests, all specimens fatigued with ASNA2026 fastener

The crack propagation rates for the mating aluminium layers are of a similar order of magnitude for both cracks propagating around the holes and cracks propagating *from* the edges of the holes.

7.1.4.4 Crack propagation through the thickness in the repair coupon

Specimen 2-A-4 is separated into the particular sheets after fatigue and residual strength test in order to investigate the through-the-thickness crack propagation. This specimen was fatigued with HL413VF-6 fastener and cracks initiated outside the holes in the mating surface layer. Cracks were not found in the deeper aluminium layers which were not damage by fretting. The glass fiber layers provide a barrier against crack propagation through the thickness. Figure 7.1.4.11 shows the crack lengths in the mating layers of both sheets, in rivet rows 1 and 4 respectively. Figure 7.1.4.12 relates the average crack length in the mating aluminium layers (upper sheet: RR1; lower sheet: RR4) to the fatigue damage rate.

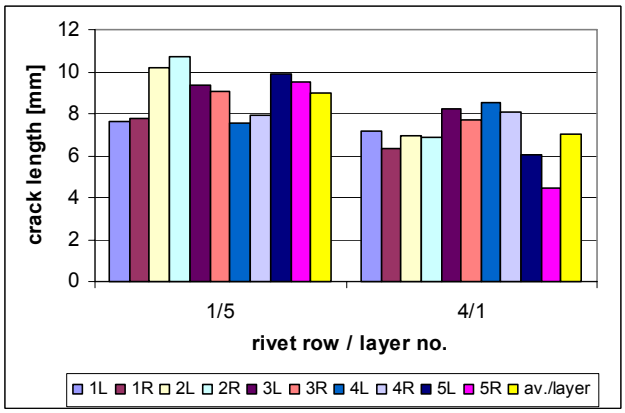

Figure 7.1.4.11. Fatigue crack lengths in mating aluminium layers of specimen 2-A-4 after 120000 cycles with Fmax.=58.8 kN. No cracks in other aluminium layers (fastener: HL413VF)

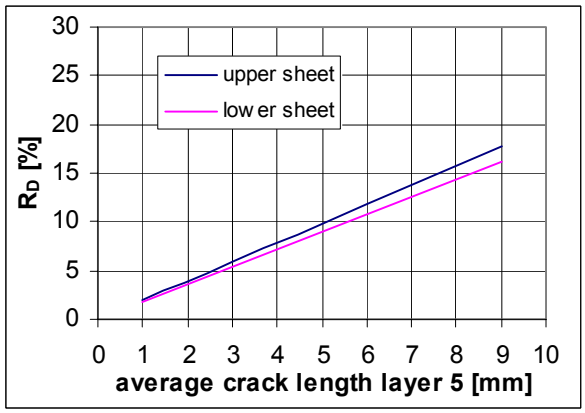

Figure 7.1.4.12. Fatigue damage rate in riveted repair sheets, related to average crack length in net section of mating aluminium layers (GLARE4A-5/4-.4, HL413VF fastener)

The fatigue crack lengths at all bore holes of specimen 2-A-46 at rivet row 1 (upper sheet) are recorded in table 7.1.3.4. The specimen belongs to the series which is fatigued with ASNA2026 fasteners and where the cracks initiated *at* the hole edges of RR1 (upper sheet) and RR4 (lower sheet). Figure 7.1.4.13 shows the crack length before the outdoor exposure and before the residual strength test for aluminium layers 2 to 5 of the upper sheet in rivet row 1. No cracks were found in aluminium layer 2. In layers 3 to 5, the latter one being the mating aluminium layer with the lower sheet, cracks are found at all ten possible locations, i.e. at both sides of all five holes in the row.

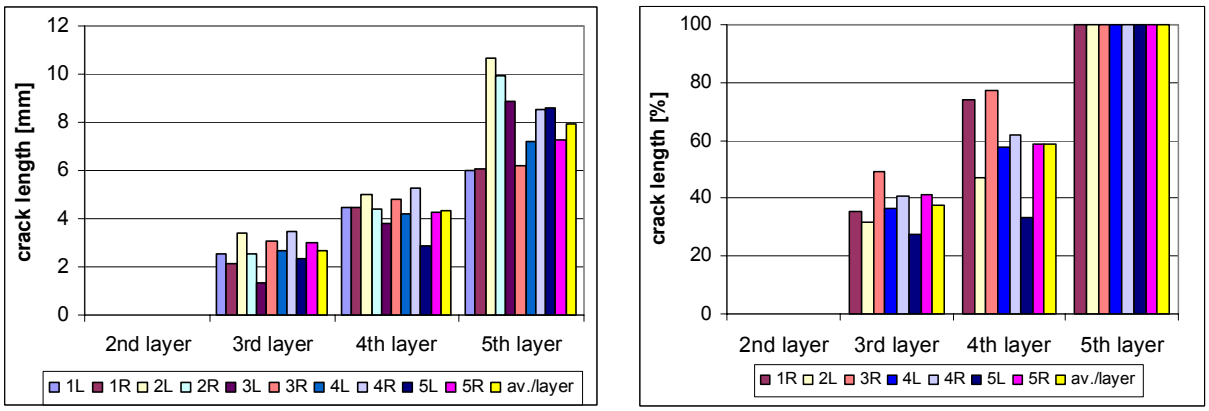

Figure 7.1.4.13. Fatigue crack lengths in specimen 2-A-46 before outdoor exposure and residual strength test, upper sheet, rivet row 1, measured values at all fatigue sensitive locations in left diagram, crack lengths in percentages from aluminium layer 5 in right diagram (fastener: ASNA2026)

The dependency between the average crack lengths of the mating upper sheet layer (5) at rivet row 1 and the fatigue damage rate R_D is given in diagram 7.1.4.14.

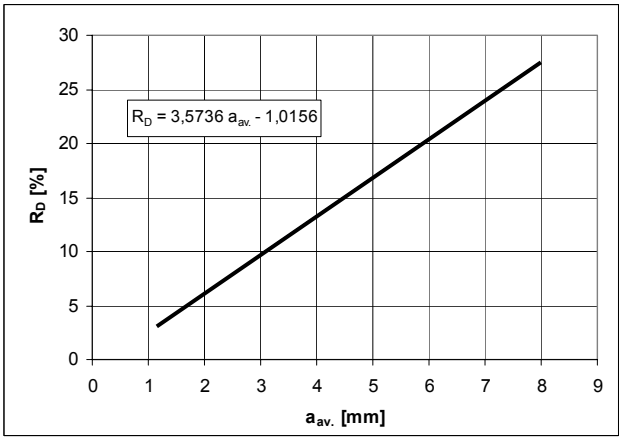

Figure 7.1.4.14. Relation between the fatigue damage rate and the average crack length of 2-A-series specimens fatigued with ASNA2026 fastener, upper sheet, RR1, aluminium layer 5

7.1.5 Miner Rule and Load spectrum factors

In this section the crack initiation life and fatigue crack growth in the circumferential joint coupon under spectrum loading is considered. It will be explored if the well-known Miner rule can be adopted for characterizing the severity of spectrum loading for this purpose. According to the Miner rule, the fatigue damage under variable-amplitude loading is characterized by:

$$D = \sum \frac{n_i}{N_i} \tag{18}$$

with n_i referring to different fatigue cycles and N_i to the corresponding fatigue life under constant amplitude loading. According to the Miner rule, fatigue failure occurs if the total damage is equal to 1. Note that the Miner rule does not consider *history effects* [27], i.e. the influence of previous load cycles on the damage increment of a particular load cycle. These effects are not discussed in detail in this paper. However, Miner values according to the relative Miner rule introduced by Schütz [26] may be useful. Schütz analysed a large amount of results of variable-amplitude tests which for spectrum loading indicated that scatter of the Miner values Sn_i/N_i at failure occurred with a mean value about 0.85. this value implies that the Miner rule then is non-conservative.

Also for GLARE constant amplitude SN data for calculation of Sn_i/N_i and fatigue test results under variable amplitude loading on the same type of specimens are necessary to calculate the Miner values which then can reveal possible spectrum effects. Variable-amplitude tests have been performed on circumferential joint specimens 2-B-103 to 2-B-105. The A340-600-EF2 stress spectrum related to strain gauge rosette 16414ABCL (see figure 3.1.4) has been used for the investigation reported in reference [24].

Calculation of stresses in aircraft longitudinal direction from strain gauge rosette 16616ABCL:

$$\sigma_{long.} = \frac{\sigma_A + \mu \times \sigma_C}{1 - \mu^2} \tag{19}$$

Note: The stress spectrum in [24] is linked to 2.4mm skin thickness, according to the panel skin thickness at the bond location of the strain gauge rosette.

A block of 1660 flights is repeatedly applied on the Airbus full scale specimen, containing different flight types, i.e. short range, medium range, long range, hard and soft flights.
For the variable spectrum tests with coupons, the test machine load spectra have been calculated under consideration of the stresses in the 2.4mm full scale specimen skin and under consideration of the specimen width. Stress ranges (double amplitudes) of 22.33 MPa have been filtered out of the spectrum (omission), in order to decrease test time. The 22.33 MPa is related to the 2.4 mm skin, related to 4.3 mm thickness (butt strap) it decreases to 12.5 MPa, which equals an applied stress amplitude of 5.6 MPa. This amplitude is far below the endurance limit of the GLARE butt strap, see figure 7.1.2.5. It may well be expected that such small cycles will no longer contribute to the fatigue damage. However, the influence of the load history on the test result, as extensively discussed by Schijve [27], remains unknown if no tests are conducted with the entire spectrum.

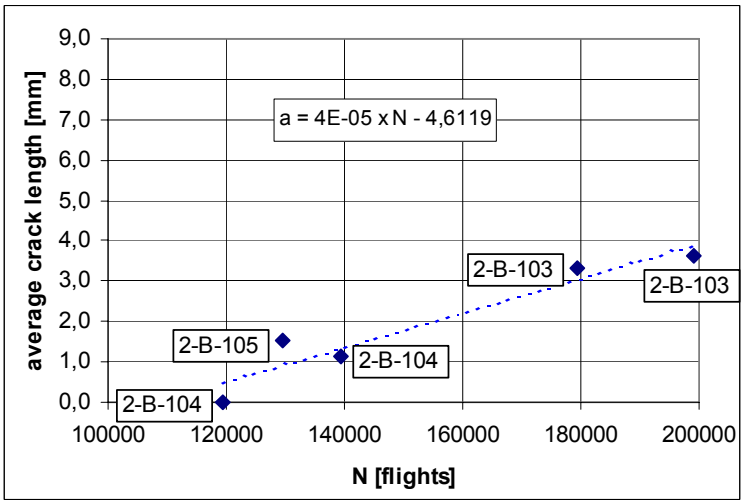

Figure 7.1.5.1. Variable amplitude crack propagation test results for circumferential joint coupon with Airbus A340-600 spectrum, butt strap mating layer, rivet rows 3 and 4, applied stress amplitude omission: 5.6 MPa

Table 7.1.5.1 contains the crack lengths measured for specimens 2-B-103 to 2-B-105. The average crack lengths and a linear regression curve are plotted in figure 7.1.5.1. The crack initiation life for both the constant amplitude and the variable amplitude results should be related to the same initiation crack length, i.e. 1.0 mm as used previously for the constant amplitude tests (Section 7.1.2).
According to the equation for the regression line in figure 7.1.5.1 the experimental crack initiation life related to the crack length 1.0 mm is:

N = (4.6119 + 1.0) / 4E-5 = 140298 flights

A calculation for crack initiation of the inner aluminium layers of a butt strap has been performed for the Airbus spectrum with the reference SN curve according to figure 7.1.2.9 with the Delft University / Airbus computer program 'FML F&DT Toolbox', release 0.93 (the same release used for the constant amplitude calculations). In view of scatter, one hundred MSD (multiple site damage) scenarios have been considered for the five critical fastener holes in the specimens. The output is recorded in Appendix J and the crack initiation lives for the MSD scenarios are shown in figure 7.1.5.2.

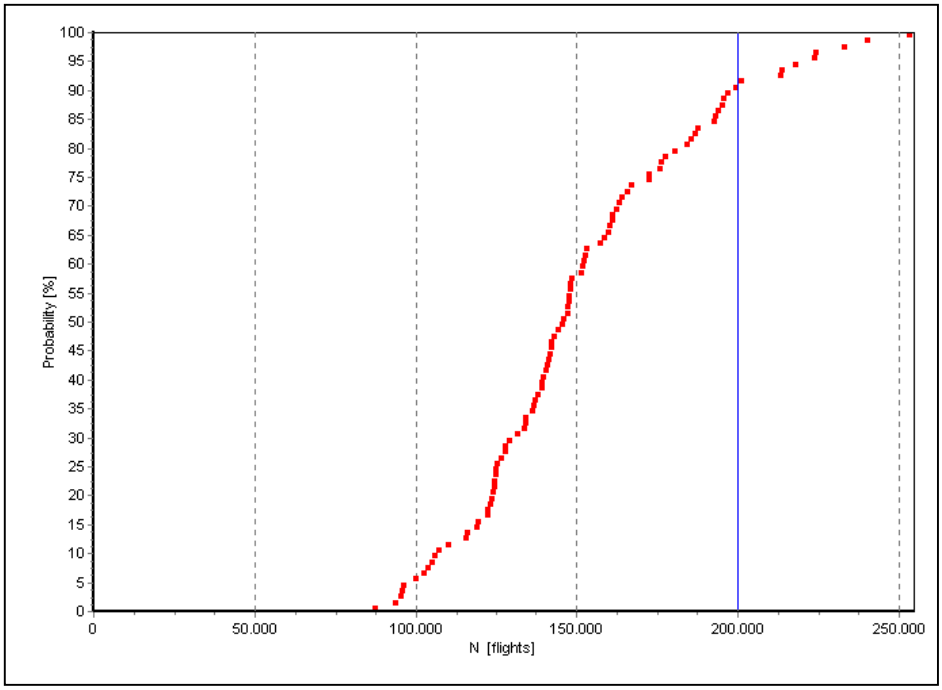

Figure 7.1.5.2. Calculated crack initiation probability for the lead crack, 100 MSD scenarios

A crack initiation life of 147000 flights is obtained for the 50% probability of failure. This result compared with the test result gives the following Miner value:

Miner value: 140298 / 147000 = 0.95

The value is close to 1, which indicates the validity for the application of damage accumulation rules for the aluminium layers of GLARE similar as for monolithic aluminium structures.

7.1.5.1 Crack initiation load spectrum factor $C_{CI(S)}$

The verification of the Miner Rule is essential for the investigation of the load spectrum factor on crack initiation. The following table contains the *applied* stresses for load case 1g + internal pressure, related to the short range (SR)-, medium range (MR)- and long range (LR) flight types:

	max. stress, t = 2.4mm	max. stress, t = 4.3mm	amplitude, R=0.1
SR flight types	78.9 MPa	44.3 MPa	19.9 MPa
MR flight types	74.3 MPa	41.5 MPa	18.6 MPa
LR flight types	75.5 MPa	42.1 MPa	18.9 MPa
average			19.1 MPa

The average stress amplitude obtained from the three different flight type groups equals 19.1 MPa. It serves as a reference stress for the determination of the spectrum factor.
The equivalent constant stress amplitude for a crack initiation life of 140298 flights (a_{av} = 1.0 mm) can be calculated with the Weibull equation contained in figure 7.1.2.5:

$$\sigma_a = 21 + \frac{231}{e^{\left(\frac{\log 140298}{3.01}\right)^{2.62}}} = 24.9MPa$$

The tested spectrum factor then becomes:

$C_{Cl(s)\ Test}$ = equivalent stress / reference stress = 24.9 MPa / 19.1 MPa = 1.30

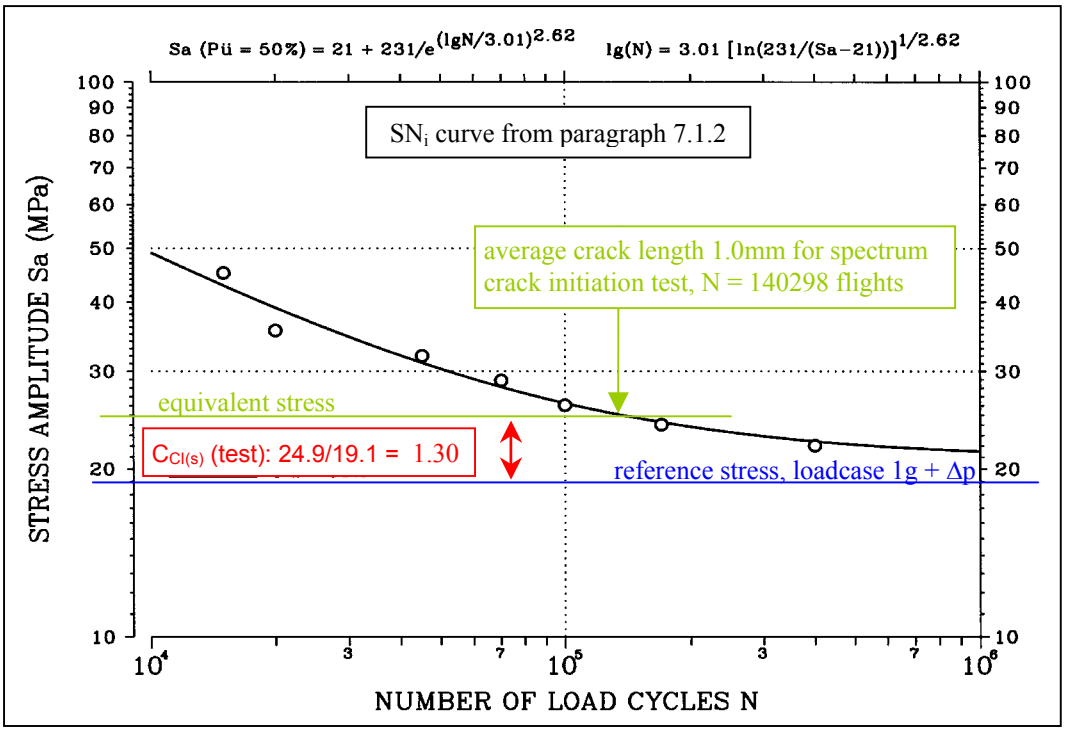

Figure 7.1.5.3. Determination of spectrum factor from tests in diagram form, applied stresses shown

A computer software which is evaluated at Airbus Deutschland, called 'cskappa' is able to calculate $C_{Cl(s)}$ - factors according to the theory provided by [14], but for more than one slope κ along a Wöhler curve. The reference point for all damage calculations is still located at N = 100000, as proposed in [14]. The associated stress level is 26 MPa amplitude, see figure 7.1.5.3.

According to reference [14] it is proposed to assume a slope of 4.5 for monolithic aluminium SN-data, if no other information is available. However, with given SN-data a more accurate calculation is possible. For the present SN-curve for the inner aluminium layer of the GLARE 2B-7/6-0.4 butt strap, the following slopes κ are determined (note: the slopes are related to applied stresses) :

for 20000 < N < 100000 : κ = 4.39
for 100000 < N < 170000 : κ = 3.72

Calculations of the spectrum factor performed with the A340-600 spectrum for different slopes:

slope κ	equivalent 1/flight stress, t=2.4mm	equiv. amplitude t=4.3mm	calculated spectrum factor = equivalent amplitude / 19.1 MPa
4.50*	88.9 MPa	22.3 MPa	1.17
3.72*	97.2 MPa	24.6 MPa	1.28
4.39/3.72#	91.4 MPa	22.9 MPa	1.20

* for all N # below/above N=100000

The *calculated* spectrum factor should be higher than the *tested* spectrum factor for a conservative prediction. This is not the case. However, when the slope is used for a prediction which is fitting best to the crack initiation life, i.e. 3.72 for the range 10000 to 170000 cycles, the spectrum factor based on test is close to the calculated one.

$$\frac{Spectrum\ \ factor\ (test)}{Spectrum\ \ factor\ (calc.)} = \frac{1.30}{1.28} = 1.02$$

The calculated spectrum factor on crack initiation is 2% un-conservative compared with the test result. Taking the small number of specimens into account as well as a conservatism due to the fact, that the SN_i-curve (constant amplitude) is generated with painted specimens and the variable amplitude tests have been performed with unpainted specimens (ref. surface condition influence, chapter 7.1.2.9), the difference is considered as neglegible.

A clear trend is observed, that the spectrum factor method can be applied for riveted GLARE joints similar as for riveted aluminium joints, using the *applied* stress level. This observation is limited to tests which are performed at constant room temperature or at variable temperature (see chapter 7.1.6). The equal slope concept (ref. chapter 7.1.2.1) is applicable for GLARE by using *applied* stress levels. The difference of the stress ratios which are *applied* on the laminate on the one hand and which are *present* in the aluminium layers of GLARE on the other hand, do not affect the reliability of the calculation method. More significant for the result is the consideration of the correct slope for the desired fatigue range.

7.1.5.2 Crack propagation load spectrum factor $C_{CP(S)}$

In the previous section it has been demonstrated that the spectrum influence on crack initiation can be calculated by application of the spectrum factor method. Consequently, provided the fatigue spectrum is known as well as a constant amplitude crack initiation SN curve for a GLARE structure, the crack initiation life under variable amplitude loading can be calculated quickly. The same investigation will be performed for a prediction of fatigue crack propagation rates in GLARE under variable load condition. The principle is illustrated in figure 7.1.5.4. With a given da/dN value obtained from variable amplitude tests, an equivalent stress level related to constant amplitude crack propagation rates is determined. The reference stress is a pre-specified value with some meaning for the spectrum, for example the 1/flight stress level. The quotient from both is the spectrum factor for crack propagation. It needs to be investigated, whether the correct crack propagation curve under *variable* load conditions can be determined by the simple addition of crack extensions which are obtained from constant amplitude data (Forman rule). Experiences made with aluminium structures have shown, that this method may be rather conservative, due to single overloads which may increase the plastic zone size in front of the crack tip and which may lead to crack retardation

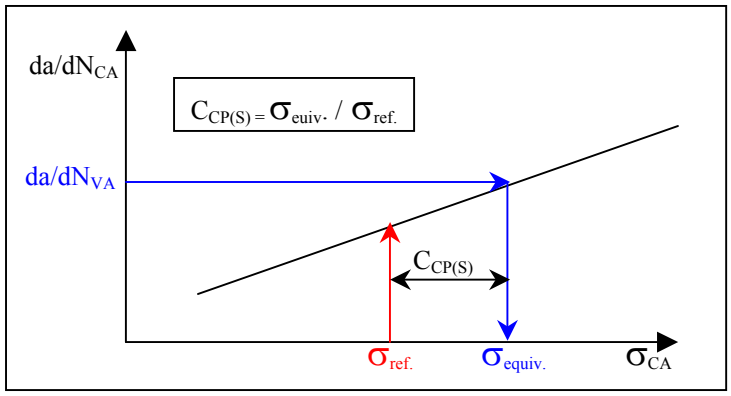

Figure 7.1.5.4. Principle to determine the spectrum factor for crack propagation

effects for the following load cycles [27]. History effects which have to be considered in the aluminium require an evaluation of the plastic zone size at any stage of the analysis.

It can be expected that the variable spectrum crack growth prediction by means of CA data is even more complicated in the GLARE laminate, due to the crack bridging effect which is added as another variable. Schijve performed some constant amplitude and variable amplitude tests with open hole specimens made of ARALL, GLARE1 and GLARE2 [36]. One crack propagation analysis compared two constant amplitude tests with one variable amplitude test, using the F-27 wing spectrum:

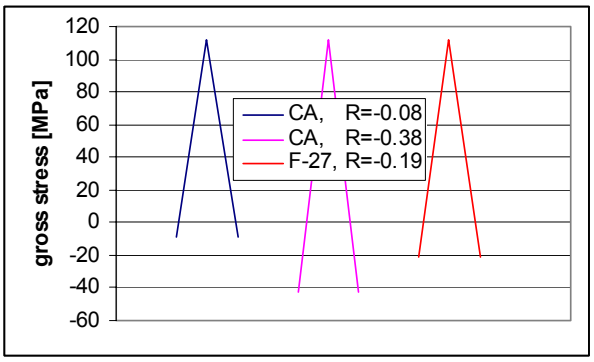

Figure 7.1.5.5. CA load cycles and the 1/flight load cycle obtained from the F-27 wing spectrum [36]

The load cycle which belongs to the F-27 spectrum is considered to occur once per flight. Other cycles involved in the spectrum should lead to additional crack propagation. From the comparison in figure 7.1.5.5 it is expected, that the crack propagation rate related to the spectrum is either the highest or that it is located between the two constant amplitude test results. In fact, the F-27 spectrum provided the *lowest* crack propagation rate of all [36]. Obviously, a history effect of other load cycles than the 1/flight cycle had a positive effect on crack growth in GLARE.

A wing load spectrum, however, is completely different compared with a pressurized fuselage spectrum. While the wing spectrum is gust and maneuver dominated with negative stresses included, the fuselage spectrum is internal pressure dominated with a limited influence of gust loads. In the following, three approximations of the spectrum influence on GLARE structures are performed:

1) The Lockheed C5 Galaxy rear upper fuselage stress spectrum

Woerden performed crack propagation tests with open hole GLARE3 specimens using the longitudinal stress spectrum of the C5 upper fuselage behind the wing [34]. The cumulative stress spectrum for 8000 flights (DSG) is plotted in figure 7.1.5.6.

The 1/flight stress, which serves as the reference stress for the spectrum, is determined with 125 MPa. The stress spectrum 'filter Elber 3' (ref. [34]) is used for a recalculation of the experimental evaluated crack propagation curve with the F&DT Toolbox, see figure 7.1.5.7. Then, constant amplitude calculations are performed with different stress levels, until the crack growth rate at constant amplitude matches the crack growth rate under the variable amplitude condition. The equivalent stress has to be increased

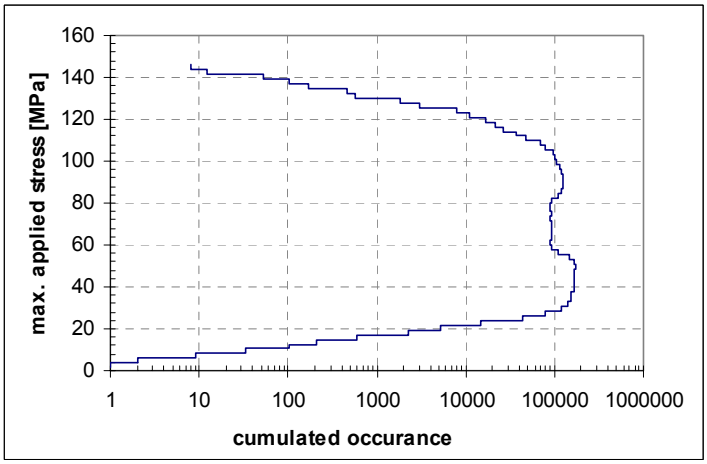

Figure 7.1.5.6. C5 Galaxy stress spectrum for 8000 flights, rear fuselage, upper shell

to a value as high as 180 MPa in order to match the variable amplitude curve.

$C_{CP(S)}$ = 180 MPa / 125 MPa = 1.44

The spectrum factor linked to the C5 spectrum is rather high for crack propagation in GLARE. For comparison, the spectrum factor is calculated for 2524 with $C_{CP(s)}$=1.0, including retardation.

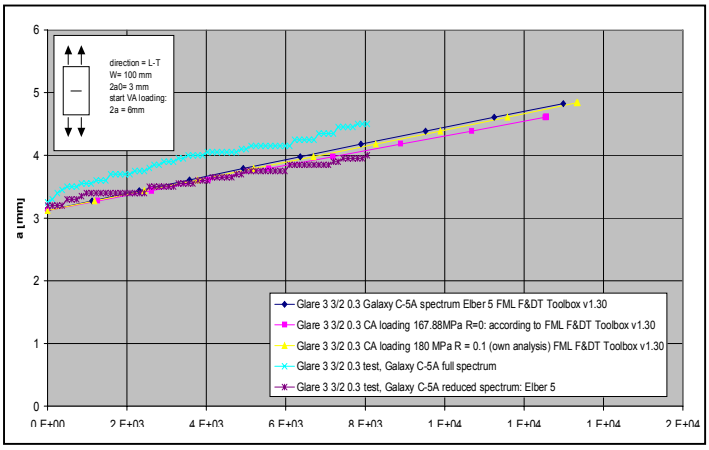

Figure 7.1.5.7. Comparison of VA test result [34], calculated VA crack propagation and CA calculation

2) A340-600, GLARE2 butt strap of experimental joint in A340-600-EF2, riveted coupon specimens

The crack propagation (average) in the mating aluminium layer of the 2-B series specimens of this research is plotted in figure 7.1.4.1. The 1/flight stress level of the A340 spectrum is 42.5 MPa (reference stress, related to 4.3mm material thickness), the obtained crack propagation rate is 4.17×10^{-5} [mm/cycle]. The information on constant amplitude crack propagation rates is limited to the values collected in figure 7.1.4.1. The factor $C_{CI(s)}$ is dependent on the curve which is used for the representation of the constant amplitude butt strap behaviour. Figure 7.1.5.8 contains the same data points as presented before, but now three curves are drawn through the available CA results. The slope of the curves is obtained from the calculations with the F&DT Toolbox:

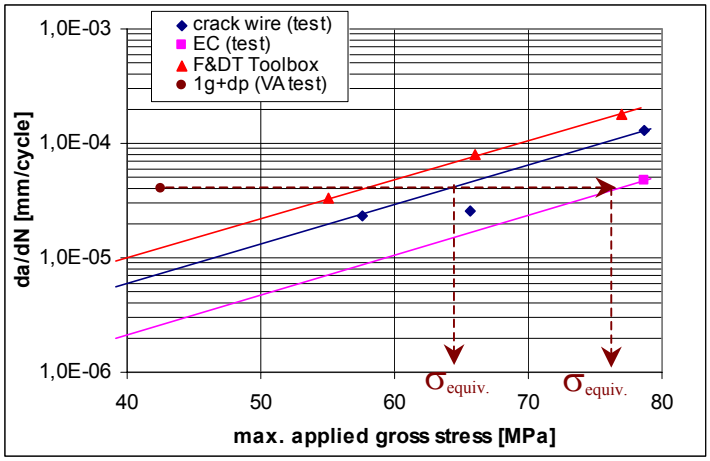

Figure 7.1.5.8. 2-B outdoor exposure specimen series, crack propagation in butt strap, mating aluminium layer, rivet row 3&4

The brown dot in figure 7.1.5.8 indicates the stress level for the 1/flight load case. Depending on the selected CA curve, it is calculated :

- if the crack wire CA test results are considered: $C_{CP(S)}$ = 64 MPa / 42.5 MPa = 1.51
- if the EC test results are considered: $C_{CP(S)}$ = 76 MPa / 42.5 MPa = 1.79

Also from this example very high $C_{CP(S)}$ factors are obtained. It is reminded, that the spectrum factor for crack initiation is 1.30, refer to the previous paragraph, and that the experience obtained from monolithic aluminium structures shows never a higher factor for crack propagation than for crack initiation.

3) The Megaliner Barrel riveted repair, GLARE4A coupons

Specimens 2-A-39 and 2-A-40 are used to evaluate a variable amplitude crack propagation curve, using the Megaliner Barrel spectrum. They are fatigued with HL413VF fastener, cracks initiated outside the holes.

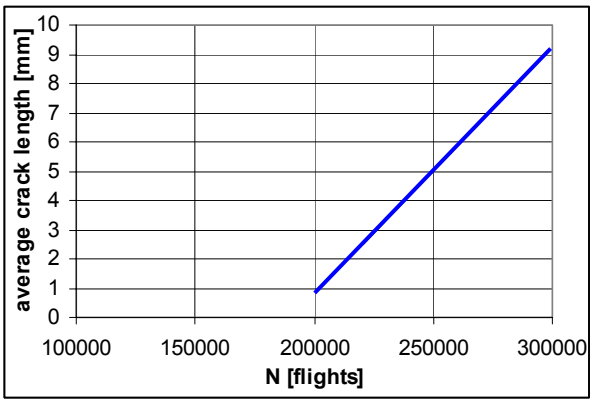

Figure 7.1.7.9. 2-A series specimens, rivet row 1, upper sheet, mating aluminium layer. Crack propagation under variable amplitude testing, cracks initiate outside the holes, HL413VF fastener

The obtained crack propagation rate for variable amplitude testing is $9x10^{-5}$ [mm/flight], see figure 7.1.7.9. The 1/flight stress level at the position of the repair at the Megaliner Barrel is 96 MPa. Under constant amplitude loading is a maximum stress level of approximately 130 MPa required in order to obtain the same crack propagation rate (R=0.1, see figure 7.1.4.9).

$C_{CP(S)}$ = 130 MPa / 96 MPa = 1.35

The three examples show relatively high spectrum factors to be considered for fatigue crack propagation in GLARE. They are higher than the spectrum factors for crack initiation and higher than calculated crack propagation spectrum factors for aluminium structures under similar conditions. Obviously there is a history effect of the fatigue delamination size to be considered. In explanation, if a relatively large delamination is present around the fatigue crack, due to the spectrum characteristic, crack propagation rates are underestimated for the following low load levels.
The phenomenological background was already discussed in chapter 6.5. Alderliesten is working on a numerical solution to take the phenomenon into account for variable amplitude fatigue crack propagation predictions [38]. It is recommended to intensify the investigation and to perform more systematic tests for verification of the final method.

For the time being it is recommended to consider an empirical factor of 1.5 for the determination of the equivalent stress for fatigue crack propagation in GLARE:

$$\sigma_{equivalent} = \sigma_{reference} \times 1.5 C_{CP(S)} \qquad (20)$$

($C_{CP(S)}$ obtained from calculation models valid for monolithic aluminium structures)

7.1.6 Variable temperature influence on riveted joint CI and CP

The influences of different *constant* temperatures on the crack initiation and crack propagation properties of elementary GLARE specimens has been investigated in chapter 6.2 and 6.3. It turned out that a high operational temperature did not affect crack initiation, but it increased the crack propagation rate significantly. Temperatures below freezing postpone the crack initiation time and decrease the crack propagation rate considerably.

A simple but conservative approximation of the temperature influence on crack propagation, based on *constant* temperature related material properties, has been discussed in chapter 6.7 for a simple PSE, i.e. a hole without significant load transfer and additional bending. It turned out that the beneficial influence of the low temperature overcompensates the detrimental influence of the high temperature for a tropical flight (high temperatures during taxi out, take off run and take off). In principle the results from elementary tests have been transferred into knock down factors and knock up factors on room temperature stresses, in order to simulate crack propagation rates measured at high and low temperatures respectively. The thermal stresses remaining after the curing cycle, the different stiffness of the resin and the fibers, and the improved material properties of 2024T3 at low temperatures have been considered. However, the different variables may cause mutually dependent variations of the material properties. This is a complex problem which can not be solved with the available specimens for the present program.

The complexity is increased for a single shear riveted joint, which experiences load transfer through the fasteners and bending of the metal sheets. Additionally, the variable fuselage skin temperature at different ground- and flight stages will not just change the curing related mean stress in GLARE, they can also lead to a different ground-air-ground cycle. Consequently, an influence on the stress *amplitude* has to be considered as well.

The influences of varying temperature in each flight is investigated experimentally with the butt strap of the circumferential joint specimens. A simplified flight load spectrum from the A340-600 rear fuselage is selected for a superposition with different temperatures. A major problem to be solved for this kind of tests is the limitation of testing time to an economically acceptable level. Therefore, several circumferential joint coupons (2-B-series) have been pre-fatigued with 60000 constant amplitude cycles at room temperature with a maximum load of 28.5 kN, stress ratio 0.1. It is the intention to fatigue these specimens close to the transition limit between crack initiation and crack propagation in order to obtain information on both, the crack initiation life and the crack propagation rates with the same specimens. Tables 7.1.6.1 and 7.1.6.2 contain the EC-measured crack lengths of the mating butt strap layer in rivet rows 3 and 4 of specimens 2-B-14 and 2-B-15 after 60000 CA cycles at room temperature. Crack initiation was detected in two to four of twenty fatigue sensitive locations. Comparative additional fatigue loading of the pre-fatigued specimens – with and without temperature variation – will indicate the possible influence of variable temperature, if any.

A longitudinal fuselage stress spectrum at the position of the circumferential joint in the A340-600 full scale specimen ‘EF2’ is selected for the investigation. The number of load peaks of this flight (type ‘MR2EYS’) is reduced to 18, in order to limit the test time. However, very short crack extensions have been observed after 75000 flights (60000 CA cycles pre-fatigue) with the initial spectrum at constant room temperature for specimen 2-B-16, see table 7.1.6.3. It was necessary to increase some stress peaks in order to create a new base line for comparison with variable temperature tests.

The increased (applied) stress spectrum is listed in table 7.1.6.4. From the GLARE family, the coefficients of thermal expansion for GLARE2 are the most deviating ones, compared with monolithic aluminium 2024T3. A test with GLARE2 material is therefore conservative and covers all other GLARE types as well. According to the method described in appendix B, the calculated curing stress which has to be considered in the aluminium layers in GLARE2 is 31 MPa for a temperature difference of –50°C (70°C material temperature), 62 MPa for –100°C (20°C material temperature) and 93 MPa for –150°C (-30°C material temperature). Figures 7.1.6.1 to 7.1.6.4 contain the measured net stresses on the mating aluminium layer, with and without variable temperature correction. The ground-air-ground (GAG) cycle is indicated between load peaks 6 and 7 for the uncorrected and between load peaks 10 and 11 for the temperature corrected stresses. Note that the peak load exceeds the yield stress, which is not unusual for a single shear GLARE joint..

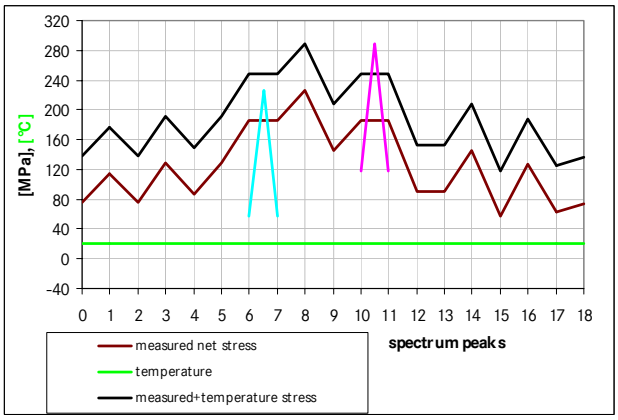

Figure 7.1.6.1. Stresses and temperature for specimen 2-B-15, tested at constant room temperature

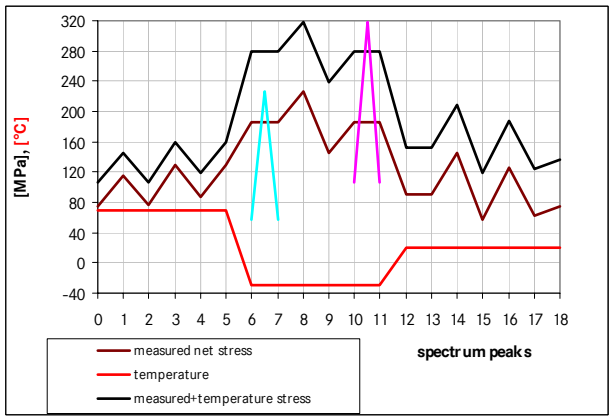

Figure 7.1.6.2. Stresses and temperature for the tropical flight type

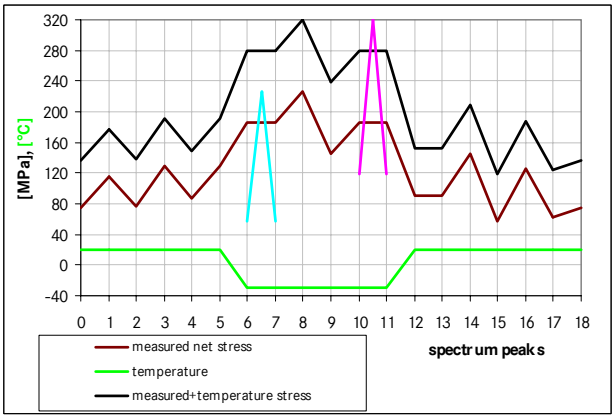

Figure 7.1.6.3. Stresses and temperature for the standard flight type

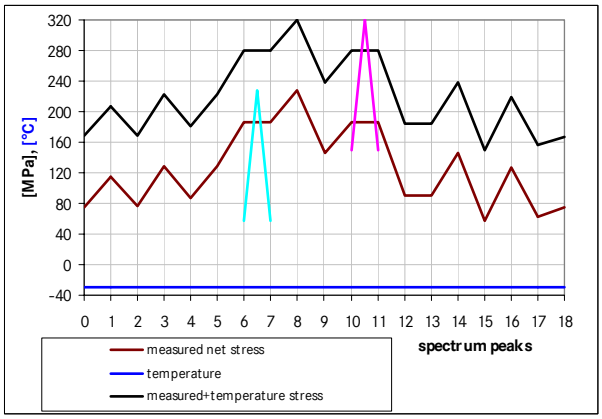

Figure 7.1.6.4. Stresses and temperature for the arctic flight type

A simple theoretical approximation of the fatigue lives can be done, using the different GAG stresses and appropriate SN-data. The latter item is solved by finding a Haigh diagram which provides approximately the crack initiation lives obtained from the constant amplitude tests (chapter 7.1.2) with the measured mating butt strap layer net stresses as input. A fitting diagram is found in the HSB for 2024T3 material and notch factor 2.5 [43].

The following table contains the calculated fatigue damages for different temperatures and 20000 flights, based on the temperature corrected ground air ground cycles, without taking the temperature related changes of the aluminium properties into account. The crack initiation life is cut by almost 50% in case of a mission mix, compared with calculated results for constant 20°C.

mission type	for GAG cycle including temperature			damage / 20000 flights	GAG cycles to failure
	σ_m [MPa]	σ_a [MPa]	damage / cycle		
tropic	213	106	5.00×10^{-5}	0.250	25800*
standard	220	100	4.00×10^{-5}	0.400	
arctic	235	85	2.50×10^{-5}	0.125	
laboratory	204	85	2.00×10^{-5}	0.400	50000

* mission mix tropic/standard/arctic: 25% / 50% / 25%

The drop of 50% in fatigue live can be completely compensated by the improved material properties at low material temperature, see chapter 6.2.

The test program with superposed mechanical- and temperature loads has a long term character, because any 10000 flights require 38 days testing time. In any case, specimens tested at constant temperature must be directly compared with specimens tested at variable temperature. The first two sets of tests are defined as follows:

Test series 1, specimens pre-fatigued with 60000 CA fatigue cycles (transition limit to crack initiation):

- specimens 2-B-14 and 2-B-17, test with variable load and variable temperature
- specimens 2-B-15 and 2-B-43, test with variable load and constant room temperature

This test series provides limited information on the influence of variable temperature on crack initiation and immediate information on the influence on crack propagation.

Test series 2, constant amplitude / variable temperature fatigue cycling:

- specimens 2-B-106, 2-B-107 and 2-B-109

The results from this test series can be compared with the SN-curve obtained from the constant amplitude tests, see figure 7.1.2.5. The influence of variable temperatures on the crack initiation live will be investigated.

A climate mission mix according to the Airbus specification [23] is specified for specimens which have to be tested with variable temperature, e.g. 2-B-14 and 2-B-26. In a sequence, 250 tropic flights are followed by 500 standard missions and 250 arctic flights.

A special test set-up is developed by EADS in order to obtain fast temperature changes [35]. The main component of the device is an electrical heater coil plate attached to a cold liquid distribution plate. Thermal contact foils between heater/cooler and test specimen allow a maximum temperature convection without restraining the specimen from deformation due to the applied structural load. The temperature of the butt strap mating aluminium layer is measured with thermo couples attached on the butt strap between the skin sheets. Because the specimen holes are filled with titanium fasteners which offer higher CTC's than GLARE it is concluded, that the required material temperature will be reached in the fasteners earlier than in the GLARE. Then, the thermal energy will spread around the boles, in all aluminium layers of the GLARE. Due to this circumstances and because the distance from the thermo couples to rivet rows 3 and 4 is just 10mm, approximately , it is assumed that the holes already obtain the desired temperature when the thermo couples measure it in the mating aluminium layer. Once the required temperature is achieved, the next sequence of structural loads is starting.

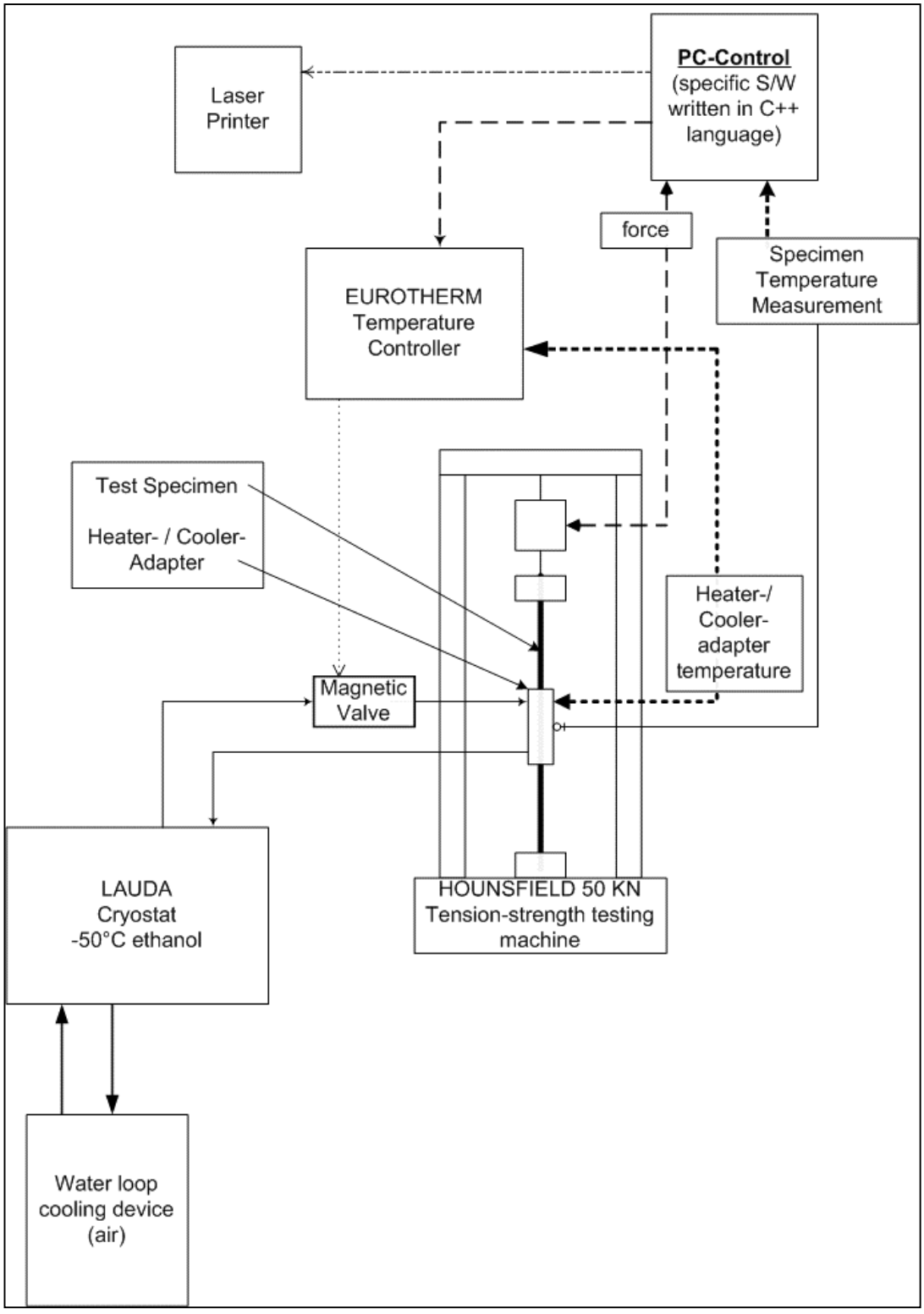

Figure 7.1.6.5 Test set-up for the variable temperature / variable load introduction [35]

Specimen 2-B-15 is the first one tested at constant room temperature (EADS Laboratories, Munich). NDT-inspections are performed in a disassembled condition after 10000, 30000 and 40000 flights by Airbus Bremen. Figure 7.1.6.6 contains the crack propagation rates of each particular crack in the mating layer of the butt strap, rivet row 3 and 4.

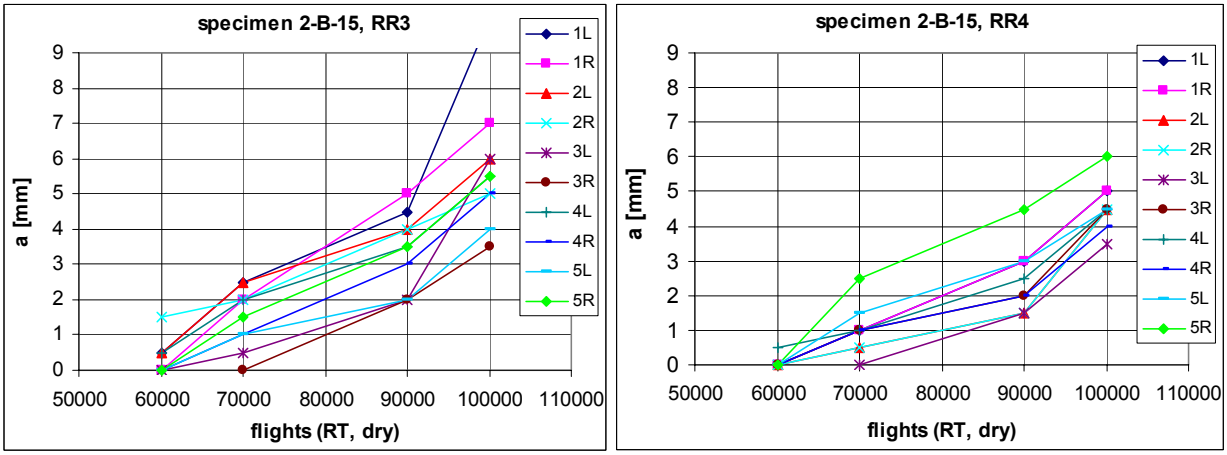

Figure 7.1.6.6. Crack lengths specimen 2-B-15, rivet rows 3 and 4 of butt strap, mating aluminium layer, tested at constant room temperature, start of variable load testing set to 60000 flights (transition limit)

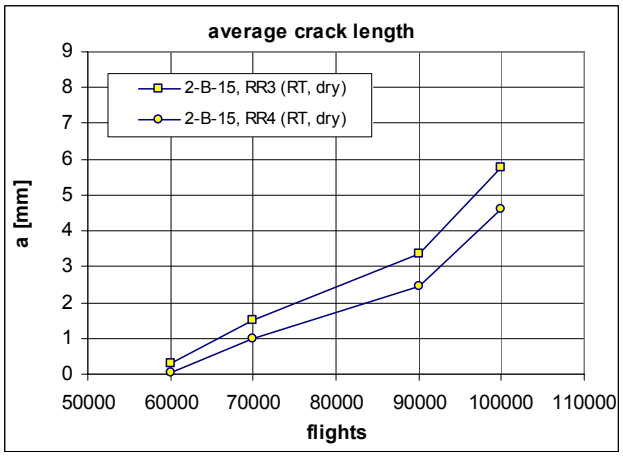

Figure 7.1.6.7. Average crack lengths of RR3 & RR4

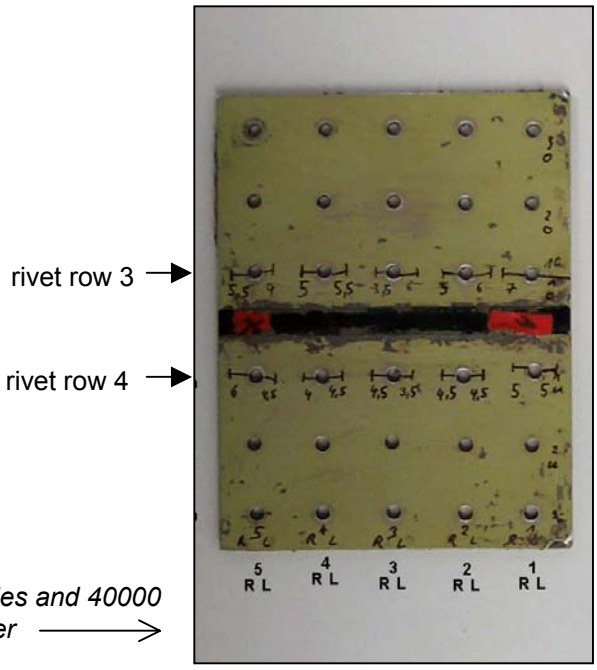

Figure 7.1.6.8. Butt strap 2-B-15 after 60000 CA cycles and 40000 flights at constant RT, view on mating aluminium layer ⟶

Figure 7.1.6.7 contains the averaged crack lengths for both rivet rows. A specific reason for the slightly increasing crack growth rates after N = 90000 flights can not be mentioned.

The same test procedure as performed with specimen 2-B-15 is repeated with specimen 2-B-14 under variable temperature conditions. Temperature and load readings are contained in attachment Q. Crack lengths measurements up to 40000 flights are shown in figure 7.1.6.9 for the particular rivet rows and in figure 7.1.6.10 for the average crack lengths in comparison to the results of specimen 2-B-15. The crack propagation rates of both specimens are quite similar (figure 7.1.6.11). From the two available specimens tested at this moment no negative influence due to variable temperature cycling on fatigue crack propagation rates can be observed. This preliminary conclusion confirms the simple approximation for an open hole presented in Section 6.7. The variable temperature test program will be continued until the end of year 2004.

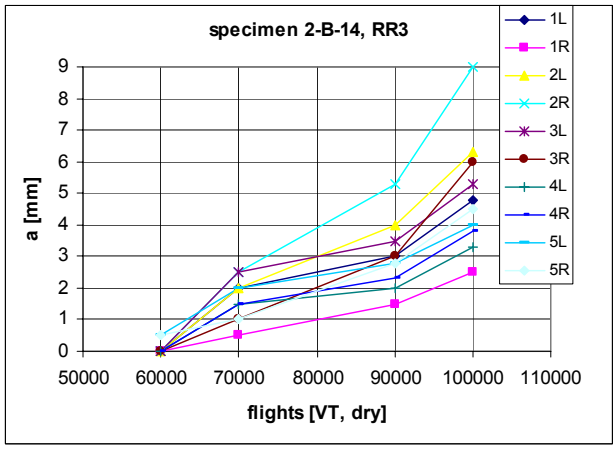

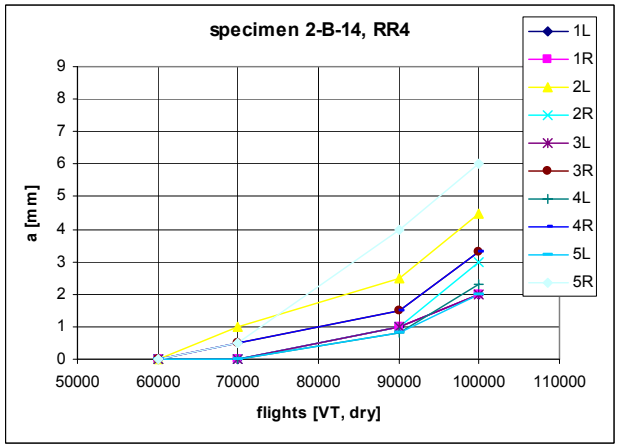

Figure 7.1.6.9. Crack lengths specimen 2-B-14, rivet rows 3 and 4 of butt strap, mating aluminium layer, tested at variable temperature, start of variable load testing set to 60000 flights (transition limit)

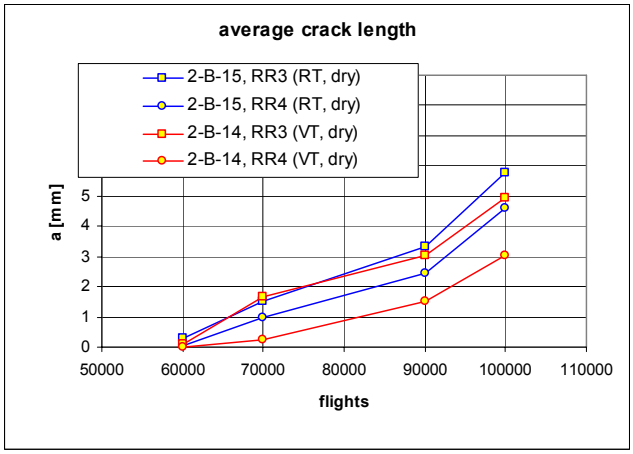

Figure 7.1.6.10. Average crack length comparison with / without variable temperature cycling

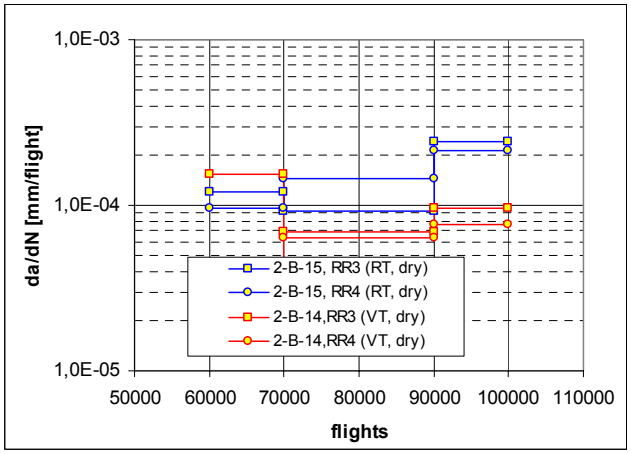

Figure 7.1.6.11. Comparison of crack propagation rates with / without variable temperature cycling

The mating aluminium layer of the butt strap from specimen 2-B-15 is removed by etching and a photo is taken from the first aluminium layer. Note that the specimen shown in figure 7.1.6.12 is turned 180 degrees compared with figure 7.1.6.8. The delamination sizes around the fatigue cracks are hard to

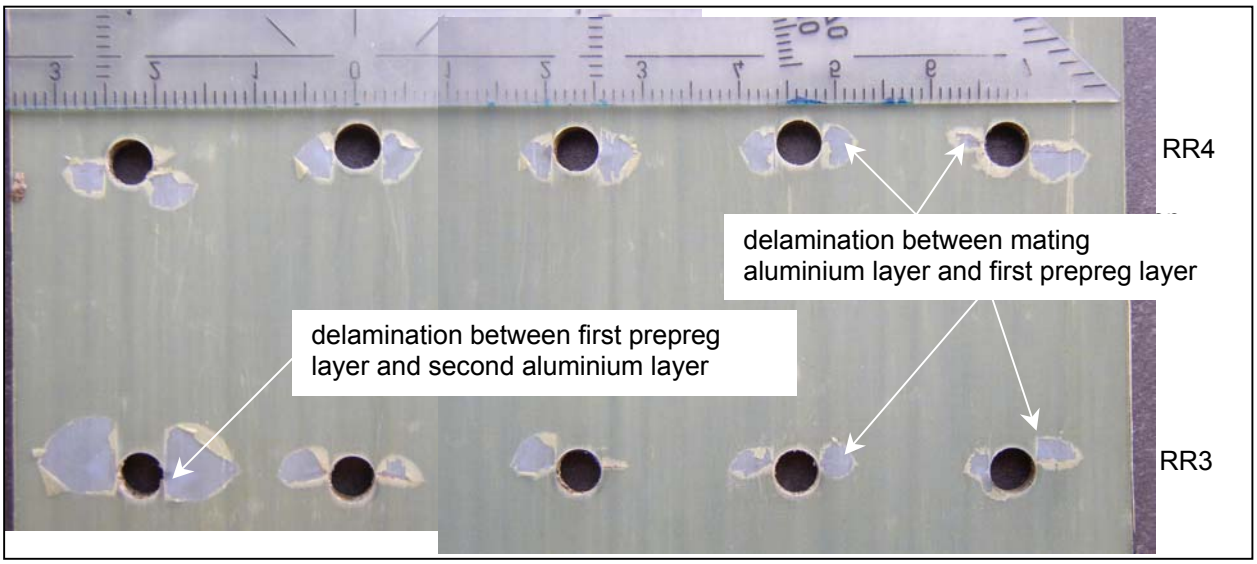

Figure 7.1.6.12. Specimen 2-B-15 after 60000 CA cycles and 40000 flights, view on the delamination shape of the butt strap between mating aluminium layer (removed) and first prepreg layer

classify, both triangular or ellipsoid shapes are observed. The fatigue cracks in the mating aluminium layer are strictly oriented perpendicular to the load direction, see figure 7.1.6.8. Surprisingly, some fatigue delaminations progressed just towards one side of the fatigue crack at some locations. It is recommended to etch the top aluminium layer of specimen 2-B-14 as well after it finishes the 40000 fatigue flights and to compare the delamination shapes with picture 7.1.6.12. Because the crack growth rates of both specimens are similar, it is expected that the delamination sizes are similar too.

Specimen 2-B-43 was fatigued to crack initiation at Delft University, exposed one year in Queensland and finally VA-fatigued at constant room temperature in the EADS laboratories Munich. Inspections are performed by Airbus Bremen as for all other specimens. The initial crack lengths at the starting point of variable amplitude fatigue cycling were slightly longer in specimen 2-B-43, compared with 2-B-15 (see figure 7.1.6.13). However, the crack propagation rates are very similar, as shown in figure 7.1.6.14.

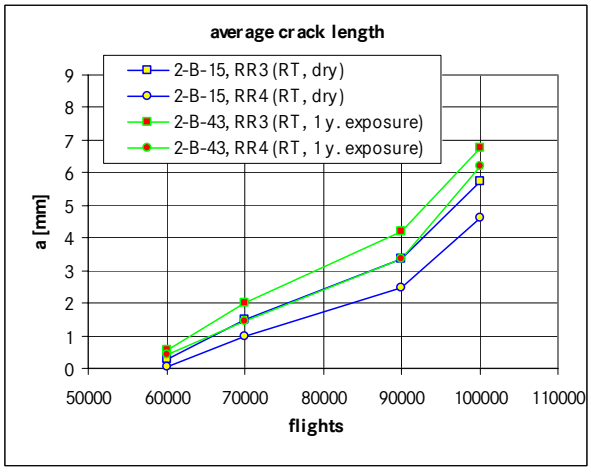

Figure 7.1.6.13. Average crack lengths for specimens 2-B-15 and 2-B-43

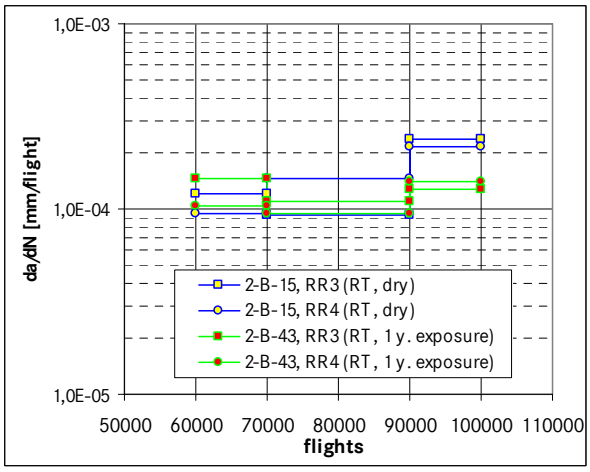

Figure 7.1.6.14. Crack propagation rates for specimens 2-B-15 and 2-B-43

After etching the mating aluminium layer of specimen 2-B-43, a similar fatigue delamination shape is found at the holes as specimen 2-B-15, which is not exposed. But the majority of delamination shapes in specimen 2-B-15 are triangular, all shapes in specimen 2-B-43 are elliptic. A change of the prepreg color from green to brown around the holes is observed, similar to specimen 3-B-37 (ref. figure 6.6.11). But different as in specimen 3-B-37, the shape of the brown area equals a circle and not an ellipse. The size of the brown colored area equals the size of the collar diameter. It is concluded that the brown area is the footprint of the chromate primer of the etched aluminium layer in the prepreg. Obviously the primer diffused into the surface of the prepreg due to the cyclic temperature change in Queensland every day. However, from the single available result it can be concluded that one year of outdoor exposure has no influence on the crack propagation rates of the tested joint.

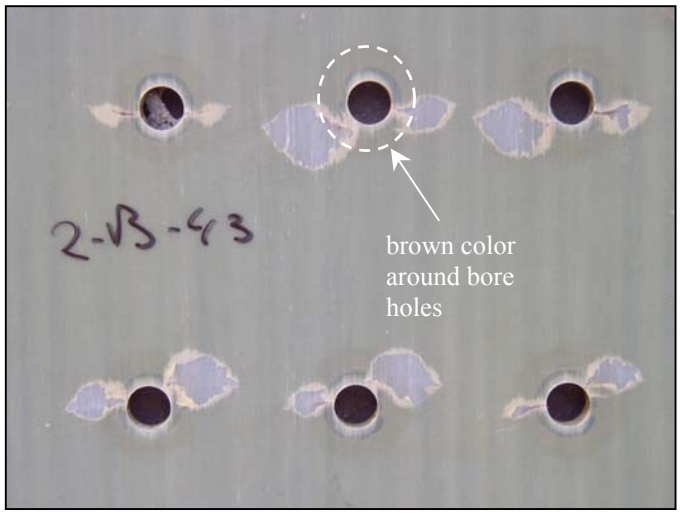

Figure 7.1.6.15. Specimen 2-B-43, prepreg condition after 1 year exposure and 40000 simulated flights at room temperature

7.1.7 Riveted joint yield strengths

It is advised in JAR/FAR 25.0305 to design aircraft structures without detrimental permanent deformations occurring at limit load. The implication of this rule for a riveted joint was already discussed on the elementary specimen basis in chapters 3.2 and 6.10. It was found, that the bearing strength leads to non-conservative yield allowables, compared with the 'rivet strength' results.

The definition of 'detrimental permanent deformation' is a matter of interpretation. At least two major aspects should be considered:

1) A permanent deformation is detrimental if movable parts (doors, air brakes, etc.) are not movable any more.
2) A permanent deformation is detrimental if the ultimate load can not be carried any longer.

The first item has obviously meaningless for riveted joints. The strength criterion 2) should be fulfilled for GLARE in both, the virgin and the fatigue damaged condition, because the ultimate failure is mainly dependent on the fiber strength. If limit load is applied and a permanent deformation is measured for a riveted joint, only a small fatigue crack extension at the holes is expected in some of the aluminium layers. The residual strength (= ultimate load capability) will be influenced insignificantly. Moreover, even an improvement is possible because the overload, introducing local plastification, may increase the following crack propagation life [34].

For riveted joints the regulation should be considered as a guideline, not as mandatory. The same applies to the rivet strength allowables according to MIL-STD-1312. Even they will not provide conservative properties if compared with a real joint. The main reason is the load transfer per rivet row, which depends on the number of rivet rows and other geometrical details. An illustration is given below. Allowable fastener loads (yield) from riveted joint coupons are compared with allowable fastener loads obtained from the rivet strength tests (ref. chapter 6.10):

7.1.7.1 **Yield strength of circumferential joint coupon specimen**

As explained in chapter 3.2, yielding is specified with 0.02 x D for each fastener. Therefore, because rivet strength specimens contain 2 fastener always, the off-set is done at 0.04 times the rivet diameter [mm]. For the circumferential joint the operator performing the displacement tests has the choice to consider either 3 rivet rows or 6 rivet rows, see figure 7.1.7.1. The displacement for the yield off-set is then either:

3 x 0.02 x 4.8mm = 0.29mm (3 rivet rows)

or

6 x 0.02 x 4.8mm = 0.58mm (6 rivet rows).

The 3 rivet row measurement is appreciated because less out of plane deformation is involved.

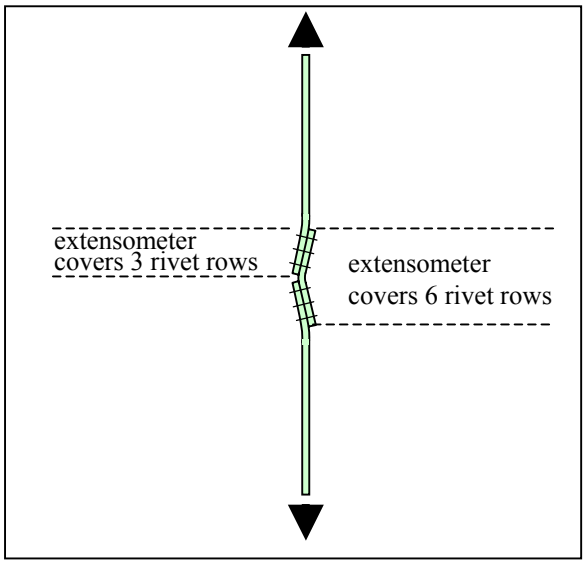

Figure 7.1.7.1

Specimen 2-B-21 belongs to the residual strength test series, it is not fatigued. A yield analysis similar as for the rivet strength specimens is performed by Airbus, for three rivet rows. With an off-set of 0.29mm a yield load of 115 kN is obtained, related to 15 fastener which transfer the load in three rivet rows.

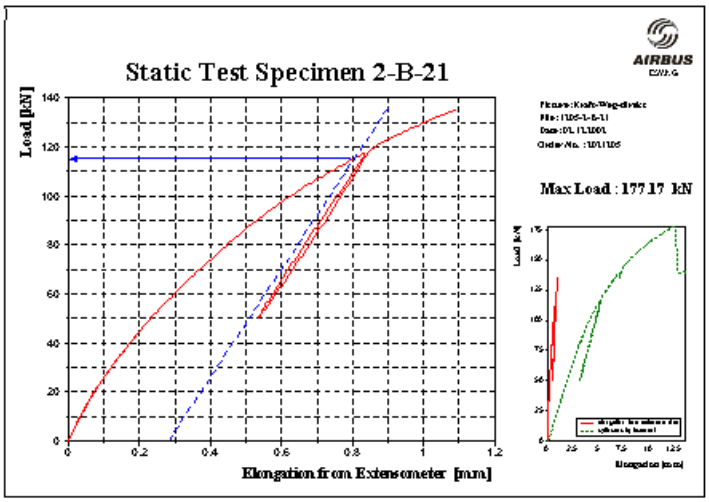

Figure 7.1.7.2. Displacement plot covering 3 rivet rows of the circumferential joint specimen 2-B-21, RT

Allowable yield load per fastener:

115000 / 15 = 7667 N

Allowable yield load per fastener obtained from rivet strength specimen (ref. chapter 6.10): 8590 N. The rivet strength specimen according to MIL-STD-1312 is overestimating the riveted joint yield strength by 12%.

In order to investigate the yield behaviour for non-virgin structures, three specimens which contain significant fatigue cracks and which have been exposed outdoors for one year are investigated in a similar way as specimen 2-B-21. However, the extensometer covers 6 rivet rows, consequently the displacement off-set which has to be considered is 0.58mm. Specimen 2-B-49 is fatigue loaded with 100000 cycles ($F_{max.}$ = 38.9 kN), specimen 2-B-50 with 200000 cycles (at least one butt strap aluminium layer completely cracked through) and specimen 2-B-51 is fatigue loaded with 400000 cycles (at least two butt strap aluminium layers completely cracked through, for details refer to chapter 7.1.8). Although the fatigue damage rates of the compared specimens are quite different, the displacement curves are identical for a wide range of load. This behaviour confirm the philosophy discussed in chapter 3, i.e. the expectation that fatigue cracks do not influence the 'fastener yield strength' if tested according to MIL-STD-1312-4.

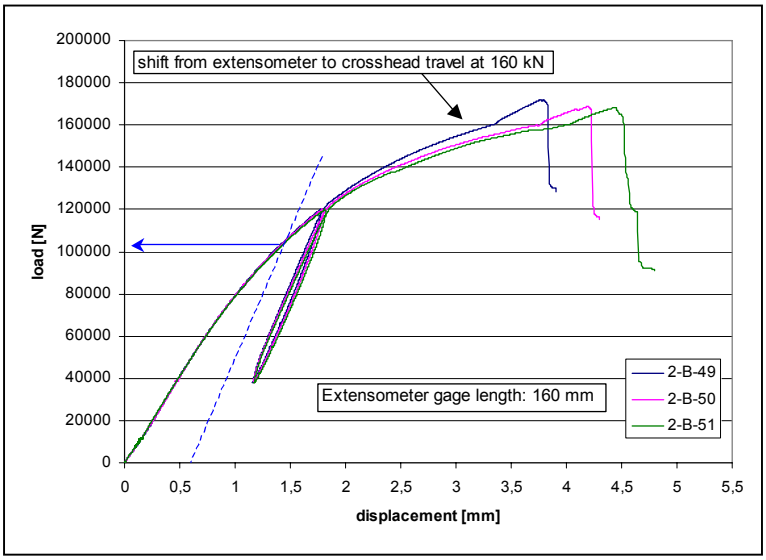

Figure 7.1.7.3. Displacement plot covering 6 rivet rows of fatigued and outdoor exposed circumferential joint specimens, fatigue damage: see chapter 7.1.8, measurement at RT

Yield load related to specimen: 105 kN.
Yield load related to one fastener: 7000 N.

It is assumed that the different determined yield loads (7667 N versus 7000 N) are dependant on the different measurement methods, i.e. the longer extensometer gap used for the measurements at specimens 2-B-49 to 2-B-51. An environmental influence is not considered at this stage of the investigation, because even 3000 hours accelerated exposure on the rivet strength specimens shows no

relevant fastener strength reduction (ref. chapter 6.10). This assumption can be verified by displacement measurements on non-fatigued circumferential joint specimens after two years and six years outdoor exposed (specimens returning in year 2004 and 2008, respectively).

7.1.7.2 Yield strength of riveted repair coupon specimen

The extensometer positioning on the riveted repair coupon is related to the overlap length of the GLARE sheets. Four rivet rows are involved with 5.6mm Hi-Lite fasteners.

Figure 7.1.7.4. Extensometer positioning on riveted repair coupon, specimen series 2-A

Displacement for yield off-set:

4 x 0.02 x 5.6mm = 0.45mm

Figures 7.1.7.5 and 7.1.7.6 show displacement plots from two specimens at different conditions, concerning fatigue damage and test temperature. However, the determined yield load is in both cases about 120 kN related to the specimen.

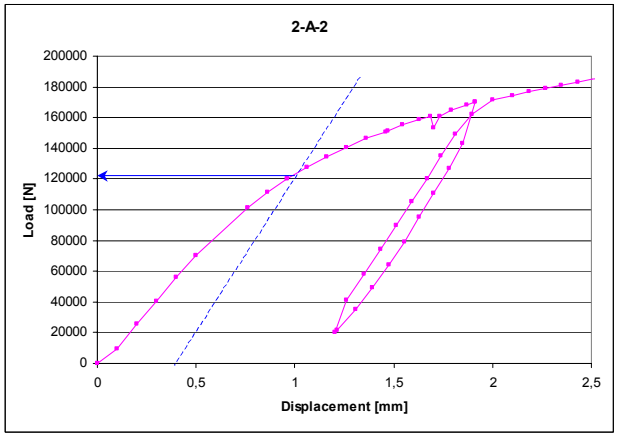

Figure 7.1.7.5. Displacement plot from specimen 2-A-2, small fatigue cracks in mating aluminium layers, displacement measured at RT

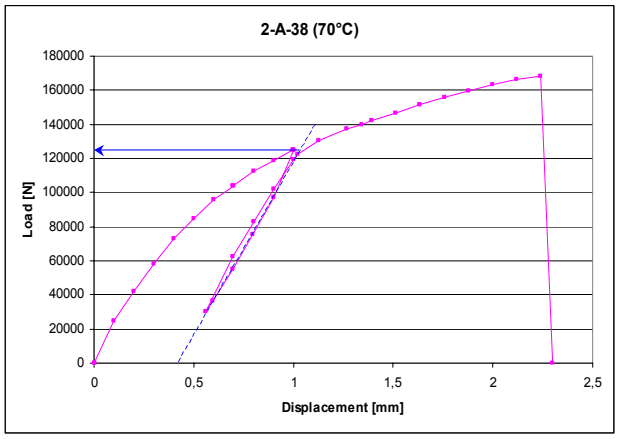

Figure 7.1.7.6. Displacement plot from specimen 2-A-38, not fatigued, displacement measured at 70°C material temperature

Because 20 fasteners are joining the two sheets, the allowable yield load per fastener equals:

120000 N / 20 = 6000 N.

Allowable yield load per fastener obtained from rivet strength specimen (ref. chapter 6.10): 7350 N. The rivet strength specimen according to MIL-STD-1312 is overestimating the riveted joint yield strength by 22.5%, if an equal load distribution between all involved fastener rows is considered. This assumption is of course not correct. It will be further discussed in frame of the joint strength justification in chapter 7.2.

No influence of the specimen temperature on fastener yield strength is observed for the joint coupon.

7.1.8 Riveted joints residual strength

7.1.8.1 Residual strength of circumferential joint coupon specimen

For most of the 2-B-series specimens severe fastener tilting and plastic deformation of the GLARE sheets is observed, followed by fastener head- or collar failure. An example of a specimen condition after residual strength testing is presented below (specimen 2-B-88, after 400000 fatigue cycles, no exposure):

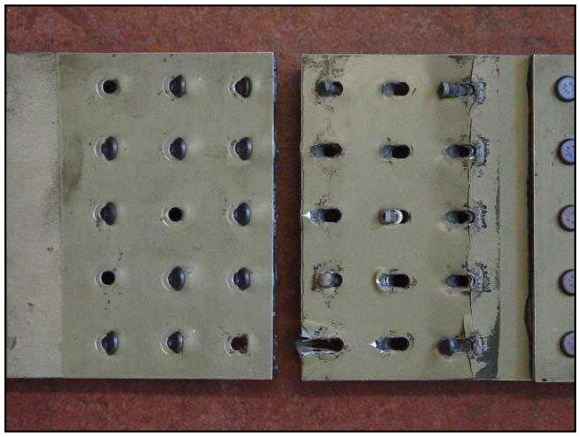

Figure 7.1.8.2a. View on specimen 2-B-88 after failure, skin sheet (left) and butt strap mating layer (right)

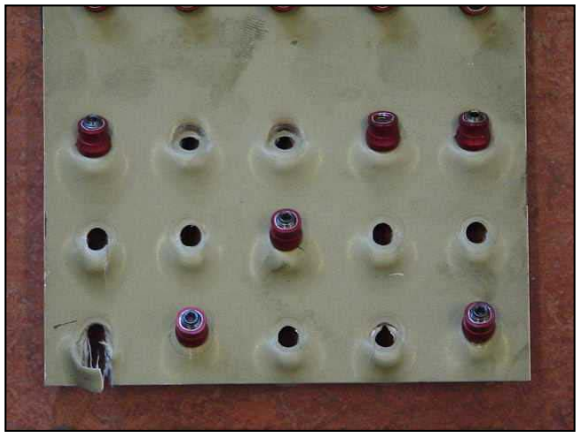

Figure 7.1.8.2b. View on specimen 2-B-88 after failure, butt strap collar side

The original 4.8mm Hi-Loks are replaced by 5.6mm Hi-Loks in specimens 2-B-24 and 2-B-92, in order to decrease the net section of the GLARE parts. Still fastener failure is the dominating failure mode, i.e. the fastener heads failed. Figure 7.1.8.3 shows the condition of specimen 2-B-24, when fastener head failure can be observed. The net section stress at failure is in the same order of magnitude as for the specimens tested with 4.8mm Hi-Loks.

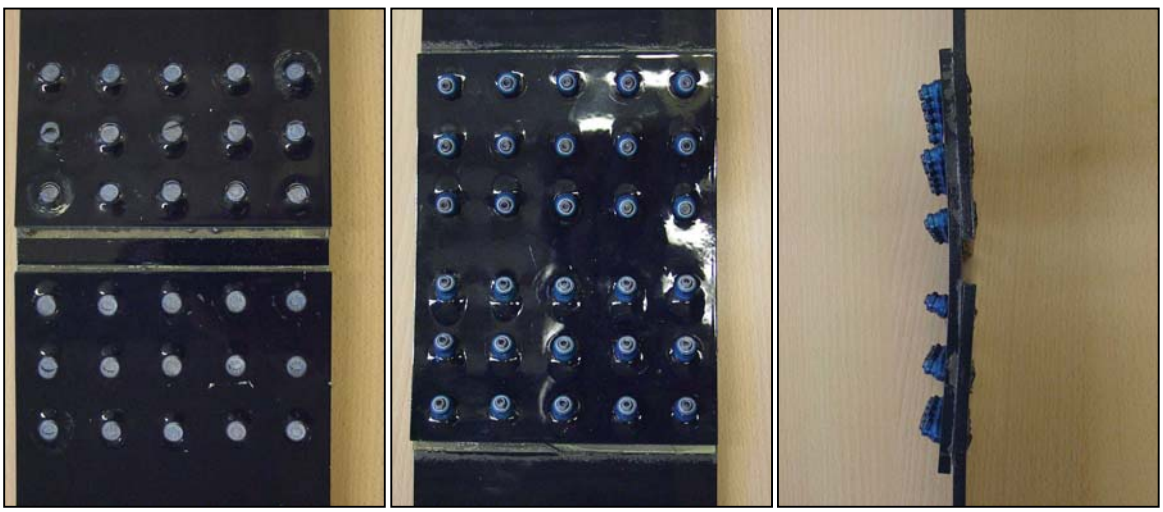

Figure 7.1.8.3: Specimen 2-B-24 with 5.6mm Hi-Loks, after the residual strength test

The following table contains the residual strength results of all tested 2-B-series specimens. The damage rates R_D were calculated with the method described in chapter 7.1.4.2, except for the specimens where the fatigue cracks linked up in the mating layer of butt strap rivet rows 3 and 4 and fatigue loading was nevertheless continued up to 400000 cycles. The fatigue damage rates for these specimens are calculated based on fractografic observations on specimens 2-B-85 (see chapter 7.1.4.2)

and 2-B-78 (see appendix R). The fatigue crack lengths of all cracks in all seven aluminium layers in rivet row 3 of its butt strap were measured.

Residual strength results 2-B-series, R_D linked to butt strap RR3 and RR4:

specimen no.	painted	N [3] [CA cycles]	$a_{av.}$ [4]	R_D [5]	failure load	gross failure stress	net failure stress
2-B-21	yes	0	0 mm	0%	177.2 kN	359 MPa	455 MPa
2-B-23	yes	0	0 mm	0%	179.1 kN	362 MPa	459 MPa
2-B-82	no	0	0 mm	0%	176.6 kN	357 MPa	453 MPa
2-B-83	no	0	0 mm	0%	178.6 kN	361 MPa	458 MPa
2-B-93	no	30000	2.19 mm	6.5%	172.7 kN	349 MPa	443 MPa
2-B-86	no	200000	7.74 mm	23.1%	170.7 kN	345 MPa	449 MPa
2-B-87	no	300000	8.98 mm	26.6%	173.7 kN	351 MPa	445 MPa
2-B-88	no	400000	link up	46,0%	186.8 kN	378 MPa	480 MPa
2-B-49 [2]	yes	100000	6.24 mm	19%	170.4 kN	345 MPa	437 MPa
2-B-76 [2]	yes	100000	6.24 mm	19%	171.8 kN	348 MPa	441 MPa
2-B-50 [2]	yes	200000	9.08 mm	27%	168.4 kN	341 MPa	433 MPa
2-B-51 [2]	yes	400000	link up	46,0%	165.4 kN	335 MPa	425 MPa
2-B-78 [2]	yes	400000	link up	46,0%	163.0 kN	330 MPa	418 MPa
2-B-24 [1]	yes	0	0 mm	0%	173.5 kN	351 MPa	466 MPa
2-B-92 [1]	no	30000	3.85 mm	12%	173.0 kN	350 MPa	465 MPa

1) Original fasteners replaced by 5.6mm Hi-Loks, type HL410V6
2) After one year accelerated exposure
3) CA load cycles at Fmax. = 38.9 kN, R=0.1
4) Average crack lengths in rivet rows 3 and 4 in butt strap mating layer
5) For RR3 and RR4, calculated (exception specimen 2-B-78: measured, see appendix R)

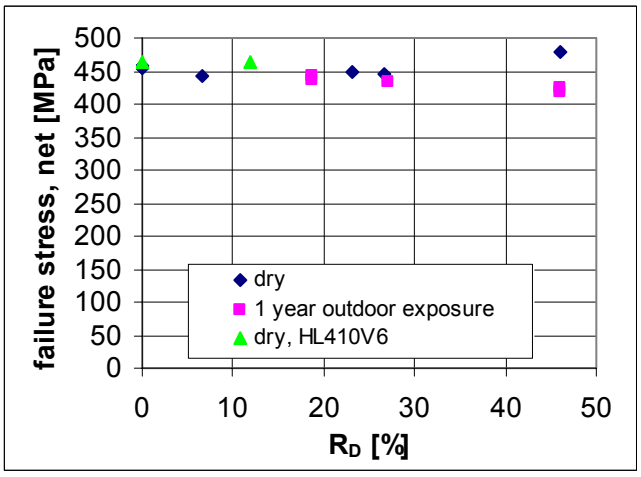

Figure 7.1.8.4: Fatigue damage rates and net residual stresses at failure for circumferential joint coupons (2-B-series), dominating failure mode: fastener failure

The residual strength parallel to the fiber orientation is almost similar for all specimens, even with high fatigue damage rates. Under consideration of the failure mode (fastener failure) the GLARE material strength should be even higher, except for specimen 2-B-78.

Specimen 2-B-78 is the only one which failed in the GLARE material, in the butt strap net section of rivet row 3. After separating the seven aluminium layers from one another by burning, markings became visible which probably indicate (significant) delamination zones (see figures 7.1.8.5 and 7.1.8.6). From the shape and size it can be concluded that the delamination markings are associated with delaminations caused by the energy release of the breaking fibers. For specimens which returned after one year exposure from Australia a ticking noise is heard by different operators at approximately 120 kN.

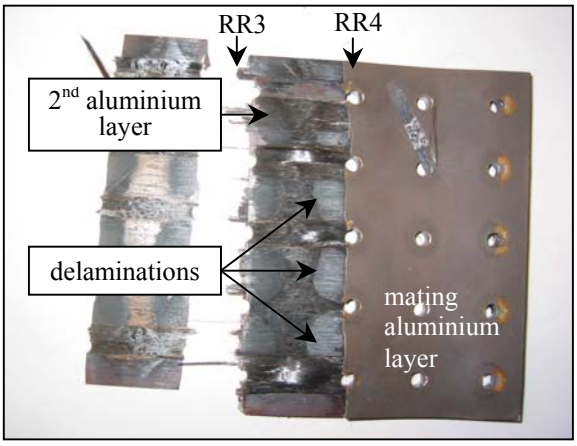

Figure 7.1.8.5. View on the butt strap of specimen 2-B-78 after burning for aluminium layer separation.

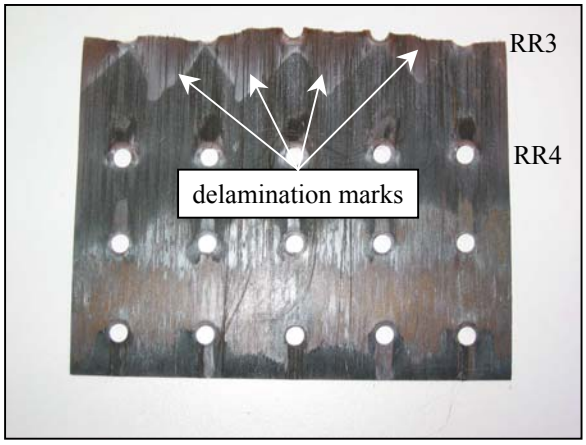

Figure 7.1.8.6. View on 1st aluminium layer of butt strap specimen 2-B-78 after burning (from previous bonding side). Delaminations visible.

Occasionally a similar noise is recorded during residual strength testing of non-exposed specimens as well, but after outdoor exposure it is much more pronounced. In order to investigate origin of the noise, specimen 2-B-77 was loaded until the same noise occured (115.5 kN). The specimen was then investigated destructively. Before the static test, the specimen had been tested until 200000 fatigue cycles (Fmax.= 38.9 kN) followed by one year outdoor exposure. Figure 7.1.8.7 shows the mating butt strap side after the static loading. The diameter of each hole in rivet rows 3 and 4, which are the highest loaded, was measured in the loading direction and transverse to the loading direction. The average calculated ovalisation (diameter in load direction divided by diameter perpendicular to load direction) is 3.4% for the holes in rivet row 3 and 4.8% for the holes in rivet row 4.

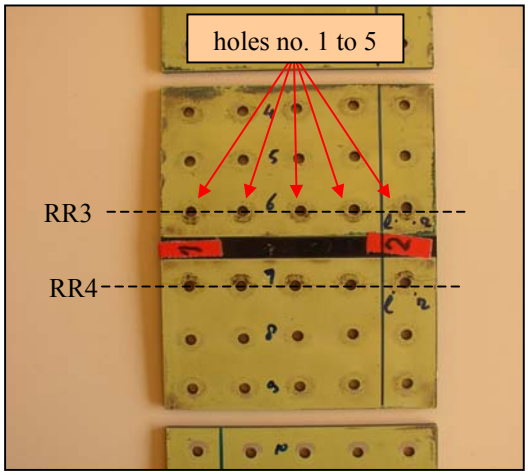

Figure 7.1.8.7. View on butt strap 2-B-77, mating surface, before destructive inspection

Cross sections just at the left and right side of two holes are made with a diamond cutter and the holes were polished until grid 5000 for observations under the Leica microscope. The investigated holes are holes no. 5 in both rivet row 3 and rivet row 4. The microscopic images are shown in figures 7.1.8.8 and 7.1.8.9.

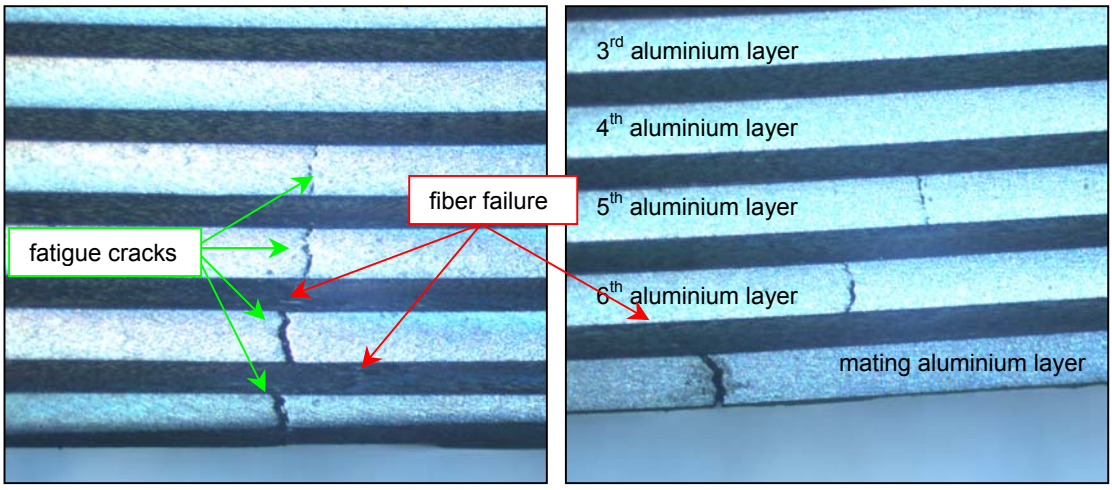

Figure 7.1.8.8. View into hole 5 (RR3), left and right side (related to load direction)

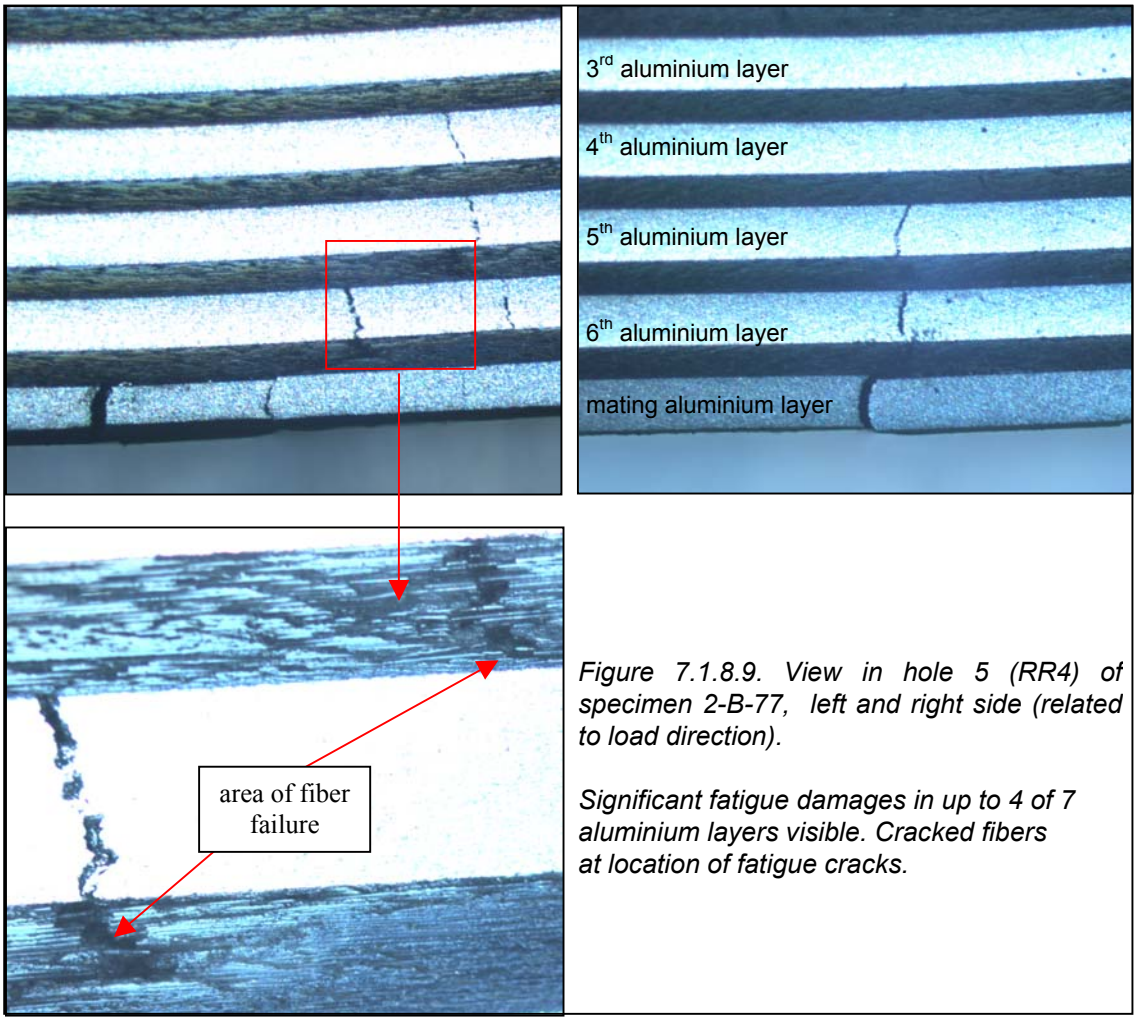

Figure 7.1.8.9. View in hole 5 (RR4) of specimen 2-B-77, left and right side (related to load direction).

Significant fatigue damages in up to 4 of 7 aluminium layers visible. Cracked fibers at location of fatigue cracks.

Failed glass fibers are found in both investigated holes, close to the fatigue cracks. From the remaining parts of the butt strap, the outer metal layer is removed by chemical etching. The results are presented in figure 7.1.8.10. Delaminations between metal and prepreg as a result of the high local bearing loads

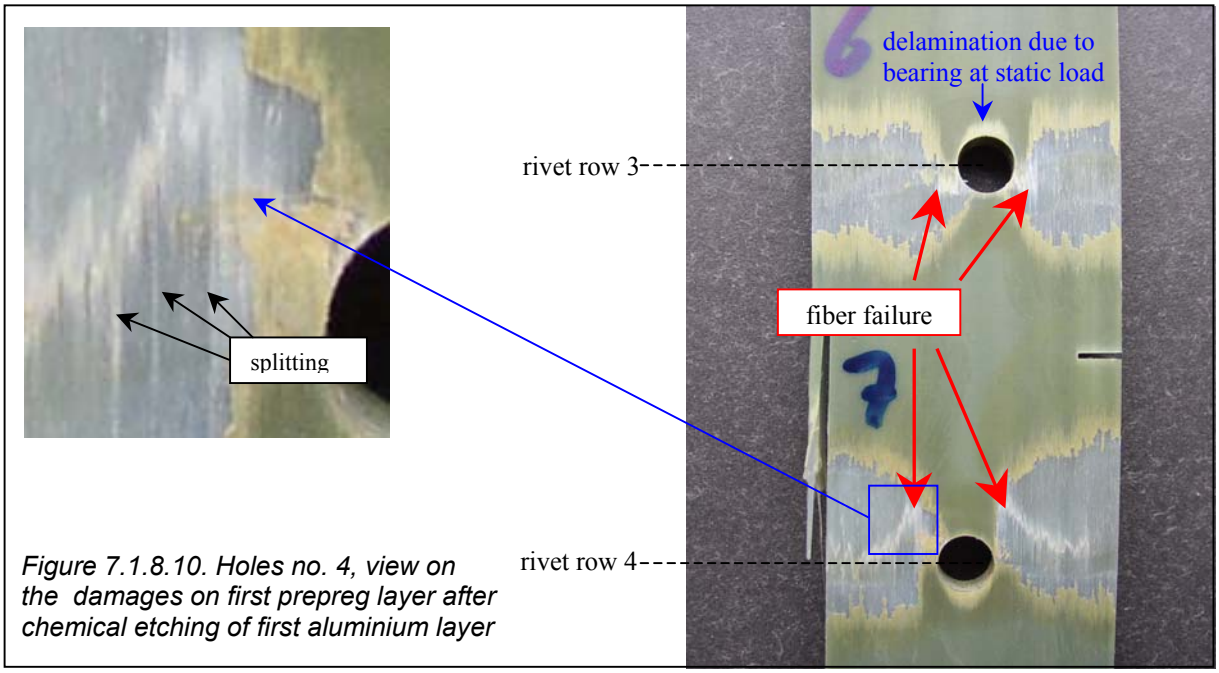

Figure 7.1.8.10. Holes no. 4, view on the damages on first prepreg layer after chemical etching of first aluminium layer

are visible at the hole edges in load direction. The net section clearly shows failed glass fibers in the area previously delaminated under the fatigue loading. The path of fiber failure is irregular. It shows failure over a significant width, apparently many times arrested by vertical splitting. This is further indicated in the magnification in figure 7.1.8.10. The fiber failure is considered to be responsible for the ticking sound heard during the residual strength tests on the specimen. The energy released by fiber failure is considered to be sufficient to generate an audible sound. The splitting behaviour, arresting fiber failure each time it occurs in the delamination area, agrees with these ticks can be heard in a test of a single specimen, rather than a single bang by failure of all fibers in a delamination area.

In figure 7.1.8.11 an overview of the remaining part of the butt strap is given. The arrows indicate the locations where fiber failure is observed. The extreme test conditions for specimens with one or more aluminium layers being completely fatigued require a review of the stress levels in the fiber prepregs. In

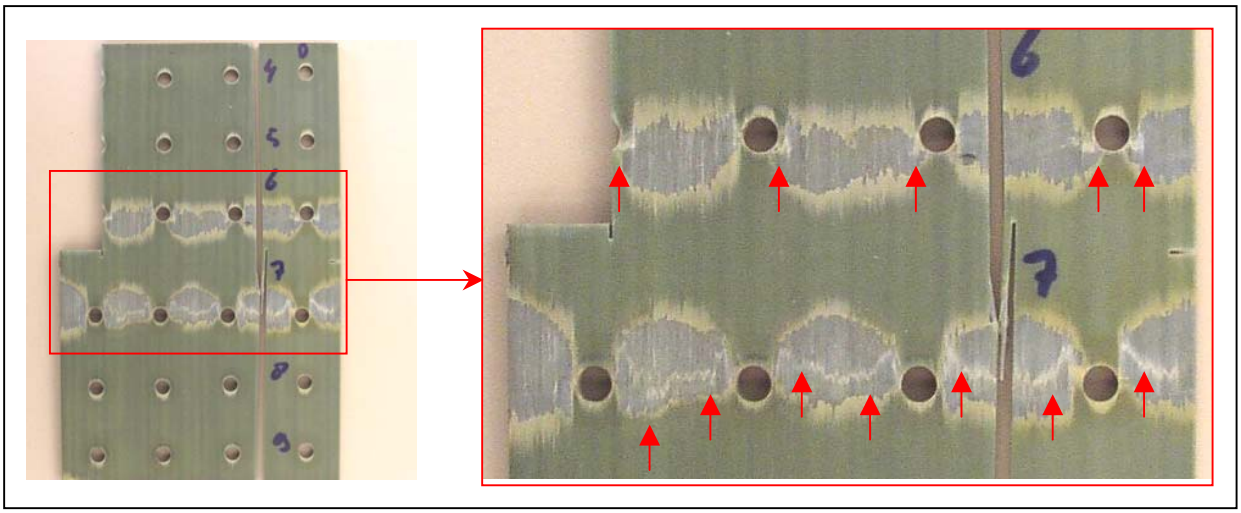

Figure 7.1.8.11. Cracked fibers in first prepreg layer of butt strap 2-B-77 after fatigue loading, outdoor exposure and static loading

fact, the stress distribution in a single shear net section with severe fatigue damages is influenced by a number of variables and requires a rather complex finite element modelling. Variables to be considered are at least the load redistribution through the laminate due to fatigue cracks, the resulting difference in structural deformation, the bearing load redistribution at the fastener / aluminium layer interfaces due to the fatigue cracks and the influence of the load redistributions on the stress concentrations around the holes. Additionally, most of the aluminium layers are loaded in the plastic region and the compression curing stress is released, if a fatigue crack is present. The problem is highly non-linear.

In order to get a first impression about the stress levels involved, a *linear* extrapolation is performed for applied loads up to 160 kN, based on strain gauge measurements on the mating butt strap aluminium layer between two holes on specimen 2-B-102 (no fatigue cracks, net section), see the blue line in figure 7.1.8.12. An approximation of the stress in the first (highest loaded) prepreg layer for a

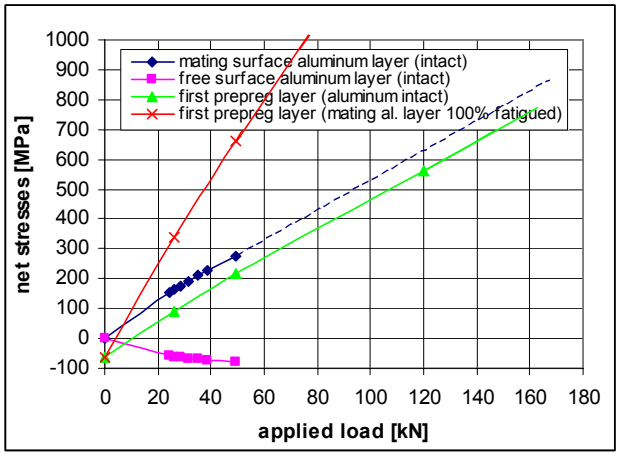

Figure 7.1.8.12. Approximation of the stresses in the butt strap rivet at rows 3 and 4, highest loaded aluminium layer and highest loaded prepreg layer, with and without fatigue cracks.

specimen without crack is based on the bending calculation discussed in chapter 7.1.4.2 and under consideration of the compression curing stress, see green line in diagram 7.1.8.12. The red line indicates the net section stress in the first fiber prepreg with the assumption, that all load from the fatigues outer aluminium layer must be carried by this fiber layer as well. With the linear approach, 1000 MPa stress in the prepreg layer is exceeded already at 75 kN applied load. At 120 kN 1500 MPa tensile stress may be reached locally in the fibers, which is the minimum failure strength according to the fiber specification. However, the yielding of the intact aluminium layers and the shift of the moment of inertia due to the lost load path (= fatigued aluminium layer) decreases the slope of the red curve. On the other hand, fatigue damages in the second aluminium layer transfer additional load in the first prepreg layer.
A non-linear finite element investigation has been performed with computer software STRESSCHECK®. A GLARE2B-7/6-.4 beam is modelled, clamped on one side and loaded with a discrete force on the other side, until 277 MPa stress is calculated for the highest loaded aluminium layer. This stress level matches the strain gauge measurement at the butt strap of specimen 2-B-102 at 50 kN applied load, see figure 7.1.8.12. The model is shown in attachment C. Subsequently, finite element knots from the concerned metal layer (277 MPa for intact specimen) and between the concerned metal layer and the adjacent prepreg layer are disconnected and the same load as before is applied on the beam. The model shall copy the butt strap net section situation under load and with one aluminium layer fatigued to link up. Stresses of more than 1200 MPa are calculated for the prepreg. A very local stress concentration is observed in the prepreg, i.e. limited to the fibers close to the (disconnected) metal layer. A high stress in all fibers which belong to the prepreg is expected. It should be recalled that yet no finite element model is available which is developed and verified for the simulation of the strains and stresses which develop in a fatigued fiber metal laminate. This is a separate task.

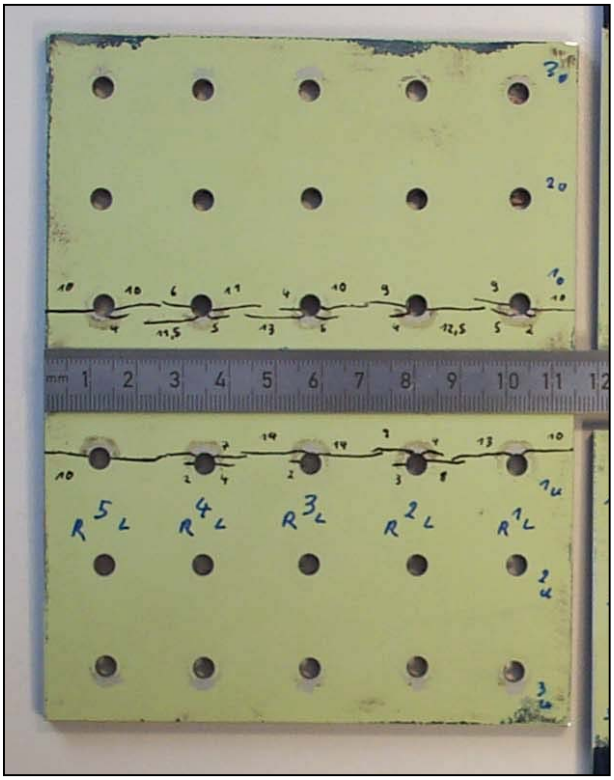

Figure 7.1.8.13. View on the mating aluminium layer of butt strap 2-B-18 after 200000 fatigue cycles and 115.5 kN static load, fatigue damages in rivet rows 3 and 4 visible

Figure 7.1.8.14. View on the first prepreg layer of the butt strap 2-B-18 after etching the mating aluminium layer, local cracked fibers in rivet rows 3 and 4 visible

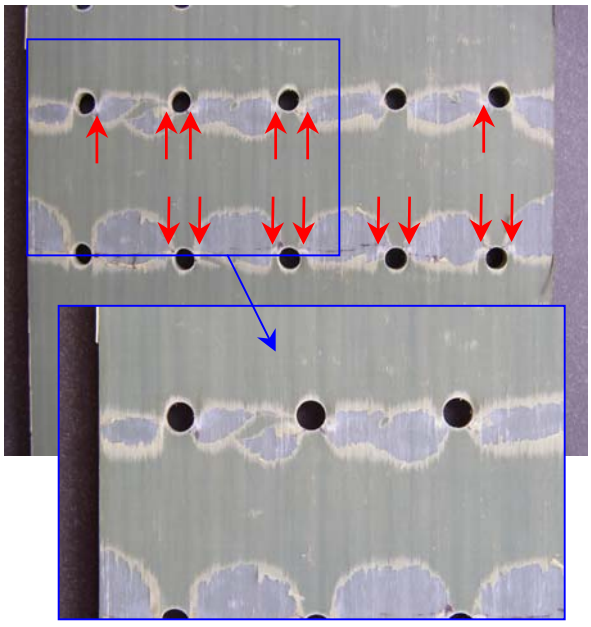

The above very simple approximations of stresses demonstrate that fiber failure must be expected under the given fatigue and load conditions of the specimen, i.e. when the ticking noise indicates a mechanical process in the structure. At the moment, it is not clear whether the one year outdoor exposure has an influence on the failure mechanism and/or the failure load, or whether a phenomenon which is present in any specimen, exposed or not, is just better audible after the outdoor exposure.
For comparison specimen 2-B-18 is fatigued similar as 2-B-77 (200000 cycles, $F_{max.}$ = 38.9 kN) and subsequently pulled to 115.5 kN, the load at which the ticking noise in specimen 2-B-77 is audible. No noise is recorded for specimen 2-B-18 during static loading. As expected, severe fatigue damages are detected in rivet rows 3 and 4 of the mating butt strap aluminium layer after disassembly of the specimen (figure 7.1.8.13). After etching this aluminium layer, cracked fibers were also found in specimen 2-B-18, although to a lower extent than in the one year outdoor exposed specimen. If the fact that just two specimens were available for this comparison is ignored (i.e. the assumption is made, that there is no scatter in the results), an influence of the one year outdoor exposure on the stress level at which fibers fail in a fatigued specimen under static load must be considered. As discussed above, a final conclusion concerning the influence of this behaviour on residual strength of GLARE is not yet possible because the 2-B series specimens fail by fastener damage.

The butt strap condition was also investigated for non-fatigued specimens. Specimen 2-B-97 is loaded up to 120kN, i.e. the load where ticking noises are heared in the heavily fatigued specimens. Specimen 2-B-98 was loaded up to 170 kN, close to the fastener failure load. The pictures in figure 7.1.8.15 show the butt strap mating aluminium layers. No particular damage is visible for specimen 2-B-97. Specimen 2-B-98 shows bearing damages and hole deformations in all rivet rows. Even fretting marks are visible around several holes from just a single applied load.
The mating aluminium layer of both butt straps were etched away and pictures were taken from the first prepreg layer, the one which experiences the highest tensile load. Small bearing damages are visible at all holes from specimen 2-B-97 and large bearing damages are observed at all holes of specimen 2-B-98, see pictures 7.1.8.16. The bearing loads destroy the prepreg locally in compression, i.e. due to fiber buckling. A magnification of 6 holes from specimen 2-B-98 is shown in picture 7.1.8.17. Fiber splitting is clearly visible for the locations where the shear loads between the fibers are maximal, tangential to the holes in load direction. The dotted boxes in picture 7.1.8.17 mark shallow areas in the net section, where fiber splitting starts.

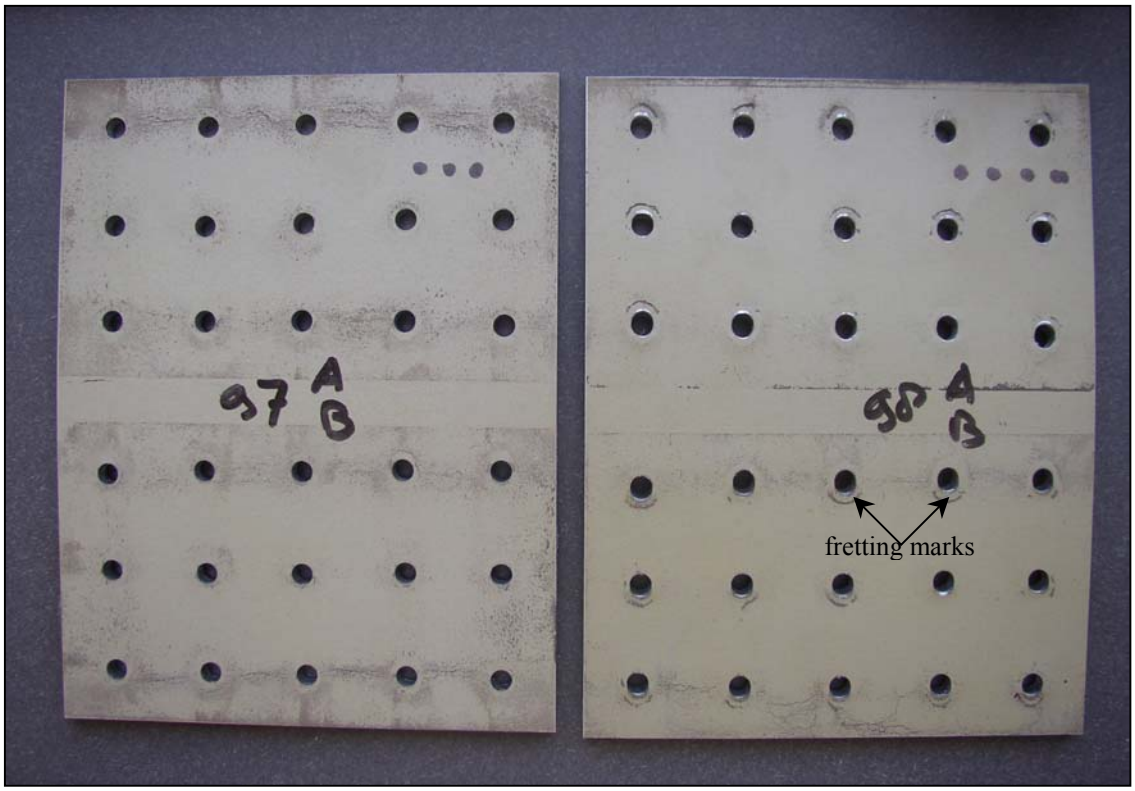

Figure 7.1.8.15. View on the butt strap mating layers of specimens 2-B-97 and 2-B-98 after static load

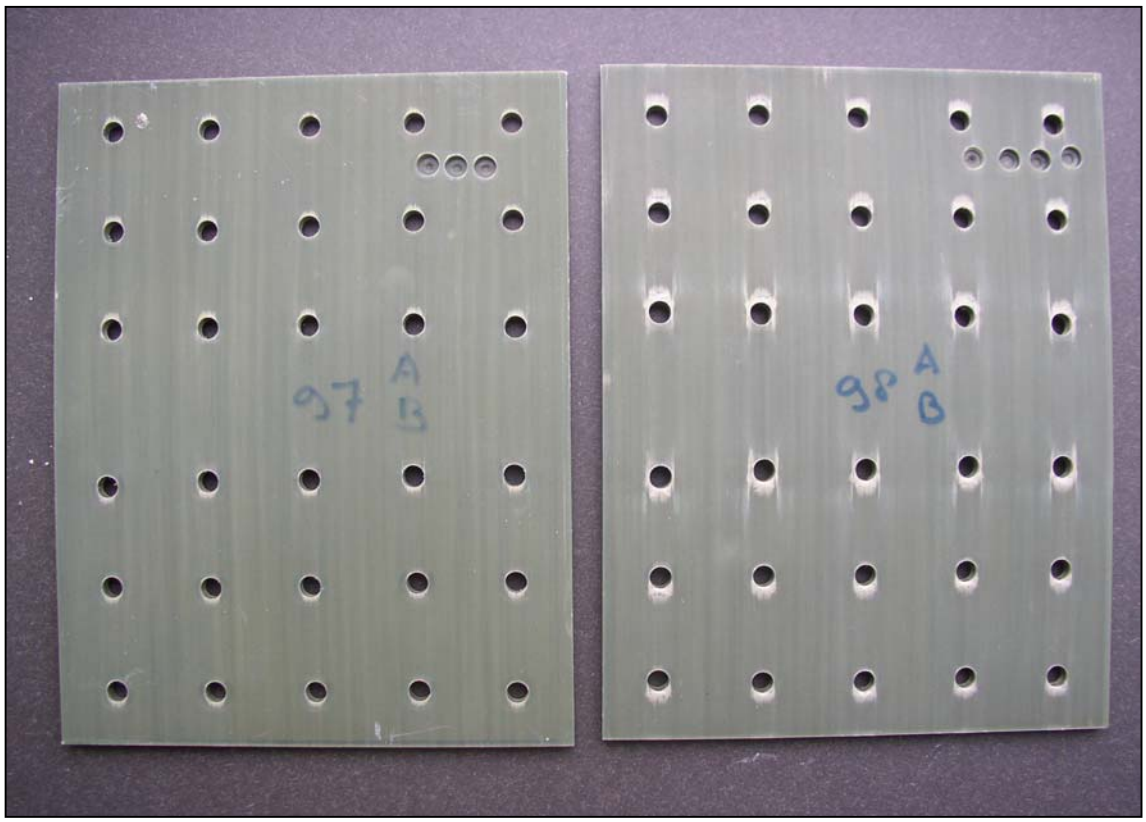

Figure 7.1.8.16. View on the first prepreg layers of specimens 2-B-97 and 2-B-98 butt straps after etching of the mating aluminium layers, specimen 2-B-97 loaded to 120 kN, specimen 2-B-98 loaded to 170kN

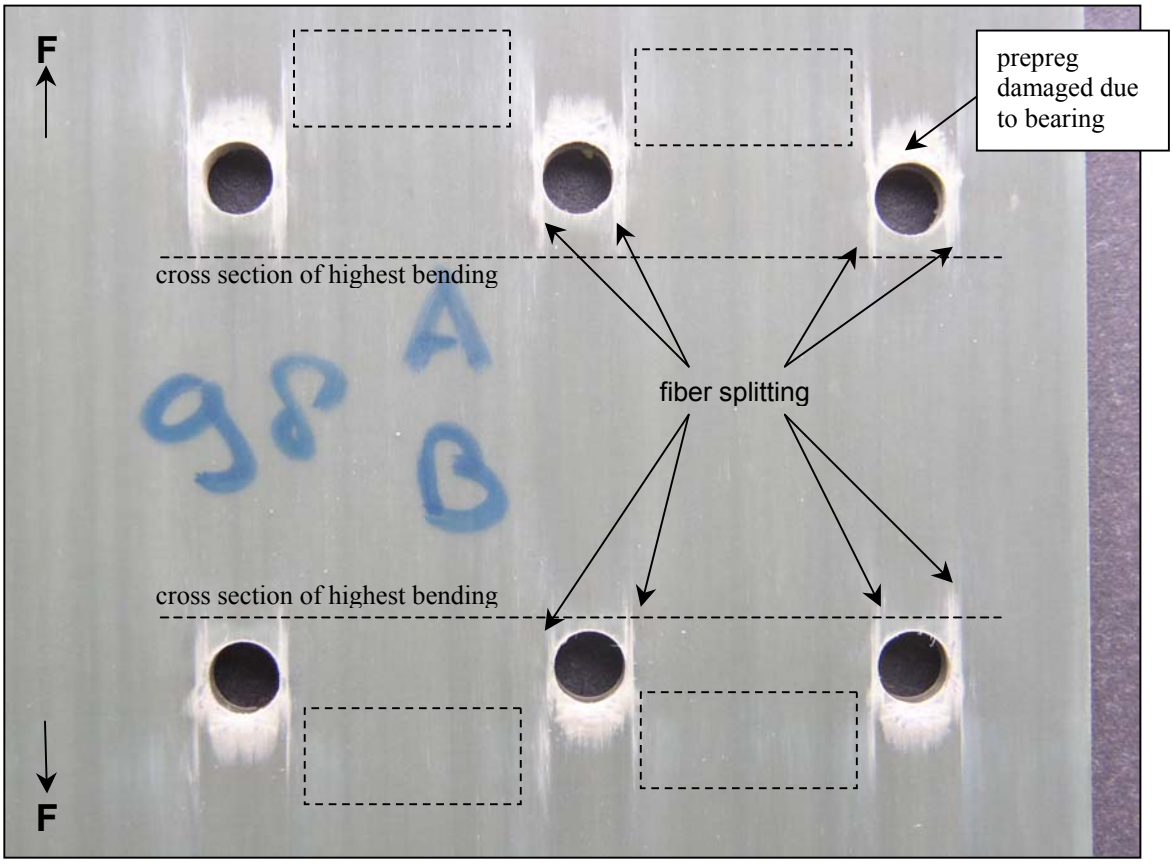

Figure 7.1.8.17. Specimen 2-B.98, magnification of part of picture 7.1.8.16, view on fiber prepreg

The circumferential joint which is investigated in this thesis is not net section failure critical. Therefore, the information about possible ageing influences on the GLARE residual strength is limited. However, a blunt notch critical butt joint is designed by the author [32] and investigated in frame of the GLARE Technology Program. Single-strap butt joint specimens were made with a GLARE3 skin and GLARE2 butt strap. These specimens were fatigue tested until different damage ratios, and afterwards exposed in an an environmental chamber 0, 1500 and 3000 hours respectively. Finally, residual strength tests were performed at room temperature. The results are presented in reference [33]. All specimens failed in the skin parts, as expected. Note, that the specimens are exposed with the fatigue cracks already being present. Figure 7.1.8.18 shows residual strength results.

A considerable influence on residual strength due to *accelerated* ageing is observed. For example at fatigue damage rate 20%, a strength reduction of 10% (mean value) is observed due to the 1500 hour accelerated aging treatment. Unfortunately, a high scatter of the results occurred after 1500 hours exposure. In fact, the data points obtained after both 1500 hours and 3000 hours ageing appears to belong to the same population. This observation matches with the results of the systematic single open hole investigation discussed in chapter 6.8. Because the weight gain investigation reported in chapter 5 of this thesis was not yet available when the program of reference [32] was defined, no 500 hour exposure is involved.

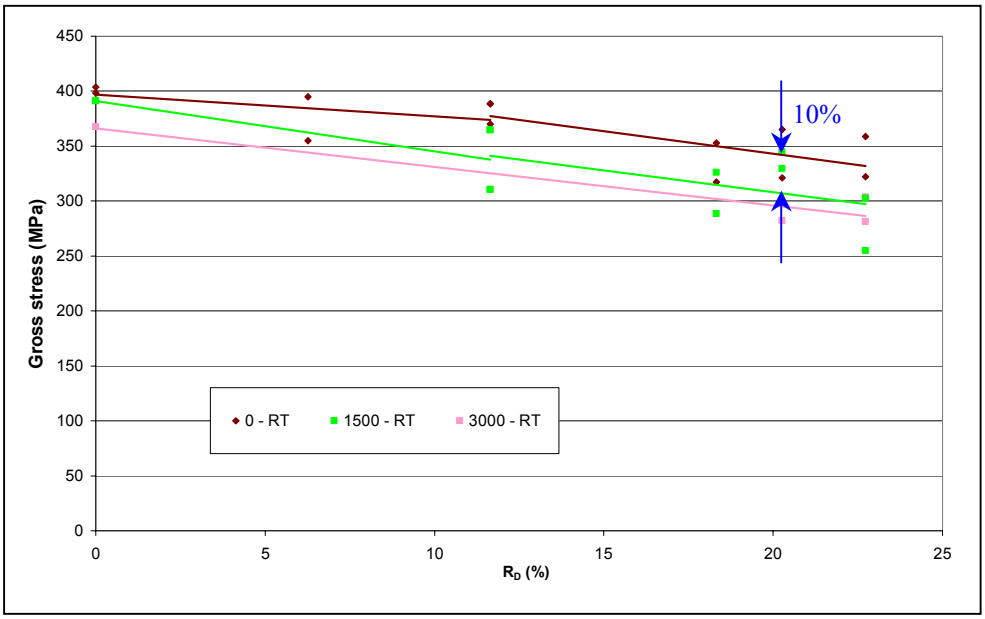

Figure 7.1.8.18. Systematic residual strength investigation at room temperature for a blunt notch critical circumferential joint, accelerated ageing 1500h and 3000h in an 70°C/85%RH environment [33].

7.1.8.2 Residual strength of riveted repair coupon specimen

The riveted repair coupons specimens are designed to fail in the net section. They fail without exception in the highest loaded rivet row of the upper GLARE4A sheet, on the countersunk side (RR1, see pictures 7.1.8.19 to 7.1.8.21). In the Megaliner Barrel Repair it would be a failure of the inner rivet row of the repair patch. Although fatigue cracks initiated outside the hole in the non-exposed specimens, they fail under static tensile load in the net section.

Note that this failure location is not expected in a full scale structure. In a full scale structure the first rivet row in the panel skin, looking from the undisturbed far field, is considered to be the critical item (RR4, lower sheet). Although not influenced by the countersunk, it is the weakest cross section of the repair, because the cross section at rivet row 1 is supported by the overlapping skin and doubler on the left and right edges. This item is further discussed in chapter 10.

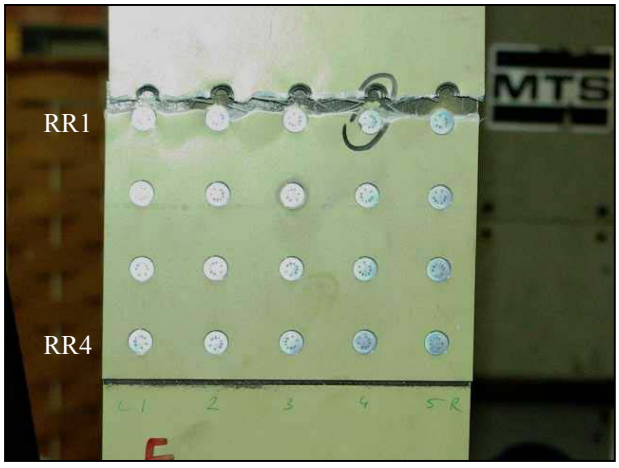

Figure 7.1.8.19. Specimen 2-A-1, front side after the residual strength test

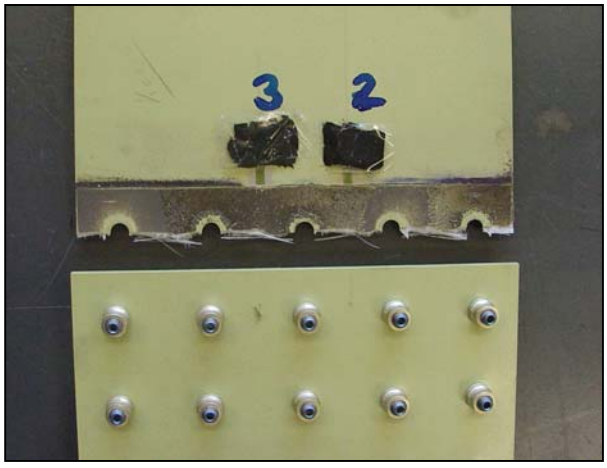

Figure 7.1.8.20. Specimen 2-A-3, rear side after the residual strength test

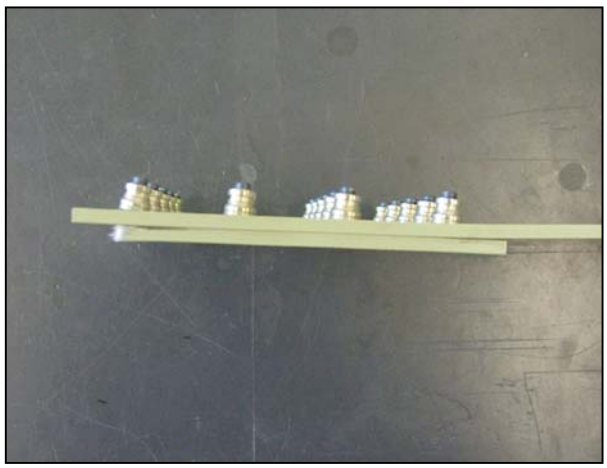

Figure 7.1.8.21. Specimen 2-A-1, side view after the residual strength test

The fastener tilting in the 7mm GLARE4 sheet package with 5.6mm Hi-Lite fastener is significantly less than observed in the 8.6mm GLARE2 package jointed with 4.8mm Hi-Loks (circumferential joint, see previous section). Three test series are conducted until summer 2003:

1) residual strength tests with different fatigue damage rates at room temperature
2) residual strength tests with different fatigue damage rates after one year outdoor exposure at room temperature
3) residual strength tests with different fatigue damage rates at 70°C material temperature

The latter test series caused clamping problems because at high temperature all specimens tend to slip through the clamping grips. The following table summarizes the test results. (Note remark 7).

Residual strength results 2-A-series, R_D linked top sheet, rivet row 1 (countersunk)

specimen no.	Fastener[7)]	N [1)] [CA cycles]	$a_{av.}$ [3)]	R_D [3)]	failure load	gross failure stress	net failure stress
2-A-1	HL413VF-6	0	0.00 mm	0.0 %	198.3 kN	404 MPa	530 MPa
2-A-2	HL413VF-6	45000	0.65 mm	1.3 %	185.9 kN	379 MPa	497 MPa
2-A-3	HL413VF-6	35000	4.11 mm	8.1 %	180.9 kN	369 MPa	483 MPa
2-A-6	HL413VF-6	27000	3.03 mm	6.0 %	182.4 kN	371 MPa	487 MPa
2-A-43 [2)]	ASNA2026	0	0.00 mm	0.0 %	197.5 kN	403 MPa	528 MPa
2-A-44 [2)]	ASNA2026	40000	3.00 mm	9.7 % [8)]	177.6 kN	362 MPa	474 MPa
2-A-45 [2)]	ASNA2026	60000	6)	6)	168.4 kN	344 MPa	450 MPa
2-A-46 [2)]	ASNA2026	80000	7.90 mm	27.4 % [8)]	153.8 kN	314 MPa	411 MPa
2-A-47 [2)]	ASNA2026	100000	6)	6)	160.1 kN	327 MPa	428 MPa
2-A-48 [2)]	ASNA2026	120000	link up	47.0 % [8)]	101.0 kN	206 MPa	270 MPa
2-A-35 [4) 5)]	HL413VF-6	0	0.00 mm	0.0 %	>171.8 kN	>350 MPa	>459 MPa
2-A-36 [4)]	HL413VF-6	90000	6.21 mm	12.2 %	163.6 kN	333 MPa	437 MPa
2-A-37 [4)]	HL413VF-6	60000	5.49 mm	10.8 %	161.6 kN	329 MPa	432 MPa
2-A-38 [4)]	HL413VF-6	120000	4.32 mm	8.5 %	168.5 kN	343 MPa	450 MPa

1) CA load cycles at Fmax. = 58.8 kN, R=0.1, exception: specimen 2-A-6: Fmax. = 64.7 kN
2) After one year accelerated exposure
3) Measured results, visible aluminium layer (non countersunk side of top sheet)
4) Residual strength test at 70°C material temperature
5) Failure at clamping
6) Not measured
7) Specimens fatigued with HL413VF fasteners fail in mating layer, only. Failure around hole, crack lengths defined according to procedure explained in chapter 7.1.3. Specimens fatigued with ASNA2026 fastener fail from hole, cracks in all aluminium layers possible
8) Destructive crack length measurements after RS test, see crack lengths recorded in table 7.1.3.3 to 7.1.3.5

Although the fatigue failure locations are different for the non-exposed specimens and the exposed specimens (section 7.1.3), the residual strength prediction method for riveted joints, proposed by Müller [1], works quite well. No influence of the 1 year exposure in Queensland on residual strength is found, see figure 7.1.8.22. Similar as for the 2-B-series specimens which have been residual strength tested after 1 year outdoor exposure, a ticking noise was audible at relatively low applied forces. Figure 7.1.8.23 contains both the net section failure stress and the stress level at which the ticking noise was heard. For the specimens which have been fatigued 100000 cycles and 120000 cycles before exposure (2-A-47 and 2-A-48), the noise appeared even in the order of the fatigue load. However, the ticking noise did no influence the residual strength result.

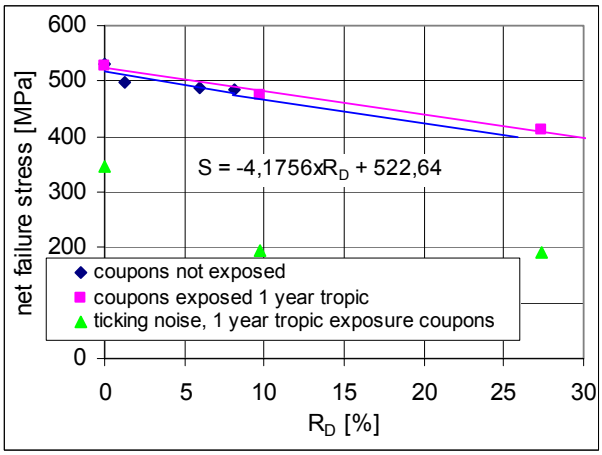

Figure 7.1.8.22. Non-exposed and 1 year exposed exposed riveted repair coupons, residual strength Consider different failure modes (ref. chapter 7.1.3)

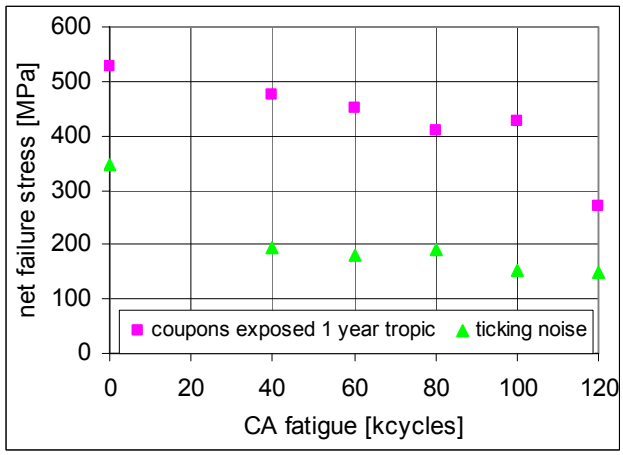

Figure 7.1.8.23. Residual strength of 1 year exposed specimens related to fatigue cycles before ageing

The fiber prepreg conditions of specimens 2-A-43 to 2-A-48 can not be investigated at rivet row 1 of the upper sheet after the residual strength test. But it can be expected that the specimen condition in the lower sheet at rivet row 4 is quite similar to the condition of rivet row 1 of the upper sheet just before net section failure. All parameters are similar between the two locations, except the smaller net section of the upper sheet due to the countersunk.

The ticking noise phenomenon was discussed for the circumferential joint specimens in connection with cracking fibers. But still there is no absolute evidence that cracking fibers are responsible for the noise. The sound is audible very early in the 2-A series specimens which returned from Australia after one year exposure (ref. figure 7.1.8.23). However, after the residual strength test it is impossible to have a closer view on the fiber condition at rivet row 1 (upper sheet) because all fibers are statically pulled to failure. According to the crack initiation and crack propagation analysis performed in the previous sections, the performance of the lower sheet in rivet row 4 is not much different compared with rivet row 1 (upper sheet). Cracks initiate earlier in the upper sheet due to the countersunk. Consequently, a further investigation of a lower GLARE sheet at rivet row 4 should add additional information concerning the failure mode(s) in the specimen series 2-A-43 to 2-A-48.

Rivet row number 1 from the severest fatigued specimen no. 2-A-48 has been investigated under an electron microscope after etching of the aluminium layers [40]. Before etching the fatigue crack lengths at the five holes were measured. The mating aluminium layer was cracked almost completely through after the 120000 fatigue cycles or before the residual strength test was performed. On the other side of the specimen five cracks with lengths between 0.25mm and 0.99mm were found. Figure 7.1.8.24 shows both sides of the specimen and indicates the investigated holes.

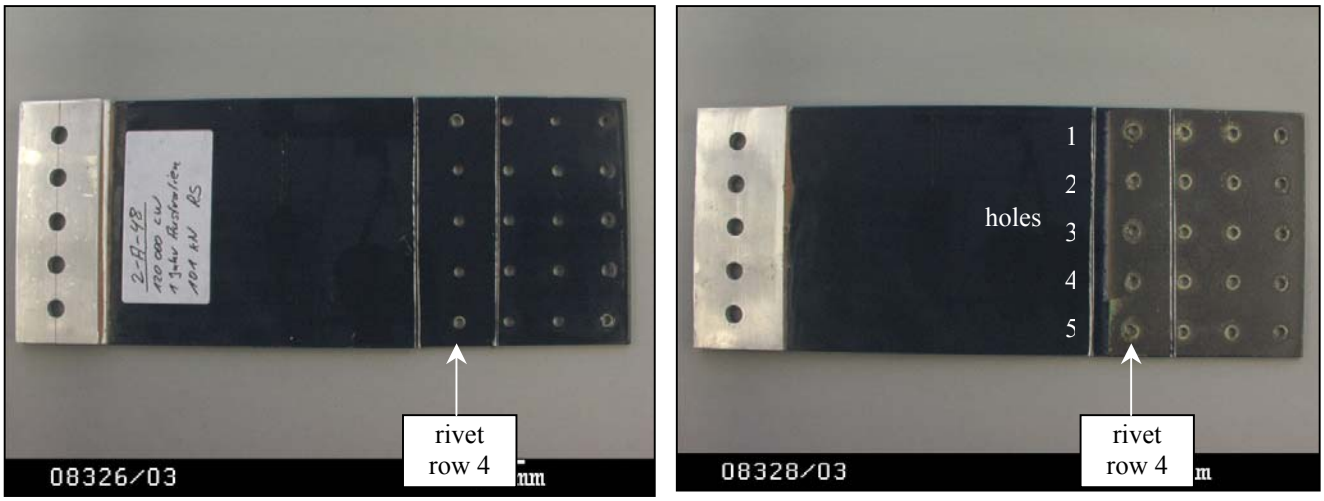

Figure 7.1.8.24. Lower sheet of specimen 2-A-48 after residual strength test, free surface on left picture, mating surface on right picture

The fatigue cracks in the mating surface aluminium layers are visible without magnification:

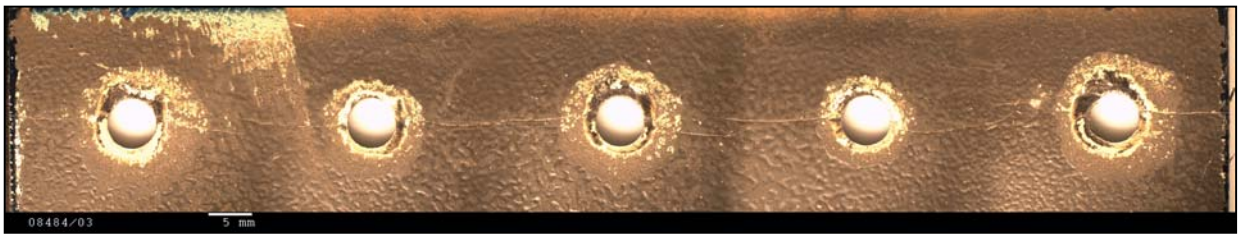

Figure 7.1.8.25. View on specimen 2-A-48, rivet row 1, mating aluminium layer

An area around holes no. 1, 2 and half of no. 3 are cut out and etched from both sides:

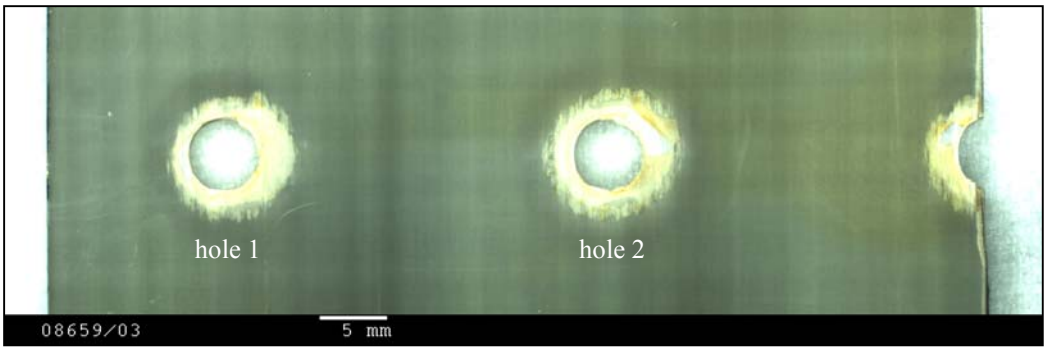

Figure 7.1.8.26. View on prepreg below free metal surface, prepreg damages around all holes

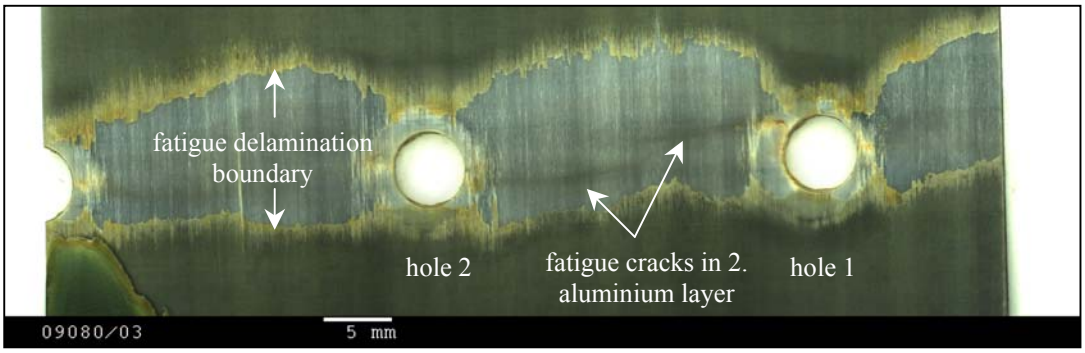

Figure 7.1.8.27. View on prepreg below mating metal surface, large fatigue delaminations

The mating aluminium layer is the one which obtained the highest fatigue loads, due to the additional bending in the single shear joint. Almost all fatigue cracks linked up in this layer. As expected, large fatigue delamination zones are observed between the mating aluminium layer and the prepreg layer (figure 7.1.8.27). Unexpected is the amount of prepreg damage in the first layer on the rear side of the specimen, see figure 7.1.8.26. It is a result of the either the residual strength load (bearing), the fastener clamping or both. However, the observation may be new because researchers usually do not inspect the lower loaded locations of a specimen.

A magnification of the no.3 hole edge shows very limited fiber failure, figure 7.1.8.28. However, the prepreg looks similar at holes 1 and 2 [40]. Specimen 2-A-48 was loaded to 101 kN when it failed, the ticking noise was observed at approximately 50 kN. If the noise is supposed to indicate fiber failure, then it is obviously independent from the *amount* of fibers which failed, because much more fibers failed in specimen 2-B-77 than in 2-A-48, but for both the noise was observed. Because no strength reduction is observed after one year outdoor exposure (figure 7.1.8.22) it is concluded that the ageing has no influence on the net section GLARE residual strength. This conclusion has to be confirmed by testing the 2-A series specimens which return from Australia in 2004 and in 2008, as well as by a close observation of the failure modes in the blunt notch specimen series (specimen series 3-). The ticking noise item is introduced by the specimens which coincidentally returned from the exposure site after just one year ageing. The present experience is insufficient for a complete understanding of the noise phenomenon.

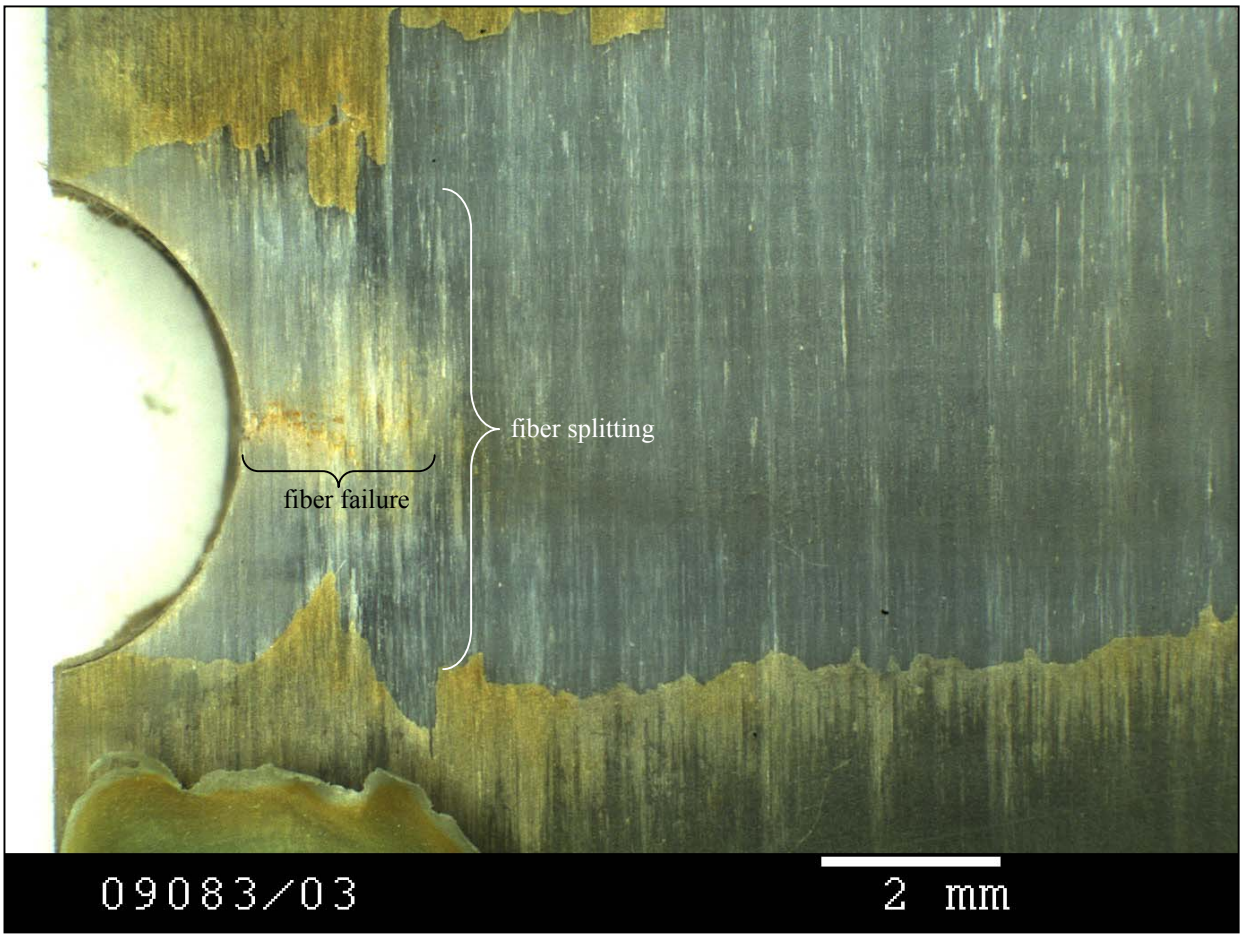

Figure 7.1.8.28. Magnification of figure 7.1.8.27, hole no. 3, limited fiber cracking in the highest loaded prepreg

7.2 Joint Strength Prediction for Aircraft PSE's

In the previous section 7.1 various properties of GLARE joints were investigated. The properties were associated with the single strap butt joint tested in the A340-600 full-scale fatigue test (see section 3.1.1) and a lap joints used in the riveted repair tested in the MegaLiner barrel test (see section 3.1.2). Several material properties have been verified, sometimes by a limited number of experiments due to long testing times involved. In such cases the results obtained should be considered as trend values.

Significant observations were obtained on the moisture weight gain prediction around holes. This has led to the conclusion that no ageing influences on strength have to be considered for long range (LR) aircraft. Even for short range (SR) aircraft, a simulation of 30 years outdoor exposure by 500 hours accelerated ageing (70°C/85%RH) would be sufficient. Also important, experimental results indicated that the scatter was low for the crack initiation fatigue life and the crack growth rate in the aluminium layers. Furthermore, varying temperature during the fatigue life did not reduce these properties. The results lead to the conclusion that no special factors have to be applied on the results obtained in a full scale fatigue test which is usually carried out in dry hangar at a comfortable temperature.

Another promising conclusion from section 7.1 applies to the comparison between calculated and experimental results for both crack initiation and crack propagation in the highest loaded aluminium layers of the riveted joints. The calculated results were obtained with the computer software 'F&DT Toolbox'. The agreement between the calculated results and the test results was excellent.

In section 7.1, data were also obtained on the static strength for relevant material properties and design allowables, and on the residual strengths as affected by the fatigue damage rate.

With the above knowledge available, the significance of this information for meeting the harmonized Federal Airworthiness Regulations / Joint Airworthiness Regulations should be considered in the present section.
The analysis of the strength prediction for the single–strap butt joint and the riveted lap joint are presented in sections 7.2.1.and 7.2.2 respectively. Attention is paid to the fatigue damage tolerance properties of both types of joints.
Note: All static design load cases are considered to apply in the temperature range 20°C to –50°C.

7.2.1 Strength prediction for the single strap butt strap in A340-600 full scale test article

Static strength calculations for the artificial butt strap, considered load direction equals flight direction:
It is assumed that the aircraft is designed according to the large damage capability. In that case, a far field stress of approximately 210 MPa should not be exceeded in the aluminium skin at limit load.

Consequently: $\sigma_{\lim,t=2.4mm} = 210\ MPa$ (gross stress)
$\sigma_{\lim,t=4.3mm} = 117\ MPa$ (gross stress)
$\sigma_{ult,t=4.3mm} = 175\ MPa$ (gross stress)

For the rear aft fuselage the maximum compression is considered to be 50% of the maximum tensile strength, because the maximum downward lift of the horizontal tail plane is approximately twice as high as the maximum upward load. Because the rear fuselage is not located between the main landing gears, the breaking case is considered to be insignificant.

$$\sigma_{\lim,comp,t=4.3mm} = -59\ MPa \qquad \text{(gross stress)}$$

Yield strength justification

(ref. FAR/JAR 25.305(a), no detrimental deformation at limit load)

Allowable yield load per fastener: 8500 N (ref. chapter 6.11, no exposure considered for LR A/C).

Load per fastener of rivet rows 3 and 4 in full scale specimen at limit load:

$$117MPa \times 4.3mm \times 22.7mm \times 0.346^{*} = 3951\ N$$

$$(^{*}34.6\%\ load\ carried\ in\ RR3\ and\ RR4,\ see\ appendix\ T)$$

- Reserve factor yield (MIL-STD-1312-4): 8500 N / 3951 N = 2.15

Remark: The yield strength allowable is conservative, because tests are performed with two GLARE2-7/6-.4 sheets, instead of one GLARE2 sheet connected to a 4mm sheet made of 2024T3 (full scale specimen condition). The higher stiffness of the aluminium sheets will increase the allowable yield stress of the joint.

Yield load per fastener obtained from coupon specimen 2-B-21: 7667 N (ref. chapter 7.1.7.1)

- Reserve factor yield (from coupon): 7667 N / 3807 N = 2.01

Failure strength justification

(ref. FAR/JAR 25.305(b) no failure at ultimate load)

Allowable blunt notch stress, not aged: 688 MPa (ref. chapter 6.9, no exposure considered for LR A/C).

Net section ultimate stress in butt strap:

175 MPa x 1.27 = 222 MPa

- Reserve factor blunt notch: 688 MPa / 222 MPa = 3.10

Significant fastener tilting is observed in thick single shear GLARE joints. A rivet pull through strength justification can be performed considering that all fastener tilt 90 degrees and the entire applied load has to be transferred in the tensile mode by the fastener and collar:

The ultimate load stress 175 MPa corresponds to a load per fastener of 5.7 kN. In the rivet pull through tests (chapter 6.12) collars failed at tensile fastener loads >8.5 kN.

- Reserve factor rivet pull through: 8.5 kN / 5.7 kN = 1.49

Failure stress obtained from specimen 2-B-21 (gross, fastener failure): 359 MPa

- Reserve factor (coupon failure): 359 MPa / 175 MPa = 2.05

Compression filled hole strength justification

(ref. FAR/JAR 25.305(a))

No compression yield is allowed at limit load. Compression yield strength GLARE2B-7/6-.4: -352 MPa (typical value divided by 1.1, ref. [31]).

Allowable compression filled hole stress (gross): -450 MPa at 80% R_D (ref. chapter 6.13).

Compression filled hole stress to be justified: -59 MPa

The experimental evaluated compression filled hole strength exceeds the compression yield strength. Consequently it can be never the critical design driver.

The following reserve factor ranking is obtained from the performed static analyses :

Rivet pull through :	1.49
Yield (coupon) :	2.01
Failure coupon :	2.05
Yield (MIL-STD) :	2.15
Blunt notch :	3.10

The calculated reserve factor for rivet pull through is obviously much too conservative, since the joint coupons fail at the fasteners and not in the rivet pull through mode.

The comparison between the reserve factors obtained from 'yield (coupon)' and 'yield (MIL-STD)' reveals that the MIL-STD test method does not lead to conservative results. However, JAR 25.305 demands no *detrimental* deformation at limit load, with the explanation that flight safety should not be jeopardized. Consequently, the 'rivet strength' results obtained from MIL-STD-1312-4 tests may serve as a design *guideline*, in the true sense of the wording.

As expected, the blunt notch strength has no use for a single shear strength justification, since it does not consider pin loads and fastener tilting, which leads to far to optimistic reserve factors.

Taking the assumptions from above into account, the following static design criteria remain important:

Tensile yield (from coupon) :	2.01
Tensile failure (from coupon) :	2.05

Fatigue & damage tolerance justification

(ref. FAR/JAR 25.571)

The bending stresses in the full scale specimen butt strap are significantly constrained by the presence of the stringer couplings, see the comparison with the coupon specimen in figure 7.2.1. For the calculation of the crack initiation life, the crack propagation rate and the residual strength of the full scale butt strap, the 'FML Toolbox' is used. The relation between normal stress and bending stress, as derived

from figure 7.2.1, is used as input for the computer program. Too conservative bending stresses as calculated by the neutral line model are then avoided.

The stress spectrum of the block of 1660 flights in the A340-600 full scale test at the location of the strain gauge rosette 16414 (ref. figure 3.1.4) is used for the calculation. It is described in reference [24] and it applies to the 2.4mm thick monolithic aluminium skin on which the strain gauge rosette has been attached. In order to convert the spectrum into gross tensile stresses in the butt strap, the stress spectrum is multiplied with a factor 2.4/4.3=0.56. This factor has to be used because the aluminium reference joint SN-data for the butt strap are also related to a thickness of 4.3mm. Hundred MSD calculations were performed. The results are presented in appendix I. Figure 7.2.2 contains the probability of crack initiation, related to a transition crack length of 1mm.

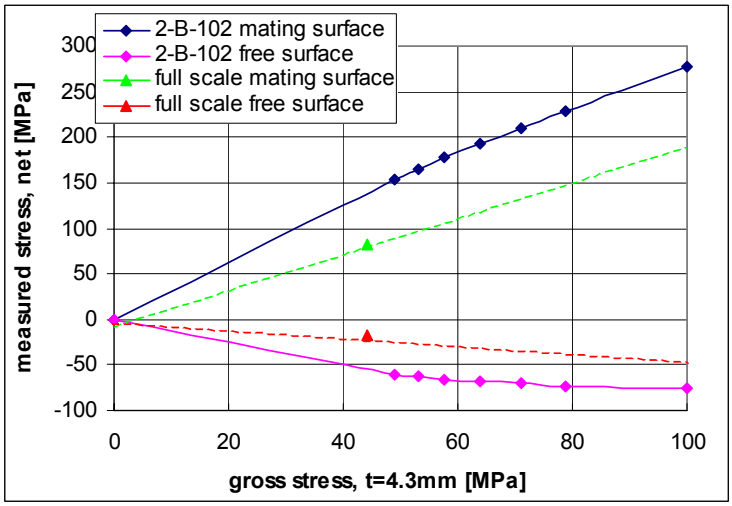

Figure 7.2.1. Stresses in the aluminium layers of the butt strap net section, rivet rows 3&4, measured in the coupon specimen and in full scale specimen (for load case 1g+Δp+10ft/s gust, ref. strain gauges 16411JL & 16413JP, see chapter 3.1)

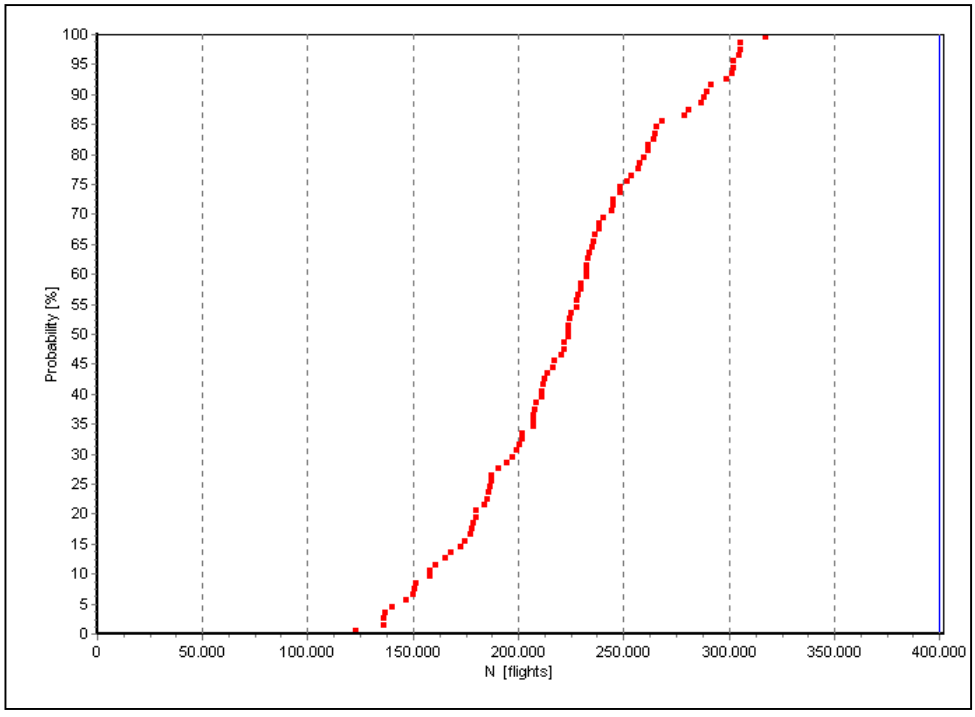

Figure 7.2.2. Probability of crack initiation for full scale specimen butt strap, 100 MSD scenarios

The crack initiation life of the mating aluminium layer of the GLARE2B-7/6-.4 butt strap at the positions of rivet rows 3 and 4 equals 217000 flights with 50% probability. A comparison with the calculation performed in chapter 7.1.5 demonstrates that conservative results are obtained with the non-stiffened coupons. With bending in the coupon specimens (blue curve in figure 7.1.2), a crack initiation life of 140000 flights was calculated. The constrained bending increases the crack initiation life by 50%.

However, the butt strap is over-designed because no crack initiation should be expected at the end of the A340-600 full scale fatigue test. The fatigue damage rate at the end of the fatigue test (50000 flights) equals:

D = 50000 flights / 217000 flights = 0.23

The maximum allowable stress level for the present design is discussed in the following. The entire fatigue stress spectrum is increased by trial and error, and crack initiation calculations are performed until a crack initiation life is obtained of approximately 20000 flights. Figure 7.2.3 shows the probability for crack initiation in the butt strap if the stress spectrum is increased by a factor 1.7.

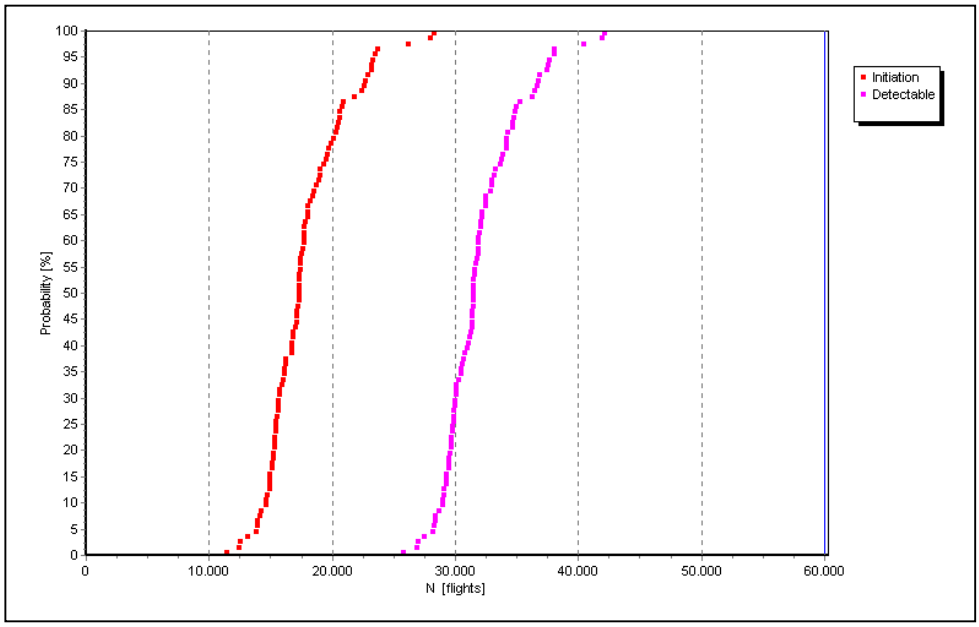

Figure 7.2.3. Probability of crack initiation for full scale specimen butt strap, 100 MSD scenarios, 8 bore holes (equals 1 stringer pitch), factor 1.7 on A340-600 stress spectrum at fuselage location C57.1

The result of the calculation is:

N_i = 17500 flights (a_i = 1mm, 50% probability)

$N_{det.}$ = 34000 flights ($a_{det.}$ = 8mm, 50% probability, $a_{det.}$ is measured from the edge of the hole (caution: the DTToolbox calculates "a" from the center of the hole).

Printed results of the calculation can be found in attachment S. One hundred different crack scenarios are calculated. As an example, results of crack scenario 1 are shown in figure 7.2.4.

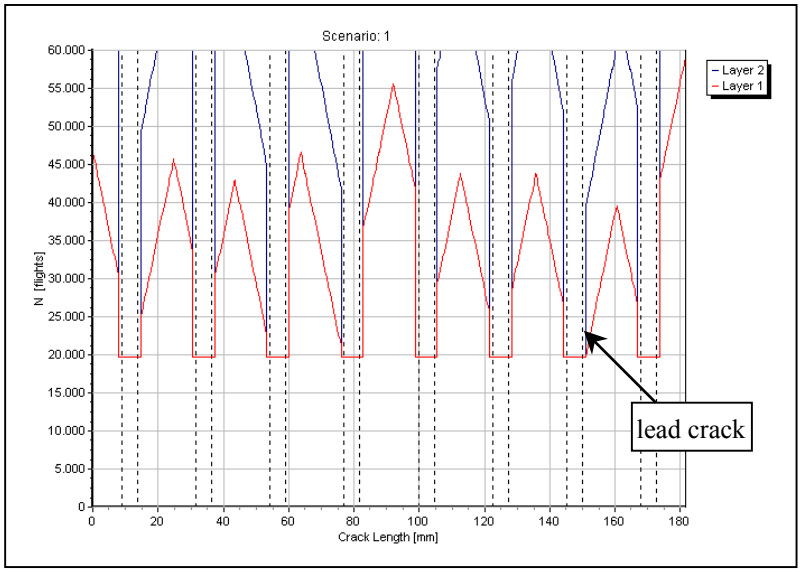

Figure 7.2.4. The first crack scenario of 100 scenarios for the GLARE2B-7/6-.4 butt strap with crack growth curves (red lines)

The design service goal of the A340-600 is 16800 flights. The fatigue damage rate after 33600 flights (2DSG A340-600) equals 1.3%. The dominating failure mode is still fastener failure, see figure 7.1.8.4.
The A340-600 EF2 full scale structure will be torn down in 2004 after 50000 simulated flights. Two panels with a width covering three stringer pitches, including stringer and stringer coupling will be cut out. It is proposed to pull some ("some" are sufficient due to the low CI scatter) fasteners in rivet rows 3 and 4 and to perform a rotating probe test inspection. No fatigue cracks are expected, according to the calculations which are calibrated by coupon tests.
The performed calculations are based on coupon data. If cracks would be found in the butt strap of the full scale specimen after 50000 flights, a test-to-structure factor between coupon and full scale structure can be calculated:

$$\frac{N_{coupon}}{N_{fullscale}} = \frac{217000\,flights}{50000\,flights} = 4.3$$

The high order of magnitude of this factor is not expected. If the butt strap is free from fatigue cracks after the 50000 flights in the full scale test, it is not possible to define a test-to-structure factor between the coupon and the full scale structure. However, the cut out panels can serve as a tool to determine the factor between a coupon and the stiffened shell.
It is proposed to continue fatigue cycling with the panels with the A340-600 load spectrum but increased by factor 1.7. Then, crack initiation is expected after 17500 x 0.8 = 14000 flights (20% damage are already introduced during the full scale test). Another inspection is recommended at this point, followed by further 16500 flights ($N_{det.}$ - N_i). Now the 8mm lead crack in the mating layer of the GLARE2B butt strap should be detectable. If this is the case, the test-to-structure factor between coupon and panel would be 1.0 because the behaviour of the full scale butt strap would be exactly predicted with the input data obtained from the coupon, including the correct bending factors as the most influencing item. Any test-to-structure factor >1.0 would cover scale effects (see chapter 2.8).

Figure 7.2.5 shows the calculated crack initiation and crack propagation of the lead crack and the average crack. The detectable crack length is defined with 8mm (input from NDT experts). It becomes detectable at approximately 2 DSG. The *average* crack length, which is determining the residual strength of the joint, is shorter than 2mm at 2 DSG. This is the reason why the residual strength is not decreased, compared with the virgin structure (and thus no knock down factors due to ageing have to be considered). Still, ultimate load capability is present.

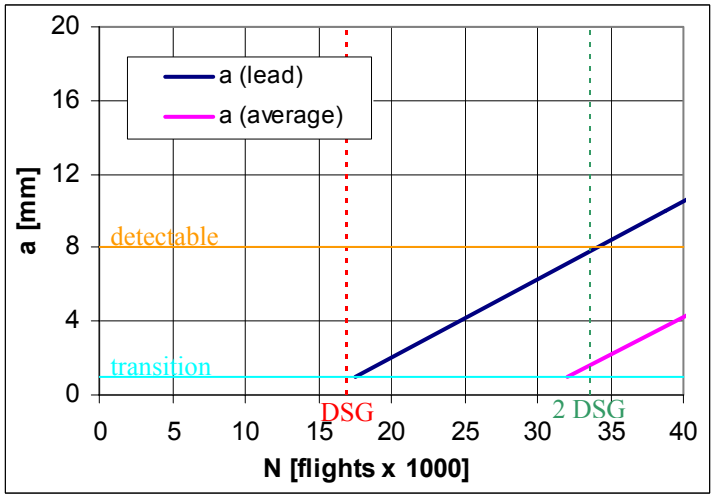

Figure 7.2.5. Predicted CI and CP life of the GLARE2B butt strap in A340-600 panel (removed from the full scale specimen), stress spectrum increased by factor 1.7, surface cracks considered

Figure 7.2.5 shows the desired test results from the proposed tests with the cut out panels from the A340-600 full scale specimen. If obtained from a full scale test specimens, the crack initiation and crack propagation lives would be divided by a scatter factor 2. This is the common factor applied on monolithic aluminium PSE's, and because the CI and CP scatter for GLARE is not larger than for the monolithic aluminium (ref. chapter 6 and 7), the same factor is adequate for GLARE. The strength justification of the butt strap for certification purposes looks similar as shown in figure 7.2.6.

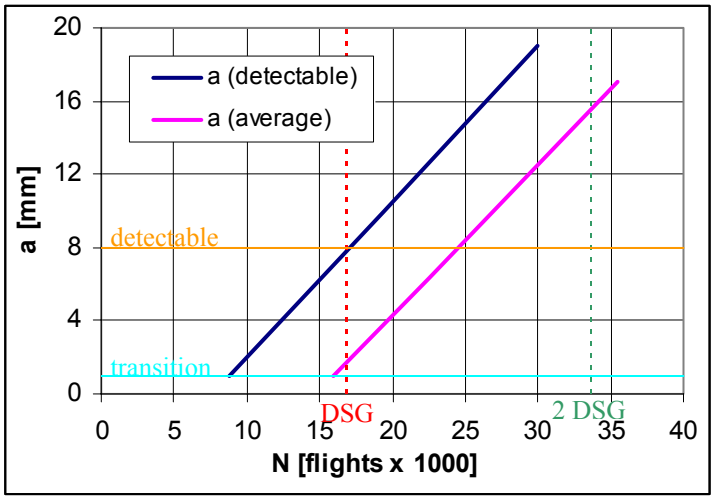

Figure 7.2.6. Factored CI and CP life of artificial GLARE2B butt strap in A340-600 panel stress spectrum increased by factor 1.7

With safety factors included, cracks become inspectable at the DSG life time, and the aircraft will then be removed from service. No scheduled inspection task is required because ultimate load capability is available at DSG with a safety factor 2.

The proposal to carry out fatigue tests with a 70% increases severity of the fatigue load spectrum % is made in order to determine the fatigue limits of the investigated GLARE2 butt strap. The author considers a non specified design rule, i.e. cracks should not initiate in the (flying) aircraft structure until ½ DSG. This limit can be met with the increased spectrum. However, the level of both static design loads and fatigue loads are interrelated. Consequently, when the fatigue spectrum is increased by 70%, the static loads should be considered to rise approximately in the same order of magnitude. The yield strength criterion is the one with the lowest reserve factor, as determined above. With 70% higher static loads, it decreases from RF=2.01 to RF=1.18.

The joint is designed by the fatigue rule: "No crack initiation before ½ DSG". Static strength is not a critical designing criterion for the joint due to the extremely high blunt notch strength of GLARE2 and the high strength of the titanium fastener.

7.2.2 Strength prediction for Megaliner Barrel repair

The strength justifcation for the riveted repair is complicated by the different crack initiation locations dependent on the fastener type in combination with specific installation errors. The item was extensively discussed in chapter 7.1.3. Apparently it was no good idea cut the expense for fasteners by 4/5 by using different fasteners in some coupons than the ones installed in the full scale structure, i.e. the ASNA2026 Hi Lite.

Static strength calculations for the riveted lap joint of the repair patch of the Megaliner Barrel test with the load in the forward direction of the fuselage. It is assumed that the structure is designed under consideration of the large damage capability. In that case, a far field stress of approximately 230 MPa should not be exceeded in the GLARE4A skin at limit load.

Consequently: $\sigma_{\lim} = 230\ MPa$ (gross stress)
$\sigma_{ult} = 345\ MPa$ (gross stress)

For the rear aft fuselage it is considered, that the maximum compression is 50% of the maximum tensile strength.

$$\sigma_{\lim,comp} = -115\ MPa$$

Yield strength justification (no yield at limit load)
(ref. FAR/JAR 25.305(a), no detrimental deformation at limit load)
Allowable yield load per fastener: 7350 N (ref. chapter 6.11, no exposure for LR A/C).
Load per fastener in full scale specimen at limit load:

230 MPa x 3.5mm x 28mm x 0.285* = 6424 N *28.5% load carried in RR1 and RR4, ref. appendix T

- Reserve factor yield (MIL-STD-1312-4): 7350 N / 5635 N = 1.14

Yield load per fastener obtained from joint coupon specimen 2-A-2: 6000 N (ref. chapter 7.1.7.2)

- Reserve factor yield (from four rivet row coupon): 6000 N / 5635 N = 1.06

Failure strength justification (no failure at ultimate load)
(ref. FAR/JAR 25.305(b), no failure at ultimate load)
Allowable blunt notch stress, non-exposed: 580 MPa (tested, ref. chapter 6.9)
Net section ultimate stress:

345 MPa x 1.25 = 431 MPa

- Reserve factor blunt notch: 1.34

Failure strength justification 'rivet strength' (MIL-STD-1312 test)

Obtained failure load per fastener: 12400 N (ref. chapter 6.11, rivet pull through, no exposure for LR A/C).

Load per fastener in full scale specimen at ultimate load:

345 MPa x 3.5mm x 28mm / 4 = 8452 N

- Reserve factor yield (MIL-STD-1312-4): 12400 N / 8452 N = 1.47

Gross failure stress obtained from specimen 2-A-1: 404 MPa (ref. chapter 7.1.8)

- Reserve factor (coupon failure, net section): 404 MPa / 345 MPa = 1.17

Compression filled hole strength justification

(ref. JAR/FAR 25.305(a))

No compression yield is allowed at limit load.

Allowable compression filled hole stress (gross): >480 MPa (tested, ref. chapter 6.13).

Maximum compression stress at limit load: 115 MPa.

The CFH strength is not designing the riveted repair.

The following reserve factor ranking is obtained from the performed static analyses :

Yield coupon :	1.06
Yield (MIL-STD) :	1.14
Failure coupon :	1.17
Blunt notch :	1.34
Failure (MIL-STD):	1.47

The rivet pull through strength is not considered because the non-fatigued coupons did neither show severe deformation before they failed in the net section nor any rivet pull through failure observed.

A similar mismatch between the yield behaviour of the joint coupon and the MIL-STD-1312 test is observed as for the GLARE2B butt joint before. The MIL-STD test is underestimating the true yield load by approximately 8%. A similar trend is observed when comparing the reserve factors for failure. The MIL-STD test is underestimating the true failure load by 30% and it provides a wrong failure mode – rivet pull through instead of net section failure.

Under consideration of the above discussed items the following static design criteria remain important:

Tensile yield (coupon) :	1.06
Tensile failure (coupon) :	1.17

The repair joint is designed to the static limits, thanks to the 4th rivet row.

Fatigue & damage tolerance justification

(FAR/JAR 25.571)

The variation of the crack initiation location of the riveted repair, depending on the fastener type and manufacturing parameters, was discussed in section 7.1.3. The SN curves for specimens with HL413VF fastener were established and an assessment was made for the specimens with ASNA2026 fastener, based on a few coupon results obtained after one year outdoor exposure. The slope of the 'HL413 curve' was used for drawing an SN curve through the single available data point for specimens fatigued with ASNA2026 fasteners. Consequently, the correct slope of the latter SN curve is uncertain (fatigue cracks initiating from hole edges).

The repair in the full scale specimen 'Megaliner Barrel' was manufactured with ASNA2026 fastener, thus crack initiation from the hole edges is expected. For repairs with repair patches of a lower or equal stiffness compared to the stiffness of the repaired skin, the outer rivet rows in the skin are the fatigue critical ones, which is rivet row 4 in the lower sheet (ref. figure 3.2.3.4). A calibration of the software 'DTToolbox' for the present problem has been performed. Test results for the joints with ASNA2026 fastener as explained above are compared to the constant amplitude crack initiation calculations at constant stress levels. The comparison is shown in figure 7.2.7.

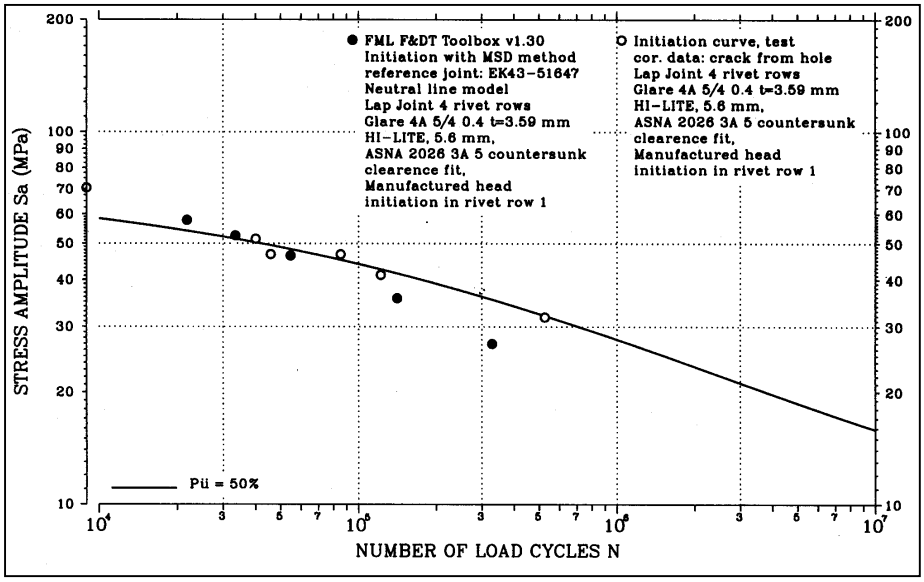

Figure 7.2.7. Riveted repair, lower sheet, RR4, comparison of crack initiation test results (constructed) with calculated results

A good correlation between the constructed test curve and the calculated data point is observed for crack initiation lives up to 50000 cycles. At a higher endurance the calculation becomes conservative.

Subsequently a prediction of the crack initiation, crack propagation and residual strength behaviour for the full scale specimen is performed, using the FML F&DT Toolbox version 1.3.

Input data for the calculation:

- Stress spectrum for 21500 Barrel flights, calibrated with the strain gauge rosette which has been bonded before the cut out has been machined and the repair patch has been applied. The stress spectrum is related to the outer aluminium layer of the GLARE4A skin, to which the strain gauges have been bonded (E = 72000 MPa).

- A correction factor for the tensile moduli, applied on stress, in order to transform the measured stresses into GLARE-stresses : 0.79.
- Bending factor 0.4 considered according to bending measurements obtained from strain gauges which bond on the Megaliner Barrel skin, close to the repair edge (ref. figure 3.1.7), and strain gauges bonded on specimen 2-A-1 at the same location.
- Transition crack length: 1mm
- The reference joint SN-curve from specimen EK43-51647 (appendix H).

The crack initiation probability for 100 MSD scenarios and 12 holes is shown in figure 7.2.8. The *calculated* crack initiation life of the outer rivet row of the Barrel skin is 40000 flights with 50% probability. The calculated detectable crack length is beyond 100000 flights ($a_{det.}$=8mm).

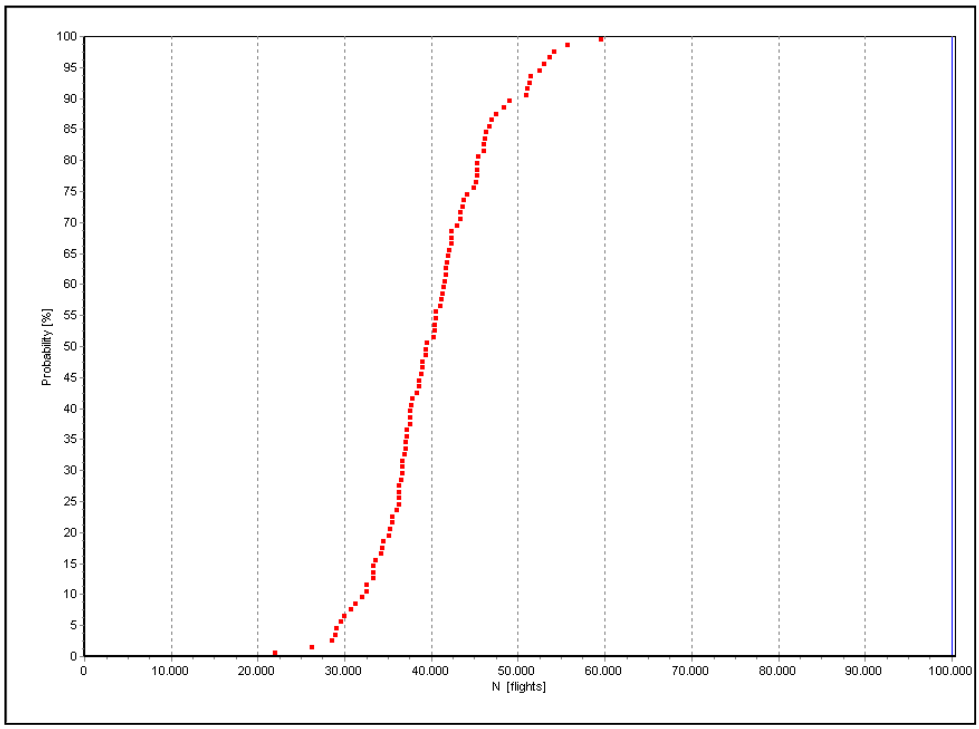

Figure 7.2.8. MSD crack initiation calculation for skin of Megaliner Barrel riveted repair, ref. appendix G

A reliable crack propagation rate for the outer aluminium layer of the GLARE4A skin is obtained from the variable amplitude tests with the 2-A series coupons, ref, chapter 7.1.7. The crack propagation rate is conservative, because the coupon specimen obtains higher bending loads than the full scale specimen repair. For the Megaliner Barrel spectrum it was found:

da/dN = 9x 10^{-5} mm/flight (ref. chapter 7.1.7)

Figure 7.2.9 contains the predicted crack initiation and crack propagation lives for the Megaliner Barrel, without safety factor. They have to be related to a Design Service Goal of 20000 flights for the specimen. According to the prediction, no cracks should be found during an inspection of the specimen after 20000 simulated flights, even if all fasteners are removed.

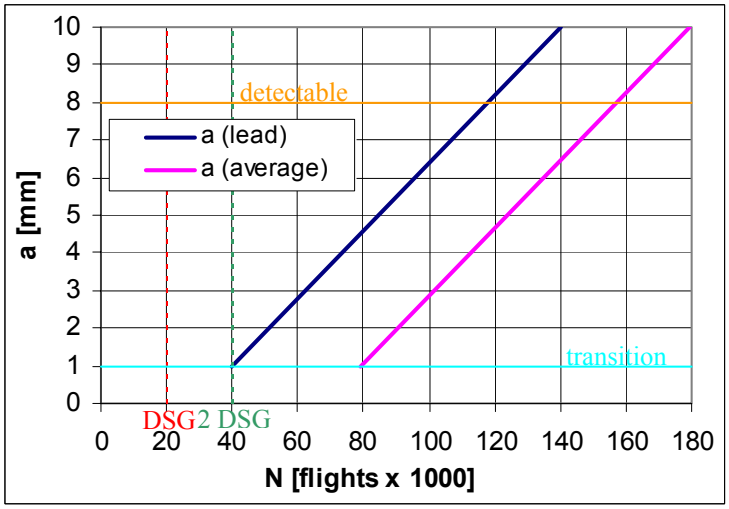

Figure 7.2.9. Fatigue prediction for the Megaliner Barrel repair, first rivet row of skin, 100 MSD scenarios

The repair patch has frequently been removed from the full scale specimen for detailed inspections, i.e. after 20000, 30000 and 43000 flights (status in September 2003). After 30000 flights, no cracks are reported, but after 43000 flights some cracks are found:

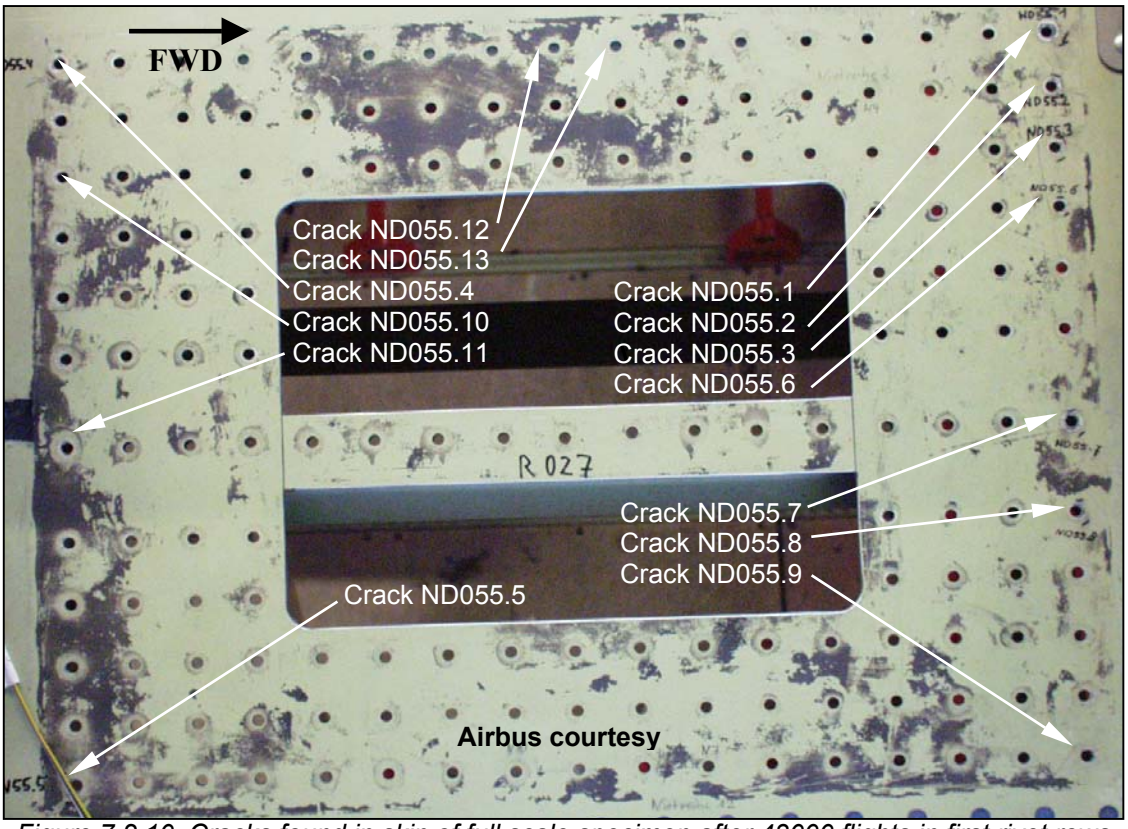

Figure 7.2.10. Cracks found in skin of full scale specimen after 43000 flights in first rivet rows in and against flight direction

Airbus inspectors reported crack initiation from the hole edges, although some fretting is observed as well. For most cracks just indications are reported, i.e. the detected crack lengths are below 0.5mm. Two cracks in the right rivet row were reported with already an 8mm crack lengths. The average crack lengths obtained from the full scale test after 43000 flights for the two rivet rows are:

- in flight direction (RH RR in figure 7.2.10): $a_{av.}$ = 1.6mm
- against flight direction (LH RR in figure 7.2.10): $a_{av.}$ < 0.5mm
  (transition crack length not yet reached)

No cracks are found in the repair patch.

The fatigue prediction which is shown in figure 2.7.9 is representing the fatigue condition of the repair close to frame 74 (rear rivet row, left side on picture 2.7.10). The forward rivet row is not covered, because the detectable crack length was achieved earlier than expected and the average crack length is longer at an earlier stage of the test. The condition of the forward rivet row is shown in figure 2.7.11, under the assumption that the two lead cracks initiated immediately after the 30000 flight inspection:

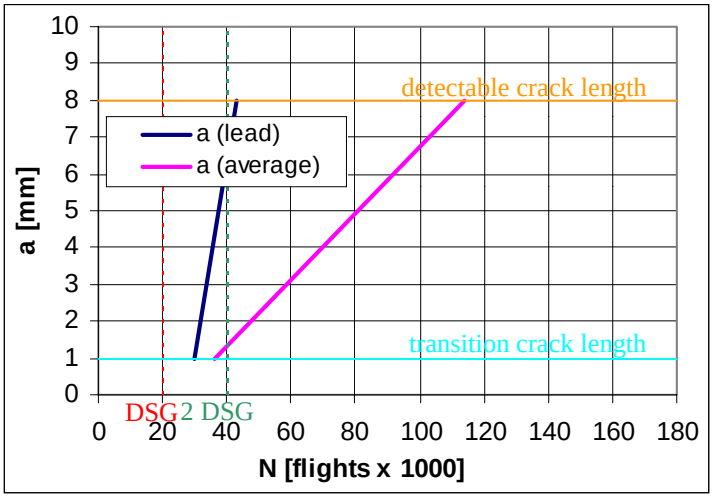

Figure 2.7.11. Fatigue condition representing the Megaliner Barrel forward rivet row of repair, damages in skin

The fatigue damage rate R_D for the forward rivet row (right side on picture 7.2.10) is related to the average crack length by using the equation developed in chapter 7.1.4, ref. figure 7.1.4.14. Two deviating aspects are accepted for the residual strength calculation. A conservatism is provided by the fact that the equation shown in figures 7.1.4.14 and 2.7.12 is related to the *countersunk* sheet of the joint, because this is the failure location obtained from the 2-A series coupons. The fatigue damage rate is lower if related to a larger net section, i.e. if related to the non-countersunk bore holes which are affected in the barrel. On the other hand, damages in the lower aluminium layers of the GLARE4A skin (i.e. not the mating aluminium layer) will initiate relatively earlier and propagate relatively faster in the full scale specimen, compared with the coupon. Consider that the stress deviation in the aluminium layers of the barrel panel is lower than for the coupon, due to the lower additional bending stress. For the present investigation it is considered that these effects compensate each other. Note that the (average) cracks link up at a = 11.2 mm.

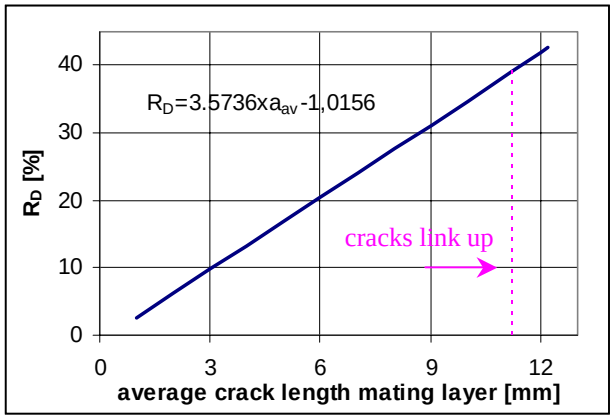

Figure 2.7.12. Forward rivet row in Megaliner Barrel skin, fatigue damage rate dependent on average crack length in mating aluminium layer

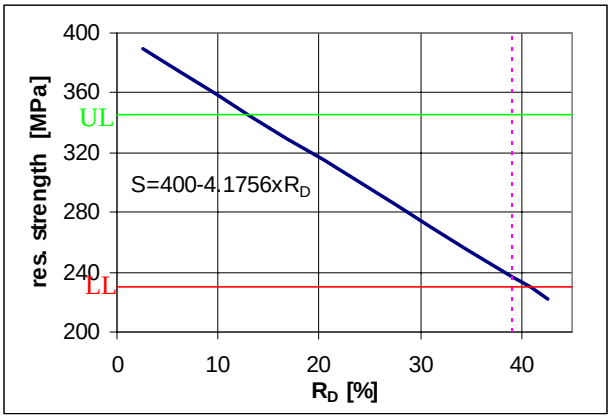

Figure 2.7.13, forward rivet row in the barrel skin, residual strength dependent on fatigue damage rate (gross stresses)

Figure 2.7.13 shows the relationship between the residual strength and the fatigue damage rate. Again this diagram is related to the countersunk side of the joint and therefore the residual strengths are

conservative. The relation between R_D and residual strength is obtained from the coupon specimens which have been tested after one year exposure in Queensland (see figure 7.1.8.22, R_D related to net stresses). The ultimate load capability is falling short below R_D=13.3% and an average crack length of 4.0mm in the mating aluminium layer of the laminate. At 40.8% R_D the point of wide spread fatigue damage (limit load capability) is reached. The collected information is now included in a fatigue diagram for PSE certification purposes. The crack initiation calculation is verified by the full scale test, the crack propagation curves have to be verified by a continuation of the Megaliner Barrel test. If the crack propagation predictions can be verified as well, all data shown in figure 2.7.11 can be divided by scatter factor 2 (scatter factor to be considered on full scale test according to FAR/JAR):

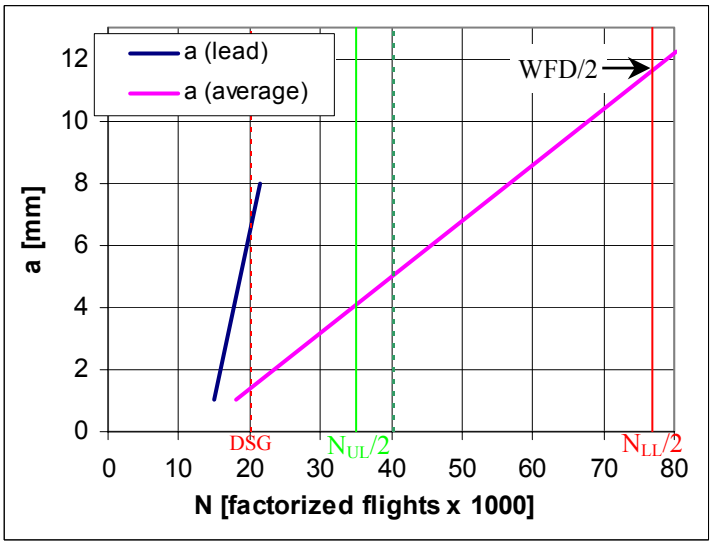

Figure 2.7.14. Fatigue strength justification plot for Megaliner Barrel repair, full scale and coupon test results considered, no ageing effects to be considered, scatter factor 2 on full scale test results and predictions included

With the factor 2 included for safety, the lead crack becomes detectable after 21500 flights, i.e. 1500 flights later then the aircraft would be removed from service. The ultimate load capability would be reached after 35000 flights and the limit load capability after 77000 flights.
Following the rules for metal structure damage tolerance, it is sufficient to validate in a full scale test that the structure is not falling short of the point of Wide Spread Fatigue Damage at the end of the test (2 x DSG). The inspection threshold N_{TH} is determined by division of N_{WFD} by a factor 2:

$$N_{TH} = N_{WFD} / 2 = 77000\, flights$$

The first directed inspection of the rivet rows is mandatory after 77000 flights for structural safety. This point is far beyond the design service goal of 20000 flights and indicates the significant structural reserve of GLARE structures. The reason for this behaviour is the long crack propagation life which moves the point of WFD and the inspection threshold far ahead of similar monolithic aluminium structures. For a long range aircraft it offers the possibility to increase the number of flight cycles without the necessity to reinforce the GLARE structure or to perform scheduled fatigue inspections. It is proposed by the author to set N_{UL} (factored) equal to the Extended Service Goal in [flights]. For the present example structure it would lead to:

$$ESG = N_{UL} / 2 = 35000\, flights$$

However, for economical reasons it can be expected that the aircraft manufacturer will perform not more than 2 DSG full scale testing for type certification, as required by FAR/JAR. For the given example, see figure 7.2.14, this would mean 40000 test flights in order to cover the DSG of 20000 flights with a scatter

factor 2. Any flight beyond the certified life requires approval from the authorities, who will probably demand more test evidence. It may therefore be clever to cut out some fatigue sensitive structural items from the full scale specimen and to store this items to continue fatigue testing with components and a final residual strength test. This procedure would require a critical review of the fatigue condition of the metallic structures connected to GLARE components. Significant fatigue damages in the aluminium structures, just below the point of wide spread fatigue damage, would imply that any further fatigue loading of a component is useless. Why should the certified fatigue life of a GLARE structure be extended, if the adjacent aluminium structure would prevent the aircraft from extended operation ?
If the above discussed situation occurs, it may be called an unbalanced design, because the fatigue life potential of GLARE is so much higher than in monolithic aluminium, but it remains unused. The high fatigue potential will be carried around as 'safety reserve'. It may be questioned whether GLARE is worth the investment under such conditions. Fortunately, it does not just offer the probably unused fatigue life but also substantial weight saving.
However, a possibility to use the high fatigue potential can occur. It is well known that some carriers use large aircraft, which are certified as a long range aircraft, for short range flights. For example Japanese Airlines fare lying Boeing 747's on short ranges. The short range profile leads to a higher demand for fatigue life which may force an aircraft manufacturer to redesign at least parts of his aircraft for the special utilization. Then, according to what has been demonstrated in this thesis, a redesign of the GLARE structures may not be necessary.
A life extension in terms of [years] would require a review of the environmental analyses and the associated knock down factors.

The investigated riveted repair joint is designed by the static yield strength criterion. However, no fatigue inspections are required through out the design life (20000 flights) of a long range aircraft. Instead, the design life can be extended. The major aspects which lead to this conclusion are summarized briefly:

- An application of the repair before the first flight is considered.
- The joint has 4 rivet rows which increases the static strengths.
- An estimated relation between static and fatigue loads.
- The yield strength which is considered as a design limit is obtained from 4 rivet row coupon tests.
- No ageing effects are considered for the long range application.
- Room temperature is considered for the applicable static failure cases.
- The crack initiation life which is obtained from the Megaliner Barrel must be considered as conservative, because the patch is removed and installed repeatedly without application of anti fretting compound after the first inspection (20000 flights). The mechanical loading without anti fretting compound can decrease the fatigue properties of a single shear joint (ref. chapter 7.1.2.9).

7.3 Conclusions

“An aircraft is considered airworthy when it is in conformity with its type design and is in a condition for safe operation.“
(Ref. FAA, see Airbus ABD0056)

The elementary investigations performed in chapter 6 are extended to a coupon specimen level in chapter 7, as a preparation for strength predictions of the two selected representative full scale structures, i.e. the GLARE2B-7/6-.4 experimental butt strap joint in the A340-600 EF2 and the repair patch on the Airbus Megaliner Barrel which implies the concept of a single-shear riveted joint. Four major items have been investigated in order to explore the influence of several factors on particular strength properties of GLARE, which are relevant for the results of full scale tests on GLARE structures carried out under room temperature conditions.

- Crack initiation scatter and crack propagation scatter in single shear GLARE joints.
- The influences of surface conditions and fastener types on fatigue failure modes and life time.
- The influence of natural ageing and variable temperature on fatigue properties.
- The validation of fatigue calculation methods which have been developed for monolithic aluminium for GLARE structures.

Scatter

The crack initiation and crack propagation scatter has been investigated with butt straps of the circumferential joint coupons (specimen series 2-B). Accounting for a geometrical factor which was discovered to influence the results, it has been verified that scatter of crack initiation period and scatter of the crack propagation rates in a rivet row of a single shear joint is not larger than observed for monolithic aluminium structures. Scatter, which may result from different aluminium lots used for manufacturing GLARE, was not a subject of this investigation.

Surface preparations of the mating surfaces of the joint

The influence of different surface preparations of the mating surfaces of single shear GLARE joints which lead to different adhesion between the mating metals and the anti fretting compound have been investigated. It includes the influences of anti fretting compound being not present or not hardened for unscheduled reasons. The influence can be significant. Crack initiation life reductions up to 33% and an increase of the crack propagation rate by a factor up to 1.3 can be observed. Due to the limited number of available specimens just trends have been observed. A *systematic* investigation of surface condition and manufacturing parameter influences on crack initiation and crack propagation is recommended.

Different fastener types and a variation of the manufacturing quality

The influence of slightly different fastener types in combination with a non-scheduled variation of manufacturing quality has been investigated. A systematic dependency of the crack initiation locations from the fastener type has been observed for the riveted repair coupon specimens. An attempt to safe money by using cheaper fasteners provided unexpected results to be considered. It is recommended to study the fatigue failure mode of any GLARE/fastener combination which shall be qualified for flying structures, also because information about the failure location is important for the NDT expert.

Natural aging

The influence of natural ageing on the fatigue and damage tolerance properties of long range aircraft is considered to be of minor importance according to the investigations performed in chapter 5. This preliminary conclusion is related to the moisture weight gain of the prepreg and the associated effect on the strength of the interlaminar properties. However, the specimens exposed in Queensland are subjected to temperature cycles at the same time. At any day the material temperature varies between approximately 20°C at night and 70°C during lunch time. Static strength, crack propagation and residual strength tests were performed on GLARE specimens which returned from Australia after one year exposure. No strength reduction was observed as predicted. But a more pronounced 'ticking noise' is audible during the residual strength test on riveted joints which have been exposed if compared to tests on specimens which were not exposed. Destructive inspections on several specimens indicated that the ticking noise should be attributed to local fiber failure which happens at locations of severe fatigue damages. The ticking noise is heard at stress levels above the maximum fatigue stress for all specimens tested so far. The phenomenon has to be carefully investigated further with the specimens which return from the outdoor exposure site in 2004 and 2008.

Blunt notch strength

The blunt notch strength decreases after 3000 hours accelerated ageing (chapter 6). The residual strength of riveted joints did not decrease after one year (=8760 hours) accelerated ageing.

Temperature effects

Fatigue spectrum tests on circumferential joint coupons at constant room temperature and with temperature cycles during each simulated flight did not show differences between the crack initiation fatigue life and the crack propagation behaviour. The crack initiation life has been calculated with accounting for the additional stress cycle due to the thermal cycling occurring in each flight (-30^0C to $+70^0$C), a stress cycle associated with the different coefficients of thermal expansion.
The calculated result indicated a decrease of the crack initiation life of 50% if compared to the calculated result for constant room temperature. Obviously, the improved 2024-T3 crack growth behaviour at temperatures below 0°C and the load redistribution from the aluminium to the fibers due to the stiff resin at low temperatures compensates the calculated disadvantage. The investigation will be continued by Airbus with additional specimens (long duration tests) until the end of 2004.

Application of calculated peak stresses at the edge of fastener holes in the mating surface layer

Basic rules used for the calculation of crack initiation in monolithic aluminium can also be applied to the aluminium layers of GLARE. It requires an accurate determination of the stresses in the particular aluminium layers. As for monolithic aluminium joints, the secondary bending stress has a significant influence on the predictions. Therefore the 'reference joint' calculation method which has been defined by Airbus and the Delft University for the calculation of crack initiation in riveted joints, is very suitable. The neutral line bending model developed by Schijve is useful for comparative predictions, although it is not necessarily very accurate for exact results of the bending stress. The model has been applied to both the aluminium reference joint and the GLARE joint to be analyzed in the same manner. Satisfactory prediction results were obtained for the GLARE joint.

Fatigue predictions for GLARE joints under variable-amplitude loading

The Relative Miner Rule is applicable for crack initiation predictions in the aluminium layers of GLARE under load spectrum conditions. The 'equal slope concept', used for the calculation of SN-data for different stress ratios R, can be applied for the aluminium layers in GLARE in the same way as for monolithic aluminium.

A helpful tool for the prediction of variable load spectra fatigue properties based on constant amplitude material data is obtained with the determination of a spectrum factor. For crack initiation it is based on the Miner rule, i.e. a comparison of the damage obtained from the total of the of stress range pairs in a flight spectrum with the damage provided by a single representative load cycle. It is shown in this thesis that the method is equally satisfactory for GLARE structures as for monolithic aluminium structures.

A prediction of crack *propagation* rates under variable load conditions is not reliable for GLARE by a simple addition of crack extensions related to single load cycles and the associated da/dN data obtained from constant amplitude tests. The variable amplitude crack propagation prediction is non-conservative with simple Δa-countings. Analysis of three different configurations led to the conclusion that the reference stress should be multiplied with an empirical factor of 1.5 for the calculation of the equivalent stress. The history effect of fatigue delamination size is believed to be a main source for the observed effect. Fatigue delamination in the wake of the crack, plastic deformation around the tip of the crack in the aluminium layer, crack opening and ΔK-threshold are complex boundary conditions for the prediction of variable amplitude crack propagation rates in GLARE. It is strongly recommended to investigate this item further.

Spectrum truncation and omission

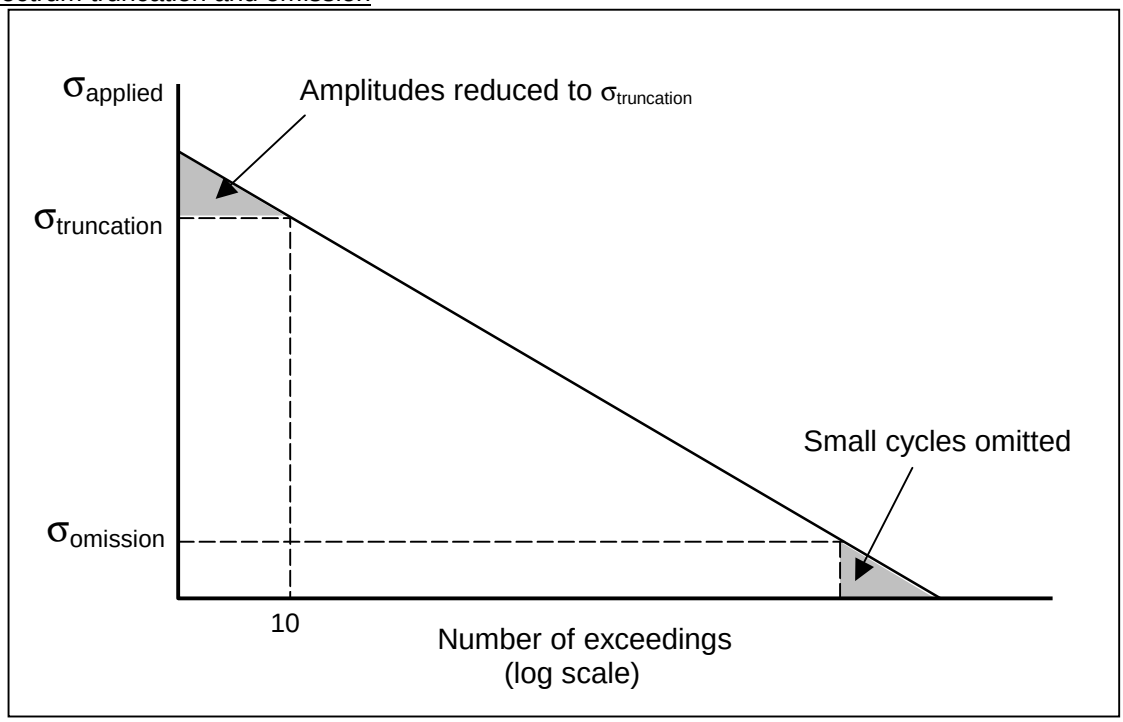

Figure 7.3.1. Load spectrum with truncation of high amplitude cycles and omission of very low amplitude cycles.

In the context of fatigue under variable-amplitude loading under flight-by-flight load histories the problem of the influences of spectrum truncation and omission should be considered. Schijve proposed to truncate load spectra at a level which will be exceeded ten times in an aircraft life [29], see figure 7.3.1. For monolithic aluminium, the effect of truncation high amplitude cycles on the crack propagation rates is

conservative, i.e. the crack will grow faster because of less retardation introduced by high peak loads. Truncating to a lower level than indicated in figure 7.3.1 will further enhance the crack growth rate which then is still more conservative. The same trend was observed by Schijve et al. [36] for GLARE 1 and GLARE2.

Omission of very small cycles is generally done for time saving on the duration of a test. The spectrum omission implies that cycles with a low amplitudes are omitted from the applied load history. The omission stress level ($\sigma_{omission}$) is selected sufficiently low to be sure that those cycles would not have contributed to the fatigue damage. Actually, it should be shown by experimental evidence that the omission is justified. Such evidence is amply available for monolithic aluminium alloy specimens, but not for fiber-metal laminates. However, the experience of the monolithic material is useful as a guide line for GLARE as well.

Static and a fatigue strength justification

A static and a fatigue strength justification is performed for both the A340-600 single-strap butt joint and the Megaliner Barrel repair. Static design stresses are estimated for the analyses. The software 'DTToolbox' works reliable for the prediction of crack initiation and crack propagation in the mating (highest loaded) aluminium layer. The program is checked with detailed test data from the coupon specimens.

Fatigue results are obtained from the Megaliner Barrel specimen for the repair for verification of the calculated results. The static yield criterion (GLARE4 repair) is providing the design limit for the repair.

Static strength prediction for the joints based on rivet strength results according to specification MIL-STD-1312 are compared with coupon results. For both, tensile yield and ultimate, the MIL-STD test provides non-conservative results. This effect is explained by the additional rivet rows in realistic joints, which lead to different load distributions per rivet row compared with the fifty/fifty load distribution which is present in a MIL-STD-1312 specimen.

In both cases, i.e. the butt strap and the repair, no scheduled fatigue inspections are required for both PSE's.

Factors to be applied on full scale structure test results

- Material scatter factor for crack initiation: similar as for monolithic aluminium
- Material scatter factor for crack propagation: similar as for monolithic aluminium
- Environmental factor on crack initiation: none
- Variable temperature on crack initiation: none (tests continue until end 2004)
- Environmental factor on crack propagation: none (to be reviewed after end of outdoor exposure test in 2008)
- Variable temperature on crack propagation: none (tests continue until end 2004)
- Environmental factor on residual strength: none (to be reviewed after end of outdoor exposure test in 2008)
- Temperature factor on residual strength of joint: none considered because the investigated PSE's are tensile load dominated and no high tensile loads occur at high temperatures.

Test result:: The residual strength drops by 12% at 70°C material temperature for fatigue damage rates from 0% to 20% (ref. chapter 10).

All valid JAR/FAR paragraphs are satisfied. There is no need to specify a special condition according to FAR/JAR 21.16 for the application of GLARE on commercial aircraft.

7.4 References

[1] An Experimental and Analytical Investigation on the Behavior of Fuselage Riveted Lap Joints, R. Müller, PhD Thesis, 1995

[2] Method for predicting the fatigue initiation life in mechanically fastened joints in GLARE sheets, J. Homan, Delft University of Technology, Report B2V-00-32, 2000

[3] Airbus F&DT Guideline

[4] Fatigue of Metallic Materials – Theory, D. Duprat, Aerospatiale Fatigue Trainings Course, 1998

[5] Feasibility of Eddy Current Inspection for detection of fatigue crack initiation in Glare joints, L. Schra, H. ten Hoeve, NLR report NLR-CR-2001-565

[6] Crack measurement methods for fatigue investigations on Glare outdoor exposure specimens, B.Borgonje, Delft University of Technology, Report B2V-02-14, 2002

[7] GTO P1.1 Durability Program, MoM EMF-932/99, 1999

[8] Richtlinien für die rechnerische Ermittlung der Lebensdauer von Bauteilen des Airbus A300, W. Goβe, Deutsche Airbus GmbH, 1969

[9] Report TN-M2111, NLR

[10] Crack Initiation and Crack Propagation Scatter in GLARE Open Hole Specimens, Th. Beumler, B. Borgonje, Delft University of Technology, Report B2V-01-26, Issue 1, 2001

[11] A380 Nachweisprogramm Längs- und Quernähte, Rißinitiierung und statistische Verteilung, Th. Beumler, Airbus Deutschland GmbH, Bericht 10L022K4700P04, 2001

[12] Ermittlung dynamischer Festigkeitskennlinien durch nichtlineare Regressionsanalyse, M. Gecks, F. Och, aus: Probleme der Festigkeitsforschung im Flugzeugbau und Bauingenieurwesen, Herausgegeben von M. Esslinger und B.Geier, 1977

[13] Calculation method for predicting the fatigue life of riveted joints, J. Homan, A. Jongebreur, ICAF 1993

[14] Aerospatiale Fatigue Manual, Document MTS005, Issue B

[15] Repair Assessment Guidelines, DaimlerChrysler Aerospace Airbus Report 10X00274450C02

[16] The Influence of the Dimensions of Riveted Lap Joints and Strap Joints on the Secondary Bending, A. Hartmann, J. Schijve, NLR Report TR 68026, 1968

[17] The Effect of Secondary Bending on the Fatigue Strength of 2024-T3 Alclad Riveted Joints, A. Hartmann, J. Schijve, NLR Report TR 69116, 1969

[18] Programm KAEPPL.FORT(SEBIANSJ) zur Berechnung der Biegespannungsanteile beim strap joint, M. Käppeler, Deutsche Airbus, 1991

[19] Crack initiation and crack propagation scatter in GLARE riveted joints, Th. Beumler, Airbus Deutschland GmbH, Report 00L022K4900P04, 2002

[20] A300B2/B4, Widespread Fatigue Damage Testing – Batch 2.1, 2.2 and 2.6 : MSD Crack Propagation – Circumferential Joints, H. Trey, EADS Airbus, Report 10X022K4751I04

[21] A300B2/B4, Widespread Fatigue Damage Testing – Batch 5 : MSD Crack Propagation – Generic tests, H. Trey, EADS Airbus, Report 10X022K4753I04

[22] A300B2/B4, Widespread Fatigue Damage Testing – Summary Report, H. Trey, EADS Airbus, Report 10X022K4758I04

[23] General environmental conditions for composites, Airbus Document ABD0087

[24] Miner Rule and Spectrum Factor Investigation on GLARE Riveted Joints, Th. Beumler, B. Borgonje, Delft University of Technology, Report B2V-02-63, 2002

[25] Cumulative damage in fatigue, A. Miner, J.Appl.Mech., Vol. 12, 1945

[26] The prediction of fatigue life in the crack initiation and crack propagation stages. A state of the art survey. W. Schütz, Eng. Fracture Mechanics, Vol. 11, 1979

[27] Fatigue of Structures and Materials, J. Schijve, Kluwer Academic Publishers, ISBN 0-7923-7013-9, 2001

[28] Fatigue predictions and scatter, J. Schijve, Delft University of Technology, Report LR-696, 1982

[29] The significance of flight-simulation fatigue tests, J. Schijve, Delft University of Technology, Report LR-466, 1985

[30] Fatigue test results of A320 and A321 circumferential butt joint panel specimens, Th. Beumler, Deutsche Airbus GmbH, Report 10D/E022K4753C04, 1991

[31] The Metal Volume Fraction Approach, G. Roebroeks, SLI Report TD-R-00-003, 2000

[32] Test program to ascertain effect of the thermal and ageing effects on GLARE lap joints and butt joints, Th. Beumler, Airbus Deutschland GmbH, Report 10L022K4801I04, 2000

[33] The effect of temperature and ageing on GLARE circumferential joints, M. Ypma, Delft University of Technology, Report B2V-02-46, 2002

[34] Fuselage Spectrum Fatigue Loading on Fiber Metal Laminates, A. Woerden, Master Thesis, Delft University of Technology, 1998

[35] Test Description of Airbus 'GLARE' Testing, W. Schwarting, EADS Space Transportation, Report LO76-RIBRE-TN-0001, 2003

[36] Flight simulation fatigue tests on notched specimens of fiber metal laminates, J. Schijve, F. Wiltink, V. van Bodegom, Delft University of Technology, Report LRV-10, 1994

[37] Werkstoffkundlicher Untersuchungsbericht, Auftrag 9721, U. Tuemena, Airbus Deutschland GmbH, 2003

[38] Load History Effects during Fatigue Crack Propagation in GLARE, R. Alderliesten, H. Woerden, Delft University of Technology, ICAF Conference 2003, Luzern, 2003

[39] Fatigue crack growth of part through the thickness cracks in GLARE3 and GLARE4B coupons, A.U. de Koning, L. Schra, revised edition of report NLR-CR-2000-078, Decmeber 2001

[40] Werkstoffkundlicher Untersuchungsbericht, Auftrag 9698, B. Fritzsche, Airbus Deutschland GmbH, 2003

[41] Fatigue Crack Propagation Tests in Surface and Part Through Cracks, Ch. Randell, Delft University of Technology, Report B2V-02-58, 2002

[42] Fatigue of Structures and Material, Jaap Schijve, Kluwer Academic Publishers, ISBN 0-7923-7013-9 (HB)

[43] Handbuch für Strukturberechnung, Band III, Kapitel 63111-01

Chapter 8-11
Returning Specimens / Panel Tests / Door Corner Cut Out

'Eins - zwei – drei, im Sauseschritt,
eilt die Zeit – wir eilen mit.'
Wilhelm Busch

8. Returning Outdoor Exposure Specimens

Specimens have been shipped to the Australien exposure site in January 2002 and in April 2002. A few specimens have been returned after one year exposure - the results from these specimens are included in the previous chapters.

The remaining specimens shall return to Delft University in three batches, i.e. after 2 years, 4 years and 6 years exposure in the years 2004, 2006 and 2008, respectively. This chapter details the particular shipment batches and the particular evaluations which have to be performed. The final conclusion shall support the definition of realistic knock down factors due to environmental ageing, to be considered for design allowables and to be applied on the full scale fatigue test article.

Returning dates of all specimens from the outdoor exposure test site, overview
(Bonded repair panels are discussed in chapter 9):

Return batch 2004, after 2 years outdoor exposure

Specimen Type	Designations	Return Date
Circumferential Joint Coupon	2-B-6	January-04
	2-B-7 to 2-B-12	January-04
	2-B-37, -38, -41, -42	January-04
	2-B-44 and 2-B-45	January-04
	2-B-52 to 2-B-57	January-04
Riveted Repair Coupon	2-A-7 to 2-A-12	April-04
	2-A-19 to 2-A-24	April-04
Blunt Notch GLARE2B	3-B-19 to 3-B-27	January-04
Blunt Notch GLARE4A	3-A-15 to 3-A-19	April-04
Bearing Specimen GLARE2B	4-B-21 to 4-B-25	January-04
Bearing Specimen GLARE4A	4-A-11 to 4-A-15	January-04
Rivet Strength GLARE2B	5-B-11 to 5-B-20	January-04
Rivet Strength GLARE4A	5-A-11 to 5-A-20	January-04
CFH GLARE2B	6-B-13 to 6-B-15	April-04
CFH GLARE4A	6-A-10 to 6-A-12	April-04
Rivet Pull Through GLARE2B	7-B-16 to 7-B-25	April-04
Rivet Pull Through GLARE4A	7-A-16 to 7-A-25	April-04
Riveted Repair Panel	11-RR-2 & 11-RR-3	April-04
Thick Adhered Specimen	14-B-13 to 14-B-18	January-04

Return batch 2006, after 4 years outdoor exposure

Specimen Type	Designations	Return Date
Circumferential Joint Coupon	2-B-1 to 2-B-5 2-B-39 to 2-B-40 2-B-72	January-06
Bonded Repair Panel	12-BR-03	April-06

Return batch 2008, after 6 years outdoor exposure

Specimen Type	Designations	Return Date
Circumferential Joint Coupon	2-B-29 to 2-B-36 2-B-46 to 2-B-48 2-B-58 to 2-B-2-B-71 2-B-73 to 2-B-75	January-08
Riveted Repair Coupon	2-A-13 to 2-A-18 2-A-25 to 2-A-30	April-08
Blunt Notch GLARE2B	3-B-28 to 3-B-38	January-08
Blunt Notch GLARE4A	3-A-20 to 3-A-24	April-08
Bearing Specimen GLARE2B	4-B-26 to 4-B-30	January-08
Bearing Specimen GLARE4A	4-A-16 to 4-A-20	January-08
Rivet Strength GLARE2B	5-B-21 to 5-B-30	January-08
Rivet Strength GLARE4A	5-A-21 to 5-A-30	January-08
CFH GLARE2B	6-B-16 to 6-B-18	April-08
CFH GLARE4A	6-A-16 to 6-A-19	April-08
Rivet Pull Through GLARE2B	7-B-26 to 7-B-30	April-08
Rivet Pull Through GLARE4A	7-A-26 to 7-A-30	April-08
Moisture Reference	all specimens	January-08
Riveted Repair Panel	11-RR-4 & 11-RR-5	April-08
Door Corner Cut Out	all specimens	April-08
Thick Adhered Specimen	14-B-19 to 14-B-24	January-08

8.1 Experimental tasks for returning batch in year 2004

The optical condition of all specimens before testing and the failure modes in case of ultimate tests have to be recorded. Average crack lengths definitions as in previous chapters. All tests to be conducted at room temperature if not specified differently.

Specimen No.	Test to be performed	Reference / Comparison	Remarks
2-B-6	Crack propagation CA, $F_{max.}$=38.9kN	Corrosion Inspection + absorption determination	
2-B-7	Crack propagation CA, $F_{max.}$=38.9kN	Compare with results from 7.1.4	Crack lengths before exposure are recorded in table 8.1
2-B-8 to 2-B-12	Yield strength (secondary modulus) and residual strength	Compare with results from 7.1.7.1	Crack lengths before exposure are recorded in table 8.1
2-B-37 2-B-38	Crack propagation CA, $F_{max.}$=38.9kN	Compare with results from 7.1.4	Average crack lengths before exposure: 1.96mm / 1.55mm
2-B-41, -42, 2-B-44, -45	Crack propagation CA, $F_{max.}$ according to specification in table 8.1	Compare with results from 7.1.4	Crack lengths before exposure are recorded in table 8.1
2-B-52	Yield strength (secondary modulus) and residual strength	Compare with results from 7.1.7.1	Specimen not pre-fatigued

Experimental tasks for returning batch in year 2004, cont'd

Specimen No.	Test to be performed	Reference / Comparison	Remarks
2-B-53 2-B-56	Yield strength (second. modulus) and residual strength in compression	No data base without exposure available	Average crack lengths before exposure are recorded in table 8.1
2-B-57	Crack propagation, variable amplitude and variable temperature	Compare with results from 7.1.6	Average crack lengths before exposure recorded in table 8.1
2-A-7 to 2-A-12	Crack propagation CA at different stress levels	Compare with results from 7.1.4	Average crack lengths before exposure (calculated): 0.5mm
2-A-19 to 2-A-24	Residual strength	Compare with results from 7.1.8.2	Average crack lengths before exposure: 2-A-19: 2.18mm 2-A-20: 6.59mm 2-A-21: 0.65mm 2-A-22: 1.76mm 2-A-23: 0.21mm 2-A-24: 3.13mm
3-B-19 to 3-B-23	Residual strength	Compare with results from 6.9.2	Specimens to be milled before test, ref. 3.2.4, crack lengths before exposure recorded in table 8.2
3-B-24	Crack propagation	Compare with results from specimens 3-B-37 and 3-B-38	Ref. 6.7, crack lengths before exposure in table 8.2
3-B-25 to 3-B-27	Blunt notch strength	Compare with results from 6.9.2	Specimens to be milled before test, ref. 3.2.4, specimens not pre-fatigued
3-A-15 to 3-A-18	Residual strength	Compare with results from 6.9.2	Specimens to be milled before test, ref. 3.2.4, crack lengths before exposure recorded in table 8.3
3-A-19	Blunt notch strength	Compare with results from 6.9.2	Specimen to be milled before test, ref. 3.2.4, specimen not pre-fatigued
4-B-21 to 4-B-25	Bearing strength	Compare with results from 6.11	Specimens not pre-fatigued
4-A-11 to 4-A-15	Bearing strength	Compare with results from 6.11	Specimens not pre-fatigued
5-B-11 to 5-B-15	Rivet strength	Compare with results from 6.11	Specimens not pre-fatigued
5-B-16 to 5-A-20	Rivet strength at 70°C	Compare with results from 6.11	Specimens not pre-fatigued
5-A-11 to 5-A-15	Rivet strength	Compare with results from 6.11	Specimens not pre-fatigued
5-A-16 to 5-A-20	Rivet strength at 70°C	Compare with results from 6.11	Specimens not pre-fatigued

Experimental tasks for returning batch in year 2004, cont'd

Specimen No.	Test to be performed	Reference / Comparison	Remarks
6-B-16 to 6-B-18	Compression filled hole tests	Compare with results from chapter 6.13	Crack lengths before exposure recorded in table 6.13.1a
6-A-16 to 6-A-18	Compression filled hole tests	Compare with results from chapter 6.13	Crack lengths before exposure recorded in table 6.13.1b
7-B-16 to 7-B-20	Rivet pull through tests	Compare with results from chapter 6.12	Crack lengths before exposure recorded in table 6.12.1a
7-B-21 to 7-B-25	Rivet pull through tests at 70°C	Compare with results from chapter 6.12	Crack lengths before exposure recorded in table 6.12.1a
7-A-16 to 7-A-20	Rivet pull through tests	Compare with results from chapter 6.12	Crack lengths before exposure recorded in table 6.12.1b
7-A-21 to 7-A-25	Rivet pull through tests at 70°C	Compare with results from chapter 6.12	Crack lengths before exposure recorded in able 6.12.1b
11-RR-2	1) Rivet 2 stringer on specimen 2) Calibrate specimen with Megaliner Barrel 1/flight stress 3) Cycle specimen 50000 Megaliner Barrel flights, no truncation, no omission 4) Disassemble repair patch and measure crack lengths. 5) Reassemble specimen with ASNA2026-3A fasteners, no new sealant required. 6) Perform residual strength test at room temperature.	Compare with results from chapter 10	
11-RR-3	1) Disassemble repair patch and measure crack lengths. 2) Reassemble specimen with ASNA2026-3A fasteners, no new sealant required. 3) Perform residual strength test at room temperature.	Compare with results from chapter 10, and with specimen 11-RR-2	
13-1 & 13-2	CI & CP	Compare with results from B2V-00-54	
14-B-13 to 14-B-18	Remove fastener, pull to failure	Compare with results from chapter 4.5	

8.2 Experimental tasks for returning batch in year 2006

The optical condition of all specimens before testing and the failure modes in case of ultimate tests have to be recorded. Average crack lengths definitions as in previous chapters. All tests to be conducted at room temperature if not specified differently.

Specimen No.	Test to be performed	Reference / Comparison	Remarks
2-B-1 to 2-B-5	Yield strength (second. modulus) and tensile residual strength test	Compare with results from 7.1.7.1	Average crack lengths before exposure are recorded in table 8.1
2-B-39	Crack propagation, variable amplitude and variable temperature	Compare with results from 7.1.6	Average crack lengths before exposure: 0.68mm
2-B-40	Crack propagation CA, $F_{max.}$=38.9kN	Compare with results from 7.1.4	Average crack lengths before exposure: 0.94mm
2-B-72	Yield strength (second. modulus) and tensile residual strength test	Compare with results from 7.1.7.1	Average crack lengths before exposure are recorded in table 8.1

8.3 Experimental tasks for returning batch in year 2008

The optical condition of all specimens before testing and the failure modes in case of ultimate tests have to be recorded. Average crack lengths definitions as in previous chapters. All tests to be conducted at room temperature if not specified differently.

Specimen No.	Test to be performed	Reference / Comparison	Remarks
2-B-29 to 2-B-36	Establish SN_i-curve by trial and error	Compare with results from chapter 7.1.3	All specimens un-fatigued before exposure
2-B-46 to 2-B-48	Crack propagation CA, $F_{max.}$=38.9kN	Compare with results from chapter 7.1.4	Average crack lengths before exposure are recorded in table 8.1
2-B-58 to 2-B-63	Yield strength (secondary modulus) and residual strength	Compare with results from chapter 7.1.7.1	Fatigue loading before exposure, all specimens loaded at Fmax.=38.9kN 2-B-58: N=0 kcycles 2-B-59: N=100 kcycles 2-B-60: N=200 kcycles 2-B-61: N=300 kcycles 2-B-62: N=400 kcycles 2-B-63: N=500 kcycles
2-B-64 to 2-B-69	Yield strength (secondary modulus) and residual strength in compression	Compare with results after 2 years exposure	Fatigue loading before exposure, all specimens loaded at Fmax.=38.9kN 2-B-64: N=0 kcycles 2-B-65: N=100 kcycles 2-B-66: N=200 kcycles 2-B-67: N=300 kcycles 2-B-68: N=400 kcycles 2-B-69: N=500 kcycles

Experimental tasks for returning batch in year 2008, cont'd

Specimen No.	Test to be performed	Reference / Comparison	Remarks
2-B-70	Yield strength (secondary modulus) and residual strength	Compare with results from chapter 7.1.7.1	Specimen not fatigued before exposure
2-B-71	Yield strength (secondary modulus) and residual strength	Compare with results from chapter 7.1.7.1	Average crack lengths approximately 7.5mm
2-B-73 and 2-B-74	Yield strength (secondary modulus) and residual strength	Compare with results from chapter 7.1.7.1	Average crack lengths before exposure are recorded in table 8.1
2-B-75	Yield strength (secondary modulus) and residual strength	Compare with results from chapter 7.1.7.1	Cracks linked up before exposure, specimen was cycled 400000 times at Fmax = 38.9kN
2-A-13 to 2-A-18	Crack propagation CA at different stress levels	Compare with results from chapter 7.1.4	Average crack lengths before exposure (calculated): 0.5mm
2-A-25 to 2-A-30	Residual strength	Compare with results from chapter 7.1.8.2	Measure fatigue crack length after residual strength tests
3-B-33	Crack propagation	Compare with results from specimens 3-B-37 and 3-B-38	Ref. 6.7, crack lengths before exposure in table 8.2
3-B-28 to 3-B-32	Residual strength	Compare with results from chapter 6.9.2	Specimens to be milled before test, ref. 3.2.4, crack lengths before exposure recorded in table 8.2
3-B-34 to 3-B-36	Blunt notch strength	Compare with results from chapter 6.9.2	Specimens to be milled before test, ref. chapter 3.2.4, specimens not pre-fatigued
3-A-20 to 3-A-23	Residual strength	Compare with results from chapter 6.9.2	Specimens to be milled before test, ref. chapter 3.2.4, crack lengths before exposure recorded in table 8.3
3-A-24	Blunt notch strength	Compare with results from chapter 6.9.2	Specimen to be milled before test, ref. 3.2.4, specimen not pre-fatigued
4-B-26 to 4-B-30	Bearing strength	Compare with results from chapter 6.11	Specimens not pre-fatigued
4-A-16 to 4-A-20	Bearing strength	Compare with results from chapter 6.11	Specimens not pre-fatigued
5-B-21 to 5-B-25	Rivet strength	Compare with results from 6.11	Specimens not pre-fatigued
5-B-26 to 5-A-30	Rivet strength at 70°C	Compare with results from chapter 6.11	Specimens not pre-fatigued
5-A-21 to 5-A-25	Rivet strength	Compare with results from chapter 6.11	Specimens not pre-fatigued
5-A-26 to 5-A-30	Rivet strength at 70°C	Compare with results from chapter 6.11	Specimens not pre-fatigued

Experimental tasks for returning batch in year 2008, cont'd

Specimen No.	Test to be performed	Reference / Comparison	Remarks
6-B-16 to 6-B-18	Compression filled hole tests	Compare with results from chapter 6.13	Crack lengths before exposure recorded in table 6.13.1a
6-A-16 to 6-A-18	Compression filled hole tests	Compare with results from chapter 6.13	Crack lengths before exposure recorded in table 6.13.1b
7-B-26 to 7-B-30	Rivet pull through tests	Compare with results from chapter 6.12	Crack lengths before exposure recorded in table 6.12.1a
7-A-26 to 7-A-30	Rivet pull through tests	Compare with results from chapter 6.12	Crack lengths before exposure recorded in table .12.1b
11-RR-4	1) Rivet 2 stringer on specimen 2) Calibrate specimen with Megaliner Barrel 1/flight stress 3) Cycle specimen 50000 Megaliner Barrel flights, no truncation, no omission 4) Disassemble repair patch and measure crack lengths. 5) Reassemble specimen with ASNA2026-3A fasteners, no new sealant required. Perform residual strength test at room temperature.	Compare with results from chapter 10, and with specimens 11-RR-2 and 11-RR-3	
11-RR-5	1) Disassemble repair patch and measure crack lengths. 2) Reassemble specimen with ASNA2026-3A fasteners, no new sealant required. 3) Perform residual strength test at room temperature.	Compare with results from chapter 10, and with other specimens	
14-B-19 to 14-B-24	Remove fastener, pull to failure	Compare with results from chapter 4.5	

9. Bonded Repair

Nowadays, “reparability” is an important design case which is also well recognized by the airlines for any new materials. Chapters 9 and 10 are dealing with the repair technology for GLARE used as the material for the skin of an aircraft fuselage. The present chapter 9 covers an investigation on bonded repairs patches and chapter 10 is associated with riveted repairs.

A riveted repair has been applied to the Megaliner Barrel structure (panel D1), see sections 3.1.1 with an evaluation of the properties in Chapter 7. It was then decided to apply a bonded repair at a similar position on the barrel test article, but just at the opposite side of the structure. The panel at this position is made of GLARE4A-5/4-.4ssc material with a GLARE2A stringer attached. A bonded repair of this panel serves as a reference for 5 flat panels with a similar GLARE skin and a bonded repair patch. Three of the 5 panels are exposed outdoors since April 2002. The other two panels have been fatigue tested in order to observe possible crack growth and delamination damage. The purpose of the tests is to examine possible degradations of the repair strength either due to the environmental exposure, due to fatigue of due to the superposition of both. The loading conditions, the repair technology, strain measurements, FEM calculations and initial fatigue test results are described and evaluated.

A dominating load case in this area is the 1g+ Δp+10ft/s vertical gust and due to fuselage bending the main load direction occurs in the longitudinal direction. The circumferential stress caused by the internal pressure is low due to the relatively high skin thickness. The high longitudinal loads in the full scale specimen require the selection of GLARE4 for the repair doubler, although for practical reasons GLARE3 doublers are recommended by the author in order to avoid problems in service with respect to available GLARE types. Some standardization of GLARE repairs is advisable. Even more important, it would prevent that GLARE4 is applied on an aircraft in the wrong direction (90°rotated).
The damage is repaired by applying an elliptical GLARE patch, see figure 9.1. Some undefined damage is removed by a cut out in the barrel skin with the dimensions 60mm x 60mm, corner radii 8mm. Previous fatigue experience concerning the behaviour of bonded repaired structures at the location of the doubler run outs (edges) was limited to thinner GLARE materials. Kuijpers found no cracks in a GLARE3-4/3-.4 with a bonded structure (skin and doubler) made of GLARE3-3/2-.4 (t=1.7mm) after 150000 fatigue cycles at 150 MPa applied load [1].
The once per flight stress applied on the barrel is lower, but the stiffness step significantly larger than for Kuijpers tests due to the 3.5mm thick skin and repair patch. *Before* the cut out has been machined into the barrel skin, a strain gauge rosette was bonded on the outside at that very location. The following strains have been measured for the load case 1g+ Δp+10ft/s vertical gust:

Aircraft length direction: 1520mm/m
Fuselage circumferential direction: 469µm/m
45 degree: 948µm/m

As a result, the stress in aircraft length direction in the undamaged barel skin is:

$$\sigma = \frac{1520 \times 0.072 + 0.3 \times 469 \times 0.072}{1 - 0.3^2} = 131\ MPa$$

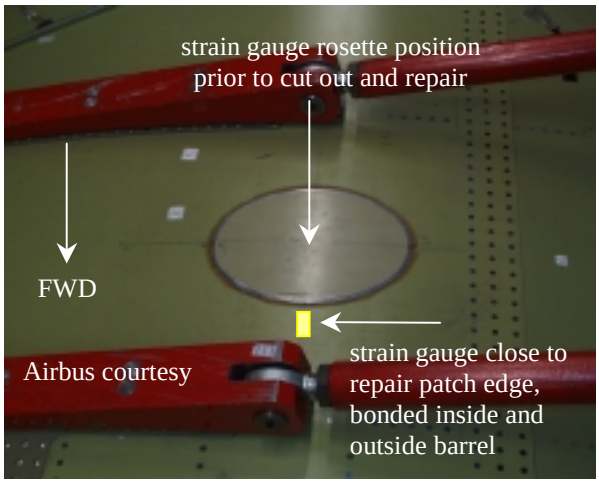

Figure 9.1. Bonded repair patch on Megaliner Barrel, view from outside, between frames 73 & 74

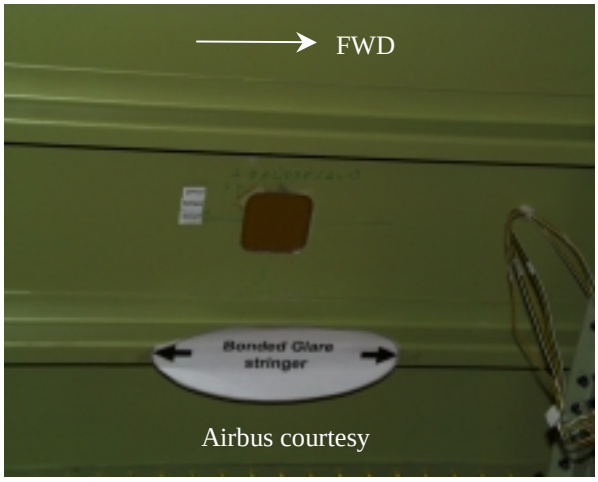

Figure 9.2. Cut out below bonded repair patch, view from inside, between stringer 3 & 4

In the undamaged GLARE4A-5/4-.4 skin the corresponding stress is:

$$\sigma = \frac{1520 \times 0.0569 + 0.3 \times 469 \times 0.0569}{1 - 0.3^2} \times 56900 = 103\ MPa$$

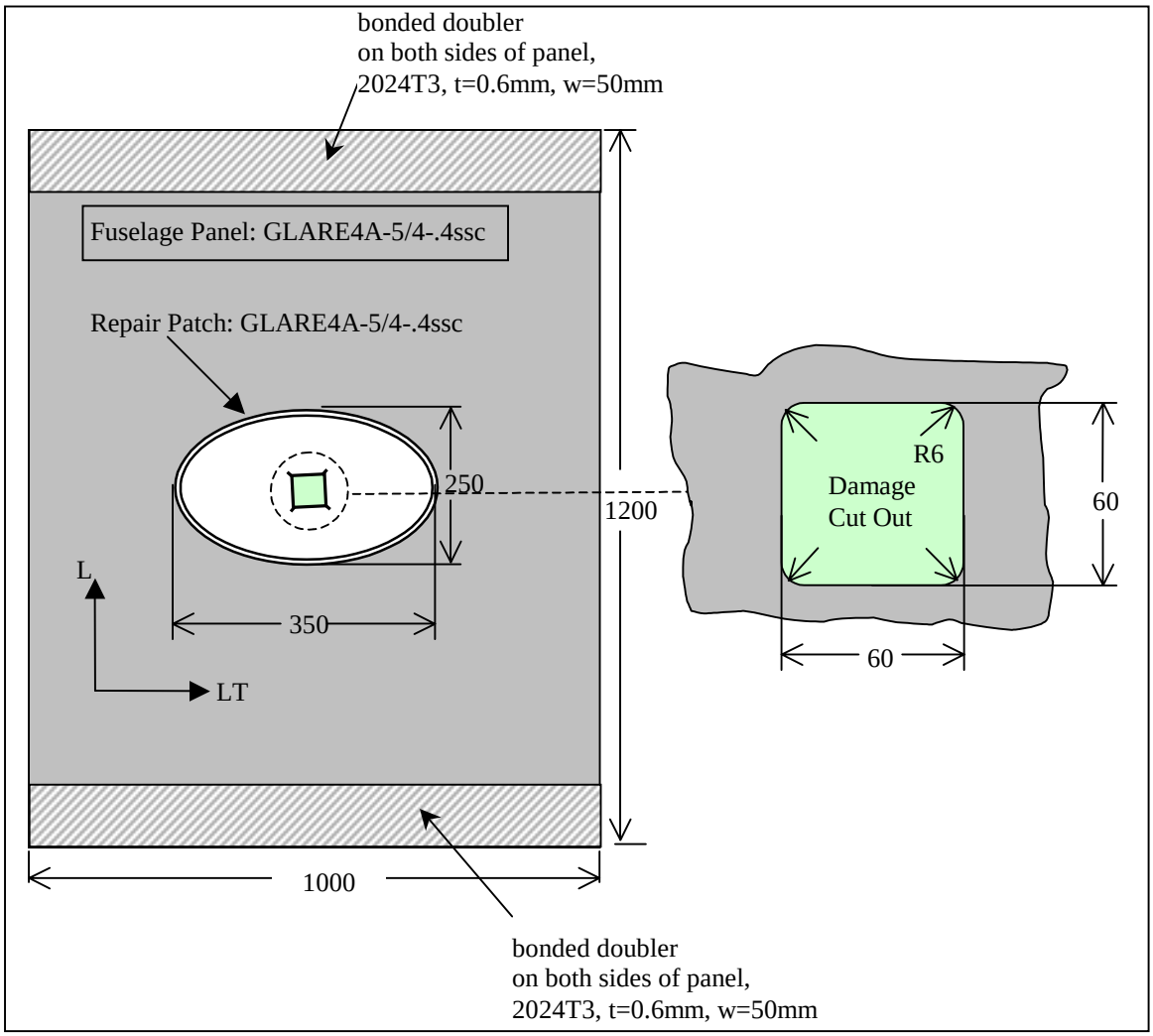

Figure 9.3. Non-stiffened bonded repair patch panel, test series 12-BR

Trials to calculate the required patch dimensions with the USAF / TU Delft computer program `CALCUREP´ failed. The program was not able to handle both the high allowable fatigue stress (input: 140 MPa) and the high allowable static stress (input: 315 MPa) for GLARE4A.
Because the repair panel tests with the similar design should be performed parallel to the Megaliner Barrel test – with and without ageing – it was decided to define the patch dimensions according to the limits of the available test equipment. Load-wise it turned out that a width of 1m should not be exceeded for the test panels.. In order to obtain a relation of panel width to patch width, which allows a representative stress distribution around the patch, the patch width was limited to 350mm (perpendicular to the main load direction). An oval patch is chosen in order to avoid stress peaks at corners. The patch length (in load direction) is defined with 250mm, see figure 9.3.

The production of the repair patches encompasses the following steps for both the Megaliner Barrel and the flat panels:

- Drilling four 12mm holes at the cut out edge position.
- Sawing straight lines from hole to hole.
- Deburring the edges of the cut out.
- Sawing the repair patch in ovaloid shape.
- Grinding champfer in repair patch edges.
- Bending repair patch in Barrel radius (for Barrel repair, only).
- Surface preparation and bonding the patches (for details see appendix K).

Figure 9.4. Repair doubler for Megaliner Barrel before bending to final shape

9.1 Flat panel tests

Five flat panel specimens have been manufactured with the designations 12-BR-01 to 12-BR-05. Unfortunately the 12mm holes have been drilled into the GLARE shells by untrained personnel, which resulted in significant deformations of the bore holes. A microscopic investigation of one of the 60mm x 60mm cut out parts was performed in order to determine the local damage due to wrong drilling, see figures 9.7 and 9.8. Delaminations through the prepregs are observed in depths of more than 10mm from the bore hole edge.

Some of the panels have been drilled form the clad-side to the unclad side and some the other way round. The bonding was intended between the clad surface of the skin panel and the unclad surface of the repair patch, for all panels. The local bulging at the cutout corners on the clad side provides a challenge for the bonding operation, since there was no way to form the deformation back. Consequently, the resin distribution after curing is not expected to be the optimum for those panels.

Figure 9.5. Bore holes at back side of panel

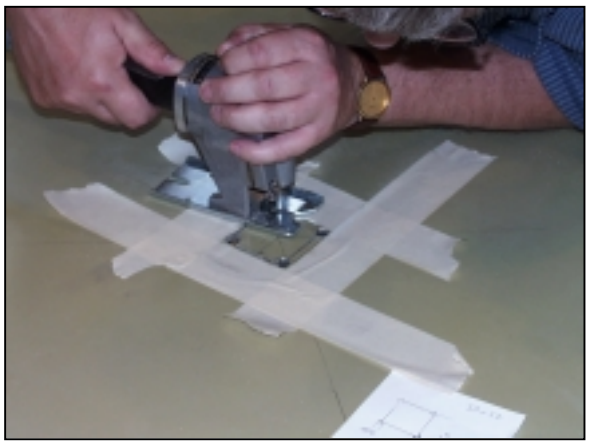

Figure 9.6. Sawing the cut out

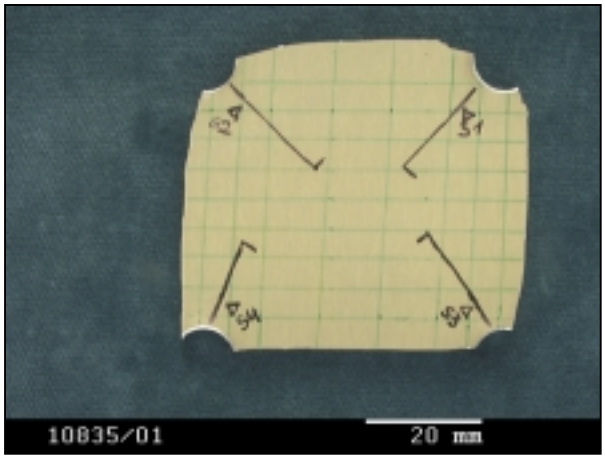

Figure 9.7. Sawed out part with marks for micro-fractographic cuts (flat panel)

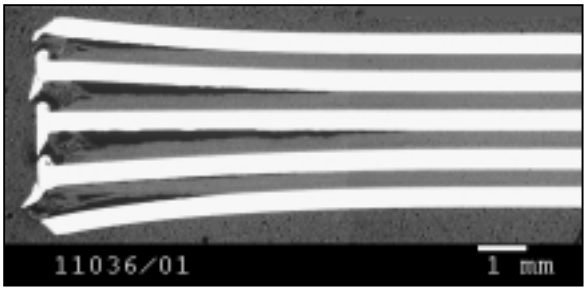

Figure 9.8. Bore hole edge of sawed out part (flat panel), delaminations between all aluminum layers

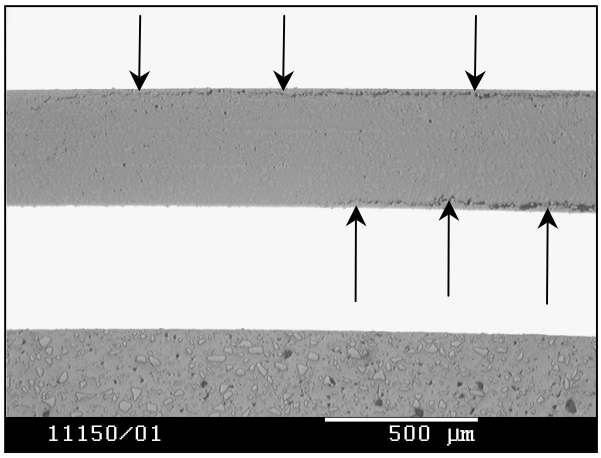

Figure 9.9. Magnification of delamination

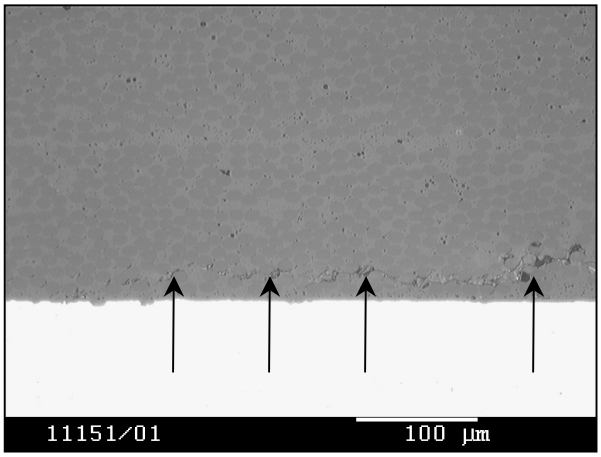

Figure 9.10. Cohesive delamination in prepreg

The particular shells have been either bonded with the portable Heathcom® device, similar as the patch on the Megaliner Barrel, or in an autoclave cycle at 3 bar pressure :

specimen no.	painted *	delamination in cut out corners**	curing tool	outdoor exposure
12-BR-01	no	severe	Heathcom®	no
12-BR-02	yes	significant	Heathcom®	2 years
12-BR-03	yes	limited	autoclave	4 years
12-BR-04	yes	significant	autoclave	6 years
12-BR-05	yes	severe	autoclave	no

* no paint at bond line skin – doubler ** due to drilling operation

All non-stiffened panels except no. 12-BR-01 have been C-scanned after bonding:

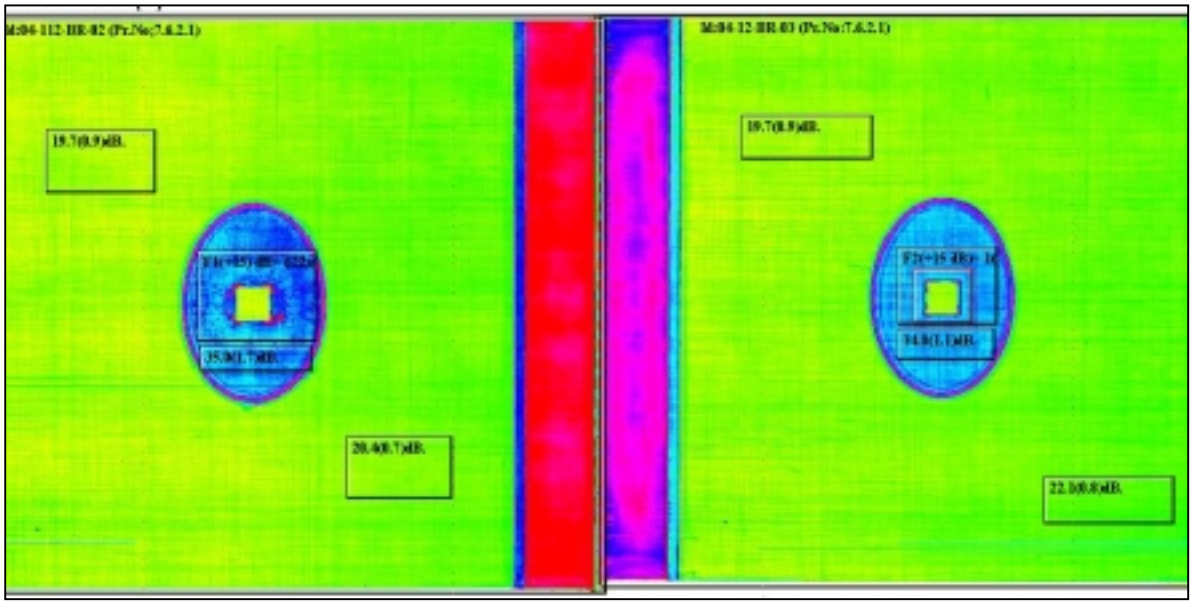

Figure 9.11. C-scan image from specimens 12-BR-02 (left) and 12-BR-03 (right)

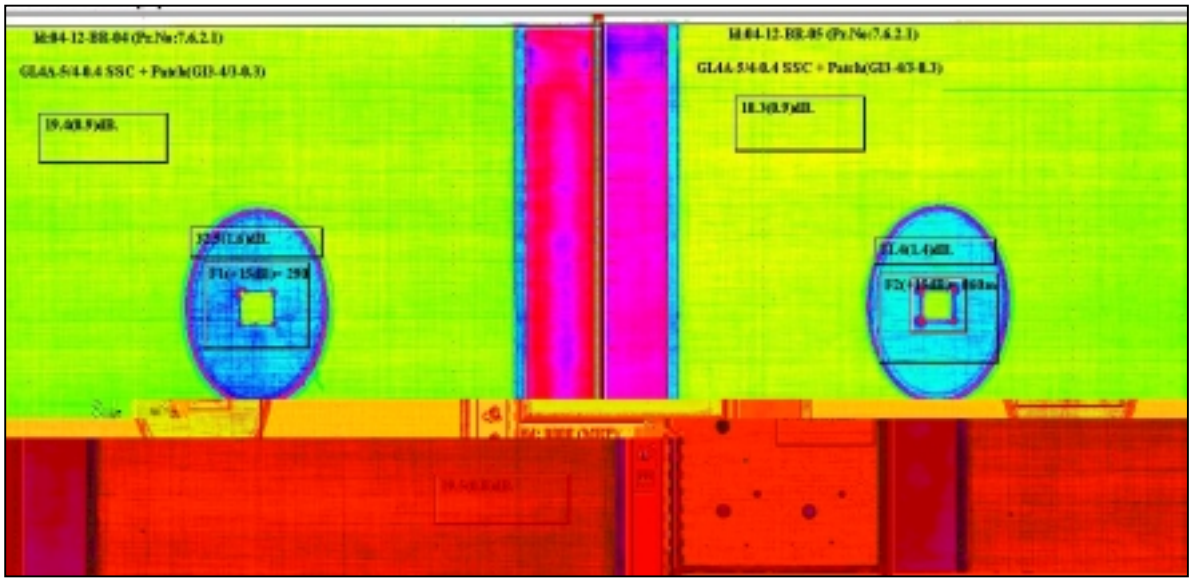

Figure 9.12. C-scan image from specimens 12-BR-04 (left) and 12-BR-05 (right)

Material identification numbers for skin panels: 101940-1, 181950-1, 181951-1, 101940-2, 191953-1.
Material identification numbers for patches: 181950-3, 181950-2

Bond film used for Megaliner Barrel: FM73.
Bond film used for unstiffened panels: FM94.
The bond film properties are considered to be similar.

The delaminations in the cut out corners are clearly visible on the scan images, see the red dots in figures 9.11 and 9.12. A delaminated GLARE should offer higher crack initiation lives than a non-delaminated material, since the curing stresses are released and tensile stress level in the aluminum layers decrease, locally. Here, the very poor drilling quality (figure 9.8) introduced micro cracks before the fatigue test started, which leads to the expectation of a decreased crack initiation life. In any case, the fatigue behaviour of the cut out radii can not be representative for a repair, which is performed according to the aircraft industry manufacturing standards.

Panel 12-BR-01 is constant amplitude loaded with a maximum load of 420 kN, which equals an applied maximum stress of 120 MPa. The stress ration R equals 0.1. This stress level covers a spectrum factor ($C_{Cl(S)}$) of 1.25 related to load case 1g+Δp+10ft/s vertical gust, as calculated for the concerned location with SN slope κ=4.5. Strain gauges are applied on the various locations on both sides of the panel.

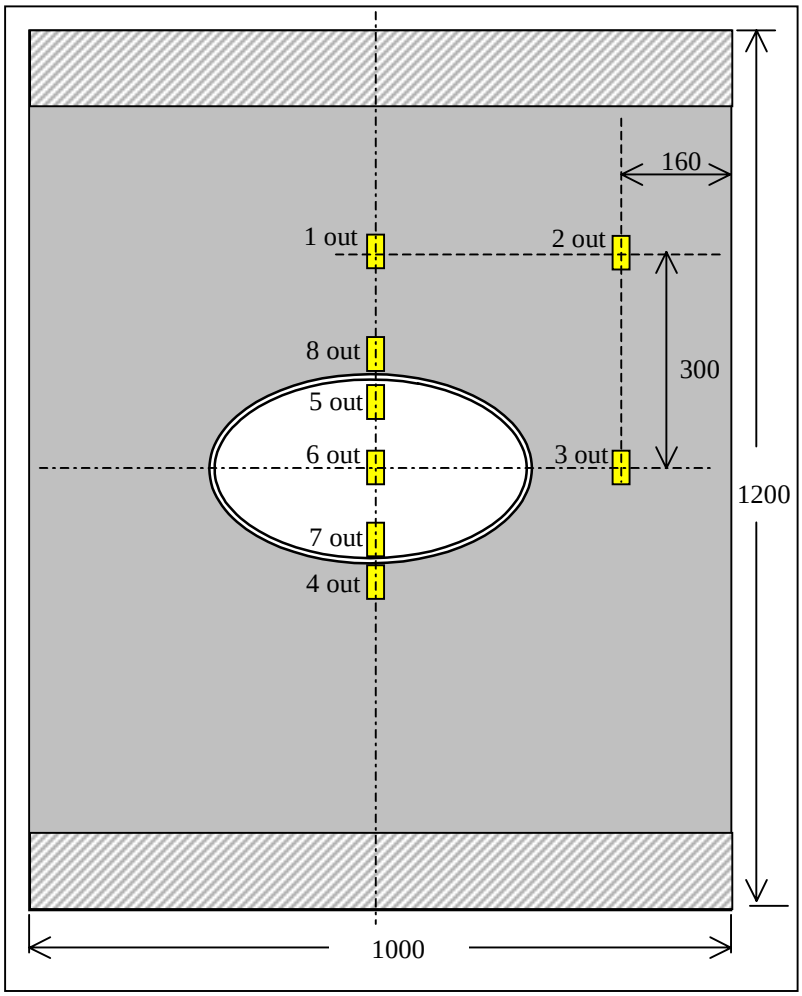

Figure 9.13. Strain gauge locations on the 'outside' of the panel, i.e. the side where the patch is attached. At the positions of strain gauges 1-, 2-, 3- and 4-out, strain gauges are bonded on the inner side as well

Figure 9.14 contains the strains which have been measured before fatigue testing. It is observed that the strain levels measured by strain gauges 2 and 3 at the inside and outside respectively, are almost equal. At these locations the panel remains practically unaffected by the repair. Neither a load redistribution nor a bending effect is observed. In width direction, eleven percent higher loads are measured in the panel center than towards the edges (compare stresses at position 1 with stresses at position 2).
Stresses E*ε are calculated for the 'far field' strain gauges at 420 kN applied load, elasticity modulus for GLARE4A: 56900 MPa:

strain gauge	1 out	1 in	2 out	2 in	3 out	3 in
stress [MPa]	128.6	129.2	115.1	122.0	114.5	119.3

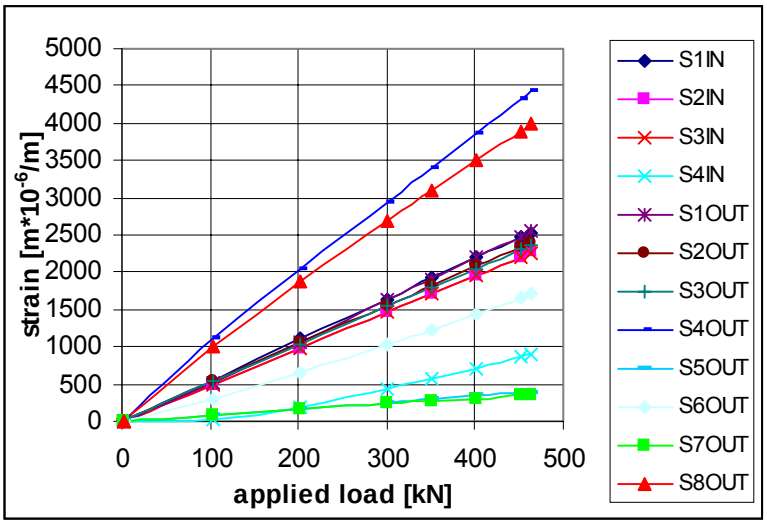

Figure 9.14. Strains at specimen 12-BR-01 before the fatigue test

As expected, the stresses are low at positions 5, 6 and 7, on the top of the repair patch. Obviously a signifycant portion of the load is transferred through the patch around the cut out, which is the argument for the oval shape of the patch with a relative large extension perpendicular to the load.
The upper skin sheet just in front of the repair patch run out is the highest loaded location. Strain gauges '4 out' and '8 out' are bonded as close to the patch edge as possible. Stresses E*ε are calculated for 420 kN applied load with the elasticity modulus for 2024 (72000 MPa), in order to obtain the applied stresses in the concerned aluminum layer:

strain gauge	4 out	4 in	8 out
stress [MPa]	289.9	55.3	262.7

The strain at position 4 in front of the patch exceeds the yield strain of 2024T3. Note: The curing stresses are not included in the measured strains !

After 55000 fatigue cycles the first delamination became detectable below strain gauge 7 by the Fokker bond test. NDT inspectors reported a fast delamination growth between the repair panel skin and the repair patch, i.e. at the metal/metal bond line. The delamination growth is shown in appendix P. It extended from the patch edge towards the cutout within 25000 cycles. Strain measurements have been performed periodically. As illustrated by figure 9.15, the bending stress is more and more decreasing in time (compare strain gauges 4in and 4out, figure 9.15), which indicates that the load transfer from the skin into the patch vanishes. At the same time as the delamination starts growing (figure 9.1.15, Delam.4out and Delam.8out), the strain gauges on the patch edge become unloaded (strain gauges 5out and 7out).

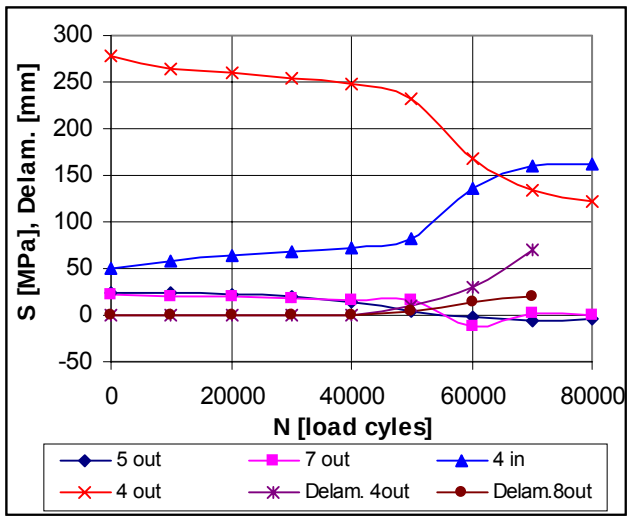

Figure 9.15. Panel 12-BR-01, stresses at particular locations (measured strains at 400 kN applied load, related to E= 72000 MPa) and delamination sizes, measured from the patch edge towards the center of the specimen

It was decided to remove the patch from panel 12-BR-01 carefully, in order to bond a new patch on it for further tests. It turned out that the delamination did not occur between skin and patch, as reported, but between the outer aluminum layer and the first prepreg layer of the skin, see figure 9.16 and 9.17.

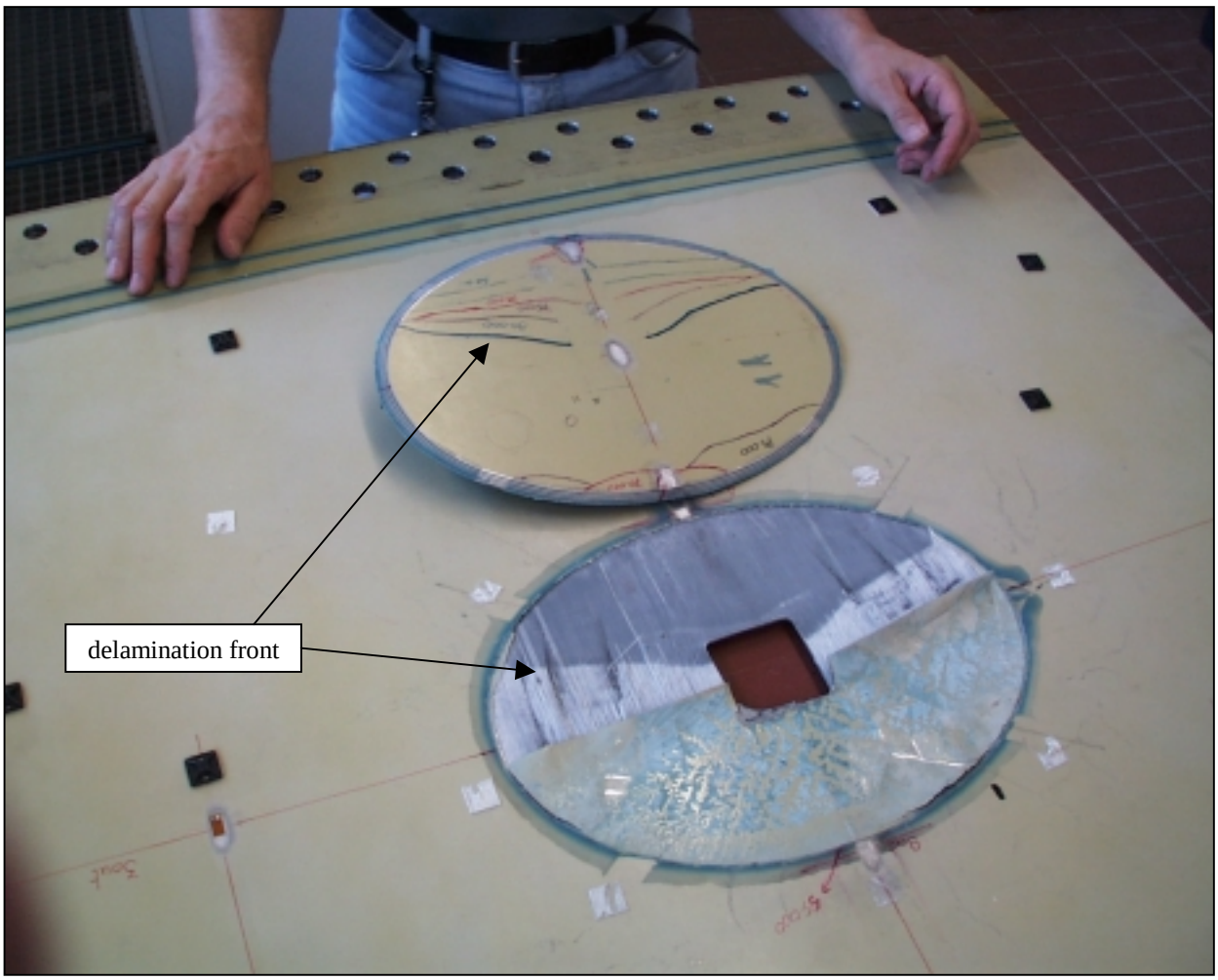

Figure 9.16. Delamination in panel 12-BR-01

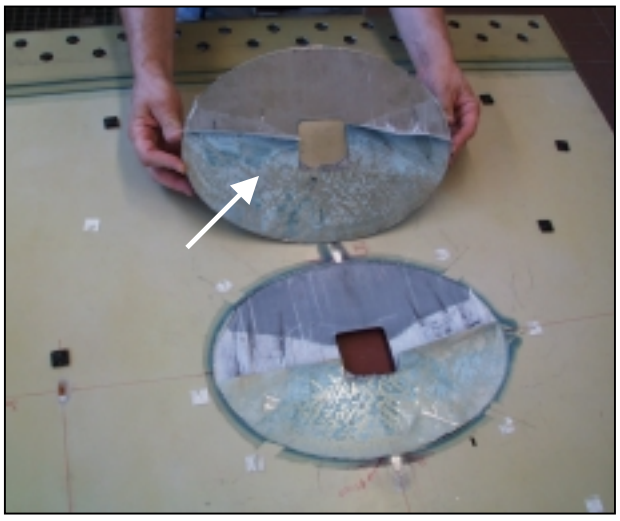

Figure 9.17. Upper skin aluminum foil still bonding on repair patch (arrow)

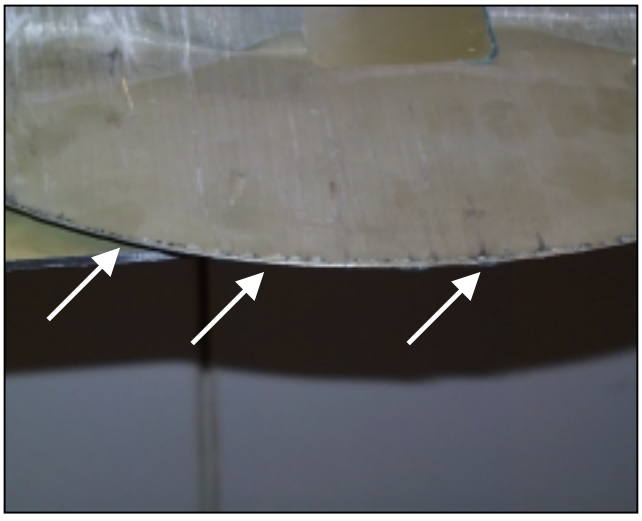

Figure 9.18. Multiple fatigue cracks in upper skin sheet

Multiple fatigue cracks initiated in the upper aluminum layer of the GLARE4A skin along the oval patch edge and linked up, see figure 9.18.

In view of the *real* failure mode the stress mapping shown in figure 9.15 has a different meaning. The sudden decrease of bending stress after approximately 40000 fatigue cycles indicates the link-up of the fatigue cracks and the start of the delamination growth. Consequently, fatigue cracks must have initiated earlier, probably as early as between 10000 and 20000 cycles. The representative fatigue result can be found in HSB sheet 63111-01 for 2024 material and stress concentration factor 2.5. With the measured stresses at strain gauge '4 out', a crack initiation life of 17000 cycles can be predicted for the outer aluminum layer of the skin panel.

The influence of the delamination on the panel top side has also been monitored by photo elastic layers bonded on the inner panel side (see reference [2] and appendix P). A complex stress pattern develops at the bonded patch edge with growing delamination. After a through crack is present in the outer aluminum layer of the skin, loads are transferred from this aluminum layer into the outer prepreg layer and from there back into the repair patch. The skin material net section decreases at this location in depth direction, leading to a higher strain on the inside of the panel also. Left and right hand side from the cut out, strains increase with the ongoing test because the patch carries less load with the growing delamination.

As expected due to the delaminations originating from the wrong drilling (figure 9.8), the cut out corners are sensitive to fatigue. Cracks in two corners are measured after 80000 cycles, one with a length of 1.6mm, the other one with a length of 8.3mm. They propagate under an angle of approximately 45 degrees related to the fiber orientations.

A second fatigue test is performed with panel 12-BR-05, before the real failure mode of panel 12-BR-01 was discovered. The maximum load is limited to 370 kN (maximum stress related to the skin cross section: 106 MPa). Panel 12-BR-05 shows the same behaviour as panel 12-BR-01. Unexpected, the strain variation which is explained by delamination growth, is observed almost after the similar number of load cycles in panel 12-BR-05, compared with panel -01. However, the delamination sizes increased slower.

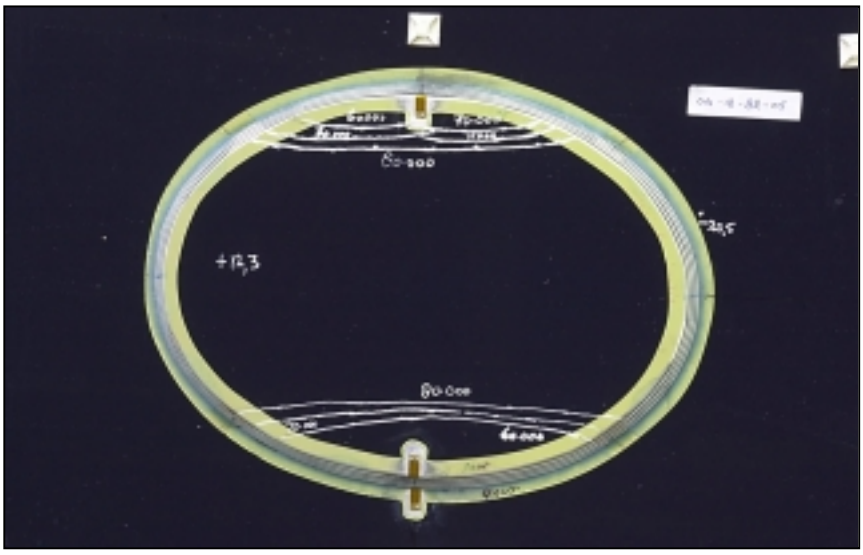

Figure 9.19. Panel 12-BR-05, delamination growth as function of load cycles

Figure 9.20 contains the measured stresses close to the patch edge on the skin and on the patch edge. The strain gauge locations are similar as on panel 12-BR-01 (ref. figure 9.13). The fatigue stress in the concerned aluminum layer of the skin is 40 MPa lower in specimen 12-BR-05 (strain gauge 4out). Without consideration of the curing stresses, this difference would make the difference between yielding and not yielding. A yielded aluminum layer right after the first fatigue cycle (12-BR-01) would explain the longer crack initiation life. However, the autoclave curing cycle introduces additional tensile stresses in

the aluminum layers of the GLARE and an unknown internal stress system remains after curing the bonded patch on the skin.

Visually measured fatigue crack lengths from the cut out corners in the inner aluminum layer of the skin panel are shown in figure 9.21. Note that panel 12-BR-05 is the panel with the more severe drilling damage, see C-scan in figure 9.12.

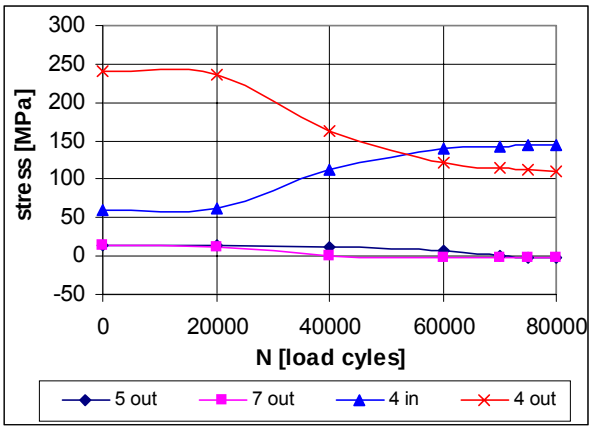

Figure 9.20. Panel 12-BR-05, stresses at particular locations (measured strains at 370 kN applied load, related to E= 72000 MPa)

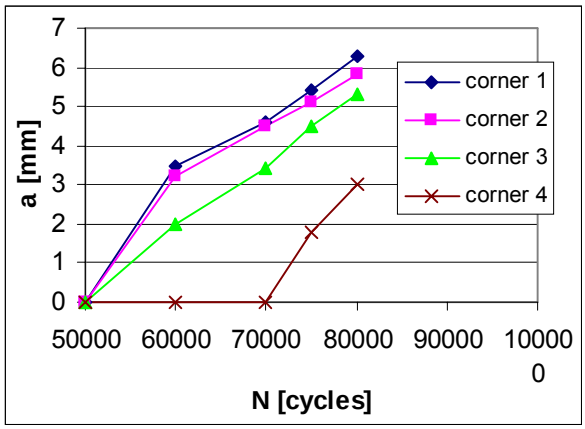

Figure 9.21. Panel 12-BR-05, crack lengths at cut out corners, cracks propagating under 45 degrees in relation to the fiber orientations

9.2 Finite element calculations

The repair panels are modeled with the p-version of the finite element software StressCheck®. It is applicable for the problem, since laminates composed of thin structures can be modeled and calculated with high accuracy. However, in order to limit the number of elements to a 'workable' size, the center three aluminum layers and the prepreg in between of both, the skin panel and the repair patch, are simulated in one sub-element. The two outer aluminum layers and the three prepreg layers between the outer aluminum layers and the center sub-laminate are modeled as separate elements. In total, 840 finite elements have been modeled in order to copy the unstiffened bonded panels. Figure 9.22 shows the (quarter) model, loaded with 420kN (max. fatigue load specimen 12-BR-01).

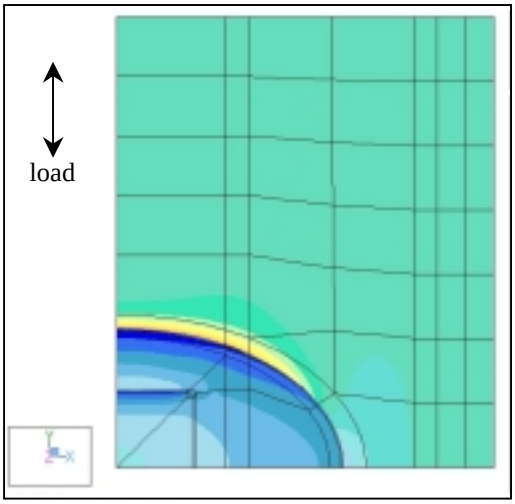

Figure 9.22. FE model of non-stiffened panel, nonlinear calculation results, stresses in aluminum

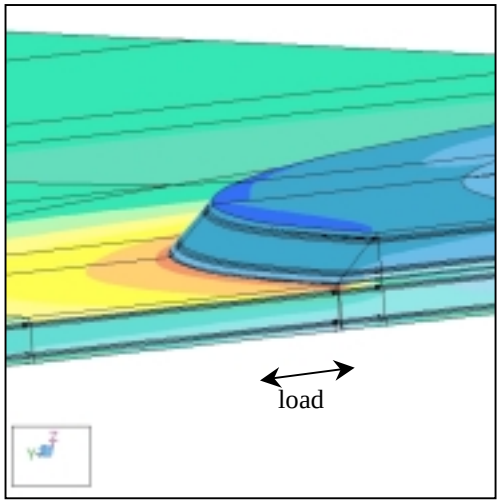

Figure 9.23. Magnification of skin location at the repair patch edge, stresses in aluminum layers

The colors indicate strains in the upper aluminum layer of the skin panel. The stress concentration in front of the bonded patch can be clearly identified. However, the 'far field' is dominated by the green color, representing a strain level of 2000 to 2500 μm/m (114 – 142 MPa for GLARE4A-5/4-.4). A comparison between measurement and calculation is presented in figures 9.24 and 9.25.

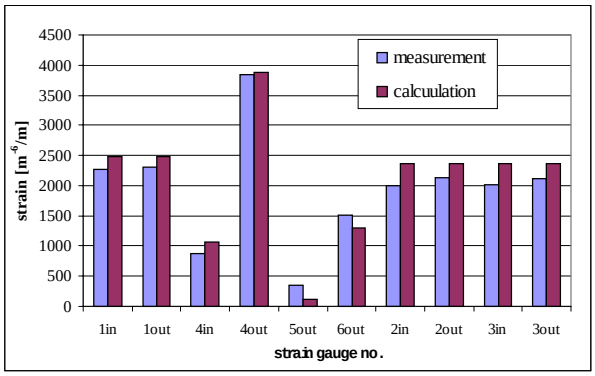

Figure 9.24. Comparison of strains, measurement and calculation

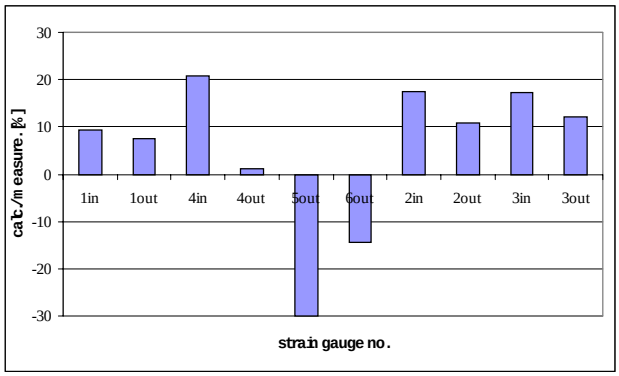

Figure 9.25. Calculated strain / measured strain

Strains at all locations are calculated conservatively, except for strain gauges 5 and 6. Strain gauge no. 5 is located on the top of the patch edge, a position at which not much load is expected. The absolute strain level is low for both measurement and calculation. Because this location is of no particular relevance to a fatigue prediction, the calculation result is acceptable. The non conservative prediction for the location of strain gauge 6 is of less importance as well. Because no strain gauge is bonded on the inside (at position 6), it remains unclear whether the computer software calculates either the load transfer from the skin into the patch non-conservatively or the bending stress incorrectly. However, if multiplied with a tensile elasticity modulus of 72000 MPa a measured stress of 108 MPa is found and a calculated stress of 90 MPa for the aluminium layer to which strain gauge 6out is attached. Both values are not critical for an unnotched structure.

The accuracy for strain gauges 1, 2 and 3 is important in order to validate the correct load distribution at the undisturbed locations of the panel. Note that a very small bending stress is measured at all three locations, but not calculated. The best calculation accuracy is found for the fatigue critical location at strain gauge 4 out. It can be concluded that software StressCheck® offers acceptable finite element calculation results with the here evaluated model.

9.3 Bonded patch on the Megaliner Barrel full scale specimen

Strain gauges are bonded on the Megaliner Barrel similar to positions '4 in' and '4 out' on the flat panels, i.e. on the skin in front of the repair patch in load direction. Measured at the 1/flight load, the stresses in the top aluminum layer of the skin are significantly lower compared with those in the panel. In a similar way as observed in the panels, the bending stress vanishes with the ongoing test time and similar as for the panels (see figure 9.26), the NDT experts did not report a finding for a long period. However, with the stress in the outside skin aluminum layer, which has been measured after 1732 Barrel flights (157 MPa) and the 2024T3 SN data for stress concentration 2.5, a crack initiation life of approximately 200000 *cycles* would be determined (mean stress: 86 MPa, stress amplitude: 70 MPa). Under consideration of a spectrum factor 1.25 (calculated for the investigated location and spectrum), this

value would drop to 80000 *flights* (mean stress: 108 MPa, stress amplitude: 88 MPa). Both results do not comply with fatigue crack initiation within 10000 to 20000 flights, which may be expected in view of the strain gauge readings.

The outer aluminum layer of the Barrel fuselage skin was found to be cracked similar as observed for the panels after 43000 flights in July 2003. However, no delamination was found. Because no damage was reported after 30000 flights and because the NDT specialists new exactly how to detect a possible damage due to the panel test experiences, it must be concluded that the crack initiated between 30000 and 43000 flights.

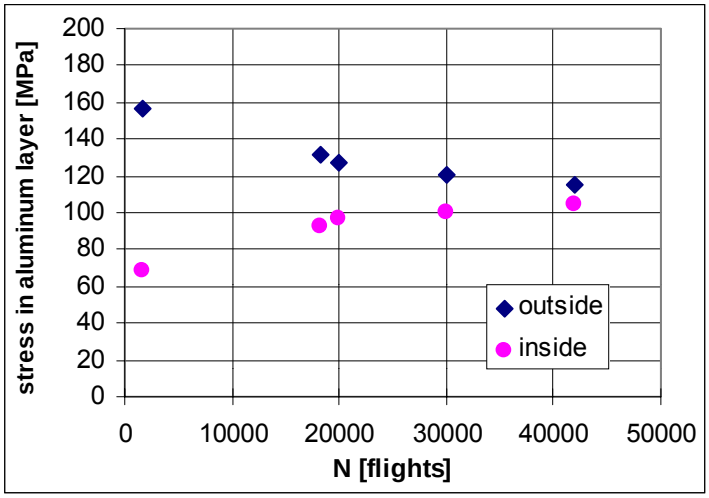

Figure 9.26. Stresses in aluminum layers of Megaliner Barrel skin, close to repair patch edge

9.4 Conclusions and returning specimens

Specimens 12-BR-02 to 12-BR-04 have been sent to the outdoor exposure test site at a time when delamination between skin panel and repair patch of specimen 12—BR-01 has been reported by the NDT experts. Any influence due to natural ageing was supposed to be an influence on the metal/metal bond line, consequently.

Meanwhile some lessons have been learned. The high stress concentration in the outer aluminum layer of the panel skin at the run out of the repair patch leads to an aluminum layer fatigue failure, which is followed by a delamination between the fatigued aluminum layer and the adjacent fiber prepreg. The fatigue sensitive locations have a distance of at minimum 90mm from the cut out edges and, taking the diffusion rates which have been discussed in chapter 4 of this thesis into account, moisture will never in an aircrafts life penetrate in the upper prepreg layer towards these fatigue sensitive locations. Consequently, an influence due to moisture on the GLARE prepreg is not expected. It remains a possible influence on both, the GLARE prepregs and the metal/metal bond, due to the constant variation of temperature, However, the maximum material temperature never exceeds 65°C at the test site (ref. chapter 5). Yet no literature reports a detrimental influence on bonding strength for 120°C curing systems due to thermal cycling between 20°C and 65°C.

The bond line between skin panel and repair patch will absorb moisture during outdoor exposure. The metal/metal bond, however, is a very reliable joining technology, which is proven by in-flight experiences of several commercial aircrafts (e.g. A300 and A310) during the past 30 years. An influence on strength due to the outdoor exposure in Queensland is not expected.

The crack initiation life of the panels can be calculated with SN data for notch factor 2.5. The full scale repair could be not recalculated. The reason for the decreasing bending stress in the fuselage skin at the doubler run out with the proceeding test is not clarified. It is recommended to perform a systematic

analytic and experimental investigation on the fatigue life of GLARE at bondend doubler run outs. Three variables have to be considered:

- the material types to be combined
- the material thickness of the bonded components skin & doubler
- the stress levels to be applied

Until no further know how is available for the prediction of the fatigue life of bonded GLARE/GLARE structures, their application should be limited to thin material combinations at locations of low stress levels.

For the returning specimens a different test procedure is recommended by the author, due to the structural behaviour observed on panels 12-BR-01 and 12-BR-05 and on the Megaliner Barrel repair. It should be focused on two major items:

a) The stress level which leads to an acceptable fatigue life (i.e. no crack initiation before 40000 flights) of the given design should be determined.
b) The influence of a row of blind fasteners around the bonded patch edge should be investigated. The rivets may reduce the peel force between the skin outer aluminum layer and the adjacent fiber prepreg layer, after fatigue crack initiation. Therefore, they should restrain the delamination growth.

The panels can be returned from Queensland according to the availability of test capacity at Delft University, independent from the exposure time. For cost reasons, the three panel should be shipped in one batch.
Proposed test procedure for returning panels:

Panel 12-BR-02:

- Attach strain gauges at positions 4 and 8, similar as on previous panels
- Fatigue panel with Megaliner Barrel load spectrum, maximum: 50000 flights. Calibration: 1520μm/m for strain gauges 4out and 8out, respectively, at load case 1g+Δp+10ft/sVG.
  Inspect every 5000 flights for fatigue crack initiation and delamination, C-scan inspection strongly recommended.
- Perform a residual strength test after last inspection.

Panel 12-BR-03:
Repeat sequence used for 12-BR-03 with 10% reduction of load spectrum.

Panel 12-BR-04:

- Install one rivet row of countersunk blind fastener at the bonded doubler specimen edge, details to be defined.
- Repeat sequence used for previous specimens with either 100% or 90% load spectrum. Decision to be made based on results obtained from previous specimens.

9.5 References

[1] Influence of doubler thickness and design on fatigue and residual strength, P. Kuijpers, Delft University of Technology, report B2V-00-20, 2000

[2] NLR Note from W. t'Hart to Th. Beumler, March 14, 2002

10. Riveted Repair Panels

The aim of the investigation reported in this chapter is to consider the relation between the results of a full-scale test and tests on panels with a similar structural configuration. The structural detail considered in this chapter for an experimental comparison is the repair patch applied on the Megaliner Barrel structure described in section 3.1.2 with properties evaluated in chapter 7. The results should contribute to the determination of test-to-structure factors. For this purpose 5 panel tests are carried out. One panel has already been tested up to final failure. The other ones are now exposed to the outdoors environment in Australia. Further testing of these panels will be carried out later.

The chapter starts with a description of the panel. General comments on the relation between specimen tests and full-scale tests are given in section 10.2. Results of the panel already tested are given in section 10.3, followed by a comparison with the behaviour of the similar coupon in the Megaliner Barrel test (section 10.4). The residual strength of the panel is presented in section 10.5 and conclusions are recapitulated in section 10.6.

10.1 Specimen design and test program

The geometry of the five non-stiffened panels which copy the Megaliner Barrel repair is presented in figure 10.1.

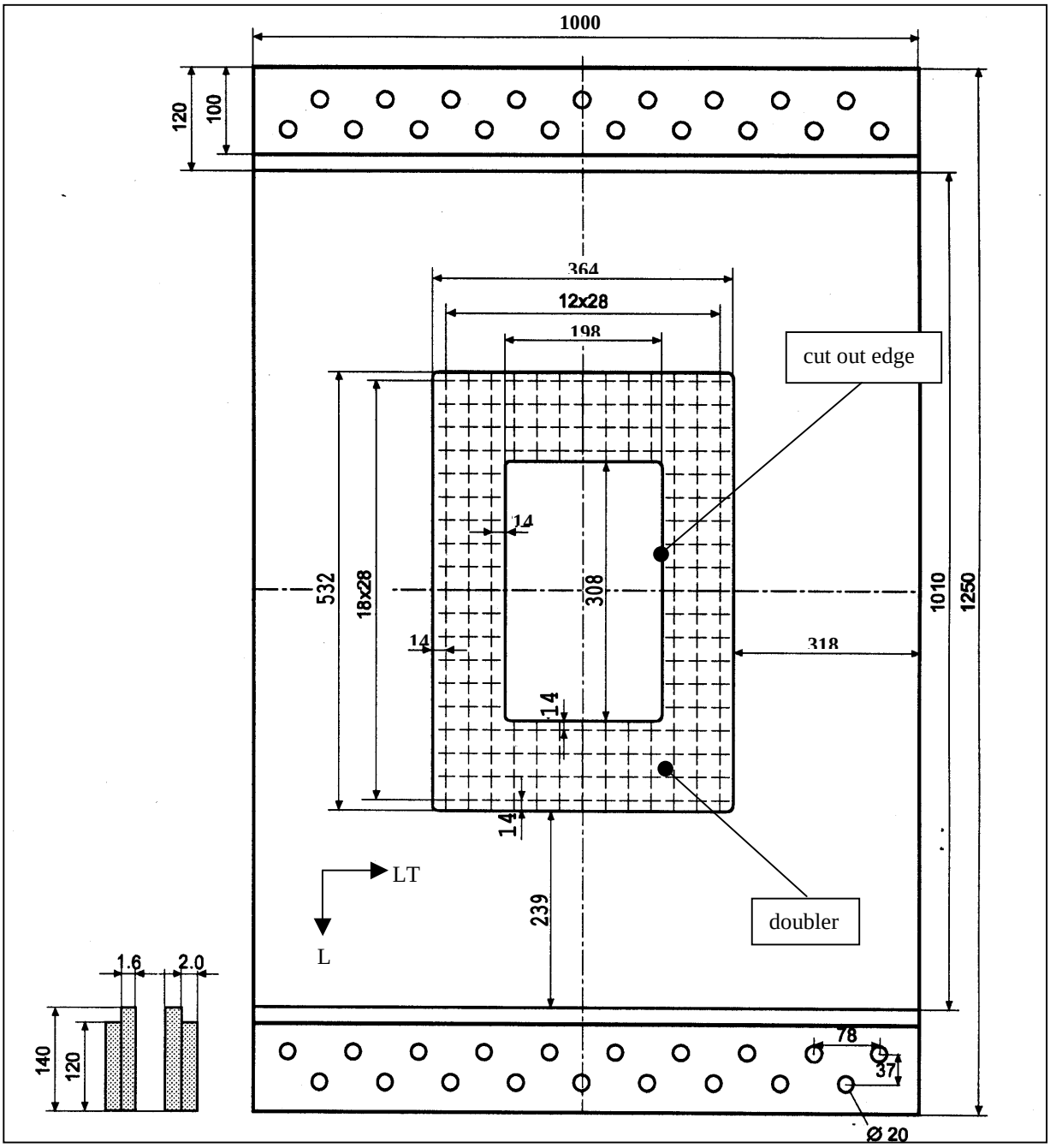

Figure 10.1. Repair panel specimen, series 11-RR

Skin and patch material: GLARE4A-5/4-.4, singe side clad, jointed with anti fretting compound.
Fasteners & collars for fatigue tests: HL413VF-6-5 / HL93-6 (cost reasons), installed dry.
Fasteners & collars for residual strength tests: ASNA2026 & ASNA2528-3A, installed dry.

Specimen designations: 11-A-1 to 11-A-5 The tasks performed by the particular specimens are contained in the following table:

specimen identification	specimen contribution					
	painted	CI	CP	RS	outdoor exposure	remarks
11-RR-1		X	X	X	no	
11-RR-2	X	X	X	X	2 years	exposure before fatigue loading
11-RR-3	X	X	X	X	2 years	exposure after fatigue loading
11-RR-4	X	X	X	X	6 years	exposure before fatigue loading
11-RR-5	X	X	X	X	6 years	exposure after fatigue loading

CI: specimen scheduled for crack initiation investigations

CP: specimen scheduled for crack propagation investigations

RS: specimen scheduled for residual strength investigations

10.2 The influence of stiffener and stiffness

If more details of a test on specimen are exactly similar to details of the aircraft structure, the closer the test result will be in comparison to results of the full scale test. The escalation of specimen types and loading conditions in comparison to the full scale structures is compiled in the table below. All types of specimens can be loaded with either constant or variable amplitude spectra. The application of compression loads of a spectrum on slender specimens usually requires specific suspensions (anti buckling guides), which is often avoided for economical reasons. Depending on the particular load spectrum, clipping of compression loads increases the crack initiation life and decreases the crack propagation rate [1]. The classification given in the table applies to the longitudinal loads in the rear upper fuselage of a civil aircraft, i.e. for the fuselage pressurization cycle and the 1g-load dominated spectrum with contribution of gust loads. The situation for both the front fuselage and the rear fuselage investigated in the circumferential direction are different.

Specimen type	Bi-axial loading	Stiffener	Curvature	Variable temperature
coupon	not possible	no	no	possible but time consuming
flat panel	almost impossible, load introduction problems	possible	no	possible, very time consuming
curved panel	usual, includes internal pressure	usual	yes	unusual, very time consuming

A good correlation for circumferential joints was found by Beumler between the results of stiffened, uniaxial and constant amplitude loaded panels and full scale test result [2] (aluminium structures). With the correct spectrum factor on the far field stress considered, almost identical results were obtained for both, the full scale specimen and the stiffened shells. However, the load transmission between skin, butt strap, stringer and stringer coupling was very complicated as indicated by a detailed finite element analyses [3]. Curvature and biaxiality obviously do not play a significant role for the simulation of the butt joint fatigue strength of the stiffened shell.

The scale factor to be applied on stress for aluminium at RT [2] became:

$$C_{CI(SC)}\left(\frac{stiffened\ \ flat\ panel}{full\ scale\ test}\right)\approx 1.03$$

(related to reference load case 1g+Δp+10ft/s vertical gust)

In the same report [2] the ratio between the stress levels of both a full scale test result and a coupon specimen result for the determination of similar fatigue lives is evaluated, both specimens have been made of aluminium 2024T3:

$$C_{CI(SC)}\left(\frac{coupon}{full\ scale\ test}\right)\approx 1.27$$

(related to reference load case 1g+Δp+10ft/s vertical gust)

It turned out that more fatigue cycles were required to obtain specimen failure in a coupon specimen rather than in the stiffened shell. This result disagrees with expectations if the higher bending stresses in the coupon are taken into account, compared to bending in the stiffened panel. The result may be associated with different specimen sizes, i.e. a load redistribution is possible between cracked and non-cracked locations in a panel (MSD in panel width direction) but not in a coupon of a limited width. It should also be considered that both aluminium full scale specimens and aluminium panels are usually inspected for crack initiation. The coupon fatigue result is related to the specimen failure. Consequently, the coupon result includes a portion of crack propagation life. According to Müller [4] the crack propagation life portion can cover up to 15% of the coupon life to failure (in aluminium specimens), an item which decreases the deviation between the above shown scale factors. However, the discovery that aluminium coupons can obtain higher fatigue lives than similar full scale structures is a wide experience in the fatigue community, worth to be implemented as an (engineering) scale factor.

In the absence of similar tests as available for monolithic aluminium it should be discussed whether a GLARE structure behaves in a different way. The bending measurements in chapter 2.8 show a significant increase of the bending stress for the coupon, which has been cut out of the panel. Is this behaviour related to the lower stiffness of GLARE ? For clarification a circumferential joint specimen has been manufactured, which has a similar design as the GLARE outdoor exposure specimen series 2-B (see chapter 3.2.3.1), but with 3.8mm aluminium skin sheets serving as ‘skin’ parts. The butt straps are again made of GLARE2B-7/6-.4, the specimen is shown in figure 10.2. Instead of 4.8mm protruded head Hi-Loks, 4.8mm countersunk Hi-Locks have been installed (DAN6). The influence of the different fastener head geometries on the butt strap stresses is negligible.

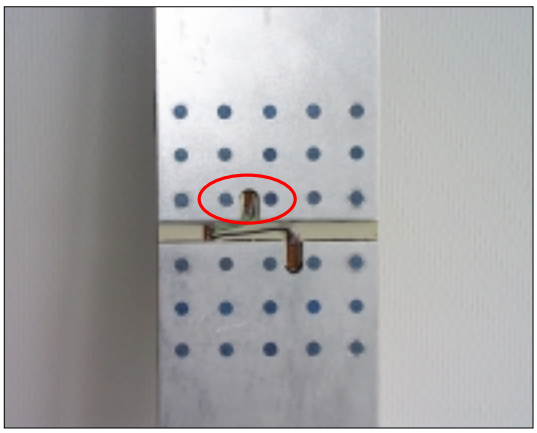

Figure 10.2. Butt joint specimen with aluminium skin and GLARE strap

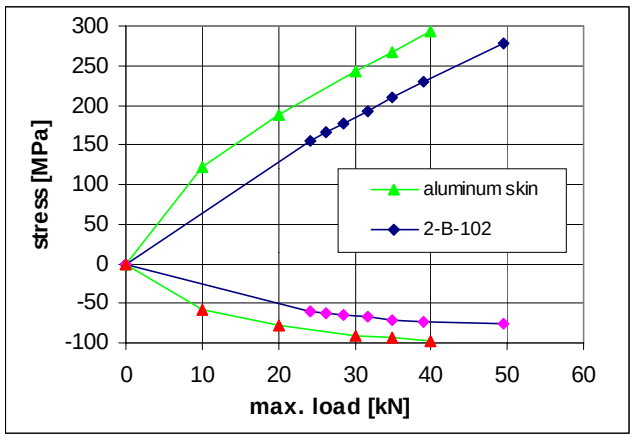

Figure 10.3. Stresses in the aluminium layers of butt the strap net section, E = 72000 MPa

Figure 10.3 shows the measured stresses in the net section of rivet row 3 (which is similar to rivet row 4). The stresses are related to the tensile modulus of material 2024T3. The slope of the curves is almost identical.

The bending factor for specimen with aluminium skin: $k_{bending} = 1.99$

The bending factor for specimen with GLARE skin: $k_{bending} = 1.94$

The *absolute* stress level in the GLARE butt strap which is attached to the aluminium skin is higher than in the butt strap of specimen 2-B-102. This effect is related to the load distribution between the rivet rows. Due to the higher stiffness of the aluminium skin sheets, the center rivet row of both sides of the specimen is unloaded and the outer rivet rows obtain a higher normal stress.

Another comparison of the bending behaviour of pure GLARE structures with pure aluminium structures of similar design is conducted with two lap joint specimens. Figure 10.4 shows a three rivet row lap joint specimen made of GLARE3-5/4-.4 (t=3.0mm) and figure 10.5 an identical specimen, but made of 3.2mm 2024T3. The net stresses are measured on the lower sheet and lower rivet row at both sides. Again, the slope of the curves is almost identical (figure 10.6), which indicates an identical bending behaviour of both materials. Note that the *absolute* stress values are approximately 15% higher for GLARE (E=57700 MPa) at a similar applied load in this comparison, due to the lower stiffness of GLARE.

The bending behaviour of structures of similar design and geometry is not dependent on the material. It is concluded, that the different stiffness of both, monolithic aluminium and GLARE, have no influence on the scale factor.

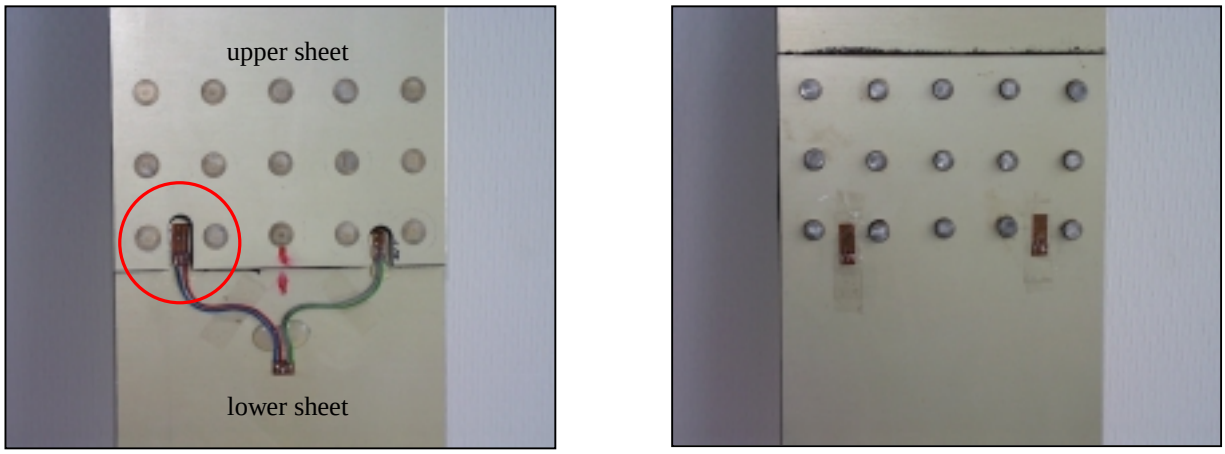

Figure 10.4. GLARE3.5/4-.4 lap joint specimen with attached strain gauges

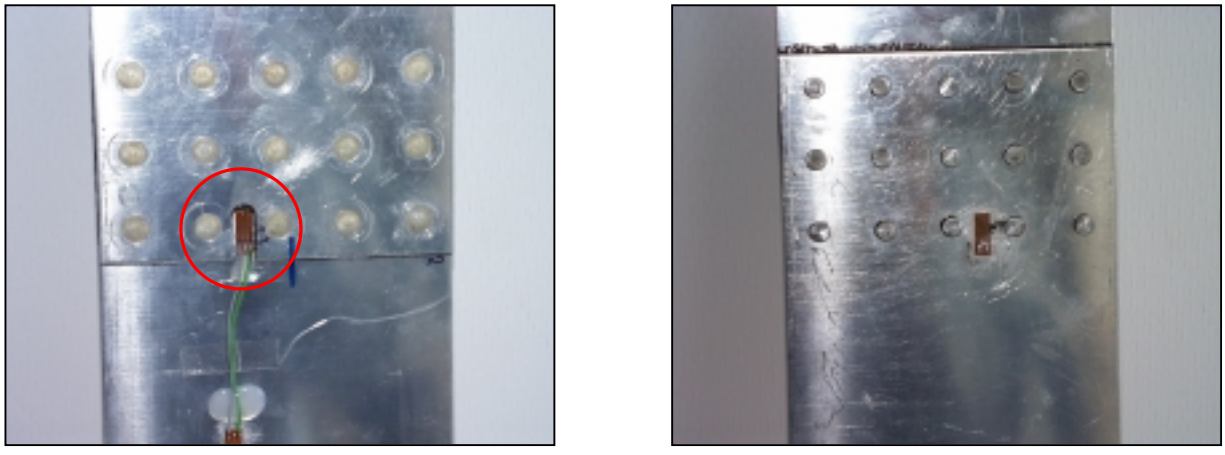

Figure 10.5. 2024T3 lap joint specimen with attached strain gauges

Although the experimental butt strap in the A340-600 full scale specimen is attached to an aluminium skin which causes higher load transfer in rivet rows 3 and 4 due to the load distribution through the rivet rows, positive and negative stresses with lower magnitudes are measured in the full scale specimen, compared with the coupon (see figure 10.7). This effect must be linked to both, the influence of the stiffeners and the curvature of the full scale test article.

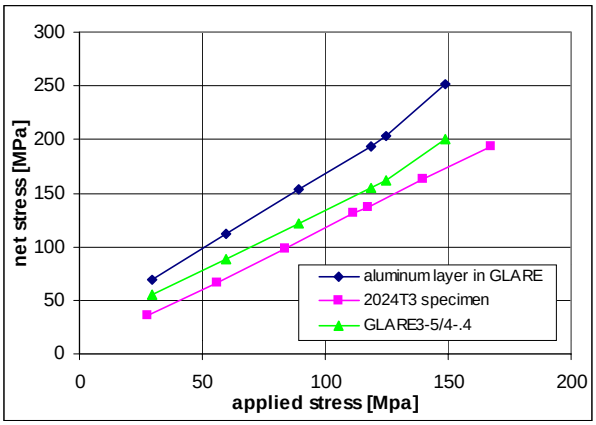

Figure 10.6. Lap joint stresses, lower sheet, mating surface, locations acc. to red circles in sketches above

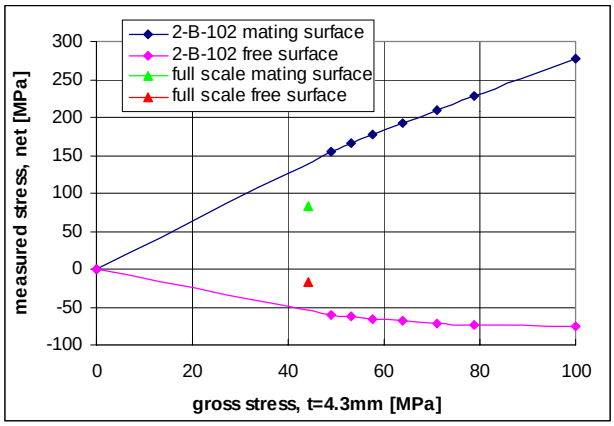

Figure 10.7. Comparison of net section stresses in butt strap coupon and full scale specimen A340-600 EF2 at load case 1g+Δp+10ft/s vertical gust. Stresses in aluminium layer of GLARE butt strap.

A compilation of the major conclusions of this paragraph is given below:

- Stiffener and panel curvature have a significant influence on the bending stress of a butt strap.
- The bending behaviour ($k_{bending}$) is independent from the type of butt strap material.
- The scale factor (on stress) between a stiffened panel and a full scale structure is close to 1.0 for internal pressure and 1g dominated spectra with significant gust loads.
- The scale factor (on stress) between coupon and a full scale structure is in the order of 1.27 for internal pressure and 1g dominated spectra with significant gust loads.

10.3 Repair panel specimen 11-RR-01

The Megaliner Barrel repair is simulated with the non-stiffened panel series 11-RR. Strain gauges according to the positions specified in figure 10.8 are bonded on specimen 11-RR-1. This panel is fatigue loaded to 420 kN (R=0.1), which corresponds to a calculated applied stress of 120 MPa. Strain gauges are bonded on both sides of the panel at similar locations. Note that strain gauges no. 4 and no. 5 are bonded as close to the doubler edge and skin edge as possible. At the same locations (no.4 and 5) strain gauges have been bonded on coupon specimen 2-A-1.

All strain gauges at positions 1, 2 and 3 show strains between 1888 µm/m (3out) and 2127 µm/m (1in), see figure 10.9. If multiplied with the tensile modulus for GLARE4A-5/4-.4, the calculated applied stress of 120 MPa is almost met (figure 10.10). The similarity of strains indicate that the repair width is balanced with the panel width, because an equal force flow can be observed through the repair patch and around the repair patch. This behaviour is also linked to the fact that both, the skin and the patch, are made of the same material.

The stresses in the aluminium layers of the GLARE parts close to the rivet field are shown in figure 10.11. Slightly higher stresses are measured on the inner side of the patch compared with the outer side of the skin. Significant bending stresses have been developed.

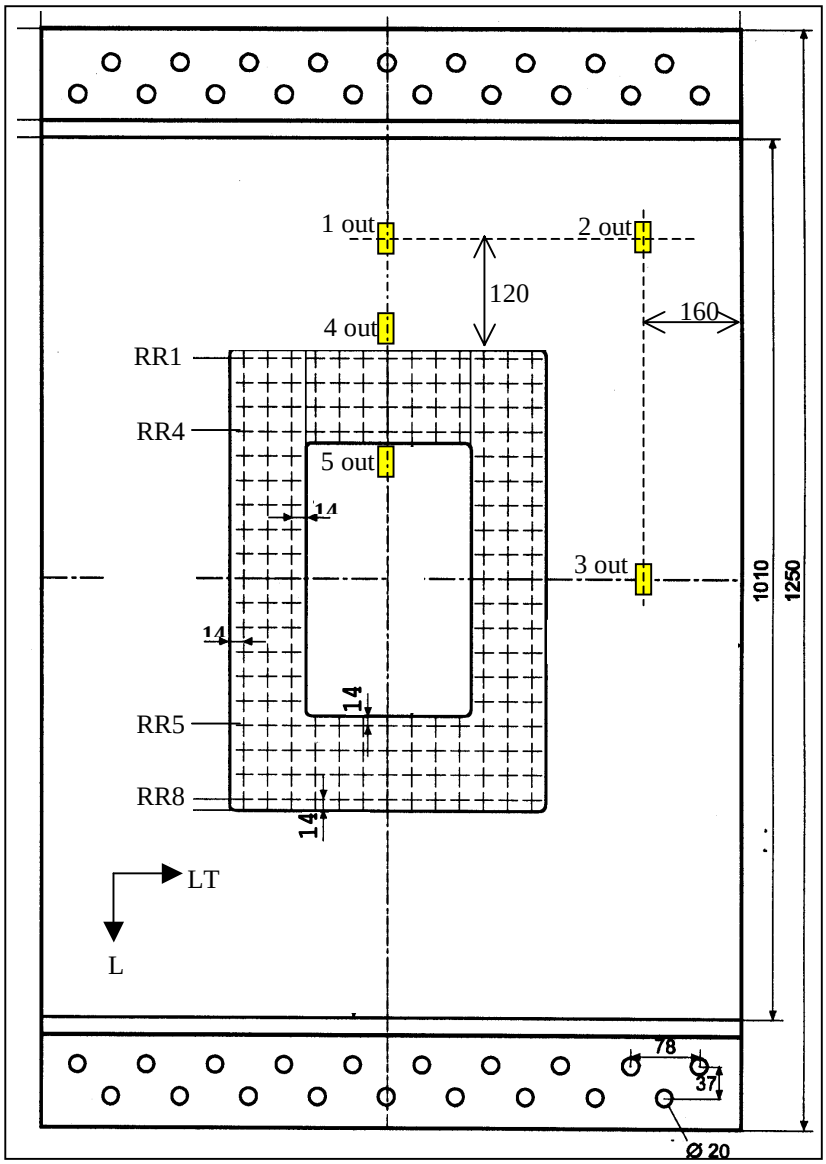

Figure 10.8. Strain gauge positions on panel 11-RR-1

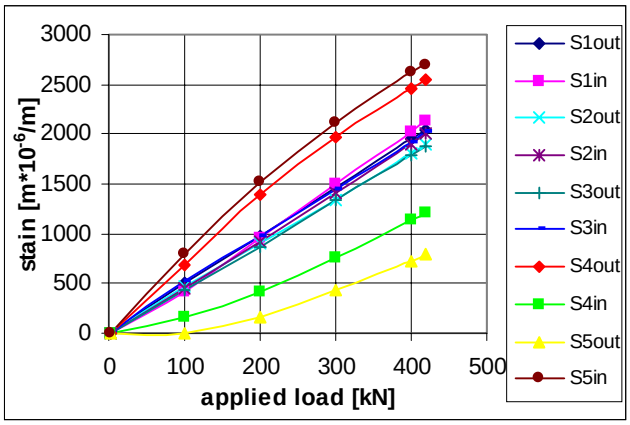

Figure 10.9. Strains at panel 11-RR-1

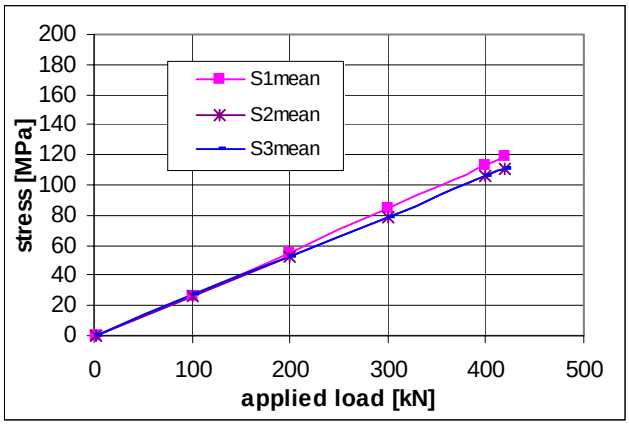

Figure 10.10. Mean stresses at positions 1, 2 and 3, tensile modulus: 56900 MPa

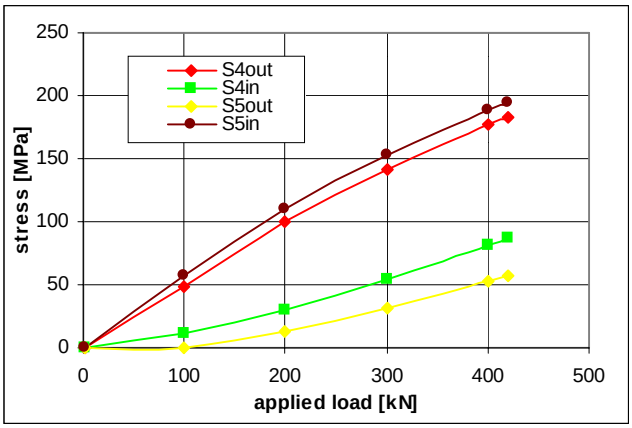

Figure 10.11. Panel 11-RR-01, stresses in aluminium layers, tensile modulus: 72000 MPa

10.4 Comparison with coupon and Megaliner Barrel results

Figure 10.12 compares the aluminium layer stresses at strain gauge positions 4 and 5 from panel 11-RR-1 with the measurements on coupon 2-A-1 and the Megaliner Barrel structure at load case 1g+Δp+10ft/s vertical gust (1/flight stress level). Note that the strain gauges at the Barrel are located close to the stringer.

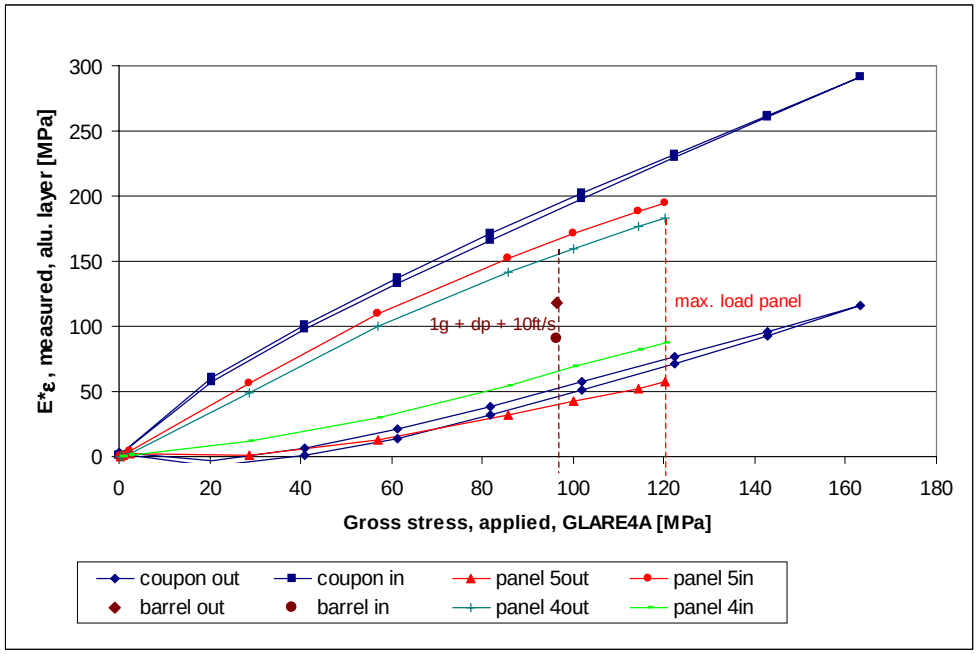

*Figure 10.12. Stresses E*ε in aluminium layers on repaired skin, in front of the repair patch, E = 72 GPa*

The ratios of the measured tensile stresses in the GLARE aluminium layers at the 1/flight level are:

$$\frac{coupon}{barrel} \approx 1.7 \qquad \frac{unstiffened\ panel}{barrel} \approx 1.4$$

At similar *applied* stress levels, the additional bending stress is lower in the panel than in the coupon. From this point of view, a higher crack initiation life is expected for the panel than for the coupon.

Panel 11-RR-1 is cycled 80000 times with $F_{max.}$ = 420 kN ($\sigma_{applied}$ = 120 MPa) and stress ratio R=0.1. HL413VF fastener have been installed for the fatigue sequence for cost reasons. After disassembly, fatigue cracks are found in similar locations as in the 2-A series coupons (ref. chapter 7.1.3), i.e. some fretting is observed and cracks initiate outside the bore holes. Figures 10.13 and 10.14 show the fatigue cracks in rivet row 1 in the panel and in rivet row 4 in the patch. The crack shapes look similar in rivet rows 5 and 8 (see also table 10.1).

Note: All panels are manufactured and three of them fatigued (11-RR-01, -03 and –05) *before* the detailed coupon results became available.

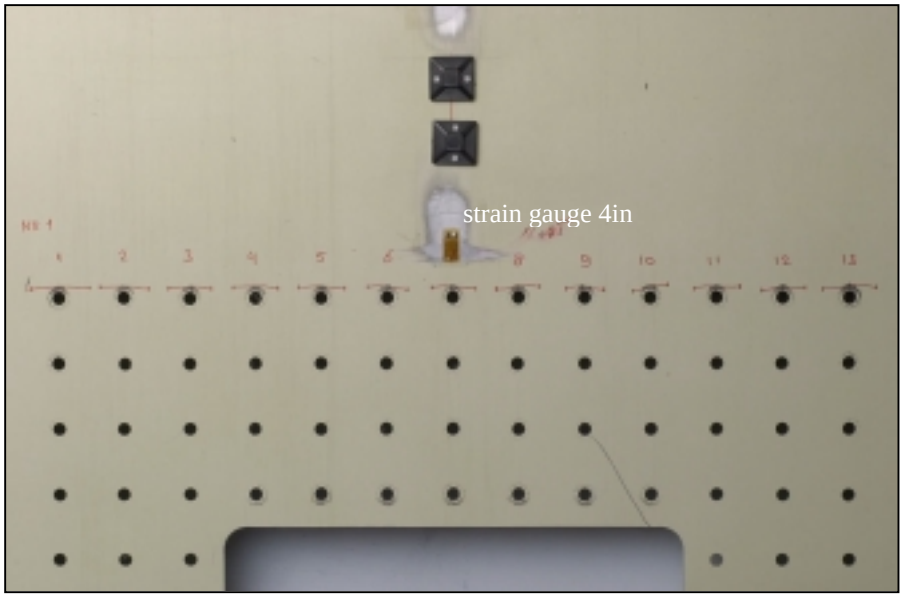

Figure 10.13. Fatigue cracks in skin panel, rivet row 1

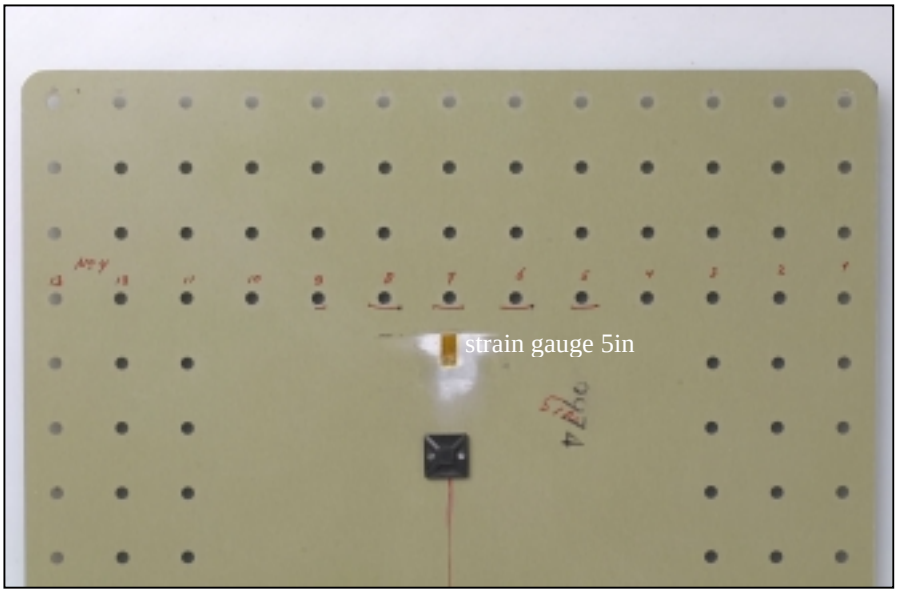

Figure 10.14. Fatigue cracks in repair patch, rivet row 4

Average total crack length in skin, rivet row 1, mating layer, after 80000 fatigue cycles: 2a = 19.23mm.
Average crack length in rivet row 1, mating layer, according to definition chapter 7.1.3: a = 6.82mm.
Fatigue cracks are almost limited to the mating aluminium layer, similar as for the coupon specimen series 2-A (with HL413VF-6-5 fastener).

Average total crack length in patch, rivet row 4, mating layer, after 80000 fatigue cycles: 2a = 18.15mm.
Average crack length in rivet row 4, mating layer, according to definition chapter 7.1.3: a = 6.28mm.

The specimen condition after 80000 constant amplitude fatigue cycles shall be recalculated with the data obtained from the coupon specimens (2-A series):

For 120 MPa applied stress (R=0.1):
N_i (coupon) = 55000 cycles (ref. figure 7.1.3.7)
da/dN = 10^{-4} mm/cycle (ref. figure 7.1.4.9) → N_{CP} (coupon) = 68000 cycles from 0mm to 6.82mm
N_{tot} (coupon) = 55000 + 68000 = 123000 cycles

The combined crack initiation and crack propagation life of the panel is lower than for the coupon, which disagrees with expectations based on physical arguments, but which confirms the observations on monolithic specimens [2].

In an iterative calculation 130 MPa applied stress is determined as representative level for the coupon, which leads to the same fatigue condition as panel 11-RR-01 after 80000 flights.

Calculation of scale factor (on stress) between coupon and non-stiffened panel for similar applied stress levels :

$$C_{CI(SC)}\left(\frac{coupon}{non-stiffened\ panel}\right)=\frac{130}{120}=1.08$$

The prediction of crack initiation and crack propagation lives in a non-stiffened GLARE panel can be performed by using coupon test results under consideration of scale factor 1.08, which is to be applied on the coupon stress. A scale factor related to the Megaliner Barrel test result (ref. chapter 7.2) can not be established, since the crack location is different due to the different fastener used.

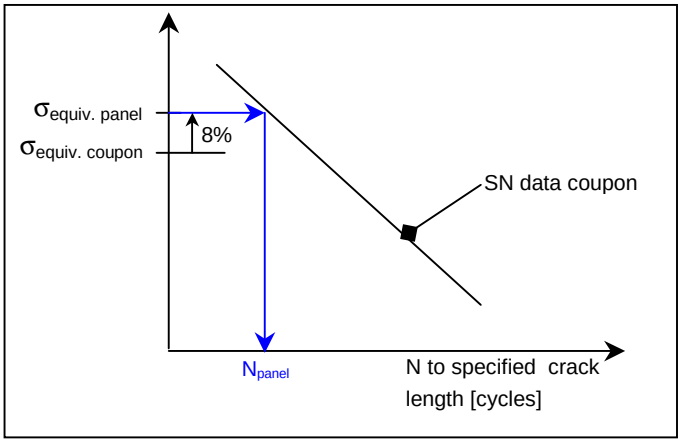

Figure 10.15. Riveted GLARE4A repair, scale factor between non-stiffened panel and coupon

10.5 Residual strength

Repair panel 11-RR-01 obtained a fatigue damage rate R_D of 20% prior to the residual strength test. It is pulled to failure at 70°C and failed through rivet row 8, i.e. in the net section of the highest loaded rivet row of the panel.

Failure load: 1250 kN.

Calculated failure stresses:	net stress:	468 MPa
	gross stress:	357 MPa

The gross stress failure load is still above the estimated ultimate load for the PSE (345 MPa, ref. chapter 7.2). Figure 10.16 relates the panel failure stress to the coupon results recorded in paragraph 7.1.8.2 of this thesis. The obtained applied failure stress is higher for the panel than for the coupon specimens, a behaviour which is attributed to the possibility of load redistribution from the blunt notch location to the non-notched cross section left and right from the riveting field.

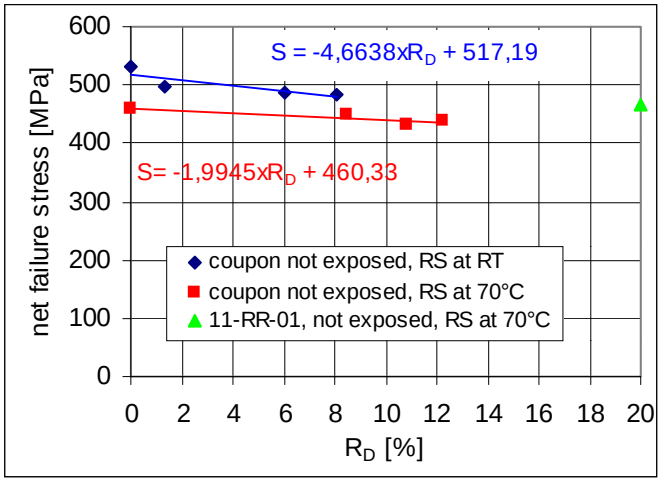

Figure 10.16. Net section failure stresses related to fatigue damage rates, coupons fail on countersunk side, panel 11-RR-01 fails on non-countersunk side, fastener HL413VF, influence of temperature

10.6 Conclusions for returning specimens

Due to the fastener mix used in the repair coupons (specimen series 2-A), the repair panels (specimen series 11-RR) and the Megaliner Barrel, respectively, another fatigue determining variable has to be considered. It is therefore proposed to keep the applied fatigue stress level and the number of fatigue cycles constant for all outdoor exposed panels.

For panels 11-RR-02 and 11-RR-04, which are not fatigued before outdoor exposure, it is proposed to exchange fastener rows 1,4,5 and 8 before starting the fatigue test. ASNA2026 fastener have to replace the HL413VF fastener. It is proposed to remove the repair patch after 40000 cycles and 80000 cycles for a detailed crack inspection. Items of interest are the crack initiation location and the crack lengths. Airbus Deutschland developed non destructive inspection methods which are very sensitive for the here discussed problem. It is appreciated to cooperate with Airbus for the analyses. Finally, a residual strength test with both panels at room temperature is proposed.

Panels 11-RR-03 and 11-RR-05 should be similar fatigue damaged as specimen 11-RR-01. The repair patches have to be removed for crack inspection. Finally, the patches have to be fastened on the skin panels again and residual strength tests shall be performed at 70°C, in order to allow a direct comparison with specimen 11-RR-01 and in order to determine environmental influences, if present. All activities have to be performed fast in order to avoid that the panels dry out.

10.7 References

[1] The significance of flight simulation fatigue tests, J. Schijve, Delft University of Technology, Report LR-466, 1985

[2] Fatigue test results of A320 and A321 circumferential butt joint panel specimens, Th. Beumler, Deutsche Airbus GmbH, Report 10D/E022K4753C04, 1991

[3] Finite Element Calculations for a Stringer Reinforced Butt Joint, J. Seegers, Delft University of Technology, Master Thesis, 1992

[4] An Experimental and Analytical Investigation on the Behavior of Fuselage Riveted Lap Joints, R. Müller, Delft University of Technology, PhD Thesis, 1995

11. Door Corner Cut Out Specimens

11.1 Objective and test

Cut outs in fuselage skin panels are locations of stress concentration and therefore they belong to the group of Principal Structural Elements. However, the stress concentration factor is close to 1.0, which increases the stress allowable to values of 150 MPa to 200 MPa once per flight, depending on the aircraft Design Service Goal and the target inspection intervals.

A stress distribution develops with the peak at the cut out, decreasing towards the far field. However, a bore hole located close to the cut out turned out to be *the* fatigue critical item for some applications in the past.

Airbus uses standardized door corner cut out specimens with an A300 door corner radius in order to simulate the stress distribution present in the Airbus widebody aircraft, see figures 11.1. The specimen can be manufactured as a single sheet, in a combination of sheet materials, e.g. an aluminium/titanium combination and with different bore hole / fastener combinations located at different distances from the cut out radius edge. Fatigue tests with similar specimens but made of different GLARE types have been initiated by Airbus in frame of GRP [1] and conducted by Delft University. Preliminary test results are reported in reference [2]. The applied maximum force was calibrated with strain gauges located at the radius edge. Related to the tensile elasticity modulus of the particular sheet material 180 MPa should not be exceeded. As expected, all tested specimens failed from the 4.8mm bore hole. Some crack initiation and crack propagation results are presented in figure 11.4. Cracks initiate between 55000 and 65000 load cycles and propagate slowly towards the door

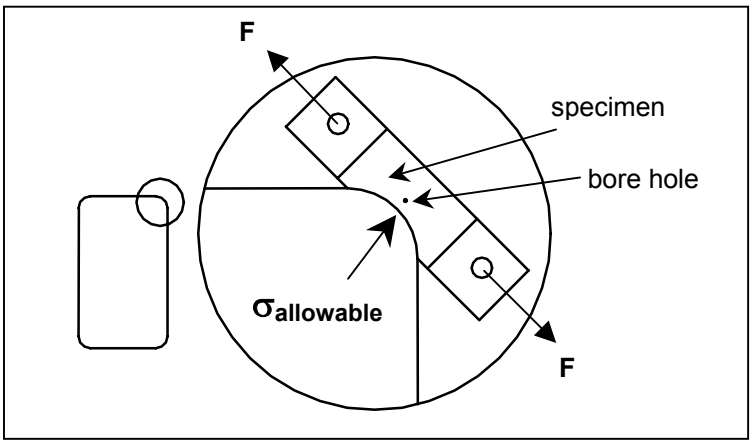

Figure 11.1. Door corner cut out specimen representing aircraft design and stress distribution

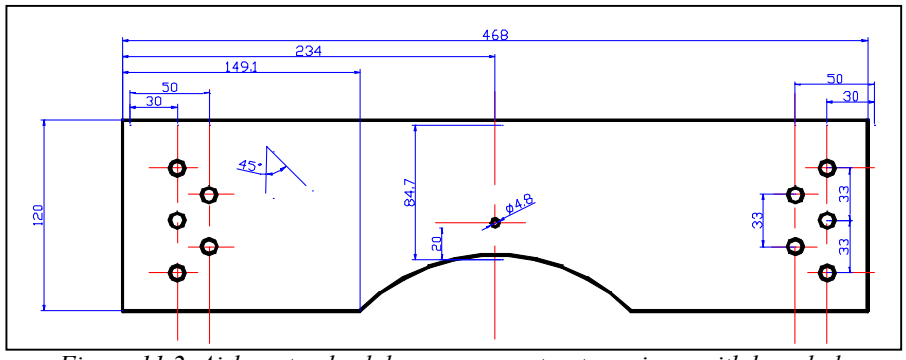

Figure 11.2. Airbus standard door corner cut out specimen with bore hole

Figure 11.3. Outdoor exposure specimen 13-1

corner cut out edge. For a rotated GLARE3 for example (prepreg layers parallel and perpendicular to load direction, equals GLARE6 application in aircraft), a crack initiated at the bore hole after 60000 cycles. With the assumption of a detectable crack length of 8mm, the total fatigue life sums up to 130000 load cycles.

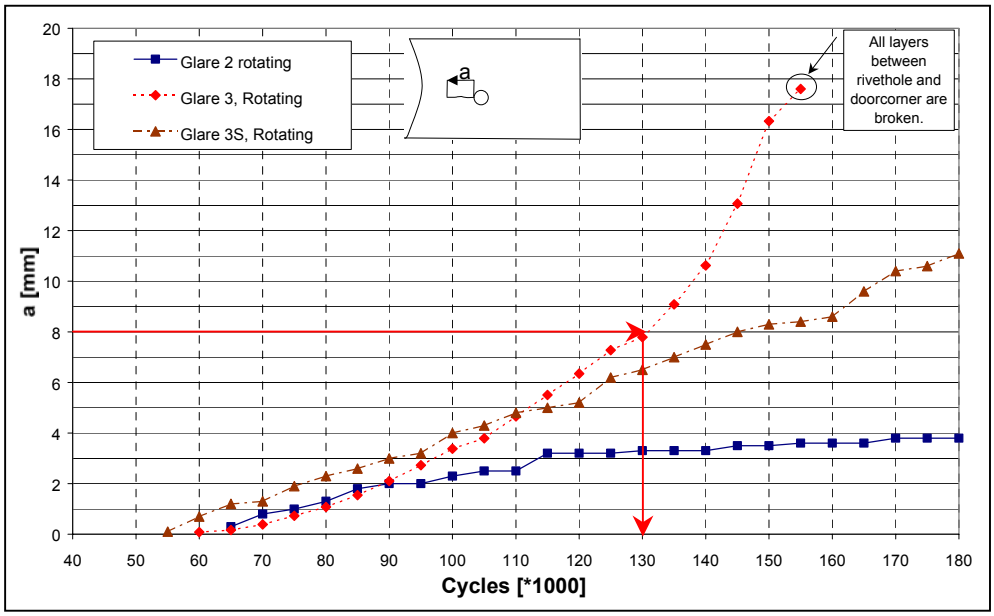

Figure 11.4. Fatigue behaviour of non-exposed GLARE specimens [2]

A fatigue strength justification would look as follows. Assumptions:

- One CA load cycle equals one aircraft flight, i.e. no spectrum factor to be considered.
- Safety factor 5 on crack initiation to be applied, since no full scale test result available.
- Safety factor 2 on crack propagation to be applied, since CP scatter always low.
- The residual strength of the structure is sufficient (limit load capability) until the detectable crack length is obtained.

Then:

N_{CI} = 60000 LC / 5 = 12000 flights
N_{CP} = (130000-60000 LC) / 2 = 35000 flights

First fatigue inspection:
N_{TH} = 12000 + 35000 = 47000 flights

The structure would be free from inspection for aircraft with Design Service Goals below 47000 flights.

The low sensitivity of the GLARE edges to environmental influences is discussed in chapter 4.1. For a verification two GLARE3 specimens are manufactured according to the design shown in figure 11.2. They are milled and drilled *after* application of the surface protection system, i.e. both, the door corner cut out edges and the bore holes are not protected at all (see picture 11.3). The specimens are supposed to be returned from the outdoor exposure site in 2008, after 6 years exposure. It is recommended to test them similar as the dry specimens before [1] and to compare the results with TU Delft report [2].

11.2 References

[1] Thermal and ageing effects on door cutouts, T. de Vries, Airbus Deutschland GmbH, Report-No. 10 L 022 K4 700 I04

[2] Fatigue allowable for the door corners, W. Brüggemann, J. de Kanter, Delft University, interim test report B2V-00-54

Summary and Conclusions

All statements collected in this section are related to GLARE made of 2024T3 metal and FM94/S-glass prepreg.

The present thesis demonstrates that an aircraft structure made of GLARE can be certified with the present airworthiness regulations for monolithic aluminium according to FAR/JAR 25, although the potential crack initiation life of GLARE structures is shorter than for monolithic 2024T3 at similar stress levels. The crack initiation life in this thesis is defined as the life until a crack length of 1 mm. Microcrack growth until 1 mm is not significantly affected by fiber crack bridging, and it was again confirmed in various tests that the crack growth rate for larger cracks is approximately constant and in fact very low. This turned out to be important for a GLARE structure in order to meet the present airworthiness regulations for aluminium aircraft structures.

The critical property for the dimensions of a riveted GLARE joint is the yield strength in order to satisfy FAR/JAR 25.0305(a), which does not allow “detrimental” permanent deformation at limit load. It is shown that the yield strength of riveted joints is lower if determined with tests according to the MIL-STD-1312-4 standard. However, it is recommended to ignore this result because the permanent deformation is not detrimental. (Note: A deformation is “detrimental” if either movable structures are affected or if ultimate load capability can not achieved. Both items are not relevant for a riveted joint.)
Tests with riveted joints has demonstrated that the yield strength of these joints is neither affected by fatigue cracks nor by natural ageing (1 year). It is recommended to continue the present investigation after 2 years and 6 years outdoor exposure.

Diffusion coefficients for moisture absorption in GLARE3 are determined for both rectangular specimens and the bore of a hole. Predictions of moisture concentrations around GLARE3 holes are based on weight gain measurements obtained from outdoor exposure tests. It is tentatively concluded that 500 hours accelerated exposure in a 70°C/85%RH environmental chamber simulates thirty years of short range aircraft operation. The simulation of long range missions would require even less hours of accelerated exposure. The calculations have to be reviewed at the end of the outdoor exposure program Initiated in the frame of this study.

Constant amplitude crack initiation in GLARE made of 2024T3 aluminium at temperatures between -30°C and –55°C has been postponed. At 70°C the crack initiation life is almost similar compared to room temperature results.
Crack propagation under constant amplitude loading is significantly faster at high temperatures, e.g. 70°C, compared to room temperature results. Crack propagation rates decrease significantly at temperatures below zero. The crack propagation rates are dependent on the fatigue delamination size in the laminate.
Complex variable amplitude / variable temperature crack initiation and crack propagation tests are performed. An influence of the variable temperature on fatigue crack initiation or fatigue crack propagation was not observed.

Crack opening in a fatigued GLARE specimen increases after 1000 hours artificial exposure in a 70°C/85%RH environment. The shear strength of the prepreg decreases. The strength reduction is not considered to be relevant for an aircraft structure during a life time of 30 years.

The Relative Miner Rule is applicable for GLARE structures in a similar way as for monolithic aluminium structures.

The simple non-interaction addition of crack length increments in each cycle of a variable-amplitude load history, which is supposed to be equal to da/dN values obtained in constant amplitude tests, does not lead to conservative crack propagation rates if compared to results of variable amplitude tests. Further research on the history effects of fatigue spectra on crack growth in GLARE is required. Special attention has to be paid to the development of the fatigue delamination size.

The residual strength of GLARE riveted joints can be predicted for tensile net section failure and rivet pull through failure. The failure mode depends on the fatigue crack length. The tensile net section strength is dependent on ageing, the rivet pull through strength is not. Due to the high bending deformation in single shear joints with fatigue cracks, very high stresses occur in some of the fiber layers which leads to local fiber failure at loads significantly below the failure load.

The influence of moisture traveling in the load direction (parallel to the fibers) seems to be more determining for the blunt notch strength than the moisture absorption perpendicular to the load direction (i.e. in the net section). It is concluded that the diffusion in fiber direction leads to earlier fiber splitting and consequently to an earlier failure of the laminate.

The compression filled-hole strength is almost independent from fatigue cracks and from ageing.

Fastener types and fastener fit have a significant influence on the crack initiation life.

Scatter of both crack initiation and crack propagation in a riveted joint of a GLARE structure is not higher than in monolithic aluminium joint.

At the end of a full scale fatigue test (duration 2 x Design Service Goal) fatigue cracks in GLARE structures will not be detectable in most cases, but the ultimate load capability will still be present. The point of Wide Spread Fatigue Damage and the (factored) Inspection Threshold must be extrapolated from the full scale fatigue test beyond the DSG. Therefore, fatigue crack propagation must be monitored in full scale fatigue test Principle Structural Elements. This demands the development of improved online inspection methods compared to the procedures from the previous century.

At relevant stress levels bonded repairs on GLARE panels fail early in fatigue of the outer aluminium layer of the panel. The failure can be detected by a delamination inspection of the panel from the inside if the repair patch is bonded on the outside. It is recommended to establish a set of allowable fatigue stresses for bonded repairs which are dependent on stress levels and the stiffness of the jointed materials.

Samenvatting en Conclusies

Alle onderstaande conclusies hebben betrekking op GLARE dat als metaal-vezel laminaat is opgebouwd uit dunne 2024-T3 platen met tussenliggende FM94/S-glass prepreg-lagen.

Het beschreven onderzoek heeft aangetoond dat een vliegtuigconstructie met GLARE als material gecertificeerd kan worden volgens de bestaande FAR/JAR 25 voorschriften, hoewel de levensduur voor scheurinitiatie bij eenzelfde spanningsniveau korter kan zijn dan voor een 2024-T3 constructie. Deze levensduur is gedefinieerd als de periode tot er een microscheur is van 1 mm. Tot deze scheurlengte wordt de groei nog niet noemenswaardig beinvloed door de vezels. Bij verdergaande scheurgroei is dat wel het geval, waarbij als gevolg van “fiber crack bridging” de scheurgroei-snelheid erg laag wordt en vrijwel constant blijft. Dit werd in het huidige onderzoek bevestigd. Dat is essentieel voor het voldoen aan de huidige luchtwaardigheidseisen voor lichtmetalen vliegtuigconstructies.

De cruciale eigenschap voor het dimensioneren van GLARE klinkverbindingen heeft betrekking op blijvende vervorming van de constructie, die volgens het FAR/JAR 25.0305(a) voorschrift niet mag leiden tot “detrimental permanent deformation at limit load”. Proeven volgens de MIL-STD-1312-4 specificatie wezen uit dat blijvende vervorming in de klinkverbindingen wel optrad, maar dat die niet als “detrimental” beschouwd kan worden, en derhalve geen consequenties heeft voor het voldoen aan de voorschriften.
Proeven op klinkverbindingen hebben ook aangetoond dat de weerstand tegen blijvende vervorming niet wordt beinvloed door vermoeiingsscheuren, ook niet na een natuurlijke veroudering van een jaar in een buitenexpositie in Australie onder tropische omstandigheden. Aangeraden wordt dit ook nog te onderzoeken na een expositieperiode van 2, respectievelijk 6 jaar.

Om de invloed van vochtigheid op de eigenschappen van GLARE te bepalen zijn diffusie-coefficienten bepaald voor de absorptie van waterdamp in de prepreg-lagen, zowel bij vochtopname aan de rand van een plaatvormig proefstuk als in de boring van een klinknagelgat. Berekeningen zijn uitgevoerd om de waterdampverdeling rond gaten in GLARE te voorspellen. Verificatie vond plaats met metingen van de gewichtstoename. Voorlopig mag worden geconcludeerd dat een kunstmatige veroudering gedurende 500 uur in een proefopstelling bij een temperatuur van 70^0C en een relatieve vochtigheid van 85% vergeleken kan worden met een veroudering van een korte-afstandvliegtuig in 30 jaar. Voor een lange-afstandsvliegtuig is een kortere kunstmatige veroudering voldoende. De uitgevoerde berekeningen zullen verder worden geverifiëerd na afloop van het buiten-expositie programma.

Scheurinitiatie-proeven met een constante-amplitude belasing zijn op GLARE bij temperaturen tussen -30^0C en -55^0C nog niet uitgevoerd. Maar bij $+70^0$C zijn de resultaten vergelijkbaar met die bij kamertemperatuur. Scheurgroeiproeven bij een constante-amplitude belasing geven bij verhoogde temperatuur wel een snellere scheurgroei. Maar bij temperaturen onder het vriespunt is de scheurgroeisnelheid lager dan bij kamertemperatuur. Proeven met een vlucht-simulatie belasting en een tijdens iedere vlucht gesimuleerd temperatuursverloop gaven geen indicaties van een mogelijke invloed van de temperatuur op de scheurinitiatie en de scheurgroei.

Het openen van een vermoeiingsscheur neemt toe na 1000 uur kunstmatige veroudering. De afschuifsterkte van de prepreg neemt af. Maar deze afname is ook na een vliegtuiggebruik van 30 jaar niet van betekenis.

De zgn. Relatieve Miner regel is van toepassing op GLARE constructies op een soortgelijke manier als voor metalen constructies.

De eenvoudige sommering van scheurlengte-incrementen in iedere belastingswisseling van een variabele-amplitude belastingshistorie, die gelijk wordt gesteld aan de corresponderende scheurgroeisnelheid in constante-amplitude proeven, leidt niet tot conservatieve voorspellingen van de scheurgroei in proeven met een veranderlijk-amplitude belasting. Verder onderzoek is voor GLARE gewenst. Speciale aandacht moet dan worden besteed aan de grootte van gedelamineerde zones.

De reststerkte van GLARE klinkverbindingen kan worden voorspeld voor bezwijken op trek in de netto doorsnede en voor “rivet pull through” als bezwijkvorm. De bezwijkvorm is afhankelijkvan de lengte van aanwezige vermoeiingsscheuren. Het bezwijken op trek is gevoelig voor veroudering, de “rivet pull through” bezwijkvorm is dat niet. Als gevolg van hoge buigvervormingen in een geklonken lapnaad met vermoeiingsscheuren treden erg hoge spanningen op in sommige vezellagen waardoor vezelbreuk kan optreden bij een spanningsniveau duidelijk lager dan de bezwijksterkte.

De invloed van de waterdampdiffusie in de belasingsrichting, evenwijdig met de vezelrichting, is belangrijker voor de “blunt notch” sterkte dan de vochtopname in de richting loodrecht op de vezels. Waargenomen is dat waterdampdiffusie in de vezelrichting eerder tot vezelbreuk leidt en daardoor tot een lagere sterkte van het laminaat.

De sterkte op druk bij aanwezigheid van een gat is ongevoelig voor vermoeiingsscheuren vanuit het gat. Ook veroudering heeft daarop geen invloed.

Het type klinknagel en de passing van de nagel in het gat hebben een significante invloed op de scheurinitiatie-levensduur.

Spreiding van de scheurinitiatie-levensduur en de scheurgroeisnelheid bij GLARE klinkverbindingen is niet hoger dan bij aluminium klinkverbindingen.

Na het voltooien van de ware-grootte vermoeiingsproef op een volledige constructie bij het bereiken van tweemaal de gewenste levensduur zullen er in de GLARE constructiedelen onzichtbare scheurtjes aanwezig zijn. De vereiste stekte zal nog aanwezig zijn. De mogelijkheid van “Wide Spread Fatigue Damage” en “threshold inspection periods” moeten onder ogen worden gezien. Dat vereist dat de groei van vermoeiingsscheuren in de belangrijke onderdelen gemeten moet worden. Daarvoor moeten verbeterde inspectiemethoden worden ontwikkeld.

About the Author

The mystery of how it is possible to keep hundreds of tons of mass flying and the elegance of some of the airborne vehicles (F-104, B727, TU-144) kept the author fascinated when he was a boy. At the age of 16 he started to fly gliders including the famous “Spatz”, an oldtimer which was designed and built in the 1950´s.

A relation to air transport was continued during the military service, when the author joined the long range reconnaissance troops and practiced parachuting. Unforgotten are the jumps out of a DC3 Dakota from the Royal Danish Air Force into a very cold winter night and the long run through the fuselage of a Fokker Friendship for the individual who is the last in the row to jump.

The author graduated as an aircraft engineer in February 1987, witnessed the birth of his first daughter at the end of March and started to work as an engineer at Messerschmidt Bölkow Blohm in April. He was associated to the Fatigue and Damage Tolerance office to which he still belongs, although the company was renamed seven times during the years (at present: Airbus Deutschland GmbH).

In the first moment fatigue and damage tolerance seemed to be a mystery similar as the one mentioned before. During the time when the author was responsible for the C-160 fatigue life extension program in Hamburg he learned from his colleague Kalman Hoffer to avoid talking about “fatigue calculations” but instead to use the phrase “fatigue estimations”. To perform a reliable but not too conservative fatigue estimation requires a lot of experience from tests and in-service occurrences. This experience can not be compensated by any analytics. The author had the advantage to belong to the group of Hans-Jürgen Schmidt who is (he may apologize) a kind of moving library which contains the experience of 40 years fatigue and damage tolerance experience of Airbus fuselage structures. This circumstance allowed the required training on the job.

The author worked on both specific design work and non specific design work. In the non specific section he associated Nikolaus Ohrloff from MBB to look for into GLARE applications for Airbus in 1988. During the 90´s he initiated and/or lead several GLARE related projects, e.g. the design and test of a 3D curved rear pressure bulkhead part of the A340 (including splice type I), fire resistance tests for the A320 APU cover, the application of a GLARE panel in an German Air Force A310 and the establishment of the Megaliner Barrel with a significant portion of GLARE. In the GLARE research program he represented Airbus in the certification, fatigue, durability and repair groups.

In September 1999, after an intensive discussion with Professor Dr. Schwarmann during a flight from Toulouse to Hamburg, the author agreed with Professor Vogelesang from the Delft University of Technology to start a PhD thesis. “Just write down what you did on GLARE during all the years” was the advice of the Professor. However, it became a little bit more complex and much more expensive than expected.

12. Tables

Typical Material Properties

Table 1

	unit	mvf	Glare 2A mvf= 0,762 L	Glare 2A mvf= 0,762 LT	Glare 2B mvf= 0,651 L	Glare 2B mvf= 0,651 LT	Glare 3 mvf= 0,643 L	Glare 3 mvf= 0,643 LT	Glare 4A mvf= 0,571 L	Glare 4A mvf= 0,571 LT	Glare 4B mvf= 0,571 L	Glare 4B mvf= 0,571 LT
Tensile ultimate strength	MPa		895	360	322	1075	678	666	873	556	566	863
Tensile yield stress	MPa		344	239	242	312	287	260	299	229	257	271
Tensile modulus	GPa		66,8	56,5	49,1	64,2	56,4	56,2	56,9	50,1	50,1	56,9
Compressive yield	MPa		347	271	218	387	292	298	317	271	253	336
Compressive modulus	GPa		68,3	60,1	53,7	65,7	58,9	59,6	57,9	52,7	52,7	57,9
shear yield	MPa		131	131	113	113	115	115	104	104	104	104
shear modulus	GPa		18,3	18,3	13,9	13,9	16,4	16,4	14,2	14,2	14,2	14,2
bearing yield, 2% (e/D=3)	MPa		717	583	532	728	680	680	646	582	582	646
bearing ultimate, failure (e/D=3)	MPa		1054	1049	978	985	1018	1018	946	981	981	946
blunt notch (net stress)	MPa		602	300	272	673	481	467	579	396	409	566
specific weight	Kg/dm_3		2,58	2,58	2,49	2,49	2,48	2,48	2,42	2,42	2,42	2,42

Chapter 3
Outdoor Exposure Test Program

Table 3.2.1, moisture reference specimens, GALRE3-2/1-.2

specimen identification	specimen contribution					
	painted	drilled	fastener installed	accelerated exposure	outdoor exposure	remarks
8-1-P & 8-2-P	X				X	
8-3-PH & 8-4-PH	X	X			X	
8-5-PF & 8-6-PF	X	X	X		X	
8-7					X	
8-18-H & 8-19-H		X			X	
8-T2-H		X		X		70°C / 85%RH
8-8-F		X	X	X		70°C / 85%RH
8-9-FP	X	X	X	X		70°C / 85%RH, painted after fastener installation
8-20-H		X		X		90°C / 95%RH
8-21-H		X		X		30°C / 70%RH
8-14-H56		X		X		70°C / 85%RH, bore hole diameter 5.6mm

Table 3.2.2, thick adhered specimens, GLARE2-2/1-8.0

specimen identification	specimen painted	exposure	test temperature
14-B-1 to 14-B-6	no	-	RT
14-B-7 to 14-B-12	yes	3000h, 70°C, 85%RH	RT
14-B-13 to 14-B-18	yes	outdoor, 2 years	RT
14-B-19 to 14-B-24	yes	outdoor, 6 years	RT

Table 3.2.3.1, GLARE2B-7/6.4 circumferential joint specimen identifications and tasks

specimen identification	specimen contribution							
	painted	CI	CP	RS	scatter		outdoor exposure	remarks
2-B-1 to 2-B-5	X		X	X			4 years	no. 1: CP curve contribution
2-B-6	X		X	X			6 years	
2-B-7 to 2-B-11	X	X	X	X			2 years	SN curve contribution
2-B-12	X			X			2 years	
2-B-13 to 2-B-17	X	X	X					variable loads & temperature
2-B-18	X	X						static test / ticking noise
2-B-19 to 2-B-27	X	X	X					variable loads & temperature
2-B-28	X	X	X		X			crack wire measurements
2-B-29 to 2-B-36	X			X			6 years	
2-B-37 & 2-B-38	X	X	X				2 years	
2-B-39	X	X	X				4 years	SN curve contribution
2-B-40	X	X	X				4 years	
2-B-41, -42 & -44	X	X	X				2 years	SN curve contribution
2-B-43	X	X					1 year	CP after outdoor exposure
2-B-45	X	X	X				2 years	SN curve contribution
2-B-46	X	X	X		X		6 years	
2-B-47 & 2-B-48	X	X	X		X		6 years	SN curve contribution
2-B-49 to 2-B-51	X	X	X	X			1 year	CP curve contribution
2-B-52	X			X			2 years	
2-B-53 to 2-B-57	X	X	X	X	X		2 years	SN curve contribution
2-B-58	X			X			6 years	
2-B-59 to 2-B-63	X		X	X			6 years	
2-B-64	X			X			6 years	
2-B-65 to 2-B-69	X		X	X			6 years	
2-B-70	X			X			6 years	
2-B-71	X		X	X			6 years	
2-B-72	X			X			4 years	
2-B-73 to 2-B-75	X		X	X			6 years	
2-B-76 to 2-B-78	X		X	X			1 year	
2-B-79 to 2-B-81			X					crack wire tests
2-B-82 to 2-B-84								TBD
2-B-85 to 2-B-89		X	X	X				
2-B-90		X	X	X				sealant inspection
2-B-91, -93, -94			X	X				
2-B-92, -95, -96			X	X				TBD
2-B-97 & 2-B-98								fiber cracking investigation
2-B-99 to 2-B-101		X	X					vacuum technology
2-B-102								strain measurements
2-B-103 to 2-B-108		X	X					variable amplitude

Table 3.2.3.2, GLARE4A-5/4-.4ssc repair coupon specimen identifications and tasks

specimen identification	specimen contribution							
	painted	CI	CP	RS	scatter		outdoor exposure	remarks
2-A-1				X				
2-A-2 to 2-A-6		X	X	X				
2-A-7 to 2-A-12	X	X	X				2 years	
2-A-13 to 2-A-18	X	X	X				6 years	
2-A-19 to 2-A-24	X	X	X	X			2 years	
2-A-25 to 2-A-30	X	X	X	X			6 years	
2-A-31 to 2-A-34		X			X			contribution SN curve
2-A-35 to 2-A-38								TBD
2-A-39 & 2-A-40	X	X						variable amplitude
2-A-41 to 2-A-42								specimen lost
2-A-43 to 2-A-48	X	X	X	X			1 year	
2-A-49 to 2-A-51	X	X						variable amplitude

CI: specimen used for crack initiation investigations

CP: specimen used for crack propagation investigations

RS: specimen used for residual strength investigations

Table 3.2.4.1, GLARE2B-7/6.4 blunt notch specimen identifications and tasks

specimen identification	specimen contribution							
	painted	CI	CP	RS	scatter	accelerated exposure	outdoor exposure	remarks
3-B-1		X	X	X	X			
3-B-2			X	X				
3-B-3			X	X				
3-B-4			X	X				all layers inspected for cracks
3-B-5			X	X				specimen lost
3-B-5R			X	X				
3-B-6			X	X				
3-B-7 to 3-B-9				X				
3-B-10		X	X	X	X	X		
3-B-11		X	X	X	X	X		
3-B-12	X		X	X		X		
3-B-13	X		X	X		X		
3-B-14	X		X	X		X		
3-B-15	X		X	X		X		
3-B-16	X			X		X		strain gauge measurements
3-B-17 & -18	X			X		X		
3-B-19 to 3-B-24	X		X	X			2 years	
3-B-25 to 3-B-27	X			X			2 years	
3-B-28 to 3-B-33	X		X	X			6 years	
3-B-34 to 3-B-36	X			X			6 years	
3-B-37	X		X			x		
3-B-38			X			x		

Table 3.2.4.2, GLARE4A-5/4.4ssc blunt notch specimen identifications and tasks

specimen identification	specimen contribution							
	painted	CI	CP	RS	scatter	accelerated exposure	outdoor exposure	remarks
3-A-1 to -6		X	X	X				
3-A-7 to -9				X				
3-A-10 to 3-A -13	X		X	X		X		
3-A-14	X			X		X		
3-A-15 to 3-A -18	X		X	X			2 years	
3-A-19	X			X			2 years	
3-A-20 to 3-A -23	X		X	X			6 years	
3-A-24	X			X			6 years	

CI: specimen used for crack initiation investigations

CP: specimen used for crack propagation investigations

RS: specimen used for residual strength investigations

Table 3.2.5, bearing specimen identifications and tasks

specimen identification	specimen contribution				
	painted	test temperature	accelerated exposure	outdoor exposure	remarks
4-B-1 to 4-B-5		RT			GLARE2B-7/6-.4
4-B-6 to 4-B-10	X	RT	3000 h		GLARE2B-7/6-.4
4-B-11 to 4-B-15	X	RT	1500 h		GLARE2B-7/6-.4
4-B-16 to 4-B-20	X	70º C	3000 h		GLARE2B-7/6-.4
4-B-21 to 4-B-25	X	RT		2 years	GLARE2B-7/6-.4
4-B-26 to 4-B-30	X	RT		6 years	GLARE2B-7/6-.4
4-A-1 to 4-A-5		RT			GLARE4A-5/4-.4ssclad
4-A-6 to 4-A-10	X	RT	3000 h		GLARE4A-5/4-.4ssclad
4-A-11 to 4-A-15	X	RT		2 years	GLARE4A-5/4-.4ssclad
4-A-16 to 4-A-20	X	RT		6 years	GLARE4A-5/4-.4ssclad

Table 3.2.6, rivet strength specimen identifications and tasks

specimen identification	specimen contribution				
	painted	test temperature	accelerated exposure	outdoor exposure	remarks
5-B-1 to 5-B-5		RT			GLARE2B-7/6-.4
5-B-6 to 5-B-10		RT	X		GLARE2B-7/6-.4
5-B-11 to 5-B-15	X	RT		2 years	GLARE2B-7/6-.4
5-B-16 to 5-B-20	X	70º C		2 years	GLARE2B-7/6-.4
5-B-21 to 5-B-25	X	RT		6 years	GLARE2B-7/6-.4
5-B-26 to 5-B-30	X	70º C		6 years	GLARE2B-7/6-.4
5-A-1 to 5-A-5		RT			GLARE4A-5/4-.4ssclad
5-A-6 to 5-A-10		RT	X		GLARE4A-5/4-.4ssclad
5-A-11 to 5-A-15	X	RT		2 years	GLARE4A-5/4-.4ssclad
5-A-16 to 5-A-20	X	70º C		2 years	GLARE4A-5/4-.4ssclad
5-A-21 to 5-A-25	X	RT		6 years	GLARE4A-5/4-.4ssclad
5-A-26 to 5-A-30	X	70º C		6 years	GLARE4A-5/4-.4ssclad

Table 3.2.7, compression filled hole specimen identifications and tasks

specimen identification	specimen contribution						
	painted	CI	CP	RS	test temperature	outdoor exposure	remarks
6-B-1 to 6-B-3		X	X	X	RT		GLARE2B-7/6-.4
6-B-4 to 6-B-6		X	X	X	80º C		GLARE2B-7/6-.4
6-B-7 to 6-B-9	X	X	X	X	RT	1 year	GLARE2B-7/6-.4
6-B-10 to 6-B-12	X	X	X	X	RT	1y + 500h	GLARE2B-7/6-.4
6-B-13 to 6-B-15	X	X	X	X	RT	2 years	GLARE2B-7/6-.4
6-B-16 to 6-B-18	X	X	X	X	RT	6 years	GLARE2B-7/6-.4
6-A-1 to 6-A-3		X	X	X	RT		GLARE4A-5/4-.4ssclad
6-A-4 to 6-A-6		X	X	X	80º C		GLARE4A-5/4-.4ssclad
6-A-7 to 6-A-9	X	X	X	X	RT	1 year	GLARE4A-5/4-.4ssclad
6-A-10 to 6-A-12	X	X	X	X	RT	2 years	GLARE4A-5/4-.4ssclad
6-A-13 to 6-A-15	X	X	X	X	RT	1y + 500h	GLARE4A-5/4-.4ssclad
6-A-16 to 6-A-18	X	X	X	X	RT	6 years	GLARE4A-5/4-.4ssclad

Table 3.2.8, rivet pull through specimen identifications and tasks

specimen identification	specimen contribution						
	painted	CI	CP	RS	test temperature	outdoor exposure	remarks
7-B-1 to 7-B-5		X	X	X	RT		GLARE2B-7/6-.4
7-B-6 to 7-B-10		X	X	X	70º C		GLARE2B-7/6-.4
7-B-11 to 7-B-15	X	X	X	X	RT	1 year	GLARE2B-7/6-.4
7-B-16 to 7-B-20	X	X	X	X	RT	2 years	GLARE2B-7/6-.4
7-B-21 to 7-B-25	X	X	X	X	70º C	2 years	GLARE2B-7/6-.4
7-B-26 to 7-B-30	X	X	X	X	RT	6 years	GLARE2B-7/6-.4
7-A-1 to 7-A-5		X	X	X	RT		GLARE4A-5/4-.4ssclad
7-A-6 to 7-A-10		X	X	X	70º C		GLARE4A-5/4-.4ssclad
7-A-11 to 7-A-15	X	X	X	X	RT	1 year	GLARE4A-5/4-.4ssclad
7-A-16 to 7-A-20	X	X	X	X	RT	2 years	GLARE4A-5/4-.4ssclad
7-A-21 to 7-A-25	X	X	X	X	70º C	2 years	GLARE4A-5/4-.4ssclad
7-A-26 to 7-A-30	X	X	X	X	RT	6 years	GLARE4A-5/4-.4ssclad

Chapter 4
Accelerated Diffusion

Table 4.2.1a, weight gain results [g] for GLARE3-4/3-.3 specimen, l=60mm, w=40mm, 30ºC/70%RH

exposure time [h]	ID 39-1	ID 39-2	weight [g] (30°C/70%RH) ID 39-3	ID 39-4	ID 39-5	average
0	11,4963	11,4866	11,4850	11,5188	11,5484	11,5070
8	11,4966	11,4868	11,4830	11,5191	11,5488	11,5069
24	11,4969	11,4871	11,4855	11,5191	11,5491	11,5075
48	11,4972	11,4875	11,4855	11,5194	11,5493	11,5078
72	11,4976	11,4875	11,4857	11,5197	11,5498	11,5081
96	11,4976	11,4876	11,4857	11,5196	11,5484	11,5078
168	11,4977	11,4877	11,4859	11,5199	11,5497	11,5082
200	11,4977	11,4877	11,4858	11,5199	11,5497	11,5082
384	11,4980	11,4882	11,4864	11,5203	11,5501	11,5086
576	11,4983	11,4882	11,4867	11,5203	11,5504	11,5088
768	11,4985	11,4885	11,4869	11,5203	11,5506	11,5090
1008	11,4989	11,4890	11,4871	11,5210	11,5509	11,5094
1500	11,4995	11,4895	11,4877	11,5214	11,5515	11,5099
2000	11,4996	11,4898	11,4881	11,5218	11,5517	11,5102
2500	11,5002	11,4902	11,4884	11,5220	11,5522	11,5106
3000	11,5007	11,4907	11,4888	11,5226	11,5526	11,5111
3500	11,5011	11,4910	11,4891	11,5228	11,5529	11,5114
4146	11,5011	11,4913	11,4894	11,5231	11,5533	11,5116
5000	11,5020	11,4917	11,4899	11,5238	11,5540	11,5123
5500	11,5020	11,4919	11,4903	11,5238	11,5540	11,5124
6000	11,5022	11,4921	11,4903	11,5242	11,5542	11,5126
6500	11,5023	11,4923	11,4905	11,5244	11,5544	11,5128
7000	11,5026	11,4927	11,4908	11,5247	11,5546	11,5131

Table 4.2.1b, weight gain results [g] for GLARE3-4/3-.3 specimen, l=60mm, w=40mm, 70ºC/70%RH

exposure time [h]	weight [g] (70°C/70%RH)					
	ID 39-6	ID 39-7	ID 39-8	ID 39-9	ID 39-10	average
0	11,5394	11,5903	11,5658	11,5385	11,5225	11,5513
8	11,5396	11,5906	11,5662	11,5387	11,5228	11,5516
24	11,5398	11,5908	11,5663	11,5389	11,5231	11,5518
48	11,5402	11,5911	11,5666	11,5394	11,5236	11,5522
72	11,5405	11,5916	11,5670	11,5396	11,5237	11,5525
96	11,5407	11,5919	11,5673	11,5400	11,5242	11,5528
168	11,5411	11,5921	11,5677	11,5403	11,5244	11,5531
200	11,5412	11,5924	11,5679	11,5406	11,5247	11,5534
384	11,5421	11,5934	11,5690	11,5415	11,5263	11,5545
576	11,5420	11,5942	11,5697	11,5424	11,5268	11,5550
768	11,5435	11,5950	11,5701	11,5429	11,5268	11,5557
1008	11,5446	11,5955	11,5709	11,5435	11,5275	11,5564
1500	11,5455	11,5967	11,5721	11,5445	11,5286	11,5575
2000	11,5460	11,5972	11,5726	11,5453	11,5292	11,5581
2500	11,5472	11,5983	11,5735	11,5462	11,5301	11,5591
3000	11,5480	11,5992	11,5744	11,5470	11,5309	11,5599
3500	11,5482	11,5996	11,5748	11,5474	11,5313	11,5603
4146	11,5489	11,6002	11,5754	11,5479	11,5319	11,5609
5000	11,5498	11,6010	11,5761	11,5489	11,5330	11,5618
5500	11,5501	11,6015	11,5767	11,5492	11,5332	11,5621
6000	11,5506	11,6020	11,5768	11,5494	11,5335	11,5625
6500	11,5509	11,6021	11,5772	11,5498	11,5341	11,5628
7000	11,5512	11,6026	11,5776	11,5501	11,5343	11,5632

Table 4.2.1c, weight gain results [g] for GLARE3-4/3-.4 specimen, l=100mm, w=25mm, 70ºC/85%RH

exposure time	weight [g] (70°C/85%RH)							
	ID 1	ID 2	ID 3	ID 4	ID 5	ID 6	ID 7	average
0 h	14,8496	14,7417	14,8263	14,8130	14,7608	14,8052	14,7840	14,7972
528 h	14,8590	14,7509	14,8366	14,8226	14,7701	14,8149	14,7938	14,8068
1002 h	14,8616	14,7540	14,8390	14,8260	14,7736	14,8178	14,7977	14,8100
1506 h	14,8620	14,7539	14,8389	14,8257	14,7732	14,8180	14,7970	14,8098
1630 h	14,8633	14,7552	14,8404	14,8273	14,7752	14,8194	14,7986	14,8113
1988 h	14,8653	14,7570	14,8423	14,8290	14,7768	14,8212	14,8002	14,8131
2496 h	14,8678	14,7593	14,8447	14,8317	14,7795	14,8239	14,8028	14,8157
3041 h	14,8696	14,7610	14,8464	14,8332	14,7809	14,8254	14,8043	14,8173
3501 h	14,8682	14,7594	14,8445	14,8316	14,7793	14,8236	14,8027	14,8156
3715 h	14,8708	14,7623	14,8475	14,8343	14,7820	14,8264	14,8054	14,8184
3863 h	14,8716	14,7630	14,8485	14,8350	14,7829	14,8272	14,8062	14,8192
4002 h	14,8719	14,7635	14,8489	14,8353	14,7833	14,8276	14,8068	14,8196
4289 h	14,8733	14,7650	14,8500	14,8366	14,7846	14,8291	14,8080	14,8209
4481 h	14,8740	14,7657	14,8510	14,8376	14,7855	14,8299	14,8086	14,8218
5013 h	14,8750	14,7665	14,8519	14,8387	14,7867	14,8306	14,8097	14,8227
5683 h	14,8760	14,7672	14,8527	14,8392	14,7875	14,8319		14,8258
6210 h	14,8761	14,7680	14,8532	14,8398	14,7883	14,8324		14,8263
6693 h	14,8774	14,7691	14,8540	14,8407	14,7891	14,8330		14,8272
7246 h	14,8780	14,7695	14,8546	14,8410	14,7898	14,8340		14,8278

Table 4.2.1d, weight gain results [g] for GLARE3-4/3-.3 specimen, l=60mm, w=40mm, 90ºC/95%RH

exposure time [h]	weight [g] (90°C/95%RH) ID 39-11	ID 39-12	ID 39-13	ID 39-14	ID 39-15	average
0	11,5208	11,5509	11,5536	11,5929	11,5392	11,5515
8	11,5218	11,5521	11,5548	11,5929	11,5404	11,5524
27	11,5226	11,5529	11,5555	11,5953	11,5413	11,5535
51	11,5244	11,5558	11,5574	11,5972	11,5434	11,5556
75	11,5261	11,5564	11,5587	11,5981	11,5442	11,5567
99	11,5269	11,5577	11,5615	11,6001	11,5469	11,5586
171	11,5283	11,5588	11,5612	11,6015	11,5472	11,5594
267	11,5302	11,5604	11,5632	11,6049	11,5489	11,5615
362	11,5327	11,5633	11,5662	11,6074	11,5541	11,5647
556	11,5346	11,5651	11,5681	11,6088	11,5551	11,5663
835	11,5381	11,5686	11,5717	11,6122	11,5582	11,5698
1009	11,5394	11,5698	11,5727	11,6137	11,5595	11,5710
1505	11,5434	11,5739	11,5775	11,6178	11,5636	11,5752
2008	11,5439	11,5749	11,5775	11,6186	11,5646	11,5759
2176	11,5440	11,5752	11,5781	11,6189	11,5646	11,5762
2511	11,5446	11,5754	11,5787	11,6189	11,5648	11,5765
3015	11,5455	11,5765	11,5800	11,6206	11,5653	11,5776
3209	11,5455	11,5763	11,5797	11,6199	11,5646	11,5772
3517	11,5470	11,5799	11,5836	11,6217	11,5665	11,5797
4045	11,5479	11,5776	11,5844	11,6214	11,5666	11,5796
4721	11,5440	11,5839	11,5938	11,6244	11,5696	11,5831
5292	11,5609	11,5800	11,5908	11,6228	11,5687	11,5846
5776	11,5504	11,5795	11,5901	11,6208	11,5669	11,5815
6281	11,5500	11,5792	11,5898	11,6207	11,5664	11,5812

Table 4.2.2a, diffusion rates GLARE3-4/3-.3 specimen, 30ºC/70%RH (not corrected)

t [h]	sqrt(t)	Av. W [g]	dW [g]	dW [%]	dWc [%]	D [mm^2/s]
0	0,0	11,50702	0	0	0	
8	2,8	11,50686	-0,00016	-0,00139	-0,00457	
24	4,9	11,50754	0,00052	0,00452	0,01485	1,80E-06
48	6,9	11,50778	0,00076	0,00660	0,02171	1,93E-06
72	8,5	11,50806	0,00104	0,00904	0,02971	2,40E-06
96	9,8	11,50778	0,00076	0,00660	0,02171	9,63E-07
168	13,0	11,50818	0,00116	0,01008	0,03314	1,28E-06
200	14,1	11,50816	0,00114	0,00991	0,03257	1,04E-06
384	19,6	11,50860	0,00158	0,01373	0,04513	1,04E-06
576	24,0	11,50878	0,00176	0,01530	0,05028	8,61E-07
768	27,7	11,50896	0,00194	0,01686	0,05542	7,85E-07
1008	31,7	11,50938	0,00236	0,02051	0,06742	8,85E-07
1500	38,7	11,50992	0,00290	0,02520	0,08284	8,98E-07
2000	44,7	11,51020	0,00318	0,02764	0,09084	8,09E-07
2500	50,0	11,51060	0,00358	0,03111	0,10227	8,21E-07
3000	54,8	11,51108	0,00406	0,03528	0,11598	8,80E-07
3500	59,2	11,51140	0,00438	0,03806	0,12512	8,77E-07
4146	64,4	11,51160	0,00458	0,03980	0,13083	8,10E-07
5000	70,7	11,51230	0,00528	0,04589	0,15083	8,93E-07
6000	77,5	11,51260	0,00558	0,04849	0,15940	8,31E-07
7000	83,7	11,51310	0,00608	0,05284	0,17368	8,45E-07

Table 4.2.2b, diffusion rates GLARE3-4/3-.3 specimen, 70ºC/70%RH (not corrected)

t [h]	sqrt(t)	Av. W [g]	dW [g]	dW [%]	dWc [%]	D [mm^2/s]
0	0,0	11,55130	0	0	0	
8	2,8	11,55158	0,00028	0,00242	0,00242	1,44E-07
24	4,9	11,55178	0,00048	0,00416	0,01371	1,54E-06
48	6,9	11,55218	0,00088	0,00762	0,02514	2,58E-06
72	8,5	11,55248	0,00118	0,01022	0,03371	3,10E-06
96	9,8	11,55282	0,00152	0,01316	0,04342	3,85E-06
168	13,0	11,55312	0,00182	0,01576	0,05199	3,16E-06
200	14,1	11,55336	0,00206	0,01783	0,05885	3,40E-06
384	19,6	11,55446	0,00316	0,02736	0,09027	4,16E-06
576	24,0	11,55502	0,00372	0,03220	0,10627	3,85E-06
768	27,7	11,55566	0,00436	0,03774	0,12455	3,96E-06
1008	31,7	11,55640	0,00510	0,04415	0,14569	4,13E-06
1500	38,7	11,55748	0,00618	0,05350	0,17654	4,08E-06
2000	44,7	11,55806	0,00676	0,05852	0,19311	3,66E-06
2500	50,0	11,55906	0,00776	0,06718	0,22168	3,86E-06
3000	54,8	11,55990	0,00860	0,07445	0,24567	3,95E-06
3500	59,2	11,56030	0,00900	0,07791	0,25710	3,70E-06
4146	64,4	11,56090	0,00960	0,08311	0,27424	3,56E-06
5000	70,7	11,56180	0,01050	0,09090	0,29995	3,53E-06
5500	74,2	11,56210	0,01080	0,09350	0,30852	3,39E-06
6000	77,5	11,56250	0,01120	0,09696	0,31994	3,35E-06
6500	80,6	11,56280	0,01150	0,09956	0,32851	3,26E-06
7000	83,7	11,56320	0,01190	0,10302	0,33994	3,24E-06

Table 4.2.2c, diffusion rates GLARE3-4/3-.4 specimen, 70ºC/85%RH (not corrected)

t [h]	sqrt(t)	Av. W [g]	dW [g]	dW [%]	dWc [%]	D [mm^2/s]
0	0	14,79723	0	0	0	
528	23,0	14,80684	0,00961	0,06497	0,26145	4,42E-06
1002	31,7	14,80996	0,01273	0,08602	0,34615	4,08E-06
1506	38,8	14,80981	0,01259	0,08505	0,34226	2,65E-06
1630	40,4	14,81134	0,01411	0,09538	0,38383	3,08E-06
1988	44,6	14,81311	0,01589	0,10736	0,43200	3,20E-06
2496	50,0	14,81567	0,01844	0,12464	0,50154	3,44E-06
3041	55,1	14,81726	0,02003	0,13535	0,54466	3,33E-06
3501	59,2	14,81561	0,01839	0,12425	0,49999	2,44E-06
3715	61,0	14,81839	0,02116	0,14298	0,57536	3,04E-06
3863	62,2	14,81920	0,02197	0,14848	0,59750	3,15E-06
4002	63,3	14,81961	0,02239	0,15128	0,60877	3,16E-06
4298	65,6	14,82094	0,02371	0,16026	0,64490	3,30E-06
4481	66,9	14,82176	0,02453	0,16576	0,66704	3,39E-06
5013	70,8	14,82273	0,02550	0,17233	0,69346	3,27E-06
5683	75,4	14,82575	0,02632	0,17782	0,71524	3,12E-06
6210	78,8	14,82630	0,02687	0,18154	0,73018	3,16E-06
6693	81,8	14,82722	0,02778	0,18773	0,75510	3,17E-06
7246	85,1	14,82782	0,02838	0,19179	0,77141	3,16E-06

Table 4.2.2d, diffusion rates GLARE3-4/3-.3 specimen, 90ºC/95%RH (not corrected)

t [h]	sqrt(t)	Av. W [g]	dW [g]	dW [%]	dWc [%]	D [mm^2/s]
0,0	0,0	11,55148	0	0	0	
8,0	2,8	11,55266	0,00118	0,01022	0,01022	2,84E-07
26,5	5,1	11,55352	0,00204	0,01766	0,05828	2,79E-06
50,5	7,1	11,55564	0,00416	0,03601	0,11884	6,10E-06
74,5	8,6	11,55670	0,00522	0,04519	0,14912	6,51E-06
98,5	9,9	11,55862	0,00714	0,06181	0,20396	9,21E-06
170,5	13,1	11,55940	0,00792	0,06856	0,22625	6,54E-06
267,0	16,3	11,56152	0,01004	0,08692	0,28681	6,72E-06
362,0	19,0	11,56474	0,01344	0,11635	0,38393	8,88E-06
556,0	23,6	11,56634	0,01504	0,13020	0,42964	7,24E-06
834,5	28,9	11,56976	0,01846	0,15981	0,52734	7,26E-06
1009,0	31,8	11,57102	0,01972	0,17072	0,56333	6,86E-06
1505,0	38,8	11,57524	0,02394	0,20725	0,68388	6,77E-06
2008,0	44,8	11,57590	0,02460	0,21296	0,70273	5,36E-06
2176,0	46,6	11,57616	0,02486	0,21521	0,71016	5,05E-06
2511,0	50,1	11,57648	0,02518	0,21798	0,71930	4,49E-06
3015,0	54,9	11,57760	0,02630	0,22768	0,75130	4,08E-06
3209,0	56,6	11,57720	0,02590	0,22422	0,73987	3,72E-06
3517,0	59,3	11,57970	0,02840	0,24586	0,81128	4,08E-06
4045,0	63,6	11,57960	0,02830	0,24499	0,80843	3,52E-06
4721,0	68,7	11,58310	0,03180	0,27529	0,90841	3,81E-06
5292,0	72,7	11,58460	0,03330	0,28828	0,95126	3,73E-06

Table 4.2.3, diffusion rate relations for GLARE3 and GLARE2, obtained from reference [30]

temperature	GLARE3	GLARE2parallel*	GLARE2 perpendicular*
20°C	1	1,76	0,55
60°C	1	1,97	0,34
	mean value:	1,865	0,445

* diffusion direction related to fiber orientation

Table 4.3.1a, accelerated weight gain results of MRS specimen 8-21-H, climate 30ºC/70%RH

time	W [g]	sqrt(t)	dW [g]	dWprep [%]	D [mm^2/s]	dWcorr [%]	D [mm^2/s]
start	110,2257	0	0	0		(corrected)	(corrected)
8 h	110,2327	2,8	0,00700	0,00795	5,98E-06	0,00475	2,14E-06
24 h	110,2331	4,9	0,00740	0,00841	2,23E-06	0,00521	8,55E-07
48 h	110,2365	6,9	0,01080	0,01227	2,37E-06	0,00907	1,30E-06
72 h	110,2384	8,5	0,01270	0,01443	2,19E-06	0,01123	1,33E-06
96 h	110,2379	9,8	0,01220	0,01386	1,51E-06	0,01066	8,96E-07
168 h	110,2402	13,0	0,01450	0,01648	1,22E-06	0,01328	7,94E-07
200 h	110,2401	14,1	0,01440	0,01636	1,01E-06	0,01316	6,55E-07
384 h	110,2446	19,6	0,01890	0,02148	9,09E-07	0,01828	6,58E-07
575 h	110,2466	24,0	0,02090	0,02375	7,42E-07	0,02055	5,56E-07
768 h	110,2494	27,7	0,02370	0,02693	7,15E-07	0,02373	5,55E-07
1008 h	110,2520	31,7	0,02630	0,02989	6,70E-07	0,02669	5,35E-07
1500 h	110,2567	38,7	0,03100	0,03523	6,26E-07	0,03203	5,17E-07
2000 h	110,2589	44,7	0,03320	0,03773	5,38E-07	0,03453	4,51E-07
2500 h	110,2642	50,0	0,03850	0,04375	5,79E-07	0,04055	4,98E-07
3000 h	110,2692	54,8	0,04350	0,04943	6,16E-07	0,04623	5,39E-07
3500 h	110,2723	59,2	0,04660	0,05295	6,06E-07	0,04975	5,35E-07
4146 h	110,2735	64,4	0,04780	0,05432	5,38E-07	0,05112	4,77E-07
5000 h	110,2830	70,7	0,05730	0,06511	6,42E-07	0,06191	5,80E-07
5500 h	110,2874	74,2	0,06170	0,07011	6,76E-07	0,06691	6,16E-07
6000 h	110,2920	77,5	0,06630	0,07534	7,16E-07	0,07214	6,56E-07
6500 h	110,2944	80,6	0,06870	0,07807	7,09E-07	0,07487	6,52E-07
7000 h	110,2992	83,7	0,07350	0,08352	7,54E-07	0,08032	6,97E-07

Table 4.3.1b, accelerated weight gain results of MRS specimen 8-T2-H, climate 70ºC/85%RH

time	W [g]	sqrt(t)	dW [g]	dWprep [%]	D [mm^2/s]	dWcorr [%]	D [mm^2/s]
start	112,0210	0,0	0,00000	0,00000		(corrected)	(corrected)
264 h	112,0810	16,2	0,06000	0,06818	3,33E-06	0,08228	4,85E-06
504 h	112,1080	22,4	0,08700	0,09886	3,67E-06	0,11296	4,79E-06
1008 h	112,1620	31,7	0,14100	0,16023	4,82E-06	0,17433	5,70E-06
1489 h	112,2000	38,6	0,17900	0,20341	5,26E-06	0,21751	6,01E-06
2016 h	112,2410	44,9	0,22000	0,25000	5,86E-06	0,26410	6,54E-06
2499 h	112,2740	50,0	0,25300	0,28750	6,26E-06	0,30160	6,88E-06
3052 h	112,3100	55,2	0,28900	0,32841	6,68E-06	0,34251	7,27E-06
3624 h	112,3400	60,2	0,31900	0,36250	6,86E-06	0,37660	7,40E-06
4006 h	112,3560	63,3	0,33500	0,38068	6,84E-06	0,39478	7,36E-06
4493 h	112,3780	67,0	0,35700	0,40568	6,93E-06	0,41978	7,42E-06
4997 h	112,4000	70,7	0,37900	0,43068	7,02E-06	0,44478	7,49E-06
5500 h	112,4170	74,2	0,39600	0,45000	6,96E-06	0,46410	7,41E-06
6000 h	112,4310	77,5	0,41000	0,46591	6,84E-06	0,48001	7,26E-06
6504 h	112,4420	80,6	0,42100	0,47841	6,66E-06	0,49251	7,05E-06

Table 4.3.1c, accelerated weight gain results of MRS specimen 8-20-H, climate 90ºC/95%RH

time	W [g]	sqrt(t)	dW [g]	dWprep [%]	D [mm^2/s]	dWcorr [%]	D [mm^2/s]
Start	111,374	0	0	0		(corrected)	(corrected)
8 h	111,376	2,8	0,00230	0,00261	7,18E-08	0,08311	7,26E-05
26,5 h	111,392	5,1	0,01740	0,01977	1,24E-06	0,10027	3,19E-05
50,5 h	111,408	7,1	0,03420	0,03886	2,51E-06	0,11936	2,37E-05
74,5 h	111,423	8,6	0,04900	0,05568	3,50E-06	0,13618	2,09E-05
98,5 h	111,437	9,9	0,06280	0,07136	4,35E-06	0,15186	1,97E-05
170,5 h	111,465	13,1	0,09060	0,10295	5,23E-06	0,18345	1,66E-05
267 h	111,504	16,3	0,12980	0,14750	6,85E-06	0,22800	1,64E-05
362 h	111,54	19,0	0,16630	0,18898	8,29E-06	0,26948	1,69E-05
556 h	111,606	23,6	0,23200	0,26364	1,05E-05	0,34414	1,79E-05
834,5 h	111,695	28,9	0,32040	0,36409	1,34E-05	0,44459	1,99E-05
1009 h	111,739	31,8	0,36480	0,41455	1,43E-05	0,49505	2,04E-05
1505 h	111,851	38,8	0,47710	0,54216	1,64E-05	0,62266	2,17E-05
2009 h	111,918	44,8	0,54420	0,61841	1,60E-05	0,69891	2,04E-05
2176 h	111,9410	46,6	0,56690	0,64420	1,60E-05	0,72470	2,03E-05
2511,5 h	111,987	50,1	0,61260	0,69614	1,62E-05	0,77664	2,02E-05
3015 h	112,041	54,9	0,66720	0,75818	1,60E-05	0,83868	1,96E-05

Table 4.3.2, prepreg weight gain results of specimens 8-8-F and 8-9-PF, 70°C / 85%RH

t [h]	[sqrt(h)]	$dW_{8\text{-}8\text{-}F}$ [%]	$dW_{8\text{-}9\text{-}PF}$ [%]
0	0	0	0
260	16.1	0.035	-0.061
500	22.4	0.064	-0.047
1003	31.7	0.110	-0.016
1508	38.8	0.155	0.020
2040	45.2	0.192	0.043
2544	50.4	0.221	0.069
3000	54.8	0.248	0.098
3500	60.2	0.281	0.119
4007	63.3	0.303	0.134
4508	67.0	0.328	0.154
4847	70.7	0.341	0.140
5496	74.2	0.367	0.130
5999	77.5	0.393	0.140
6500	80.6	0.419	0.136
7004	83.7	0.442	0.127
7538	86.6	0.449	0.122
7993	89.4	0.475	0.140
8516	92.2	0.493	0.127

Table 4.5, failure loads of thick adhered specimens

	failure load [N]	
specimen no.	dry specimens	3000h aged specimens
14-B-1	15609	
14-B-2	15502	
14-B-3	15676	
14-B-4	15877	
14-B-6	15167	
average dry	**15566**	
14-B-7		14864
14-B-8		14000
14-B-9		14917
14-B-10		14529
14-B-11		14144
14-B-12		14368
average wet		**14470**

Chapter 5
Tropic Ageing

Table 5.2.1, long term climate record from outdoor exposure site

DEPARTMENT OF DEFENCE

DEFENCE SCIENCE AND TECHNOLOGY ORGANISATION
Aeronautical and Maritime Research Laboratory - Queensland

METEOROLOGICAL SUMMARY
1963 --- 1994

PIN GIN HILL HOT WET CLEARED SITE

	JAN	FEB	MAR	APR	MAY	JUN	JUL	AUG	SEP	OCT	NOV	DEC	YEAR
TEMPERATURE (c)													
Highest daily Maximum	40.8	38.3	38.8	34.9	32.0	31.6	30.5	33.3	34.6	36.4	41.1	40.8	41.1
Average daily Maximum	31.2	30.5	29.7	27.9	26.0	24.3	23.8	25.3	27.2	29.0	30.7	31.2	28.1
Average daily Mean	26.7	26.4	25.6	24.0	22.2	20.0	19.4	20.5	22.0	23.7	25.5	26.4	23.5
Average daily Minimum	22.8	22.9	22.3	20.7	19.1	16.4	15.7	16.3	17.4	19.0	20.9	22.0	19.6
Lowest daily Minimum	17.7	18.2	16.0	14.0	9.5	7.2	6.3	9.6	10.5	11.3	15.5	17.0	6.3
RELATIVE HUMIDITY %													
Highest daily Maximum	100	100	100	100	100	100	100	100	100	100	100	100	100
Average daily Maximum	95	96	96	96	96	95	95	95	95	95	95	95	95
Average daily Mean	82	84	85	87	86	83	82	81	79	78	78	79	82
Average daily Minimum	60	65	65	67	68	62	60	57	52	52	54	57	60
Lowest daily Minimum	17	17	16	26	28	25	11	18	11	9	4	14	4
PRECIPITATION													
Highest Monthly Rainfall (mm)	2548.0	2036.8	1226.0	1011.6	875.3	454.5	447.5	295.0	322.6	341.9	554.5	1050.0	2548.0
Average Rainfall (mm)	531.5	597.4	588.3	422.1	340.5	143.4	118.4	78.1	82.3	92.7	128.5	256.5	3379.6
Average Rain Days	17	19	20	21	19	12	13	12	10	10	10	14	177
RADIATION													
Average Sun Hours	204.2	158.8	167.7	144.4	138.9	154.3	161.6	180.0	212.7	234.0	225.0	218.7	2200.4
Average Total Global Radiation (kWhm-2)	169.5	129.2	135.2	110.4	96.8	96.4	101.6	121.8	145.7	168.7	169.5	168.7	1613.4
Average UV Radiation (kWhm-2)	8.8	6.2	5.9	6.1	5.1	4.4	4.5	5.3	6.7	7.7	7.7	8.0	76.4

Table 5.2.2, MRS outdoor weight gain measurements, absolute values

	Weights (g)								Additional Panels	Weight (g)	
	Specimen									Specimen	
Date	Calibration Weight	8-1-P	8-2-P	8-3-PH	8-4-PH	8-5-PF	8-6-PF	8-7	Date	8-18-H	8-19-H
As received 21-Dec-2001	100,0006	115,3944	115,4746	111,8930	112,5436	135,5927	135,3282	111,8133			
Pre-exposure 8-Jan-2002	100,0008	115,3992	115,4822	111,9012	112,5560	135,6029	135,3319	111,8152			
8-Apr-02	100,0017	115,3547	115,4424	111,8661	112,5263	135,5931	135,3046	111,8085	As received 2-Jul-2002	110,7901	109,8186
08. Jul 02	99,9982	115,3307	115,4138	111,8418	112,5032	135,5409	135,2717	111,7900	Pre-exp. 8-Jul-2002	110,7861	109,8145
10. Okt 02	99,9995	115,3242	115,4087	111,8430	112,5078	135,5467	135,2739	111,7774		110,7827	109,8093
08. Jan 03	100,0009	115,3495	115,4370	111,9031	112,5419	135,5829	135,3072	111,7831		110,7925	109,8168
10. Apr 03	99,9999	115,3460	115,4335	111,8758	112,5395	135,5949	135,3197	111,7717		110,7901	109,8132

Table 5.2.3, mean weight gain of open hole- and filled hole MRS, delta weight for prepreg (bore holes, corrected for absorption of paint system)

time [month]	0	3	6	9	12	15
time [h]	0	2136	4320	6576	8760	10968
time sqrt[h]	0	46,2	65,7	81,1	93,6	104,7
weight 8-7	111,815	111,809	111,7900	111,7774	111,7831	111,7717
weight P	115,441	115,399	115,372	115,366	115,393	115,390
weight PH	112,229	112,196	112,173	112,175	112,223	112,208
weight PF	135,467	135,449	135,406	135,410	135,445	135,457
weight H	110,300	110,296	110,305	110,302		
delta PH [g]		0,009	0,011	0,020	0,041	0,029
delta PF [g]		0,023	0,006	0,016	0,024	0,040
delta H [g]		0,002	0,029	0,039		

P: painted specimen
PH: painted open hole specimens
PF: painted filled hole specimen
H: unpainted open hole specimens

Table 5.2.4, temperatures and humidities on the 14th of January, 2002

time [hour]	$T_{ambient}$ [°C]	RH_{mean} [%]	f_{MRS}	T_{MRS} [°C]	M_m [%]
1	24,9	89,1	1,08	26,9	0,89
2	24,7	91,9	1,07	26,4	0,98
3	24,9	88,0	1,05	26,1	0,86
4	24,7	89,0	1,06	26,1	0,89
5	24,6	89,7	1,06	26,0	0,91
6	24,6	86,5	1,06	26,1	0,81
7	25,2	84,9	1,05	26,5	0,77
8	27,0	77,2	1,01	27,3	0,57
9	29,3	68,2	1,17	34,4	0,39
10	31,5	58,7	1,63	51,2	0,24
11	33,2	54,7	1,90	63,1	0,19
12	34,1	52,1	2,03	69,4	0,17
13	33,6	53,7	2,11	71,0	0,18
14	34,0	51,8	1,86	63,3	0,16
15	33,8	55,3	1,75	59,2	0,20
16	33,9	55,8	1,29	43,6	0,21
17	30,3	73,2	1,12	33,9	0,48
18	26,6	83,3	1,04	27,6	0,72
19	25,7	88,3	1,09	28,0	0,87
20	25,7	90,4	1,06	27,4	0,93
21	25,7	91,3	1,05	27,1	0,96
22	25,3	92,6	1,05	26,7	1,01
23	25,1	94,2	1,06	26,5	1,06
24	25,3	91,7	1,07	27,1	0,97

Table 5.2.5a, 'calibration day' diffusion, $T_{ambient}$

time	related to $T_{ambient}$		
[hour]	D [mm^2/h]	dM_t [%/h]	% contr.
1	4,87E-04	9,41E-04	5,46
2	4,78E-04	1,03E-03	5,96
3	4,86E-04	9,05E-04	5,25
4	4,78E-04	9,29E-04	5,39
5	4,73E-04	9,46E-04	5,49
6	4,75E-04	8,48E-04	4,92
7	4,97E-04	8,18E-04	4,75
8	5,74E-04	6,51E-04	3,78
9	6,86E-04	4,84E-04	2,81
10	8,12E-04	3,29E-04	1,91
11	9,25E-04	2,82E-04	1,63
12	9,94E-04	2,51E-04	1,46
13	9,53E-04	2,69E-04	1,56
14	9,84E-04	2,44E-04	1,42
15	9,68E-04	2,98E-04	1,73
16	9,80E-04	3,08E-04	1,79
17	7,45E-04	6,29E-04	3,65
18	5,57E-04	8,16E-04	4,73
19	5,17E-04	9,43E-04	5,48
20	5,18E-04	1,01E-03	5,89
21	5,18E-04	1,05E-03	6,07
22	5,03E-04	1,08E-03	6,27
23	4,92E-04	1,12E-03	6,53
24	5,03E-04	1,05E-03	6,07
	total:	1,72E-02	100,00

Table 5.2.5b, 'calibration day' diffusion, $T_{specimen}$

time	related to T_{MRS}		
[hour]	D [mm^2/h]	dM_t [%/h]	% contr.
1	5,70E-04	1,02E-03	4,76
2	5,46E-04	1,10E-03	5,13
3	5,36E-04	9,50E-04	4,45
4	5,35E-04	9,82E-04	4,60
5	5,29E-04	1,00E-03	4,68
6	5,35E-04	9,00E-04	4,21
7	5,53E-04	8,63E-04	4,04
8	5,86E-04	6,58E-04	3,08
9	1,01E-03	5,87E-04	2,75
10	3,35E-03	6,69E-04	3,13
11	7,33E-03	7,92E-04	3,71
12	1,08E-02	8,28E-04	3,87
13	1,19E-02	9,50E-04	4,44
14	7,42E-03	6,70E-04	3,14
15	5,71E-03	7,24E-04	3,39
16	1,99E-03	4,39E-04	2,05
17	9,80E-04	7,21E-04	3,37
18	6,03E-04	8,49E-04	3,97
19	6,22E-04	1,03E-03	4,84
20	5,90E-04	1,08E-03	5,07
21	5,78E-04	1,10E-03	5,17
22	5,59E-04	1,14E-03	5,33
23	5,53E-04	1,19E-03	5,58
24	5,78E-04	1,12E-03	5,25
	total:	2,14E-02	100,00

Table 5.2.6, representative short range flight missions for one day

Destination		KLM flight	GMT [h]	flight time [h]	ground time [h]	RH [%]	T [°C]
HAM	departure	1778	06:45	1.08			
AMS	arrival	1778	07:40		2.00	80	35-44
AMS	departure	1779	09:40	1.00			
HAM	arrival	1779	10:40		0.75	55	52
HAM	departure	1780	11:25	1.08			
AMS	arrival	1780	12:30		3.08	52	66-48
AMS	departure	1783	15:35	0.67			
HAM	arrival	1783	16:15		1.08	55-85	26-30
HAM	departure	1784	17:20	1.17			
AMS	arrival	1784	18:30		1.50	90	26
AMS	departure	1789	20:00	1.00			
HAM	arrival	1789	21:00		9.75	95	25-24

assumption: both cities tropic

	GMT	t ambient [°C]	t skin [°C]	RH [%]
	0	24.3	24	90
06:45	6.75	25	30	85
	6.8	-55	-30	0
07:40	7.67	-55	-30	0
	7.75	27	35	80
09:40	9.67	32.2	44	80
	9.75	-55	-30	0
10:40	10.67	-55	-30	0
	10.75	33.3	52	55
11:25	11.42	34.1	52	55
	11.5	-55	-30	0
12:30	12.5	-55	-30	0
	12.58	34.4	66	52
	14	34.2	66	52
15:35	15.58	34.6	48	52
	15.67	-55	-30	0
16:15	16.25	-55	-30	0
	16.33	29.7	30	55
17:20	17.33	26.2	26	85
	17.42	-55	-30	0
18:30	18.5	-55	-30	0
	18.58	25.7	26	90
20:00	20	25.9	26	90
	20.08	-55	-30	0
21:00	21	-55	-30	0
	21.08	25.5	25	95
	24	24.3	24	95

Table 5.2.7, representative long range flight mission for one day

Destination		KLM flight 781 local time [h]	GMT [h]	flight time [h]	ground time [h]	RH [%]	T [°C]
AMS	departure	12:45	12:45	9.50			
ARUBA	arrival	16:15	22:15		1.25	60-90	24-30
ARUBA	departure	17:30	23:30	0.67			
CURACAO	arrival	18:10	00:10		1.5	90	30
CURACAO	departure	19:40	01:40	9.00			
AMS	arrival	10:40	10:40		2.75	55	33-66

assumption: AMS is tropic

	GMT	t ambient [°C]	t skin [°C]	RH [%]
	0	-55	-30	0
evening	0.16	-55	-30	0
evening	0.33	25.9	30	90
1:40 GMT	1.67	25.6	30	90
	1.75	-55	-30	0
	10.67	-55	-30	0
	10.75	33	33	55
	11	34	54	55
	12	34.3	66	55
	12.75	33.5	65	55
	12.83	-55	-30	0
afternoon	22.25	-55	-30	0
	22.33	32.5	30	60
	23	28	28	81
	23.5	23.8	24	90
	23.58	-55	-30	0
	24	-55	-30	0

Table 5.2.8, calculation of weight gain for long range mission, empirical

Destination		KLM flight 781 local time [h]	GMT [h]	flight time [h]	ground time [h]	RH [%]	T_{am} [°C]	T_{skin} [°C]	Summer 02 [g/2002]	Autumn 02 [g/2002]	Winter 02 [g/2002]	Spring 02 [g/2002]	Summer 03 [g/2002]
									89	91	91	92	92
AMS	departure	12:45	12:45	9,50									
ARUBA	arrival	16:15	22:15		1,25	75	30	27	3,80E-04	1,28E-04	4,08E-04	3,41E-04	6,75E-04
ARUBA	departure	17:30	23:30	0,67									
CURACAO	arrival	18:10	00:10		1,5	90	26	30	6,54E-04	2,20E-04	7,03E-04	5,87E-04	1,16E-03
CURACAO	departure	19:40	01:40	9,00									
AMS	arrival	10:40	10:40		2,75	55	34	66	9,99E-04	3,37E-04	1,07E-03	8,98E-04	1,78E-03
								g/quarter:	0,0020	0,0007	0,0022	0,0018	0,0036
assumption: AMS is tropic								total g:	0,0020	0,0027	0,0049	0,0067	0,0103
								% prepreg	0,0015	0,0020	0,0036	0,0050	0,0077

Table 5.2.9, calculation of weight gain for short range mission, empirical

File 'KLMflights'									Summer 02	Autumn 02	Winter 02	Spring 02	Summer 03
Destination		KLM flight	GMT [h]	flight time [h]	ground time [h]	RH [%]	T_{am} [°C]	T_{skin} [°C]	[g/2002]	[g/2002]	[g/2002]	[g/2002]	[g/2002]
									89	91	91	92	92
HAM	departure	1778	06:45	1,08									
AMS	arrival	1778	07:40		2,00	80	30	40	5,24E-04	1,77E-04	5,64E-04	4,71E-04	9,32E-04
AMS	departure	1779	09:40	1,00									
HAM	arrival	1779	10:40		0,75	55	34	52	2,50E-04	8,44E-05	2,69E-04	2,25E-04	4,45E-04
HAM	departure	1780	11:25	1,08									
AMS	arrival	1780	12:30		3,08	52	34	57	1,01E-03	3,41E-04	1,09E-03	9,09E-04	1,80E-03
AMS	departure	1783	15:35	0,67									
HAM	arrival	1783	16:15		1,08	70	28	28	3,29E-04	1,11E-04	3,54E-04	2,96E-04	5,85E-04
HAM	departure	1784	17:20	1,17									
AMS	arrival	1784	18:30		1,50	90	26	26	6,54E-04	2,20E-04	7,03E-04	5,87E-04	1,16E-03
AMS	departure	1789	20:00	1,00									
HAM	arrival	1789	21:00		9,75	95	25	25	4,68E-03	1,58E-03	5,03E-03	4,20E-03	8,31E-03
assumption: both cities tropic								Einzelerte:	0,007	0,003	0,008	0,007	0,013
								Summe:	0,007	0,010	0,018	0,025	0,038
								% prepreg	0,006	0,007	0,013	0,018	0,028

Chapter 6
Elementary Tests

Remark: All constant amplitude fatigue tests are conducted with stress ration 0.1.

Tables 6.2.1, stiffness, temperature and stress ratio correction for aluminium layers in GLARE3-3/2-.3
Room temperature results

specimen	max. applied load [N]	σ_{max} stiffness & temperature corrected [MPa]	σ_{min} stiffness & temperature corrected [MPa]	R alumi-num	$\sigma_{max\ R=0.05}$ [MPa]	$\sigma_{a\ R=0.05}$ [MPa]	$F_{ref.}$ for Wöhler prog. [N]	N [cycles]
0	29822	558	78	0.14	526	250	36791	1
1	8448	176	40	0.23	155	74	10879	31000
2	8448	176	40	0.23	155	74	10879	34000
3	8026	168	39	0.23	148	70	10367	25000
4	8026	168	39	0.23	148	70	10367	38000
5	7603	161	39	0.24	141	67	9853	40000
6	7181	153	38	0.25	133	63	9340	34000
7	6758	146	37	0.25	126	60	8825	60000
8	5914	131	36	0.27	111	53	7798	445000
9	5069	116	34	0.29	97	46	6768	1000000

Tables 6.2.1 cont'd, 70°C results

specimen	max. applied load [N]	σ_{max} stiffness & temperature corrected [MPa]	σ_{min} stiffness & temperature corrected [MPa]	R alumi-num	$\sigma_{max\ R=0.05}$ [MPa]	$\sigma_{a\ R=0.05}$ [MPa]	$F_{ref.}$ for Wöhler prog. [N]	N [cycles]
0	31257	581	69	0.12	555	264	38848	1
1	8448	166	28	0.17	153	73	10740	28000
2	7603	151	26	0.17	139	66	9698	48000
3	7181	143	26	0.18	131	62	9177	49000
4	6758	135	25	0.18	124	59	8656	63000
5	6336	128	24	0.19	116	55	8135	62000
6	5914	120	23	0.19	109	52	7614	78000
7	5491	112	22	0.20	101	48	7092	96000
8	5280	109	22	0.20	98	46	6832	260000

Tables 6.2.1 cont'd, -55°C results

specimen	max. applied load [N]	σ_{max} stiffness & temperature corrected [MPa]	σ_{min} stiffness & temperature corrected [MPa]	R alumi-num	$\sigma_{max\ R=0.05}$ [MPa]	$\sigma_{a\ R=0.05}$ [MPa]	$F_{ref.}$ for Wöhler prog. [N]	N [cycles]
0	29822	585	97	0.17	540	257	37830	1
1	8448	196	58	0.30	164	78	11644	68000
2	8026	188	57	0.30	156	74	10943	54000
3	7803	184	57	0.31	152	72	10666	65000
4	7181	173	56	0.32	141	67	9894	120000
5	7181	173	56	0.32	141	67	9894	100000
6	6758	165	55	0.33	134	64	9368	80000
7	6336	158	54	0.34	126	60	8843	95000

Table 6.4.1, test conditions for blunt notch / scatter specimens

specimen	test frequency	maximum force	R_{GLARE}	maximum gross stress F/A_{GLARE}	max. gross stress aluminium layers*
3-B-1	10 Hz	69100 N	0.1	140 MPa	182 MPa
3-B-10	6 Hz	107500 N	0.1	218 MPa	269 MPa
3-B-11	5 Hz	88300 N	0.1	179 MPa	225 MPa
all specimens tested on 100 ton machine at room temperature					* ref. annex B

Table 6.4.2, crack length measurements specimen 3-B-1, front side, values in [mm]

cycles	1Lf	1Rf	2Lf	2Rf	3Lf	3Rf	4Lf	4Rf	5Lf	5Rf
20000	0.00	0.00	0.00	0.00	0.00	0.00	0.00	0.00	0.00	0.00
50000	0.00	1.13	0.00	0.68	0.00	0.00	0.00	0.00	0.00	0.00
80000	1.80	2.88	1.43	2.73	1.99	2.07	1.71	1.16	0.00	0.17
100000	2.90	3.94	2.95	3.92	3.40	3.55	2.92	2.41	0.77	0.91
120000	3.81	4.89	4.30	5.10	4.64	4.55	4.09	3.45	1.62	1.59
140000	4.70	5.83	5.45	6.18	5.87	5.82	5.17	4.35	2.43	2.36
160000	5.49	6.80	6.55	7.29	6.91	6.87	6.17	5.20	3.28	3.05

Table 6.4.3, specimen 3-B-1, linear extrapolation of crack propagation curves to point of crack initiation Ni (a=1mm) and crack link-up N_L (a=9mm)

Crack loc.	a = f(N)	Ni [cycles]	LOG10(Ni)	N_L [cycles]	LOG10(N_L)
1Lf	a=5E-05N-1,768	55360	4.743	215360	5.333
1Rf	a=5E-05N-1.285	45708	4.660	205708	5.313
2Lf	a=6E-05N–3.508	75133	4.876	225133	5.352
2Rf	a=6E-05N-2.145	52423	4.720	185757	5.269
3Lf	a=6E-05N-3.064	67740	4.831	201073	5.303
3Rf	a=6E-05N-2.946	65767	4.818	199100	5.299
4Lf	a=6E-05N-2.787	63120	4.800	196453	5.293
4Rf	a=5E-05N-2.698	73960	4.869	233960	5.369
5Lf	a=4E-05N-3.312	107800	5.033	307800	5.488
5Rf	a=4E-05N-3.312	107800	5.033	307800	5.488

Table 6.4.4, specimen 3-B-1, determination of probability of crack initiation
Pci = 100-100 * (3n-1) / (3m+1), m =10

n	Pci [%]	N [cycles]
10	6	45708
9	16	52423
8	26	55360
7	35	63120
6	45	65767
5	55	67740
4	65	73960
3	74	75133
2	84	107800
1	94	107800

Table 3.4.5, crack length measurements specimen 3-B-10, values in [mm]

cycles	1Lf	1Rf	2Lf	2Rf	3Lf	3Rf	4Lf	4Rf	5Lf	5Rf
15000	1.99	1.82	2.65	2.85	2.53	2.24	1.98	1.77	0.74	0.91
30000	4.80	5.14	6.41	6.68	6.41	6.14	5.75	5.57	4.06	3.85
45000	8.90	8.83	8.83	8.83	8.83	8.83	8.83	8.83	8.83	7.18

cycles	1Lr	1Rr	2Lr	2Rr	3Lr	3Rr	4Lr	4Rr	5Lr	5Rr
15000	1.69	2.04	2.12	2.16	1.44	2.05	1.08	1.77	0.76	1.09
30000	4.64	4.73	5.70	5.66	5.50	5.61	4.97	5.39	3.89	4.50
45000	8.83	8.08	8.83	8.83	8.83	8.83	8.83	8.83	6.68	8.83

Table 6.4.6, specimen 3-B-10, linear extrapolation of crack propagation curves to point of crack initiation Ni (a = 1mm) and crack link-up N_L(a = 9mm)

crack loc.	a = f(N)	Ni [cycles]	LOG10 (Ni)	N_L [cycles]	LOG10(N_L)
1Lf	a = 0,0002N - 0,82	9100	3.96	40900	4.61
1Rf	a = 0,0002N - 1,75	13750	4.14	36250	4.56
2Lf	a = 0,0003N - 1,11	7033	3.85	26300	4.42
2Rf	a = 0,0003N - 0,98	6600	3.82	26733	4.43
3Lf	a = 0,0003N - 1,11	7033	3.85	26300	4.42
3Rf	a = 0,0003N - 1,66	8867	3.95	24467	4.39
4Lf	a = 0,0002N - 1,33	11650	4.07	38350	4.58
4Rf	a = 0,0002N - 1,67	13350	4.13	36650	4.56
5Lf	a = 0,0002N - 2,58	17900	4.25	32100	4.51
5Rf	a = 0,0002N - 2,29	16450	4.22	33550	4.53
1Lr	a = 0,0002N - 2,09	15450	4.19	34550	4.54
1Rr	a = 0,0002N - 1,09	10450	4.02	39550	4.60
2Lr	a = 0,0002N - 1,16	10800	4.03	39200	4.59
2Rr	a = 0,0002N - 1,12	10600	4.03	39400	4.60
3Lr	a = 0,0002N - 2,13	15650	4.19	34350	4.54
3Rr	a = 0,0002N - 1,12	10600	4.03	39400	4.60
4Lr	a = 0,0003N - 2,79	12633	4.10	20700	4.32
4Rr	a = 0,0002N - 1,73	13650	4.14	36350	4.56
5Lr	a = 0,0002N - 2,14	15700	4.20	34300	4.54
5Rr	a = 0,0002N - 2,32	16600	4.22	34400	4.52

Table 6.4.7, specimen 3-B-10, determination of probability of crack initiation
Pci = 100-100 * (3n-1) / (3m+1), m =20

n	Pci [%]	Ni [cycles]
20	3	6600
19	8	7033
18	13	7033
17	18	8867
16	23	9100
15	28	10450
14	33	10600
13	38	10600
12	43	10800
11	48	11650
10	52	12633
9	57	13350
8	62	13650
7	67	13750
6	72	15450
5	77	15650
4	82	15700
3	87	16450
2	92	16600
1	97	17900

Table 6.4.8, crack length measurements specimen 3-B-11, values in [mm]

cycl.	1Lf	1Rf	2Lf	2Rf	3Lf	3Rf	4Lf	4Rf	5Lf	5Rf
15000	1.09	1.50	1.21	2.25	3.24	2.33	2.14	2.49	1.59	1.06
30000	2.93	3.49	2.73	4.29	5.38	4.72	4.69	4.94	3.69	3.38
45000	4.85	5.55	4.83	6.61	7.60	7.11	7.03	6.73	5.64	4.99
60000	7.03	8.60	7.91	8.90	8.90	8.90	8.90	8.90	8.90	7.16

cycl.	1Lr	1Rr	2Lr	2Rr	3Lr	3Rr	4Lr	4Rr	5Lr	5Rr
15000	1.69	1.02	2.39	2.30	2.30	2.07	1.69	1.90	0.88	0.72
30000	4.46	2.74	4.26	4.14	4.28	4.11	3.80	3.98	2.84	2.84
45000	5.37	4.44	6.27	6.22	6.25	6.01	5.55	6.01	4.39	4.58
60000	8.90	6.70	8.90	8.90	8.90	8.90	7.78	8.90	6.20	6.70

Table 6.4.9, specimen 3-B-11, linear extrapolation of crack propagation curves to point of crack initiation Ni (a = 1mm) and crack link-up N_L(a = 9mm)

crack loc.	a = f(N)	Ni [cycles]	LOG10 (N_i)	N_L [cycles]	LOG10 (N_L)
1Lf	a = 0.0001N - 0.96	19600	4.29	80400	4.91
1Rf	a = 0.0001N - 0.5367	15400	4.19	80600	4.93
2Lf	a = 0.0001N - 0.6967	17000	4.23	83000	4.92
2Rf	a = 0.0001N - 0.055	10550	4.02	89450	4.95
3Lf	a = 0.0001N + 1.0467	467	2.67	100467	5.00
3Rf	a = 0.0001N + 0.24	7600	3.88	92400	4.97
4Lf	a = 0.0002N - 0.27	12700	4.10	87300	4.94
4Rf	a = 0.0001N + 0.51	4900	3.69	95100	4.98
5Lf	a = 0.0001N - 0.41	14100	4.15	85900	4.93
5Rf	a = 0.0001N - 0.83	18300	4.26	81700	4.91
1Lr	a = 0.0001N - 0.08	10800	4.03	89200	4.95
1Rr	a = 0.0001N - 0.96	19600	4.29	80400	4.91
2Lr	a = 0.0001N + 0.07	9300	3.97	90700	4.96
2Rr	a = 0.0001N - 0.08	10800	4.03	89200	4.95
3Lr	a = 0.0001N - 0.08	10800	4.03	89200	4.95
3Rr	a = 0.0001N + 0.1233	8767	3.94	91233	4.96
4Lr	a = 0.0001N - 0.3	13000	4.11	87000	4.94
4Rr	a = 0.0001N - 0.1467	11467	4.06	88533	4.95
5Lr	a = 0.0001N - 0.8	18000	4.26	82000	4.91
5Rr	a = 0.0001N - 1.21	22100	4.34	77900	4.89

Table 6.4.10, specimen 3-B-11, determination of probability of crack initiation
Pci = 100-100 * (3n-1) / (3m+1), m =20

n	Pci [%]	Ni [cycles]
20	3	467
19	8	4900
18	13	7600
17	18	8767
16	23	9300
15	28	10550
14	33	10800
13	38	10800
12	43	10800
11	48	11467
10	52	12700
9	57	13000
8	62	14100
7	67	15400
6	72	17000
5	77	18000
4	82	18300
3	87	19600
2	92	19600
1	97	22100

Table 6.4.11, crack initiation in single hole specimens, maximum applied stress 140 MPa

Results		N (i) [cycles]	log10 (Ni)	Smax [MPa]	Sa [MPa]
OH3	Front	45000	4,653	140	63
	Back	45000	4,653	140	63
OH4	Front	39000	4,591	140	63
	Back	54000	4,732	140	63
OH5	Front	48000	4,681	140	63
	Back	52000	4,716	140	63
OH6	Front	50000	4,699	140	63
	Back	43000	4,633	140	63
OH7	Front	41000	4,613	140	63
	Back	49000	4,690	140	63
OH8	Front	43000	4,633	140	63
	Back	45000	4,653	140	63
OH9	Front	34000	4,531	140	63
	Back	49000	4,690	140	63
OH10	Front	37000	4,568	140	63
	Back	41000	4,613	140	63
OH11	Front	47000	4,672	140	63
	Back	49000	4,690	140	63
Mean crack initiation live N		45056			
Standard deviation on N		5148			
Standard deviation on log10(N)			0,051		

Table 6.4.12, crack initiation in single hole specimens, maximum applied stress 140 MPa, a =1mm

Results		Front			
		N (1mm) [cycles]	log10 (N1)	Smax [MPa]	Sa [MPa]
OH3	Left	62000	4,792	140	63
	Right	62000	4,792	140	63
OH4	Left	63000	4,799	140	63
	Right	73000	4,863	140	63
OH5	Left	57000	4,756	140	63
	Right	67000	4,826	140	63
OH6	Left	62000	4,792	140	63
	Right	73000	4,863	140	63
OH7	Left	57500	4,760	140	63
	Right	56000	4,748	140	63
OH8	Left	54500	4,736	140	63
	Right	56500	4,752	140	63
OH9	Left	57500	4,760	140	63
	Right	51500	4,712	140	63
OH10	Left	51000	4,708	140	63
	Right	60500	4,782	140	63
OH11*	Left			140	63
	Right			140	63
Mean crack initiation live N		60250			
Standard deviation on N		6327			
Standard deviation on log10(N)			0,045		

Table 6.4.13, crack initiation in single hole specimens, maximum applied stress 110 MPa

Results		N (i) [cycles]	log10 (Ni)	Smax [MPa]	Sa [MPa]	Comments
OH12	Front	127000	5,104	110	49,5	
	Back	140000	5,146	110	49,5	
OH13	Front	88000	4,944	110	49,5	
	Back	120000	5,079	110	49,5	
OH14	Front	110000	5,041	110	49,5	
	Back	120000	5,079	110	49,5	
OH15	Front	130000	5,114	110	49,5	
	Back	135000	5,130	110	49,5	
OH16	Front	83000	4,919	110	49,5	
	Back			110	49,5	PDM signal unusable
OH17	Front	-		110	49,5	No crack initiation frontside within 200000 C
	Back	101000	5,004	110	49,5	
OH18	Front	107000	5,029	110	49,5	
	Back	-		110	49,5	No crack initiation backside within 200000 C
OH19	Front	119000	5,076	110	49,5	
	Back	-		110	49,5	PDM signal unusable
OH20	Front	130000	5,114	110	49,5	
	Back	95000	4,978	110	49,5	
Mean crack initiation live N		114643				
Standard deviation on N		17157				
Standard deviation on log10(N)			0,068			

Table 6.4.14, crack initiation in single hole specimens, maximum applied stress 110 MPa, a =1mm

Results		Front				
		N (1mm) [cycles]	log10 (N1)	Smax [MPa]	Sa [MPa]	Comments
OH12	Left	155000	5,190	110	49,5	
	Right			110	49,5	No crack initiation after 169000 Cycles
OH13	Left	95000	4,978	110	49,5	
	Right	130000	5,114	110	49,5	
OH14	Left	150000	5,176	110	49,5	
	Right	143000	5,155	110	49,5	
OH15	Left	152500	5,183	110	49,5	
	Right			110	49,5	No crack initiation after 155000 Cycles
OH16	Left			110	49,5	No visual measurements available
	Right			110	49,5	
OH17	Left			110	49,5	No visual measurements available
	Right			110	49,5	
OH18	Left			110	49,5	No visual measurements available
	Right			110	49,5	
OH19	Left			110	49,5	No visual measurements available
	Right			110	49,5	
OH20	Left			110	49,5	No visual measurements available
	Right			110	49,5	
Mean crack initiation live N						
		137583				
Standard deviation on N						
		20737				
Standard deviation on log10(N)						
			0,074			

Table 6.4.15, specimen 3-B-1, determination of crack propagation rates da/dN [mm/cycle] for the particular crack locations

cycles	1L	1R	2L	2R	3L	3R	4L	4R	5L	5R
80000		5.8E-05		6.8E-05						
100000	5.5E-05	5.3E-05	7.6E-05	6.0E-05	7.1E-05	7.4E-05	6.1E-05	6.3E-05		3.7E-05
120000	4.6E-05	4.8E-05	6.8E-05	5.9E-05	6.2E-05	5.0E-05	5.9E-05	5.2E-05	4.3E-05	3.4E-05
140000	4.5E-05	4.7E-05	5.8E-05	5.4E-05	6.2E-05	6.4E-05	5.4E-05	4.5E-05	4.1E-05	3.9E-05
160000	4.0E-05	4.9E-05	5.5E-05	5.6E-05	5.2E-05	5.3E-05	5.0E-05	4.3E-05	4.3E-05	3.5E-05
mean	4.6E-05	5.1E-05	6.4E-05	5.9E-05	6.2E-05	6.0E-05	5.6E-05	5.1E-05	4.2E-05	3.6E-05
LOG10	-4.34	-4.29	-4.19	-4.23	-4.21	-4.22	-4.25	-4.30	-4.38	-4.44

Table 6.4.16, specimen 3-B-10, determination of crack propagation rates da/dN [mm/cycle] for the particular crack locations

cycl.	1Lf	1Rf	2Lf	2Rf	3Lf	3Rf	4Lf	4Rf	5Lf	5Rf
15000	1.9E-04	2.2E-04	2.5E-04	2.6E-04	2.6E-04	2.6E-04	2.5E-04	2.5E-04	2.2E-04	2.0E-04
30000	1.9E-04	2.2E-04	2.5E-04	2.6E-04	2.6E-04	2.6E-04	2.5E-04	2.5E-04	2.2E-04	2.0E-04
45000	2.7E-04	2.5E-04	1.6E-04	1.4E-04	1.6E-04	1.8E-04	2.1E-04	2.2E-04	3.2E-04	2.2E-04
mean	2.3E-04	2.3E-04	2.1E-04	2.0E-04	2.1E-04	2.2E-04	2.3E-04	2.4E-04	2.7E-04	2.1E-04
LOG10	-3.64	-3.63	-3.69	-3.70	-3.68	-3.66	-3.64	-3.63	-3.57	-3.68

cycl.	1Lr	1Rr	2Lr	2Rr	3Lr	3Rr	4Lr	4Rr	5Lr	5Rr
15000	2.0E-04	1.8E-04	2.4E-04	2.3E-04	2.7E-04	2.4E-04	2.6E-04	2.4E-04	2.1E-04	2.3E-04
30000	2.0E-04	1.8E-04	2.4E-04	2.3E-04	2.7E-04	2.4E-04	2.6E-04	2.4E-04	2.1E-04	2.3E-04
45000	2.8E-04	2.2E-04	2.1E-04	2.1E-04	2.2E-04	2.1E-04	2.6E-04	2.3E-04	1.9E-04	2.9E-04
mean	2.4E-04	2.0E-04	2.2E-04	2.2E-04	2.5E-04	2.3E-04	2.6E-04	2.4E-04	2.0E-04	2.6E-04
LOG10	-3.62	-3.70	-3.65	-3.65	-3.61	-3.65	-3.59	-3.63	-3.70	-3.59

Table 6.4.17, specimen 3-B-11, determination of crack propagation rates da/dN [mm/cycle] for the particular crack locations

cycl.	1Lf	1Rf	2Lf	2Rf	3Lf	3Rf	4Lf	4Rf	5Lf	5Rf
15000	1.2E-04	1.3E-04	1.0E-04	1.4E-04	1.4E-04	1.6E-04	1.7E-04	1.6E-04	1.4E-04	1.5E-04
30000	1.2E-04	1.3E-04	1.0E-04	1.4E-04	1.4E-04	1.6E-04	1.7E-04	1.6E-04	1.4E-04	1.5E-04
45000	1.3E-04	1.4E-04	1.4E-04	1.5E-04	1.5E-04	1.6E-04	1.6E-04	1.2E-04	1.3E-04	1.1E-04
60000	1.5E-04	2.0E-04	2.1E-04	1.5E-04	8.7E-05	1.2E-04	1.2E-04	1.4E-04	2.2E-04	1.4E-04
mean	1.3E-04	1.6E-04	1.5E-04	1.5E-04	1.3E-04	1.5E-04	1.5E-04	1.4E-04	1.6E-04	1.4E-04
LOG10	-3.88	-3.80	-3.83	-3.83	-3.90	-3.84	-3.82	-3.85	-3.79	-3.87

cycl.	1Lr	1Rr	2Lr	2Rr	3Lr	3Rr	4Lr	4Rr	5Lr	5Rr
15000	1.8E-04	1.1E-04	1.2E-04	1.2E-04	1.3E-04	1.4E-04	1.4E-04	1.4E-04	1.3E-04	1.4E-04
30000	1.8E-04	1.1E-04	1.2E-04	1.2E-04	1.3E-04	1.4E-04	1.4E-04	1.4E-04	1.3E-04	1.4E-04
45000	6.1E-05	1.1E-04	1.3E-04	1.4E-04	1.3E-04	1.3E-04	1.2E-04	1.4E-04	1.0E-04	1.2E-04
60000	2.4E-04	1.5E-04	1.8E-04	1.8E-04	1.8E-04	1.9E-04	1.5E-04	1.9E-04	1.2E-04	1.4E-04
mean	1.6E-04	1.3E-04	1.4E-04	1.5E-04	1.5E-04	1.5E-04	1.4E-04	1.6E-04	1.2E-04	1.3E-04
LOG10	-3.80	-3.90	-3.84	-3.83	-3.83	-3.82	-3.87	-3.81	-3.93	-3.88

Table 6.4.18, average crack lengths of different specimens

specimen	N [cycles]	a_{av} [mm]
3-B-1	180000	7.68
3-B-2	160000	5.96
3-B-3	140000	5.24
3-B-4	120000	4.38
3-B-5	100000	3.2
3-B-6	80000	2.75
3-B-12	140000	5.03
3-B-13	120000	4.12
3-B-14	100000	3.33
3-B-15	80000	1.43

Table 6.8.1, systematic single hole test results

Material	Specimen no.	Exp. Time [h]	Fyield [N]	Fult [N]	t [mm]
GLARE 2B	2B-0-1	0	61284,66	139422,19	4,33
	2B-0-2	0	61541,20	138869,91	4,34
	2B-0-3	0	61622,10	138419,20	4,35
	2B-0-4	0	60821,70	138192,08	4,35
	2B-0-5	0	60958,73	137648,00	4,35
	2B-500-1	500	62209,35	128666,50	4,35
	2B-500-2	500	61174,05	127086,76	4,35
	2B-500-3	500	60968,32	126879,01	4,34
	2B-500-4	500	60638,48	128328,27	4,34
	2B-500-5	500	62242,11	127267,45	4,34
	2B-1000-1	1000	61776,70	127237,40	4,35
	2B-1000-2	1000	61217,64	128929,95	4,37
	2B-1000-3	1000	61477,15	126117,95	4,35
	2B-1000-4	1000	61733,29	127805,38	4,35
	2B-1000-5	1000	60548,54	128593,70	4,42
	2B-3000-1	3000	61408,50	102041,00	4,41
	2B-3000-2	3000	61000,10	113290,00	4,41
	2B-3000-3	3000	54230,00	126974,00	4,39
	2B-3000-4	3000	54729,90	126448,00	4,40
	2B-3000-5	3000	54880,70	126553,00	4,40
GLARE 3	3-O-0-1	0	19481,18	30287,97	1,47
	3-O-0-2		19035,03	29456,01	1,47
	3-O-0-3		18928,30	30352,77	1,45
	3-O-0-4		19125,50	29276,96	1,45
	3-O-0-5		19295,96	29824,95	1,47
	3-O-500-1	500	19487,79	28614,46	1,47
	3-O-500-2	(open holes)	19390,77	28614,08	1,47
	3-O-500-3		19375,34	28493,47	1,47
	3-O-500-4		19413,56	28188,28	1,47
	3-O-500-5		19381,22	28326,24	1,47
	3-O-1000-1	1000	19576,15	28252,34	1,48
	3-O-1000-2	(open holes)	19696,22	27867,58	1,48
	3-O-1000-3		19400,57	27257,44	1,45
	3-O-1000-4		19566,31	28437,96	1,48
	3-O-1000-5		19297,80	26210,15	1,44
	3-O-3000-1	3000	22155,80	27834,40	1,48
	3-O-3000-2	(open holes)	22175,20	27769,40	1,47
	3-O-3000-3		21988,30	26277,70	1,45
	3-O-3000-4		22169,00	28561,20	1,46
	3-O-3000-5		22204,70	27353,10	1,47

Table 6.8.1, systematic single hole test results cont'd

GLARE 3	3-F-500-1	500	19345,08	29461,74	1,48
	3-F-500-2	(filled holes)	19277,03	28316,09	1,45
	3-F-500-3		19334,30	29104,79	1,45
	3-F-500-4		19211,05	28082,08	1,45
	3-F-500-5		19315,80	28376,36	1,46
	3-F-1000-1	1000	19664,94	29283,91	1,47
	3-F-1000-2	(filled holes)	19806,03	28774,39	1,46
	3-F-1000-3		19722,87	29562,18	1,45
	3-F-1000-4		19612,53	28742,33	1,45
	3-F-1000-5		19580,60	29011,19	1,48
	3-F-3000-1	3000	22145,10	26544,20	1,46
	3-F-3000-2	(filled holes)	22246,70	28756,90	1,46
	3-F-3000-3		22162,00	28499,30	1,47
	3-F-3000-4		22251,90	28941,90	1,47
	3-F-3000-5				
GLARE 4A	4A-0-1	0	50763,82	93569,12	3,56
	4A-0-2		51013,52	94758,84	3,57
	4A-0-3		50986,98	93051,44	3,59
	4A-0-4		50717,21	94727,44	3,57
	4A-0-5		50663,88	94000,04	3,59
	4A-500-1	500	50414,40	88400,28	3,60
	4A-500-2		50715,00	89803,47	3,60
	4A-500-3		50702,40	89903,37	3,60
	4A-500-4		51845,56	88811,85	3,58
	4A-500-5		52094,49	91125,47	3,59
	4A-1000-1	1000	51952,04	89199,92	3,58
	4A-1000-2		52046,39	89428,16	3,60
	4A-1000-3		51851,21	89709,57	3,61
	4A-1000-4		52079,99	89842,45	3,61
	4A-1000-5		51912,46	89530,83	3,61
	4A-3000-1	3000	47292,70	81114,20	3,61
	4A-3000-2		47466,50	80020,30	3,59
	4A-3000-3		47478,10	80041,60	3,59
	4A-3000-4		47255,60	79950,80	3,59
	4A-3000-5		47766,80	78661,40	3,60
GLARE 4B	4B-0-1	0	46750,49	66695,20	3,62
	4B-0-2		46254,55	67512,04	3,62
	4B-0-3		46709,79	67255,71	3,61
	4B-0-4		46699,95	66888,49	3,63
	4B-0-5		46276,59	66821,72	3,61
	4B-500-1	500	46297,99	63966,06	3,62
	4B-500-2		46294,37	63386,58	3,62
	4B-500-3		46261,79	63476,67	3,62
	4B-500-4		46278,40	62818,02	3,61
	4B-500-5		46217,03	63796,75	3,61
	4B-1000-1	1000	46111,27	60354,28	3,63
	4B-1000-2		46224,99	62239,52	3,62
	4B-1000-3		48943,10	63050,52	3,67
	4B-1000-4		47765,32	63112,48	3,68
	4B-1000-5		47888,60	63550,69	3,67
	4B-3000-1	3000	46334,20	59621,5	3,69
	4B-3000-2		46495,00	59893,2	3,68
	4B-3000-3		46530,00	59328,8	3,68
	4B-3000-4		46922,40	59494,6	3,66
	4B-3000-5		46400,50	59768	3,67

Table 6.9.1, specimen 3-B-4, measured crack lengths and standard deviations, values in [mm]
upper half of specimen

Layer	2L	2R	3L	3R	4L	4R	s
1	3,9	5,2	6,0	5,8	5,6	5,1	0,7
2	2,9	4,1	3,8	4,8	4,5	3,5	0,6
3	3,5	3,5	4,4	4,3	4,3	4,0	0,4
4	3,3	3,5	3,7	4,5	3,6	3,8	0,4
5	3,5	2,9	3,8	4,4	4,1	2,9	0,6
6	3,9	3,1	4,3	4,6	4,4	4,0	0,5
7	4,6	4,3	5,2	5,3	5,1	5,0	0,4

Table 6.9.2, specimen 3-B-4, measured crack lengths and standard deviations, values in [mm]
lower half of specimen

Layer	2L	2R	3L	3R	4L	4R	s
1	3,8	5,3	5,9	5,9	5,5	5,0	0,7
2	3,0	4,2	3,6	5,0	4,7	3,3	0,7
3	3,5	3,7	4,5	4,4	4,3	3,0	0,5
4	3,4	3,6	3,8	4,6	3,6	3,6	0,4
5	3,7	3,1	3,6	4,4	3,8	2,7	0,5
6	3,8	3,1	4,1	4,6	4,3	3,9	0,5
7	4,5	4,5	5,4	5,4	5,0	5,0	0,4

Table 6.9.3, specimen 3-B-4, average crack lengths calculated
from upper half and lower half of specimen, values in [mm]

Layer	2L	2R	3L	3R	4L	4R
1	3,9	5,3	6,0	5,9	5,6	5,1
2	3,0	4,2	3,7	4,9	4,6	3,4
3	3,5	3,6	4,5	4,4	4,3	3,5
4	3,4	3,6	3,8	4,6	3,6	3,7
5	3,6	3,0	3,7	4,4	4,0	2,8
6	3,9	3,1	4,2	4,6	4,4	4,0
7	4,6	4,4	5,3	5,4	5,1	5,0

Table 6.9.4, specimen 3-B-4, percentages of crack lengths of aluminium layers 2 to 6 in relation to the crack lengths measured in layers 1 and 7 for each fatigue sensitive location, values in [%]

Layer	2L	2R	3L	3R	4L	4R	max. value
1	100	100	100	100	100	100	
2	77	79	62	84	83	67	84
3	91	69	75	74	77	69	91
4	87	68	63	78	65	73	87
4	74	81	71	85	71	74	85
5	79	68	70	82	78	56	82
6	85	70	79	86	86	79	86
7	100	100	100	100	100	100	
							mean: 86

Table 6.9.5, GLARE2B specimens tested for the determination of ageing influence on residual strength

ID		Fmax [kN]	N [kcyc]	expo-sure	2L a [mm]	2R a [mm]	3L a [mm]	3R a [mm]	4L a [mm]	4R a [mm]	a av. [mm]	Tot. average [mm]
3-B-2	Front	69.1	160	no	6,10	7,05	7,59	8,15	8,03	6,95	7,31	6,81
	Rear	69.1	160	no	5,92	5,95	6,67	6,95	6,04	6,35	6,31	
3-B-3	Front	69.1	140	no	5,57	5,83	6,38	6,68	7,19	7,14	6,47	5,99
	Rear	69.1	140	no	5,58	5,07	5,93	6,27	5,14	5,08	5,51	
3-B-4	Front	69.1	120	no	3,92	4,97	5,89	5,75	5,57	4,97	5,18	5,03
	Rear	69.1	120	no	4,30	4,49	5,31	5,30	4,91	4,99	4,88	
3-B-6	Front	69.1	80	no	3,80	3,45	4,27	4,26	3,21	2,96	3,66	3,50
	Rear	69.1	80	no	3,65	3,13	3,42	3,24	3,12	3,50	3,34	
3-B-7	Front		0	no	0	0	0	0	0	0	0	0
	Rear		0	no	0	0	0	0	0	0	0	
3-B-8	Front		0	no	0	0	0	0	0	0	0	0
	Rear		0	no	0	0	0	0	0	0	0	
3-B-9	Front		0	no	0	0	0	0	0	0	0	0
	Rear		0	no	0	0	0	0	0	0	0	
3-B-10	Front	107.5	45	yes	8,83	8,83	8,83	8,83	8,83	8,83	8,83	8,83
	Rear	107.5	45	yes	8,83	8,83	8,83	8,83	8,83	8,83	8,83	
3-B-11	Front	88.3	60	yes	7,91	8,90	8,90	8,90	8,90	8,90	8,74	8,72
	Rear	88.3	60	yes	8,90	8,90	8,90	8,90	7,78	8,90	8,71	
3-B-12	Front	69.1	140	yes	5,52	5,78	5,84	5,85	5,50	5,60	5,68	5,86
	Rear	69.1	140	yes	5,44	5,89	6,76	6,25	6,07	5,83	6,04	
3-B-13	Front	69.1	120	yes	3,53	3,98	4,31	4,61	4,34	4,36	4,19	4,67
	Rear	69.1	120	yes	4,93	5,29	5,25	5,22	5,04	5,12	5,14	
3-B-14	Front	69.1	100	yes	3,50	4,01	4,21	4,17	4,10	3,45	3,91	3,94
	Rear	69.1	100	yes	4,04	4,07	4,36	4,47	3,82	3,06	3,97	
3-B-15	Front	69.1	80	yes	1,90	0,00	1,80	0,52	1,90	0,94	1,18	1,66
	Rear	69.1	80	yes	1,91	2,32	2,21	2,31	2,26	1,88	2,15	
3-B-16	Front		0	yes	0	0	0	0	0	0	0	0
	Rear		0	yes	0	0	0	0	0	0	0	
3-B-17	Front		0	yes	0	0	0	0	0	0	0	0
	Rear		0	yes	0	0	0	0	0	0	0	
3-B-18	Front		0	yes	0	0	0	0	0	0	0	0
	Rear		0	yes	0	0	0	0	0	0	0	

Table 6.9.6, corrected average crack lengths and failure stresses (gross) for fatigued dry blunt notch specimens, GLARE2B-7/6-.4

specimen	a_{av} [mm]	$a_{corr.}$ [mm]	R_D [%]	F [N]	S_{RS} [MPa]
3-B-2	6,81	6,13	68,5	132576	574
3-B-3	5,99	5,39	60,2	139164	603
3-B-4	5,03	4,53	50,6	143179	620
3-B-6	3,50	3,15	35,2	131474	569
3-B-7 to 9	0,00	0,00	0,0	164000	710

Table 6.9.7, corrected average crack lengths and failure stresses (gross) for fatigued and aged blunt notch GLARE2B-7/6-.4 specimens

specimen	a_{av} [mm]	$a_{corr.}$ [mm]	R_D [%]	F [N]	S_{RS} [MPa]
3-B-10	8,83	7,95	88,8	99743	432
3-B-11	8,72	7,85	87,7	110854	480
3-B-12	5,86	5,27	58,9	117633	509
3-B-13	4,67	4,20	47,0	123446	535
3-B-14	3,94	3,55	39,6	123386	534
3-B-15	1,66	1,49	16,7	140251	607
3-B-16 to 18	0,00	0,00	0,0	161000	697

Table 6.9.8, GLARE4A specimens tested for the determination of ageing influence on residual strength

ID	Fmax [kN]	N [kcycles]	expo-sure	2L [mm]	2R a[mm]	3L a[mm]	3R a[mm]	4L a[mm]	4R a[mm]	a av. a[mm]	tot. average a[mm]
3-A-1	67,4	40	no	3,51	3,15	2,85	3,62	3,60	2,19	3,15	3,15
3-A-2	67,4	60	no	6,70	7,06	7,55	7,01	6,65	6,58	6,93	6,93
3-A-3	58,8	160	no	12,46	12,03	12,61	12,83	12,17	12,41	12,42	12,42
3-A-4	67,4	100	no	9,38	10,18	10,22	9,98	9,40	8,51	9,61	9,61
3-A-5	67,4	50	no	4,00	4,28	3,64	4,04	3,78	3,38	3,85	3,85
3-A-6	67,4	30	no	2,01	1,62	1,47	2,25	0,97	2,60	1,82	1,82
3-A-7			no							0,00	
3-A-8			no							0,00	
3-A-9			no							0,00	
3-A-10	67,4	30	yes	1,90	2,03	3,48	3,50	2,13	2,10	2,52	2,52
3-A-11	58,8	60	yes	2,46	2,82	3,11	2,81	3,07	3,71	3,00	3,00
3-A-12	67,4	60	yes	6,35	6,28	7,24	6,88	6,67	6,24	6,61	6,61
3-A-13	58,8	120	yes	8,30	9,25	8,05	9,57	8,65	8,45	8,71	8,71
3-A-14			yes							0,00	

Cracks measured on non-countersunk side

Table 6.9.9, corrected average crack lengths and failure stresses for fatigued dry blunt notch specimens, GLARE4A-5/4-.4ssc

specimen	a_{av} [mm]	$a_{corr.}$ [mm]	R_D [%]	F [N]	S_{RS} [MPa]
3-A-3	12,42	11,38	101,6	85220	362
3-A-4	9,61	8,80	78,6	93370	397
3-A-2	6,93	6,35	56,7	97220	413
3-A-5	3,85	3,53	31,5	100430	427
3-A-1	3,15	2,89	25,8	103670	441
3-A-6	1,82	1,67	14,9	104390	444
3-A-7 to 9	0,00	0,00	0,0	125947	535

Table 6.9.10, corrected average crack lengths and failure stresses for fatigued and aged blunt notch GLARE4A-5/4-.4ssc specimens

specimen	a_{av} [mm]	$a_{corr.}$ [mm]	R_D [%]	F [N]	S_{RS} [MPa]
3-A-13	8,71	7,98	71,2	84241	358
3-A-12	6,61	6,05	54,1	89543	381
3-A-11	3,00	2,75	24,5	105101	447
3-A-10	2,52	2,31	20,6	105187	447
3-A-14	0,00	0,00	0,0	124306	529

Table 6.11.1, GLARE2B-7/6-.4, bearing strength results

ID	exposure	test temp.	dimensions [mm]						strength [MPa]	
			w	D	t_1	t_2	t_3	t_{av}	σ_{yield}	σ_{ult}
4-B-1	none	RT	24.00	4.77	4.41	4.42	4.42	4.42	498	854.7
4-B-2			24.02	4.78	4.41	4.42	4.40	4.41	527	859.5
4-B-3			23.87	4.77	4.39	4.40	4.39	4.39	511	868.6
4-B-4			23.97	4.77	4.42	4.41	4.41	4.41	570	866.2
4-B-5			23.97	4.77	4.42	4.42	4.42	4.42	522	870.0
4-B-6	3000 h accelerated	RT	24.20	4.77	4.58	4.56	4.54	4.56	538	805.0
4-B-7			24.17	4.77	4.58	4.57	4.58	4.58	522	784.6
4-B-8			24.24	4.77	4.58	4.58	4.56	4.57	- [1]	781.0
4-B-9			24.25	4.78	4.62	4.59	4.55	4.59	497	777.7
4-B-10			24.19	4.77	4.59	4.57	4.56	4.57	440	781.8
4-B-11	1500 h accelerated	RT	24.20	4.76	4.53	4.54	4.55	4.54	532	802.1
4-B-12			24.16	4.76	4.55	4.53	4.54	4.54	449	777.5
4-B-13			24.18	4.77	4.52	4.49	4.54	4.52	464	788.0
4-B-14			24.14	4.75	4.50	4.51	4.51	4.51	397	793.1
4-B-15			24.13	4.76	4.51	4.52	4.53	4.52	493	799.9
4-B-16	3000 h accelerated	70° C	24.12	4.78	4.58	4.57	4.53	4.56	- [1]	714.3
4-B-17			24.12	4.78	4.55	4.57	4.53	4.55	354	731.4
4-B-18			24.11	4.78	4.56	4.55	4.53	4.55	313	717.4
4-B-19			24.13	4.78	4.55	4.55	4.53	4.54	- [1]	- [2]
4-B-20			24.11	4.78	4.54	4.53	4.50	4.52	416	695.8

[1] no secondary modulus loop
[2] shear failure of outer aluminium layer

Table 6.11.2, GLARE4A-5/4-.4ssc, bearing strength results

ID	exposure	test temp.	dimensions [mm]						strength [MPa]	
			w	D	t_1	t_2	t_3	t_{av}	σ_{yield}	σ_{ult}
4-A-1	none	RT	27.68	5.58	3.54	3.54	3.54	3.54	562	884.7
4-A-2			28.00	5.57	3.56	3.55	3.56	3.56	565	876.0
4-A-3			27.98	5.56	3.57	3.56	3.57	3.57	580	851.5
4-A-4			28.05	5.56	3.54	3.56	3.55	3.55	572	871.6
4-A-5			27.99	5.55	3.57	3.57	3.54	3.56	572	850.9
4-A-6	3000 h accelerated	RT	28.18	5.56	3.68	3.66	3.66	3.67	510	755.2
4-A-7			28.22	5.56	3.65	3.66	3.65	3.65	542	763.5
4-A-8			28.25	5.55	3.67	3.66	3.65	3.66	546	761.8
4-A-9			28.26	5.55	3.65	3.65	3.64	3.65	514	768.7
4-A-10			28.16	5.56	3.64	3.63	3.64	3.64	539	760.9

Table 6.11.3, rivet strength test results for GLARE2B-7/6-.4 specimens

specimen	exposure	$F_{failure}$ [N]	F_{yield} [N]
5-B-1		23774	17300
5-B-2		24036	17300
5-B-3	None	24515	16000
5-B-4		24256	17700
5-B-5		24639	17600
average		24244	17180
[%]		100.0	70.9
5-B-6		23223	16300
5-B-7		23174	14200
5-B-8	3000 h	23199	15900
5-B-9	70ºC, 85%RH	23147	19400
5-B-10		23512	15000
average		23251	16160
%		95.9	66.7

Table 6.11.4, rivet strength test results for GLARE4A-5/4-.4ssc specimens

specimen	exposure	$F_{failure}$ [N]	F_{yield} [N]
5-A-1		25200	14500
5-A-2		23800	14700
5-A-3	none	23200	15000
5-A-4		26600	15000
5-A-5		25200	14300
average		24800	14700
%		100.0	59.3
5-A-6		25800	15700
5-A-7		26000	14600
5-A-8	3000 h	25400	13900
5-A-9	70ºC, 85%RH	24600	14200
5-A-10		24800	13900
average		25320	14460
%		102.1	57.1

Table 6.12.1a, rivet pull through tests, crack lengths in GLARE2B-7/6-.4 specimens

ID	F_{max} [kN]	N [cycles]	machine [kN]	f [Hz]	crack lengths [mm]				
					front L	front R	back L	back R	average
7-B-1									0.00
7-B-2	50.0	60000	60	10	1.47	1.39	1.48	1.16	1.38
7-B-3	50.0	90000	60	10	3.22	3.02	3.06	2.86	3.04
7-B-4	50.0	120000	60	10	5.91	5.28	5.57	5.27	5.51
7-B-5	50.0	160000	60	10	10.15	9.81	8.67	9.37	9.50
7-B-6									0.00
7-B-7	50.0	60000	60	10	0.28	0.75	1.63	1.28	0.99
7-B-8	50.0	90000	60	10	3.81	3.97	3.51	3.80	3.77
7-B-9	50.0	120000	60	10	5.54	4.89	4.90	5.09	5.11
7-B-10	50.0	160000	60	10	6.39	6.26	6.22	6.48	6.34
7-B-11									0.00
7-B-12	41.3	100000	60	10	0.00	0.61	0.00	0.00	0.15
7-B-13	41.3	120000	60	10	1.31	0.90	0.00	0.42	0.66
7-B-14	41.3	140000	60	10	0.00	1.55	1.29	0.00	0.71
7-B-15	50.0	160000	250	10	5.27	5.00	5.56	5.71	5.39
7-B-16									0.00
7-B-17	41.3	140000	60	10	2.49	0.82	3.39	1.59	2.07
7-B-18	41.3	180000	60	10	0.00	1.68	0.00	2.70	1.10
7-B-19	41.3	140000	250	10	2.46	2.30	2.85	2.07	2.42
7-B-20	41.3	250705	60	10	2.57	5.27	4.68	5.00	4.38
7-B-21									0.00
7-B-22	50.0	60000	60	10	1.60	1.26	0.52	0.51	0.97
7-B-23	50.0	90000	60	10	1.12	2.86	1.26	1.85	1.77
7-B-24	50.0	120000	60	10	3.45	4.36	4.67	5.07	4.39
7-B-25	50.0	160000	60	10	7.8	7.24	6.70	6.50	7.06
7-B-26									0.00
7-B-27	50.0	60000	60	10	0.37	0.00	1.98	1.69	1.01
7-B-28	50.0	90000	60	10	2.67	3.40	2.86	3.30	3.06
7-B-29	50.0	120000	60	10	4.37	4.08	5.01	5.38	4.71
7-B-30	50.0	160000	60	10	6.97	6.61	6.70	7.15	6.86

Table 6.12.1b, rivet pull through tests, crack lengths in GLARE4A-5/4-.4ssclad specimens

ID	F_{max} [kN]	N [cycles]	machine [kN]	f [Hz]	crack lengths [mm]		
					back L	back R	average
7-A-1							0.00
7-A-2	33.6	100000	60	10	4.41	4.79	4.60
7-A-3	33.6	80000	60	10	4.34	4.75	4.55
7-A-4	33.6	60000	60	10	1.62	1.46	1.54
7-A-5	33.6	40000	60	10	0.86	0.69	0.78
7-A-6							0.00
7-A-7	33.6	40000	60	10	0.19	0.41	0.30
7-A-8	33.6	60000	60	10	2.26	1.74	2.00
7-A-9	33.6	85000	60	10	3.13	3.63	3.38
7-A-10	33.6	110000	60	10	4.69	4.09	4.39
7-A-11							0.00
7-A-12	33.6	40000	60	10	0.24	0.39	0.32
7-A-13	33.6	60000	60	10	1.73	1.11	1.42
7-A-14	33.6	85000	60	10	3.51	3.75	3.63
7-A-15	33.6	110000	60	10	5.36	5.34	5.35
7-A-16							0.00
7-A-17	33.6	45000	60	10	0.85	0.51	0.68
7-A-18	33.6	60000	60	10	2.08	2.16	2.12
7-A-19	33.6	85000	60	10	4.17	3.74	3.96
7-A-20	33.6	110000	60	10	5.00	5.23	5.12
7-A-21							0.00
7-A-22	33.6	45000	60	10	1.04	1.54	1.29
7-A-23	33.6	60000	60	10	1.77	2.37	2.07
7-A-24	33.6	85000	60	10	3.49	3.74	3.62
7-A-25	33.6	110000	60	10	5.48	6.05	5.77
7-A-26							0.00
7-A-27	33.6	45000	60	10	0	1.62	0.81
7-A-28	33.6	60000	60	10	2.4	2.48	2.44
7-A-29	33.6	85000	60	10	3.51	3.4	3.46
7-A-30	33.6	110000	60	10	5.25	5.18	5.22

Table 6.12.2, rivet pull through strengths

GLARE2B-7/6-0.4			GLARE4A-5/4-0.4ssc		
ID	temperature	F_{max} [N]	ID	temperature	F_{max} [N]
7-B-1		8937.6	7-A-1		7764.8
7-B-2		8632.6	7-A-2		6384.0
7-B-3	RT	8739.4	7-A-3	RT	6660.3
7-B-4		8747.7	7-A-4		6861.2
7-B-5		8524.4	7-A-5		7367.4
7-B-6		8884.1	7-A-6		7658.5
7-B-7		8914.5	7-A-7		6819.5
7-B-8	70º C	8780.1	7-A-8	70º C	6235.5
7-B-9		8797.3	7-A-9		6118.3
7-B-10		8557.9	7-A-10		5970.1

Table 6.13.1a, fatigue crack lengths in compression filled hole specimens GLARE2B

		Fatigue tests		Crack lengths [mm]				
ID	Paint	Fmax [kN]	N [cycles]	Front L	Front R	Back L	Back R	Average
6-B-1	No		0					
6-B-2	No	13,8	100000	4,13	3,77	3,87	3,30	3,77
6-B-3	No	13,8	100000	6,88	6,66	7,01	6,58	6,78
6-B-4	No		0					
6-B-5	No	13,8	100000	3,54	4,07	3,67	4,34	3,91
6-B-6	No	13,8	100000	6,9	6,65	7,01	6,55	6,78
6-B-7	Yes		0					
6-B-8	Yes	13,8	100000	3,01	2,65	1,76	2,51	2,48
6-B-9	Yes	13,8	100000	7,85	6,65	7,94	8,2	7,66
6-B-10	Yes		0					
6-B-11	Yes	13,8	100000	3,63	3,15	3,63	4,14	3,64
6-B-12	Yes	13,8	100000	6,45	6,16	6,45	5,92	6,25
6-B-13	Yes		0					
6-B-14	Yes	13,8	100000	3,76	3,87	3,16	2,74	3,38
6-B-15	Yes	13,8	100000	6,08	4,76	5,13	5,98	5,49
6-B-16	Yes		0					
6-B-17	Yes	13,8	100000	2,66	2,51	1,45	1,16	1,95
6-B-18	Yes	13,8	100000	5,31	4,98	5,93	5,76	5,50
6-B-19R	Yes	13,8	100000	2,96	2,99	4,50	4,27	3,68

Table 6.13.1b, fatigue crack lengths in compression filled hole specimens GLARE4A

ID	S_{max} [MPa]	N [cycles]	Machine [kN]	f [Hz]	Crack lengths [mm]		
					Back L	Back R	Average
6-A-1							0.00
6-A-2	122	100000	100	10	6.25	5.00	5.63
6-A-3	122	60000	100	10	3.43	3.40	3.42
6-A-4							0.00
6-A-5	122	100000	100	10	6.12	6.27	6.20
6-A-6	122	50000	100	10	2.29	2.17	2.23
6-A-7							0.00
6-A-8	122	100000	100	10	11.2*	11.2*	11.2*
6-A-9	122	55000	100	10	2.21	3.02	2.62
6-A-10							0.00
6-A-11	122	1000	100	10	6.00	5.53	5.77
6-A-12	122	55000	100	10	2.41	2.48	2.45
6-A-13							0.00
6-A-14	122	100000	100	10	5.94	6.08	6.01
6-A-15	122	55000	100	10	1.89	1.72	1.81
6-A-16							0.00
6-A-17	122	100000	100	10	6.04	5.65	5.85
6-A-18	122	55000	100	10	2.08	2.88	2.48

* link-up

Table 6.13.2, compression filled hole test results

GLARE2B-7/6-0.4				GLARE4A-5/4-0.4ssc			
ID	**test temperature**	**σ_{max} [MPa]**	**σ_{max} [%]**	**ID**	**test temperature**	**σ_{max} [MPa]**	**σ_{max} [%]**
6-B-1	RT (as-received)	544.5	100	6-A-1	RT (as-received)	473.2	100
6-B-2		454.9	84	6-A-2		448.0	95
6-B-3		463.6	85	6-A-3		470.9	100
6-B-4	80º C (as-received)	397.9	73	6-A-4	80º C (as-received)	301.3*	64
6-B-5		396.5	73	6-A-5		269.9*	57
6-B-6		339.7*	62	6-A-6		194.0*	41
6-B-7	RT 1 year outdoor exposure	567.6	104	6-A-7	RT 1 year outdoor exposure	518.9	109
6-B-8		578.9	106	6-A-8		423.8	90
6-B-9		454.0	83	6-A-9		496.1	105

* incorrect failure mode

Chapter 7
Riveted Joint Investigations

Table 7.1.1.1, specimen 2-B-28, crack propagation data and standard deviations

rivet row	foil	N1	a1	N2	a2	N (1mm)	log N	da/dN	log da/dN
		[cycles]	[mm]	[cycles]	[mm]	[cycles]		[mm/cyc.]	
3	2	64101	0,31	250676	5,06	91203	4,96	2,55E-05	-4,59
3	5	55783	0,77	218696	5,34	63982	4,81	2,81E-05	-4,55
3	7	60336	0,84	158019	3,52	66168	4,82	2,74E-05	-4,56
3	8	74612	1,04	188035	4,04	73100	4,86	2,64E-05	-4,58
3	10	70719	1,18	260000	5,50	62832	4,80	2,28E-05	-4,64
3	11	55710	0,45	116675	2,70	70613	4,85	3,69E-05	-4,43
3	13	61467	0,90	122235	3,65	63677	4,80	4,53E-05	-4,34
						average	s		s
						70225	0,05		0,10

rivet row	foil	N1	a1	N2	a2	N (1mm)	log N	da/dN	log da/dN
		[cycles]	[mm]	[cycles]	[mm]	[cycles]		[mm/cyc.]	
4	16	88075	1,01	278585	5,01	87599	4,94	2,10E-05	-4,68
4	18	30127	0,38	212326	5,13	53909	4,73	2,61E-05	-4,58
4	19	9689	0,25	259085	4,75	51255	4,71	1,80E-05	-4,74
4	21	60000	1,00	310000	4,25	60000	4,78	1,30E-05	-4,89
4	22	52243	1,14	137681	4,39	48563	4,69	3,80E-05	-4,42
4	24	1970	0,49	325881	4,24	46022	4,66	1,16E-05	-4,94
4	25	29310	0,47	240000	5,50	51510	4,71	2,39E-05	-4,62
4	27	46257	1,12	317326	3,62	33246	4,52	9,22E-06	-5,04
						average	s		s
						54013	0,11		0,19

Table 7.1.1.2, specimen 2-B-79, crack propagation data and standard deviations

rivet row	foil	N1	a1	N2	a2	N (1mm)	log N	da/dN	log da/dN
		[cycles]	[mm]	[cycles]	[mm]	[cycles]		[mm/cyc.]	
3	2	14712	1,23	35655	3,98	12960	4,11	1,31E-04	-3,88
3	4	24615	1,54	42490	3,79	20325	4,31	1,26E-04	-3,90
3	5	32460	1,13	97944	4,13	29622	4,47	4,58E-05	-4,34
3	7	23301	1,14	56400	3,39	21242	4,33	6,80E-05	-4,17
3	10	21268	1,13	38735	3,63	20360	4,31	1,43E-04	-3,84
3	11	16304	1,04	72287	4,54	15664	4,19	6,25E-05	-4,20
3	13	15384	1,25	31863	3,00	13030	4,11	1,06E-04	-3,97
						average	s		s
						19029	0,12		0,18

Table 7.1.1.2, continued

rivet row	foil	N1	a1	N2	a2	N (1mm)	log N	da/dN	log da/dN
		[cycles]	[mm]	[cycles]	[mm]	[cycles]		[mm/cyc.]	
4	16	14083	1,52	41587	5,27	10269	4,01	1,36E-04	-3,87
4	18	9826	1,29	24780	3,79	8091	3,91	1,67E-04	-3,78
4	19	8743	1,20	35268	5,70	7564	3,88	1,70E-04	-3,77
4	21	10142	1,13	37421	5,38	9308	3,97	1,56E-04	-3,81
4	22	12345	1,27	35282	5,27	10797	4,03	1,74E-04	-3,76
4	24	11828	1,19	32215	4,94	10795	4,03	1,84E-04	-3,74
4	25	13868	1,50	29235	5,0	11673	4,07	2,28E-04	-3,64
4	27	18558	1,78	41663	4,5	12005	4,08	1,19E-04	-3,92
						average	s		s
						10063	0,07		0,08

Table 7.1.1.3, specimen 2-B-80, crack propagation data and standard deviations

rivet row	foil	N1	a1	N2	a2	N (1mm)	log N	da/dN	log da/dN
		[cycles]	[mm]	[cycles]	[mm]	[cycles]		[mm/cyc.]	
3	2	10450	1,04	48380	5,54	10113	4,00	1,19E-04	-3,93
3	4	11987	1,17	50256	5,67	10541	4,02	1,18E-04	-3,93
3	5	9176	1,02	48355	5,52	9002	3,95	1,15E-04	-3,94
3	7	15190	1,00	57730	5,57	15190	4,18	1,07E-04	-3,97
3	10	21958	1,19	50124	4,19	20174	4,30	1,07E-04	-3,97
3	13	18101	1,21	36578	3,96	16690	4,22	1,49E-04	-3,83
						average	s		s
						13618	0,13		0,05

rivet row	foil	N1	a1	N2	a2	N (1mm)	log N	da/dN	log da/dN
		[cycles]	[mm]	[cycles]	[mm]	[cycles]		[mm/cyc.]	
4	16	7960	1,03	48380	5,54	7691	3,89	1,12E-04	-3,95
4	19	7948	1,24	42805	5,99	6187	3,79	1,36E-04	-3,87
4	21	10004	0,95	33034	3,95	10388	4,02	1,30E-04	-3,89
4	24	7075	1,19	40405	5,94	5742	3,76	1,43E-04	-3,85
4	25	9934	1,13	45810	5,63	8898	3,95	1,25E-04	-3,90
4	27	13161	1,17	43002	5,17	11893	4,08	1,34E-04	-3,87
						average	s		s
						8466	0,11		0,03

Table 7.1.1.4, specimen 2-B-81, crack propagation data and standard deviations

rivet row	foil	N1	a1	N2	a2	N (1mm)	log N	da/dN	log da/dN
		[cycles]	[mm]	[cycles]	[mm]	[cycles]		[mm/cyc.]	
3	4	68363	1,36	223954	5,11	53426	4,73	2,41E-05	-4,62
3	5	81690	1,09	225489	4,34	77708	4,89	2,26E-05	-4,65
3	7	40684	0,38	200954	5,13	61603	4,79	2,96E-05	-4,53
3	8	80631	0,79	279531	5,04	90459	4,96	2,14E-05	-4,67
3	10	32668	1,04	129719	4,54	31559	4,50	3,61E-05	-4,44
3	11	38027	0,97	115016	4,47	38687	4,59	4,55E-05	-4,34
3	13	41006	0,84	159668	4,34	46431	4,67	2,95E-05	-4,53
						average	s		s
						57125	0,15		0,11

rivet row	foil	N1	a1	N2	a2	N (1mm)	log N	da/dN	log da/dN
		[cycles]	[mm]	[cycles]	[mm]	[cycles]		[mm/cyc.]	
4	16	79187	0,76	197914	4,29	87259	4,94	2,97E-05	-4,53
4	18	30127	0,38	203024	4,88	53948	4,73	2,60E-05	-4,58
4	19	47824	0,74	289062	3,99	67123	4,83	1,35E-05	-4,87
4	21	87972	0,54	224838	2,54	119451	5,08	1,46E-05	-4,84
4	22	1E+05	1,36	322178	4,86	111171	5,05	1,83E-05	-4,74
4	27	68656	0,84	346064	2,59	94019	4,97	6,31E-06	-5,20
4	25	1E+05	0,49	414289	2,24	212765	5,33	6,15E-06	-5,21
						average	s		s
						76139	0,18		0,25

Table 7.1.1.5, mean crack initiation lives and logarithmic standard deviations

specimen	rivet row	N_{mean} [cycles] (a=1mm)	$S_{(a=1mm)}$
2-B-28	3	70225	0.05
2-B-28	4	54013	0.11
2-B-28	3 + 4	61578	0.11
2-B-79	3	19029	0.12
2-B-79	4	10063	0.07
2-B-79	3 + 4	14247	0.16
2-B-80	3	13618	0.13
2-B-80	4	8466	0.11
2-B-80	3 + 4	11042	0.16
2-B-81	3	57125	0.15
2-B-81	4	76139	0.18
2-B-81	3 + 4	66632	0.21

Table 7.1.2.1, crack lengths in 2-B specimens, butt strap, mating surface layer, EC measurements
crack length clustered: 1.5mm, 2.0mm, 2.5mm, >2.5mm

	Fatigue series 1		Crack lengths row 3 [mm]										Crack lengths row 4 [mm]										a av.
ID	Fmax [kN]	N [kcycles]	1L	1R	2L	2R	3L	3R	4L	4R	5L	5R	1L	1R	2L	2R	3L	3R	4L	4R	5L	5R	[mm]
2-B-39	31.6	70	1.5	1.5	1.5	1.5	1.5	1.5	1.5	1.5	1.5	1.5	1.5	1.5	1.5	1.5	1.5	1.5	1.5	1.5	1.5	1.5	1.50
2-B-41	49.4	15	1.5	1.5	1.5	1.5	1.5	1.5	1.5	1.5	1.5	1.5	1.5	1.5	1.5	1.5	1.5	1.5	1.5	1.5	1.5	1.5	1.50
2-B-42	26.3	170	1.5	1.5	1.5	1.5	1.5	1.5	1.5	1.5	1.5	1.5	1.5	1.5	1.5	1.5	1.5	1.5	1.5	1.5	2.5	2.0	1.58
2-B-43	35	45	1.5	1.5	1.5	1.5	1.5	1.5	1.5	1.5	1.5	1.5	1.5	1.5	1.5	1.5	1.5	1.5	1.5	1.5	1.5	1.5	1.50
2-B-45	24.1	400	1.5	1.5	1.5	1.5	1.5	1.5	1.5	2.5	1.5	1.5	1.5	1.5	1.5	1.5	1.5	1.5	2.0	2.6	2.0	1.5	1.66
2-B-48	38.9	30	2.0	1.5	2.5	2.5	1.5	1.5	2.7	2.7	1.5	1.5	1.5	1.5	2.5	2.0	2.5	2.9	2.0	2.0	2.0	1.5	2.02
2-B-53	38.9	20	2.0	2.0	2.0	2.0	1.5	1.5	2.5	2.5	2.5	2.5	2.0	1.5	2.0	2.0	2.0	2.0	1.5	1.5	1.5	1.5	1.93
2-B-54	38.9	20	1.5	1.5	1.5	1.5	1.5	1.5	1.5	1.5	1.5	1.5	1.5	1.5	1.5	1.5	1.5	1.5	1.5	1.5	1.5	1.5	1.50
2-B-55	38.9	20	1.5	1.5	1.5	1.5	1.5	1.5	1.5	1.5	1.5	1.5	1.5	1.5	1.5	1.5	1.5	1.5	1.5	1.5	1.5	1.5	1.50
2-B-56	38.9	20	1.5	1.5	1.5	1.5	1.5	1.5	1.5	1.5	1.5	1.5	1.5	1.5	2.5	1.5	1.5	1.5	1.5	1.5	1.5	1.5	1.55
2-B-57	38.9	20	1.5	1.5	1.5	1.5	1.5	1.5	1.5	1.5	1.5	1.5	1.5	1.5	1.5	1.5	1.5	1.5	1.5	1.5	1.5	1.5	1.50

Table 7.1.2.2, crack lengths in butt strap, mating surface layer, optical measurements
crack length clustered: 1.5mm, 2.0mm, 2.5mm, >2.5mm

	Fatigue series 1		Crack lengths row 3 [mm]										Crack lengths row 4 [mm]										a av.
ID	Fmax [kN]	N [kcycles]	1L	1R	2L	2R	3L	3R	4L	4R	5L	5R	1L	1R	2L	2R	3L	3R	4L	4R	5L	5R	[mm]
2-B-7	28.5	100	1.5	1.5	1.5	1.5	1.5	1.5	1.5	1.5	1.5	1.5	1.5	1.5	1.5	1.5	2.5	2.0	2.5	1.5	2.5	1.5	1.68
2-B-8	28.5	100	1.5	1.5	1.5	1.5	1.5	1.5	1.5	1.5	1.5	1.5	1.5	1.5	1.5	1.5	1.5	1.5	1.5	1.5	1.5	1.5	1.50
2-B-9	28.5	100	1.5	2.0	1.5	1.5	1.5	2.0	1.5	1.5	1.5	1.5	1.5	1.5	2.5	2.0	1.5	2.0	1.5	1.5	1.5	1.5	1.65
2-B-10	28.5	100	1.5	1.5	1.5	1.5	1.5	1.5	1.5	1.5	1.5	2.0	1.5	1.5	1.5	1.5	1.5	1.5	1.5	1.5	1.5	1.5	1.53
2-B-11	28.5	100	1.5	1.5	1.5	1.5	1.5	1.5	1.5	1.5	1.5	1.5	1.5	1.5	1.5	1.5	1.5	1.5	1.5	1.5	1.5	1.5	1.50

Table 7.1.2.3, crack lengths in butt strap, mating surface layer, EC measurements
crack length clustered: 0mm, 1.5mm, 2.0mm, 2.5mm, >2.5mm

	Fatigue series 1		Crack lengths row 3 [mm]										Crack lengths row 4 [mm]										a av.
ID	Fmax [kN]	N [kcycles]	1L	1R	2L	2R	3L	3R	4L	4R	5L	5R	1L	1R	2L	2R	3L	3R	4L	4R	5L	5R	[mm]
2-B-39	31.6	70	1.5	1.5	0.0	0.0	0.0	0.0	0.0	0.0	0.0	1.5	0.0	1.5	1.5	1.5	0.0	1.5	1.5	1.5	1.5	1.5	0.83
2-B-41	49.4	15	0.0	0.0	0.0	0.0	0.0	1.5	0.0	0.0	0.0	0.0	0.0	0.0	1.5	1.5	1.5	1.5	1.5	1.5	1.5	0.0	0.60
2-B-42	26.3	170	1.5	0.0	0.0	1.5	0.0	1.5	0.0	0.0	0.0	0.0	1.5	0.0	0.0	0.0	0.0	0.0	1.5	1.5	2.5	2.0	0.68
2-B-43	35	45	0.0	1.5	0.0	1.5	0.0	1.5	0.0	0.0	0.0	0.0	0.0	0.0	1.5	0.0	1.5	1.5	1.5	0.0	0.0	0.0	0.53
2-B-45	24.1	400	0.0	0.0	1.5	1.5	0.0	0.0	1.5	2.5	0.0	1.5	1.5	0.0	0.0	0.0	0.0	1.5	2.0	2.6	2.0	0.0	0.91
2-B-48	38.9	30	2.0	1.5	2.5	2.5	1.5	1.5	2.7	2.7	0.0	0.0	1.5	1.5	2.5	2.0	2.5	2.9	2.0	2.0	2.0	1.5	1.87
2-B-53	38.9	20	2.0	2.0	2.0	2.0	1.5	1.5	2.5	2.5	2.5	2.5	2.0	1.5	2.0	2.0	2.0	2.0	1.5	1.5	0.0	0.0	1.78
2-B-54	38.9	20	1.5	1.5	0.0	0.0	1.5	1.5	1.5	1.5	0.0	1.5	1.5	1.5	1.5	1.5	1.5	1.5	1.5	1.5	0.0	1.5	1.20
2-B-55	38.9	20	0.0	1.5	1.5	0.0	1.5	1.5	1.5	1.5	0.0	0.0	0.0	0.0	1.5	0.0	1.5	0.0	0.0	0.0	1.5	1.5	0.75
2-B-56	38.9	20	0.0	1.5	0.0	1.5	1.5	1.5	0.0	1.5	0.0	0.0	0.0	0.0	2.5	1.5	1.5	0.0	0.0	1.5	1.5	1.5	0.88
2-B-57	38.9	20	0.0	1.5	0.0	0.0	1.5	1.5	0.0	0.0	0.0	0.0	1.5	1.5	0.0	0.0	0.0	0.0	1.5	1.5	1.5	0.0	0.60

Table 7.1.2.4, crack lengths in butt strap, mating surface layer, optical measurements
crack length clustered: 0mm, 1.5mm, 2.0mm, 2.5mm, >2.5mm

	Fatigue series 1		Crack lengths row 3 [mm]										Crack lengths row 4 [mm]										a av.
ID	Fmax [kN]	N [kcycles]	1L	1R	2L	2R	3L	3R	4L	4R	5L	5R	1L	1R	2L	2R	3L	3R	4L	4R	5L	5R	[mm]
2-B-7	28.5	100	1.5	1.5	0.0	0.0	1.5	1.5	0.0	1.5	0.0	0.0	0.0	0.0	0.0	0.0	2.5	2.0	2.5	1.5	2.5	1.5	1.00
2-B-8	28.5	100	0.0	1.5	0.0	1.5	0.0	0.0	0.0	0.0	0.0	1.5	0.0	0.0	0.0	0.0	1.5	0.0	1.5	0.0	0.0	0.0	0.38
2-B-9	28.5	100	0.0	2.0	0.0	1.5	1.5	2.0	0.0	0.0	0.0	0.0	1.5	0.0	2.5	2.0	1.5	2.0	0.0	0.0	0.0	1.5	0.90
2-B-10	28.5	100	0.0	0.0	0.0	0.0	0.0	0.0	0.0	0.0	1.5	2.0	0.0	0.0	1.5	0.0	1.5	0.0	0.0	0.0	0.0	0.0	0.33
2-B-11	28.5	100	1.5	1.5	0.0	0.0	0.0	1.5	0.0	0.0	0.0	0.0	0.0	0.0	0.0	0.0	0.0	0.0	0.0	0.0	0.0	0.0	0.23

Table 7.1.2.5, probability of crack length after 20000 cycles at F_{max} = 38.9 kN

specimen	n	Pcl [%]	a av [mm]
57/3	10	93,5	0,45
55/4	9	83,9	0,60
57/4	8	74,2	0,75
56/3	7	64,5	0,75
55/3	6	54,8	0,90
56/4	5	45,2	1,00
54/3	4	35,5	1,05
54/4	3	25,8	1,35
53/4	2	16,1	1,45
53/3	1	6,5	2,10
		mean value:	1,04

m = 10

Table 7.1.2.6, calculation of input data for crack initiation curves, representing the average crack length 0.6mm, 1.0mm and 1.7mm

$F_{appl.}$ [N]	$N_{appl.}$ [cyc.]	σ_{net} [1)] [MPa]	σ_{gross} [MPa]	$\sigma_{grosstemp}$ [MPa] [(12)]	$a_{average}$ [mm]	$R_{alumin.}$ (12)	ΔK_F (13) [N/mm$^{3/2}$]	da/dN (9) [mm/cyc.]	$N_{1.7}$ (14) [cycles]	$N_{1.0}$ (15) [cycles]	$N_{0.6}$ (16) [cycles]
49400	15000	277.3	256.2	318.2	0.60	0.28	395	1.70E-04	21463	17350	15000
38900	20000	228.8	212.2	274.2	1.04	0.30	340	1.11E-04	25946	19640	16036
35000	45000	210.1	195.1	257.1	0.53	0.32	319	9.64E-05	57367	49968	45740
31600	70000	193.2	179.7	241.7	0.83	0.33	300	8.08E-05	80762	72103	67155
28500	100000	177.3	165.1	227.1	0.57	0.35	282	6.92E-05	116325	106212	100433
26300	170000	165.7	154.5	216.5	0.68	0.36	268	6.15E-05	186580	175202	168700
24100	400000	153.8	143.5	205.5	0.91	0.37	255	5.43E-05	414557	401658	394288

1) measured strains in rivet rows 3&4 between fastener on mating surface, E=72000 MPa

Table 7.1.2.7, stresses on mating surface of butt strap, rivet rows 3 and 4, specimen 2-B-102, gross stresses

$F_{appl.}$ [N]	$\sigma_{appl.}$ [MPa]	$\sigma_{bending}$ [MPa]	k_b
49400	100	156	2.6
38900	79	134	2.7
35000	71	124	2.8
31600	64	116	2.8
28500	58	108	2.9
26300	53	101	2.9
24100	49	95	2.9

Table 7.1.2.8, calculated and measured crack initiation data for average crack length 1mm, probability of crack initiation 50%

$\sigma_{max.}$ [MPa]	88	77	66	59.4	55
N_{tested} [cycles]	18000	32000	65000	100000	140000
$N_{calculated}$ [cycles]	23500	38900	68000	94800	119000
$N_{calculated}$ / N_{tested}	1.31	1.22	1.04	0.95	0.85

Table 7.1.2.9, 2-B specimen series, painted, average crack lengths for rivet rows 3 and 4 on butt strap mating aluminium layer

specimen	N [cycles]	a [mm]	inspection
2-B-1	100000	4,58	EC
2-B-5	150000	2,41	EC
2-B-48	30000	1,685	EC
2-B-49	100000	5,385	EC
2-B-53	20000	1,57	EC
2-B-54	20000	0,56	EC
2-B-55	20000	0,21	EC
2-B-56	20000	0,45	EC
2-B-57	20000	0,125	EC
2-B-73	200000	8,91	optic

Table 7.1.2.10, 2-B specimen series, non-painted, average crack lengths for rivet rows 3 and 4 on butt strap mating aluminium layer

specimen	N [cycles]	a [mm]	inspection
2-B-91	30000	2,19	optic
2-B-92	30000	2,27	optic
2-B-93	30000	1,94	optic
2-B-94	30000	2,35	optic
2-B-95	30000	2,03	optic
2-B-96	30000	2,37	optic
2-B-85	100000	7,74	optic
2-B-86	200000	8,98	optic

Table 7.1.3.1, eddy current crack length measurements at specimen series 2-A, riveted repair coupon

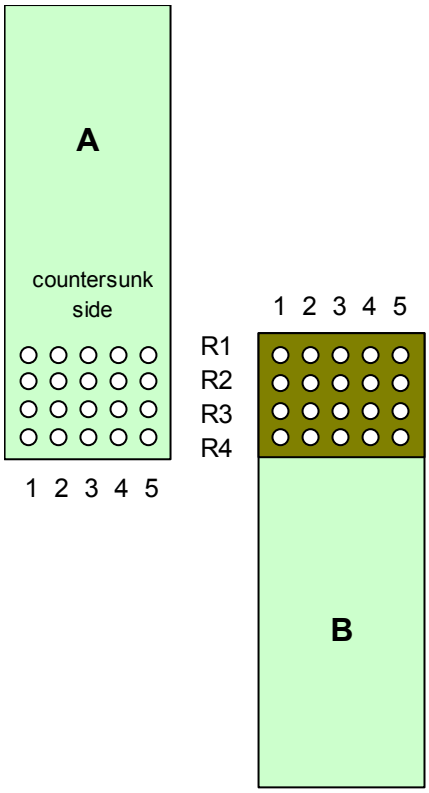

* Eddy current crack length measurements corrected according to procedure explained in chapter 7.1.2.2. All cracks contained in this table initiated *around* the bore hole !

	fatigue tests		sheet /	crack lengths [mm]										average
ID	Fmax [kN]	N [kcyc.]	riv. row	1L	1R	2L	2R	3L	3R	4L	4R	5L	5R	per row
2-A-2	58,8	45000	A/R1	0,0	0,0	1,4	1,3	0,0	0,0	0,0	0,0	2,6	1,0	0,63
			B/R4	0,0	0,0	0,0	0,0	0,0	0,0	0,0	0,0	0,0	0,0	0,00
		corrected*	A/R1	0,0	0,0	2,3	2,2	0,0	0,0	0,0	0,0	3,5	1,9	0,97
			B/R4	0,0	0,0	0,0	0,0	0,0	0,0	0,0	0,0	0,0	0,0	0,00
		65000	A/R1	0,2	0,0	2,3	1,9	0,0	0,0	0,0	0,0	3,0	1,6	0,90
			B/R4	0,0	0,0	0,0	0,0	0,0	0,0	0,0	0,0	0,0	0,0	0,00
		corrected*	A/R1	1,1	0,0	3,2	2,8	0,0	0,0	0,0	0,0	3,9	2,5	1,33
			B/R4	0,0	0,0	0,0	0,0	0,0	0,0	0,0	0,0	0,0	0,0	0,00
2-A-3	58,8	90000	A/R1	0,5	3,6	3,8	4,5	4,1	3,0	1,9	4,2	6,5	6,5	3,86
			B/R4	3,9	5,0	3,9	3,6	2,5	3,1	3,5	3,7	0,0	0,0	2,92
		camera	A/R1	1,6	4,0	4,2	4,6	4,8	3,2	2,5	4,3	6,6	7,1	4,27
		corrected*	B/R4	4,8	5,9	4,8	4,5	3,4	4,0	4,4	4,6	0,0	0,0	3,60
2-A-4	58,8	55000	A/R1	0,0	0,0	3,7	3,4	0,8	0,6	0,0	0,0	3,3	2,6	1,44
			B/R4	0,0	0,0	0,0	0,0	0,0	0,0	0,6	0,0	0,0	0,0	0,06
		corrected*	A/R1	0,0	0,0	4,6	4,3	1,7	1,5	0,0	0,0	4,2	3,5	1,95
			B/R4	0,0	0,0	0,0	0,0	0,0	0,0	1,5	0,0	0,0	0,0	0,15
		120000	A/R1	6,8	7,0	9,4	9,9	8,6	7,9	6,8	6,8	8,9	8,3	8,04
			B/R4	6,6	5,6	5,7	6,1	7,0	7,2	7,9	7,1	5,3	3,4	6,19
		corrected*	A/R1	7,7	7,9	10,3	10,8	9,5	8,8	7,7	7,7	9,8	9,2	8,89
			B/R4	7,5	6,5	6,6	7,0	7,9	8,1	8,8	8,0	6,2	4,3	7,04

Table 7.1.3.1 continued

ID	fatigue tests		sheet /	crack lengths [mm]										average
	Fmax [kN]	N [kcyc.]	riv. row	1L	1R	2L	2R	3L	3R	4L	4R	5L	5R	per row
2-A-5	58,8	65000	A/R1	1,4	0,2	2,4	2,4	0,6	3,0	3,2	2,4	3,5	3,5	2,26
			B/R4	2,9	1,6	2,0	1,5	0,4	2,5	3,6	2,0	1,6	1,1	1,92
		corrected*	A/R1	2,3	1,1	3,3	3,3	1,5	3,9	4,1	3,3	4,4	4,4	3,11
			B/R4	3,8	2,5	2,9	2,4	1,3	3,4	4,5	2,9	2,5	2,0	2,77
		90000	A/R1	3,4	2,1	4,3	4,6	3,1	4,9	5,3	4,5	6,3	5,6	4,41
			B/R4	5,2	4,8	3,4	4,6	4,6	5,4	6,0	4,7	5,1	4,1	4,79
		corrected*	A/R1	4,3	3,0	5,2	5,5	4,0	5,8	6,2	5,4	7,2	6,5	5,26
			B/R4	6,1	5,7	4,3	5,5	5,5	6,3	6,9	5,6	6,0	5,0	5,64
2-A-6	64,7	27000	A/R1	0,0	0,0	0,0	0,6	0,0	0,0	0,0	0,0	0,0	0,6	0,12
			B/R4	0,0	0,0	0,0	0,0	0,0	0,0	0,0	0,0	0,0	0,0	0,00
		corrected*	A/R1	0,0	0,0	0,0	1,5	0,0	0,0	0,0	0,0	0,0	1,5	0,29
			B/R4	0,0	0,0	0,0	0,0	0,0	0,0	0,0	0,0	0,0	0,0	0,00
		60000	A/R1	1,2	1,3	3,0	4,6	2,4	2,1	2,6	3,6	4,3	5,3	3,04
			B/R4	2,3	3,1	2,5	2,2	0,1	1,1	2,3	2,2	0,0	0,0	1,58
		corrected*	A/R1	2,1	2,2	3,9	5,5	3,3	3,0	3,5	4,5	5,2	6,2	3,89
			B/R4	3,2	4,0	3,4	3,1	1,0	2,0	3,2	3,1	0,0	0,0	2,26
2-A-19	51,8	100000	A/R1	0,0	0,5	0,0	0,0	0,0	0,0	0,0	0,0	0,0	1,3	0,18
			B/R4	0,0	0,0	0,0	0,0	0,0	0,0	0,0	0,0	0,0	0,0	0,00
		corrected*	A/R1	0,0	1,4	0,0	0,0	0,0	0,0	0,0	0,0	0,0	2,2	0,35
			B/R4	0,0	0,0	0,0	0,0	0,0	0,0	0,0	0,0	0,0	0,0	0,00
		200000	A/R1	0,0	1,1	0,5	0,5	0,0	0,0	0,0	0,0	0,9	4,7	0,77
			B/R4	2,2	2,5	5,4	4,4	2,8	2,8	0,0	0,9	0,6	2,3	2,39
		corrected*	A/R1	0,0	2,0	1,4	1,4	0,0	0,0	0,0	0,0	1,8	5,6	1,20
			B/R4	3,1	3,4	6,3	5,3	3,7	3,7	0,0	1,8	1,5	3,2	3,16
2-A-20	40,0	1000000	A/R1	6,5	4,8	4,5	5,2	0,0	0,0	0,0	3,9	3,9	0,0	2,88
			B/R4	11,2	6,2	5,0	5,4	2,2	2,7	0,0	2,6	0,0	1,6	3,69
		corrected*	A/R1	7,4	5,7	5,4	6,1	0,0	0,0	0,0	4,8	4,8	0,0	3,39
			B/R4	12,1	7,1	5,9	6,3	3,1	3,6	0,0	3,5	0,0	2,5	4,37
	58,8	50000	A/R1	11,2	9,2	8,0	7,9	1,8	1,3	0,8	6,7	7,3	1,9	5,61
			B/R4	11,2	10,7	8,7	8,6	4,2	6,4	0,0	6,5	0,0	4,0	6,03
		corrected*	A/R1	12,1	10,1	8,9	8,8	2,7	2,2	1,7	7,6	8,2	2,8	6,46
			B/R4	12,1	11,6	9,6	9,5	5,1	7,3	0,0	7,4	0,0	4,9	6,71
2-A-21	40,0	500000	A/R1	0,0	0,0	0,0	0,0	0,0	1,2	0,0	2,2	0,0	0,0	0,34
			B/R4	1,6	0,0	1,0	0,6	1,3	0,0	0,0	0,0	0,0	0,0	0,45
		corrected*	A/R1	0,0	0,0	0,0	0,0	0,0	2,1	0,0	3,1	0,0	0,0	0,51
			B/R4	2,5	0,0	1,9	1,5	2,2	0,0	0,0	0,0	0,0	0,0	0,79
2-A-22	58,8	60000	A/R1	0,0	0,0	0,0	0,0	0,0	0,0	0,0	0,0	0,0	0,0	0,00
			B/R4	1,6	0,5	0,0	0,0	0,0	0,0	0,0	0,0	0,0	0,0	0,21
		corrected*	A/R1	0,0	0,0	0,0	0,0	0,0	0,0	0,0	0,0	0,0	0,0	0,00
			B/R4	2,5	1,4	0,0	0,0	0,0	0,0	0,0	0,0	0,0	0,0	0,38
		90000	A/R1	3,0	0,7	0,8	0,0	2,8	0,5	0,2	1,7	3,9	2,8	1,64
			B/R4	3,0	2,0	0,0	0,0	0,0	1,3	0,0	0,9	0,0	0,3	0,75
		corrected*	A/R1	3,9	1,6	1,7	0,0	3,7	1,4	1,1	2,6	4,8	3,7	2,41
			B/R4	3,9	2,9	0,0	0,0	0,0	2,2	0,0	1,8	0,0	1,2	1,18

Table 7.1.3.1 continued

ID	fatigue tests		sheet /	crack lengths [mm]										average
	Fmax [kN]	N [kcyc.]	riv. row	1L	1R	2L	2R	3L	3R	4L	4R	5L	5R	per row
2-A-23	58,8	80000	A/R1	0,2	0,0	0,8	0,0	0,7	0,0	0,0	0,0	0,0	0,0	0,17
			B/R4	0,0	0,0	0,0	0,0	0,0	0,0	0,0	0,0	0,0	0,0	0,00
		corrected*	A/R1	1,1	0,0	1,7	0,0	1,6	0,0	0,0	0,0	0,0	0,0	0,43
			B/R4	0,0	0,0	0,0	0,0	0,0	0,0	0,0	0,0	0,0	0,0	0,00
2-A-24	58,8	120000	A/R1	5,3	1,6	3,8	3,1	1,7	1,7	2,5	2,0	2,2	1,0	2,49
			B/R4	3,1	1,5	1,1	0,0	3,0	3,3	3,1	3,3	0,0	4,0	2,24
		corrected*	A/R1	6,2	2,5	4,7	4,0	2,6	2,6	3,4	2,9	3,1	1,9	3,34
			B/R4	4,0	2,4	2,0	0,0	3,9	4,2	4,0	4,2	0,0	4,9	2,92
2-A-31	58,8	45000	A/R1	0,0	0,0	1,3	1,9	0,0	0,0	0,0	0,0	1,8	2,1	0,71
			B/R4	0,0	0,0	0,0	0,0	0,5	0,1	0,0	0,0	1,2	0,5	0,23
		corrected*	A/R1	0,0	0,0	2,2	2,8	0,0	0,0	0,0	0,0	2,7	3,0	1,05
			B/R4	0,0	0,0	0,0	0,0	1,4	1,0	0,0	0,0	2,1	1,4	0,57
	51,8	200000	A/R2	7,5	8,6	8,6	8,6	8,6	9,5	10,6	8,6	8,6	9,2	8,81
			B/R5	9,2	7,0	3,2	9,3	9,4	8,6	8,6	8,6	8,6	10,8	8,29
		corrected*	A/R2	7,9	9,0	9,0	9,0	9,0	9,9	11,0	9,0	9,0	9,6	9,21
			B/R5	9,6	7,4	3,6	9,7	9,8	9,0	9,0	9,0	9,0	11,2	8,69
2-A-32	58,8	45000	A/R1	0,0	0,0	2,3	1,9	0,0	0,0	0,0	0,0	0,0	1,5	0,57
			B/R4	0,0	0,0	0,0	0,0	0,0	0,0	0,0	0,0	0,0	0,0	0,00
		corrected*	A/R1	0,0	0,0	3,2	2,8	0,0	0,0	0,0	0,0	0,0	2,4	0,83
			B/R4	0,0	0,0	0,0	0,0	0,0	0,0	0,0	0,0	0,0	0,0	0,00
	58,8	70000	A/R2	9,2	8,6	8,6	12,8	5,7	3,8	7,2	5,2	12,0	9,2	8,21
			B/R5	5,6	8,5	2,9	3,0	3,9	3,3	7,7	10,3	4,2	6,1	5,52
		corrected*	A/R2	9,6	9,0	9,0	13,2	6,1	4,2	7,6	5,6	12,4	9,6	8,61
			B/R5	6,0	8,9	3,3	3,4	4,3	3,7	8,1	10,7	4,6	6,5	5,92
2-A-33	58,8	45000	A/R1	0,0	1,4	0,0	0,0	0,0	0,0	0,0	0,0	0,0	0,8	0,22
			B/R4	0,0	0,0	0,0	0,0	0,0	0,0	0,0	0,0	0,0	0,0	0,00
		corrected*	A/R1	0,0	2,3	0,0	0,0	0,0	0,0	0,0	0,0	0,0	1,7	0,39
			B/R4	0,0	0,0	0,0	0,0	0,0	0,0	0,0	0,0	0,0	0,0	0,00
	58,8	45000	A/R2	9,2	11,0	4,5	6,4	7,8	8,1	8,1	5,4	9,2	9,2	7,87
			B/R5	5,9	7,4	6,4	6,2	6,9	7,1	5,6	7,5	4,9	9,2	6,68
		corrected*	A/R2	9,6	11,4	4,9	6,8	8,2	8,5	8,5	5,8	9,6	9,6	8,27
			B/R5	6,3	7,8	6,8	6,6	7,3	7,5	6,0	7,9	5,3	9,6	7,08
2-A-34	58,8	45000	A/R1	1,6	2,2	0,0	0,0	0,0	0,0	0,0	0,0	2,3	1,9	0,80
			B/R4	0,0	0,0	0,0	0,0	0,0	0,0	0,0	1,0	0,0	0,0	0,10
		corrected*	A/R1	2,5	3,1	0,0	0,0	0,0	0,0	0,0	0,0	3,2	2,8	1,14
			B/R4	0,0	0,0	0,0	0,0	0,0	0,0	0,0	1,9	0,0	0,0	0,19

Table 7.1.3.2, crack initiation results for repair coupon specimens, which form SN_i-curves

Top sheet, rivet row 1, mating aluminium layer

Specimen	Fmax [kN]	Sa [MPa]	N [cycles]	$a_{av.}$ [mm]
2-A-6	64700	59,4	27000	0,29
2-A-2	58800	54,0	45000	0,97
2-A-22	58800	54,0	60000	0,00
2-A-19	51800	47,6	100000	0,35
2-A-21	40000	36,7	500000	0,51

Bottom sheet, rivet row 4, mating surface layer

Specimen	Fmax [kN]	Sa [MPa]	N [cycles]	$a_{av.}$ [mm]
2-A-6	64700	59,4	40000	0,00
2-A-4	58800	54,0	55000	0,15
2-A-22	58800	54,0	60000	0,38
2-A-19	51800	47,6	100000	0,00
2-A-21	40000	36,7	500000	0,79

7.1.3.3, fatigue crack length in specimen 2-A-44, rivet row 1, upper GLARE4 sheet, measured after one year outdoor exposure (Queensland) and residual strength test. Measured cross section is failed cross section. Unit: [mm]

2-A-44	1			2			3			4			5		
	Left	Hole	Right	Left	Hole	Right	Left	Hole	Right	Left	Hole	Right	Left	Hole	Right
1st layer	0,00	8,35	0,00	0,00	8,29	0,00	0,00	8,50	0,00	0,00	8,29	0,00	0,00	8,29	0,00
2nd layer	0,00	6,43	0,00	0,00	6,43	0,00	0,00	6,50	0,00	0,00	6,44	0,00	0,00	6,21	0,00
3rd layer	0,00	5,50	0,00	1,61	5,56	0,64	0,00	5,65	0,67	0,00	5,70	1,17	0,50	5,55	1,61
4th layer	1,07	5,46	0,56	2,41	5,61	1,73	1,75	5,48	1,73	0,84	5,43	2,43	1,80	5,53	2,51
5th layer	1,90	5,44	0,81	3,27	5,58	3,06	3,25	5,43	3,26	3,04	5,56	2,95	3,89	5,48	4,27

7.1.3.4, fatigue crack length in specimen 2-A-46, rivet row 1, upper GLARE4 sheet, measured after one year outdoor exposure (Queensland) and residual strength test. Measured cross section is failed cross section. Unit: [mm]

2-A-46	1			2			3			4			5		
	Left	Hole	Right	Left	Hole	Right	Left	Hole	Right	Left	Hole	Right	Left	Hole	Right
1st layer	0,00	8,29	0,00	0,00	8,34	0,00	0,00	8,02	0,00	0,00	8,46	0,00	0,00	8,35	0,00
2nd layer	0,00	6,16	0,00	0,00	5,96	0,00	0,00	6,13	0,00	0,00	6,27	0,00	0,00	6,37	0,00
3rd layer	2,55	5,50	2,15	3,42	5,46	2,55	1,36	5,42	3,05	2,64	5,46	3,47	2,36	5,57	3,03
4th layer	4,44	5,30	4,46	5,02	5,45	4,40	3,83	5,17	4,80	4,17	5,14	5,30	2,87	5,48	4,29
5th layer	6,02	5,50	6,04	10,69	5,52	9,91	8,90	5,29	6,23	7,22	5,44	8,54	8,58	5,40	7,30

7.1.3.5, fatigue crack length in specimen 2-A-48, rivet row 1, upper GLARE4 sheet, measured after one year outdoor exposure (Queensland) and residual strength test. Measured cross section is failed cross section. Unit:[mm]

2-A-48	1			2			3			4			5		
	Left	Hole	Right	Left	Hole	Right	Left	Hole	Right	Left	Hole	Right	Left	Hole	Right
1st layer	0,00	n.m.	0,00	0,00	n.m.	0,00	0,00	n.m.	0,00	0,00	n.m.	0,00	0,00	n.m.	0,00
2nd layer	0,00	n.m.	0,87	2,16	n.m.	2,23	1,22	n.m.	2,16	1,40	n.m.	1,60	2,23	n.m.	2,43
3rd layer	4,24	n.m.	4,15	5,69	n.m.	5,63	4,97	n.m.	5,72	5,47	n.m.	5,48	5,45	n.m.	5,48
4th layer	6,56	n.m.	5,96	8,47	n.m.	7,65	7,74	n.m.	7,77	8,13	n.m.	7,57	7,64	n.m.	8,19
5th layer	11,25	n.m.	11,25	11,24	n.m.	11,24	11,36	n.m.	11,36	11,28	n.m.	11,28	11,30	n.m.	11,30

n.m: not measured

Table 7.1.4.1, crack propagation rates in repair coupons

Top sheet, rivet row 1, mating aluminium layer

$F_{max.}$ [N]	$S_{max.}$ [MPa]	RR1 unpainted	RR1 painted
40000	81,6	5,76E-06	6,88E-06
51800	105,7	8,50E-06	1,02E-05
58800	120	1,80E-05	4,23E-05
64700	132	1,13E-04	1,35E-04

Bottom sheet, rivet row 4, mating surface layer

$F_{max.}$ [N]	$S_{max.}$ [MPa]	RR4 unpainted	RR4 painted
40000	81,6	7,16E-06	2,64E-06
51800	105,7	3,16E-05	1,17E-05
58800	120	1,15E-04	4,23E-05
64700	132	1,13E-04	4,17E-05

Table 7.1.5.1, crack length measurements for variable amplitude circumferential joint specimens, butt strap mating aluminium layer, rivet rows 3 and 4, crack lengths in [mm]

specim.	flights	r. row	1L	1R	2L	2R	3L	3R	4L	4R	5L	5R	Av./row
2-B-103	179280	R3	4.45	3.25	3.85	3.25	3.85	3.65	4.05	3.85	2.55	2.95	3.57
		R4	2.25	2.55	3.25	4.25	4.05	4.25	2.55	3.25	2.45	1.95	3.08
	199200	R3	4.95	4.20	4.15	4.20	4.25	3.90	4.10	4.35	2.20	3.25	3.96
		R4	2.25	2.55	3.90	4.25	4.45	4.25	2.55	3.75	2.45	2.35	3.28
2-B-104	119520	R3	0.00	0.00	0.00	0.00	0.00	0.00	0.00	0.00	0.00	0.00	0.00
		R4	0.00	0.00	0.00	0.00	0.00	0.00	0.00	0.00	0.00	0.00	0.00
	139440	R3	1.95	0.00	1.45	1.55	1.95	0.00	0.00	0.00	0.00	0.00	0.69
		R4	2.35	1.35	1.85	1.05	1.05	2.05	1.15	1.95	1.25	1.65	1.57
2-B-105	129480	R3	1.85	0.00	2.25	0.95	1.45	1.25	1.55	1.85	1.55	1.25	1.40
		R4	2.45	0.00	2.65	2.35	1.55	2.95	1.15	1.55	0.00	2.15	1.68

Table 7.1.6.1,
specimen 2-B-14, crack lengths in butt strap, rivet rows 3 and 4, mating layer, after 60000 CA cycles at room temperature

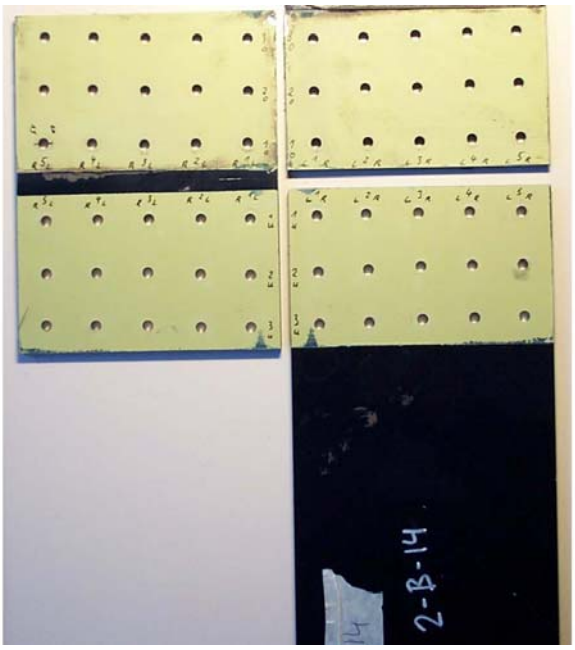

Crack lengths in [mm]

	fatigue sensitive locations at bore holes									
	1L	1R	2L	2R	3L	3R	4L	4R	5L	5R
RR3	-	-	-	-	-	-	-	-	<1	<1
RR4	-	-	-	-	-	-	-	-	-	-

Table 7.1.6.2,
specimen 2-B-15, crack lengths in butt strap, rivet rows 3 and 4, mating layer, after 60000 CA cycles at room temperature

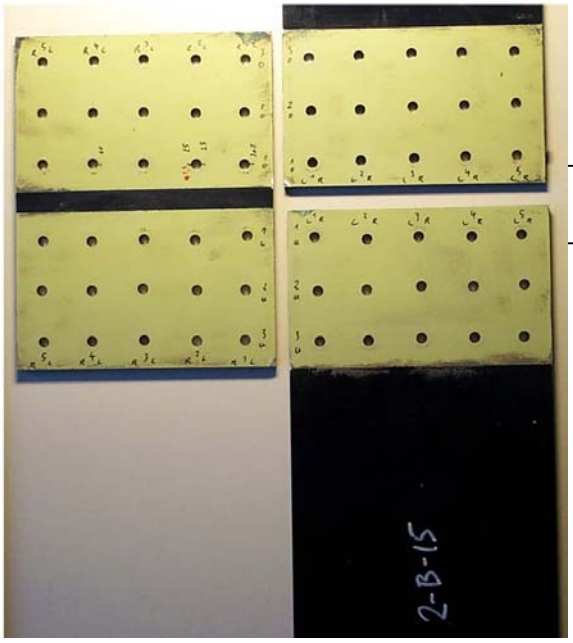

Crack lengths in [mm]

	fatigue sensitive locations at bore holes									
	1L	1R	2L	2R	3L	3R	4L	4R	5L	5R
RR3	<1	-	<1	1.5	-	-	<1	-	-	-
RR4	-	-	-	-	-	-	-	-	-	-

Table 7.1.6.3, specimen 2-B-16, crack lengths in butt strap, rivet rows 3 and 4, mating layer, after 60000 CA cycles and 75000 simplified flights (A340-600 flight type MR"EYS) at room temperature, crack lengths in [mm]

	fatigue sensitive locations at bore holes									
	1L	1R	2L	2R	3L	3R	4L	4R	5L	5R
RR3	2.5	2	<1	<1	2	2	2	2	2	-
RR4	1.5	2	2	2	2	2	2.5	1.5	2	3.5

Table 7.1.6.4, variable amplitude and variable temperature spectra (increased loads)
for circumferential joint coupon tests (S: applied gross stress)

stress peak	S [MPa] (t=4.3mm)	T [°C] standard	T [°C] tropic	T [°C] arctic	force [N]
0	15,4	20	70	-30	7604
1	31,6	20	70	-30	15594
2	15,7	20	70	-30	7742
3	37,5	20	70	-30	18515
4	20,3	20	70	-30	10029
5	37,5	20	70	-30	18515
6	61,4	20	70	-30	30307
7	61,4	-30	-30	-30	30307
8	78,1	-30	-30	-30	38573
9	44,7	-30	-30	-30	22042
10	61,4	-30	-30	-30	30307
11	61,4	-30	-30	-30	30307
12	21,9	20	20	-30	10828
13	21,9	20	20	-30	10828
14	44,7	20	20	-30	22042
15	7,8	20	20	-30	3830
16	36,5	20	20	-30	18019
17	10,3	20	20	-30	5070
18	15,1	20	20	-30	7467

Chapter 8
Returning Outdoor Exposure Specimens

Table 8.1, specimen series 2-B, eddy crack length measurements before outdoor exposure, cracks at rivet rows 3 and 4 in mating butt strap layer

			Crack measurements													
	Fatigue tests		Measurement method		Crack lengths [mm]										Average	Total
ID	Fmax [kN]	N [kcycles]		Row	1L	1R	2L	2R	3L	3R	4L	4R	5L	5R	per row	average
2-B-1	38,9	100	Eddy current	R3	4,9	3,4	5,8	3,3	4,3	3,7	6,0	3,5	4,9	4,7	4,45	4,58
				R4	3,7	2,7	5,5	6,6	4,2	3,5	3,4	3,9	7,7	5,9	4,71	
			Eddy current	R3	5,8	4,3	6,7	4,2	5,2	4,6	6,9	4,4	5,8	5,6	5,30	5,43
			(corrected)	R4	4,6	3,6	6,4	7,5	5,1	4,4	4,3	4,8	8,6	6,8	5,56	
2-B-2	38,9	200	Eddy current	R3	*	*	*	*	*	*	*	*	*	*	9,08	9,08
				R4	*	*	*	*	*	*	*	*	*	*	9,08	
			Eddy current	R3	*	*	*	*	*	*	*	*	*	*	9,08	9,08
			(corrected)	R4	*	*	*	*	*	*	*	*	*	*	9,08	
2-B-3	38,9	300	Microscope	R3	9,6	3,8	8,8	7,7	7,9	8,8	8,0	9,0	9,0	9,6	8,21	7,98
				R4	9,6	3,5	9,4	3,3	9,8	8,9	7,4	7,8	8,1	9,6	7,74	
2-B-4	38,9	400	Microscope	R3	9,6	3,2	8,2	9,4	7,4	9,0	9,0	9,0	9,0	9,6	8,32	8,70
				R4	9,6	9,0	9,0	9,0	9,0	9,0	9,0	9,0	9,0	9,6	9,08	
2-B-5	38,9	150	Eddy current	R3	2,1	3,0	2,7	2,1	2,1	1,4	2,5	2,6	2,1	1,9	2,25	2,41
				R4	2,6	1,7	2,7	2,2	3,8	2,9	3,2	2,2	1,4	3,0	2,57	
			Eddy current	R3	3,0	3,9	3,6	3,0	3,0	2,3	3,4	3,5	3,0	2,8	3,10	3,26
			(corrected)	R4	3,5	2,6	3,6	3,1	4,7	3,8	4,1	3,1	2,3	3,9	3,42	
2-B-6	38,9	150	Eddy current	R3	*	*	*	*	*	*	*	*	*	*	9,08	9,08
				R4	*	*	*	*	*	*	*	*	*	*	9,08	
			Eddy current	R3	*	*	*	*	*	*	*	*	*	*	9,08	9,08
			(corrected)	R4	*	*	*	*	*	*	*	*	*	*	9,08	
2-B-7	28,5	100	Microscope	R3	0,8	0,7	0,0	0,0	0,9	0,6	0,0	0,7	0,0	0,0	0,37	0,76
				R4	0,0	0,0	0,0	0,0	2,5	1,6	2,3	1,5	2,2	1,4	1,15	
	38,9	50	Microscope	R3	2,5	0,7	1,0	0,0	2,3	1,0	0,0	2,6	0,0	1,8	1,19	1,46
				R4	0,0	0,0	0,0	0,0	3,1	2,8	2,9	2,7	2,9	2,9	1,73	
			Eddy current	R3	2,3	0,7	0,0	0,0	1,5	0,5	0,0	1,8	0,0	1,3	0,81	1,16
				R4	0,0	0,0	0,8	0,0	3,1	2,1	2,5	2,2	2,1	2,3	1,51	
			Eddy current	R3	3,2	1,6	0,0	0,0	2,4	1,4	0,0	2,7	0,0	2,2	1,32	1,71
			(corrected)	R4	0,0	0,0	1,7	0,0	4,0	3,0	3,4	3,1	3,0	3,2	2,11	

Table 8.1, continued

					Crack measurements											
	Fatigue tests		Measurement method		Crack lengths [mm]										Average	Total
ID	Fmax [kN]	N [kcycles]		Row	1L	1R	2L	2R	3L	3R	4L	4R	5L	5R	per row	average
2-B-8	28,5	100	Microscope	R3	0,0	0,6	0,0	1,1	0,0	0,0	0,0	0,0	0,0	1,1	0,28	0,22
				R4	0,0	0,0	0,0	0,0	0,3	0,0	1,3	0,0	0,0	0,0	0,16	
	38,9	100	Microscope	R3	3,4	3,0	0,9	3,1	2,7	2,5	3,5	3,0	2,8	2,9	2,78	2,80
				R4	2,8	2,6	2,2	3,2	3,0	2,8	3,4	2,5	3,1	2,5	2,81	
			Eddy current	R3	5,9	6,0	3,7	4,3	7,3	7,1	6,0	5,4	3,4	4,8	5,39	6,15
				R4	9,6	8,6	3,0	5,3	8,2	7,6	4,7	6,8	7,8	7,4	6,90	
			Eddy current	R3	6,8	6,9	4,6	5,2	8,2	8,0	6,9	6,3	4,3	5,7	6,24	6,95
			(corrected)	R4	9,6	9,5	3,9	6,2	9,1	8,5	5,6	7,7	8,7	8,3	7,67	
2-B-9	28,5	100	Microscope	R3	0,0	1,8	0,0	0,5	1,5	1,9	0,0	0,0	0,0	0,0	0,57	0,76
				R4	1,5	0,0	2,2	1,9	1,4	1,8	0,0	0,0	0,0	0,7	0,95	
	38,9	200	Microscope	R3	9,6	9,0	9,0	9,0	9,0	9,0	9,0	9,0	9,0	2,0	8,32	8,51
				R4	9,6	9,0	9,0	9,0	9,0	10,2	3,9	9,0	9,0	9,6	8,70	
			Eddy current	R3	*	*	*	*	*	*	*	*	*	*	9,08	9,08
				R4	*	*	*	*	*	*	*	*	*	*	9,08	
			Eddy current	R3	*	*	*	*	*	*	*	*	*	*	9,08	9,08
			(corrected)	R4	*	*	*	*	*	*	*	*	*	*	9,08	
2-B-10	28,5	100	Microscope	R3	0,0	0,0	0,0	0,0	0,0	0,0	0,0	0,0	1,2	1,6	0,28	0,26
				R4	0,0	0,0	1,5	0,0	0,8	0,0	0,0	0,0	0,0	0,0	0,23	
	38,9	250	Microscope	R3	9,6	12,0	1,5	6,9	7,8	12,5	5,4	0,8	3,6	9,6	6,97	8,03
				R4	9,6	9,0	9,0	9,0	9,0	9,0	9,0	9,0	9,0	9,6	9,08	
			Eddy current	R3	*	*	*	*	*	*	*	*	*	*	9,08	9,08
				R4	*	*	*	*	*	*	*	*	*	*	9,08	
			Eddy current	R3	*	*	*	*	*	*	*	*	*	*	9,08	9,08
			(corrected)	R4	*	*	*	*	*	*	*	*	*	*	9,08	
2-B-11	28,5	100	Microscope	R3	1,3	0,7	0,0	0,0	0,0	0,4	0,0	0,0	0,0	0,0	0,24	0,12
				R4	0,0	0,0	0,0	0,0	0,0	0,0	0,0	0,0	0,0	0,0	0,00	
	38,9	300	Eddy current	R3	*	*	*	*	*	*	*	*	*	*	9,08	9,08
				R4	*	*	*	*	*	*	*	*	*	*	9,08	
			Eddy current	R3	*	*	*	*	*	*	*	*	*	*	9,08	9,08
			(corrected)	R4	*	*	*	*	*	*	*	*	*	*	9,08	
2-B-37	38,9	30	Microscope	R3	2,1	2,8	2,1	0,9	1,5	2,3	2,1	2,0	2,2	1,1	1,91	1,96
				R4	2,4	1,7	1,1	2,2	1,8	2,4	1,8	2,1	2,4	2,2	2,01	
2-B-38	38,9	30	Microscope	R3	2,7	1,4	2,3	2,3	1,4	1,0	1,0	1,3	0,6	1,1	1,51	1,55
				R4	1,5	0,7	0,8	1,4	0,7	0,7	2,8	2,5	2,7	2,0	1,58	
2-B-39	31,6	70	Microscope	R3	2,3	2,0	0,8	0,7	0,6	0,5	0,9	1,0	0,6	0,8	1,02	0,68
				R4	0,0	0,0	0,0	0,0	0,0	0,0	0,0	0,0	1,7	1,7	0,34	
			Eddy current	R3	1,1	0,9	0,0	0,0	0,0	0,0	0,0	0,0	0,0	0,2	0,22	0,32
				R4	0,0	0,2	0,2	0,2	0,0	0,3	0,3	0,2	1,4	1,4	0,42	
			Eddy current	R3	2,0	1,8	0,0	0,0	0,0	0,0	0,0	0,0	0,0	1,1	0,48	0,79
			(corrected)	R4	0,0	1,1	1,1	1,1	0,0	1,2	1,2	1,1	2,3	2,3	1,10	
2-B-40	38,9	30	Microscope	R3	1,4	1,6	1,3	2,2	1,5	0,9	1,3	0,6	0,3	0,3	1,14	0,94
				R4	0,0	0,0	0,0	0,0	1,6	0,0	1,9	2,3	1,5	0,0	0,73	

Table 8.1, continued

	Fatigue tests		Crack measurements													
			Measurement method		Crack lengths [mm]										Average	Total
ID	Fmax [kN]	N [kcycles]		Row	1L	1R	2L	2R	3L	3R	4L	4R	5L	5R	per row	average
2-B-41	49,4	15	Microscope	R3	0,8	0,7	0,8	0,7	0,5	1,0	0,6	0,6	0,8	0,8	0,73	0,90
				R4	1,3	0,6	1,0	1,0	1,5	1,4	1,2	1,2	0,8	0,6	1,06	
			Eddy current	R3	0,0	0,0	0,0	0,0	0,0	0,5	0,0	0,0	0,0	0,0	0,05	0,25
				R4	0,0	0,0	0,9	0,2	1,0	0,8	0,7	0,6	0,2	0,0	0,44	
			Eddy current	R3	0,0	0,0	0,0	0,0	0,0	1,4	0,0	0,0	0,0	0,0	0,14	0,59
			(corrected)	R4	0,0	0,0	1,8	1,1	1,9	1,7	1,6	1,5	1,1	0,0	1,04	
2-B-42	26,3	170	Microscope	R3	0,0	0,0	0,0	0,6	0,0	1,1	0,0	0,0	0,0	0,0	0,17	0,52
				R4	1,8	0,0	0,0	0,0	0,0	0,0	0,9	1,5	2,4	2,1	0,87	
			Eddy current	R3	0,6	0,0	0,0	0,1	0,0	1,0	0,0	0,0	0,0	0,0	0,17	0,41
				R4	0,7	0,0	0,0	0,0	0,0	0,0	0,6	1,0	2,3	1,8	0,64	
			Eddy current	R3	1,5	0,0	0,0	1,0	0,0	1,9	0,0	0,0	0,0	0,0	0,43	0,75
			(corrected)	R4	1,6	0,0	0,0	0,0	0,0	0,0	1,5	1,9	3,2	2,7	1,07	
2-B-43	35	45	Eddy current	R3	0,0	0,7	0,0	0,1	0,0	0,6	0,0	0,0	0,0	0,0	0,14	0,17
				R4	0,0	0,0	0,3	0,0	0,4	0,9	0,3	0,0	0,0	0,0	0,19	
			Eddy current	R3	0,0	1,6	0,0	1,0	0,0	1,5	0,0	0,0	0,0	0,0	0,40	0,46
			(corrected)	R4	0,0	0,0	1,2	0,0	1,3	1,8	1,2	0,0	0,0	0,0	0,53	
2-B-44	28,5	100	Microscope	R3	0,0	0,0	2,2	2,2	1,7	2,2	1,7	2,6	1,1	2,1	1,58	1,29
				R4	0,4	0,0	2,0	2,2	1,3	0,6	1,5	0,0	1,1	0,9	1,00	
2-B-45	24,1	400	Eddy current	R3	0,0	0,0	0,6	1,0	0,0	0,0	1,1	2,1	0,0	0,1	0,49	0,66
				R4	0,7	0,0	0,0	0,0	0,0	1,4	2,0	2,6	1,6	0,0	0,83	
			Eddy current	R3	0,0	0,0	1,5	1,9	0,0	0,0	2,0	3,0	0,0	1,0	0,92	1,09
			(corrected)	R4	1,6	0,0	0,0	0,0	0,0	2,3	2,9	3,5	2,5	0,0	1,26	
2-B-46	38,9	30	Microscope	R3	2,0	2,4	2,0	0,8	1,0	0,8	2,6	2,2	1,2	2,3	1,73	1,63
				R4	1,8	1,0	1,4	0,7	1,0	1,6	1,6	2,6	1,8	1,7	1,52	
2-B-47	38,9	30	Microscope	R3	0,6	0,8	1,9	0,8	0,0	0,5	0,8	1,8	0,0	0,0	0,72	0,64
				R4	0,8	0,0	0,7	0,0	0,6	0,4	0,9	0,8	0,9	0,5	0,56	
2-B-48	38,9	30	Eddy current	R3	1,6	1,1	2,4	2,4	1,0	1,4	2,7	2,7	0,0	0,0	1,53	1,69
				R4	1,2	1,5	2,4	2,0	2,5	2,9	2,0	1,7	1,6	0,6	1,84	
			Eddy current	R3	2,5	2,0	3,3	3,3	1,9	2,3	3,6	3,6	0,0	0,0	2,21	2,45
			(corrected)	R4	2,1	2,4	3,3	2,9	3,4	3,8	2,9	2,6	2,5	1,5	2,69	
2-B-49	38,9	100	Eddy current	R3	6,4	6,0	6,5	5,1	6,5	3,2	5,3	4,5	7,3	4,0	5,48	5,39
				R4	3,3	2,6	6,7	6,4	5,7	7,2	5,2	5,1	6,3	4,4	5,29	
			Eddy current	R3	7,3	6,9	7,4	6,0	7,4	4,1	6,2	5,4	8,2	4,9	6,33	6,24
			(corrected)	R4	4,2	3,5	7,6	7,3	6,6	8,1	6,1	6,0	7,2	5,3	6,14	
2-B-50	38,9	200	Eddy current	R3	*	*	*	*	*	*	*	*	*	*	9,08	9,08
				R4	*	*	*	*	*	*	*	*	*	*	9,08	
			Eddy current	R3	*	*	*	*	*	*	*	*	*	*	9,08	9,08
			(corrected)	R4	*	*	*	*	*	*	*	*	*	*	9,08	
2-B-51	38,9	400	Microscope	R3	*	*	*	*	*	*	*	*	*	*	9,08	9,08
				R4	*	*	*	*	*	*	*	*	*	*	9,08	

Table 8.1, continued

					Crack measurements											
	Fatigue tests		Measurement method		Crack lengths [mm]										Average	Total
ID	Fmax [kN]	N [kcycles]		Row	1L	1R	2L	2R	3L	3R	4L	4R	5L	5R	per row	average
2-B-53	38,9	20	Eddy current	R3	2,0	1,9	1,8	2,0	1,2	1,5	2,1	2,1	2,4	2,5	1,95	1,57
				R4	1,6	1,2	1,9	1,8	1,6	1,8	1,1	0,9	0,0	0,0	1,19	
			Eddy current	R3	2,9	2,8	2,7	2,9	2,1	2,4	3,0	3,0	3,3	3,4	2,80	2,34
			(corrected)	R4	2,5	2,1	2,8	2,7	2,5	2,7	2,0	1,8	0,0	0,0	1,87	
2-B-54	38,9	20	Eddy current	R3	0,2	0,1	0,0	0,0	1,3	0,9	0,1	0,3	0,0	0,4	0,33	0,56
				R4	1,3	0,8	1,5	1,4	0,5	0,2	0,9	1,1	0,0	0,2	0,79	
			Eddy current	R3	1,1	1,0	0,0	0,0	2,2	1,8	1,0	1,2	0,0	1,3	0,93	1,24
			(corrected)	R4	2,2	1,7	2,4	2,3	1,4	1,1	1,8	2,0	0,0	1,1	1,56	
2-B-55	38,9	20	Eddy current	R3	0,0	0,3	0,2	0,0	0,2	0,1	0,7	0,6	0,0	0,0	0,21	0,21
				R4	0,0	0,0	0,6	0,0	0,7	0,0	0,0	0,0	0,6	0,2	0,21	
			Eddy current	R3	0,0	1,2	1,1	0,0	1,1	1,0	1,6	1,5	0,0	0,0	0,72	0,64
			(corrected)	R4	0,0	0,0	1,5	0,0	1,6	0,0	0,0	0,0	1,5	1,1	0,55	
2-B-56	38,9	20	Eddy current	R3	0,0	0,5	0,0	0,4	0,8	0,9	0,0	0,5	0,0	0,0	0,31	0,45
				R4	0,0	0,0	2,1	0,9	0,2	0,0	0,0	0,8	0,8	1,1	0,59	
			Eddy current	R3	0,0	1,4	0,0	1,3	1,7	1,8	0,0	1,4	0,0	0,0	0,74	0,92
			(corrected)	R4	0,0	0,0	3,0	1,8	1,1	0,0	0,0	1,7	1,7	2,0	1,10	
2-B-57	38,9	20	Eddy current	R3	0,0	0,2	0,0	0,0	0,4	0,1	0,0	0,0	0,0	0,0	0,07	0,13
				R4	0,7	0,1	0,0	0,0	0,0	0,0	0,2	0,4	0,4	0,0	0,18	
			Eddy current	R3	0,0	1,1	0,0	0,0	1,3	1,0	0,0	0,0	0,0	0,0	0,33	0,47
			(corrected)	R4	1,6	1,0	0,0	0,0	0,0	0,0	1,1	1,3	1,3	0,0	0,61	
2-B-73	38,9	200	Microscope	R3	9,6	9,0	9,0	9,0	9,0	9,0	9,0	9,0	9,0	9,6	9,08	8,91
				R4	9,6	9,0	9,0	10,8	3,7	9,0	9,0	9,0	9,0	9,6	8,74	
2-B-74	38,9	300	Microscope	R3	*	*	*	*	*	*	*	*	*	*	9,08	9,08
				R4	*	*	*	*	*	*	*	*	*	*	9,08	

Table 8.2, specimen series 3-B, crack lengths before outdoor exposure

					Crack measurements												Holes 2/3/4	
	Fatigue tests		Measurement		Crack lengths										Average	Total	Average	Total
ID	Fmax[kN]	N [cycles]	method	Side	1L	1R	2L	2R	3L	3R	4L	4R	5L	5R	per row	average	per row	average
3-B-19	69,1	180000	Camera	Front	6,55	7,31	7,86	7,93	8,53	7,76	7,29	6,64	5,54	2,65	6,81	7,59	7,67	8,43
				Rear	6,24	6,88	8,51	8,83	9,50	9,05	9,86	9,40	8,17	7,27	8,37		9,19	
3-B-20	69,1	160000	Camera	Front	3,30	5,38	6,23	6,53	7,46	8,02	7,57	7,07	5,81	5,18	6,26	6,51	7,15	7,43
				Rear	4,95	5,56	6,68	7,36	8,68	8,42	7,87	7,24	5,87	5,11	6,77		7,71	
3-B-21	69,1	140000	Camera	Front	4,32	4,95	5,99	6,12	6,47	6,55	5,88	5,66	4,61	4,07	5,46	5,80	6,11	6,49
				Rear	4,97	5,46	6,64	6,77	7,46	7,77	6,75	5,86	5,08	4,68	6,14		6,88	
3-B-22	69,1	120000	Camera	Front	4,48	4,91	5,53	6,40	6,34	6,70	5,69	5,60	3,87	3,85	5,34	5,05	6,04	5,76
				Rear	3,99	4,38	5,30	5,46	5,85	5,98	5,45	4,85	3,13	3,32	4,77		5,48	
3-B-23	69,1	100000	Camera	Front	0,98	3,09	4,12	4,18	5,11	4,70	3,76	3,96	2,54	3,12	3,56	3,57	4,31	4,39
				Rear	2,04	2,95	4,19	4,57	5,18	5,01	3,94	3,99	2,67	1,27	3,58		4,48	
3-B-24	69,1	80000	Camera	Front	0,92	1,53	2,72	2,00	3,09	3,30	3,11	2,63	2,92	2,09	2,43	2,45	2,81	2,93
				Rear	2,07	2,03	2,97	3,63	3,21	3,03	2,50	3,00	1,89	0,39	2,47		3,06	
3-B-25				Front	0,00	0,00	0,00	0,00	0,00	0,00	0,00	0,00	0,00	0,00	0,00	0,00	0,00	0,00
				Rear	0,00	0,00	0,00	0,00	0,00	0,00	0,00	0,00	0,00	0,00	0,00		0,00	
3-B-26				Front	0,00	0,00	0,00	0,00	0,00	0,00	0,00	0,00	0,00	0,00	0,00	0,00	0,00	0,00
				Rear	0,00	0,00	0,00	0,00	0,00	0,00	0,00	0,00	0,00	0,00	0,00		0,00	
3-B-27				Front	0,00	0,00	0,00	0,00	0,00	0,00	0,00	0,00	0,00	0,00	0,00	0,00	0,00	0,00
				Rear	0,00	0,00	0,00	0,00	0,00	0,00	0,00	0,00	0,00	0,00	0,00		0,00	
3-B-28	69,1	180000	Camera	Front	6,14	7,62	9,09	9,20	###	8,64	9,16	9,75	9,15	7,97	8,71	8,59	9,37	9,46
				Rear	5,99	7,14	8,93	9,45	###	9,37	9,71	9,66	7,58	6,80	8,48		9,54	
3-B-29	69,1	160000	Camera	Front	6,12	6,79	7,96	8,57	9,01	8,50	8,52	7,36	5,61	4,10	7,25	7,25	8,32	8,31
				Rear	3,98	5,59	7,19	8,53	8,52	9,06	8,61	7,93	6,78	6,33	7,25		8,31	
3-B-30	69,1	140000	Camera	Front	5,88	7,36	9,29	9,42	9,90	###	9,42	9,05	7,45	5,93	8,39	7,74	9,54	9,06
				Rear	4,49	5,07	7,20	9,13	9,38	9,84	8,43	7,51	5,61	4,29	7,10		8,58	
3-B-31	69,1	120000	Camera	Front	4,77	4,90	6,68	6,39	7,72	8,41	8,53	8,48	8,48	7,29	7,17	7,25	7,70	8,01
				Rear	5,41	5,75	7,27	7,98	8,76	9,21	8,75	7,90	6,53	5,74	7,33		8,31	
3-B-32	69,1	100000	Camera	Front	3,90	3,48	6,07	5,78	6,79	6,49	6,46	6,18	4,33	4,72	5,42	5,35	6,30	6,11
				Rear	3,73	4,20	5,36	5,72	6,46	6,37	6,15	5,50	4,61	4,67	5,28		5,93	
3-B-33	69,1	80000	Camera	Front	3,41	3,34	3,56	3,06	4,83	4,45	4,50	4,21	2,29	3,32	3,70	3,83	4,10	4,28
				Rear	3,98	3,86	4,41	4,35	5,06	5,14	3,95	3,87	2,43	2,62	3,97		4,46	
3-B-34				Front	0,00	0,00	0,00	0,00	0,00	0,00	0,00	0,00	0,00	0,00	0,00	0,00	0,00	0,00
				Rear	0,00	0,00	0,00	0,00	0,00	0,00	0,00	0,00	0,00	0,00	0,00		0,00	
3-B-35				Front	0,00	0,00	0,00	0,00	0,00	0,00	0,00	0,00	0,00	0,00	0,00	0,00	0,00	0,00
				Rear	0,00	0,00	0,00	0,00	0,00	0,00	0,00	0,00	0,00	0,00	0,00		0,00	
3-B-36				Front	0,00	0,00	0,00	0,00	0,00	0,00	0,00	0,00	0,00	0,00	0,00	0,00	0,00	0,00
				Rear	0,00	0,00	0,00	0,00	0,00	0,00	0,00	0,00	0,00	0,00	0,00		0,00	

Table 8.3, specimen series 3-A, crack lengths before outdoor exposure

				Crack measurements											Holes 2/3/4
	Fatigue tests		Measurement	Crack lengths [mm]											Average
ID	Fmax [kN]	N [kcycles]	method	1L	1R	2L	2R	3L	3R	4L	4R	5L	5R	Average	per row
3-A-15	58,8	40	Camera	0,00	0,00	1,57	0,00	1,16	0,00	0,62	0,61	0,89	0,59	0,54	0,66
3-A-16	67,4	45	Camera	3,61	3,60	3,92	4,33	4,77	4,77	4,34	3,54	1,90	2,38	3,72	4,28
3-A-17	58,8	80	Camera	3,59	3,30	4,27	4,18	4,55	4,27	5,24	4,91	3,80	3,37	4,15	4,57
3-A-18	67,4	80	Camera	6,86	7,33	9,51	9,32	9,02	10,13	9,78	9,67	9,18	8,26	8,91	9,57
3-A-19														0,00	
3-A-20	58,8	40	Camera	0,00	0,00	0,00	0,00	0,00	0,92	0,00	0,00	0,00	0,00	0,09	0,15
3-A-21	58,8	60	Camera	1,77	1,19	3,04	3,01	4,55	4,38	4,47	4,46	2,52	1,95	3,13	3,99
3-A-22	67,4	60	Camera	4,02	5,06	6,53	6,20	6,82	7,04	6,33	6,65	5,48	5,68	5,98	6,60
3-A-23	58,8	120	Camera	5,58	5,98	7,18	8,28	8,63	9,06	8,46	8,26	7,05	6,31	7,48	8,31
3-A-24														0,00	

Cracks measured on non-countersunk side

Chapter 10
Riveted Repair Panels

Table 10.1, crack lengths in rivet rows of panel 11-RR-01, after 80000 fatigue cycles at 120 MPa applied gross stress. Fastener position: see figure 10.8, 10.13 and 10.14. Crack lengths 2a in [mm].

fastener no.	RR1	RR4	RR5	RR8
	skin mating layer	patch mating layer	patch mating layer	skin mating layer
1	25.5	-	-	24.5
2	21.0	-	-	23.0
3	18.5	-	-	18.0
4	19.0	-	-	17.0
5	19.5	11.5	13.0	16.5
6	17.0	14.0	14.0	15.0
7	19.0	13.0	16.0	15.0
8	18.5	13.5	12.5	14.0
9	16.5	4.0	9.0	16.5
10	15.0	-	-	15.5
11	19.5	-	-	20.0
12	18.5	-	-	20.0
13	22.5	-	-	20.0

13. Appendices

A
CA Crack Initiation Calculations for Circumferential Joint

Reference TU Delft / Airbus Computer Program `JOINT´, Release 0.93

Calculation for maximum stress 55 MPa

Loads
Remote tensile (gross) loads in sheet 1:
Factor on loads: 1.000
Smax = 55.00 MPa
R = 0.100
No Limit Load

Joint Data
Number of holes in a rows: 5
Butt Joint

Number of rivet rows in sheet 1:	3
Number of rivet rows in sheet 2:	3
Rivet pitch in sheet 1:	22.7 mm
Rivet pitch in sheet 2:	22.7 mm
Rivet row distance in sheet 1:	22.7 mm
Rivet row distance in sheet 2:	22.7 mm
Rivet row distance between sheet 1 and 2:	28.0 mm
Rivet diameter in sheet 1:	4.80 mm
Rivet diameter in sheet 2:	4.80 mm

Fastener Data
Hi-Lok, steel/titanium - high interference - collar side
Applied factor on life: 1.18
Load Transfer: 36.2% 27.7% 36.2% / 36.2% 27.7% 36.2%

Analyzed Location
Last row in strap between sheet 1 and strap
Sheet 1

FML lay-up:	Glare 2B-7/6-0.4
Thickness:	4.396 mm
Alloy:	2024T3
Prepreg:	S2-glass, FM-94/BR127, 120°C curing
Orientation:	Rolling direction in Al layers perpendicular to loading direction

Sheet 2

FML lay-up:	Glare 2B-7/6-0.4
Thickness:	4.396 mm
Alloy:	2024T3
Prepreg:	S2-glass, FM-94/BR127, 120°C curing
Orientation:	Rolling direction in Al layers perpendicular to loading direction

Butt Strap

FML lay-up:	Glare 2B-7/6-0.4
Thickness:	4.396 mm
Alloy:	2024T3
Prepreg:	S2-glass, FM-94/BR127, 120°C curing
Orientation:	Rolling direction in Al layers perpendicular to loading direction

Reference Curve
EK43-51649 (2024T3)

MSD Analysis
Number of scenarios: 100

Results
Initiation (lead crack):
Layer 1:
Mean: N = 1.19E+05 cycles
StdDev: s = 7.82E-02
Layer 2:
Mean: N = 2.21E+05 cycles
Layer 3:
Mean: N = 4.84E+05 cycles
Layer 4:
Mean: N = 1.93E+06 cycles
Layer 5:
Mean: N = 6.99E+29 cycles
Layer 6:
Mean: N = 6.99E+29 cycles
Layer 7:
Mean: N = 6.99E+29 cycles

Endurance:
Mean: N = 1.21E+05 cycles
StdDev: s = 6.55E-02
Calculation stopped after 1.00E+05 cycles

Residual strength:
Mean: S = 0.00E+00
StdDev: s = 0.00E+00

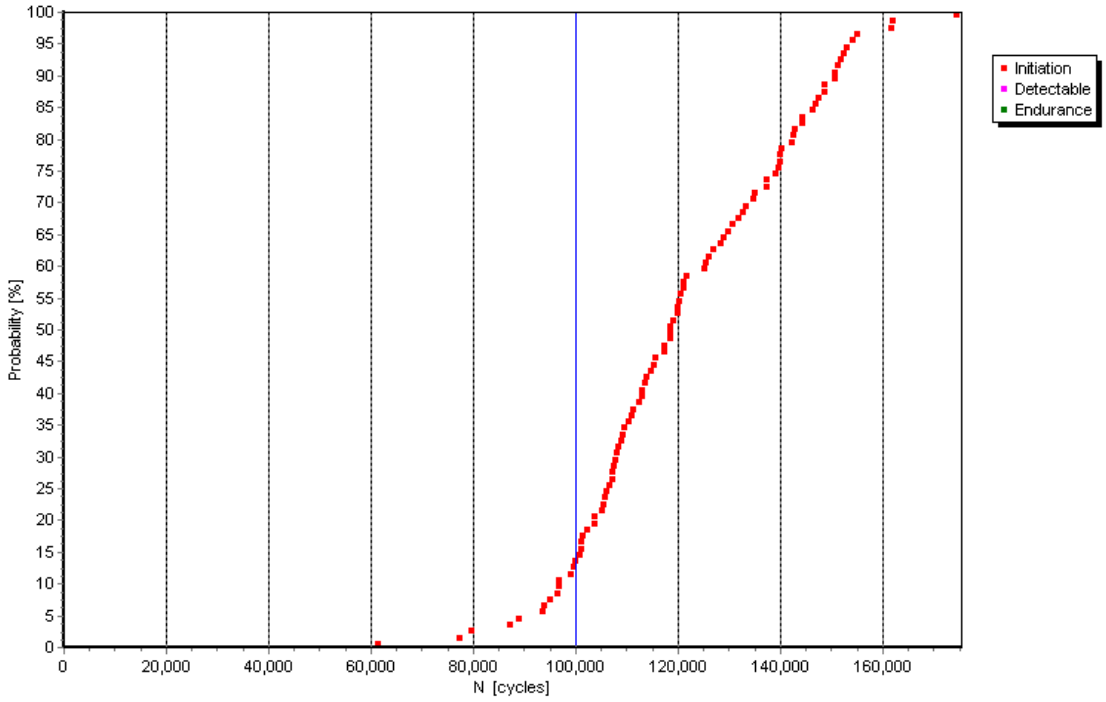

Calculation for maximum stress 59.4 MPa

Loads
Remote tensile (gross) loads in sheet 1:
Factor on loads: 1.000
Smax = 59.40 MPa
R = 0.100
No Limit Load

Joint Data
Number of holes in a rows: 5
Butt Joint

Number of rivet rows in sheet 1:	3
Number of rivet rows in sheet 2:	3
Rivet pitch in sheet 1:	22.7 mm
Rivet pitch in sheet 2:	22.7 mm
Rivet row distance in sheet 1:	22.7 mm
Rivet row distance in sheet 2:	22.7 mm
Rivet row distance between sheet 1 and 2:	28.0 mm
Rivet diameter in sheet 1:	4.80 mm
Rivet diameter in sheet 2:	4.80 mm

Fastener Data
Hi-Lok, steel/titanium - high interference - collar side
Applied factor on life: 1.18
Load Transfer: 36.2% 27.7% 36.2% / 36.2% 27.7% 36.2%

Analyzed Location
Last row in strap between sheet 1 and strap
Sheet 1

FML lay-up:	Glare 2B-7/6-0.4
Thickness:	4.396 mm
Alloy:	2024T3
Prepreg:	S2-glass, FM-94/BR127, 120°C curing
Orientation:	Rolling direction in Al layers perpendicular to loading direction

Sheet 2

FML lay-up:	Glare 2B-7/6-0.4
Thickness:	4.396 mm
Alloy:	2024T3
Prepreg:	S2-glass, FM-94/BR127, 120°C curing
Orientation:	Rolling direction in Al layers perpendicular to loading direction

Butt Strap

FML lay-up:	Glare 2B-7/6-0.4
Thickness:	4.396 mm
Alloy:	2024T3
Prepreg:	S2-glass, FM-94/BR127, 120°C curing
Orientation:	Rolling direction in Al layers perpendicular to loading direction

Reference Curve
EK43-51649 (2024T3)

MSD Analysis
Number of scenarios: 100

Results
Initiation (lead crack):
Layer 1:
Mean: N = 9.48E+04 cycles
StdDev: s = 7.58E-02
Layer 2:
Mean: N = 1.75E+05 cycles
Layer 3:
Mean: N = 3.71E+05 cycles
Layer 4:
Mean: N = 1.18E+06 cycles
Layer 5:
Mean: N = 7.07E+29 cycles
Layer 6:
Mean: N = 7.07E+29 cycles
Layer 7:
Mean: N = 7.07E+29 cycles

Endurance:
Mean: N = 1.05E+05 cycles
StdDev: s = 3.31E-02
Calculation stopped after 1.00E+05 cycles

Residual strength:
Mean: S = 0.00E+00
StdDev: s = 0.00E+00

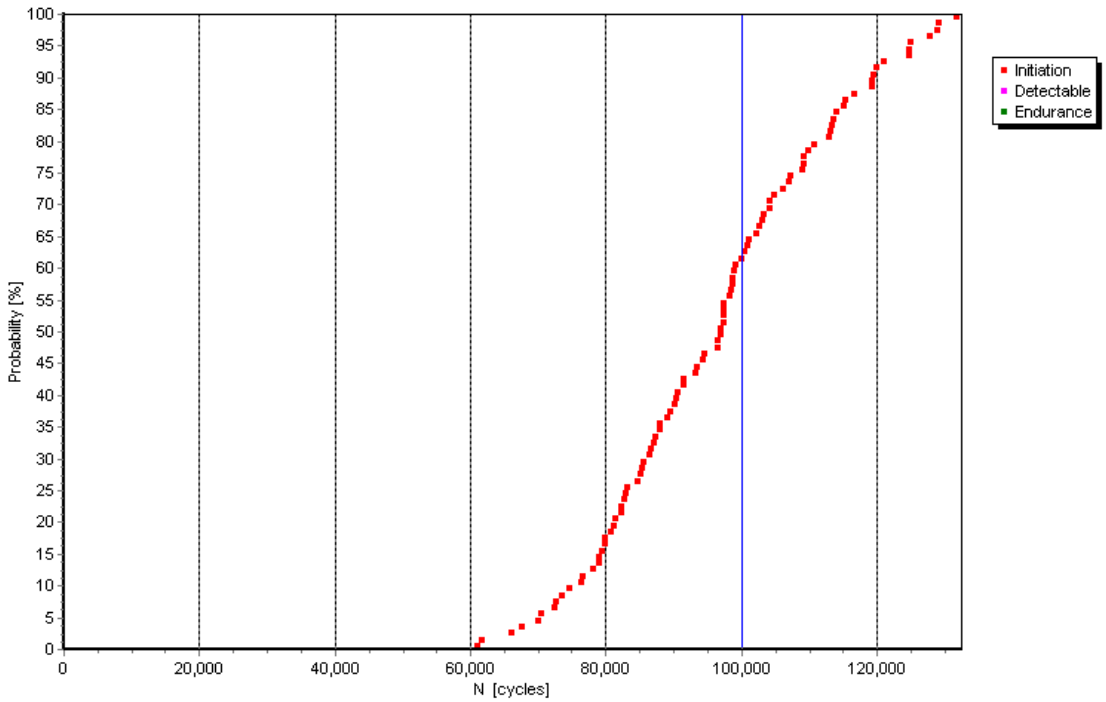

Calculation for maximum stress 66 MPa

Loads
Remote tensile (gross) loads in sheet 1:
Factor on loads: 1.000
Smax = 66.00 MPa
R = 0.100
No Limit Load

Joint Data
Number of holes in a rows: 5
Butt Joint

Number of rivet rows in sheet 1:	3
Number of rivet rows in sheet 2:	3
Rivet pitch in sheet 1:	22.7 mm
Rivet pitch in sheet 2:	22.7 mm
Rivet row distance in sheet 1:	22.7 mm
Rivet row distance in sheet 2:	22.7 mm
Rivet row distance between sheet 1 and 2:	28.0 mm
Rivet diameter in sheet 1:	4.80 mm
Rivet diameter in sheet 2:	4.80 mm

Fastener Data
Hi-Lok, steel/titanium - high interference - collar side
Applied factor on life: 1.18
Load Transfer: 36.2% 27.7% 36.2% / 36.2% 27.7% 36.2%

Analyzed Location
Last row in strap between sheet 1 and strap
Sheet 1

FML lay-up:	Glare 2B-7/6-0.4
Thickness:	4.396 mm
Alloy:	2024T3
Prepreg:	S2-glass, FM-94/BR127, 120°C curing
Orientation:	Rolling direction in Al layers perpendicular to loading direction

Sheet 2

FML lay-up:	Glare 2B-7/6-0.4
Thickness:	4.396 mm
Alloy:	2024T3
Prepreg:	S2-glass, FM-94/BR127, 120°C curing
Orientation:	Rolling direction in Al layers perpendicular to loading direction

Butt Strap

FML lay-up:	Glare 2B-7/6-0.4
Thickness:	4.396 mm
Alloy:	2024T3
Prepreg:	S2-glass, FM-94/BR127, 120°C curing
Orientation:	Rolling direction in Al layers perpendicular to loading direction

Reference Curve
EK43-51649 (2024T3)

MSD Analysis
Number of scenarios: 100

Results
Initiation (lead crack):
Layer 1:
Mean: N = 6.80E+04 cycles
StdDev: s = 7.76E-02
Layer 2:
Mean: N = 1.27E+05 cycles
Layer 3:
Mean: N = 2.61E+05 cycles
Layer 4:
Mean: N = 7.06E+05 cycles
Layer 5:
Mean: N = 7.07E+29 cycles
Layer 6:
Mean: N = 7.07E+29 cycles
Layer 7:
Mean: N = 7.07E+29 cycles

Endurance:
Mean: N = 1.00E+05 cycles
StdDev: s = 0.00E+00
Calculation stopped after 1.00E+05 cycles

Residual strength:
Mean: S = 0.00E+00
StdDev: s = 0.00E+00

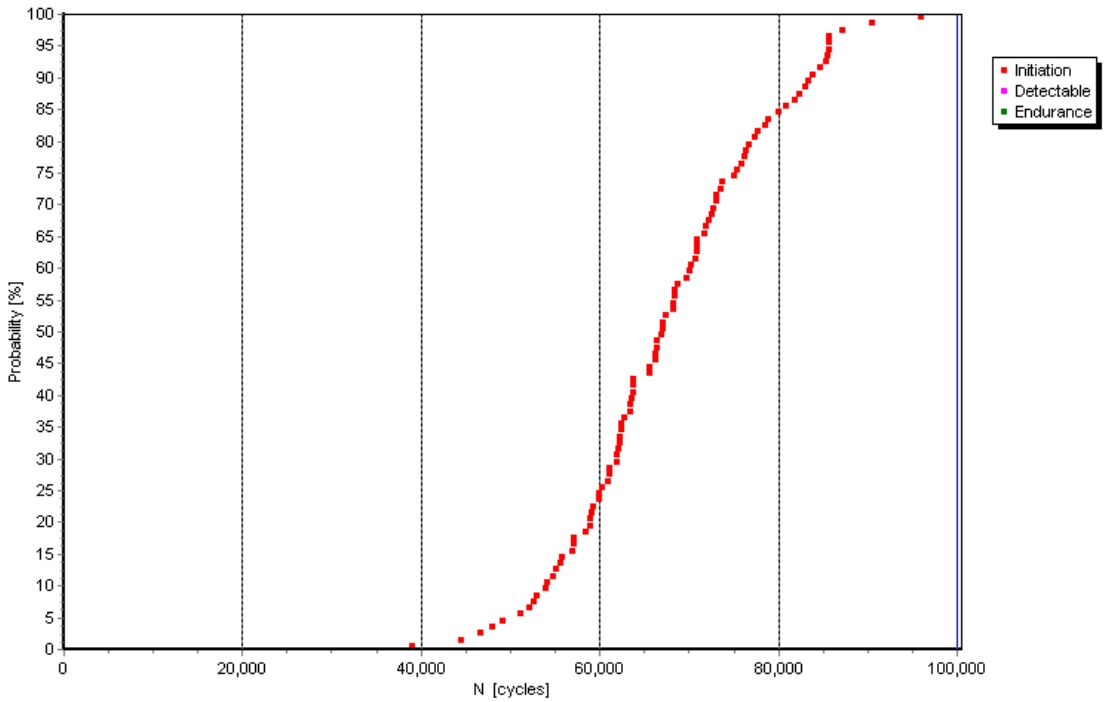

Calculation for maximum stress 77 MPa

Loads
Remote tensile (gross) loads in sheet 1:
Factor on loads: 1,000
Smax = 77,00 MPa
R = 0,100
No Limit Load

Joint Data
Number of holes in a rows: 5
Butt Joint

Number of rivet rows in sheet 1:	3
Number of rivet rows in sheet 2:	3
Rivet pitch in sheet 1:	22,7 mm
Rivet pitch in sheet 2:	22,7 mm
Rivet row distance in sheet 1:	22,7 mm
Rivet row distance in sheet 2:	22,7 mm
Rivet row distance between sheet 1 and 2:	28,0 mm
Rivet diameter in sheet 1:	4,80 mm
Rivet diameter in sheet 2:	4,80 mm

Fastener Data
Hi-Lok, steel/titanium - high interference - collar side
Applied factor on life: 1,18
Load Transfer: 36,2% 27,7% 36,2% / 36,2% 27,7% 36,2%

Analyzed Location
Last row in strap between sheet 1 and strap
Sheet 1

FML lay-up:	Glare 2B-7/6-0,4
Thickness:	4,396 mm
Alloy:	2024T3
Prepreg:	S2-glass, FM-94/BR127, 120°C curing
Orientation:	Rolling direction in Al layers perpendicular to loading direction

Sheet 2

FML lay-up:	Glare 2B-7/6-0,4
Thickness:	4,396 mm
Alloy:	2024T3
Prepreg:	S2-glass, FM-94/BR127, 120°C curing
Orientation:	Rolling direction in Al layers perpendicular to loading direction

Butt Strap

FML lay-up:	Glare 2B-7/6-0,4
Thickness:	4,396 mm
Alloy:	2024T3
Prepreg:	S2-glass, FM-94/BR127, 120°C curing
Orientation:	Rolling direction in Al layers perpendicular to loading direction

Reference Curve
EK43-51649 (2024T3)

MSD Analysis
Number of scenarios: 100

Results
Initiation (lead crack):
Layer 1:
Mean: N = 3,89E+04 cycles
StdDev: s = 8,38E-02
Layer 2:
Mean: N = 7,42E+04 cycles
Layer 3:
Mean: N = 1,51E+05 cycles
Layer 4:
Mean: N = 3,65E+05 cycles
Layer 5:
Mean: N = 1,76E+06 cycles
Layer 6:
Mean: N = 6,77E+29 cycles
Layer 7:
Mean: N = 6,77E+29 cycles

Endurance:
Mean: N = 1,00E+05 cycles
StdDev: s = 0,00E+00
Calculation stopped after 1,00E+05 cycles

Residual strength:
Mean: S = 0,00E+00
StdDev: s = 0,00E+00

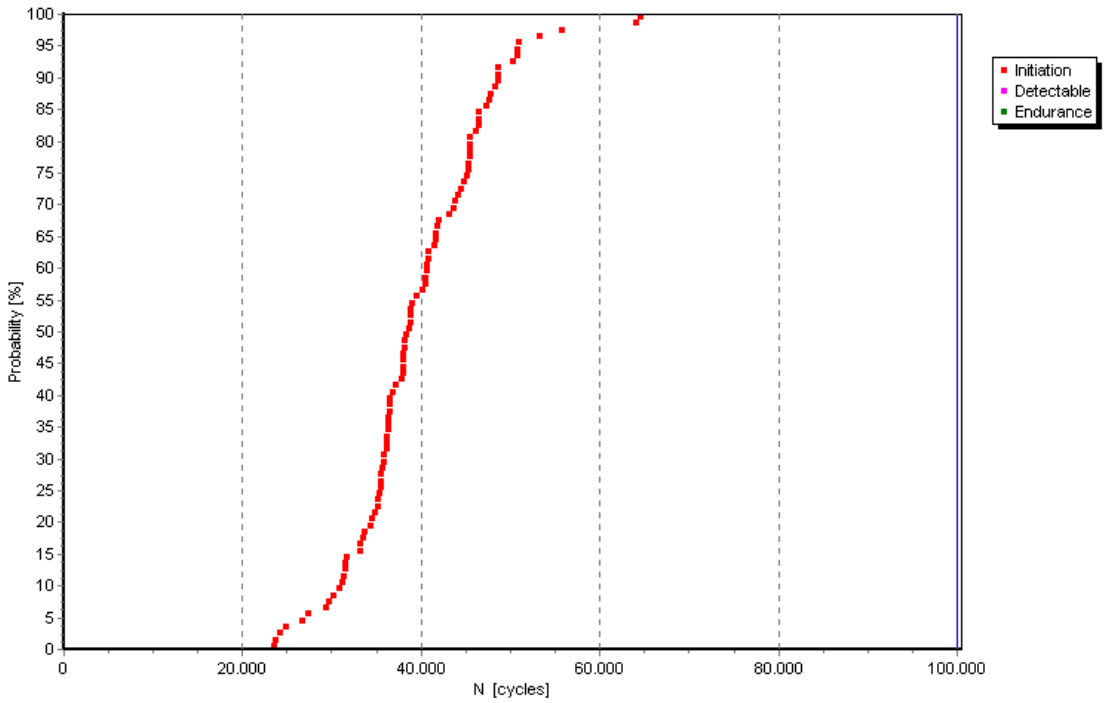

Calculation for maximum stress 88 MPa

Loads
Remote tensile (gross) loads in sheet 1:
Factor on loads: 1.000
Smax = 88.00 MPa
R = 0.100
No Limit Load

Joint Data
Number of holes in a rows: 5
Butt Joint

Number of rivet rows in sheet 1:	3
Number of rivet rows in sheet 2:	3
Rivet pitch in sheet 1:	22.7 mm
Rivet pitch in sheet 2:	22.7 mm
Rivet row distance in sheet 1:	22.7 mm
Rivet row distance in sheet 2:	22.7 mm
Rivet row distance between sheet 1 and 2:	28.0 mm
Rivet diameter in sheet 1:	4.80 mm
Rivet diameter in sheet 2:	4.80 mm

Fastener Data
Hi-Lok, steel/titanium - high interference - collar side
Applied factor on life: 1.18
Load Transfer: 36.2% 27.7% 36.2% / 36.2% 27.7% 36.2%

Analyzed Location
Last row in strap between sheet 1 and strap

Sheet 1

FML lay-up:	Glare 2B-7/6-0.4
Thickness:	4.396 mm
Alloy:	2024T3
Prepreg:	S2-glass, FM-94/BR127, 120°C curing
Orientation:	Rolling direction in Al layers perpendicular to loading direction

Sheet 2

FML lay-up:	Glare 2B-7/6-0.4
Thickness:	4.396 mm
Alloy:	2024T3
Prepreg:	S2-glass, FM-94/BR127, 120°C curing
Orientation:	Rolling direction in Al layers perpendicular to loading direction

Butt Strap

FML lay-up:	Glare 2B-7/6-0.4
Thickness:	4.396 mm
Alloy:	2024T3
Prepreg:	S2-glass, FM-94/BR127, 120°C curing
Orientation:	Rolling direction in Al layers perpendicular to loading direction

Reference Curve
EK43-51649 (2024T3)

MSD Analysis
Number of scenarios: 100

Results
Initiation (lead crack):
Layer 1:
Mean: N = 2.35E+04 cycles
StdDev: s = 8.90E-02
Layer 2:
Mean: N = 4.69E+04 cycles
Layer 3:
Mean: N = 9.69E+04 cycles
Layer 4:
Mean: N = 2.25E+05 cycles
Layer 5:
Mean: N = 7.60E+05 cycles
Layer 6:
Mean: N = 6.76E+29 cycles
Layer 7:
Mean: N = 6.76E+29 cycles

Detectable (lead crack):
Mean: N = 2.62E+04 cycles
StdDev: s = 7.70E-02

Endurance:
Mean: N = 5.00E+04 cycles
StdDev: s = 1.30E-14
Calculation stopped after 5.00E+04 cycles

Residual strength:
Mean: S = 0.00E+00
StdDev: s = 0.00E+00

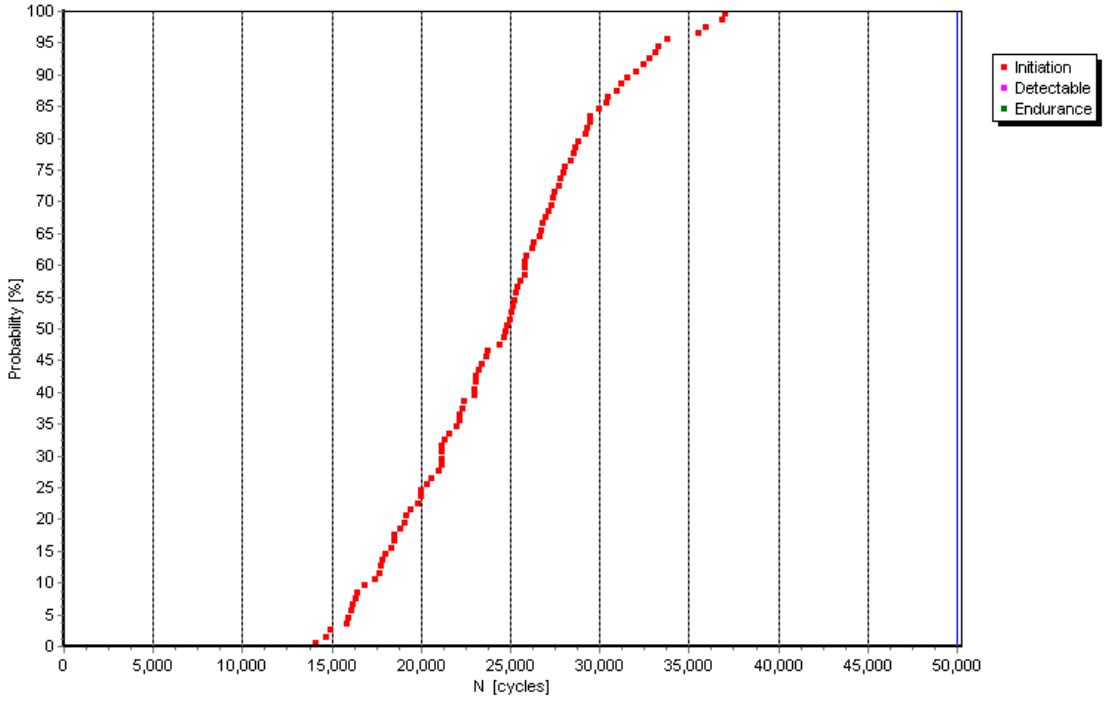

B
Calculation of Stresses in the Aluminium Layers of GLARE2B-7/6-.4 Specimens

Reference chapter 6.2

The calculation of stresses in the aluminum layers of GLARE has been invented by Kieboom [1]. The stress level is dependant on the external load, the stiffnesses of both, the aluminum layers and the glass fiber prepregs, and the applied material temperature. However, since the crack initiation life of GLARE increases at temperatures below zero degrees Celsius, it is recommended to investigate the material behaviour at room temperature in order to take a conservative approach.

$$\sigma_m = \sigma_{m,curing} + \sigma_{m,applied} \quad (1)$$

$$\sigma_{m,curing} = A_m \times \Delta T \times (CTE_{laminate} - CTE_m) \quad (2)$$

$$\sigma_{m,applied} = \sigma_t \times t_t / (t_m + (E_c/E_m) \times t_c) \quad (3)$$

The stiffness matrix can be calculated with

$$A_m = \begin{bmatrix} \frac{E_m}{1-\nu_m^2} & \frac{\nu_m \cdot E_m}{1-\nu_m^2} \\ \frac{\nu_m \cdot E_m}{1-\nu_m^2} & \frac{E_m}{1-\nu_m^2} \end{bmatrix} = 0.10864 \times 10^6 \text{ MPa.} \quad (4)$$

The curing temperature for GLARE is 120°C, the room temperature in the laboratory at Delft University is estimated with 20°C.

Temperature difference ΔT: 100 °C.

Thickness t_t for GLARE2B-7/6-.4: 4.3mm
Thickness t_m for GLARE2B-7/6-.4: 2.8mm
Thickness t_c for GLARE2B-7/6-.4: 1.5mm

Elasticity modulus E_m for 2024 [18]: 72000 MPa
Elasticity modulus E_c for the prepreg [34]: 48900 MPa

Gross section A_g= 493.6mm^2
Net section A_n = 390.4mm^2

CTE_{2024} = 2.25E-05 1/°C [1]
$CTE_{laminate}$ = 1.68E-05 1/°C [35]

Calculation of applied gross stresses and net stresses in tabular form:

Specimen	F_{max}	S_{tgross}	S_{tnet}	$S_{m\ curing}$	$S_{m\ app.\ gross}$	$S_{m\ app.\ net}$	$S_{m\ gross}$	$S_{m\ net}$
Unit	N	[MPa]	[MPa]	[MPa]	[MPa]	[MPa]	[MPa]	[MPa]
3-B-1	69100	140	177	62	158	199	220	261
3-B-10	107500	218	276	62	245	310	307	372
3-B-11	88300	179	226	62	202	255	263	317

C
FEM Calculations for Fatigue Cracked GLARE2B-7/6-.4

Reference chapter 7.1.8.1

A beam is composed as GLARE2B-7/6-.4 material with the FE software STRESSCHECK® :

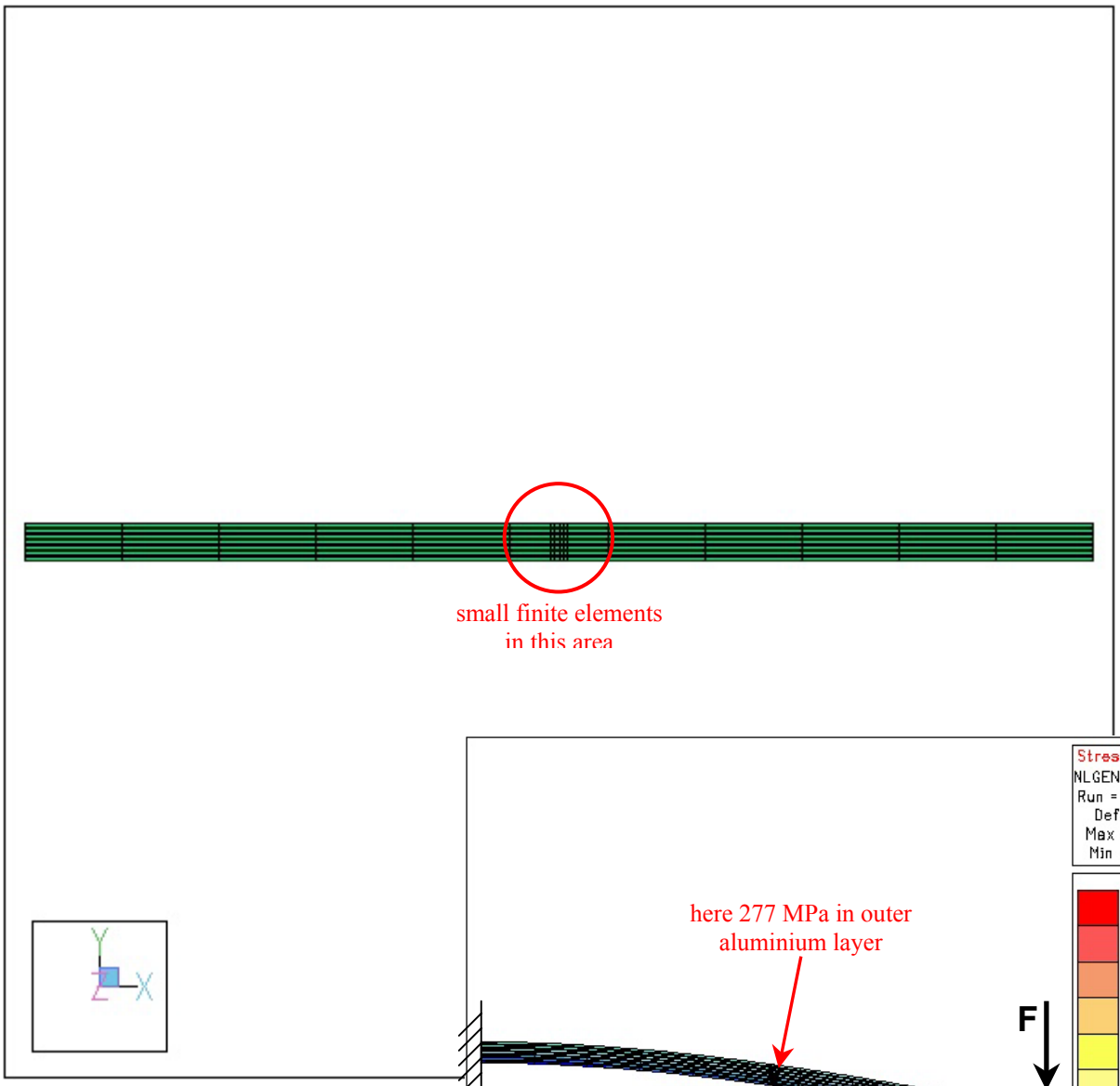

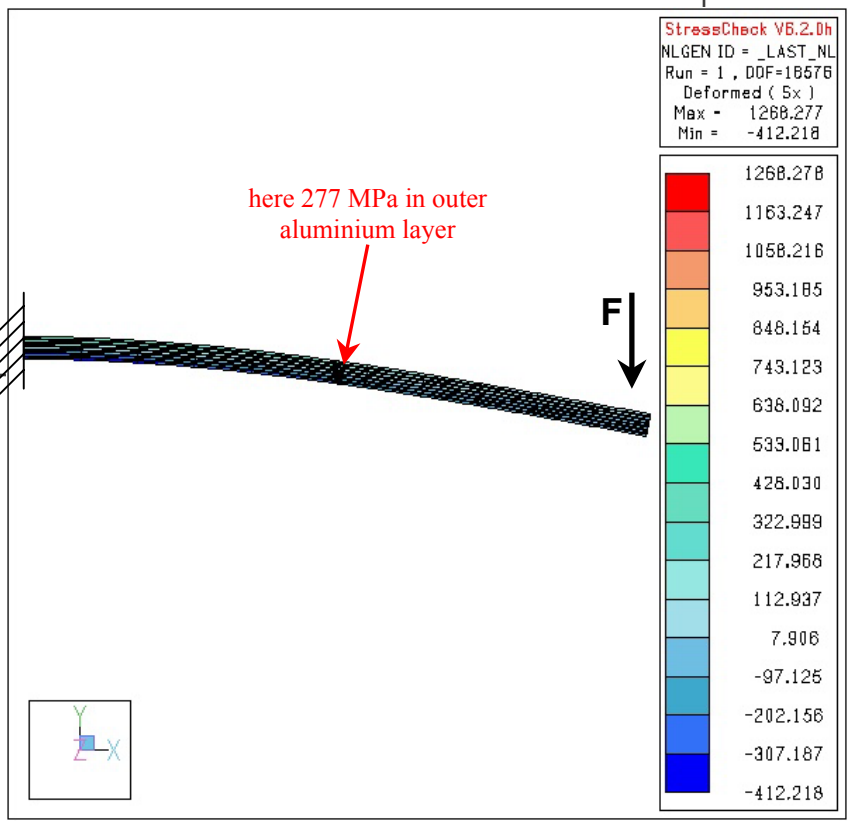

The GLARE beam is clamped on the left side and a load is applied on the right side, until 277 MPa is achieved in the non fatigue outer aluminum layer of the laminate at the small element location :

Then, the outer aluminum layer is cut, simulating a fatigue crack. Two finite elements representing the top aluminum layer on both sides of the 'crack' are disconnected from the first prepreg layer, and the same load is applied as on the non-fatigued model before :

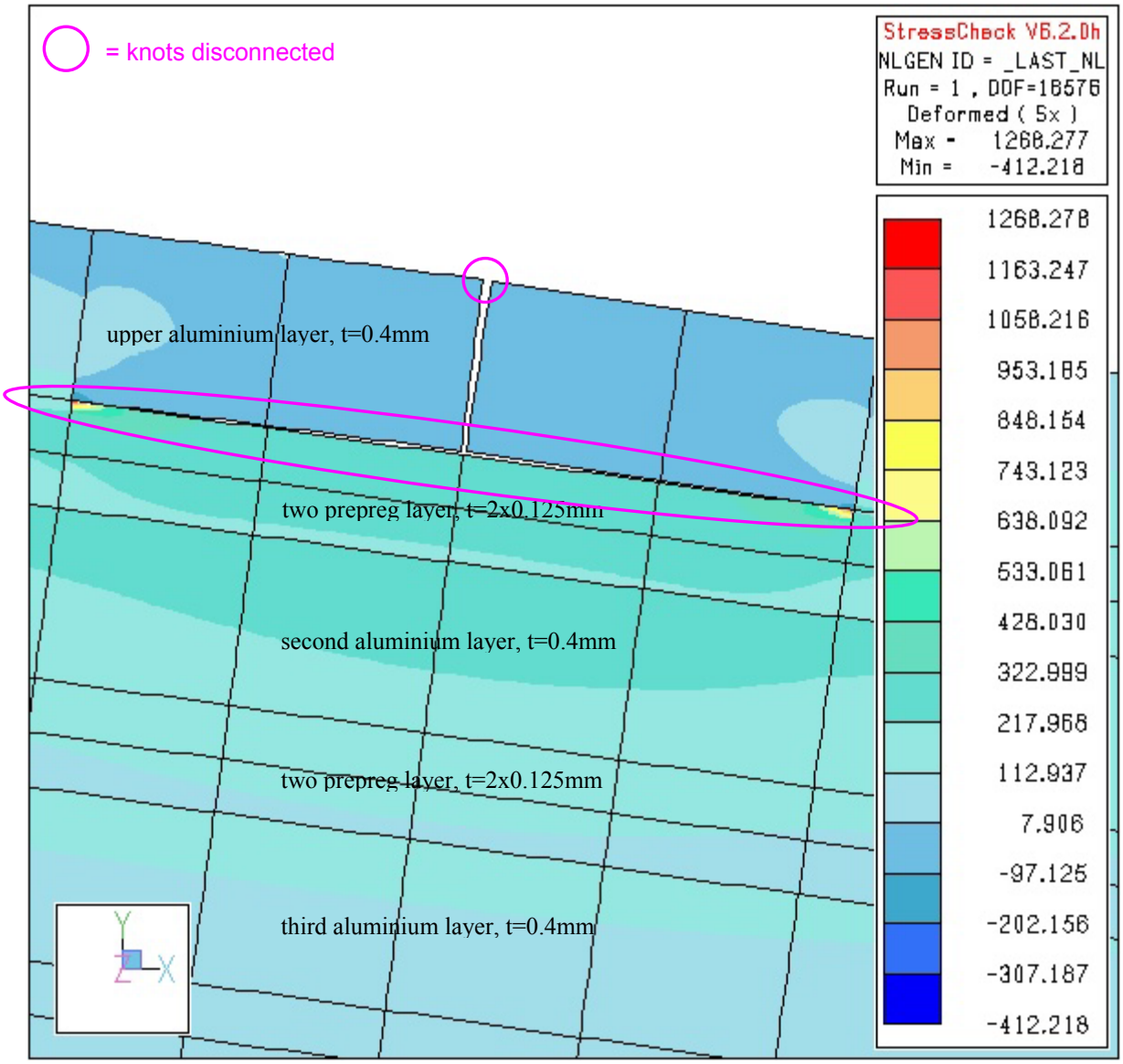

The non-linear calculation shows local stress concentrations in the fibers at the bond line between the disconnected upper aluminum layer (representing the fatigue delamination) and the first fiber prepreg. The local fiber stresses exceed 1200 MPa. Fiber failure is expected at stress values > 1500 MPa, according to the material specification.

D
Determination of Prepreg Weight Gain in MRS

Reference chapters 4 and 5

The prepreg weight of a moisture reference specimen with open holes is determined as follows:

l = 130 mm
w = 130 mm
t_{layer} = 0.133 mm
n = 20 layers
r = 2.4 mm
m = 25 holes

$\rho_{prepreg} = 1.98\ 10^{-3}$ g/mm^3

$V_{prepreg} = (l \times w - m \times \pi \times r^2) \times n \times t = (130 \times 130 - 25 \times \pi \times (2.4)^2) \times 20 \times 0.133$
$= 43751$ mm^3

$m_{prepreg} = V_{prepreg} \times \rho_{prepreg} = 44954 \times 1.98\ 10^{-3} = 86.6$ g

This value can then be used to calculate the weight increase as a percentage of prepreg weight.

As an extra check, the weight of the aluminum layers is determined:

l = 150 mm
w = 150 mm
t_{layer} = 0.2 mm
n = 2 layers
r = 2.4 mm
m = 25 holes

$\rho_{Al} = 2.67\ 10^{-3}$ g/mm^3

$V_{Al} = (l \times w - m \times \pi \times r^2) \times n \times t = (150 \times 150 - 25 \times \pi \times (2.4)^2) \times 2 \times 0.2$
$= 8819$ mm^3

$m_{Al} = V_{Al} \times \rho_{Al} = 8819 \times 2.67\ 10^{-3} = 23.5$ g

The total weight of the specimen with open holes should therefore be approximately 110.1 g. This is somewhat lower than the actual weight of specimen T2 at the start of exposure, which was 112.021 g. This small difference can be the result of the extra adhesive that was used to bond the edges of the specimens. Other causes might be some deviations in specimen dimensions or the presence of moisture.
The weight of a Lok-Bolt with collar and washer is approximately 0.88 g, therefore the total weight of the fasteners is 25 x 0.88 = 22.0 g. As a result, the calculated weight of the specimen with fasteners should be approximately 110.1 + 22.0 = 132.1 g. This is somewhat higher than the weight of specimen 8-8, which was 130.969 g at the start of exposure.
If it is assumed that without the paint, specimen 8-9 is similar to 8-8, then the weight of the paint can be determined by their weight difference. At the start of accelerated exposure this would have been 136.008 – 130.969 = 5.039 g.

E
Meteorological Record 14.1.2002

Reference chapter 5

Meteorological data provided by DSTO						
Date	Time	Dry Bulb (°C)	Wet Bulb (°C)	Wind Direction (°)	Solar(MJ/m²)	Rain(mm)
14. Jan 02	00:00	24,3	23,4	323	35	
14. Jan 02	00:10	24,7	23,5	323	35	
14. Jan 02	00:20	24,5	23,5	323	33	
14. Jan 02	00:30	24,6	23,5	324	34	
14. Jan 02	00:40	25,7	23,5	301	36	
14. Jan 02	00:50	25,6	23,6	236	34	
14. Jan 02	01:00	25,2	23,9	221	33	
14. Jan 02	01:10	24,8	23,8	222	31	
14. Jan 02	01:20	24,5	23,8	221	29	
14. Jan 02	01:30	24,4	23,7	222	28	
14. Jan 02	01:40	24,5	23,6	222	26	
14. Jan 02	01:50	24,5	23,7	221	25	
14. Jan 02	02:00	25,1	23,4	221	26	
14. Jan 02	02:10	25,2	23,5	221	26	
14. Jan 02	02:20	25,0	23,5	221	25	
14. Jan 02	02:30	24,8	23,4	221	25	
14. Jan 02	02:40	24,6	23,4	221	24	
14. Jan 02	02:50	24,6	23,3	221	24	
14. Jan 02	03:00	25,1	23,3	222	24	
14. Jan 02	03:10	24,9	23,4	222	23	
14. Jan 02	03:20	24,8	23,1	222	21	
14. Jan 02	03:30	24,5	23,3	222	22	
14. Jan 02	03:40	24,8	23,1	222	23	
14. Jan 02	03:50	24,6	23,6	222	23	
14. Jan 02	04:00	24,3	23,5	177	19	
14. Jan 02	04:10	24,3	23,5	177	17	
14. Jan 02	04:20	24,3	23,3	177	18	
14. Jan 02	04:30	24,5	23,3	180	20	
14. Jan 02	04:40	24,9	22,9	310	21	
14. Jan 02	04:50	25,1	23,1	272	23	
14. Jan 02	05:00	24,7	23,4	268	23	
14. Jan 02	05:10	24,4	23,3	243	21	
14. Jan 02	05:20	24,6	22,9	216	23	
14. Jan 02	05:30	24,7	22,8	211	22	
14. Jan 02	05:40	24,7	22,7	178	22	
14. Jan 02	05:50	24,7	22,7	215	22	
14. Jan 02	06:00	24,6	22,7	119	26	
14. Jan 02	06:10	24,4	22,9	118	29	
14. Jan 02	06:20	24,6	22,9	118	58	
14. Jan 02	06:30	24,9	23,3	118	96	
14. Jan 02	06:40	25,0	23,5	164	139	
14. Jan 02	06:50	26,0	23,6	154	184	
14. Jan 02	07:00	26,8	23,8	160	240	
14. Jan 02	07:10	27,4	23,7	162	211	
14. Jan 02	07:20	27,0	23,6	268	137	

14. Jan 02	07:30	26,3	23,8	268	172	
14. Jan 02	07:40	27,0	23,6	279	200	
14. Jan 02	07:50	26,9	24,0	254	185	
14. Jan 02	08:00	27,7	24,8	273	367	
14. Jan 02	08:10	29,1	24,7	158	529	
14. Jan 02	08:20	29,3	24,5	265	547	
14. Jan 02	08:30	29,2	24,7	214	521	
14. Jan 02	08:40	29,4	24,5	263	567	
14. Jan 02	08:50	29,9	24,5	238	551	
14. Jan 02	09:00	30,4	24,5	186	598	
14. Jan 02	09:10	30,8	24,5	290	585	
14. Jan 02	09:20	30,9	24,7	215	542	
14. Jan 02	09:30	31,4	24,7	270	578	
14. Jan 02	09:40	32,2	25,2	92	629	
14. Jan 02	09:50	31,9	25,2	145	584	
14. Jan 02	10:00	32,6	25,7	46	612	
14. Jan 02	10:10	33,0	25,8	63	723	
14. Jan 02	10:20	32,7	25,5	84	610	
14. Jan 02	10:30	33,2	25,6	61	803	
14. Jan 02	10:40	33,3	25,6	15	850	
14. Jan 02	10:50	33,4	25,6	151	881	
14. Jan 02	11:00	34,0	25,8	124	911	
14. Jan 02	11:10	34,1	25,7	38	807	
14. Jan 02	11:20	33,8	25,7	42	607	
14. Jan 02	11:30	34,3	26,2	128	697	
14. Jan 02	11:40	34,1	25,8	339	445	
14. Jan 02	11:50	34,2	26,1	347	598	
14. Jan 02	12:00	34,3	26,4	11	528	
14. Jan 02	12:10	33,7	25,9	345	474	
14. Jan 02	12:20	33,4	25,9	100000	444	
14. Jan 02	12:30	33,1	25,8	327	372	
14. Jan 02	12:40	32,6	25,2	336	463	
14. Jan 02	12:50	33,4	25,3	288	848	
14. Jan 02	13:00	34,4	26,0	6	914	
14. Jan 02	13:10	33,5	25,4	355	575	
14. Jan 02	13:20	33,6	25,5	341,0	667	
14. Jan 02	13:30	34,2	25,9	301,0	837	
14. Jan 02	13:40	33,8	25,6	70,0	556	
14. Jan 02	13:50	34,2	25,9	8,0	845	
14. Jan 02	14:00	34,2	26,1	5,0	602	
14. Jan 02	14:10	34,5	26,3	304,0	711	
14. Jan 02	14:20	34,1	26,6	99999,9	432	
14. Jan 02	14:30	33,8	26,3	354,0	530	
14. Jan 02	14:40	33,5	26,4	337,0	469	
14. Jan 02	14:50	32,9	26,1	10,0	442	
14. Jan 02	15:00	33,4	26,2	41,0	599	
14. Jan 02	15:10	33,8	26,6	325,0	505	
14. Jan 02	15:20	33,9	26,4	22,0	563	
14. Jan 02	15:30	34,5	26,7	39,0	757	
14. Jan 02	15:40	34,6	26,7	332,0	611	
14. Jan 02	15:50	34,1	26,6	9,0	412	
14. Jan 02	16:00	33,2	26,4	308,0	116	
14. Jan 02	16:10	32,9	26,6	302,0	87	
14. Jan 02	16:20	32,1	26,4	279,0	54	
14. Jan 02	16:30	29,7	25,7	344,0	84	
14. Jan 02	16:40	28,4	26,4	323,0	191	

14. Jan 02	16:50	28,1	26,3	297,0	133	0,5
14. Jan 02	17:00	28,0	25,9	271,0	146	
14. Jan 02	17:10	27,9	26,3	232,0	110	
14. Jan 02	17:20	27,0	24,2	114,0	79	
14. Jan 02	17:30	26,2	23,8	147,0	110	
14. Jan 02	17:40	25,8	23,4	207,0	89	
14. Jan 02	17:50	25,8	23,5	188,0	77	
14. Jan 02	18:00	25,7	23,8	188,0	79	
14. Jan 02	18:10	25,9	24,2	294,0	68	
14. Jan 02	18:20	25,7	24,2	294,0	49	
14. Jan 02	18:30	25,7	24,3	294,0	32	
14. Jan 02	18:40	25,6	24,2	244,0	24	
14. Jan 02	18:50	25,5	24,2	265,0	18	
14. Jan 02	19:00	25,7	24,4	317,0	14	
14. Jan 02	19:10	25,7	24,5	311,0	12	
14. Jan 02	19:20	25,5	24,5	311,0	12	
14. Jan 02	19:30	25,7	24,4	311,0	13	
14. Jan 02	19:40	25,6	24,4	257,0	12	
14. Jan 02	19:50	25,8	24,5	286,0	12	
14. Jan 02	20:00	25,9	24,6	290,0	11	
14. Jan 02	20:10	25,8	24,8	2,0	12	
14. Jan 02	20:20	25,7	24,6	2,0	11	
14. Jan 02	20:30	25,8	24,7	2,0	11	
14. Jan 02	20:40	25,8	24,5	334,0	11	
14. Jan 02	20:50	25,5	24,5	333,0	11	
14. Jan 02	21:00	25,5	24,5	295,0	11	
14. Jan 02	21:10	25,6	24,5	295,0	10	
14. Jan 02	21:20	25,4	24,4	295,0	10	
14. Jan 02	21:30	25,3	24,4	295,0	9	
14. Jan 02	21:40	25,2	24,4	295,0	9	
14. Jan 02	21:50	25,2	24,3	295,0	9	
14. Jan 02	22:00	25,1	24,3	295,0	9	
14. Jan 02	22:10	25,1	24,4	295,0	9	
14. Jan 02	22:20	25,0	24,4	295,0	10	
14. Jan 02	22:30	25,0	24,4	295,0	10	
14. Jan 02	22:40	25,0	24,4	206,0	11	
14. Jan 02	22:50	25,1	24,3	248,0	11	
14. Jan 02	23:00	25,2	24,2	233,0	12	
14. Jan 02	23:10	25,3	24,2	254,0	12	
14. Jan 02	23:20	25,5	24,3	260,0	12	
14. Jan 02	23:30	25,4	24,3	267,0	11	
14. Jan 02	23:40	25,3	24,3	180,0	11	
14. Jan 02	23:50	25,3	24,4	180,0	11	
	min	24,3	22,7		9	0,5
	max	34,6	26,7		914,0	0,5
	average	28,1	24,6		234,5	0,5

F
CA Crack Propagation Calculations for Circumferential Joint Coupon

Reference TU Delft / Airbus Computer Program `JOINT´, Release 0.93

See results for one of 100 MSD calculation results for maximum stress 55 MPa:

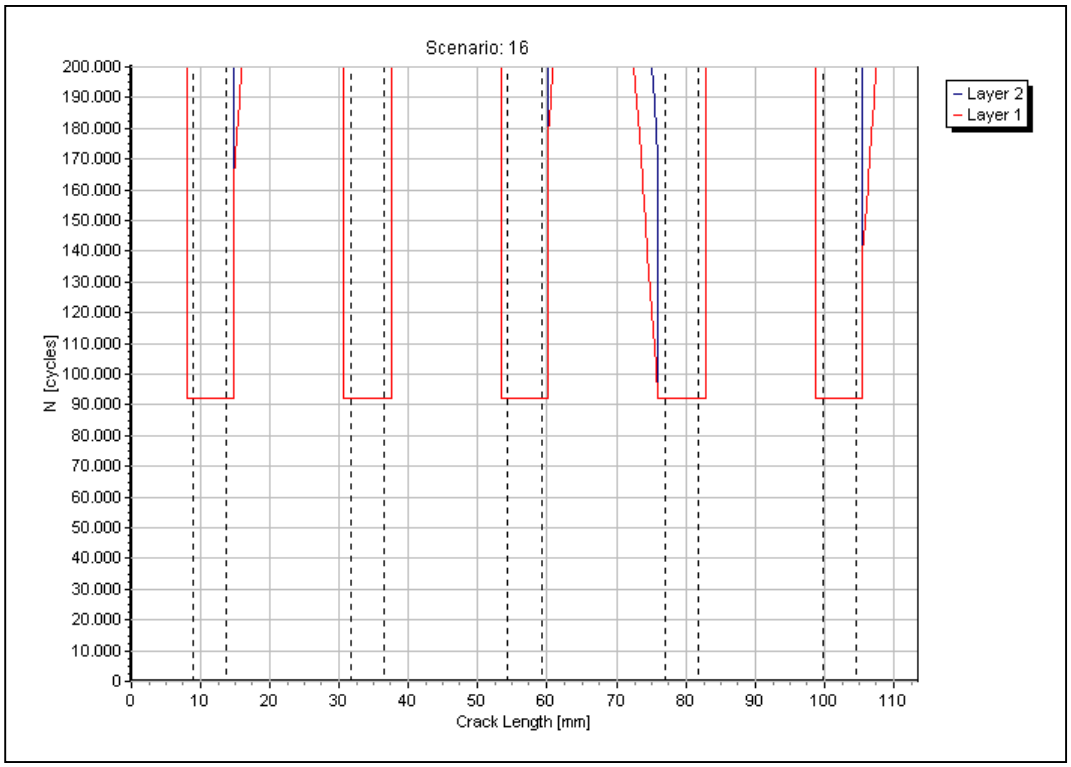

One of 100 MSD calculation results for maximum stress 66 MPa:

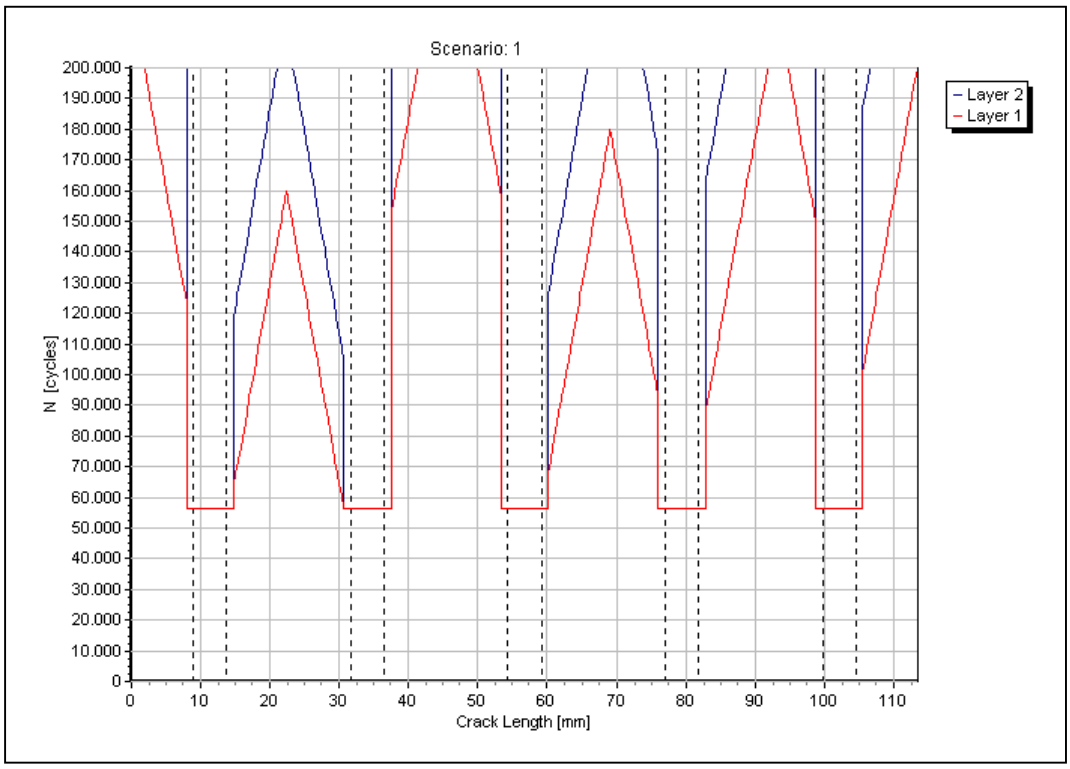

One of 100 MSD calculation results for maximum stress 77 MPa:

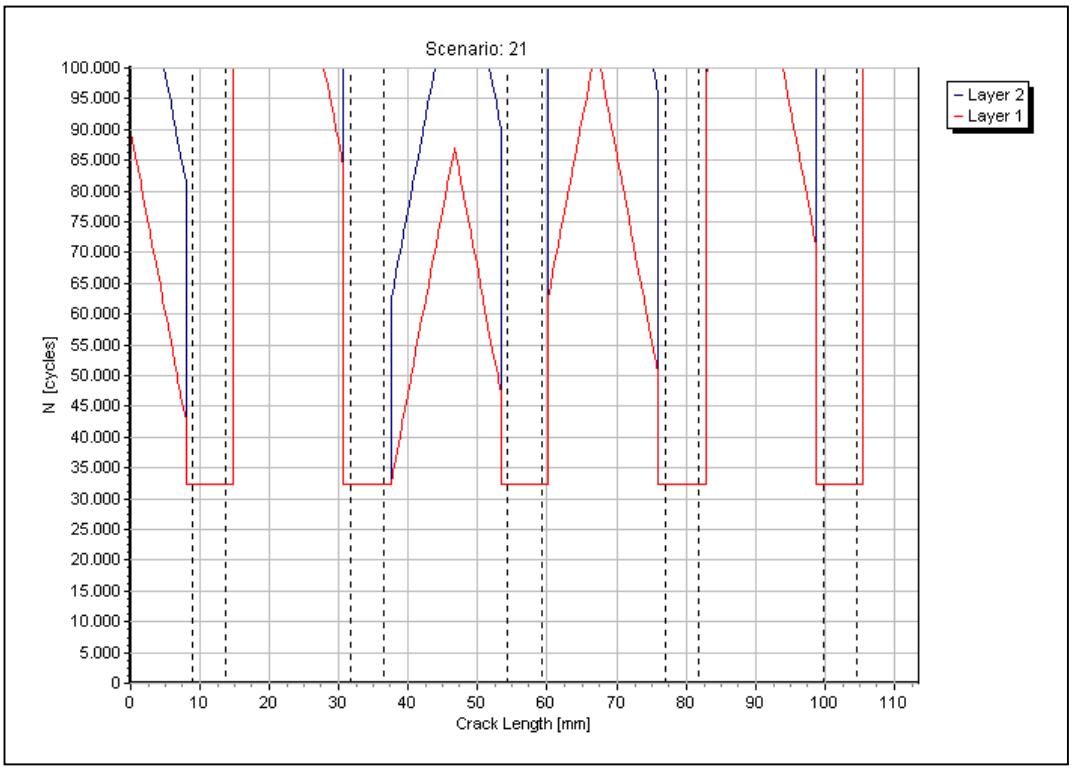

One of 100 MSD calculation results for maximum stress 88 MPa:

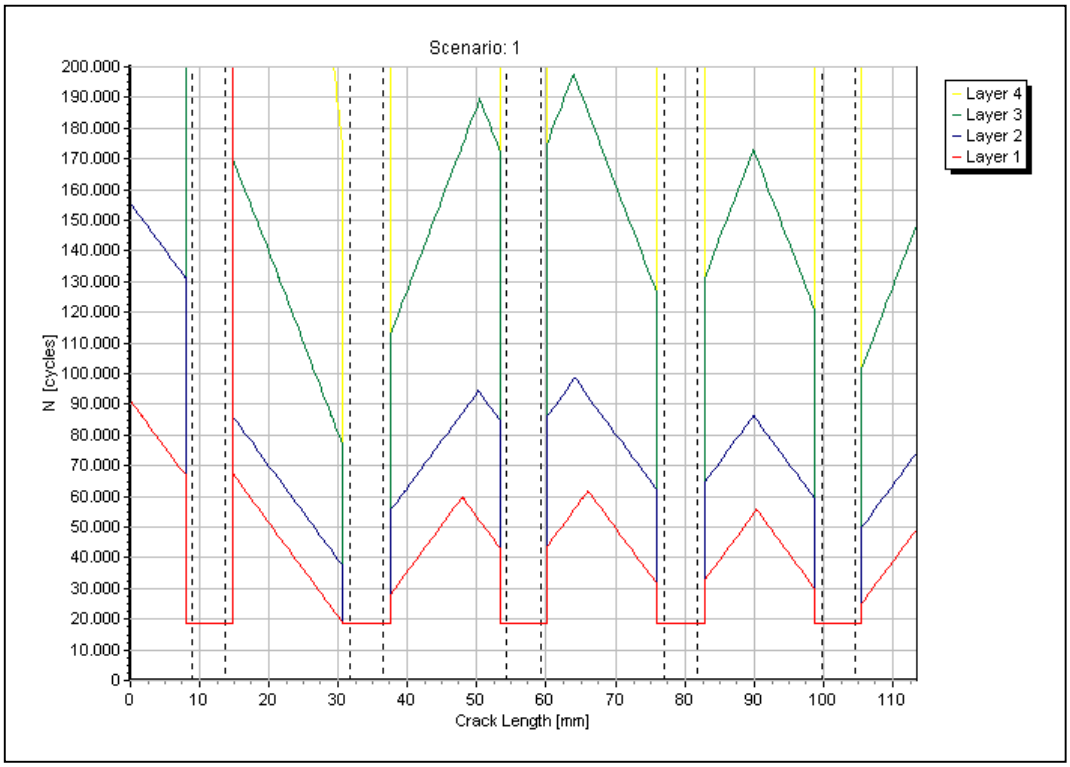

G
Strength Calculation for Megaliner Barrel Repair

Reference chapter 7.2.2

TU Delft / Airbus Computer Program `JOINT´, Release 1.30

Project
Description: Mechanically Fastened Joint
File: specimen 2-A-X-VA-29.8-26.fjt

Joint Data
Type: Lap Joint
Number of rivet rows: 4
Rivet pitch: 28,0 mm
Rivet row distance: 28,0 mm
Rivet diameter: 5,60 mm

Fastener Data
ASN A2026, Hi-Lite - no interference - collar side
Load transfer: 30,9% 19,1% 19,1% 30,9% (Swift's formula for rivet flexibility)

Analyzed Location
Last row in sheet 2

Sheet 1
FML lay-up: Glare 4A-5/4-0,4
Thickness: 3,596 mm
Alloy: 2024T3
Prepreg: S2-glass, FM-94/BR127, 120°C curing
Orientation: Rolling direction in Al layers parallel to loading direction (L-T)

Sheet 2
FML lay-up: Glare 4A-5/4-0,4
Thickness: 3,596 mm
Alloy: 2024T3
Prepreg: S2-glass, FM-94/BR127, 120°C curing
Orientation: Rolling direction in Al layers parallel to loading direction (L-T)

Reference Curve
EK43-51647 (2024T3 Alclad)

Loads
Remote tensile (gross) loads in sheet 1:
Factor on loads: 0,790
Flights in spectrum: 21500

Design Load = 230,000 MPa

Environment
Temperature: 20°C

Calculation options
Maximum growth increment: 10,0 %
Transition initiation-propagation: 1,00 mm
Detectable crack length: 10,80 mm
Propagation Limit: 2,00E+05 cycles/flights
Number of MSD scenarios: 100
Link up criterion: 90% of fastener pitch
Secondary bending: User data

Results

Initiation (lead crack):
Layer 1:
Mean: N = 4,04E+04 flights
Std Dev: s = 7,67E-02
Layer 2:
Mean: N = 5,74E+04 flights
Layer 3:
Mean: N = 6,40E+04 flights
Layer 4:
Mean: N = 7,14E+04 flights
Layer 5:
Mean: N = 7,96E+04 flights

Endurance:
Mean: N = 2,00E+05 flights
Std Dev: s = 2,62E-18

H
SN data from specimen Ek43-51647

Aluminum reference joint for Megaliner Barrel repair calculation

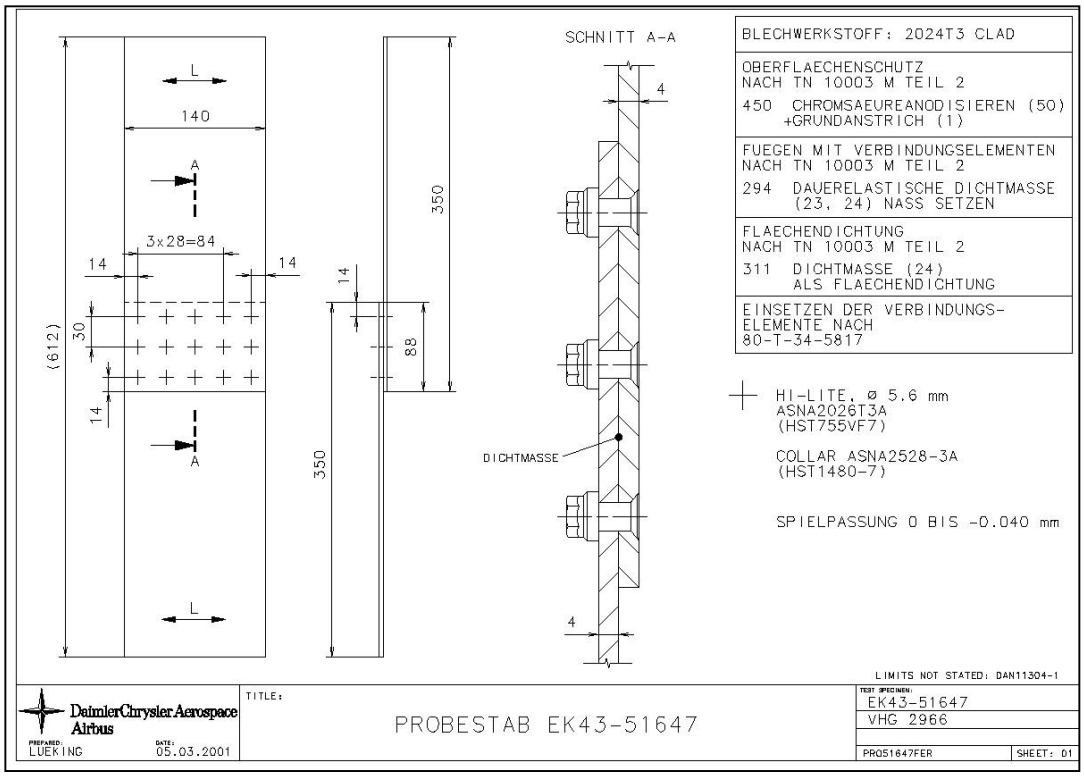

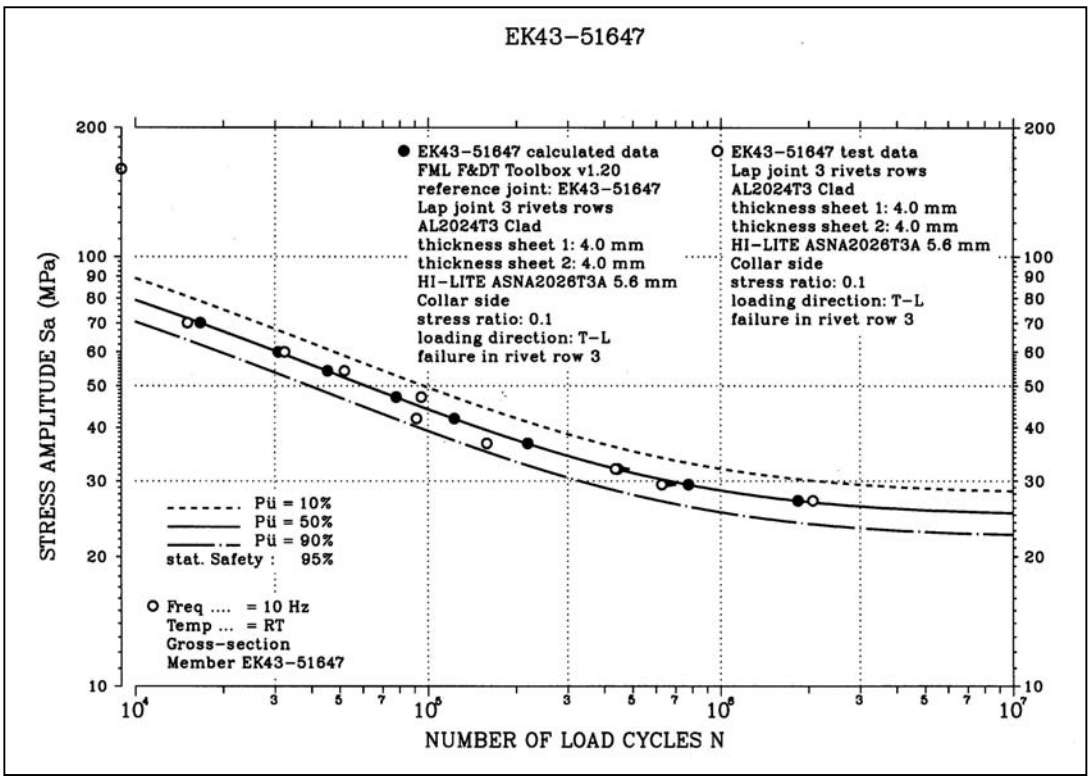

I

F&DT Calculation for A340-600 Artificial GLARE2 Butt Strap

Reference TU Delft / Airbus Computer Program `JOINT´, Release 0.93

Loads
Remote tensile (gross) loads in sheet 1:
Factor on loads: 0,560
Flights in spectrum: 1660

Limit Load = 175,000 MPa

Joint Data
Number of holes in a rows: 5
Butt Joint
Number of rivet rows in sheet 1: 3
Number of rivet rows in sheet 2: 3
Rivet pitch in sheet 1: 22,7 mm
Rivet pitch in sheet 2: 22,7 mm
Rivet row distance in sheet 1: 22,7 mm
Rivet row distance in sheet 2: 22,7 mm
Rivet row distance between sheet 1 and 2: 29,0 mm
Rivet diameter in sheet 1: 4,80 mm
Rivet diameter in sheet 2: 4,80 mm

Fastener Data
Hi-Lok, steel/titanium - high interference - collar side
Applied factor on life: 1,18
Load Transfer: 36,2% 27,7% 36,2% / 36,2% 27,7% 36,2%

Analyzed Location
Last row in strap between sheet 1 and strap
Sheet 1

FML lay-up: Glare 2B-7/6-0,4
Thickness: 4,396 mm
Alloy: 2024T3
Prepreg: S2-glass, FM-94/BR127, 120°C curing
Orientation: Rolling direction in Al layers perpendicular to loading direction

Sheet 2
FML lay-up: Glare 2B-7/6-0,4
Thickness: 4,396 mm
Alloy: 2024T3
Prepreg: S2-glass, FM-94/BR127, 120°C curing
Orientation: Rolling direction in Al layers perpendicular to loading direction

Butt Strap
FML lay-up: Glare 2B-7/6-0,4
Thickness: 4,396 mm
Alloy: 2024T3
Prepreg: S2-glass, FM-94/BR127, 120°C curing
Orientation: Rolling direction in Al layers perpendicular to loading direction

Reference Curve
EK43-51649 (2024T3)

MSD Analysis
Number of scenarios: 100

Results

Initiation (lead crack):
Layer 1:
Mean: N = 2,17E+05 flights
StdDev: s = 9,34E-02
Layer 2:
Mean: N = 4,61E+05 flights
Layer 3:
Mean: N = 1,38E+06 flights
Layer 4:
Mean: N = 1,12E+08 flights
Layer 5:
Mean: N = 3,85E+29 flights
Layer 6:
Mean: N = 3,85E+29 flights
Layer 7:
Mean: N = 3,85E+29 flights

Endurance:
Mean: N = 4,00E+05 flights
StdDev: s = 3,92E-18
Calculation stopped after 4,00E+05 schedules

J

VA Crack Propagation Calculations for Circumferential Joint Coupon

Reference TU Delft / Airbus Computer Program `JOINT´, Release 0.93

Factor 0.56 applied in order to account for thickness relation: strain gauge measurement position / butt strap thickness (2.4/4.3).

Stress spectrum according to appendix A.

Loads
Remote tensile (gross) loads in sheet 1:
Factor on loads: 0,560
Flights in spectrum: 1660
N Smax Smin
No Limit Load

Joint Data
Number of holes in a rows: 5
Butt Joint
Number of rivet rows in sheet 1: 3
Number of rivet rows in sheet 2: 3
Rivet pitch in sheet 1: 22,7 mm
Rivet pitch in sheet 2: 22,7 mm
Rivet row distance in sheet 1: 22,7 mm
Rivet row distance in sheet 2: 22,7 mm
Rivet row distance between sheet 1 and 2: 28,0 mm
Rivet diameter in sheet 1: 4,80 mm
Rivet diameter in sheet 2: 4,80 mm

Fastener Data
Hi-Lok, steel/titanium - high interference - collar side
Applied factor on life: 1,18
Load Transfer: 36,2% 27,7% 36,2% / 36,2% 27,7% 36,2%

Analyzed Location
Last row in strap between sheet 1 and strap
Sheet 1

FML lay-up: Glare 2B-7/6-0,4
Thickness: 4,396 mm
Alloy: 2024T3
Prepreg: S2-glass, FM-94/BR127, 120°C curing
Orientation: Rolling direction in Al layers perpendicular to loading direction

Sheet 2
FML lay-up: Glare 2B-7/6-0,4
Thickness: 4,396 mm
Alloy: 2024T3
Prepreg: S2-glass, FM-94/BR127, 120°C curing
Orientation: Rolling direction in Al layers perpendicular to loading direction

Butt Strap
FML lay-up: Glare 2B-7/6-0,4
Thickness: 4,396 mm
Alloy: 2024T3
Prepreg: S2-glass, FM-94/BR127, 120°C curing
Orientation: Rolling direction in Al layers perpendicular to loading direction

Reference Curve
EK43-51649 (2024T3)

MSD Analysis
Number of scenarios: 100

Results
Initiation (lead crack):
Layer 1:
Mean: N = 1,47E+05 flights
StdDev: s = 9,94E-02
Layer 2:
Mean: N = 3,70E+05 flights
Layer 3:
Mean: N = 1,16E+06 flights
Layer 4:
Mean: N = 1,93E+08 flights
Layer 5:
Mean: N = 1,13E+29 flights

Layer 6:
Mean: N = 1,13E+29 flights
Layer 7:
Mean: N = 1,13E+29 flights

K
Preparation of Flat Bonded Repair Panels for Bonding
(Airbus facilities, Bremen)

Appendix to chapter 9

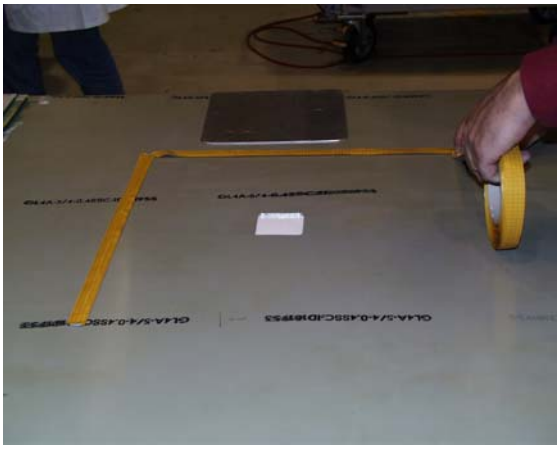

Rear side of repair panel

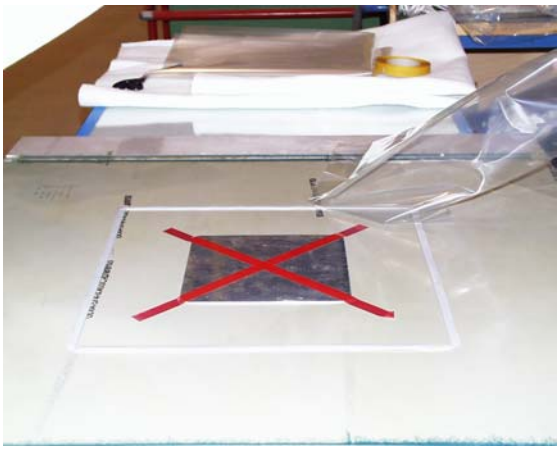

Rear side of repair panel
tightened with aluminium sheet

Rear side of repair panel,
application of bleeder material and
subsequently vacuum foil

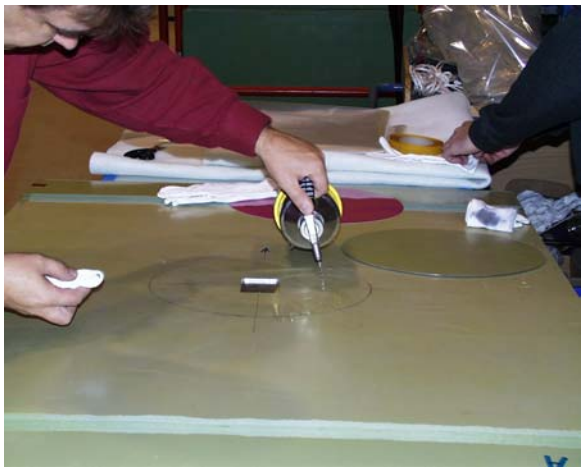

Front side of panel, application of cleaning agent according to Airbus technical instruction 80-T-35-0014

Cleaning of bonding surface

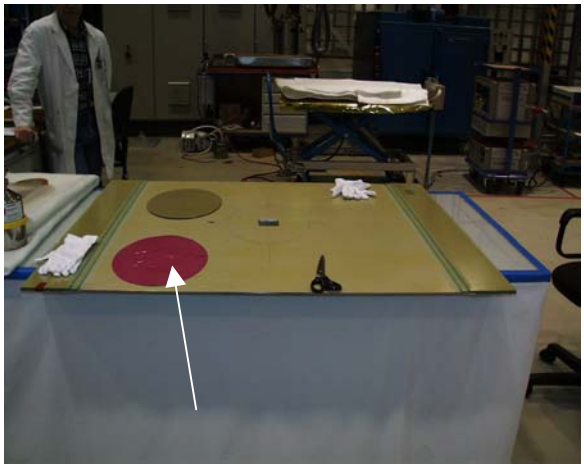

FM94 K06 bonding film cut to shape

Fixation of GLARE patch in order to avoid movement during curing

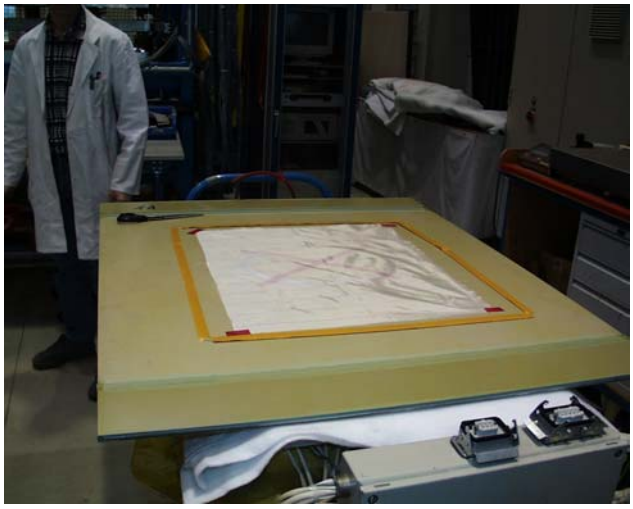

Application of bleeding material

Fixation of thermo couples

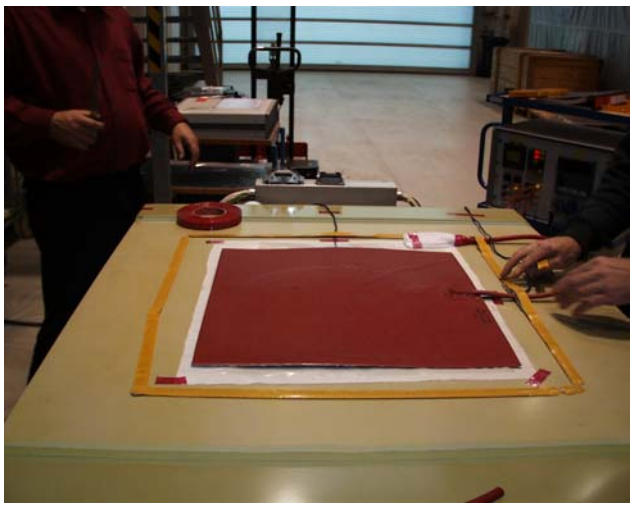

Application of heating rubber

Application of vacuum foil, thereafter start of curing with Heatcom® device, low vacuum pressure
(for specimens 12-BR-1 and 12-BR-2)

For specimens 12-BR-03 to 12-BR-05: curing in autoclave at 3 bar vacuum pressure

L
One Dimensional Diffusion Depth Calculation Results, Computer Program W8GAIN, GLARE3 Open Bore Holes, Environment 70°C/85%RH, t = 28mm, D = 4.8mm

Data used for diffusion depth directions 0 degree and 90 degree from bore hole

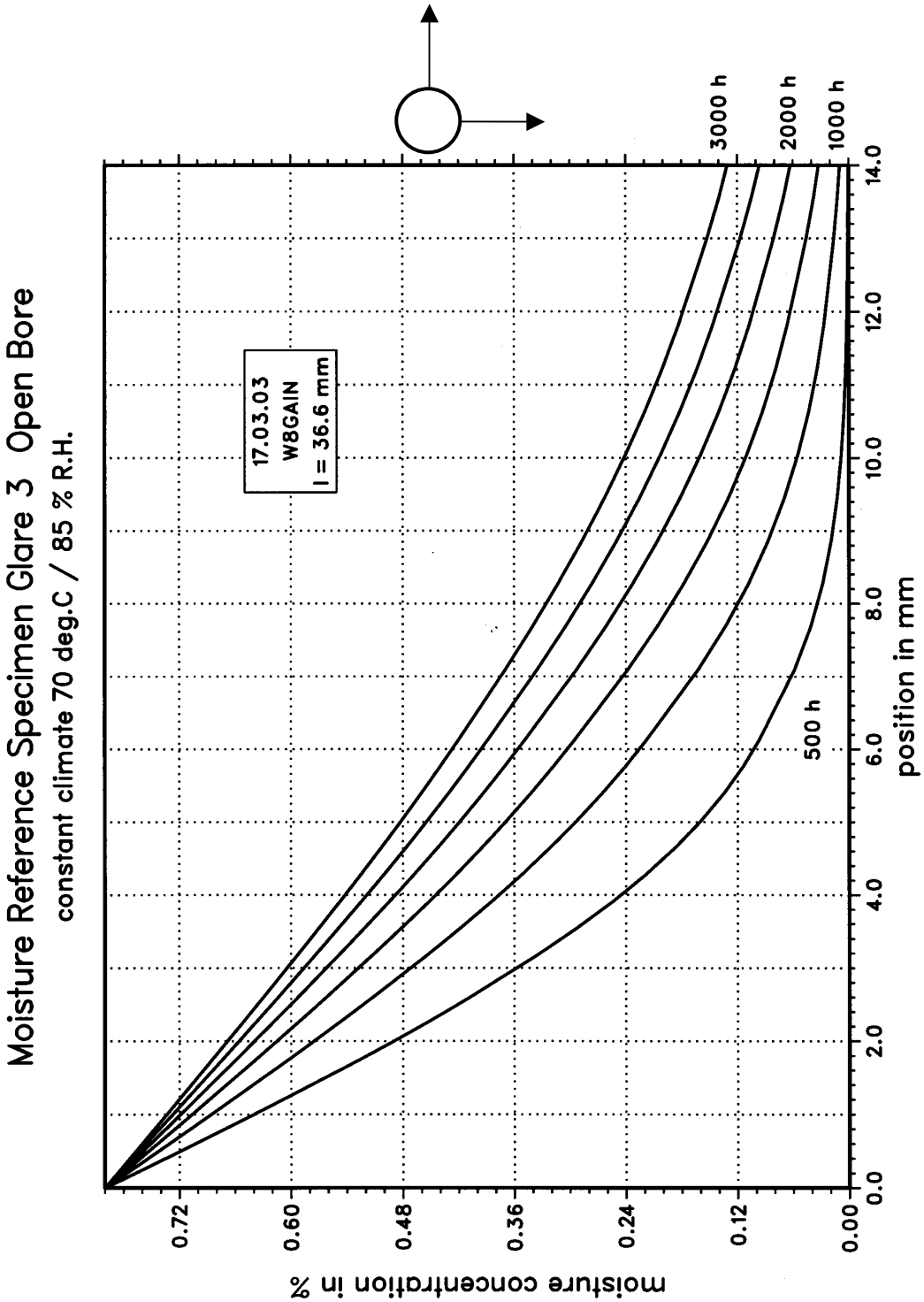

Data used for diffusion depth directions 22.5 degree and 67.5 degree from bore hole

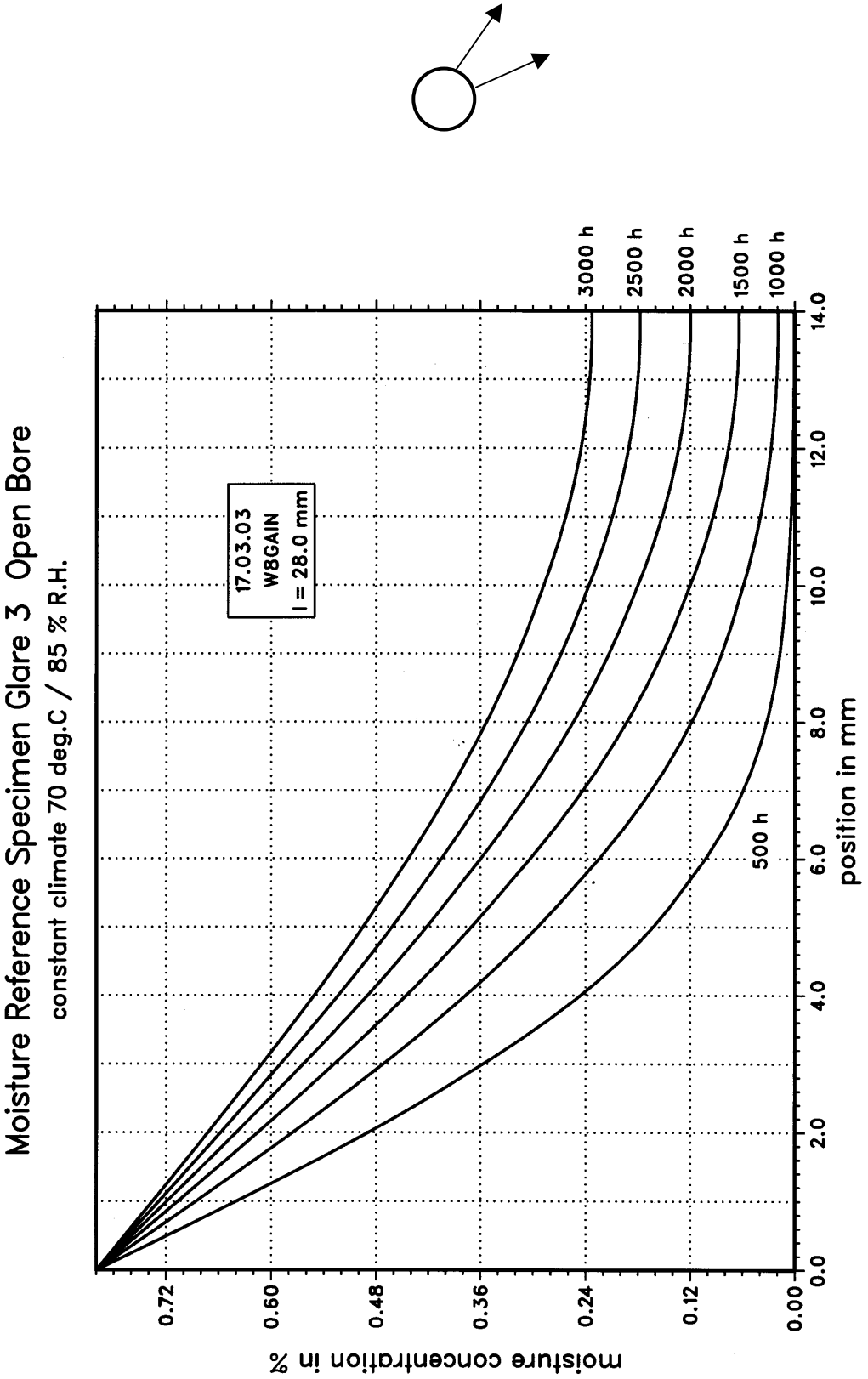

Data used for diffusion depth directions 45 degree from bore hole

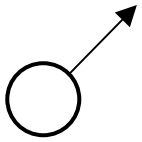

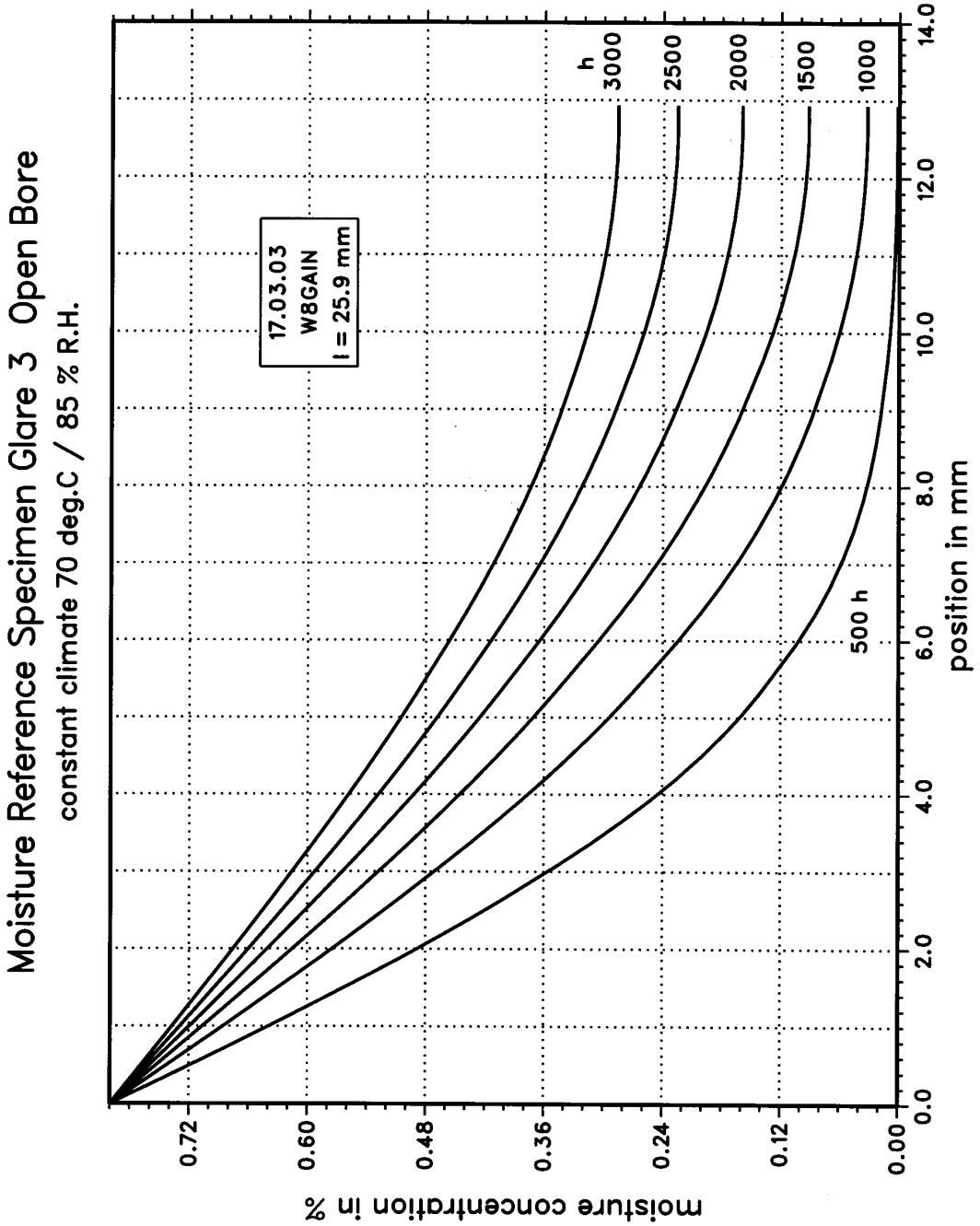

M
One Dimensional Diffusion Depth Calculation Results, Computer Program W8GAIN, GLARE3 Filled Bore Holes, Environment 70°C/85%RH, t = 28mm, D = 4.8mm

Data used for diffusion depth directions 0 degree and 90 degree from bore hole

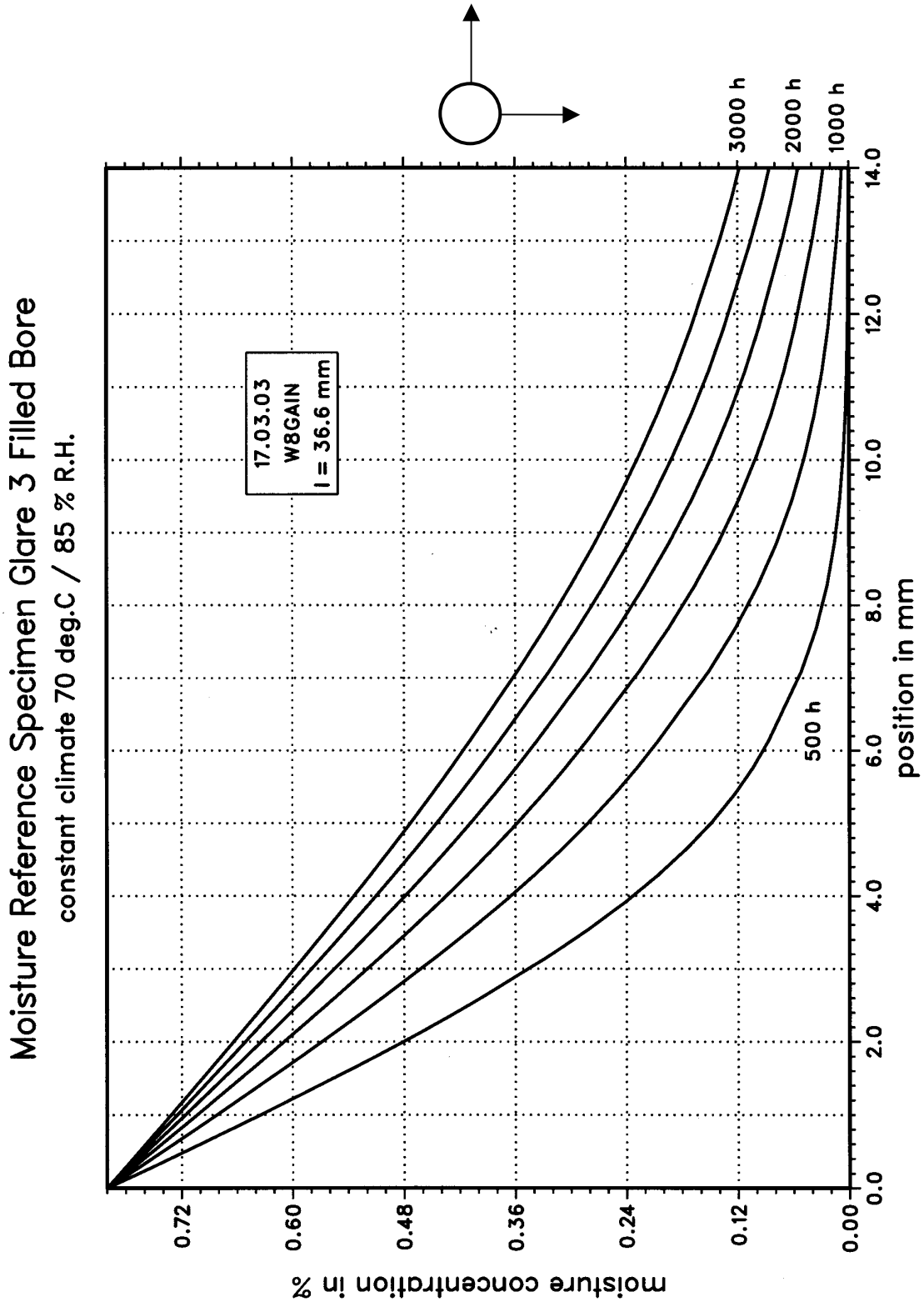

Data used for diffusion depth directions 22.5 degree and 67.5 degree from bore hole

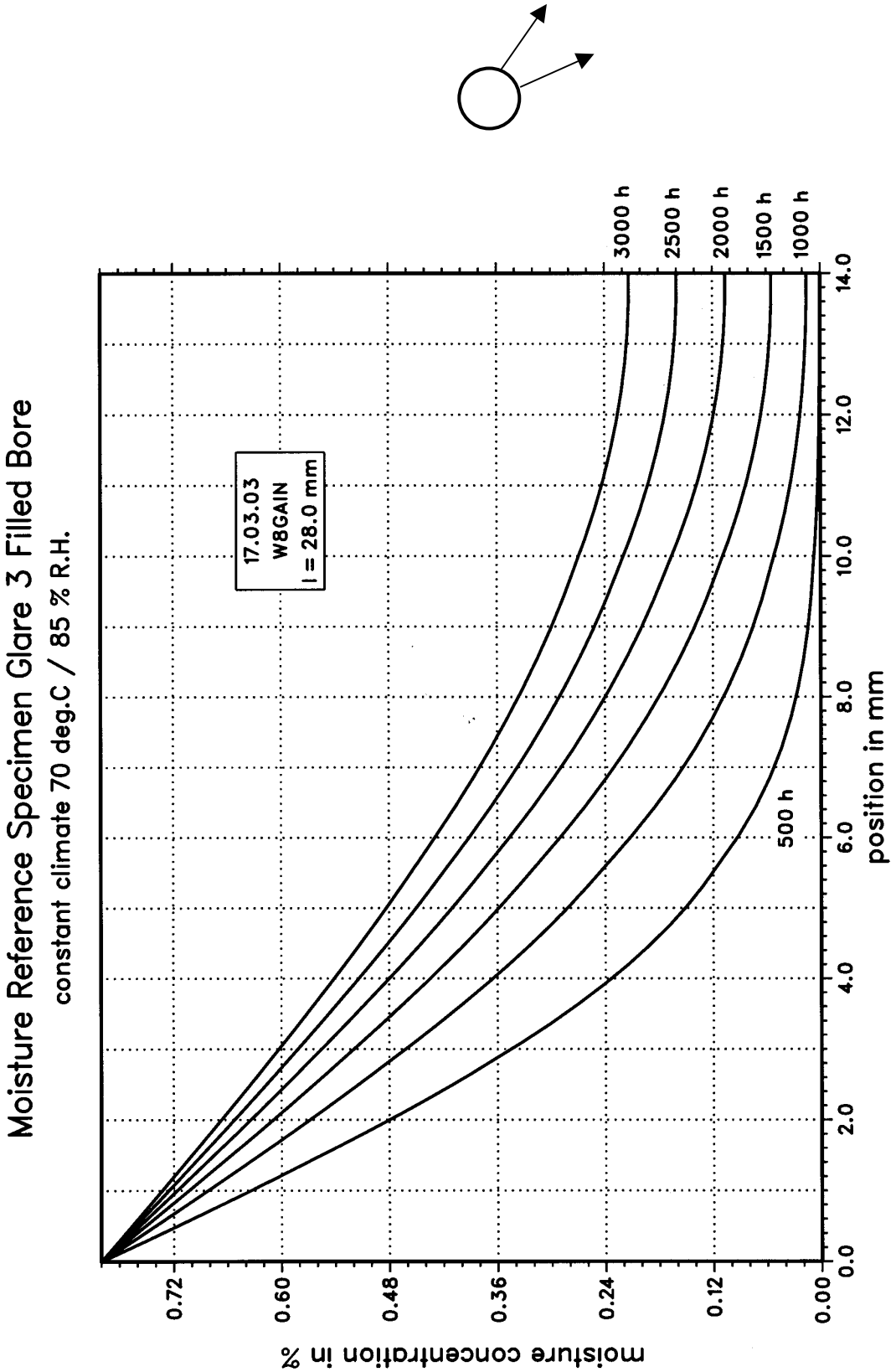

Data used for diffusion depth directions 45 degree from bore hole

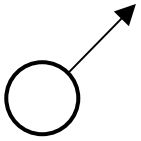

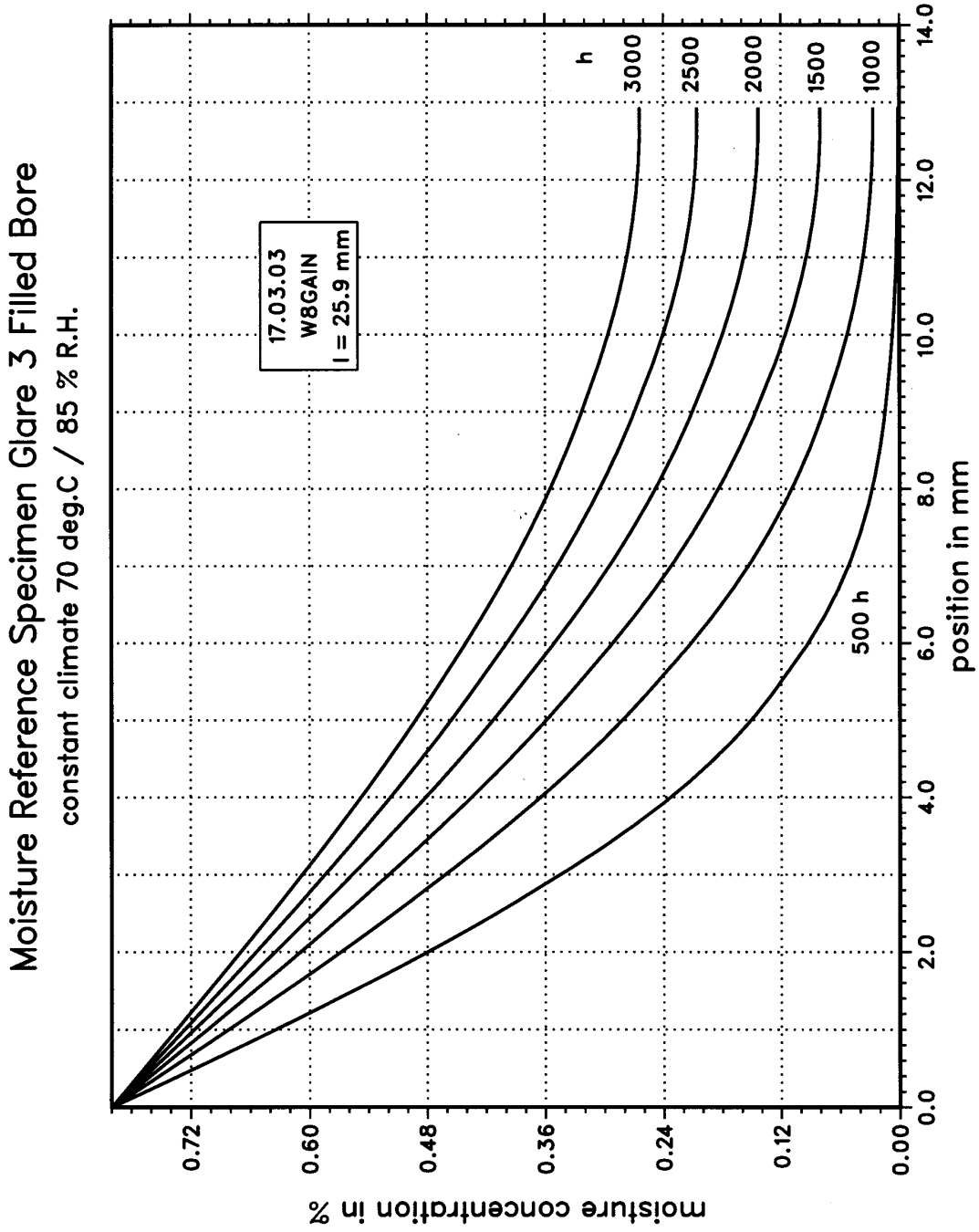

N
One Dimensional Diffusion Depth Calculation Results, Computer Program W8GAIN, GLARE3 Open Bore Holes, Environment 70°C/85%RH, t = 22.7mm, D = 4.8mm

Data used for diffusion depth directions 0 degree and 90 degree from bore hole

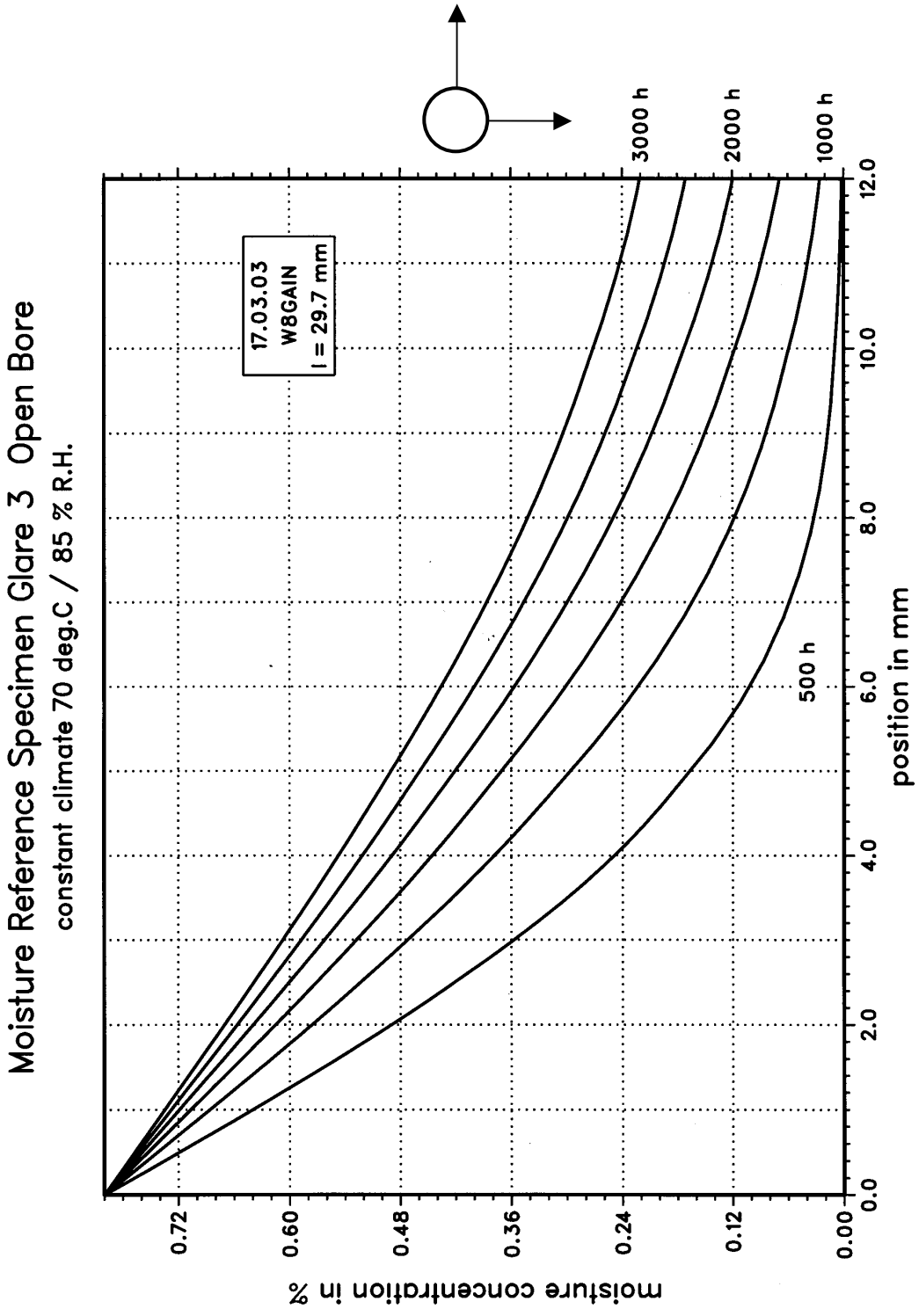

Data used for diffusion depth directions 22.5 degree and 67.5 degree from bore hole

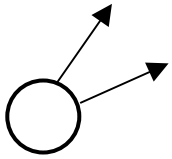

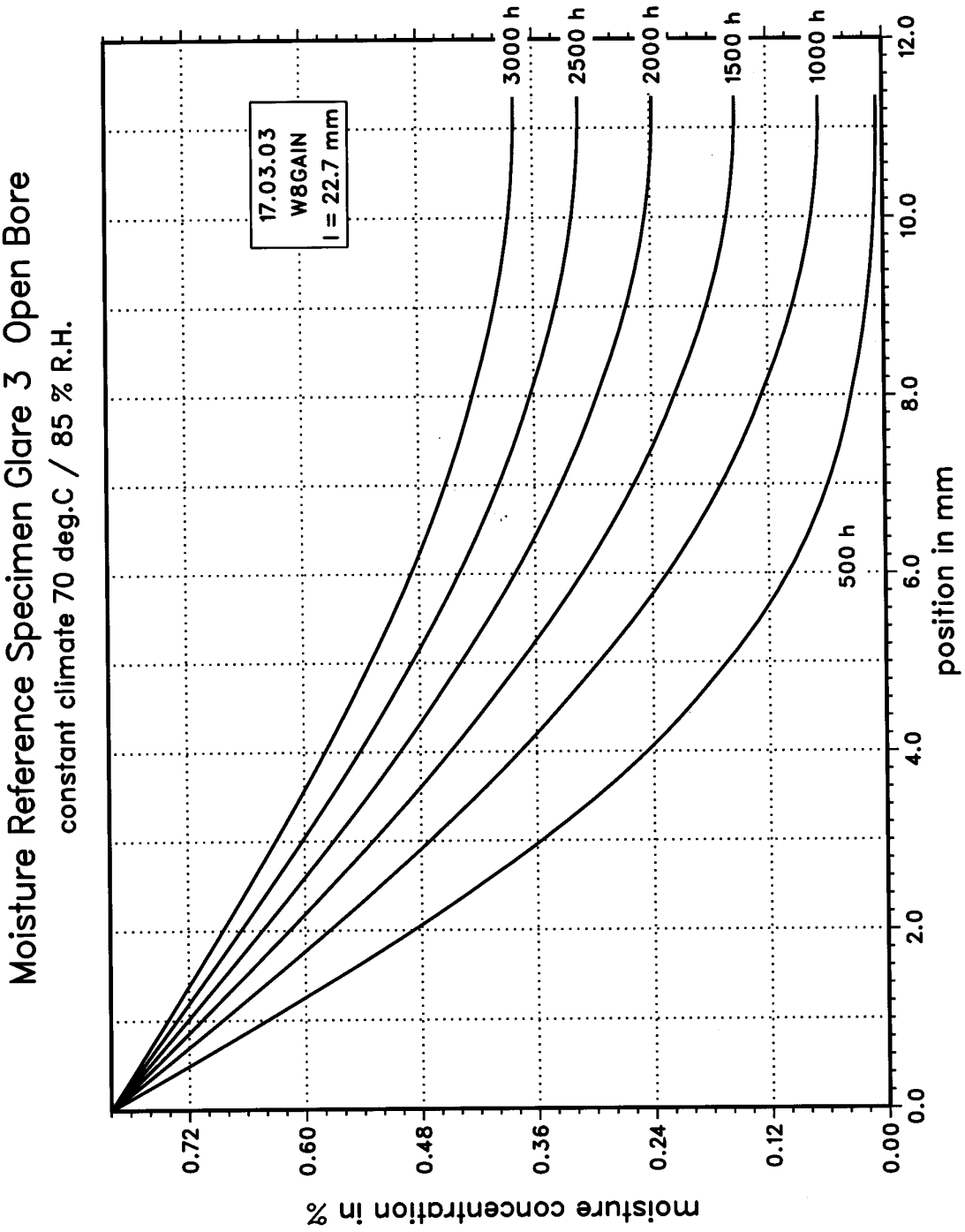

Data used for diffusion depth directions 45 degree from bore hole

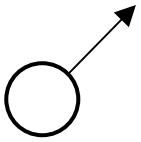

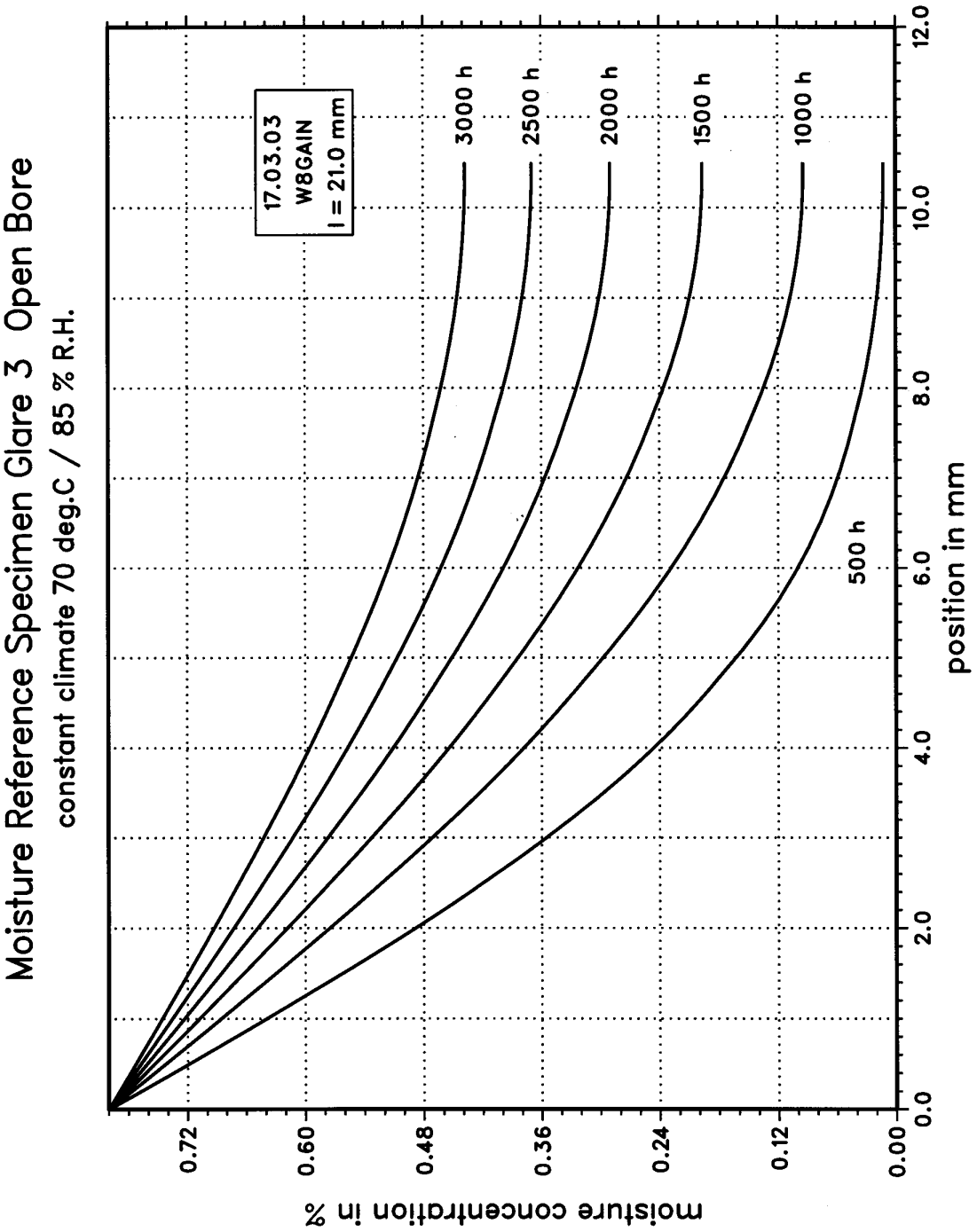

O
Blunt Notch specimen SEM Pictures

Appendix to chapter 6.8.2

The following pictures show cross sections from (different) blunt notch specimens which have been exposed in a 70°C/85%RH environment for 0, 500, 1000 and 3000 hours, respectively,
followed by static loading up to yield, 70% failure load, 80% failure load, 90% failure load and 98% failure load, respectively.

Specimen material: GLARE4A-5/4-.4, loaded in L-direction.

Specimens design :

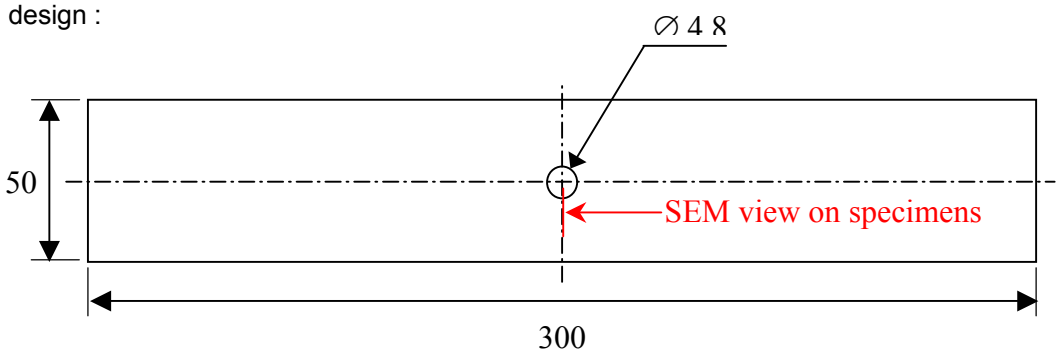

No exposure, **yield load,** magnification 22

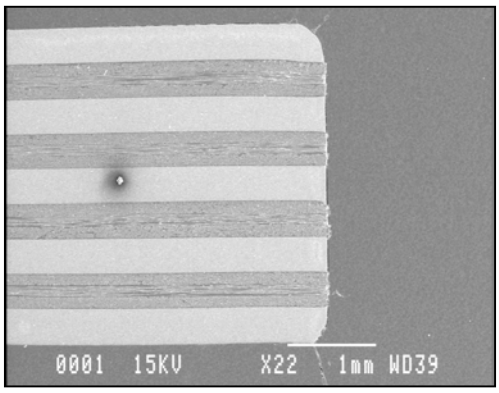

500 h exposure, yield load, magnification 22

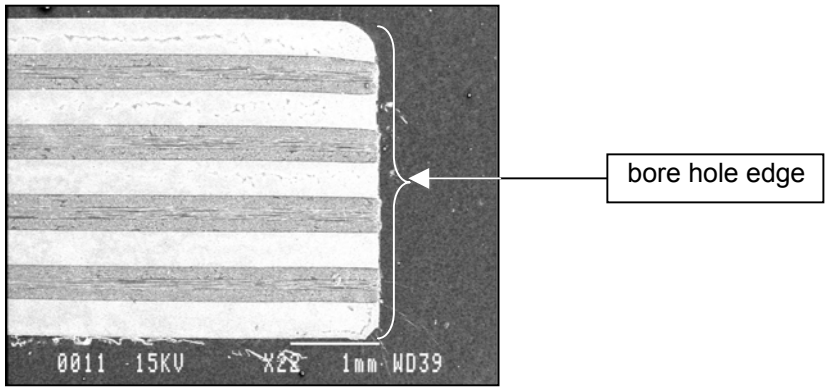

1000 h exposure, yield load

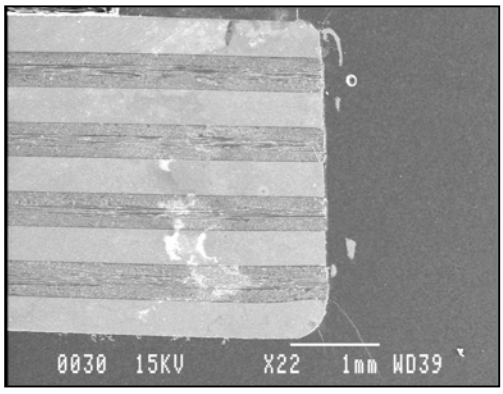

magnification 22

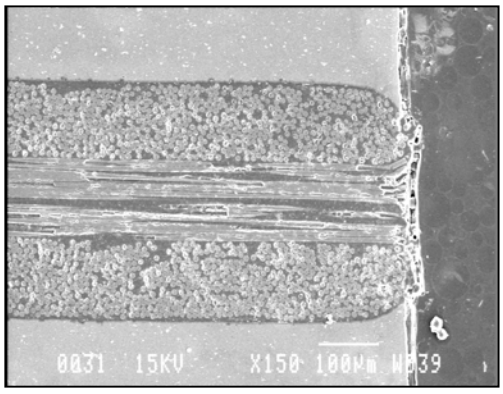

magnification 150

3000 h exposure, yield load

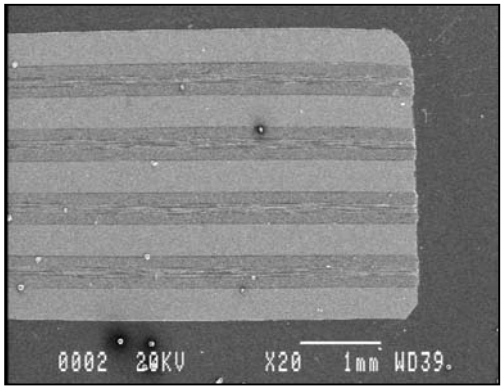

magnification 20

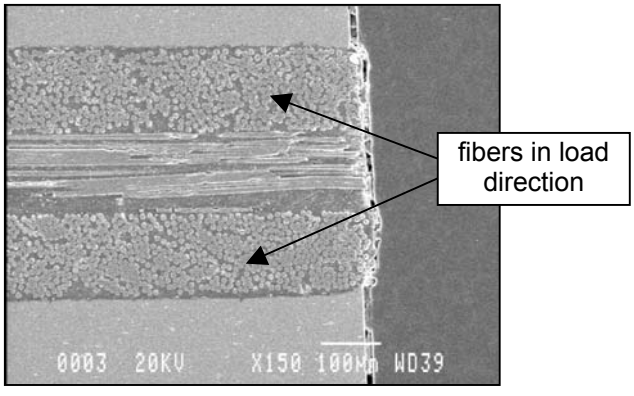

magnification 150

No exposure, **70% failure load,** magnification 22

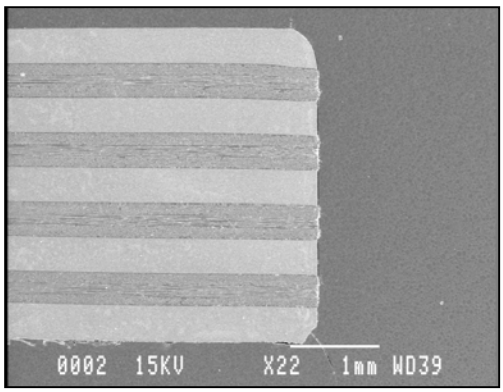

500 h exposure, 70% failure load, magnification 22

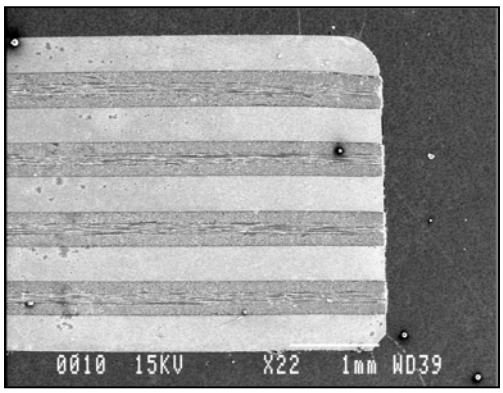

1000 h exposure, 70% failure load

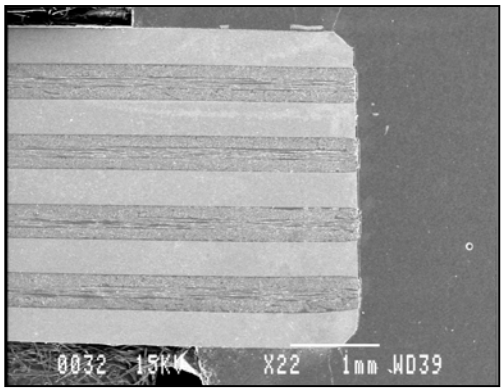

magnification 22

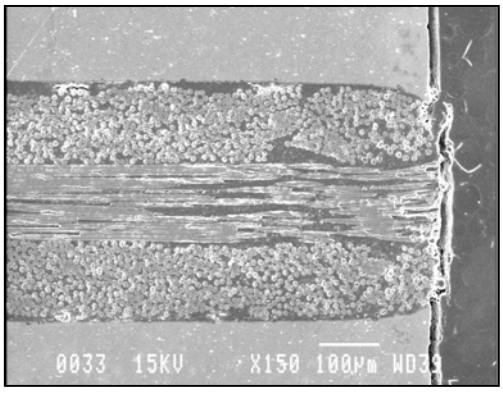

magnification 150

3000 h exposure, 70% failure load

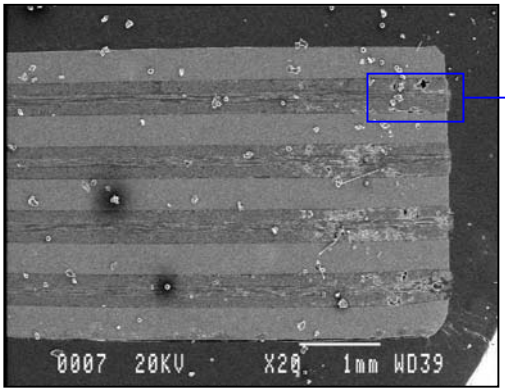

magnification 20

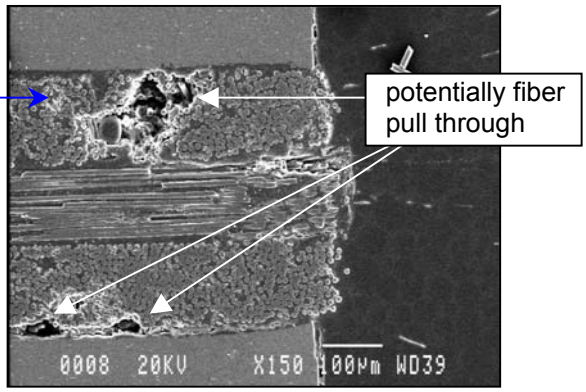

magnification 150

This page 80% failure load

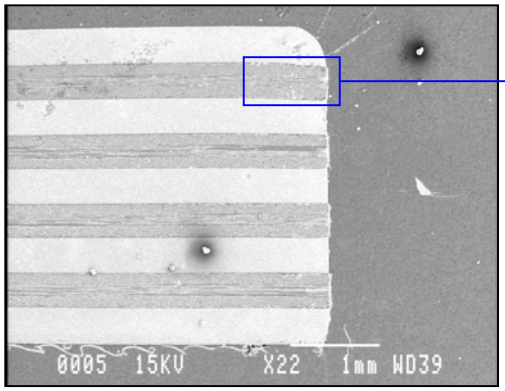

No exposure, magnification 22

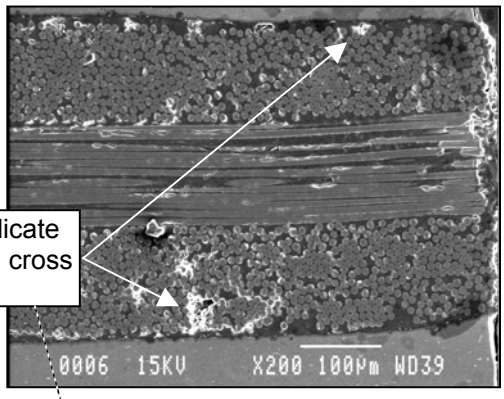

No exposure, magnification 200

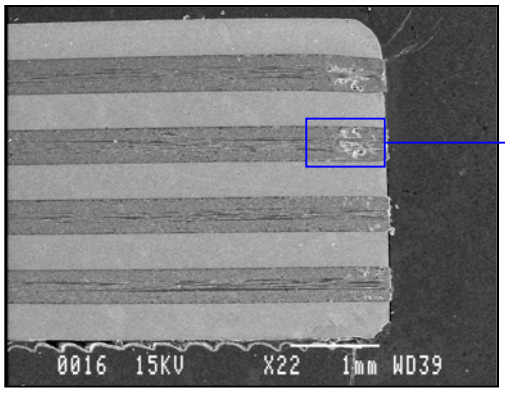

500 h exposure, magnification 22

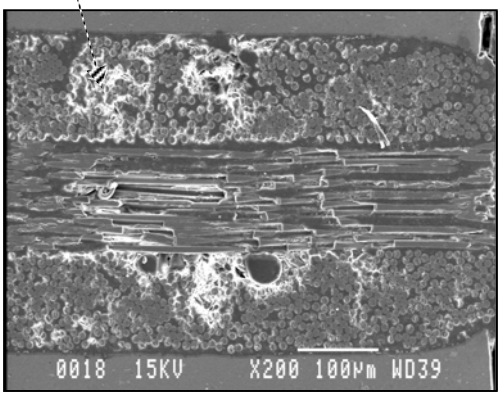

500 h exposure, magnification 200

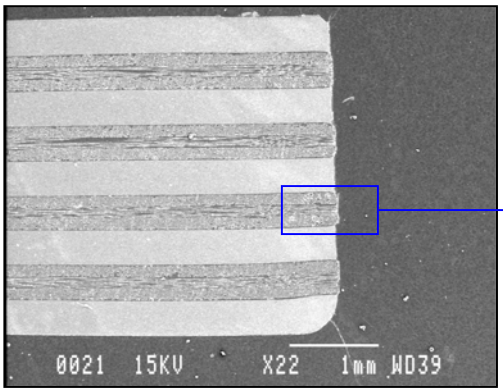

1000 h exposure, magnification 22

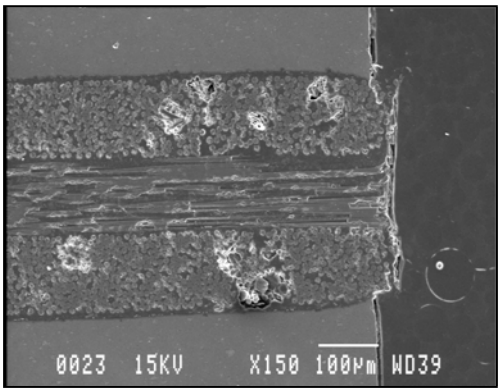

1000 h exposure, magnification 150

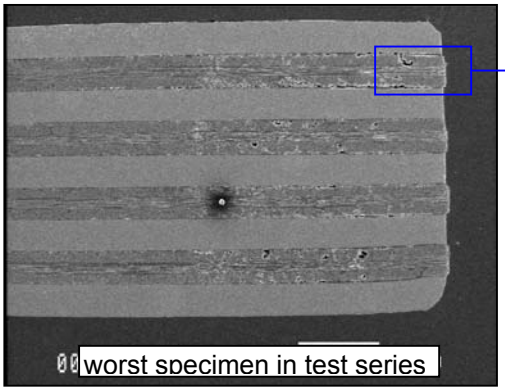

3000 h exposure, magnification 20

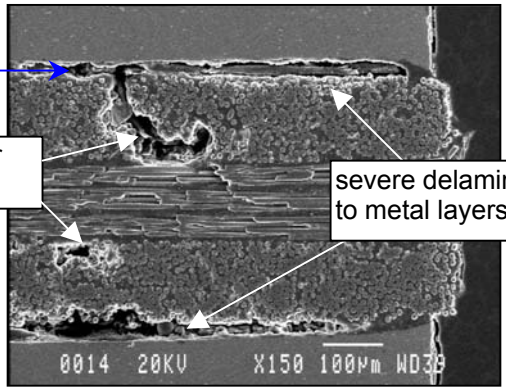

3000 h exposure, magnification 150

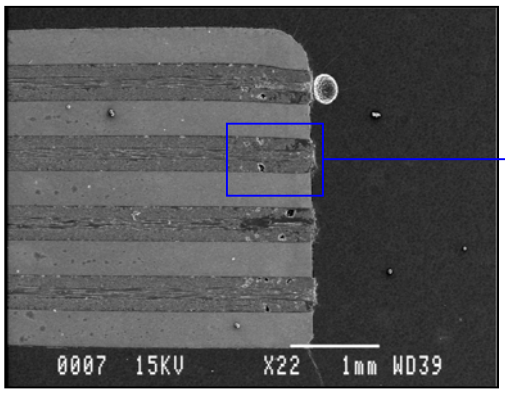

This page 90% failure load

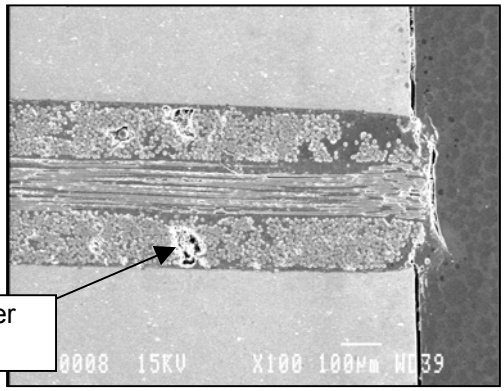

potentially fiber pull through

No exposure, magnification 22

No exposure, magnification 100

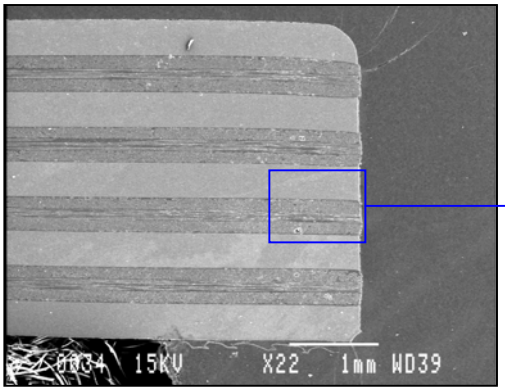

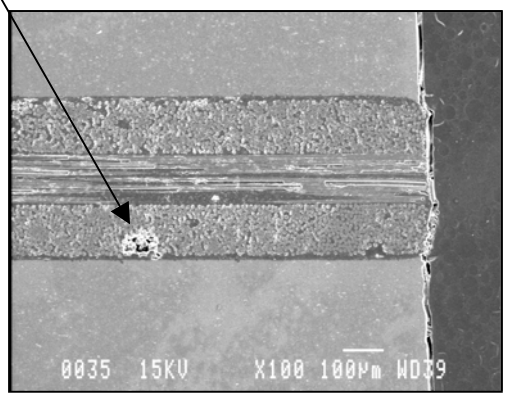

500 h exposure, magnification 22

500 h exposure, magnification 100

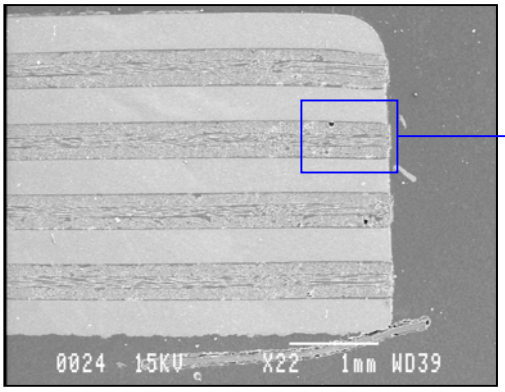

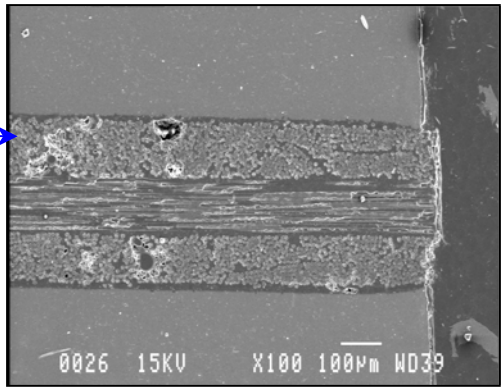

1000 h exposure, magnification 22

1000 h exposure, magnification 100

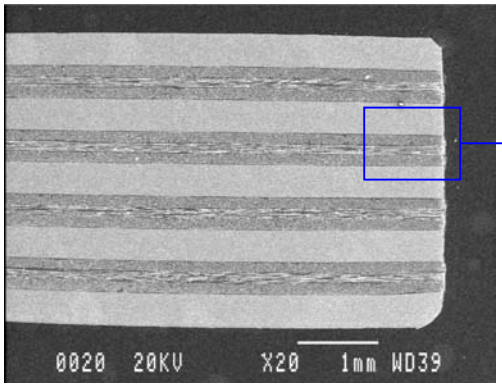

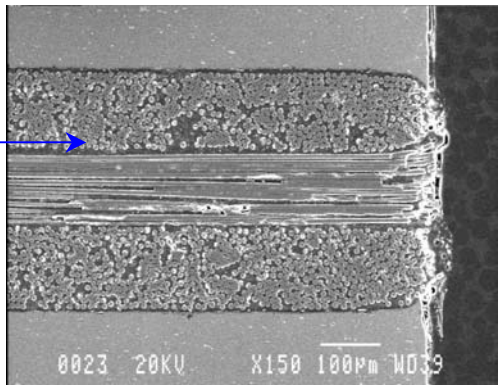

3000 h exposure, magnification 20

3000 h exposure, magnification 150

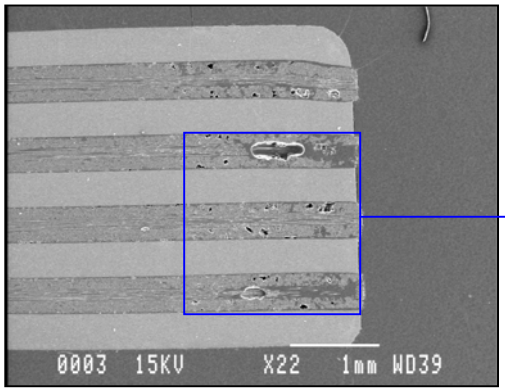

This page 98% failure load

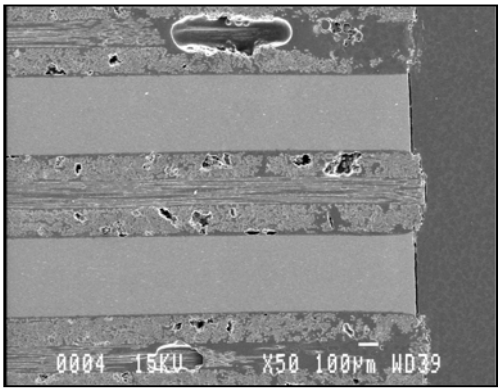

No exposure, magnification 22

No exposure, magnification 50

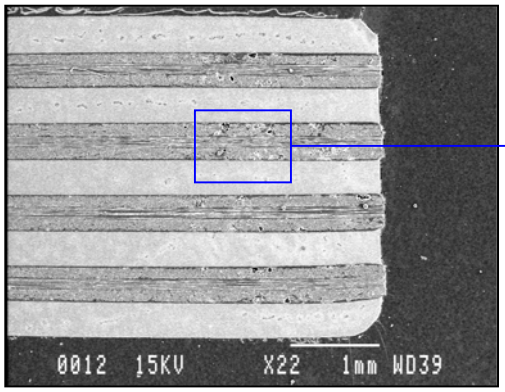

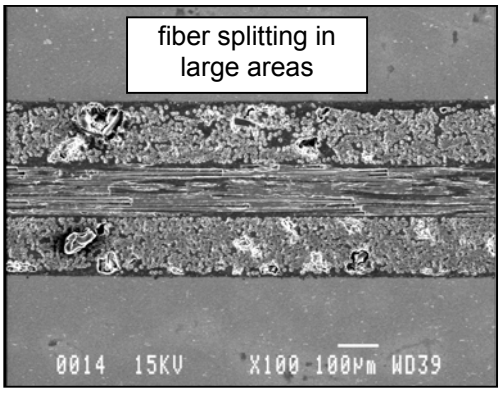

500 h exposure, magnification 22

500 h exposure, magnification 100

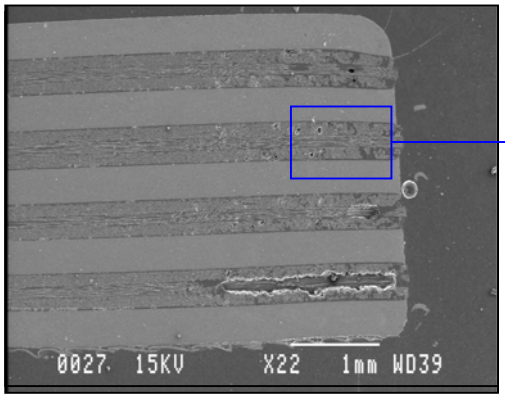

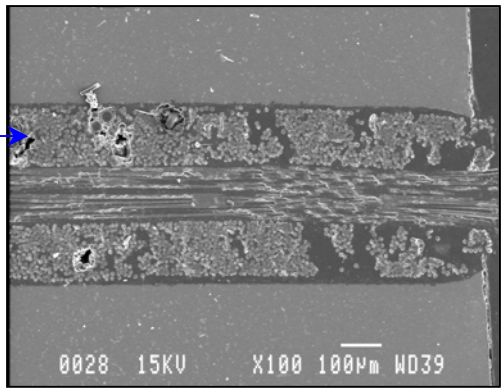

1000 h exposure, magnification 22

1000 h exposure, magnification 100

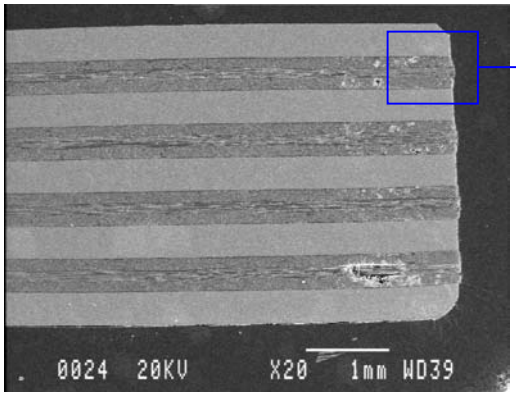

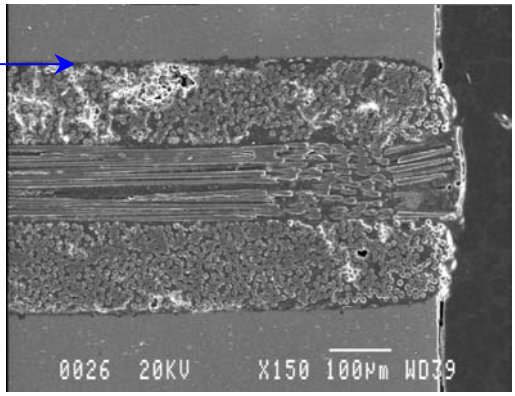

3000 h exposure, magnification 20

3000 h exposure, magnification 150

yield load after
3000 h exposure,
magnification 1000

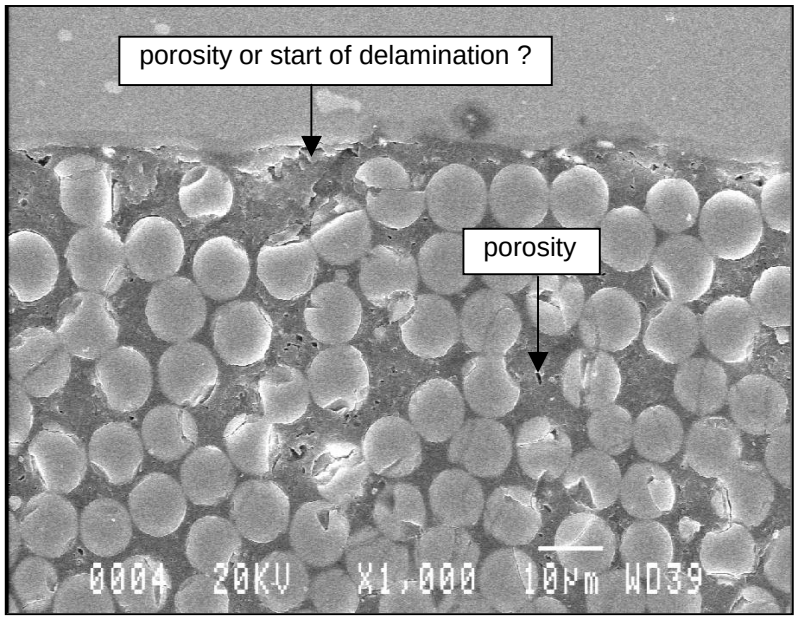

70% failure load after
3000 h exposure,
magnification 1000

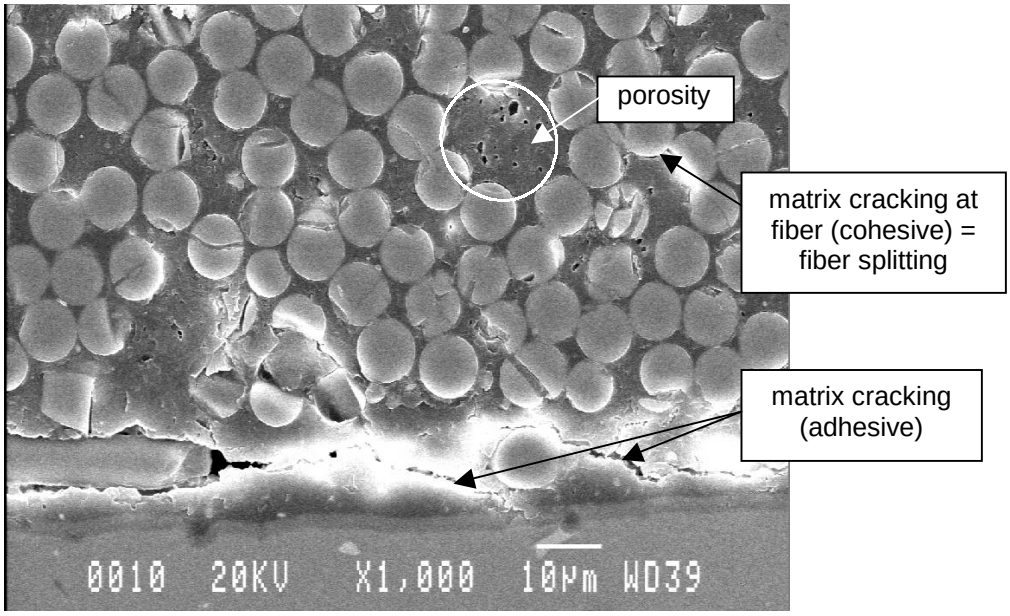

98% failure load after
3000 h exposure,
magnification 1000

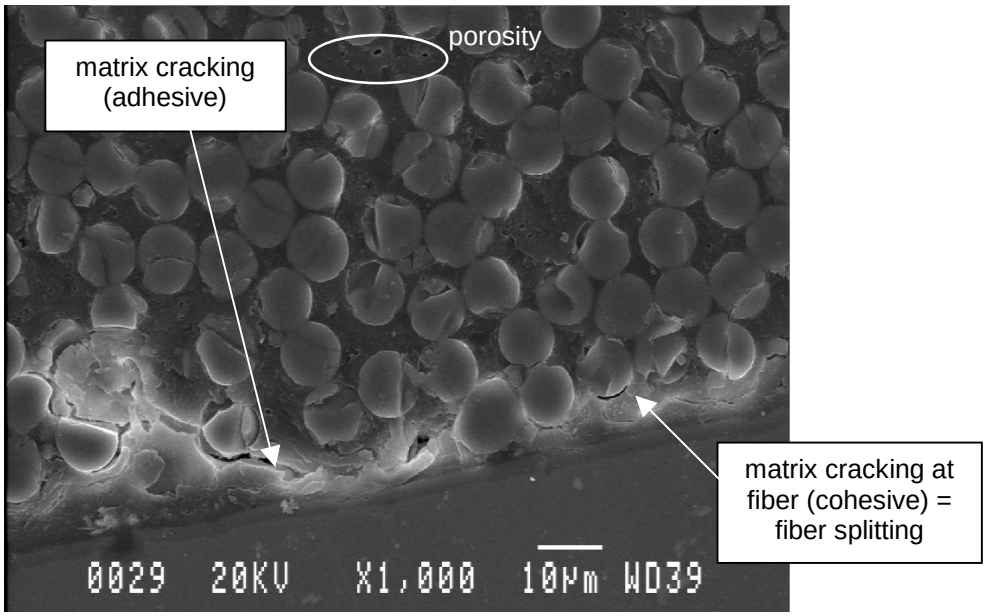

P
Photoelastic Measurements preformed on Bonded Repair Panel 12-BR-01 at NLR Facilities

Attachment to chapter 9

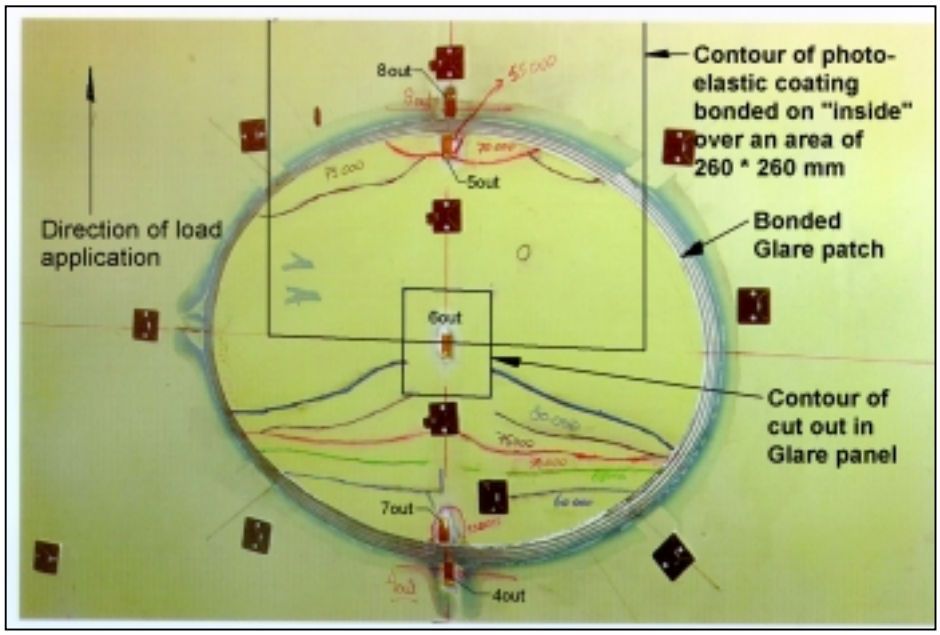

Photo elastic measurements illustrate delamination extension with increased fatigue life :

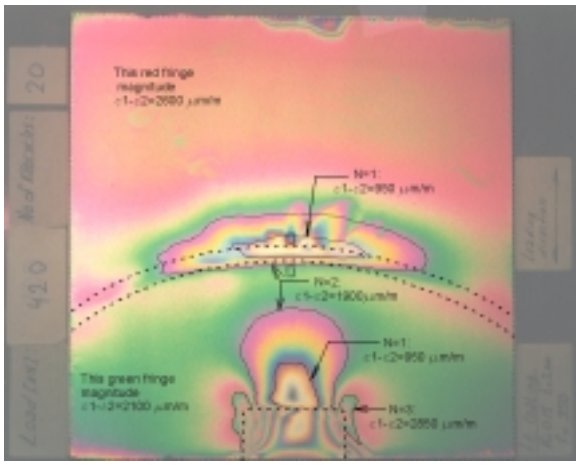

… after 20000 cycles

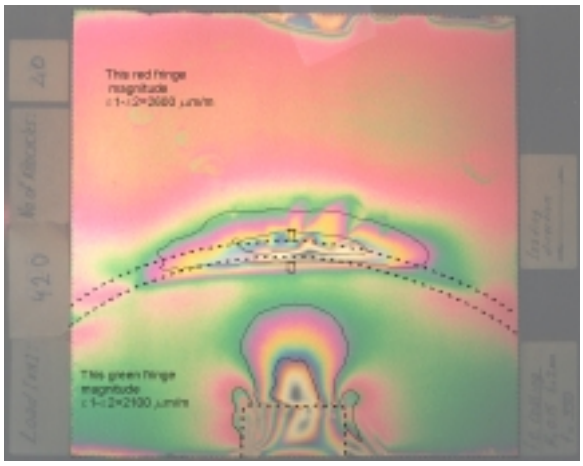

… after 40000 cycles

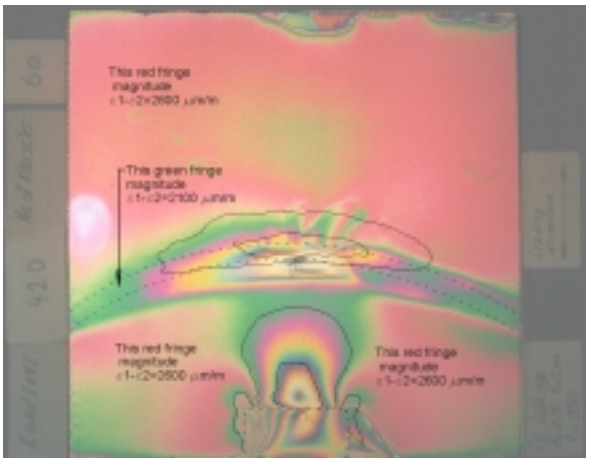

… after 60000 cycles

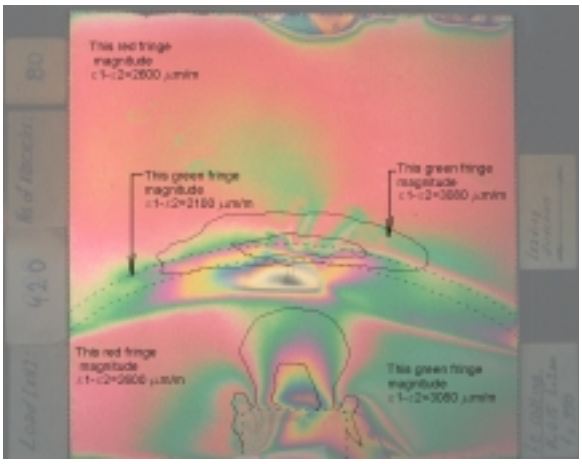

… after 80000 cycles

Q
Variable Temperature and Load Readings, Tests performed at ASTRIUM Facilities

Attachment to chapter 7.1.6

The thermal expansion/shrinking during heating/cooling of the specimens requires a continuous assessment of the force control, see the standard mission plot for 1½ flight: cycles :

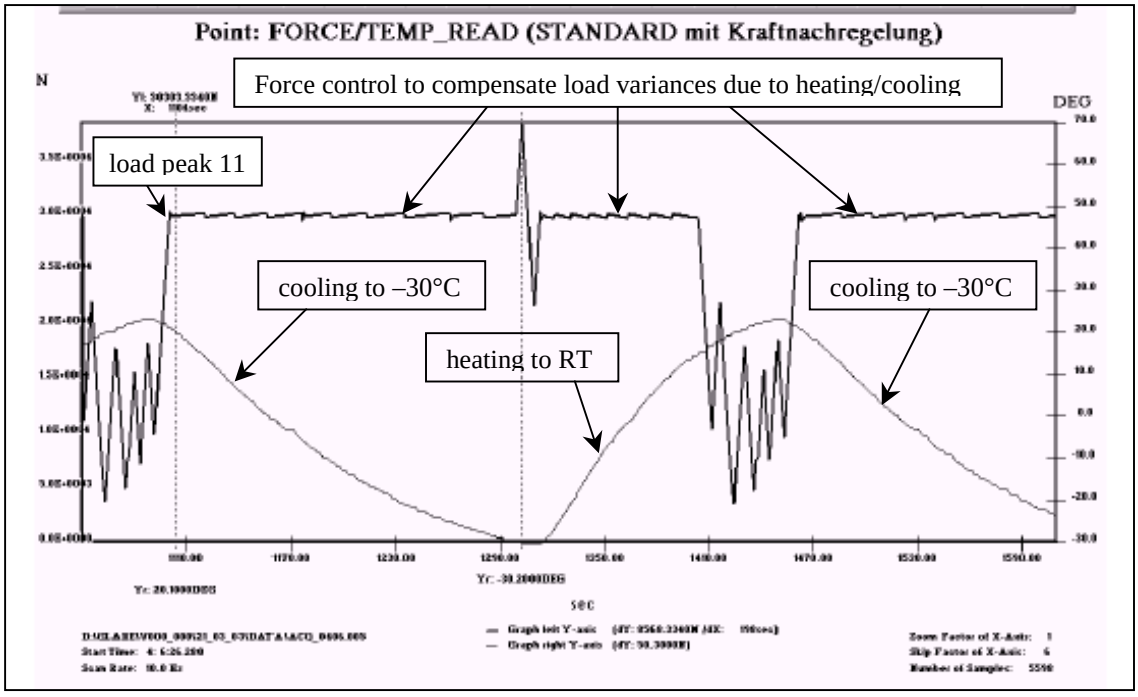

If there would be influence of the thousands of small load peaks on the fatigue behaviour of the specimens it may be hard to interprete them. Therefore, it was decided to include the thermal forces as variable to obtain the particular target force in the spectrum at the end of a heating or cooling cycle. See standard mission without assessment of force control due to specimen expansion/shrinking:

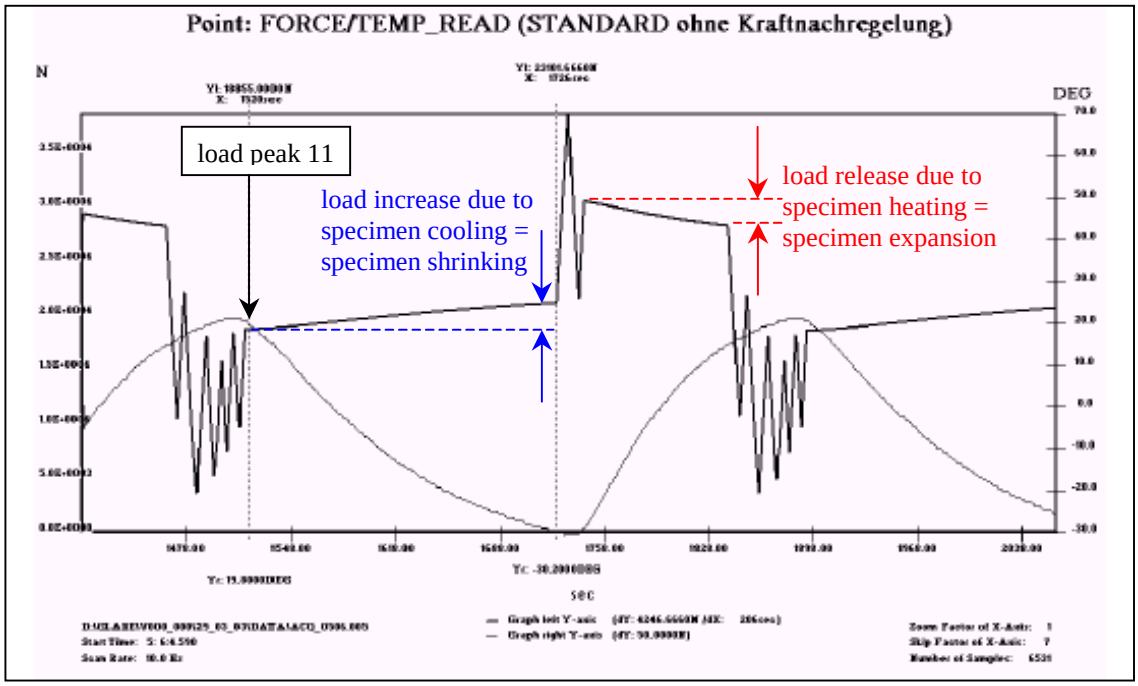

The arctic flight is performed at constant –30°C specimen temperature. Temperature related deformation are no item. See 2½ arctic flight sequences :

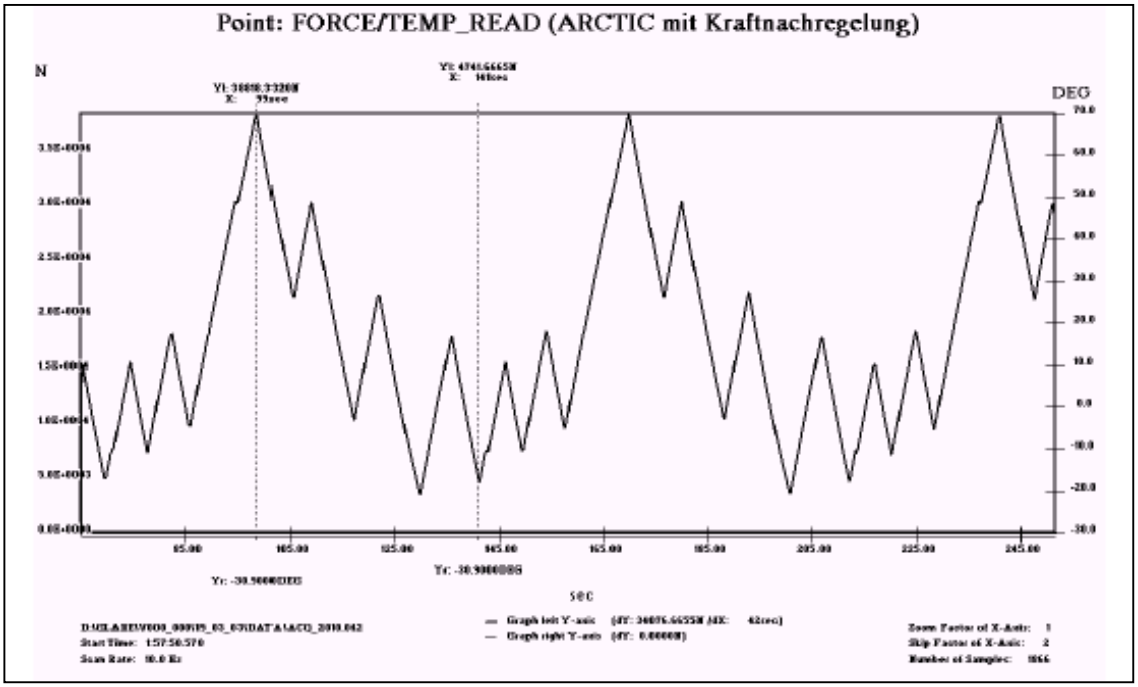

1½ tropic flight cycles, thermal forces included in order to match target load after cooling or heating, respectively :

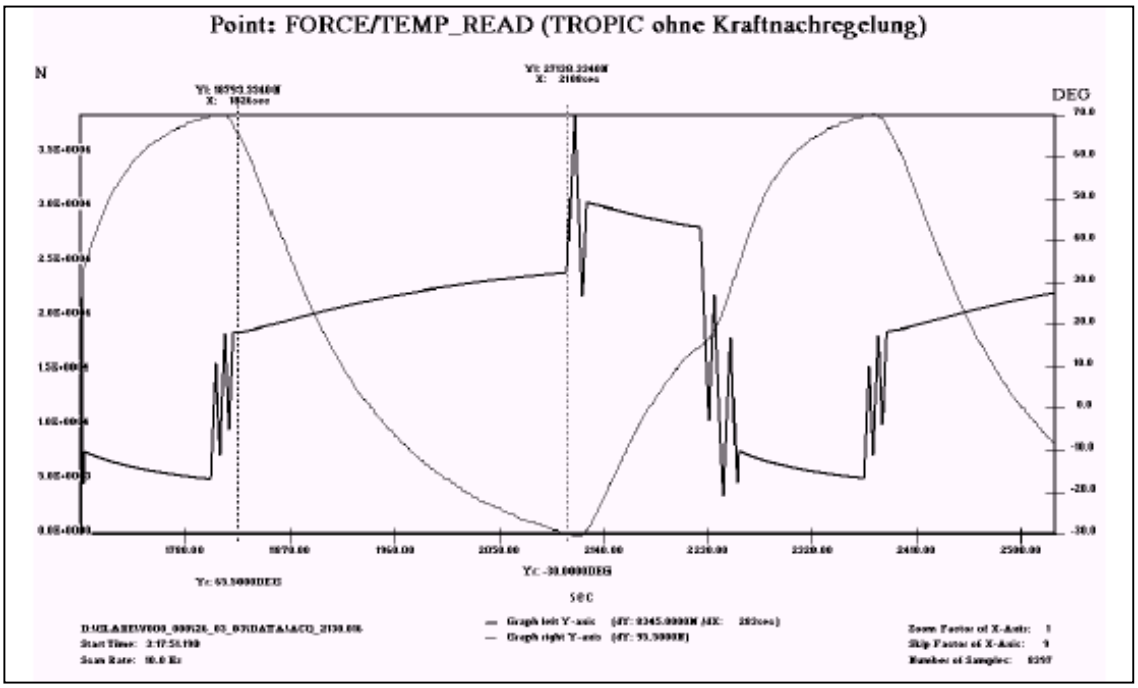

R
Microfractografic Investigation of Specimen 2-B-78
Reference: Airbus, werkstoffkundlicher Untersuchungsbericht, 9597

Attachment to chapter 7.1.7.1

Specimen 2-B-78 was fatigue cycled 400000 times with a maximum force of 38.9 kN (R=0.1), exposed from January 2002 to January 2003 in Queensland and pulled to failure. Failure load: 163 kN. Failure location: GLARE2B-7/6-.4 butt strap, rivet row 3. Failure mode: net section. The crack lengths in all bore holes are determined for all fatigue sensitive locations by Airbus Deutschland:

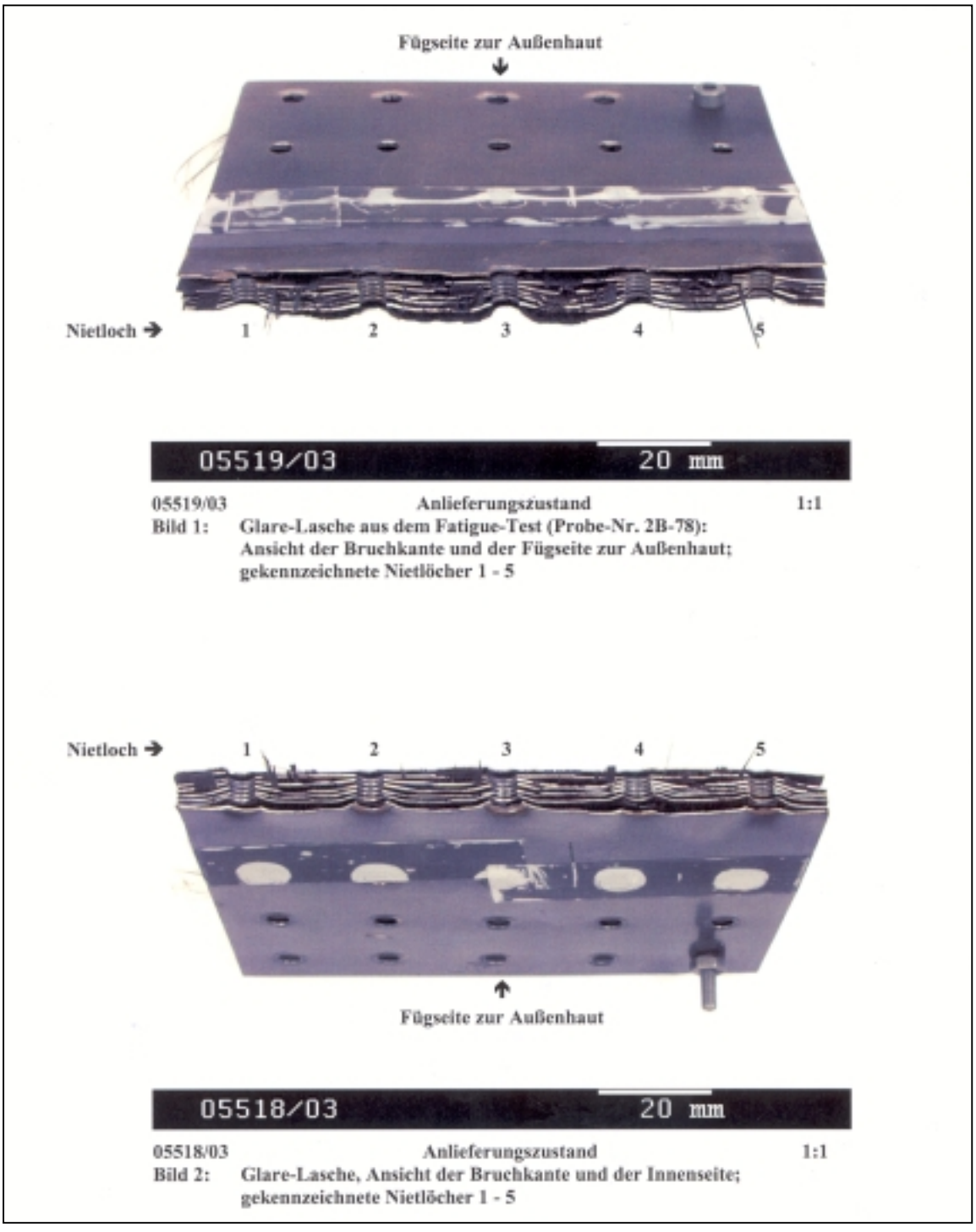

Ermüdungsrisslängen (in mm)
Nietloch 1

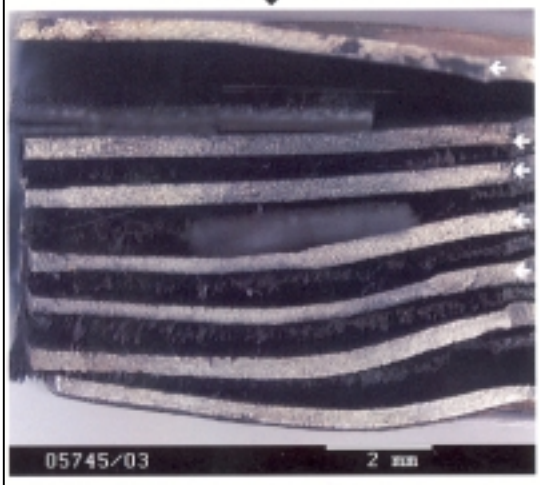

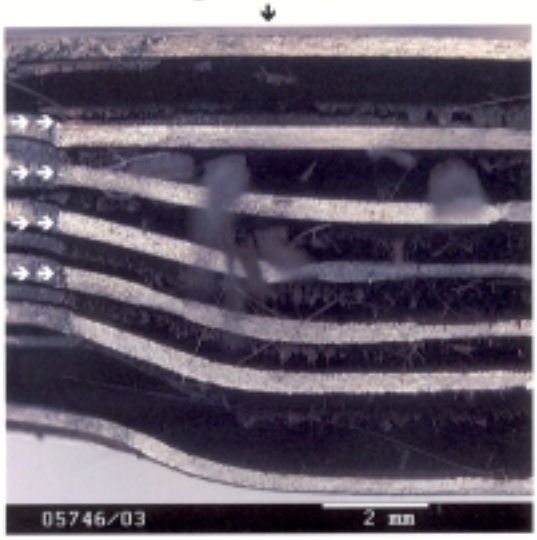

durchgängig		
	9,34	
durchgängig		
	8,35	8,44
	4,08	4,27
	1,82	1,80

05745/03 10:1
Bild 3: Ermüdungsrisse ausgehend vom Nietloch 1, Risslängen makroskopisch gemessen (Det. v. Bild 1 und 2)

0574603 10:1
Bild 4: Ermüdungsrisse ausgehend vom Nietloch 1, Risslängen makroskopisch gemessen (Det. v. Bild 1 und 2)

Ermüdungsrisslängen (in mm)
Nietloch 2

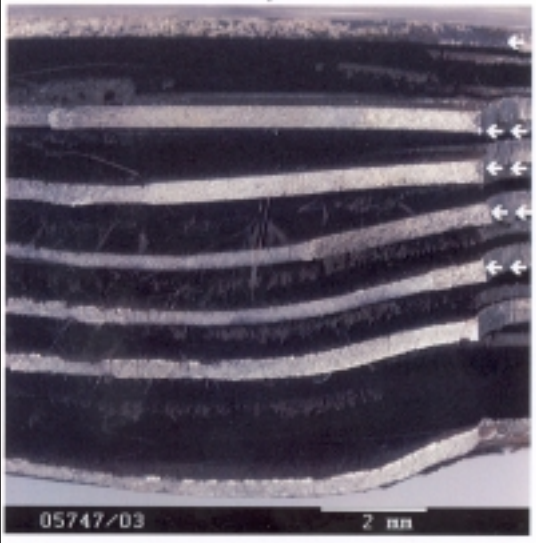

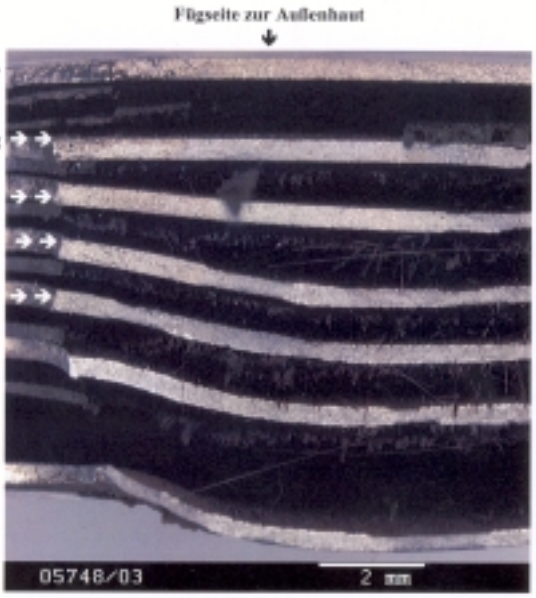

durchgängig		
	8,23	
durchgängig		
	6,48	7,51
	3,51	2,92
	1,08	1,20

05747/03 10:1
Bild 5: Ermüdungsrisse ausgehend vom Nietloch 2, Risslängen makroskopisch gemessen (Det. v. Bild 1 und 2)

0574803 10:1
Bild 6: Ermüdungsrisse ausgehend vom Nietloch 2, Risslängen makroskopisch gemessen (Det. v. Bild 1 und 2)

Ermüdungsrisslängen (in mm)
Nietloch 3

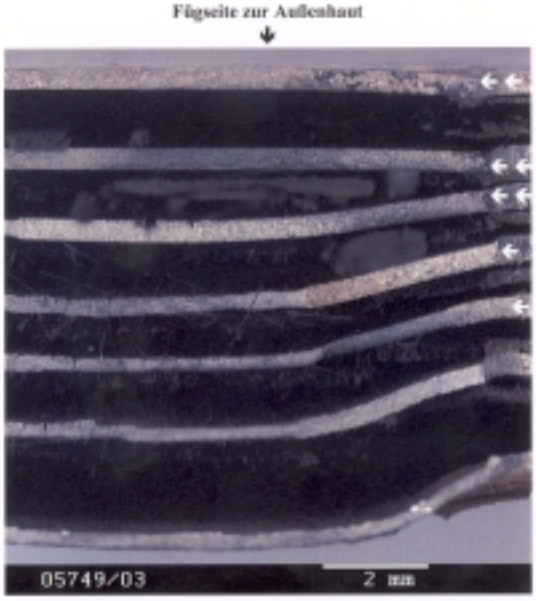

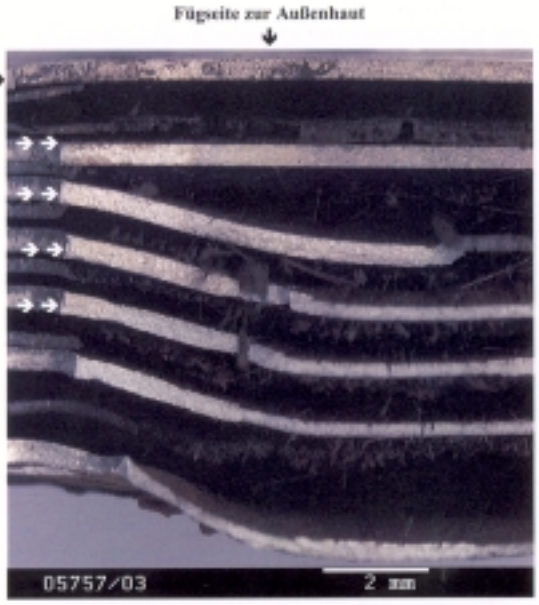

durchgängig		durchgängig
	9,15	
durchgängig		
9,00	7,01	
3,83	3,35	
1,45	0,87	

05749/03 10:1
Bild 7: Ermüdungsrisse ausgehend vom Nietloch 3, Risslängen makroskopisch gemessen (Det. v. Bild 1 und 2)

05757/03 10:1
Bild 8: Ermüdungsrisse ausgehend vom Nietloch 3, Risslängen makroskopisch gemessen (Det. v. Bild 1 und 2)

Ermüdungsrisslängen (in mm)
Nietloch 4

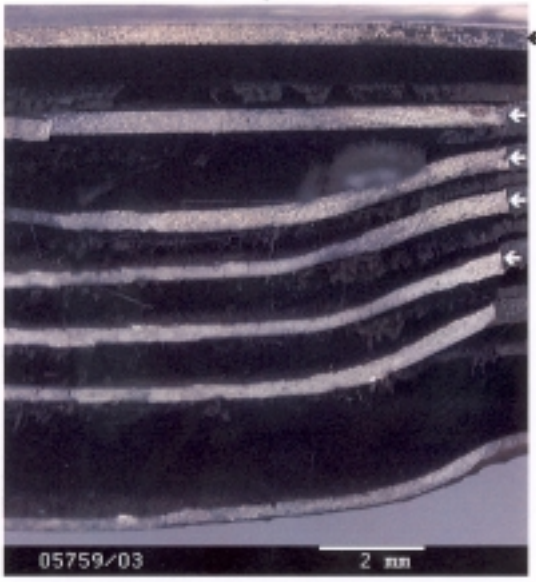

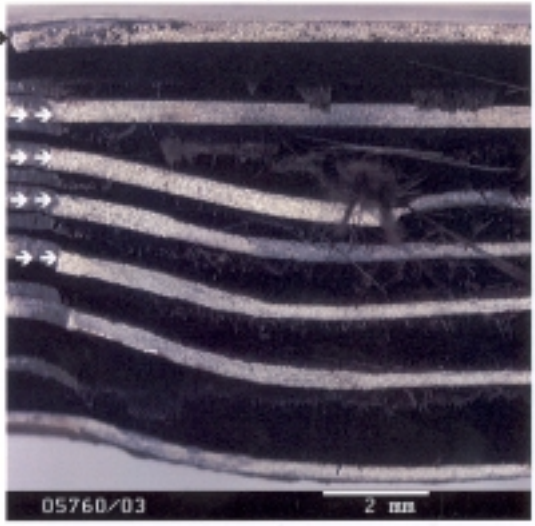

durchgängig		durchgängig
8,75	9,78	
6,80	6,75	
2,93	2,36	
0,84	0,49	

05759/03 10:1
Bild 9: Ermüdungsrisse ausgehend vom Nietloch 4, Risslängen makroskopisch gemessen (Det. v. Bild 1 und 2)

05760/03 10:1
Bild 10: Ermüdungsrisse ausgehend vom Nietloch 4, Risslängen makroskopisch gemessen (Det. v. Bild 1 und 2)

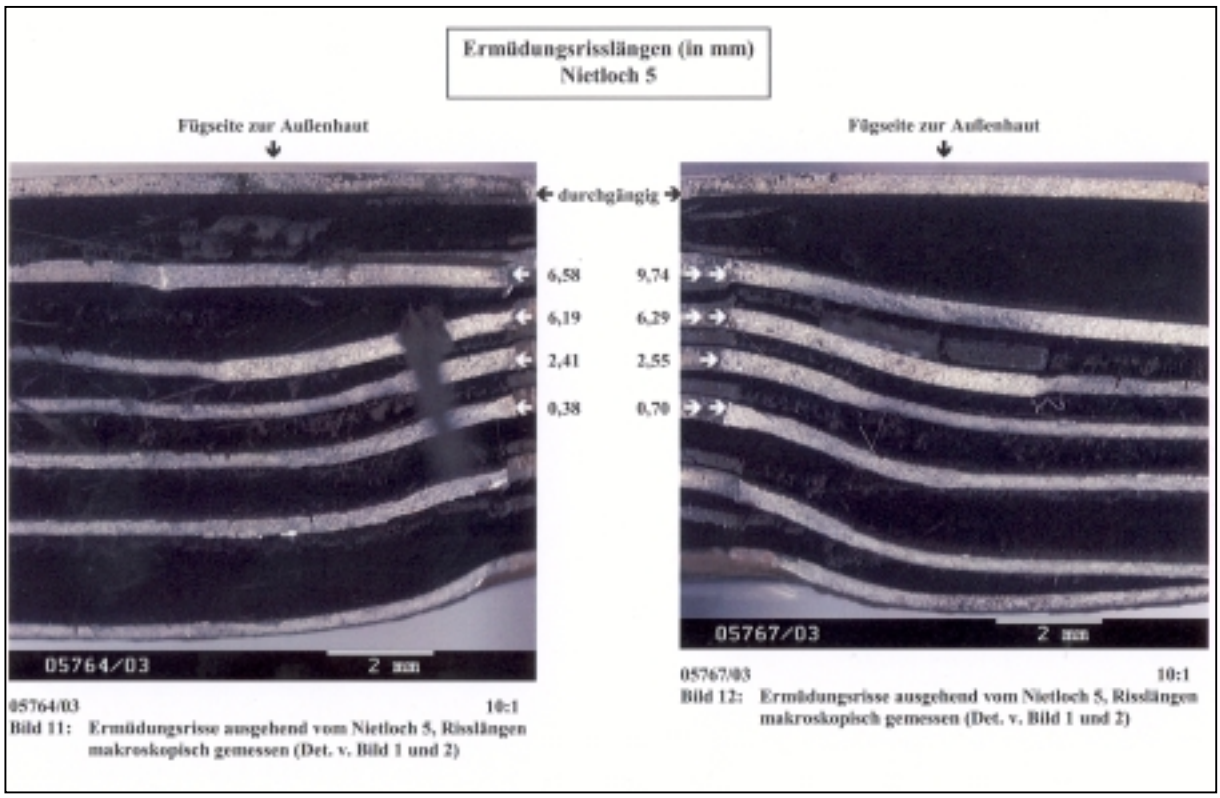

05764/03 10:1
Bild 11: Ermüdungsrisse ausgehend vom Nietloch 5, Risslängen makroskopisch gemessen (Det. v. Bild 1 und 2)

05767/03 10:1
Bild 12: Ermüdungsrisse ausgehend vom Nietloch 5, Risslängen makroskopisch gemessen (Det. v. Bild 1 und 2)

S

Circumferential Joint Calculation for A340 Butt Strap

(Stress spectrum increased by factor 1.7 related to measurements)

Attachment to chapter 7.2.1

Loads

Remote tensile (gross) loads in sheet 1:

Factor on loads: 0,950

Flights in spectrum: 1660

N	Smax [MPa]	Smin [MPa]
1	98,700	8,100
1	95,200	8,100
1	94,600	8,100
1	93,800	8,100
1	92,800	8,100
1	91,200	8,100
1	96,500	13,900
1	96,500	14,400
2	90,000	8,100
2	95,200	13,400
1	89,500	8,100
2	89,300	8,100
1	94,600	13,500
1	94,600	13,900
1	88,000	8,100
4	87,600	8,100
1	92,800	13,500
1	87,200	8,100

2	92,800	13,900
1	90,000	11,400
2	86,700	8,100
1	91,500	13,100
1	91,300	13,400
1	91,200	13,500
1	91,500	13,900
2	85,700	8,100
1	91,300	13,900
8	85,500	8,100
4	91,200	13,900
1	88,600	11,400
4	84,900	8,100
5	84,200	8,100
1	89,300	13,500
1	87,200	11,400
3	89,500	13,900
10	89,300	13,900
3	92,800	17,600
9	82,900	8,100
2	88,600	13,900
10	82,700	8,100
2	91,300	16,800
1	85,700	11,400
5	88,000	13,900
1	87,600	13,500
4	88,600	14,600
1	88,600	14,900
22	87,600	13,900
11	91,200	17,600
5	87,200	13,900
18	81,300	8,100
11	86,700	13,900
1	84,200	11,400
1	85,500	13,500
4	89,500	17,600
11	85,700	13,900
27	89,300	17,600
52	85,500	13,900
12	88,000	16,700
1	82,700	11,400
23	84,900	13,900
26	84,200	13,900
66	87,600	17,600
12	87,200	17,200
29	86,700	17,600
49	82,900	13,900
1	82,900	14,100
63	82,700	13,900
32	85,700	17,200
156	85,500	17,600
110	81,300	13,900
65	84,900	17,600
1	81,300	14,100
77	84,200	17,600
146	82,900	17,600
188	82,700	17,600
329	81,300	17,600
15	71,600	11,400
12	71,600	13,500
4	71,600	13,900
26	71,600	14,100
12	71,600	15,200
6	71,600	15,400

1	68,300	15,900
1	65,400	13,900
4	68,300	17,600
102	65,400	15,900
113	65,400	17,600
78	65,400	17,800
68	65,400	18,200
37	65,400	18,400
1	63,300	16,400
1	62,000	15,200
11	62,000	15,400
2	60,000	14,300
1	60,000	14,600
2	60,000	14,700
2	60,000	14,900
2	71,400	26,400
1	60,000	15,000
2	63,300	18,500
1	71,400	26,800
1	71,400	26,900
5	62,000	17,600
2	71,400	27,200
1	60,000	15,900
1	60,000	16,400
90	62,000	18,500
6	60,000	16,700
2	60,000	16,800
7	71,400	28,400
9	60,000	17,200
31	60,000	17,600
3	67,200	24,900
17	71,400	29,600
7	60,000	18,200
1	57,000	15,200
40	71,400	29,700
3	63,300	21,700
53	60,000	18,500
3	56,600	15,200
26	56,700	15,400
26	67,200	26,100
310	71,400	30,700
4	55,900	15,200
11	55,900	15,400
267	62,000	21,700
12	57,500	17,200
4	55,900	15,900
17	60,000	20,100
32	57,500	17,600
4	67,200	27,500
109	57,500	18,000
1	55,400	15,900
4	57,000	17,600
3	56,700	17,600
3	56,600	17,600
2	56,700	17,800
1	57,000	18,200
1	56,600	17,800
42	67,200	28,400
109	56,700	18,200
3	56,600	18,200
69	56,700	18,400
5	55,900	17,600
40	57,500	19,200
9	56,600	18,400

74	57,500	19,400
2	55,400	17,600
755	67,200	29,400
67	55,900	18,200
35	55,900	18,400
92	57,500	20,300
1	55,400	18,200
317	55,900	18,800
1	95,400	58,400
205	57,500	20,500
6	57,000	20,000
213	56,700	20,000
3	55,400	18,800
48	56,600	20,000
93	57,500	21,000
329	56,700	20,200
188	55,900	19,400
18	49,700	13,500
61	57,500	21,600
19	57,500	23,100
513	54,500	20,100
156	55,900	21,600
673	54,500	20,300
72	54,000	20,300
14	49,700	16,300
4	49,700	16,500
1	91,300	58,200
439	55,900	23,100
21	44,000	11,400
3	90,100	57,600
1	94,000	62,500
14	49,300	18,300
4	48,700	17,700
1	92,700	62,100
1	55,700	25,300
1	89,600	59,600
2	55,700	26,100
5	55,700	26,200
2	55,700	26,300
8	44,900	15,800
1	55,700	26,600
28	44,300	15,200
3	88,800	59,800
1	55,700	27,400
2	55,700	27,900
3	90,400	62,800
2	88,300	61,000
19	55,700	28,600
1	91,000	64,000
46	55,700	29,100
5	64,500	37,900
4	87,300	61,100
371	55,700	29,500
3	87,400	61,300
1	91,600	65,700
2	91,400	65,500
3	91,300	65,400
92	44,400	18,500
1	91,300	65,600
2	91,600	65,900
2	91,500	65,800
1	88,300	62,700
4	91,100	65,600
2	90,800	65,900

2	87,600	62,700
3	87,300	62,600
88	45,000	20,300
3	83,100	58,500
1	85,900	61,400
1	87,600	63,300
737	55,900	31,800
1	90,500	66,400
2	90,400	66,300
396	49,000	25,000
4	44,400	20,500
8	40,100	16,400
13	40,100	16,600
54	40,000	16,600
21	40,600	17,200
109	39,200	15,900
2	90,100	66,900
3	90,000	66,800
2	86,400	63,300
4	44,400	21,700
7	85,500	63,100
2	89,900	67,600
1	89,500	67,200
5	55,900	33,600
1	89,700	67,400
1	89,400	67,200
5	84,800	62,600
1	90,000	67,800
7	86,300	64,200
88	44,400	22,300

Limit Load = 117,000 MPa

Joint Data

Number of holes in a rows: 8
Butt Joint
Number of rivet rows in sheet 1: 3
Number of rivet rows in sheet 2: 3
Rivet pitch in sheet 1: 22,7 mm
Rivet pitch in sheet 2: 22,7 mm
Rivet row distance in sheet 1: 22,7 mm
Rivet row distance in sheet 2: 22,7 mm
Rivet row distance between sheet 1 and 2: 34,0 mm
Rivet diameter in sheet 1: 4,80 mm
Rivet diameter in sheet 2: 4,80 mm

Fastener Data

Hi-Lok, steel/titanium - high interference - collar side
Applied factor on life: 1,18
Load Transfer: 36,2% 27,7% 36,2% / 36,2% 27,7% 36,2%

Analyzed Location

Last row in strap between sheet 1 and strap
Sheet 1

FML lay-up: Glare 2B-7/6-0,4
Thickness: 4,396 mm
Alloy: 2024T3
Prepreg: S2-glass, FM-94/BR127, 120°C curing
Orientation: Rolling direction in Al layers perpendicular to loading direction

Sheet 2

FML lay-up: Glare 2B-7/6-0,4
Thickness: 4,396 mm
Alloy: 2024T3

Prepreg: S2-glass, FM-94/BR127, 120°C curing
Orientation: Rolling direction in Al layers perpendicular to loading direction

Butt Strap
FML lay-up: Glare 2B-7/6-0,4
Thickness: 4,396 mm
Alloy: 2024T3
Prepreg: S2-glass, FM-94/BR127, 120°C curing
Orientation: Rolling direction in Al layers perpendicular to loading direction

Reference Curve
EK43-51649 (2024T3)

MSD Analysis
Number of scenarios: 100

Results
Initiation (lead crack):
Layer 1:
Mean: N = 1,75E+04 flights
StdDev: s = 7,43E-02
Layer 2:
Mean: N = 3,47E+04 flights
Layer 3:
Mean: N = 8,14E+04 flights
Layer 4:
Mean: N = 2,93E+05 flights
Layer 5:
Mean: N = 2,26E+06 flights
Layer 6:
Mean: N = 1,05E+29 flights
Layer 7:
Mean: N = 1,05E+29 flights

Detectable (lead crack):
Mean: N = 3,19E+04 flights
StdDev: s = 4,08E-02

Endurance:
Mean: N = 6,00E+04 flights
StdDev: s = 4,36E-19
Calculation stopped after 6,00E+04 schedules

T
Calculation of Load Distribution in Rivet Rows

Used software: FORTRAN software “Josef” from Airbus Deutschland GmbH

Calculation for GLARE2B butt strap, rivet rows 3 and 4:

```
1       GLARE2B-7/6-.4 Circumferential Joint
0        3- REIHIGE NIETUNG.
0       HAUTSTOSS
0
       E- MODUL DES BLECHES 2:   6420.00   N/MM**2
       E- MODUL DES BLECHES 1:   6420.00   N/MM**2
0
0       ABSTAND DER NIETREIHEN L(1) BIS L(N-1) IN MM.
       22.500   22.500
0
0       DATEN DER NIETUNG:
      NIET TYP  T1    T2   W1    W2      EN        EC
        1   1  4.30  4.30 22.50 22.50   11000.0    7200.0
        2   1  4.30  4.30 22.50 22.50   11000.0    7200.0
        3   1  4.30  4.30 22.50 22.50   11000.0    7200.0
0       NIET TYP  D     DNK   DKE   DC   DSENK   RIVET STIFFNESS
        1   1  4.80 10.00  4.80 10.00   .00       .2904E-03
        2   1  4.80 10.00  4.80 10.00   .00       .2904E-03
        3   1  4.80 10.00  4.80 10.00   .00       .2904E-03
0
0       ERGEBNISSE DER RECHNUNG:
       NIETKRAFT R 1/P=   .346   <- rivet rows 3 and 4 carry 34.6% of the to be transfered load
       NIETKRAFT R 2/P=   .308
       NIETKRAFT R 3/P=   .346
0
0       SSF   TEIL  NIET     KT     PHI
       10.39   1    1      1.29    1.54
        7.83   1    2      1.29    1.54
        6.47   1    3      1.29    1.54
        6.47   2    1      1.29    1.54
        7.83   2    2      1.29    1.54
       10.39   2    3      1.29    1.54
```

Calculation for GLARE4A-5/4-.4 Megaliner Barrel skin, outer rivet row of repair:

```
1       Megaliner Barrel GLARE4A-5/4-.4 Repair
0        4- REIHIGE NIETUNG.
0       HAUTSTOSS
0
       E- MODUL DES BLECHES 2:   5690.00   N/MM**2
       E- MODUL DES BLECHES 1:   5690.00   N/MM**2
0
0       ABSTAND DER NIETREIHEN L(1) BIS L(N-1) IN MM.
       28.000   28.000   28.000
0
0       DATEN DER NIETUNG:
      NIET TYP  T1    T2   W1    W2      EN        EC
        1   1  3.50  3.50 28.00 28.00   11000.0    7200.0
        2   1  3.50  3.50 28.00 28.00   11000.0    7200.0
        3   1  3.50  3.50 28.00 28.00   11000.0    7200.0
        4   1  3.50  3.50 28.00 28.00   11000.0    7200.0
0       NIET TYP  D     DNK   DKE   DC   DSENK   RIVET STIFFNESS
        1   1  5.60 13.00  5.60 13.00 13.00       .3057E-03
        2   1  5.60 13.00  5.60 13.00 13.00       .3057E-03
        3   1  5.60 13.00  5.60 13.00 13.00       .3057E-03
        4   1  5.60 13.00  5.60 13.00 13.00       .3057E-03
0
0       ERGEBNISSE DER RECHNUNG:
       NIETKRAFT R 1/P=   .285  <- outer rivet row carries 28.5% of the to be transfered load
       NIETKRAFT R 2/P=   .215
       NIETKRAFT R 3/P=   .215
       NIETKRAFT R 4/P=   .285
0
0       SSF   TEIL  NIET     KT     PHI
        8.27   1    1      1.26    1.11
        6.00   1    2      1.26    1.11
        4.71   1    3      1.26    1.11
        3.99   1    4      1.26    1.11
        6.59   2    1      1.26    1.02
        6.67   2    2      1.26    1.02
        7.96   2    3      1.26    1.02
       10.88   2    4      1.26    1.02
```

U
QVA-Z10-46-03

Qualitätssicherungsverfahrensanweisung

Daimler-Benz Aerospace Airbus

Bestimmung der Schälkraft von Klebstoffen im Rollenschälversuch (Bell)

QVA–Z10–46–03

1. Ausgabe: 30.08.96
Ausgabe:

Determination of the Peel Strength of Adhesives in Floating Roller Pell Tests (BELL)

Determination de la resistance a l'ecaillage de colles a l'essai d'ecaillage a l'aide de rouleaux

Ersatz für:
74–T–FG10–04
1. Ausgabe, 29.04.85

Inhaltsverzeichnis

Diese QVA wurde aufgrund der Umstellung der Handbuchsystematik in Anlehnung an die DIN EN ISO 9001 und der damit verbundenen neuen Numerierungssystematik redaktionell überarbeitet.

Eine fachliche Veränderung am Inhalt dieser Anweisung erfolgte nicht.

Eine vollständige Gegenüberstellung der Anweisungen 74–T– zu QVA ist der QVA–Z02–00–11 zu entnehmen.

geprüft: Neugebauer
LQM Neugebauer

1 Zweck der Anweisung

Dieses Prüfverfahren dient zur Ermittlung der Schälkraft von Klebungen. Es eignet sich nicht für Klebstoffe, deren Schälkraft nach dieser Anweisung ≦ 30 N ist.

Dieses Prüfverfahren kann eingesetzt werden

a) zur Beurteilung der Güte von Klebstoffen.

b) zur vergleichenden Beurteilung von Einflüssen auf die Festigkeit, die aus der Wahl der Verfahrensbedingungen herrühren können;

c) zur vergleichenden Beurteilung von Einflüssen auf die Festigkeit, die aus der Lagerung und Behandlung der Probekörper herrühren können, d. h. zur Beurteilung der Beständigkeit der Klebungen gegen äußere Einflüsse.

2 Geltungsbereich

MBB Unternehmensbereich Transport– und Verkehrsflugzeuge

3 Zusätzlich anzuwendende Anweisungen

80–T–34–9000	Kleben struktureller Verbindungen
DIN 51 220	Werkstoffprüfmaschinen – Begriff, Allgemeine Richtlinien, Klassen–einteilung
DIN 51 221	Zugprüfmaschinen

4 Verantwortlichkeiten

Verantwortlich für die Einhaltung dieser Anweisung sind die Org.–Einheiten, die mit der Probenherstellung, der Durchführung der Prüfung und Auswertung der Prüfergebnisse beauftragt werden.

5 Begriffe

a) Schälkraft Fs : ist die mittlere Trennkraft nach Abschnitt 6.6.1.

b) Standard–Probetafel : ist ein aus zwei Blechen hergestellter Prüfkörper, aus dem die einzelnen Probekörper entnommen werden.

c) Bruchart : Zur Beurteilung der Klebung wird die Bruchfläche nach folgenden Kriterien eingeteilt:

			Kurzbezeichnung
Adhäsionsbruch	:	Klebstoff oder Haftgrundmittel löst sich von der Metalloberfläche	A
Klebstoff–Kohäsionsbruch	:	Bruch in der Klebstoffschicht	K
Haftgrundmittel–Kohäsionsbruch	:	Bruch in der Haftgrundmittelschicht	P
Haftgrundmittel–Klebstoffbruch	:	Bruch in der Grenzschicht Haft–grundmittel/Klebstoff	PK

6 Bestimmung der Schälkraft von Klebstoffen im Rollenschälversuch (Bell)

6.1 Allgemeines

Die für die Untersuchung benötigten Probekörper werden einer Standard–Probetafel entnommen, die unter festgelegten und kontrollierten Bedingungen geklebt worden ist. Die Blechlagen der Probekörper werden in einer Rollenschälvorrichtung (nach Abbildung 3) in der Zugprüfmaschine voneinander abgeschält und die dafür benötigte Trennkraft ermittelt.

Die im Rollenschälversuch ermittelte Schälkraft darf nicht mit den Schälkräften, die nach anderen Prüfverfahren (z. B. nach dem CIBA– oder Klettertrommelschälversuch) bestimmt wurden, direkt verglichen werden.

6.2 Herstellung der Probekörper

Die Probekörper nach der Abbildung 1 werden frühestens 2 Stunden nach dem Aushärten des Klebstoffes aus der Standard–Probetafel nach Abbildung 2 parallel und rechtwinklig gesägt und so gekennzeichnet, daß die Zuordnung eindeutig zu erkennen ist und Verwechslungen ausgeschlossen sind. Beim Sägen sind die Bedingungen (Schnittgeschwindigkeit, Zähnezahl, Schränkung) so zu wählen, daß die Erwärmung der Klebung infolge Reibung möglichst gering gehalten wird.

Für die Herstellung der Standard–Probetafel sind 0,5 mm und 1,6 mm dicke Bleche der Aluminiumlegierung 3.1364.5 (2024 T3 clad) zu verwenden.

Die Vorbehandlung der Klebflächen sowie das Kleben Standard–Probetafeln geschieht nach den Angaben des 80–T–34–9000.

6.3 Anzahl der Probekörper

Mindestens 6.

6.4 Prüfeinrichtungen

a) Es ist eine Zugprüfmaschine nach DIN 51 221 Blatt 2 zu verwenden, die den allgemeinen Richtlinien für Werkstoffprüfmaschinen nach DIN 51 220 Klasse 1 und bezüglich der Prüfkraftanzeige der Klasse 1 nach DIN 51 221 Blatt 1 entspricht. Die Zugprüfmaschine muß mit einer Einrichtung zur Aufzeichnung des Kraft–Weg–Diagrammes ausgestattet sein. Der Kraftmeßbereich ist so zu wählen, daß die Schälkraft zwischen 10 und 90% des gewählten Meßbereichs liegt.

   Für die Bestimmung der Schälkraft bei erhöhter oder tiefer Temperatur muß die Zugprüfmaschine mit geeigneter Kammer mit entsprechender Temperaturregulierung vorhanden sein, die eine Einhaltung der Prüftemperatur über die Dauer der Prüfung auf ± 3°C gestattet.

b) Rollenschälvorrichtung nach Abbildung 3.

6.5 Durchführung der Prüfung

6.5.1 Bestimmung der Klebflächen

Die Breite der Klebfläche ist an jedem Probekörper auf 0,1 mm genau zu messen.

6.5.2 Prüfen bei Raumtemperatur

Der Probekörper ist in die in die Zugprüfmaschine eingehängte Rollenschälvorrichtung einzulegen, die Kraftanzeige auf Null abzugleichen und dann das abgewinkelte Ende des Probekörpers in die andere Klemme der Prüfmaschine so einzuspannen, daß eine gleichmäßige und mittige Krafteinleitung gewährleistet wird (siehe Abbildung 3). Dann wird der Probekörper mit einer gleichbleibenden Geschwindigkeit von 75 bis 100 mm/Minute über eine Länge von mindestens 150 mm abgeschält.

Während des Schälvorganges muß die Schälkraft in Abhängigkeit vom Spannkopfweg durch die Prüfmaschine in einem Schäldiagramm aufgezeichnet werden.

6.5.3 Prüfen bei erhöhter und tiefer Temperatur

Das Erwärmen des Probekörpers auf die Prüftemperatur hat mit einer Aufheizgeschwindigkeit von 6 bis 10°C/Minute zu erfolgen. Die Abkühlgeschwindigkeit ist beliebig. Der Probekörper ist 10 Minuten auf Prüftemperatur zu halten, bevor der Prüfvorgang einsetzt.

Die Temperatur ist mit einem Thermoelement, das an einer geeigneten Stelle des Probekörpers, abgeschirmt von der Wärmequelle, angebracht ist, zu überwachen.

Die Prüfung geschieht nach Abschnitt 6.5.2.

6.6 Prüfergebnisse

6.6.1 Bestimmung der mittleren Schälkraft

Die mittlere Schälkraft ist über eine Schällänge von 125 mm zu bestimmen, indem eine geschätzte Mittelwertlinie in das Diagramm eingezeichnet wird, wie es Abbildung 4 zeigt. Von der Mittelwertbildung ist der Anfangsbereich des Schäldiagrammes, der einer Schällänge von 10 mm nach dem ersten Maximum entspricht, auszuschließen. In Schieds–fällen ist die mittlere Schälkraft durch Planimetrieren zu bestimmen.

6.6.2 Beurteilung des Bruches

Die Anteile der einzelnen Brucharten (siehe Abschnitt 3 c) in Prozent der gesamten Klebflächen sind für jeden Probekörper abzuschätzen und im Prüfprotokoll anzugeben.

7 Dokumentation

Für betriebliche Prüfungen im Rahmen der Wareneingangsprüfung und Fertigungsüberwachung ist ein Prüfprotokoll zu verwenden, auf dem die ermittelte Schälkraft anzugeben ist.

Bei Reklamationen oder Entwicklungsversuchen ist ein ausführliches Prüfprotokoll zu erstellen, das folgende Angaben zu enthalten hat:

- Vollständige Bezeichnung des Klebstoffsystems, einschließlich Typ, Herstellercode, Herstellungsdatum, Chargennummer, Rollen–Nr., Werkstoffdatenblatt usw.
- Vollständige Angaben zum verwendeten Fügeteilwerkstoff einschließlich der wirklichen Streckgrenze in der Richtung der Belastung bei der Klebstoffprüfung.
- Einzelheiten der Vorbehandlung des Fügeteilwerkstoffes zum Kleben.
- Verarbeitungs– und Härtebedingungen, einschließlich Angaben, ob im Autoklav oder in der Presse gehärtet, Preßdruck, Aufheizzeit, Härtezeit und Temperatur usw.
- Anzahl der geprüften Probekörper.
- Auslagerungsbedingungen und Prüftemperatur.
- Typ der Prüfmaschine und Prüfgeschwindigkeit.
- Angaben zu den einzelnen Probekörpern, einschließlich genaue Abmessungen und mittlere Schälkraft.
- Bruchart, einschließlich des geschätzten Anteiles an Kohäsions– und/oder Adhäsions–, bzw. Klebstoff/Haftgrundmittel–Bruches in Prozent der Bruchfläche.
- Mittel–, Mindest– und Höchstwert der Schälkraft der Prüfreihe.
- Jede Abweichung von dieser Anweisung bei der Durchführung der Prüfung ist ausführlich zu beschreiben.

Qualitätssicherungsverfahrensanweisung **QVA–Z10–46–03**

Bestimmung der Schälkraft von Klebstoffen
im Rollenschälversuch (Bell)

1. Ausgabe: 30.08.96

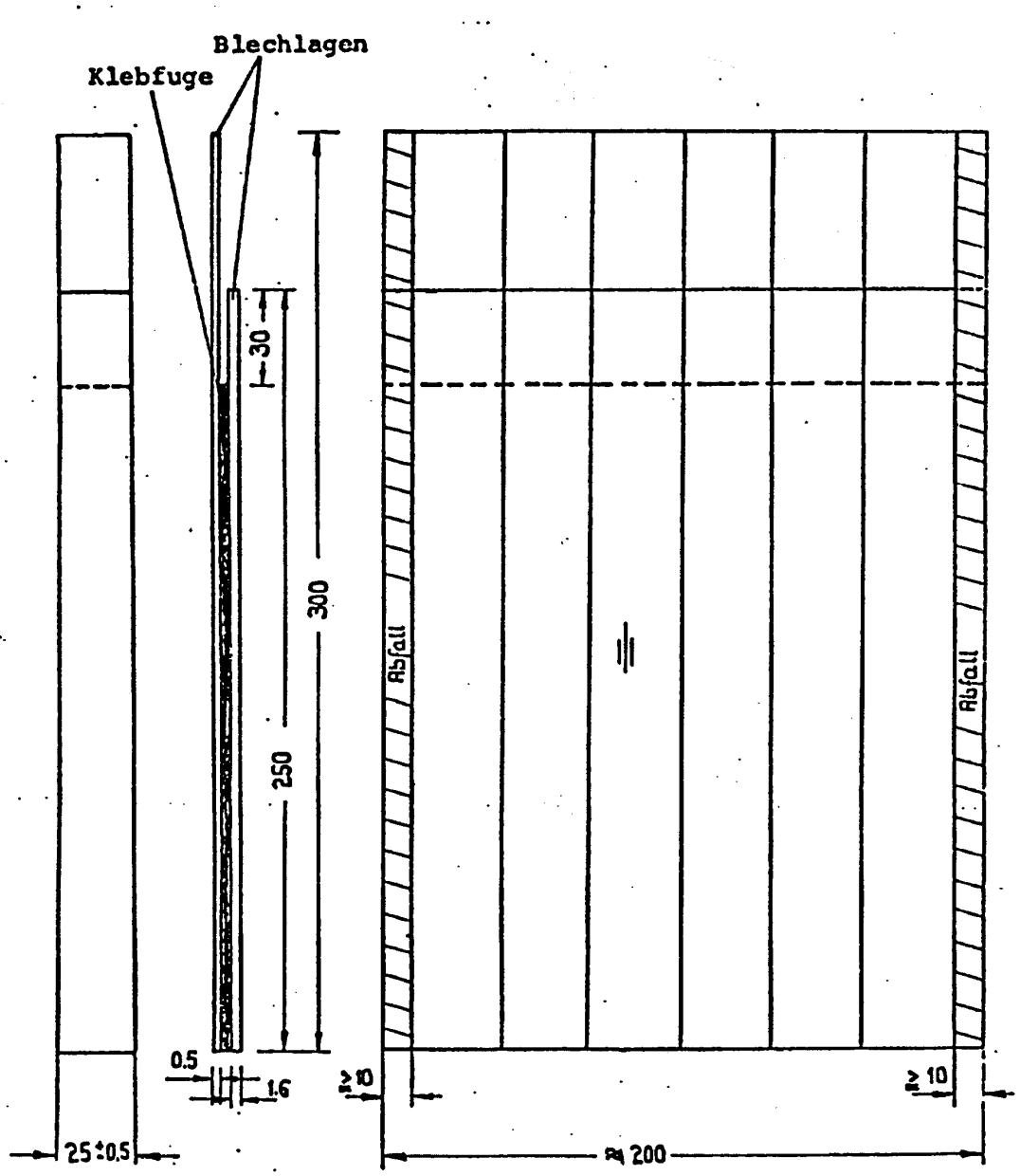

Abbildung 1:
Probekörper

Abbildung 2:
Standard-Probetafel und Schema der Probeentnahme

Walzrichtung

Qualitätssicherungsverfahrensanweisung **QVA–Z10–46–03**

Bestimmung der Schälkraft von Klebstoffen
im Rollenschälversuch (Bell)

1. Ausgabe: 30.08.96

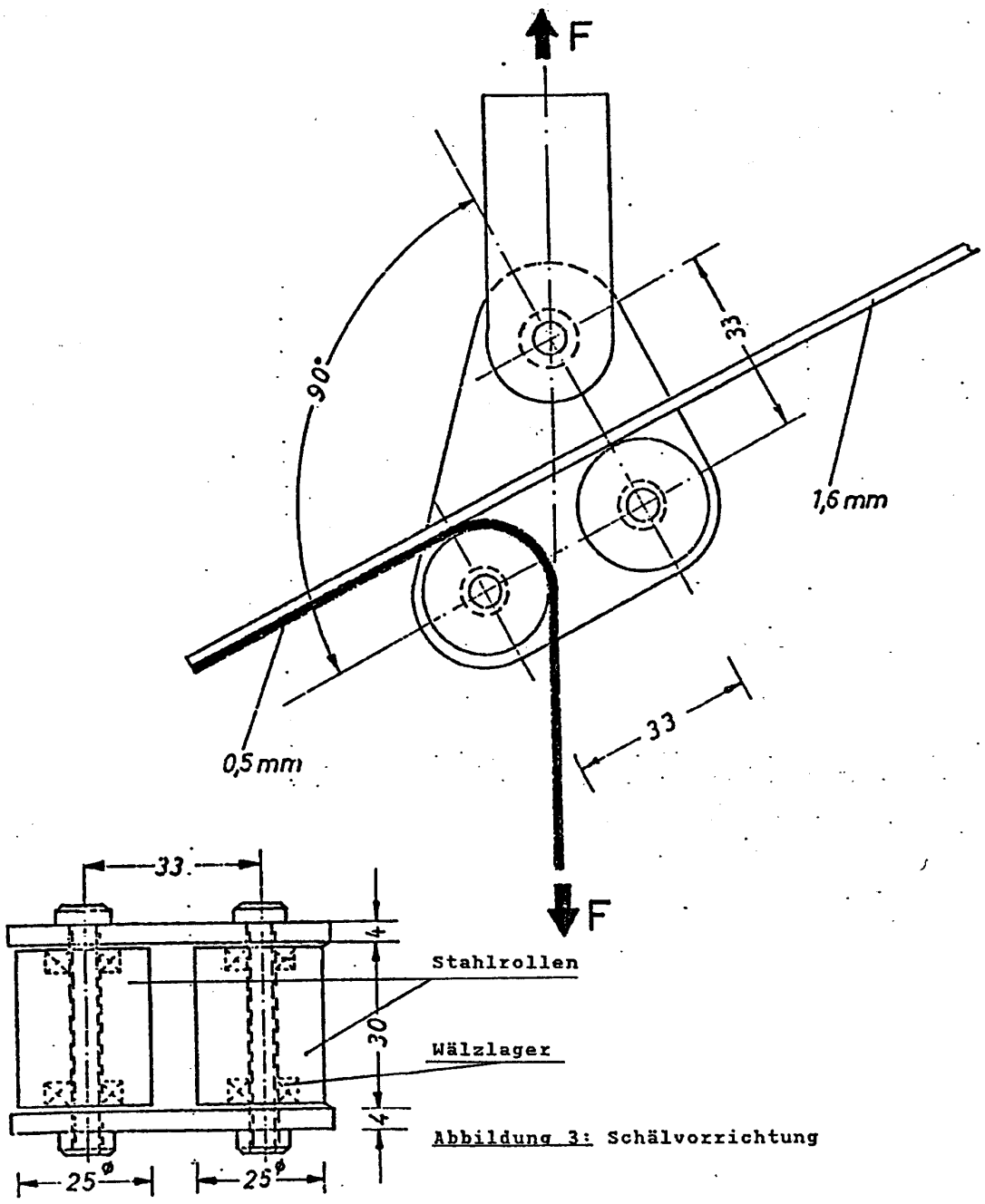

Abbildung 3: Schälvorrichtung

Qualitätssicherungsverfahrensanweisung **QVA–Z10–46–03**

Bestimmung der Schälkraft von Klebstoffen
im Rollenschälversuch (Bell)

1. Ausgabe: 30.08.96

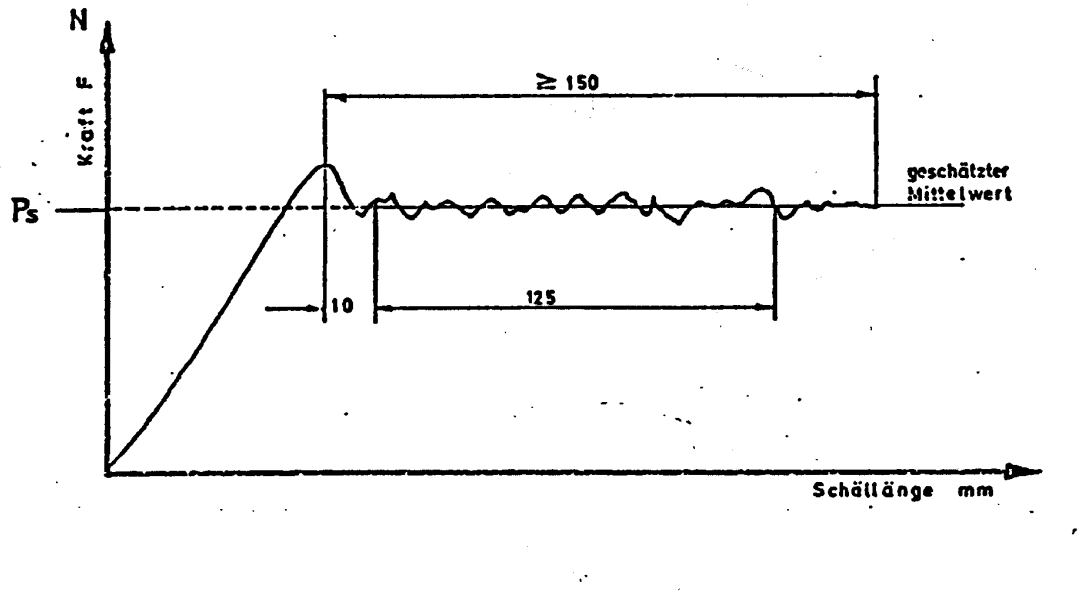

Abbildung 4: Schäldiagramm

V
Airbus Crack Wire Test Results

Example of crack propagation measurements on specimen 2-B-series butt straps, performed by Airbus. Reference chapter 7.1.1.

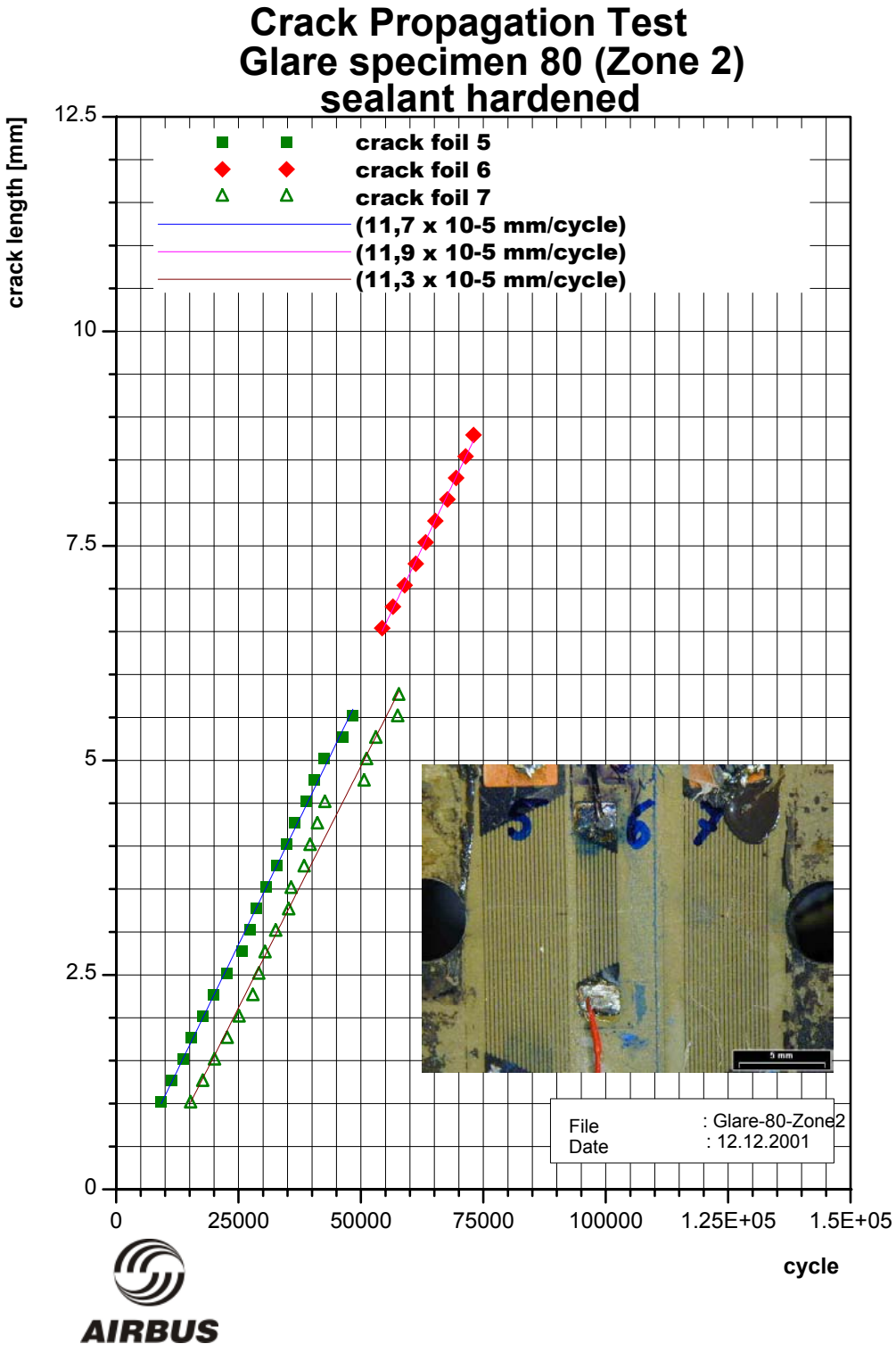

The Faculty of Aerospace Engineering of the Delft University of Technology broke the ground for the GLARE material application on aircraft structures. Professor Dr. Vlot concluded in 2001 his book “GLARE – History of the development of a new aircraft material” with the sentences:
“The influences on GLARE’s further development are so diverse, and so many, that the small circle of people who once sat down at the Delft coffee table together do not fully control GLARE anymore. GLARE is on its own.”

This book is addressing the most important items which have to be considered if a structural material develops from the laboratory status to an aircraft application. The ultimate proof for the material is the certification as part of an aircraft component by the dedicated Airworthiness Authorities. Therefore, relevant FAR/JAR25 paragraphs and strength prediction and justification methods are discussed for the GLARE application. Included in the analysis are predictions of the long term behaviour of GLARE, supported by an outdoor exposure program. The environmental influences on material properties, design values and on the strength justification methods are investigated and validated with test specimens which copy the design of Airbus full scale test specimens.

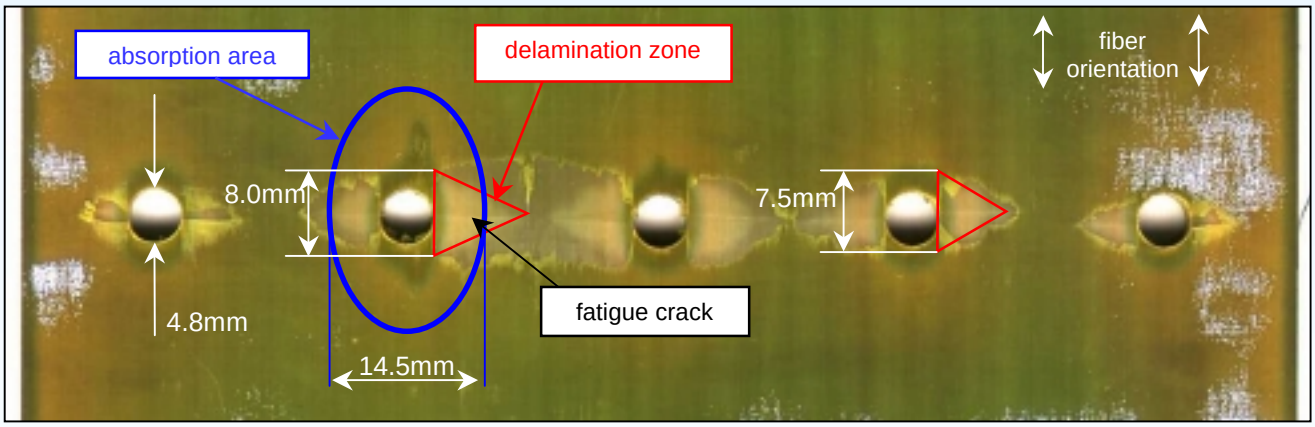

DELFT AEROSPACE
FACULTY OF AEROSPACE ENGINEERING